Redox Regulation of Type Iα PKA in the Heart

Hathaway, Natasha

Awarding institution:
King's College London

Title: Redox Regulation of Type I PKA in the Heart

Author: Natasha Hathaway

Redox Regulation of Type Iα PKA in the Heart

Natasha Hathaway

Kings College London
Department of Cardiology
Cardiovascular Division
The Rayne Institute
St Thomas' Hospital
London SE1 7EH

Thesis undertaken for the degree of

Doctor of Philosophy

ABSTRACT

The two regulatory RIα subunits of cAMP-dependent protein kinase (PKA) form interprotein disulfides during oxidative stress which is associated with kinase activation. PKA classical activation involves cAMP binding to the regulatory subunits causing release of catalytic subunits which phosphorylate substrates. Presence of substrate sensitises Type I PKA to cAMP. PKA subcellular localisation is determined by regulatory subunits binding A-kinase anchoring proteins (AKAPs), with RIα oxidation enhancing their binding. I assessed whether thioredoxin (Trx) redox recycles disulfide RIα back to its reduced state. In adult rat ventricular myocytes (ARVMs) pre-treatment with diamide (inducing disulfide) potentiated isoprenaline-induced cardiac Troponin I phosphorylation. Inhibition of monoamine oxidase (MAO), which metabolises monoamines to generate hydrogen peroxide (H_2O_2), blocked monoamine-induced RIα oxidation. Echocardiography revealed that RIα Cys17Ser 'redox-dead' knock-in (KI) mouse (which I verified cannot form disulfides) hearts had larger left ventricles during diastole and systole and demonstrated systolic dysfunction. Cytosolic RIα disulfide translocated to membrane and myofilament in isolated WT hearts in response to oxidant. Dual-specificity AKAP (D-AKAP) 1, D-AKAP2, AKAP220 and α / β tubulin were not co-purified with WT or KI RIα after cAMP-affinity capture. LC-MS/MS showed that the PKA substrates, alpha-enolase and ChChd3 did co-purify, but the AKAPs associated with these (myomegalin and sphingosine kinase interacting protein, respectively) were not co-captured. Trx recycled disulfide RIα back to its reduced state shown by an RIα-dependent decrease in NADPH fluorescence and RIα disulfide accumulation in ARVMs treated with Trx reductase inhibitors. In conclusion, whilst monoamines classically elevate cAMP to activate PKA, their degradation by MAO generates H_2O_2 which induces disulfide formation. Disulfide RIα translocates from cytosol to membrane and myofilament in response to oxidant, but whether this is due to an increased affinity for AKAPs remains unclear. Disulfide-induced sensitisation of PKA to cAMP is consistent with the idea it increases RIα affinity for AKAPs, so targeting PKA close to substrate to enable substrate-induced activation.

I lovingly dedicate this thesis to my dad, John Hathaway, who passed away in 2010. He was always there for me and was always so proud of me for studying a PhD.

'I know you are going through a difficult patch at the moment but I don't think you realise how proud we are of you, you are something else!!!

Dad xx'

ACKNOWLEDGEMENTS

I would like to thank my supervisor Professor Philip Eaton for his guidance, encouragement, support and also his enthusiasm about my work throughout the PhD ‘marathon’.

Fellow laboratory members also deserve a big thank you for sharing their knowledge and for giving advice and guidance in experiments; Dr. Rebecca Charles, Dr. Joe Burgoyne, Dr. Oleksandra Prysyazhna, Dr. Olena Rudyk and Dr. Ewald Schroder.

In addition, I would like to thank my friends at the Rayne Institute for being there to talk to about any problems or worries and for making working at the Rayne even more enjoyable; Karen, Dina, Alex, Becky, Denise, Abbi, Ike and Ellen.

I would also like to thank my sister, mum and Tony for their continued support and for believing in me.

Finally I would like to thank my fiancé Andrew for putting up with me being stressed and for motivating me to write my thesis especially during my maternity leave. I would also like to thank my daughter Zara-Louise for showing me what life is all about after my dad passing away and for giving me the goal of making her proud of me.

TABLE OF CONTENTS

LIST OF FIGURES

LIST OF TABLES

LIST OF ABBREVIATIONS

A	Amps
ADP	adenosine diphosphate
AKAP	A-kinase anchoring protein
AKB	PKA-binding domain
Ala	alanine
AP-1	activator protein 1
APS	ammonium persulfate
ARF	adenosine diphosphate (ADP)-ribosylation factor
ARVMs	adult rat ventricular myocytes
ASK1	apoptosis signal-regulating kinase 1
ATP	adenosine-5'-triphosphate
Au	gold
AUC	area under the curve
BH_4	(6R)-5, 6, 7, 8 - tetrahydro-L-biopterin
BIG1	Brefeldin A-inhibited guanine nucleotide-exchange protein 1
BIG2	Brefeldin A-inhibited guanine nucleotide-exchange protein 2
bp	base pairs
bpm	beats per minute
C	carbon
Cα	PKA catalytic subunit α isoform
Ca^{2+}	calcium
CaBP(1, 2)	Ca^{2+} binding protein 1, Ca^{2+} binding protein 2
$CaCl_2$	calcium chloride

cAMP	3′,5′-cyclic monophosphate
cDNA	complementary deoxyribonucleic acid
CF	coronary flow
cGMP	cyclic guanosine monophosphate
ChChd3	coiled-coil-helix-coiled-coil-helix domain-containing protein 3
Cl	chlorine
cMyBP-C	cardiac myosin binding protein C
CNC	carney complex
COX-2	cyclooxygenase-2
CPP	coronary perfusion pressure
CREB	cAMP response element-binding protein
CTnT	cardiac troponin T
cTnI	cardiac troponin I
Cu	copper
Cys	cysteine
d	diastole
D-AKAP(1a,b,c,d,2)	dual-specificity A-kinase anchoring protein (1a,b,c,d, 2)
DD	dimerisation / docking domain
DNA	deoxyribonucleic acid
dNTPs	deoxynucleoside triphosphates
DTPA	diethylene triamine pentaacetic acid
DTT	dithiothreitol
DUOX	dual oxidase
EC	excitation-contraction

E. coli	*Escherichia coli*
EDP	end diastolic pressure
EDTA	ethylenediaminetetraacetic acid
epac1	exchange protein directly activated by cAMP
ERK	extracellular signal-regulated kinase
FAD	flavin adenine dinucleotide
Fe	iron
Fe-S	iron-sulfur
FMN	flavin mononucleotide
g	gram
GAPDH	glyceraldehyde 3-phosphate dehydrogenase
GDP	guanosine diphosphate
GEP	guanine nucleotide-exchange protein
Gly	glycine
Gpx	glutathione peroxidase
GSH	reduced glutathione
GSSG	oxidised glutathione
GSK	glycogen synthase kinase
GTP	guanosine triphosphate
H	hydrogen
H^+	hydrogen ion
HCl	hydrochloric acid
HET	heterozygous
His	histidine
H_2O	water
H_2O_2	hydrogen peroxide

HRP	horse radish peroxidase
IP	intraperitoneally
IQGAP1	IQ domain GTPase-activating protein 1
IU	international unit
IVS	intraventricular septal width
JNK	c-Jun N-terminal kinase
KCl	potassium chloride
KDa	kilodalton
Kg	kilogram
KH	K-homology
KH_2PO_4	potassium dihydrogen sulphate
KI	knock-in
KO	knock-out
L	litre
LC-MS/MS	liquid chromatography-tandem mass spectrometry
LD_{50}	lethal dose, 50%
LTCC	L-type Ca^{2+} channel
LVAW	left ventricular anterolateral wall
LVID	left ventricular internal dimension
LVP	left ventricular pressure
LVDP	left ventricular developed pressure
LVPW	left ventricular posterior wall
m	metre
M	molar
mAKAP	muscle-specific AKAP
MAO	monoamine oxidase

MAPK	mitogen-activated protein kinase
mg	milligram
$MgCl_2$	magnesium chloride
$MgSO_4.7H_2O$	magnesium sulfate heptahydrate
min	minutes
ml	millilitre
mm	millimetre
mmHg	millimetres of mercury
M-mode	motion-mode
mM	millimolar
Mn	manganese
mRNA	messenger ribonucleic acid
ms	millisecond
m / s	metres per second
MSK-1	mitogen- and stress-activated protein kinase 1
Mw	molecular weight
N	nitrogen
Na^+	sodium ion
NaCl	sodium chloride
NAD^+	oxidised nicotinamide adenine dinucleotide
NADH	reduced nicotinamide adenine dinucleotide
$NaHCO_2$	sodium hydrogen carbonate
NFκB	nuclear factor kappa-light-chain-enhancer of activated B cells
NHE-3	Na+ / H+ exchanger 3
NHERF(-1/ -3)	Na+ / H+ exchanger regulatory co-factor(-1 /-3)

NKA	Na+ / K+ ATPase
nM	nanomolar
No.	number
NO	nitric oxide
NOS	nitric oxide synthase
NOX	NADPH oxidase
O / O_2	oxygen
$O_2^{\bullet-}$	superoxide
OD	optical density
$OH^{\bullet}$	hydroxyl radical
$ONOO^{\bullet}$	peroxynitrite
OPA1	optic atrophy 1
P	phosphorus
PAP7	PKA-associated protein 7
PBR	peripheral-type benzodiazepine receptor
PBS	phosphate buffered saline
PBS-T	phosphate buffered saline with 0.1 % Tween-20
PCR	polymerase chain reaction
PDE	phosphodiesterase
PDE4D3	phosphodiesterase 4D3
PDGF	platelet-derived growth factor
PDK	phosphoinositide-dependent protein kinase
PI3K	phosphoinositide-3 kinase
PKA	protein kinase A/ cAMP-dependent protein kinase
PK_a	acid dissociation constant
PKC	protein kinase C

PKD	protein kinase D
PKG	protein kinase G, cGMP-dependent protein kinase
PLB	phospholamban
PLC	phospholipase C
PLM	phospholemman
PP1	protein phosphatase 1
PP2A	protein phosphatase 2A
Pro	proline
Prx	peroxiredoxin
Pt	platinum
PTP	protein-tyrosine phosphatase
PVDF	polyvinylidene fluoride
Rcf	relative centrifugal force
Ref-1	redox factor 1
RFU	relative fluorescence units
RI	regulatory subunit I
RNS	reactive nitrogen species
ROS	reactive oxygen species
rpm	revolutions per minute
RVXF	arginine-valine-any residue-phenylalanine
RyR	ryanodine receptor
s	systolic
S	sulphur
S-AKAP84	spermatid A-kinase anchoring protein 84
SDS	sodium dodecyl sulphate

SDS-PAGE	sodium dodecyl sulfate polyacrylamide gel electrophoresis
secs	seconds
SeCys	selenocysteine
SEM	standard error of the mean
Ser	serine
SERCA	sarcoplasmic reticulum Ca^{2+}-ATPase
SFRS17A	splicing factor arginine / Ser-rich 17A
sGC	soluble guanylate cyclase
SphK	sphingosine kinase
SPHKAP	sphingosine kinase interacting protein
SR	sarcoplasmic reticulum
Srx	sulfiredoxin
StAR	steroidogenesis acute regulatory protein
TAE	tris acetate buffer with EDTA
TEMED	tetramethylethylenediamine
Thr	threonine
TnC	troponin C
TNFα	tumour necrosis factor
Trx	thioredoxin
TrxR	thioredoxin reductase
TXNIP	thioredoxin interacting protein
Tyr	tyrosine
U	units
V	volts
VLCD	very long-chain specific acyl-CoA dehydrogenase

WT	wild-type
w / v	mass / volume
XDH	xanthine dehydrogenase
XO	xanthine oxidase
Zn	zinc
^{o}C	degrees celcius
^{o}	degrees
µl	microlitre
%	percent
5-HT	5-hydroxytryptamine, serotonin
8-Br-cAMP	8-bromoadenosine 3′,5′-cyclic monophosphate
8-AEA-cAMP-agarose	(2- aminoethylamino) adenosine- 3', 5'- cyclic monophosphate immobilized on agarose
3-UTR	the three prime untranslated region

1 GENERAL INTRODUCTION

1.1 Generation of reactive oxygen species and reactive nitrogen species

Reactive oxygen species (ROS) is a catch-all term for a variety of free radicals (species with unpaired electrons) and molecules derived from molecular oxygen (O_2) that are generated through a sequence of reduction reactions. As shown in Figure 1.1, one electron reduction of O_2 generates superoxide ($O_2^{\bullet -}$), which can then undergo further sequential one electron reduction steps to hydrogen peroxide (H_2O_2), the hydroxyl radical ($OH^{\bullet}$) and then water (H_2O). ROS and species derived from nitric oxide (NO) can react to form secondary reactants known as reactive nitrogen species (RNS). For example, peroxynitrite ($ONOO^{\bullet}$) forms when NO and $OH^{\bullet}$ react. In addition, NO can be reduced to the nitroxyl ion (NO^-).

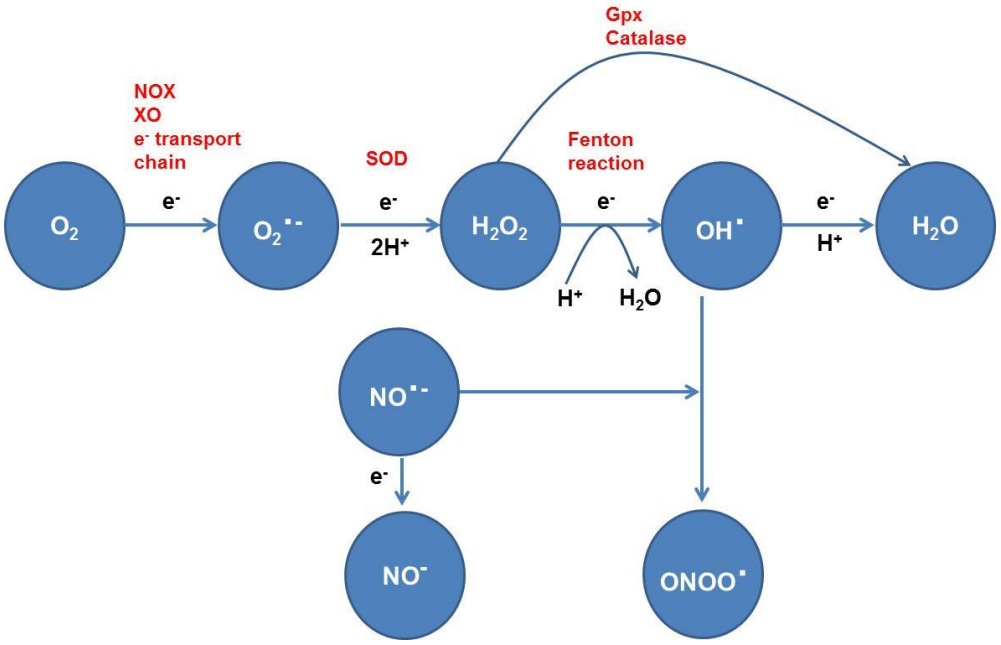

Figure 1.1 Generation of ROS and RNS.

O_2 can be sequentially reduced to superoxide (O_2•-), hydrogen peroxide (H_2O_2), the hydroxyl radical ($OH^{\bullet}$) and then water (H_2O) via a series of one electron (e^-) reduction steps. $O_2^{\bullet -}$ generation from O_2 can be catalysed by multiple enzyme systems including NADPH oxidases (NOX), xanthine oxidase (XO) and the electron transport chain. Superoxide dismutase (SOD) catalyses reduction of $O_2^{\bullet -}$ to H_2O_2 which can then be further reduced to $OH^{\bullet}$ during the Fenton reaction. H_2O_2 can also be decomposed to H_2O by antioxidant enzymes such as glutathione peroxidase (Gpx) and catalase. $OH^{\bullet}$ reacts with nitric oxide ($NO^{\bullet -}$) to form peroxynitrite ($ONOO^{\bullet}$) or is reduced to the nitroxyl ion (NO).

ROS generation has been studied extensively in phagocytic cells where NADPH oxidase (phox) is activated during engulfment of microbes to generate the 'oxidative burst'. Phox consists of a membrane-bound flavocytochrome *b*558, which is a complex made up of a flavin and haem-binding glycoprotein (gp91phox) and another subunit p22phox, several cytosolic regulators (p47phox, p67phox and p40phox) and also a small GTPase, Rac1 or Rac2.[1] Upon stimulation, the cytosolic subunits translocate to the membrane and interact with membrane-associated subunits leading to the transfer of an electron from NADPH to molecular O_2, forming $O_2^{\bullet-}$ which can then dismutate to H_2O_2, as explained below.[2] Various homologues of gp91phox have been identified in humans, designated as the NADPH oxidase (NOX) family, although the precise composition of NOX enzymes and their physiological roles are still being determined. The family consists of NOX1, NOX2 (formerly termed gp91phox), NOX3, NOX4, NOX5 and the dual oxidases, DUOX1 and DUOX2, which have an N-terminal extracellular peroxidase-like domain and a gp91phox-like oxidase portion.[1] Platelet-derived growth factor (PDGF) binds to the PDGF receptor causing autophosphorylation of tyrosine (Tyr) 740 and Tyr751 of the receptor and the binding and consequent activation of phosphoinositide 3-kinase (PI3K). The products of PI3K activity, phosphatidylinositol (3,4,5) trisphosphate and phosphatidylinositol 3,4-bisphosphate, bind to βPix, a guanine nucleotide exchange factor, which catalyses the exchange of guanosine diphosphate (GDP) for GTP, required for Rac activation and consequent NOX1 activation.[3] Epidermal growth factor also activates NOX1 via PI3K, βPix and Rac,[4] and generates H_2O_2.[5] Other stimuli for NOX activation include the pro-inflammatory cytokines interleukin-1β or interferon- γ,[6] and the vasoconstrictor angiotensin II which causes increased $O_2^{\bullet-}$ production in vascular smooth muscle associated with development of hypertension.[7]

As already considered, H_2O_2 may be generated by dismutation of $O_2^{\bullet-}$ involving its single electron reduction, which can occur spontaneously or through catalysis by superoxide dismutase (SOD), as shown below in reaction A. There are three mammalian isoforms of SOD; copper (Cu) / zinc (Zn) SOD (SOD1) located in the cytosol, manganese (Mn) SOD (SOD2) located in the mitochondria, and extracellular SOD (SOD3). In addition to producing H_2O_2, SOD enzymes also protect against $O_2^{\bullet-}$

cytotoxicity. $O_2^{\bullet-}$ reacts rapidly with NO to form $ONOO^{\bullet}$, potentially attenuating NO bioavailability and signalling.[8] $ONOO^{\bullet}$ also reacts with select Tyr residues to generate nitrotyrosine, which may also mediate dysfunction. This may also explain why in part increased NOX activity (producing $O_2^{\bullet-}$) is associated with impaired NO-mediated endothelial function, and increased risk of atherosclerosis, a condition in which the artery wall thickens and hardens due to accumulation of fatty materials.[9, 10]

(A) $2\ H^+ + 2\ O_2^{\bullet-} \longrightarrow H_2O_2 + O_2$

H_2O_2 can be further reduced to $OH^{\bullet}$ by the Fenton reaction,[11] (shown below in reaction B) which, for example in the mitochondria, can be catalysed by reduced transition metals present in the electron transport chain complexes (described later). The Fenton reaction is driven by the reduction of Fe^{3+} by $O_2^{\bullet-}$ regenerating Fe^{2+} (reaction C below).

(B) $Fe^{2+} + H_2O_2 \longrightarrow Fe^{3+} + OH^- + OH^{\bullet}$

(C) $Fe^{3+} + O_2^{\bullet-} \longrightarrow Fe^{2+} + O_2$

Another major source of ROS is the xanthine oxidoreductase system, which consists of two forms, xanthine dehydrogenase (XDH) and xanthine oxidase (XO), which are interconvertible by proteolysis. Both forms degrade purines by metabolising hypoxanthine to xanthine and xanthine to uric acid. The difference is that XO only reduces O_2, whereas XDH reduces O_2 and also NAD^+, having a higher affinity for NAD^+. Oxidation of reduced XO yields H_2O_2 as well as $O_2^{\bullet-}$.[12] Both increased XO activity and reduced SOD3 activity have been shown to contribute to increased oxidative stress and consequent endothelial dysfunction in patients with congestive heart failure.[13]

$O_2^{\bullet-}$ may be generated during aerobic respiration when single electrons leak from the mitochondrial electron transport chain and react with molecular O_2. The mitochondrial electron transport chain couples the transfer of electrons from NADH or succinate to molecular O_2 (reducing it to H_2O) with the transfer of H^+ ions across the membrane. The transmembrane proton gradient provides the energy required for phosphorylation of

adenosine diphosphate (ADP) to ATP by ATP synthase. As shown in Figure 1.2, the electron transport chain is made up of four electron-transporting complexes (I – IV) and one H^+-translocating ATP synthetic complex. Complex I (the NADH ubiquinone oxidoreductase) and complex III (the ubiquinol-cytochrome *c* oxidoreductase) are considered to be the major sources of $O_2^{\bullet-}$ in the chain,[14] as illustrated in Figure 1.2. Complex III releases $O_2^{\bullet-}$ to both sides of the inner mitochondrial membrane, whereas complex I only releases $O_2^{\bullet-}$ into the mitochondrial matrix.[15] The one electron transfer to molecular O_2 to generate $O_2^{\bullet-}$ is mediated by electron carriers present in the complexes of the electron transport chain. The electron carriers present in complex I are the flavin mononucleotide (FMN), the iron-sulfur (Fe-S) centers (N1a, N1b, N2, N3, N4, N5), and an unknown number of semiquinones. There is controversy about the source of $O_2^{\bullet-}$ in complex I, with evidence for it being fully reduced FMN,[16, 17] Fe-S centres N1a,[18] or N2,[19] the ubisemiquinones which are spin-coupled with Fe-S centre N2,[20] or both FMN and a semiquinone.[21] The electron carriers in complex III are the Rieske Fe-S center, cytochromes b_L, b_H and c_1 and the semiquinones at centers "*i*" and "*o*" and investigators agree that the source of $O_2^{\bullet-}$ in complex III is the Q_o semiquinone.[22, 23]

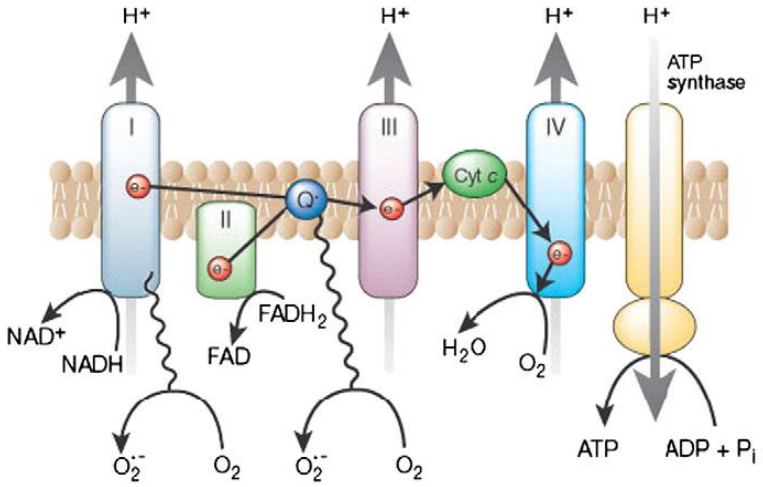

Figure 1.2 Generation of $O_2^{\bullet-}$ at complex I and III of the mitochondrial electron transport chain (adapted from Schaffer *et al*.[24]).

NADH is oxidised to NAD^+ transferring its electrons to complex I followed by coenzyme Q (ubiquinone) forming ubiquinol (Q). Electron carriers in complex I can also transfer electrons to molecular O_2 to form $O_2^{\bullet-}$. Succinate may also be oxidised to generate electrons for complex II (via flavin adenine dinucleotide **(**FAD)) followed by ubiquinone. Electrons are removed from ubiquinol and transferred to complex III, another major source of $O_2^{\bullet-}$, followed by cytochrome c (Cyt c). Electrons are then transferred to complex IV, which transfers the electrons to molecular O_2 to form H_2O. Whilst electrons are transferred along the chain, protons are pumped into the intermembrane space creating a proton gradient across the membrane. This gradient provides the energy to drive production of ATP by ATP synthase.

H_2O_2 can be reduced to H_2O and O_2 by catalase (as shown in reaction D below), or it can be reduced to H_2O by glutathione peroxidase (Gpx), a process fuelled by reduced glutathione (GSH) which is oxidised to GSSG, as shown in reaction E below. Catalase is localised in mitochondria and peroxisomes and Gpx is also localised in mitochondria as well as the cytosol suggesting that H_2O_2 generated in the mitochondria, for example, may be reduced in the mitochondria itself or diffuse across the membrane into the cytosol for reduction there.[14, 25, 26] Peroxiredoxins (Prxs) are also peroxidases that decompose H_2O_2 but they are reduced by thioredoxin (Trx) rather than GSH (as is the case for Gpx), which will be discussed in detail later.

(D) $2\ H_2O_2 \longrightarrow H_2O + O_2$

(E) $H_2O_2 + 2\ GSH \longrightarrow 2\ H_2O + GSSG$

Catalase, SOD, Gpx and 2-Cys Prxs (explained later) are all examples of antioxidant enzymes which are able to compete with other oxidisable substrates to inhibit or slow the oxidation of these substrates. Non-enzymatic antioxidants include α-tocopherol, β-carotene, GSH and ascorbate (vitamin C).[27]

NO synthase (NOS) enzymes catalyse the oxidation of L-arginine to L-citrulline generating NO. NO biosynthesis also requires the reducing agent (6*R*)-5, 6, 7, 8 - tetrahydro-L-biopterin (BH_4) and NADPH. Electrons are transferred from NADPH to the heme in the amino-terminal oxygenase domain of NOS via flavin adenine dinucleotide (FAD) and FMN in the carboxy-terminal reductase domain of the enzyme. There are three isoforms of NOS namely endothelial NOS (eNOS), inducible NOS (iNOS) or neuronal NOS (nNOS), all of which are dimeric. Healthy cardiac myocytes express eNOS and nNOS whilst iNOS expression is induced during inflammation in conditions such as heart failure. eNOS is the dominant form of NOS in the vasculature and NO generation can be stimulated by circulating factors such as acetylcholine, bradykinin, and adenosine or shear stress due to flowing blood. NO is important in activation of cGMP-dependent protein kinase (PKG) for endothelium-dependent vasodilation and blood pressure regulation (as explained later), and is also important in platelet activation, inflammation and thrombosis.[28-30]

All three isoforms of NOS are susceptible to 'uncoupling' where $O_2^{\bullet-}$ is generated rather than NO. eNOS uncoupling can occur due to depletion of the cofactor BH_4, as a result of its oxidation / degradation by $ONOO^{\bullet}$ to form cofactor-inactive pterins.[31] Uncoupling of eNOS can also result from oxidation of its Zn-thiolate complex by $ONOO^{\bullet}$. The Zn-thiolate complex stabilises the dimer interface of eNOS,[32] but interaction with $ONOO^{\bullet}$ releases Zn from the complex and promotes formation of disulfides between the subunits, reducing dimer stability and causing uncoupling of eNOS resulting in $O_2^{\bullet-}$ production.[33] Other mechanisms for eNOS uncoupling are depleted L-arginine levels, or increased levels of the endogenous eNOS inhibitor asymmetric dimethyl-L-arginine.[34] S-glutathionylation (formation of a mixed disulfide with glutathione (GSH), explained later) of eNOS also uncouples the enzyme producing $O_2^{\bullet-}$.[35] Uncoupled eNOS and therefore the consequential reduced NO

bioavailability results in endothelial dysfunction and is associated with conditions such as atherosclerosis,[28] and hypertension.[36]

1.2 Redox signalling

If ROS levels increase or levels of antioxidant 'defences' such as catalase, Gpx, Trx or SOD decrease, redox homeostasis is no longer maintained and there is a shift towards pro-oxidising conditions commonly known as oxidative stress. At high levels, ROS can damage proteins,[37] nuclear and mitochondrial deoxyribonucleic acid (DNA) resulting in accelerated cell death and unregulated cell proliferation,[38] as well as lipids resulting in altered cell membrane permeability.[39] Oxidative stress has been widely implicated in ageing,[40] cancer,[41, 42] and cardiovascular diseases such as hypertension,[43] injury during ischaemia and reperfusion,[44] as well as progression to hypertrophy and heart failure.[45] However, it is now known that oxidants are also produced in healthy tissue, where controlled levels play a key role in redox signalling (summarised in Figure 1.3).

Redox signalling may be defined as 'a regulatory process where the signal is delivered by redox chemistry' and this signalling can induce functional responses such as increased expression of antioxidant enzymes or altered activity of antioxidants, such as Prx as discussed later to sustain redox homeostasis and protect the cell from oxidative damage.[27] Redox signalling can also play regulatory physiological roles other than protection against oxidative stress, as considered below when the redox regulation of 3′,5′-cyclic monophosphate (cAMP)-dependent protein kinase (PKA) and cGMP-dependent protein kinase (PKG) are discussed. These crucial regulatory roles of oxidants may help explain why antioxidant therapies have been generally unsuccessful or even dangerous in some cases,[37, 38] as these reducing molecules may intercept the oxidants and prevent them from 'hitting' their regulatory targets and achieving their important homeostatic roles.

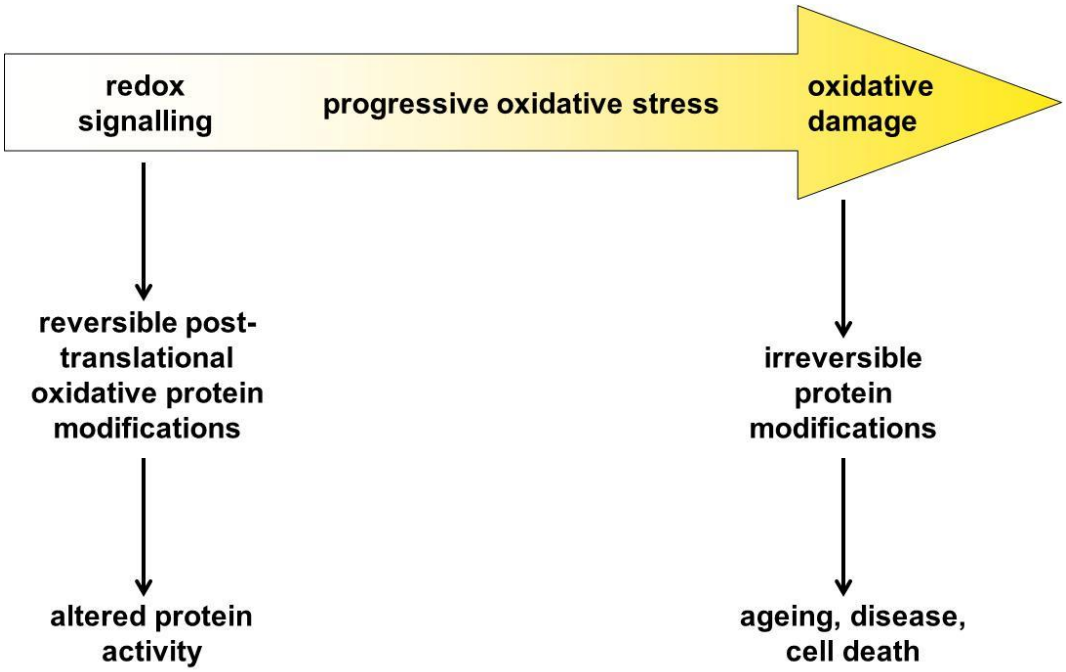

Figure 1.3 Schematic showing consequences of low and high levels of oxidants.

Low levels of oxidants play a key role in redox signalling which involves reversible oxidative protein modifications and can lead to altered protein activity. As the level of oxidants increases oxidative stress occurs and very high unregulated levels of oxidants can result in oxidative damage and irreversible protein modifications leading to ageing, disease and cell death.

1.3 Oxidative modifications of Cysteine thiols

Redox signalling can involve post-translational oxidative protein modifications allowing the transduction of an oxidant signal into a response (Figure 1.3). Methionine is an amino acid that can be reversibly oxidised to methionine sulfoxide by a range of ROS as well as be irreversibly oxidised to methionine sulfone.[39] Tyr can be nitrated by $ONOO^{\bullet}$ to form nitrotyrosine, with some evidence that this can be reversed by a denitrase.[40] As these amino acid modifications can be reversed, there may be potential for post-translational regulation.

Cysteine (Cys) contains a thiol group (S-H) on its side chain which is potentially reactive with oxidants. Oxidants such as H_2O_2 only react efficiently with thiols when they are deprotonated to the thiolate anion (S^-) state. The redox properties of a protein

thiol depend on its surrounding tertiary structure and its solvent environment. For example, the presence of adjacent positively charged amino acid lowers the acid dissociation constant (pK_a) of the thiol because these basic residues deprotonate it to S^-. These low pK_a thiols are likely to be principal targets for H_2O_2 at physiological pH.[41] Likewise, an 'acid-base' motif of flanking acidic (aspartic acid, glutamic acid) and basic (arginine, histidine (His), lysine) residues has been shown to be predictive of Cys thiols susceptible to S-nitrosylation (described below).[42] The side chain thiol of a typical Cys thiol has a pK_a of 8.0 meaning at physiological pH (~7.3) essentially none of it is ionised to the S^- state and so it is not reactive with oxidants. However, when in a deprotonating environment the pK_a of the thiol decreases. If the thiol pK_a lowers to 7.3, 50 % of it will be in the reactive state at physiological pH. The dependence of a Cys thiols reactivity on its pK_a means that some thiols are oxidant reactive whilst indeed most Cys thiols are not. This provides a basis for selective oxidant signalling. In summary, most proteins do not have Cys residues that react efficiently with physiological concentrations of oxidants whereas certain redox-active proteins do.

Figure 1.4 focuses on some examples of oxidative modifications of Cys thiols. H_2O_2 reversibly reacts with S^- to form a sulfenic acid (Protein-SOH) which can then be further irreversibly oxidised to sulfinic acid (Protein-SOOH) and then sulfonic acid (Protein-SO_2OH).[43] Under mild oxidising conditions, a sulfenic acid intermediate can react with a second reduced thiol to form a disulfide (Protein-S-S-Protein). This is reversible, and the disulfide can be either interprotein or intraprotein (i.e. between thiols in two proteins or between thiols in one protein respectively).[44] Similarly, mixed disulfides can form between a protein thiol and a thiol on a small Cys containing molecule such as GSH, which is known as S-glutathionylation.[43] Disulfide formation is important in preventing irreversible oxidation of thiols to the sulfinic / sulfonic acid forms. As already mentioned, the addition of the NO moiety to a Cys thiol produces an S-nitrosothiol (SNO) and this is known as S-nitrosylation (also referred to as S-nitrosation). The NO moiety may be provided by NO itself, nitrosothiols, nitrite or metal NO complexes, and de-nitrosylation can be performed by Trx,[42] as discussed in Chapter 6. S-nitrosylated proteins, like sulfenates, can also react with additional thiols to yield disulfides.

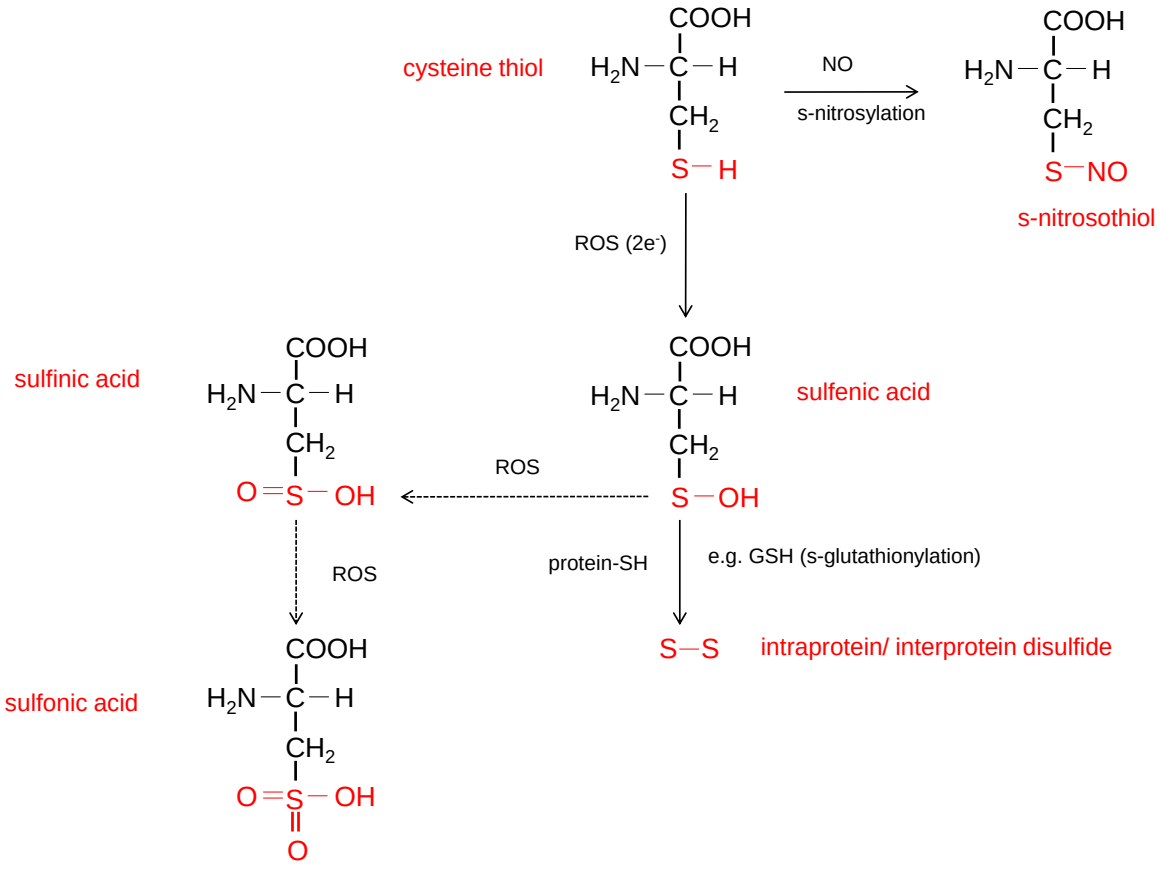

Figure 1.4 Examples of oxidative modifications of the Cys thiol.

Cys thiols may be S-nitrosylated to an S-nitrosothiol by addition of the nitric oxide (NO) moiety, reversibly oxidised to sulfenic acid, irreversibly oxidised to sulfinic or sulfonic acids or react with other protein thiols such as glutathione (GSH, known as S-glutathionylation) to form disulfides (intraprotein (between thiols of the same protein) or interprotein (between thiols of different proteins)). The unbroken line represents reversible modifications by Trx or glutaredoxin, whereas the broken line represents irreversible modifications.

1.4 Reversal of oxidative Cys thiol modifications

As already mentioned, some thiol modifications such as disulfides and S-nitrosothiols can be reversed enzymatically. Glutaredoxin (Grx) is able to reduce disulfides using two mechanisms (Figure 1.5). One mechanism uses the two Cys thiols in its active site, whereby one of the Cys thiols forms an interprotein disulfide with the oxidised substrate (step 1) which is then resolved by the other Cys thiol of Grx to form an intraprotein

disulfide in Grx (step 2). GSH then reduces this disulfide to form a mixed disulfide (step 3), which is then further reduced by GSH to form glutathione disulfide (GSSG) and regenerate reduced Grx (step 4). GSH is then regenerated by glutathione reductase using NADPH (step 5). The second mechanism for reduction of disulfides by Grx involves the thiol in the more N-terminal active site Cys of Grx being S-glutathionylated and then reduced by GSH (steps 6 and 4).[45] Trx is a universal disulfide reductase that catalyses thiol-disulfide exchange reactions by a similar mechanism that will be discussed in more detail in Chapter 6.

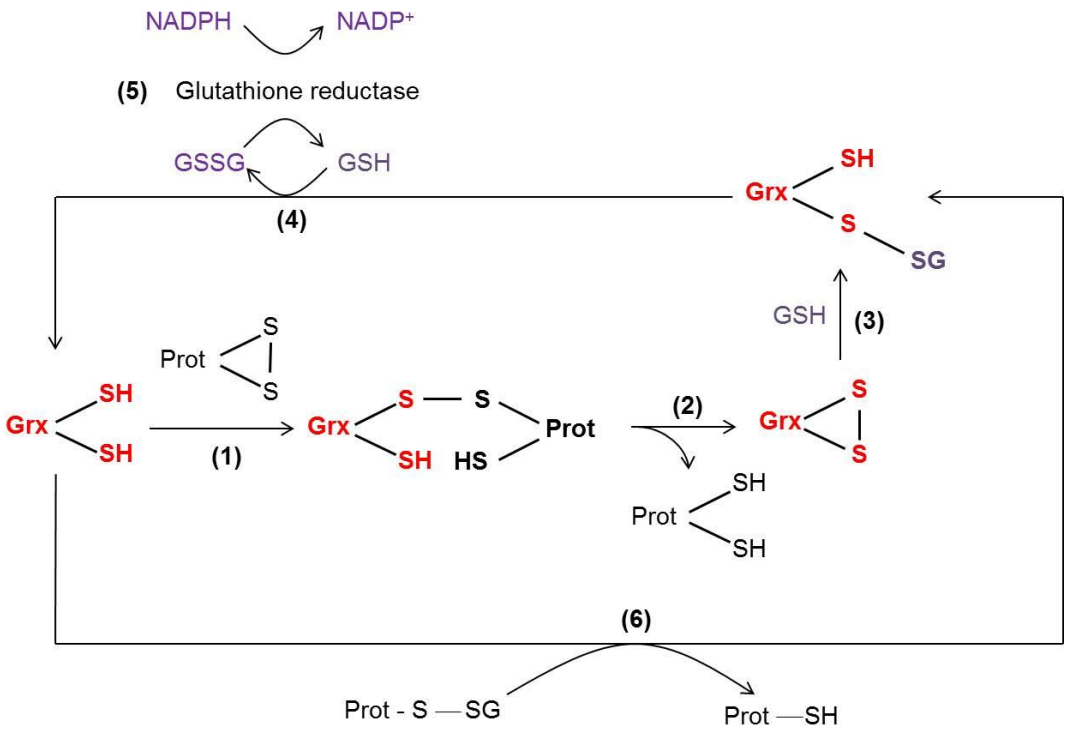

Figure 1.5 Mechanisms of protein disulfide reduction by Grx.

(1) Grx forms an interprotein disulfide with the oxidised substrate protein. (2) This is attacked by the resolving Cys thiol to form an intraprotein disulfide in Grx and reduced substrate protein. (3) GSH then forms a mixed disulfide with Grx. (4) Another GSH reduces this disulfide to regenerate reduced Grx and form GSSG. (5) GSH is regenerated from GSSG by glutathione reductase using NADPH. (6) Grx can also reduce protein disulfides by using one of its active site Cys thiols and forming a mixed disulfide which can then be reduced by GSH (same as (4)).

1.5 Examples of proteins modified by Cys thiol oxidation

Oxidant-reactive Cys thiols are found widely in many types of proteins including ion channels, signalling molecules and structural proteins, enabling their redox regulation. Numerous oxidation-sensitive proteins have been identified and some examples are shown in Table 1.1, which focuses specifically on signalling proteins that are regulated via thiol oxidation.

Protein	Modification	Result	References
2-Cys Prx	sulfinic acid	inactivation	[46]
MEKK1	S-glutathionylation	inactivation	[47]
p38α	interprotein disulfide	p38α phosphorylation	[48]
JNK	S-nitrosylation	inhibition	[49]
ASK1	interprotein disulfide S-nitrosylation	activation inactivation	[50] [51]
PKCγ (H_2O_2) **PKC α, β_{II}, ε, ζ ($O_2^{\cdot-}$)** **PKC (α, ε, β_1, γ, ζ)** **PKC**	disulfide disulfide S-glutathionylation S-nitrosylation	activation activation inactivation inactivation	[52] [53] [54, 55] [56]
PKA RI **PKA catalytic domain** **PKA RII and catalytic domain**	interprotein disulfide S-glutathionylation interprotein disulfide	activation inactivation inactivation	[57] [58] [59]
PKGIα	interprotein disulfide	activation	[60]
PTPB1	sulfenylamide S-glutathionylation	inactivation inactivation	[61, 62] [63]
MKP3	multiple disulfides	inactivation	[64]
RPTPα	interprotein disulfide cyclic sulfenylamide	inactivation inactivation	[65, 66] [67]
PTEN	intraprotein disulfide mixed disulfide	inactivation inhibition	[68] [69]
Yap1/Gpx3	interprotein / intraprotein disulfide	Yap1 activation	[70, 71]
OxyR	intraprotein disulfide	activation	[72-74]
c-Jun	S-glutathionylation	inhibition	[75, 76]
HSF1	intraprotein disulfide	inactivation	[77, 78]
NEMO **IKK** **p65** **p50**	interprotein disulfide S-nitrosylation S-nitrosylation S-nitrosylation	inhibition of IKK activation inhibition of IKK inhibition of NF*k*B gene transcription inhibition of NF*k*B DNA binding	[79] [80] [81, 82] [83]

Table 1.1. Table of example signalling proteins modified by thiol oxidation.

The table shows the type of Cys thiol oxidative modification that occurs in the protein and functional consequences and references to support these.

A number of signalling proteins have been identified as being responsive to H_2O_2 but the molecular mechanism has not always been clearly established (i.e. the specific post-translational oxidative modification). A functional response is often not defined. For example, Yang *et al.*,[84] showed that H_2O_2 induced Akt activation, but there was no molecular insight as to how H_2O_2 did this; this being a common scenario. In contrast, the molecular structural basis for the redox regulation of some redox-regulated proteins, such as Prx, PKG and PKA are at least in part understood as discussed in more detail below.

Prxs: Prx enzymes are ubiquitous thiol-containing Trx peroxidase antioxidant enzymes which reduce H_2O_2 to H_2O. Mammals have three classes which differ in the number and location of their Cys residues: typical 2-Cys (PrxI - PrxIV), atypical 2-Cys (PrxV) or 1-Cys Prxs (PrxVI),[46] but all isoforms contain a redox sensitive Cys which is termed the peroxidatic Cys.[85]

The first step in the catalytic cycle (Figure 1.6) for all isoforms is the oxidation of the peroxidatic Cys thiol to a sulfenic acid by reacting with H_2O_2. Typical 2-Cys Prxs exist as homodimers,[85] and contain a conserved NH_2-terminal Cys and a COOH-terminal Cys,[86] so following sulfenic acid formation, the resolving Cys thiol at the COOH-terminal of the adjacent monomer of the homodimer reacts with the sulfenic acid intermediate to form an interprotein disulfide. This disulfide is stable and can be reduced by Trx. In contrast, atypical 2-Cys Prxs are monomeric and so intraprotein disulfide bonds form between Cys thiols within the same polypeptide, again via a sulfenic acid intermediate. 1-Cys Prxs only have the conserved peroxidatic Cys but no resolving protein thiols. Instead the sulfenic acid form is resolved by the thiol in GSH,[85] forming an S-glutathiolate, an adduct that is reduced by Grx.

2-Cys Prxs can be inactivated by hyperoxidation of the peroxidatic Cys thiol to a sulfinic acid. For this hyperoxidation to occur, Prx must be turning over its catalytic cycle i.e. Trx must be present as well as H_2O_2. The Trx system may be required to expose or destabilise the Cys sulfenic acid for hyperoxidation by H_2O_2.[87] 2-Cys Prxs are believed to be more sensitive to hyperoxidation than other Prx classes because of interaction between the conserved YF and GGLG motifs. This interaction inhibits attack

of the Cys sulfenic acid by the resolving Cys thiol, slowing the rate of disulfide formation and increasing the probability of further oxidation by H_2O_2 to a Cys sulfinic acid.[85] Inactivation of 2-Cys Prxs by H_2O_2 allows accumulation of H_2O_2 and so H_2O_2-mediated signalling.[46] 2-Cys Prxs therefore function as 'flood gates' which, when active keep basal levels of H_2O_2 low, but when inactivated by increased levels of H_2O_2 during oxidative stress, this enables potentiated H_2O_2-mediated signal transduction.[85] However, it is unclear why other peroxidases not inactivated by this hyperoxidation mechanism do not prevent the 'gates' opening, providing an argument against the floodgate hypothesis.

Cys sulfinic acid formation is generally considered to be irreversible in most proteins, but the activity of 2-Cys Prxs after inhibitory sulfinic acid formation specifically can be restored by an enzyme known as sulfiredoxin (Srx).[86] Srx takes the γ-phosphate of ATP and transfers it to Prx sulfinic acid.[46, 88, 89] Transfer of the phosphate to Prx leads to phosphorylation and formation of a sulfinic acid phosphoryl intermediate in Prx,[46, 88] which then forms an interprotein thiosulfinate intermediate with Cys99 of Srx,[90, 91] or thiols such as GSH.[88] This thiosulfinate is then reduced by GSH or Trx.[89] In mammals, sestrin 2, a member of a protein family whose expression is regulated by p53, has been identified as another enzyme that can reverse hyperoxidised PrxI.[92] Reversal of sulfinic acid formation allows the termination of H_2O_2-mediated signalling and restores peroxidase activity, lowering H_2O_2 levels and so 'shuts-off' oxidant signalling.[86] This background information about the redox regulation of 2-Cys Prx enzymes is potentially useful in understanding PKA RIα. This is because RIα is also an antiparallel homodimer that forms a double disulfide during oxidative stress, as discussed below.

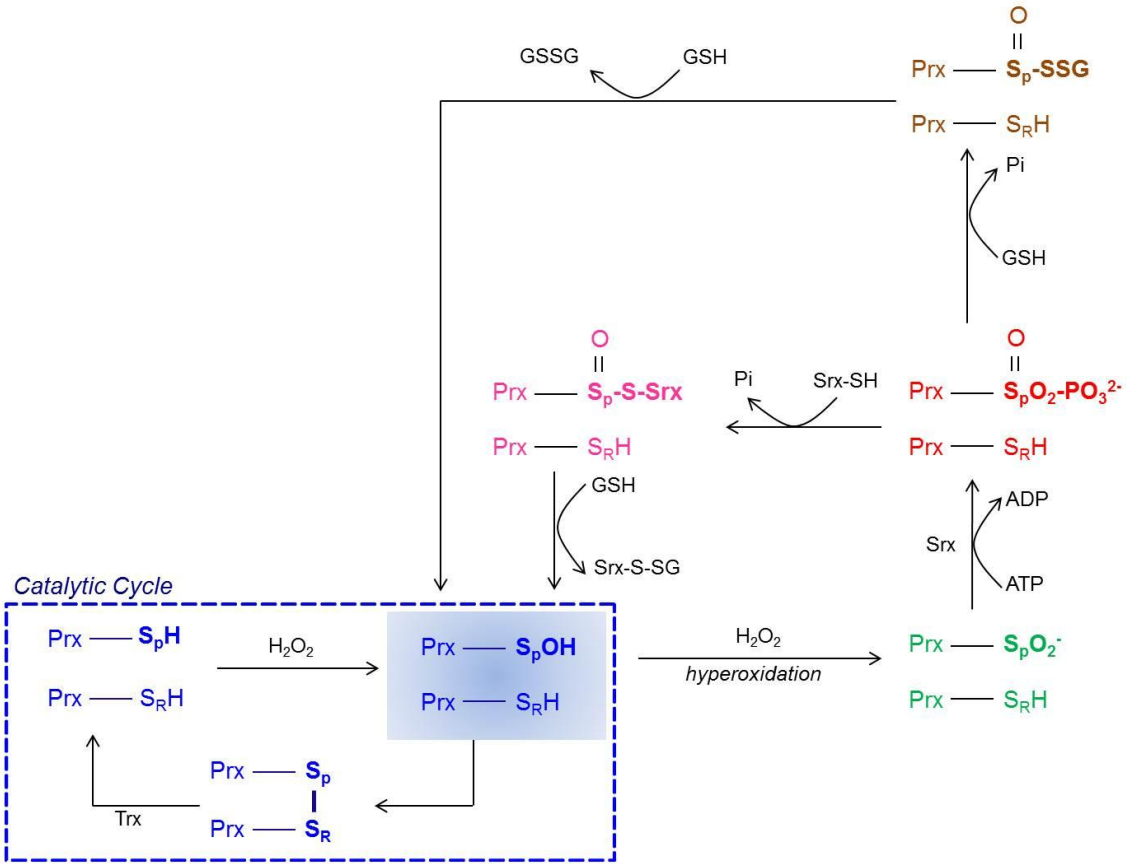

Figure 1.6 Oxidation of Prx and reduction of the sulfinic acid product by Srx (adapted from Jonsson et al. 2008,[89, 91]).

The catalytic cycle (in blue) of typical 2-Cys Prxs involves oxidation of the thiol (S_pH) of the peroxidatic Cys by H_2O_2 to a sulfenic acid (S_pOH) intermediate. This intermediate is then resolved by the thiol (S_RH) of a Cys on the adjacent monomer to form a disulfide bond which is reduced by Trx.[85] Some Prxs are sensitive to hyperoxidation by H_2O_2 and so the sulfenic acid intermediate is further oxidised to sulfinic acid ($S_pO_2^-$, in green).[46, 87] Srx is able to specifically target this and restore Prx activity. This process involves the transfer of a phosphate from ATP to Prx to form a sulfinic acid phosphoryl intermediate (Prx-$S_pO_2PO_3^{2-}$, in red).[46, 88, 89] This then forms a thiosulfinate bond with Srx,[90, 91] (in pink) or thiols such as GSH (in brown).[88] The complexes are then reduced by Trx or GSH forming the Prx sulfenic acid intermediate,[89] and the catalytic cycle can occur.

PKG: The classical mode of activation of PKG involves NO binding to the haem group of soluble guanylate cyclase (sGC) in smooth muscle, activating the kinase and increasing the conversion of GTP to cGMP.[93] The second messenger cGMP then binds to and allosterically activates PKG.[94] There are two types of PKG in mammalian cells; PKG I and PKG II. PKG I is highly expressed in smooth muscle as two isoforms (Iα and Iβ) that have identical catalytic and regulatory domains, but differ in their first ~100 amino acids.[95] PKG Iα exists basally as a parallel aligned 75 kDa homodimer with each subunit containing a C-terminal catalytic domain and an N-terminal regulatory domain. The subunits are held together by a leucine zipper in the regulatory domain and aligned PKG Iα molecules have Cys42 residues in close proximity.[96] Members of my research laboratory showed that H_2O_2 caused the formation of an interprotein disulfide linkage between the two Cys42 residues. PKG Iα disulfide formation directly activates PKG Iα increasing its affinity for substrates. This activation is independent of the classical NO-sGC-cGMP pathway, and contributed to H_2O_2-induced vasorelaxation of the coronary vasculature.[60] This oxidant-induced activation pathway also contributes to sGC-independent vasorelaxation induced by transnitrosylating NO donors.[97] In follow-up studies, a PKG Iα Cys42Ser 'redox-dead' KI mouse was found to be basally hypertensive,[98] and deficient in its vasodilatory blood pressure-lowering response to the thiol-oxidising drug nitroglycerin.[99] Disulfide formation represents a novel mechanism for direct cGMP-independent PKG Iα activation.

PKA: The structure and activity of PKA can also be regulated by oxidation, and is the primary focus of this thesis. After providing an overview of PKA structure and regulation, I will review current evidence as to its redox regulation.

***Regulatory subunit isoforms*:** PKA is a tetramer of two regulatory subunits and two catalytic subunits (Figure 1.7). There are two types of regulatory subunit; RI and RII and their presence defines Type I and Type II PKA respectively. There are also α and β isoforms of RI and RII encoded by different genes on different chromosomes. The open reading frames of RIα and RIβ are 75 % identical in nucleotide sequence and both proteins are 380 amino acids long and are 82 % identical in amino acid sequence.[100]

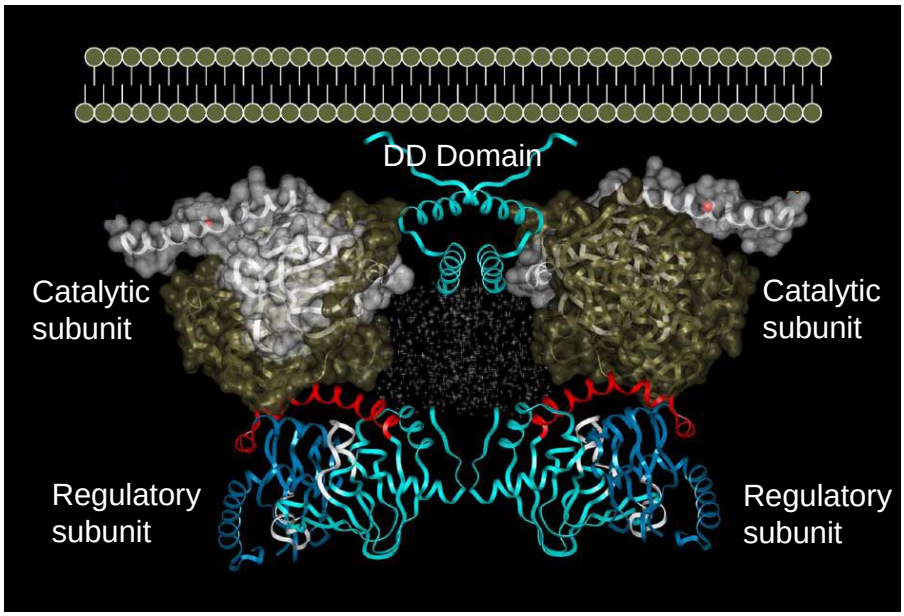

Figure 1.7 Model of the RIIβ holoenzyme based on small angle X-ray scattering (adapted from Taylor 2005,[101]).

All PKA holoenzymes consist of two catalytic subunits and two regulatory subunits. This figure also shows the dimerisation / docking (DD) domain important for dimerisation of the regulatory subunits and A-kinase anchoring protein (AKAP) binding, which determines PKA localisation e.g. allows PKA to anchor to membranes.

Regulatory subunit structure: All isoforms of the regulatory subunit have the same domain organisation (Figure 1.8). They have two C-terminal cAMP-binding domains (A and B) which couple cAMP binding to kinase activation and a linker region which contains phosphorylation sites. They also have SH3 binding domains and a pseudosubstrate inhibitor region which binds to the active site of the catalytic subunit, preventing it from phosphorylating substrates. Type II PKA can be autophosphorylated in its inhibitor region whereas Type I PKA cannot as the phosphorylated serine (Ser) residue is replaced with alanine (Ala). The regulatory subunits also have an N-terminal dimerisation / docking (DD) domain which dimerises RI or RII, and also determines PKA localisation via its binding to A-kinase anchoring proteins (AKAPs), as discussed in Chapter 5 (also see Figure 1.7).

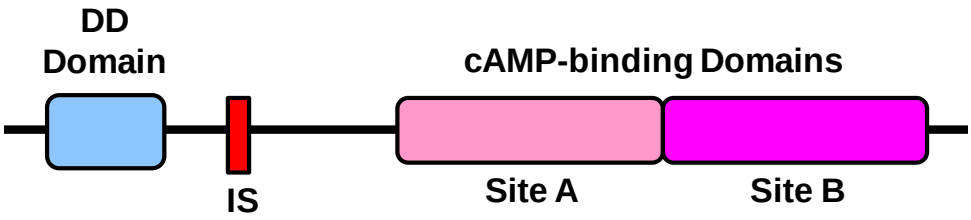

Figure 1.8 Domain organisation of PKA regulatory subunit.

It consists of a dimerisation / docking (DD) domain, which is important in dimerising the regulatory subunits and binding to A-kinase anchoring proteins (AKAPs) to determine PKA localisation, as well as a pseudosubstrate inhibitor site (IS) and cAMP-binding domains (A and B).

The DD domain refers to residues 12 - 61 in RIα, 14 - 62 in RIβ and 1 - 44 in RIIα / β. The DD domain of RIα (Figure 1.9) contains two Cys residues, RIβ contains three and there are none in the RIIα or β isoforms. I am primarily interested in RIα because it forms a disulfide dimer during oxidative stress,[57] and is constitutively expressed in the heart, whereas RIβ is restricted to neural tissue,[100] and the alignment of the Cys residues doesn't allow for disulfide formation. Solution nuclear magnetic resonance revealed that the DD domain of both RIIα and RIα is an X-type four helix bundle,[102] (as shown in Figure 1.9) where each subunit contains two helices (helix 1 and helix 2) separated by a turn.[103] As discussed later, each subunit contains two Cys residues (Cys16 and Cys37) which form disulfides during oxidative stress.[57] Dual-specificity AKAPs (D-AKAPs, explained in Chapter 5) bind at the region directly flanked by the two Cys residues, so as part of my PhD studies I assessed the logical possibility that disulfide formation may modulate AKAP binding to RIα.

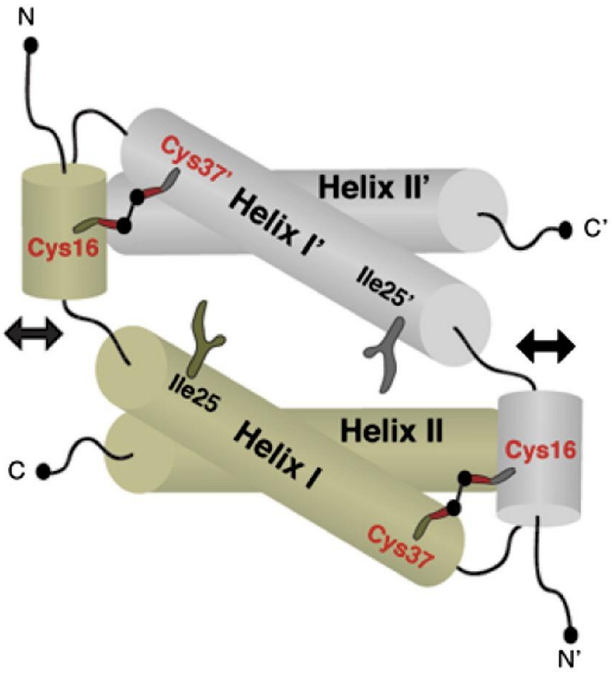

Figure 1.9 DD domain of RIα.[104]

The DD domain of both RIIα and RIα is an X-type four helix bundle as each subunit contains two helices (helix 1 and helix 2) separated by a turn. Each subunit contains two Cys residues (Cys16 and Cys37) which form disulfides during oxidative stress. D-AKAPs bind at the region flanked by the Cys residues so it is possible that disulfide formation may modulate AKAP binding to RIα.

Classical mode of PKA activation: As shown in Figure 1.10, the classical mode of PKA activation involves ligands binding to G_S-coupled receptors, e.g. catecholamines binding to β adrenoceptors. This causes the conversion of GDP to GTP which then activates adenylate cyclase which converts ATP to cAMP. cAMP binds to cAMP-binding domain B of PKA regulatory subunits causing a conformational change that allows cAMP to access cAMP-binding domain A. cAMP binding to domain A induces dissociation of catalytic subunits which catalyse the transfer of a phosphates to Ser / threonine (Thr) residues of substrates.[105] PKA signalling continues until phosphodiesterases hydrolyse cAMP, the catalytic subunit is inhibited by protein kinase inhibitor peptide,[106] or phosphatases dephosphorylate PKA substrates to return their activity to basal. G_S-coupled receptors, G-proteins and adenylate cyclase are also

compartmentalised to regulate where PKA signalling occurs. PKA itself is compartmentalised by binding to specific AKAPs, which help enable co-ordinated signalling by this kinase, explained in Chapter 5.

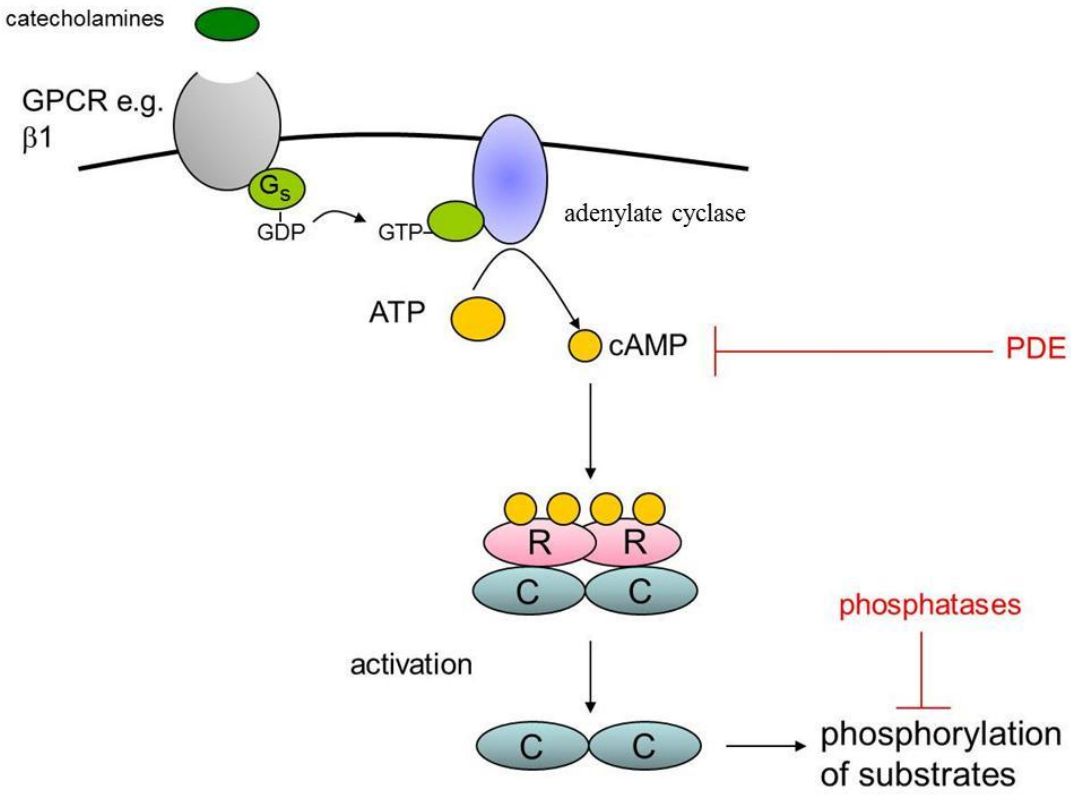

Figure 1.10 Classical mode of PKA activation.

GPCR activation e.g. catecholamine stimulation of the β1 adrenoceptor leads to conversion of GDP to GTP which activates adenylate cyclase to catalyse the conversion of ATP to cAMP. cAMP binds to the regulatory (R) subunits of the PKA tetramer, causing dissociation of the catalytic (C) subunits and phosphorylation of substrates. PKA signalling can be regulated by PDEs which break down cAMP, and phosphatases which dephosphorylate PKA substrates.

PKA catalyses the phosphorylation of a number of proteins involved in regulating a highly diverse range of physiological processes. A prominent example is glycogen metabolism in the liver, whereby PKA is activated by glucagon causing it to phosphorylate and activate glycogen phosphorylase kinase. This then phosphorylates and activates glycogen phosphorylase, which phosphorylates glycogen resulting in its breakdown to yield glucose. PKA also phosphorylates and inhibits glycogen synthase

resulting in inhibited glycogen synthesis contributing to increased glucose levels. PKA is therefore important in maintaining glucose homeostasis.[107] PKA also plays a role in promoting cell survival,[108] or promoting apoptosis,[109] depending on the cell-type. For example, in lymphoid cells, induction of the pro-apoptotic protein Bim_{EL} is a key event in cAMP-mediated apoptosis,[109] and the mechanism for this was shown to be PKA regulatory subunits binding to Bim_{EL} positioning it close to PKA catalytic subunits for catalysis of Bim_{EL} phosphorylation and therefore protection from proteosomal degradation.[110] Inhibition of apoptosis by PKA was observed in neuronal cells,[108] as well as endothelial cells during ischaemic late preconditioning.[111] Preconditioning is repeated intermittent short episodes of ischaemia that protects the myocardium against a subsequent longer otherwise injurious ischaemic insult and it is classed into early phase (lasting 2 - 3 hours) then late phase (lasting 2 - 3 days).[112] Phosphorylation of Akt (which then stimulates eNOS activity) by PKA and PI3K is important in protecting cells against ischaemia-induced cell death during late preconditioning.[111] My particular focus in this thesis, which will become evident later, is PKA's role in increasing the force and rate at which the heart beats, to elevate cardiac output. PKA achieves this by phosphorylating a number of Ca^{2+}-handling and sarcomeric proteins. These events and their redox regulation will be discussed in detail in Chapter 4.

Catalytic subunit oxidation: The catalytic subunit of PKA contains Cys thiols at positions 199 and 343. Cys199 is located in the activation loop but is not involved in catalysis and is protected from modification when the catalytic subunit is bound to regulatory subunits. At physiological pH, Cys199 is more reactive than Cys343, which is located in the C-terminus outside the catalytic domain.[58] Diamide, a thiol selective oxidant that induces disulfides, inhibited PKA activity,[58, 106] but recombinant catalytic subunit mutants with a Cys199 to Ala mutation (Cys199Ala) were resistant to this diamide-induced inhibition, suggesting Cys199 oxidation was responsible for the inactivation. In wild-type (WT) catalytic subunits inhibition could be reversed by dithiothreitol (DTT) suggesting that a disulfide bond was involved, which was identified as an internal disulfide between Cys199 and Cys343 (Figure 1.11).[58]

In the presence of diamide and GSH, the catalytic subunit forms a disulfide with GSH (S-glutathionylation) and this could be reversed by Grx.[58]

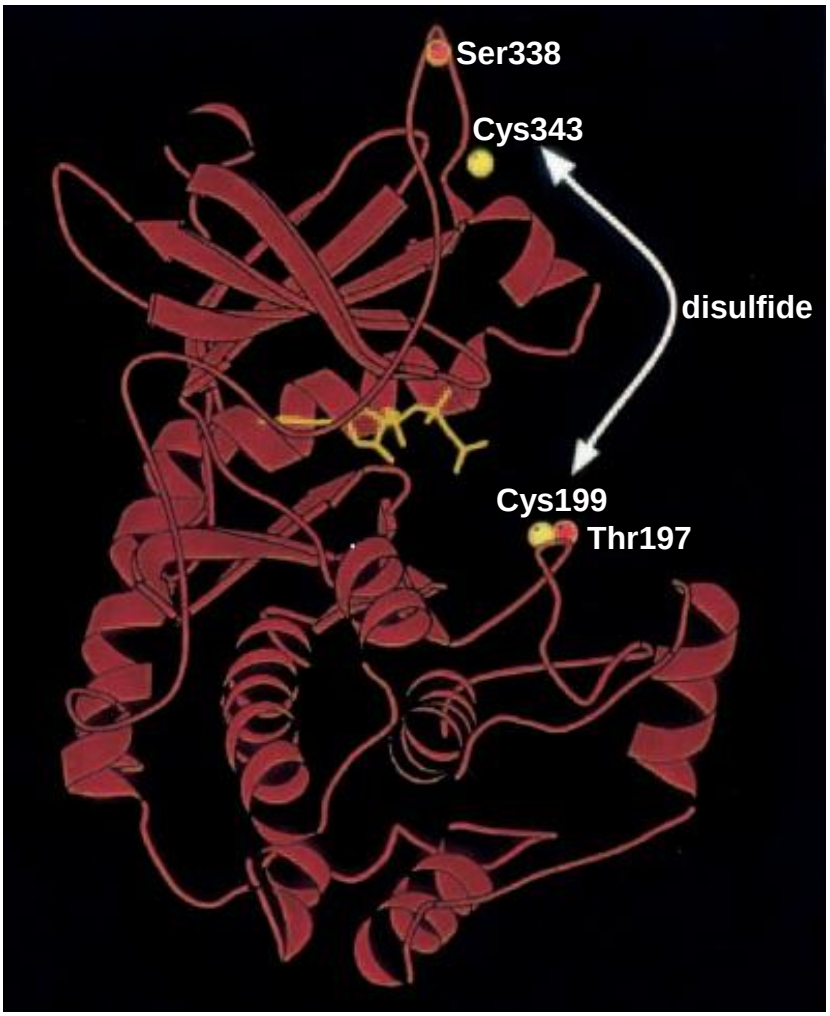

Figure 1.11 PKA catalytic subunit.[113]

Phosphorylation sites in the catalytic subunit are indicated by red circles (Ser338 and Thr197) and the Cys residues are indicated by two yellow circles. An intraprotein disulfide forms between Cys199 and Cys343, sensitising the catalytic subunit to dephosphorylation.

The catalytic subunit contains regulatory phosphorylation sites; Thr197 (in the activation loop) and Ser338 (near the C-terminus). Phosphorylation of Thr197, most probably by phosphoinositide-dependent protein kinase (PDK),[114, 115] is essential for optimal PKA activity involving the generation of a stable binding surface for RI.[113] Cys199Ala catalytic subunit mutants were inactivated by phosphatases,

whereas WTs were resistant to the inactivation. This demonstrates that Cys199, located proximal to the phosphate on Thr197, is involved in the resistance to dephosphorylation. Also, re-phosphorylation of PKA by PDK-1 was preferential when the catalytic subunit was reduced, suggesting that the redox state of PKA may determine its phosphorylation state.[113]

Regulatory subunit oxidation: Initially, the RIα dimer was thought to contain a constitutive double disulfide.[116] However, previous studies from my research laboratory showed, using diagonal electrophoresis with proteomic analysis, the disulfides only form in cellular RIα in response to oxidants.[57] Disulfides also are not necessary for dimerisation.[117] However, RIα prepared *in vitro* and kept in the absence of reducing agents does contain the disulfide due to air-mediated oxidation. RII also exists as a dimer but does not form disulfides consistent with the absence of Cys residues in the DD domain.

Diamide induced a biphasic response to PKA agonists in HeLa cells. Up to 100 μM diamide reversibly enhanced agonist-induced PKA activity, but this increase in activity did not involve increased adenylate cyclase activity (i.e. changes were independent of cAMP levels), or direct activation of PKA by diamide. The enhanced PKA activity was suggested to be a result of inactivation of a phosphatase that dephosphorylates PKA substrates.[106] H_2O_2 added exogenously or generated endogenously in adipocyte cell membranes via insulin stimulation caused Cys97 in the RII subunit and Cys199 in the catalytic subunit to form an interprotein disulfide. This modification prevented PKA activation upon cAMP addition and inhibited lipolysis.[59]

Previously, work from my research laboratory demonstrated that in adult rat ventricular myocytes (ARVMs) and isolated rat hearts, elevated levels of H_2O_2 caused the two RIα subunits of PKA to form interprotein disulfides,[57] (shown in Figure 1.12) as did the transnitrosylating NO donor nitrocysteine.[97] As shown in Figure 1.12, RIα subunits lie antiparallel to each other in the dimeric complex,[118] so Cys17 of one monomer is positioned opposite Cys38 of the other monomer. I do not know for certain whether Cys17 is the sensing thiol (i.e. the thiol that is oxidised first by H_2O_2), but this is rational in the context of the peroxidatic Cys in 2-Cys Prxs (as described above, see

Figure 1.6). The sensing thiol of one subunit (Cys17 in Figure 1.12) is likely oxidised to a sulfenic acid intermediate, which is then attacked by the resolving Cys thiol of the other subunit (Cys38 in Figure 1.12) to form an interprotein disulfide dimer. If this occurs on both Cys thiols of each RIα subunit, a double disulfide will form.

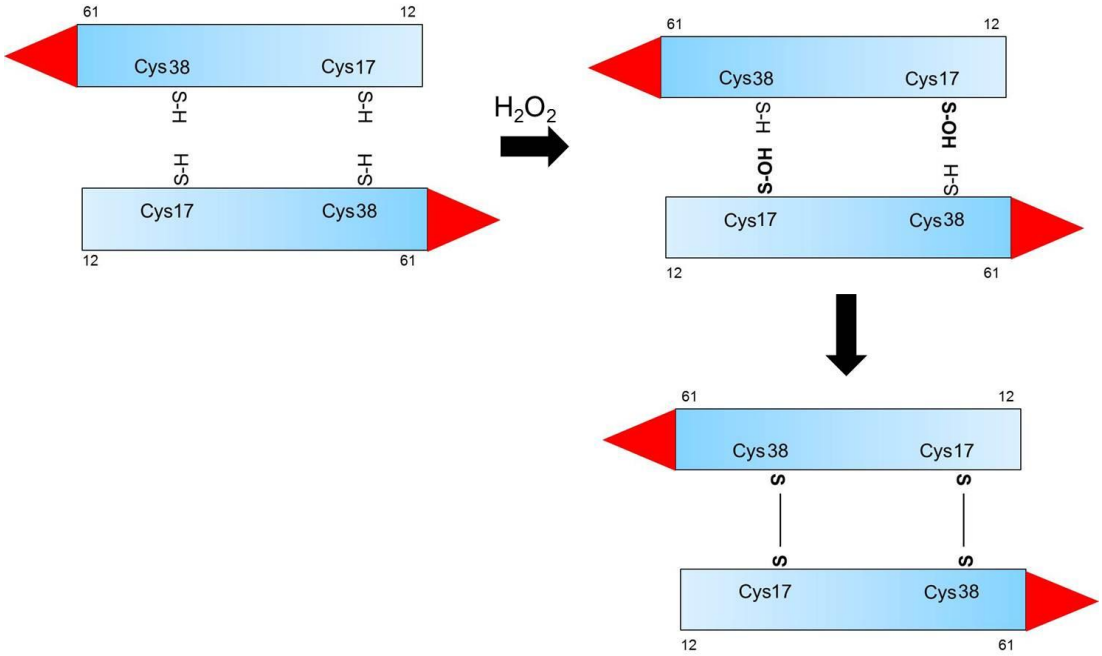

Figure 1.12 Proposed mechanism for RIα disulfide formation.

This schematic shows the DD domains of the RIα subunits (residues 12 - 61) lying antiparallel to each other so Cys38 and Cys17 are opposite each other. H_2O_2 causes the sensing thiol (e.g. Cys17, S-H) to form a sulfenic acid intermediate (S-OH) which is then resolved by the opposite Cys (e.g. Cys38) thiol to form interprotein disulfides (S-S).

Recombinant RIα disulfide *in vitro* is highly resistant to reduction with concentrations of 50 mM DTT or more required for significant reduction. Furthermore, adding urea to unfold the protein does not lower the concentration of DTT required. This suggests that the disulfides are well shielded from the cell's reducing environment.[117] Also, mutating Tyr19 or His23, which are in close proximity to the disulfide, interferes with disulfide formation so these residues may help stabilise the disulfide.[119]

In isolated rat hearts, disulfide dimerisation of RIα induced translocation to the myofilament compartment and the nucleus, potentially positioning PKA closer to its substrates. RIα disulfide formation seemed to activate PKA, independently of cAMP, as

demonstrated by increased phosphorylation of PKA substrates and increased myocyte contractility. However, these phosphorylation events were not blocked efficiently by the PKA inhibitor H89. Also, no 'simple' *in vitro* demonstration of disulfide-activation of the kinase was provided.[57]

Interestingly, neither intraprotein disulfide formation or S-glutathionylation of the catalytic subunit of PKA, nor interprotein disulfide formation between the regulatory subunits and catalytic subunits of PKA have been observed in cardiac tissue samples prepared by members of my research laboratory. These oxidative modifications have not been identified using multiple screening approaches for cardiac proteins susceptible to Cys-targeted oxidation.[120-123] These observations that seemingly contradict those in the literature,[58, 59] may be a result of different model systems. In addition, perhaps, RIα oxidation serves to first activate the kinase, with subsequent catalytic subunit inactivation serving as a regulatory 'off-switch'. This would avoid chronic PKA activation during oxidative stress.

1.6 Primary aims of this thesis

PKA RIα disulfide formation during cardiovascular oxidative stress warrants further study as we do not fully understand the physiological significance of this process. Consequently the over-arching goal of my PhD studies is to increase our knowledge of this oxidation event. My work addresses some of the many remaining questions with regards to the biochemistry, cell biology and implications for cardiovascular physiology that ensue as a result of disulfide oxidation of PKA RIα.

Comparisons will be made between hearts from a novel Cys17Ser RIα 'redox-dead' knock-in (KI) mouse line which, in theory, will not form a disulfide in response to oxidative stress, and hearts from WT mice to determine the contribution of this oxidative event to function of PKA specifically and function of the heart in general.

I plan to use the mutant KI mouse, biochemical and cell biological approaches to address the following, which will be discussed in more detail in subsequent chapters:

1. Whether the Cys17Ser RIα KI mouse, which is unable to form a disulfide, has a cardiac phenotype

2. Whether RIα disulfide formation synergises or counteracts the classical mode of PKA activation by cAMP

3. Whether there are AKAPs that selectively bind disulfide-oxidised RIα

4. Whether the Trx system reverses RIα disulfide back to the reduced thiol state

2 GENERAL METHODS & DEVELOPMENT OF METHODS

2.1 GENERAL METHODS

2.1.1 Reagents

Unless stated otherwise, reagents were obtained from Sigma Aldrich.

2.1.2 Generation of a novel 'redox dead' Cys17Ser RIα knock-in (KI) mouse

Mice constitutively expressing RIα Cys17Ser (knock-in, KI) were generated for us on a pure C57BL/6 background by TaconicArtemis. A targeting vector was constructed, which involved polymerase chain reaction (PCR) amplification of the murine Prkar1 region, introducing the Cys17Ser mutation into exon2 (the translation initiation codon) by site directed mutagenesis and inserting an FRT-flanked neomycin selection marker (to allow for selection of transfected embryonic stem cells) close to the mutation to favour homologous recombination. Then screening by Southern blot was carried out to identify if homologous recombination had occurred followed by validation of the positive clones. Embryonic stem cell transfection was then carried out followed by chimera generation. The chimeras were directly bred with an Flp deletor for the *in-vivo* deletion of the selection marker. As the embryonic stem cells always go germline, chimeras can be directly bred to the deletor in order to obtain germline transmission and selection marker deletion at the same time.

2.1.3 Breeding of mice

Mice were set up as heterozygous : heterozygous breeding pairs to generate wild-type (WT) or KI mice. Mice were bred at 6 - 7 weeks old and able to breed for ~6 months. Gestation lasted ~3 weeks and then the mice were weaned at 3 weeks old.

2.1.4 Genotyping of mice

The genotype of each mouse was determined by isolating deoxyribonucleic acid (DNA) from a small piece of mouse ear tissue using the Qiagen DNAeasy tissue kit. PCR was then performed followed by DNA electrophoresis.

Ear-clipping: Ears of mice were clipped to provide the tissue for DNA isolation and clipped in such a way that each mouse could be identified i.e. each mouse was numbered and then either right, left or right and left ear-clipped etc. The clipping was stored in the freezer until DNA isolation was carried out.

DNA isolation: The standard protocol provided in the Qiagen DNAeasy tissue kit was followed. All the DNeasy mini spin columns, collection tubes and buffers (of an undisclosed proprietary composition) were provided in this kit (unless stated otherwise).

The mouse ear clipping was placed in an Eppendorf tube. 180 µl ATL buffer and 20 µl proteinase K were added. The mixture was vortexed and incubated at 55 ºC on a shaker (1000 rpm) overnight. The next morning, the samples were removed from the incubator and vortexed. 400 µl buffer AL - ethanol (1:1 ratio, Fisher Scientific) mixture was added to each sample and vortexed. The mixture was then pipetted into the DNeasy mini spin column placed in a new collection tube and centrifuged at 10000 rpm for 1 min. The flow-through was then discarded and the spin column was placed in a new collection tube. 500 µl buffer AW1 was then added to each sample and centrifuged at 10000 rpm for 1 min. The flow-through was then discarded and the spin column placed in a new collection tube. 500 µl Buffer AW2 was then added and the sample centrifuged at 10000 rpm for 3 min. The flow-through was then discarded and the spin column placed into a 1.5 ml Eppendorf tube. 200 µl of buffer AE was then pipetted onto the DNeasy membrane and after 1 min incubation at room temperature was centrifuged at 10000 rpm for 1 min. The DNA elute (flow-through) was now ready for PCR.

PCR: The genotype of each mouse was identified by first using a PCR reaction developed by TaconicArtemis (Figure 2.1). The volume of each reagent required for one reaction (i.e. one sample) is shown in Table 2.1. A master-mix was made where these volumes (except that of DNA) were multiplied by the number of samples to be analysed

and added to an Eppendorf tube on ice. The master-mix was then split into the number of samples to be analysed (36 µl) and the DNA was added (4 µl). The samples were then placed in the thermal cycler (Eppendorf) and the program detailed in selected and started. When the program was finished, the samples were held at 4 ºC.

Reagent	Volume for one PCR reaction (µl)
5 x green GoTaq flexi buffer (Promega)	10
25 mM $MgCl_2$ (Promega)	4
10 mM dNTPs (Promega)	1
5 µM PKA primer 1 (Invitrogen) **GCT TTC CTT TAC CAA GCA GG**	1
5 µM PKA primer 2 (Invitrogen) **GTC TGT GAG TCA CAC TGA CC**	1
Taq (5 U / µl) (Promega)	0.4
nucleotide free H_2O	35.6
DNA elute	4

Table 2.1 Volumes of reagents required for one PCR reaction.

First a master-mix was made which had all the reagents present except DNA and then 36 µl of this was added to 4 µl DNA.

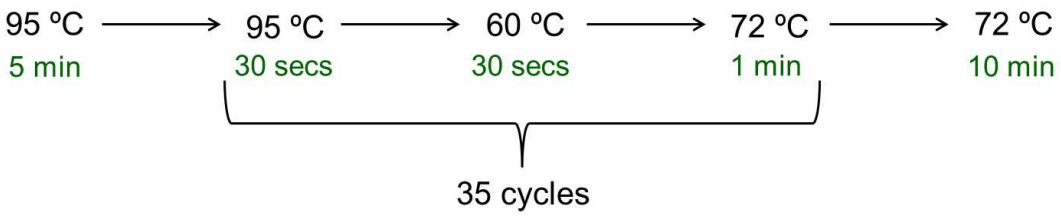

Figure 2.1 Details of PCR reaction program.

Temperatures and period the reagents were incubated at each temperature are shown.

DNA electrophoresis: After PCR, the genotype of the mouse was determined by carrying out DNA electrophoresis. 4 g agarose and 200 ml 1 x tris acetate buffer with ethylenediaminetetraacetic acid (EDTA) (TAE) (50 x TAE (1 l): 242 g Tris base, 57.1 ml glacial acetic acid, 18.6 g EDTA) was heated in microwave for ~2 min to make a 5 % agarose gel and then 5 µl of GelRed^{TM} Nucleic Acid Gel Stain (Biotium) (stains DNA) was added. The mixture was poured into the electrophoresis tank and allowed to set. 1 x TAE was then poured over the gel. The PCR products were loaded (15 µl of each) on the agarose gel and in the first lane the 100 bp DNA step ladder (Promega) was loaded (5 µl). The gel was run at 160 V for 30 min or until the samples had run far enough through the gel.

Analysis of PCR products: The gel was removed from the tank and placed in the GelDock system which imaged and photographed the gel. Fragments were expected at 385 bp for WT, 548 bp for KI and both 385 bp and 548 bp for heterozygous genotypes (see Figure 2.2).

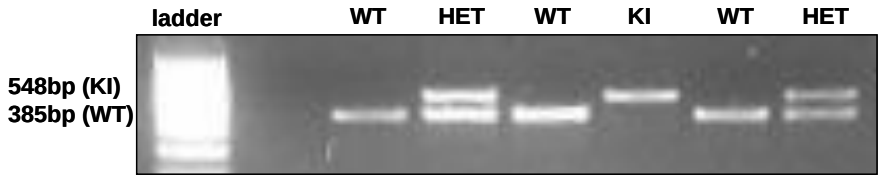

Figure 2.2 Agarose gel showing size of PCR products for identifying WT, KI and HET mice.

The upper band (548 bp) represents knock-in (KI), the lower band (385 bp) represents wild-type (WT) and both bands represent a heterozygous (HET) mouse.

2.1.5 Langendorff heart perfusion

Mouse heart excision: WT and KI mice (14 - 16 weeks old) were anaesthetised with pentobarbital (45 mg / kg intraperitoneally (IP)) and anti-coagulated with heparin (1000 IU / kg IP). Hearts were rapidly excised and placed in cold Krebs-Henseleit bicarbonate buffer (K-HB) (described below).

Heart cannulation: The aorta was located and cut just below the aortic arch. The heart was then 'hung' by inserting a cannula (connected to the perfusion rig and made from a

20-gauge blunted needle) into the aorta, tying it on securely. This meant that the heart was retrogradely perfused. The pressure of the perfusion medium in the aorta closes the aortic valve so it flows into the ostium and the coronary vessels.

Perfusion medium: Hearts were perfused with K-HB. This contained 118.5 mM NaCl, 25 mM $NaHCO_3$, 4.7 mM KCl, 1.2 mM $MgSO_4.7H_2O$, 1.2 mM KH_2PO_4, 11 mM glucose and 1.4 mM $CaCl_2$. It was gassed with 95 % O_2 and 5 % CO_2 and maintained at 37 ºC by the heated water jacket around the buffer reservoir (Figure 2.3). The K-HB was circulated around the system and passed through a heated glass coil to maintain the K-HB at 37 ºC.

Parameters measured during perfusion: After the heart was cannulated, the coronary flow was increased (driven by a peristaltic pump) until a coronary perfusion pressure (CPP) of 80 mmHg was reached. CPP was continuously measured by a pressure transducer and maintained at 80 mmHg throughout the perfusion period by the computer-driven peristaltic pump controller (Figure 2.3). After the CPP was set, the left atrium was removed from the heart and a small hole made so that a small balloon (made of cling-film, Figure 2.4A) could be inserted into the left ventricle (Figure 2.4B). This was then inflated by filling with water via a Hamilton syringe. The balloon was also connected to a pressure transducer so left ventricular pressure (LVP) could be measured (Figure 2.4C). End diastolic pressure (EDP) and left ventricular developed pressure (LVDP) were also calculated. Hearts were paced at 600 bpm via a pacing wire connected to a pacing box. All parameters were recorded on the computer using LabChart 7 (ADInstruments).

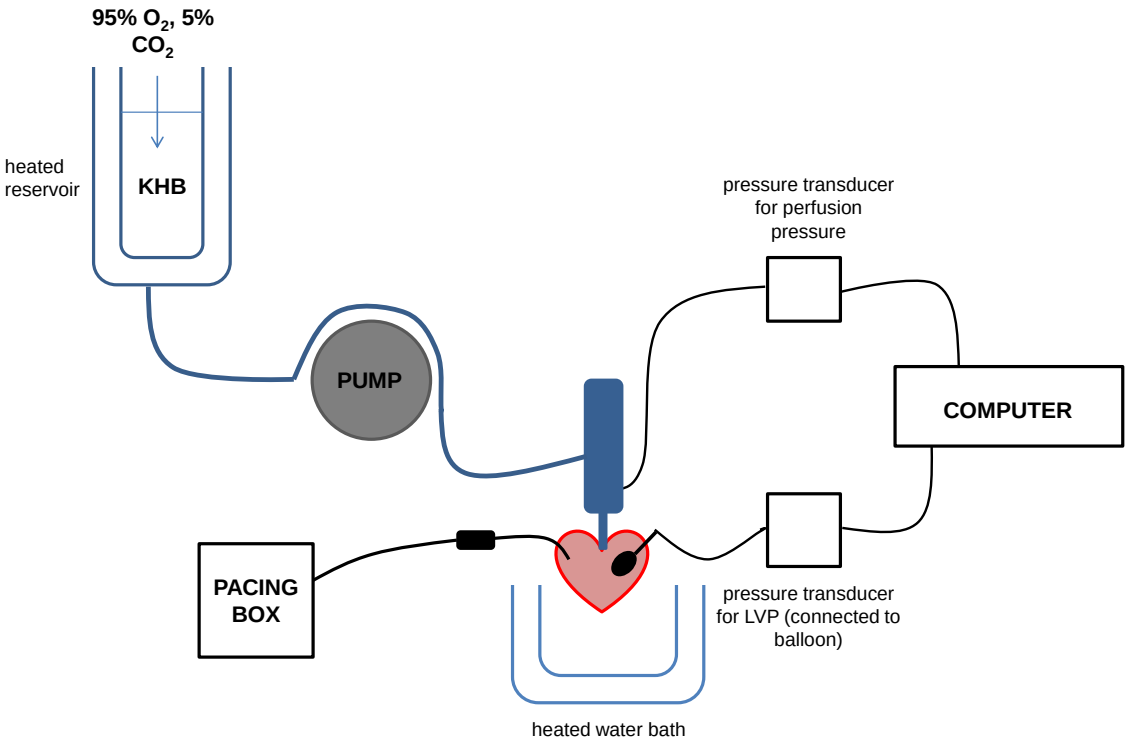

Figure 2.3 Set-up for Langendorff mouse heart perfusion.

Heated reservoirs were filled with K-HB which then flowed through a peristaltic pump (to control coronary flow rate) to the heart. The heart was immersed in a water bath to maintain its temperature at 37 ºC. The CPP was set to 80 mmHg (measured by pressure transducer) and a balloon was inserted into the left ventricle and inflated. As the heart contracts and relaxes, pressure changes are measured by the pressure transducer connected to the balloon and LVP was recorded on the computer. The heart was also paced at 600 bpm by a pacing box.

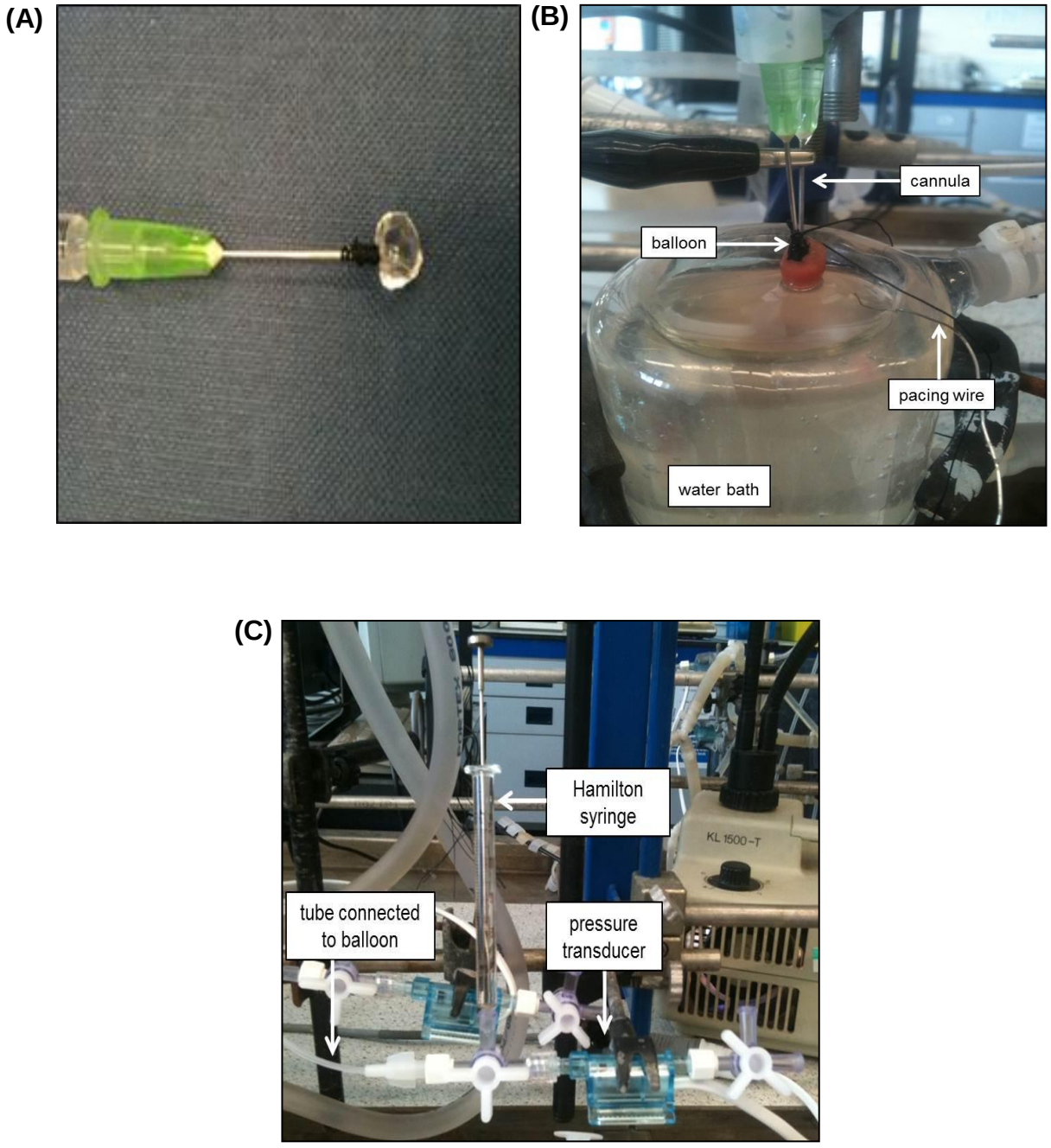

Figure 2.4 Measuring LVP in the Langendorff mouse heart.

(A) A small balloon was made out of cling-film (B) After the heart was cannulated and perfusion pressure set to 80 mmHg, the balloon was inserted into the left ventricle (C) The balloon was inflated (using Hamilton syringe) and LVP was recorded by a pressure transducer connected to the computer.

Stability period: Hearts were perfused with K-HB for a total period of 40 min. During the first 20 min adjustments were made when needed, such as inflating the balloon to maintain EDP. During the subsequent 20 min stabilisation period no adjustments were made and function should have been stable. This approach was used to make sure that WT and KI hearts were stable.

Inclusion criteria: In initial training experiments I checked that I was able to perfuse hearts with similar criteria to those recommended by others,[124] (Figure 2.5). Thus after a 20 min stabilisation period, to be included in a study, individual hearts had to have a coronary flow of 1 - 5 ml / min, an EDP of 4 - 10 mmHg and an LVDP above 60 mmHg. I achieved these criteria during my training before moving on to studies using WT and KI hearts. During training I also checked there was no 'changing the line effect'. By no changing the line effect I mean that when the line supplying the heart with K-HB is switched to another line also supplying the heart with K-HB there is no change in function (Figure 2.6). If there was a changing the line effect the coronary flow rate through each line and their temperatures were re-checked (they should be the same), and then if nothing seemed to resolve the problem, the perfusion setup was washed with 10 % hydrochloric acid (HCl) and then boiling water. Hearts were included in the study if they weren't 'cycling' during the stability period. By 'cycling' I mean a cyclical pattern of increasing and decreasing function as shown in Figure 2.7, where the LVDP, EDP and coronary flow change. Other laboratories,[124, 125] have also reported this in mouse hearts. The severity and duration of the cycling can vary and its occurrence is unpredictable. A possible reason for contractile cycling is a substrate deficiency as addition of pyruvate (a substrate for the heart to produce energy) to the K-HB stops cycling.[124, 125]

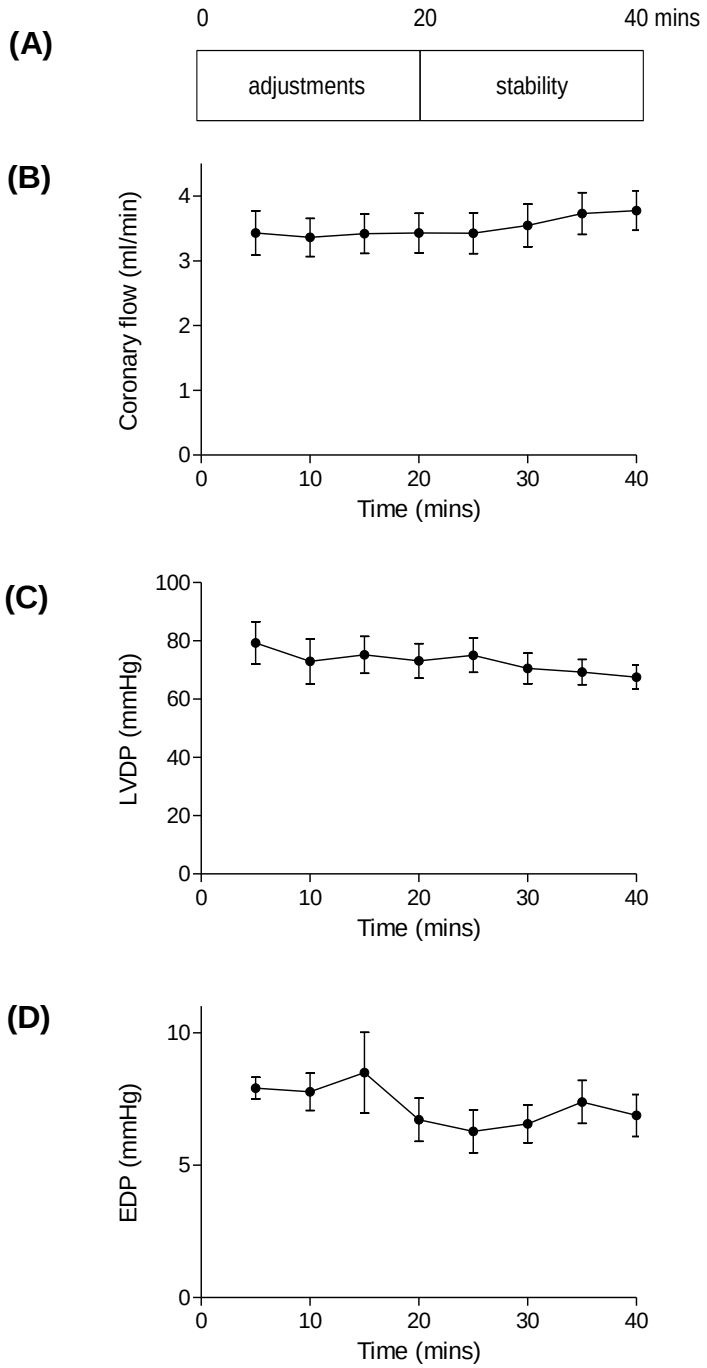

Figure 2.5 Stability of Langendorff-perfused C57BL/6 mouse hearts over a 40 min period.

(A) Adjustments, such as balloon inflation, were only made during the first 20 min of aerobic perfusion after which no adjustments were made; the hearts must stabilise. (B) Graph of average coronary flow during the 40 min perfusion period (n=9 ± SEM) (C) Graph of average LVDP (D) Graph shows average EDP. In my hands, during the stability period, coronary flow was 3 - 4 ml / min, LVDP was 60 - 80 mmHg and EDP was 6 - 9 mmHg and these are all within the recommended inclusion criteria.

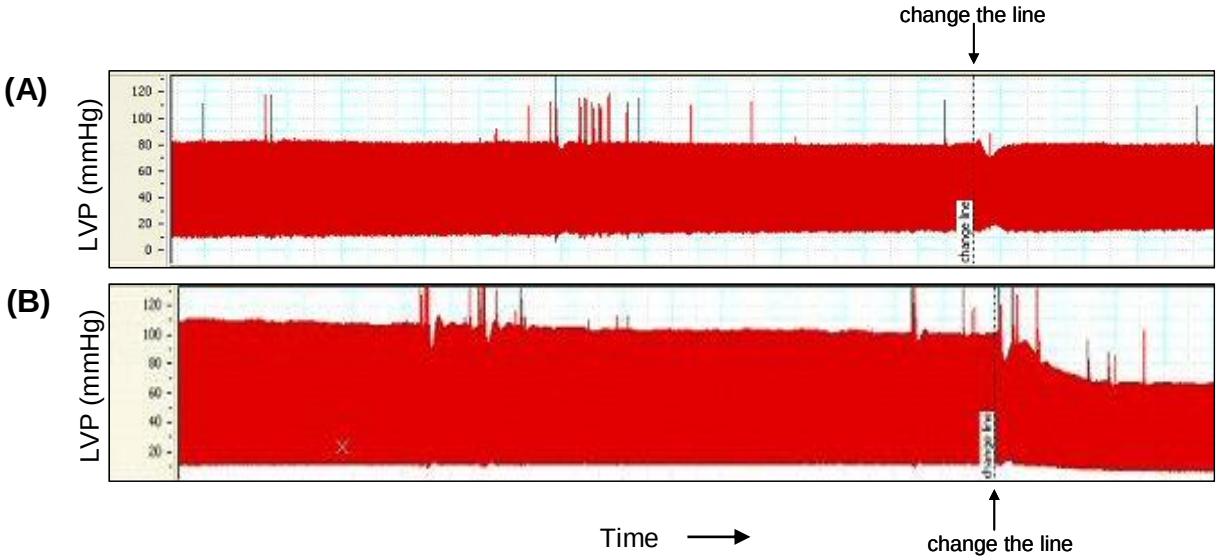

Figure 2.6 'Changing the line effect'.

Hearts were perfused with K-HB for 40 min and then the line was changed so that the heart was perfused with K-HB from a different reservoir. LabChart traced LVP during the stability period and then after the line was changed. (A) Changing the line has no effect on LVP (B) Changing the line caused a decrease in LVP. This must be rectified before using the set-up for experiments.

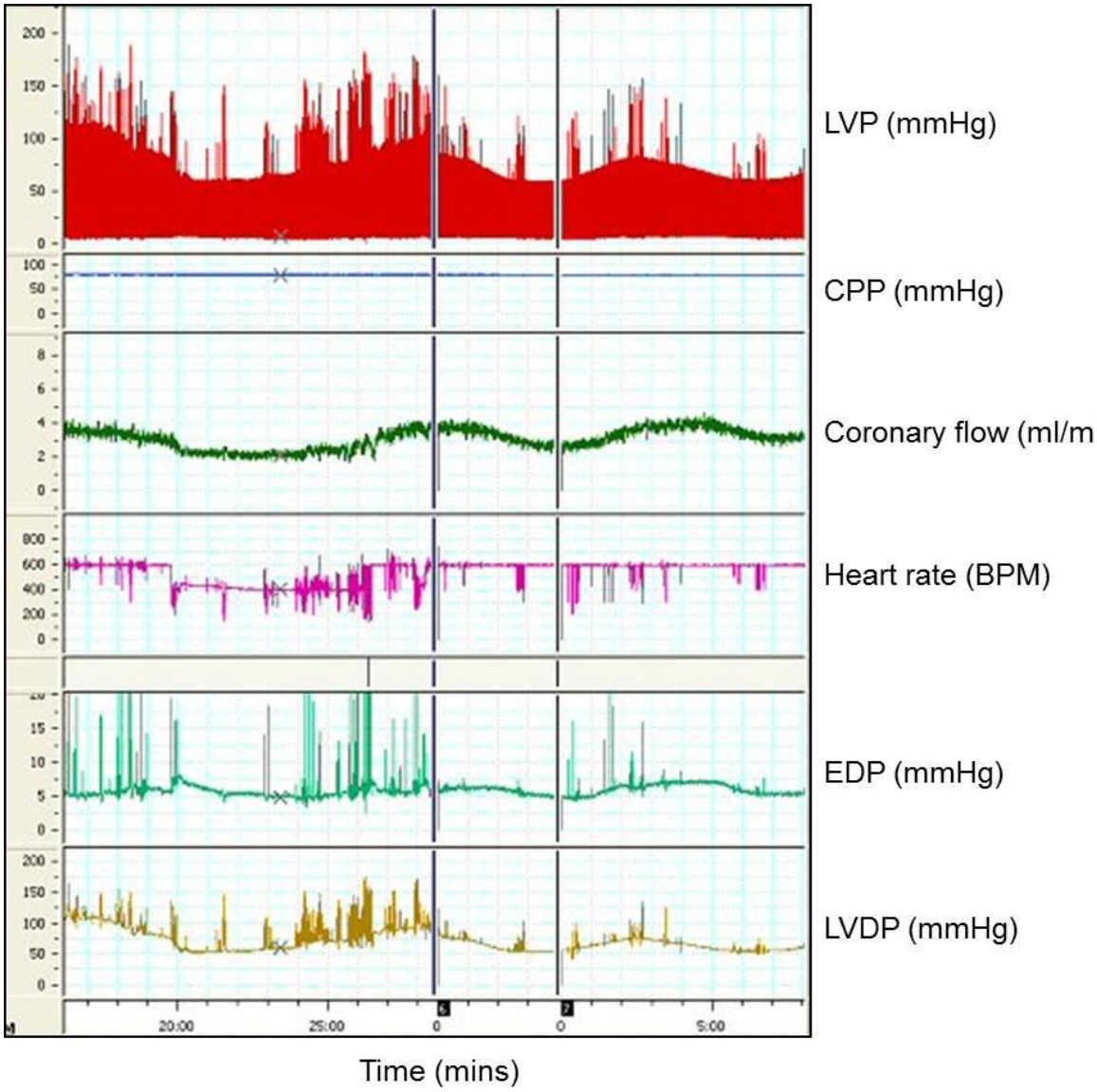

Figure 2.7 'Cycling' in the Langendorff-perfused mouse heart.

LabChart traced LVP, coronary perfusion pressure (CPP), coronary flow, heart rate, EDP and LVDP over 40 min in the Langendorff-perfused heart. This representative part of a trace shows that coronary flow, EDP and LVDP are all increasing then decreasing again over time, function is not stabilising so hearts that did this were excluded from analysis.

2.1.6 Tissue homogenisation

Organs such as heart (after excision or Langendorff perfusion studies) or other tissues were stored in liquid nitrogen until subsequent analysis. Typically it was weighed and then 10 ml of homogenisation buffer was added per g tissue. The homogenisation buffer was 100 mM Tris-HCl pH 7.4 with 100 mM maleimide, 200 µM phenylmethanesulfonylfluoride (PMSF, a protease inhibitor), phosphatase inhibitor cocktail 2 (1:100) and 100 µM EDTA. Tissue was homogenised on ice using a Polytron grinder until all tissue was fully homogenious. The homogenate was then added to an equal volume of non-reducing SDS sample buffer (100 mM Tris HCl pH 6.8, 4 % SDS, 20 % glycerol, bromophenol blue) with 100 mM maleimide or reducing SDS sample buffer (i.e. supplemented with 5 % β-mercaptoethanol).

2.1.7 SDS-polyacrylamide gel electrophoresis (PAGE)

SDS polyacrylamide gels were made with a stacking gel on top of a resolving gel (see Table 2.2). The volume of acrylamide was adjusted according to the percentage gel required. For proteins of a low molecular weight a higher percentage resolving gel was used. Samples were centrifuged at 25000 rcf for 2 min before loading. Unless stated otherwise, 10 µl of each sample was loaded into the wells of the gel. The gels were placed into two gel or four gel electrophoresis tanks (BioRad) filled with 1 x running buffer (10 x running buffer (1 l): 30 g tris base, 144 g glycine) with 0.1 % SDS, and run at a constant voltage of 180 - 210 V until the protein had run off the gel (shown by the SDS sample buffer dye front running off).

	5 % resolving gel (ml)	10 % resolving gel (ml)	15 % resolving gel (ml)	Stacking gel (ml)
30 % acrylamide	1.67	3.33	5	0.9
Water	4.33	2.67	1	4
TEMED	0.01	0.01	0.01	0.01
10 % SDS (w / v) in water	0.1	0.1	0.1	0.1
1 M Tris HCl, pH 8.8	3.8	3.8	3.8	-
10 % (w / v) APS in water	0.09	0.09	0.09	0.07
1 M Tris HCl, pH 6.8	-	-	-	0.72

Table 2.2. Composition of different percentage resolving gels and the stacking gel.

The volume of acrylamide and water in the resolving gel was adjusted for different percentage gels but the composition of the stacking gel did not change.

2.1.8 Western blotting

PVDF membranes were soaked in methanol for 5 min followed by transfer buffer (100 ml transfer buffer : 10 ml 10 x running buffer, 0.1 ml 10 % SDS, 20 ml methanol, make up to 100 ml with water). The protein was then transferred from the gel to the membrane using a semi-dry transfer blotter (BioRad). This was achieved by making a 'sandwich' as shown in Figure 2.8. Transfer was for 38 min at a constant voltage of 10 V and 0.25 A per gel being transferred in the blotter. The membrane will now be referred to as a blot.

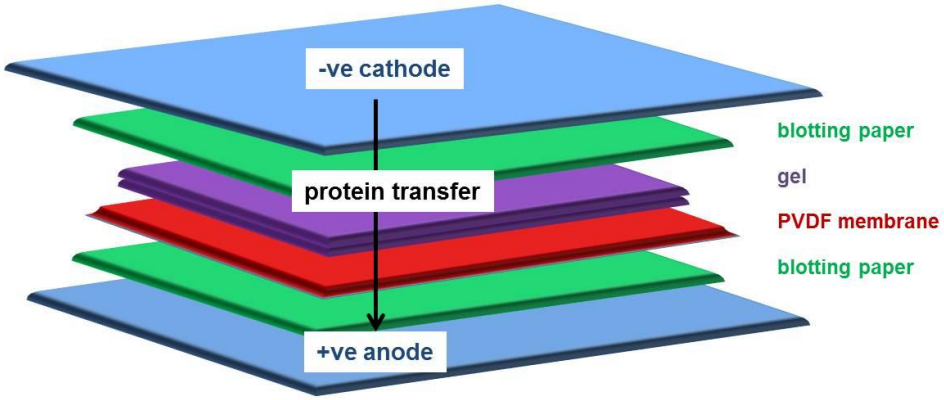

Figure 2.8 Western blotting set-up.

To transfer protein from the gel to the membrane after SDS-PAGE, a 'sandwich' is made where six sheets of blotting paper soaked in transfer buffer are placed on the anode of the blotter, the membrane soaked in transfer buffer is placed on top of this then the gel is placed on top of the membrane. Another six sheets of blotting paper soaked in transfer buffer are placed on top of the gel. Air bubbles are rolled out of the sandwich. Finally, the lid (cathode) coated in transfer buffer is placed on the sandwich and the voltage set at 10 V for 38 min. Protein is transferred from the gel to the membrane.

2.1.9 Immunoblotting

Blots were typically blocked overnight at 4 ºC on a shaker in 5 % milk in PBS with 0.1 % Tween-20 (PBS-T). The blot was then incubated with 10 ml primary antibody (diluted in 5 % milk in PBS-T), washed for 1 hour (four 15 min washes) in PBS-T and then incubated with horse radish peroxidase (HRP)-linked secondary antibody (1:1000 in 5 % milk in PBS-T, 10 ml) for 1 hour, followed by another wash for 1 hour. Details of the primary and secondary antibodies will be described in the specific methods section for each chapter.

2.1.10 Enhanced chemiluminescence

Proteins were visualised by incubating the blots with enhanced chemiluminescence reagent (GE Healthcare) for 1 min, placing them in a cassette and then, in a dark room, exposing hyperfilm to them.

2.1.11 Densitometry

The film was scanned and the maximum optical density (OD) of each band on the film was calculated using Gel Pro-Analyzer 3.1.

2.1.12 Coomassie Brilliant Blue staining of proteins on the PVDF membrane

After the proteins were visualised on the blot and the film was labelled, the blot was washed in de-ionised water and then immersed in Coomassie Brilliant Blue stain (0.2 % Coomassie Brilliant Blue R-250, 7.5 % acetic acid, 50 % ethanol) for 5 min on a shaker. This stains all protein bands on the blot. The Coomassie Blue was replaced with de-staining solution (50 % methanol, 1 % acetic acid), which was changed regularly. The blot was de-stained until the proteins were more visible. This procedure was performed to check that protein transfer from the gel to blot was efficient and also to check loading was similar between lanes, so an accurate comparison could be made between different samples loaded on the same gel.

2.1.13 Heart fractionation

Protocol: 500 µl of heart homogenate (without SDS sample buffer present) was added to an Eppendorf tube, and centrifuged at 25000 rcf for 5 min at 4 °C. The supernatant (cytosol-enriched fraction) was then removed and added to 500 µl non-reducing (with 100 mM maleimide) or reducing (with 5 % β-mercaptoethanol) SDS sample buffer. The pellet was then re-suspended in 500 µl homogenisation buffer with 1 % Triton X-100 and centrifuged at 25000 rcf for 5 min at 4 °C. The supernatant (membrane-enriched fraction) was removed and added to 500 µl non-reducing (with 100 mM maleimide) or reducing (with 5 % β-mercaptoethanol) SDS sample buffer. The pellet (myofilament-enriched fraction) was re-suspended in 1000 µl non-reducing (with 100 mM maleimide) or reducing (with 5 % β-mercaptoethanol) SDS sample buffer.

Checking for markers of the heart fractions: To assess whether the fractionation protocol was successful, WT hearts were Langendorff-perfused for 45 min with K-HB and homogenised and fractionated (as above). SDS-PAGE and Western blotting were carried out. Blots were probed for glyceraldehyde 3-phosphate dehydrogenase

(GAPDH, marker of cytosol), the α1 subunit of the Na^+/K^+ ATPase (marker of membrane) and telethonin (marker of myofilament) as shown in Table 2.3.

Antibody	Code	Company	Species	Conc.	Incubation period
GAPDH (V-18)	sc-20357	Santa Cruz Biotechnology	goat	1:1000	1 hour at room temperature
ATPase (Na^+/K^+) alpha-1 subunit	α6F	Developmental Studies Hybridoma Bank	mouse	1:1000	1 hour at room temperature
Telethonin (G-11)	sc-25327	Santa Cruz Biotechnology	mouse	1:1000	overnight at 4 ºC

Table 2.3. Antibodies to markers of fractions of heart.

GAPDH is a marker of the cytosolic fraction, Na^+/K^+ ATPase α-1 subunit is a marker of membrane and telethonin is a marker of myofilament. The table shows the company from which the antibody was purchased and the product code, the species the antibody was raised in and so the secondary antibody to be used and also the concentration the antibody was used at (in 5 % milk in PBS-T) and for how long.

Figure 2.9 shows that GAPDH was only present in the cytosol, the α1 subunit of the Na^+/K^+ ATPase was only present in the membrane and telethonin was only present in the myofilament. Therefore the fractionation protocol successfully generated cytosol-, membrane- and myofilament-enriched fractions.

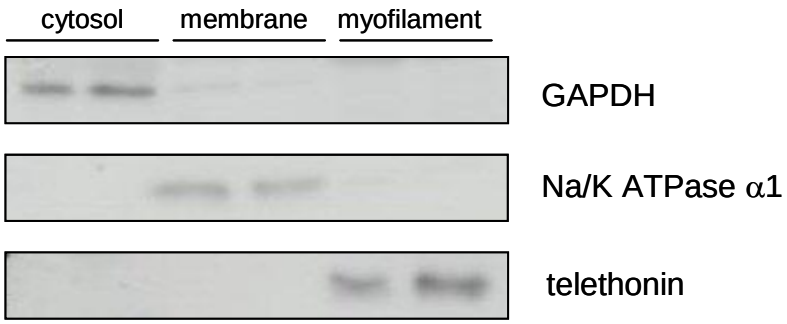

Figure 2.9 Confirmation that the heart fractionation protocol was successful.

WT hearts (n=2) were Langendorff-perfused for 45 min and then homogenised. The homogenate was fractionated in cytosol-, membrane- and myofilament-enriched fractions. SDS-PAGE and Western blotting were carried out and then blots were probed for GAPDH, Na^+/K^+ ATPase α1 or telethonin. GAPDH was present in the cytosol-enriched fraction only, Na^+/K^+ ATPase α1 was only present in the membrane-enriched fraction and telethonin was only present in the myofilament-enriched fraction, as expected, confirming that the protocol was successful.

2.1.14 Isolation of adult rat ventricular myocytes (ARVMs)

Adult rat ventricular myocytes (ARVMs) were isolated from adult male Wistar rats by Dr. Shiney Reji. In this protocol, hearts were excised, perfused for 5 min with modified K-HB solution (Solution A; 130 mM NaCl, 0.4 mM NaH_2PO_4, 0.75 mM $CaCl_2$, 4.2 mM 2-[4-(2-hydroxyethyl)piperazin-1-yl]ethanesulfonic acid (HEPES), 1.4 mM MgCl, 220 mM taurine, 4.5 mM KCl, 10 mM creatine and 10 mM glucose, pH 7.3, 37 ºC) and then perfused for 4 min with Ca^{2+}-free solution A containing 100 µM ethylene glycol tetra acetic acid (EGTA). The heart was then perfused for 8 min with solution A containing 100 µM $CaCl_2$ and 1 mg / ml collagenase. The ventricles were cut into small pieces and incubated in 10 ml collagenase solution (gassed with 100 % O_2, 37 ºC) for ~ 10 min until the digestion was complete. This mixture was then filtered through nylon gauze to separate isolated ARVMs from undigested ventricular tissue. The filtrate was then allowed to settle for 10 min. The pellet was then re-suspended in 500 µM Ca^{2+} with 1 % bovine serum albumin (BSA). ARVMs were again left to settle and the supernatant replaced with 30 ml solution A containing 1 mM $CaCl_2$.

Freshly isolated ARVMs: After the above procedure, ARVMs were left to settle at room temperature for 2 hours. Typically, ARVMs from a single rat heart isolation were

divided so each aliquot contained ~2 % of the isolation in a 500 µl total volume. After treatment, ARVMs were centrifuged at 1000 g for 0.5 min, the supernatant was removed and the pellet was re-suspended in 250 µl of SDS sample buffer containing 100 mM maleimide.

Overnight-cultured ARVMs: After isolation, ARVMs were left to stabilise at room temperature for 30 min before being washed in 50 ml modified M199 containing 100 IU / ml penicillin / streptomycin, 5 mM taurine, 2 mM creatine and 2 mM carnitine. The ARVMs were again left to settle before re-suspension in fresh modified M199 (approximately 25 ml of modified M199 was added to the pellet from ~50 % of a rat heart). Laminin (from Engelbreth-Holm-Swarm murine sarcoma basement membrane, Sigma, diluted 15 µg / ml in sterile PBS) was added to each well of the culture plate (1 ml / well for a twelve well plate and 2 ml / well for a six well plate) and left for 1 hour. The laminin was then removed and the cell suspension was pipetted into each well (1 ml / well for a twelve well plate or 2 ml / well for a six well plate). The ARVMs were incubated at 37 ºC and in 5 % CO_2 for 1.5 hours. After this time, the M199 medium was removed, to remove any non-adherent ARVMs, and replaced with fresh modified M199. The ARVMs were incubated at 37 ºC and in 5 % CO_2 overnight before treatment studies the following day.

2.1.15 Statistics

Mean values are expressed ± SEM. Statistical analyses were carried out using GraphPad Prism 5. Unless stated otherwise, differences between two groups were analysed by a T-test. Differences between three or more groups were analysed using an analysis of variance (ANOVA) followed by a T-test. Differences were considered statistically significant if the confidence level was more than 95 % ($p<0.05$) and were denoted by *.

2.2 DEVELOPMENT OF METHODS

During the studies described in this thesis a number of methodological issues hampered my progress. There were significant early issues with identifying an antibody that detects both redox states of RIα, as well as problems detecting reduced monomeric RIα after storing samples in the freezer and in ARVMs after overnight culture. The experiments carried out to troubleshoot, better-define and overcome these methodological issues are described below as well as the results and conclusions.

2.2.1 Screening for an antibody that detects both redox states of PKA RIα

The PKA RIα antibody (Calbiochem) Brennan *et al.*,[57] used to assess RIα disulfide formation is no longer available. Therefore, my initial aim was to find an alternative antibody that detects both redox states of PKA RIα. Previous studies investigating the redox regulation of PKG Iα made us aware that the oxidation state can markedly influence the affinity of antibodies. For example, antibodies to PKG Iα selectively bind the reduced form, and others the oxidised form.[126]

Methods: Freshly isolated ARVMs were left untreated or treated with 1, 100 or 1000 μM H_2O_2 for 5 min. Samples were then prepared in non-reducing SDS sample buffer containing 100 mM maleimide. SDS-PAGE and Western blotting were carried out and then the blots were incubated with the primary antibodies listed in Table 2.4 at the concentrations and for the periods stated. The blots were then incubated with an HRP-conjugated secondary antibody appropriate for the species the primary antibody originated from (also listed in Table 2.4) and antibody binding was visualised as described previously (see section 2.1.10).

Antibody name	Code	Company	Species	Conc.	Incubation time
PKA Iα/β reg (H-90)	sc-28893	Santa Cruz Biotechnology	rabbit	1:1000	1 hour
PKA RIα	610610	BD Transduction Laboratories	mouse	1:500	overnight
PKA Iα reg (3546c2a)	sc-81641	Santa Cruz Biotechnology	mouse	1:1000	3 hours
PKA RIα	ab38936	Abcam	rabbit	1:1000	3 hours
PKA RIα	ab65013	Abcam	rabbit	1:1000	overnight
PKA RIα subunit	SA-285	Biomol International	chicken	1:1000	overnight
PKA Iα reg (C-14)	sc-18800	Santa Cruz Biotechnology	goat	1:500	overnight
PKA RI (immunogen is RIα)	610165	BD Transduction Laboratories	mouse	1:5000	1 hour

Table 2.4. **Details of anti-PKA RIα antibodies screened to identify an antibody that detects both redox states of RIα.**

This table shows the company from which each antibody was purchased, its purchase code, the species it was raised in (and so the secondary antibody to be used), the concentration the antibody was used at and the incubation period. The incubation was at room temperature except for overnight incubation, which was at 4 ºC.

Results: Figure 2.10 shows that some antibodies simply failed to detect any protein, namely Santa Cruz sc-28893 and Santa Cruz sc-18800, and another antibody (Abcam ab38936) detected a non-specific band at too high a molecular weight to be disulfide dimeric RIα. Some antibodies detected a decrease in monomer with increasing H_2O_2 concentration but without a corresponding increase in the anticipated disulfide dimer (BD Transduction laboratories 610610, Santa Cruz sc-81641, Biomol International SA-

285). There was no detectable change in the monomeric RIα signal with H_2O_2 treatment for the antibody from Abcam (ab65013), consistent with this not detecting PKA RIα. However, eventually an antibody (BD Transduction Laboratories 610165) was identified that clearly detected both redox states of RIα and showed a marked loss of monomer and concomitant increase in disulfide dimer with increasing H_2O_2 concentration. This was used in subsequent studies monitoring the thiol-disulfide redox state of RIα.

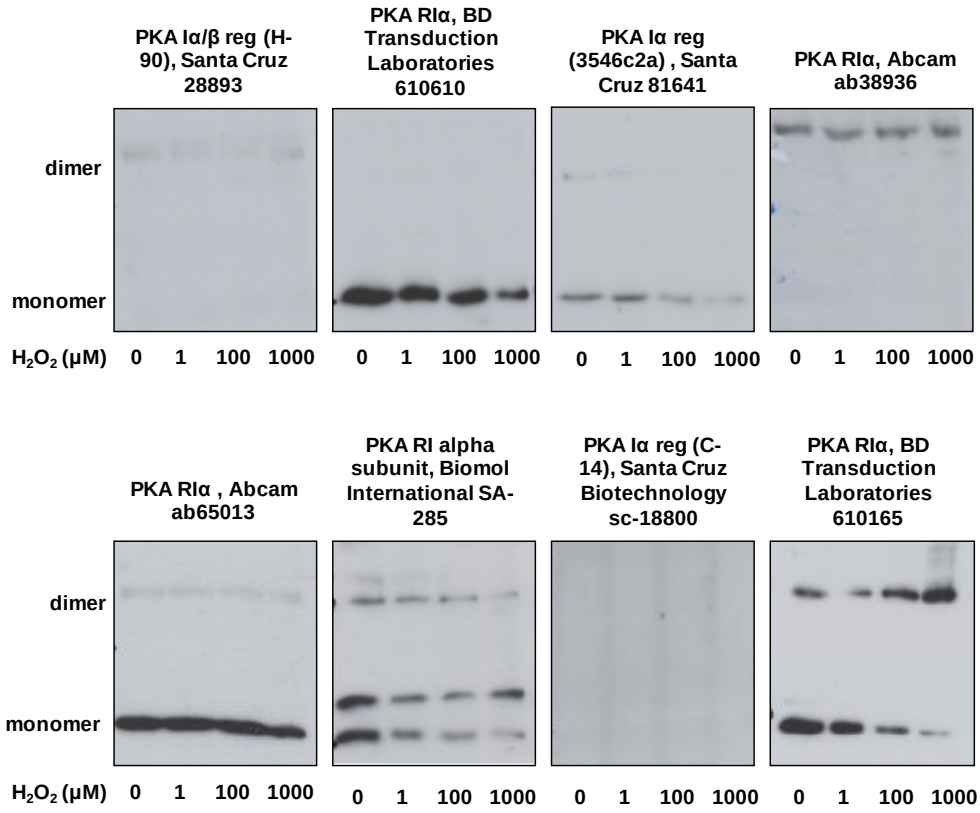

Figure 2.10 Antibody detection of PKA RIα disulfide dimer formation.

Freshly isolated ARVMs were treated with 0 - 1000 μM H_2O_2 for 5 min. SDS-PAGE was then carried out followed by Western blotting, probing blots with the antibodies described above. The PKA RIα antibody from BD Transduction Laboratories (610165) was the only one that detected loss of RIα monomer with reciprocal formation of RIα disulfide dimer in response to treatment with increasing concentration of H_2O_2 and so was the chosen antibody for use in subsequent studies.

Conclusions: Commercially available RIα antibodies vary immensely in their ability to detect both redox states of RIα. This may be because oxidative modification of RIα alters the epitope and so the antibody may not bind oxidised RIα protein with the same affinity as when it was in the reduced state. Antibody 610165 (BD Transduction Laboratories) was primarily used in subsequent studies, unless stated otherwise, when a Western blot was probed for PKA RIα.

2.2.2 Effect of sample storage time on detection of RIα monomer and dimer

It is often necessary to re-run samples, and is important that the redox state of RIα remains the same, or is unaltered during storage which involved freezing at 20 ºC.

Methods: Samples were prepared in non-reducing SDS sample buffer (with 100 mM maleimide) and SDS-PAGE and Western blotting were carried out. The blots were probed for PKA RIα. The same samples were stored in the freezer (for ~1 or ~2 months) and then re-analysed using the same procedure. The samples analysed in this way were (1) homogenate of hearts excised from C57BL/6 mice and Langendorff-perfused with K-HB for 45 min or K-HB for 40 min followed by 50 or 100 µM H_2O_2 for 5 min or (2) freshly isolated ARVMs left untreated or treated with 0.5 mM diamide for 5 min. All methods are described in more detail in section 2.1.

Results: Figure 2.11A shows that there was both RIα monomer and disulfide dimer present basally in control hearts; in most cases more monomer than dimer. The percentage disulfide increased in hearts when they were perfused with H_2O_2 (Figure 2.11Ai). However, after storage of the samples in the freezer for just under a month, the blot (Figure 2.11Aii) had to be exposed for a longer time to get the same intensity disulfide dimer signal as in Figure 2.11Ai, and even at this higher exposure, there was very little reduced RIα monomer detected compared to Figure 2.11Ai. Figure 2.11B shows that approximately equal amounts of RIα monomer and disulfide dimer were present in control ARVMs. Treatment with 0.5 mM diamide caused the entire RIα pool to become disulfide dimeric. However, when the same samples were run approximately two months later, for similar signal intensity for RIα disulfide dimer, no reduced monomer was detected. Even when the exposure time was increased, the signal for RIα

monomer was blurred and less intense compared to when the samples were run two months before. Clearly, storing the sample at -20 ºC for several weeks results in loss of reduced monomeric RIα which is not associated with concomitant increase in disulfide dimer.

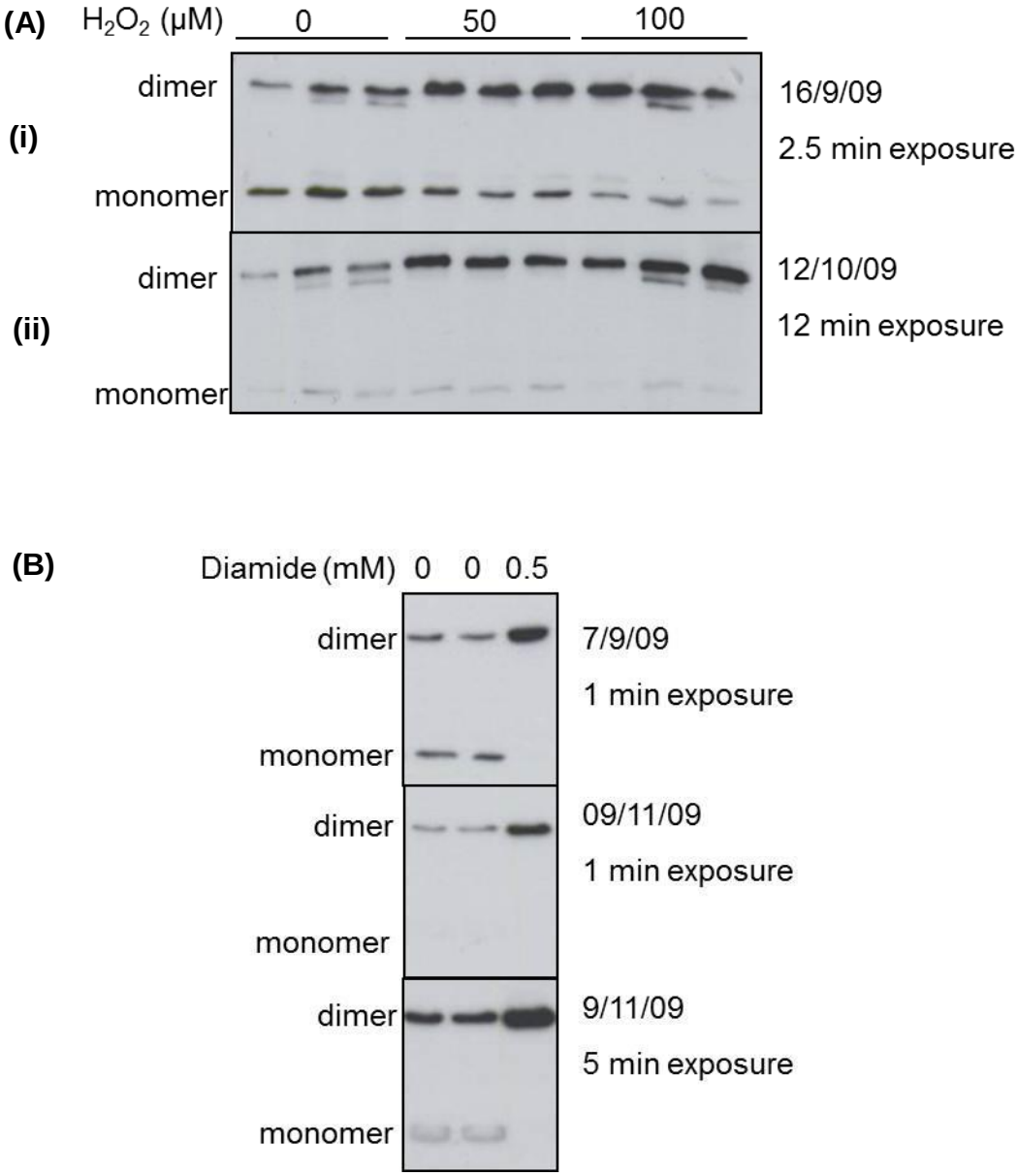

Figure 2.11 Detection of PKA RIα redox state in samples after storage in the freezer.

(A) C57BL/6 hearts were perfused for 45 min with K-HB or 40 min with K-HB then 5 min H_2O_2 (50 or 100 μM) (i) Western blot of the samples run on a gel the same day the samples were prepared probed for PKA RIα (ii) Western blot of the same samples run on a gel a month later (B) Freshly isolated ARVMs were left untreated or treated with 0.5 mM diamide for 5 min. Top blot shows PKA RIα in samples run on a gel on the same day the samples were prepared and middle and bottom blots are for the same samples run on a gel ~ two months later and film was exposed for 1 min or 5 min. Less RIα monomer was detected in samples after storage but detection of disulfide dimer was not affected.

Conclusions: The detection of reduced monomeric RIα redox state was hampered by time-dependent changes in the sample during storage in the freezer. This was not because of oxidation to the disulfide dimer form as there was still a difference in dimer abundance between untreated control and oxidant-treated samples after time in storage. It also was not sample-type specific, as this reduced detection of monomeric RIα was demonstrated in both heart homogenate and freshly isolated ARVM samples. A possible explanation is that the RIα antibody (BD Transduction Labs 610165) may have a higher affinity for disulfide dimeric RIα than reduced monomeric RIα, and this may be exacerbated by the presence of maleimide in the SDS sample buffer. Time in storage may allow maleimide in the SDS sample buffer to react with the RIα thiols and the antibody may not detect the alkylated monomer as well as the non-alkylated monomer. Due to this finding, samples were typically analysed within a few days of preparation.

2.2.3 Effect of overnight culture on RIα disulfide in ARVMs

RIα redox state in freshly isolated ARVMs and overnight-cultured ARVMs

Methods: ARVMs were isolated and aliquoted into two groups. One group was cultured overnight as described in section 2.1, and the other left for 2 hours before experimental treatments and were considered 'freshly' isolated cells. ARVMs in both groups were left untreated or treated with 0.5 mM diamide for 5 min. Samples were then prepared by adding non-reducing sample buffer containing 100 mM maleimide. SDS-PAGE and Western blotting were carried out as described in 2.1. Blots were probed for PKA RIα.

Results: Figure 2.12 shows a clear difference in redox state of RIα between overnight-cultured and freshly isolated ARVMs. As expected, in untreated freshly isolated ARVMs there was approximately equal abundance of RIα monomer and disulfide dimer present. 0.5 mM diamide caused the entire pool of RIα to shift to the disulfide dimer form. However, unexpectedly, in untreated control overnight-cultured ARVMs there was only RIα disulfide dimer present; no reduced monomer. 0.5 mM diamide increased the signal for disulfide dimeric RIα but as there was no monomeric RIα

present in overnight-cultured control ARVMs suggests an increase in RIα protein abundance. This blot clearly illustrates that culturing ARVMs overnight causes a loss of monomeric RIα.

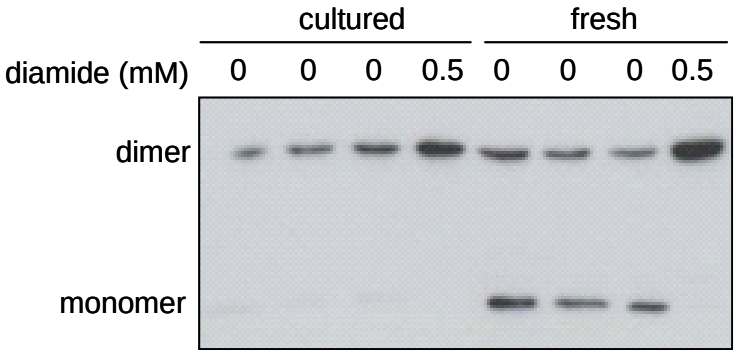

Figure 2.12 PKA RIα in overnight-cultured and freshly isolated ARVMs.

ARVMs were left untreated or treated with 0.5 mM diamide for 5 min. SDS-PAGE and Western blotting were carried out and blots were probed for PKA RIα. RIα monomer was absent in control overnight-cultured ARVMs unlike in control freshly isolated ARVMs, which had equal amounts of RIα monomer and disulfide dimer.

Conclusions: Reduced RIα monomer was detected in freshly isolated ARVMs but not in overnight-cultured ARVMs. An increase in RIα disulfide in response to oxidant treatment was still observed in overnight-cultured ARVMs, similar to in freshly isolated ARVMs, suggesting an increase in RIα protein expression in overnight-cultured ARVMs. This *de novo* protein synthesis is difficult to explain and has not been observed in other model systems. After further investigation, the 'changing the medium' step in the culture protocol appeared to cause the complete loss of reduced monomer in overnight-cultured ARVMs and an associated decrease in total RIα protein. Expression of the kinase PKG Iα has been shown to be suppressed in cultured vascular smooth muscle cells resulting in a dedifferentiated phenotype.[127] Alternatively, perhaps RIα is exiting the cell so total RIα protein decreases. There is evidence that cells can secrete PKA into the extracellular space.[49] Maleimide in the sample buffer, as discussed with time in storage, is not the reason why I do not observe the monomeric form of RIα in ARVMs cultured overnight as all samples were analysed within 24 hours of preparation. Another possible explanation is that RIα disulfide dimerisation may be important in

adhesion of ARVMs to the laminin coated plate so non-adhered cells (which have RIα present as monomer) are removed when the culture medium is changed, leaving RIα disulfide dimer only present in adherent cells. Another explanation may be anoikis, which is programmed cell death induced when anchorage-dependent cells detach from the extracellular matrix. When the culture medium is changed the cells may detach and RIα may dimerise and then the cells may die.

The explanation for absence of monomer is complicated and could be a combination of the factors above. A solution to this issue is to use another cell type or using freshly isolated ARVMs for experiments, which was the solution of choice in my studies in this thesis. Examples highlighting this problem of absence of RIα monomer in overnight-cultured ARVMs are shown in Chapters 4 and 6.

3 INITIAL CARDIAC CHARACTERISATION OF A NOVEL PKA RIα KNOCK-IN MOUSE

3.1 Introduction

RIα homozygous null mutant embryos have developmental abnormalities and so die early in embryogenesis. They have increased basal PKA activity due to lack of regulatory inhibition of the catalytic subunit, but can be partially rescued by deletion of the α isoform of the catalytic subunit (Cα).[128] In RIα knockout (KO) animals on a Cα KO background the total abundance of catalytic subunit was reduced and so catalytic activity was more controlled and basal or 3′,5′-cyclic monophosphate (cAMP)-stimulated PKA activity was lower. This resulted in improved development but the genotype was still lethal.[129] Similarly, Cα homozygous null mice survive through embryogenesis but die early after birth.[130]

Carney complex (CNC) is a multiple endocrine neoplasia characterised by spotty skin pigmentation typically on the face together with Schwannomas, which are benign tumours made up of Schwann cells of the peripheral nervous system. Myxomas (tumours of the heart) are also characteristic and a major cause of mortality. Endocrine tumours may also form, most commonly occurring in the adrenal glands.[131, 132] In ~75 % of patients with CNC, a mutation in *PRKAR1A* that inactivated PKA RIα was the cause.[133] Most of the mutations in *PRKAR1A* result in a premature stop codon leading to messenger RNA (mRNA) instability and degradation.[132, 134] Many of the CNC mutations are located in the dimerisation / docking (DD) domain (Figure 3.1),[132] a region in RIα that contains the pair of disulfides that form during oxidative stress.[57] Consequently the cysteine 17 serine (Cys17Ser) mutation present in the KI mouse I investigated in these studies is located within the DD domain. In tumours with these RIα inactivating mutations, basal PKA activity was shown to be unaltered but activity induced by cAMP was enhanced i.e. the tumours were more sensitive to cAMP.[135]

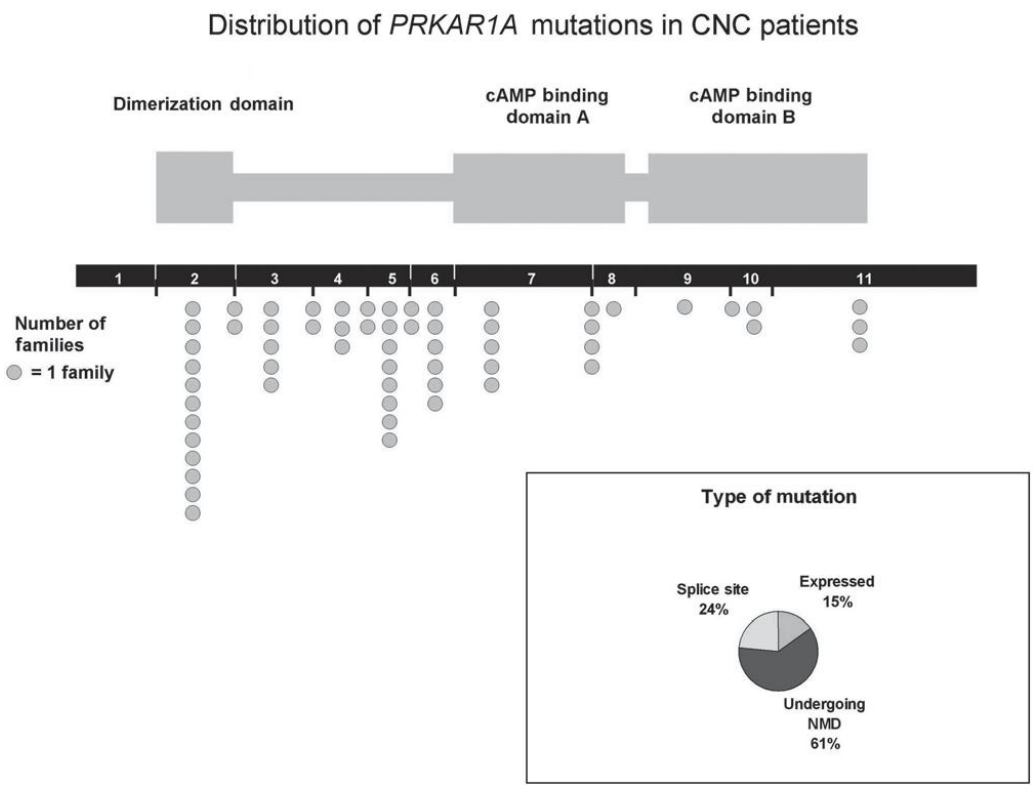

Figure 3.1 Location of mutations in *PRKARIA* in patients with CNC.[132]

Each circle represents one family unit with a mutation in that region. Of particular note is the number of families with mutations in the DD domain which is where the Cys17 mutated in the KI mouse is located. NMD= nonsense-mediated mRNA decay.

A number of mouse models have been developed to study CNC. Kirschner *et al.* showed that heterozygous mutations in *PRKARIA* resulted in tumourigenesis highlighting PKA RIα's role as a tumour suppressor. Mice with a mutation in exon 2 of *PRKAR1A*, a modification frequently seen in CNC patients, develop Schwannomas and bone lesions with similar histology to those seen in human CNC. Similarly, mice with facial neural crest tissue-specific KO of *PRKAR1A* also develop Schwannomas.[136] Pituitary-specific KO mice also develop tumours, although with a long latency.[131] Mice with cardiomyocyte-specific ablation of *PRKAR1A* die during embryogenesis due to aberrant cardiac development. Their hearts have myxomas and they also have elevated total and free PKA activity, which results in down-regulation of transcription factors required for cardiogenesis.[137] The increase in activity was found to be due to uncontrolled catalytic subunit activity which is normally suppressed by RIα.[131]

In my studies, the influence of RIα disulfide formation on cardiac 'function' was investigated primarily by the characterisation of a novel Cys17Ser RIα 'redox-dead' KI mouse line. I refer to this mouse line as 'redox dead' as Cys17 in each RIα subunit has been mutated to a Ser (Figure 3.2) so theoretically the regulatory subunits cannot form disulfides in response to oxidative stress.

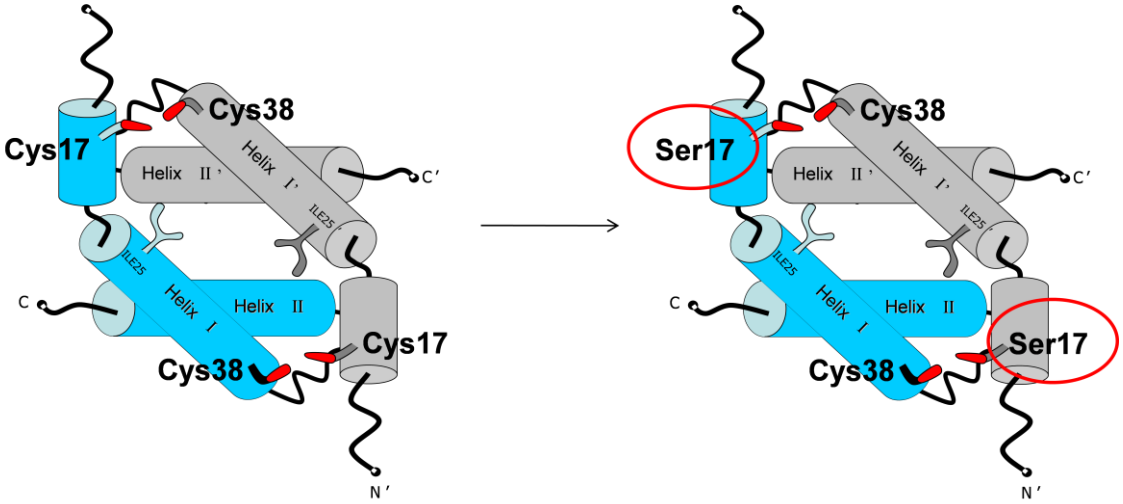

Figure 3.2 Diagram of Cys17Ser 'redox-dead' KI RIα.

Cys17 has been replaced with a Ser, so theoretically disulfides cannot form with the Cys38 residues.

I hypothesised that Cys17Ser mutant mice that cannot form RIα disulfides would still be regulated by classical stimulation of PKA by cAMP. This was reasoned because disulfide RIα is not generally present in tissues under basal conditions as an oxidant is required, but the PKA is responsive to β agonist-induced PKA activation via elevated cAMP.[57] Furthermore, the anti-parallel dimeric RIα state is not disrupted by mutating either or both Cys residues involved in disulfide formation.[116]

My research laboratory chose to solely mutate Cys17, as opposed to both Cys17 and Cys38, when generating the transgenic mouse. This was because a single amino acid change is more conservative compared to a two amino acid change. Furthermore, at the time of choosing which RIα 'redox dead' mouse to generate, the effect of mutating the redox-sensitive Cys thiols in the DD domain of RIα on binding to dual-specificity A-

kinase anchoring proteins (D-AKAPs) had been investigated. As discussed in more detail in Chapter 5, D-AKAP1 and D-AKAP2 are proteins that bind to the DD domain of RI and RII subunits and determine PKA localisation with substrates PKA phosphorylates. AKAP binding is crucial to the coordination of PKA function. Banky *et al.* showed that mutating both Cys17 and Cys38 to alanine abolished D-AKAP1 binding to RIα,[116] and Huang *et al.* showed this double mutation also abolished D-AKAP2 binding to RIα,[138] suggesting that the dual amino acid change caused a conformational change that itself altered normal PKA function. Therefore, a dual mutant mouse was not considered to be a viable option. Similarly, the same research group (Taylor's laboratory) showed that mutation of Cys38 to histidine (His) had a more marked effect on the conformation of RIα (such that it attenuated D-AKAP1 / D-AKAP2 binding to RIα) than solely mutating Cys17 to His, which did not alter binding to the D-AKAPs.[116, 138] In addition, mutating Cys to Ser in the KI mouse was envisaged not to have a marked effect as both side chains of these amino acids are hydrophilic and of a similar size. Overall the transgenesis to produce a Cys17Ser RIα KI mouse line introducing a single atom (sulfur to oxygen) alteration was considered the best option.

The primary aim of this chapter was to characterise the novel Cys17Ser RIα KI mouse which was achieved by addressing the following:

1. Whether KI RIα forms the disulfide bonds a wild-type (WT) does during oxidative stress. I hypothesise it will not because Ser17 cannot be oxidised so cannot form a disulfide with the adjacent Cys38.

2. Whether the Cys17Ser mutation in RIα causes any compensatory changes in expression of other PKA subunits or protein kinases. It is important to establish whether the abundance of proteins is the same in WT and KI mice allowing me to dis-count such potential changes as a reason for any differences I may identify between genotypes. For this reason it was also important to determine whether there were any compensatory changes in abundance of other PKA subunits in the KI mouse. The abundance of cGMP-dependent protein kinase (PKG) Iα was also analysed as this is also activated by

oxidation to a disulfide form,[60] and has roles in excitation-contraction coupling and smooth muscle relaxation by phosphorylating some of the same substrates as PKA. The abundances of the following enzymes were also compared between genotypes: p38 mitogen-activated protein kinase (MAPK), protein kinase C (PKC) (ε, α, δ), protein kinase D (PKD), Akt, cyclooxygenase-2 (COX-2) and extracellular signal-regulated kinase (ERK).

3. Whether the inability to form RIα disulfide results in a compensatory increase in RIα abundance in the heart and other organs (kidney, liver, lung, brain and pancreas). The Cys17Ser RIα mutation is global and PKA has roles in multiple tissues (Chapter 4). At the outset, I don't anticipate the expression of RIα to be different between WT and KI organs.

4. Whether RIα disulfide alters basal cardiac and coronary vascular function. RIα disulfide has been associated with increased PKA activity and increased phosphorylation of cardiac proteins.[57] I hypothesise that there will be a difference in basal function between WT and KI hearts because there may be some RIα disulfide in WT basally but RIα will all be reduced in KI. I therefore expect PKA activity to be higher in WT than KI basally and so phosphorylation of PKA substrates higher too.

3.2 Methods

3.2.1 *In vitro* treatment of heart homogenate with diamide

Male and female hearts were perfused with K-HB for 45 min and then homogenised as described in Chapter 2.1. The homogenate was treated with 0.5 mM diamide (a thiol-specific oxidant that selectively induces disulfide formation) for 5 min or left untreated for 5 min (control). The homogenate was then added to an equal volume of non-reducing (with 100 mM maleimide) or reducing (i.e. with 5 % β-mercaptoethanol) SDS sample buffer.

3.2.2 *Ex vivo* treatment of heart homogenate with H_2O_2

Male and female WT and KI hearts were perfused with K-HB for 40 min followed by 50 μM H_2O_2 for 5 min and then homogenised and added to non-reducing SDS sample buffer (with 100 mM maleimide) as described in Chapter 2.1.

3.2.3 Excising organs and analysis of RIα abundance

After the heart was excised for Langendorff perfusion, the lung, kidney, liver, pancreas and brain were removed, homogenised as the heart was (described in Chapter 2.1) and added to reducing SDS sample buffer. SDS-PAGE and Western blotting were carried out with blots probed for PKA RIα. The relative expression of RIα in WT and KI was assessed by comparing pairs of samples. This approach was used as analysis was carried out on different days, which precludes absolute quantitative analysis.

3.2.4 Probing for specific proteins in WT and KI heart homogenate

Homogenates of Langendorff-perfused (K-HB for 45 min) male WT and KI hearts were analysed for abundance of different enzymes and PKA subunits by adding reducing SDS sample buffer (i.e. with 5 % β-mercaptoethanol) to the homogenate and carrying out SDS-PAGE and Western blotting. Blots were probed with the antibodies shown in Table 3.1.

Antibody	Purchase code	Company	Species	Conc.	Incubation period (hours)
p38 MAP kinase	#9212	Cell Signalling Technology	rabbit	1:1000	3
cGKIα (E-17)	sc-10338	Santa Cruz Biotechnology	goat	1:1000	1
PKCε (C-15)	sc-214	Santa Cruz Biotechnology	rabbit	1:1000	1
PKCα (C-20)	sc-208	Santa Cruz Biotechnology	rabbit	1:1000	1
PKCδ (C-17)	sc-213	Santa Cruz Biotechnology	rabbit	1:1000	1
PKA RII	06-411	Upstate cell signalling solutions	goat	1:1000	1
PKD/PKCμ	#2052	Cell Signalling Technology	rabbit	1:1000	3
PKA catalytic subunit	610980	BD Biosciences	mouse	1:1000	1
Akt	#9272	Cell Signalling Technology	rabbit	1:1000	1
COX-2	160126	Cayman Chemical	mouse	1:1000	3
ERK 1/2 (p44/42 MAPK)	#9102	Cell Signalling Technology	rabbit	1:1000	2
PRKAR1B	WH0005575M5	Sigma Aldrich	mouse	1:1000	1

Table 3.1. Antibodies to different proteins used to compare their abundance in male WT and KI hearts.

The table shows the name of the antibody, the company from which it was purchased (and product code) and the species it was raised in. The table also shows the concentration of antibody the blot was probed with and the incubation period at room temperature.

3.2.5 Measuring heart weight

After the heart was excised it was placed in cold K-HB and weighed on a zeroed weighing balance (fresh heart weight). In some studies, the heart was frozen in liquid nitrogen after Langendorff perfusion and then weighed (frozen heart weight).

3.2.6 Echocardiography

An echocardiogram uses sound waves to give a two-dimensional picture of the heart enabling measurement of cardiac dimensions and cardiac function. This was carried out by Dr. Oleksandra Prysyazhna. Six WT and six KI male mice of ~26 g in body weight were anaesthetised by placing in a box supplied with isoflurane (~4 %, 0.75 % O_2). They were then removed, weighed and a mask supplying isoflurane (~2.5 %) was placed on the mouse. Heart rate was monitored and maintained at ~520 bpm. The mouse was placed on a heated table and temperature of the mouse was monitored and maintained at approximately 37 ºC. Hair was removed from the chest and abdomen and ultrasound transmission gel was applied on to which the probe was placed. The long and short axes of the heart were imaged in different modes, as outlined below.

The long axis of the heart (axis of heart is horizontal) was measured when the aorta was positioned to the right opposite the apex and one papillary muscle was visible (Figure 3.3). This was visualised using motion-mode (M-mode) which produces a one-dimensional view of the cardiac structures moving over time. The short axis of the heart was visualised by rotating the probe 90º from the long axis position so the biggest ventricular lumen could be visualised. Ideally, both papillary muscles were visible (Figure 3.4).

Transmission gel was applied to the right side of the mouse's chest and the probe placed on the chest such that the ultrasound beam was parallel with the direction of flow of blood through the aorta (white dotted line on Figure 3.5). A vertical line was drawn on the image (red line in Figure 3.5) near to the first vessel of the aortic arch and so that it had a slope of ~50 º to the white dotted line which enables measurements of blood flow. This is called Doppler mode and assesses blood flow velocity by measuring the change

in frequency between transmitted sound waves and sound waves reflected from blood cells moving away from or towards the probe.

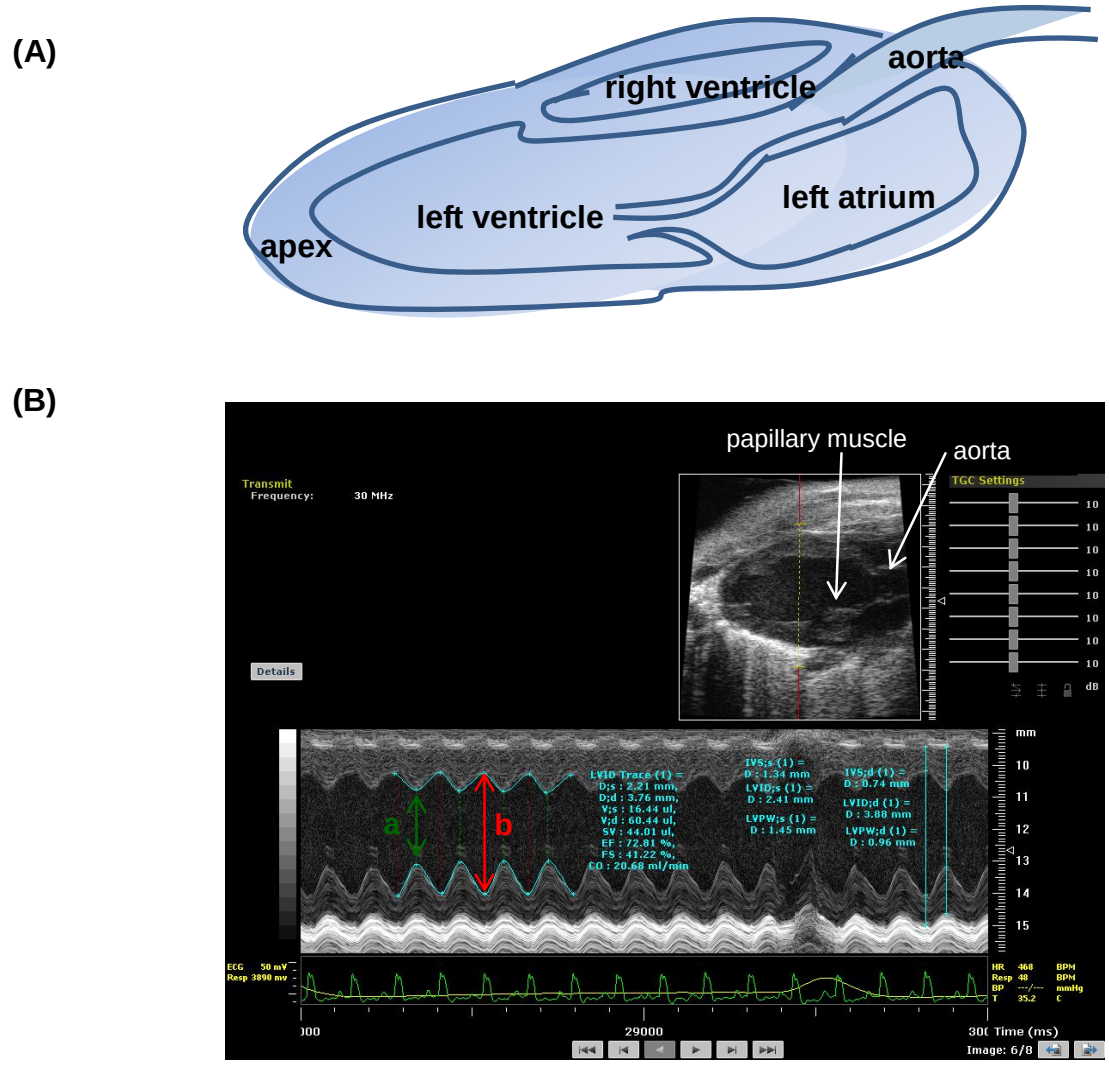

Figure 3.3 Long axis of the heart.

(A) The heart is positioned so that the aorta is positioned to the right opposite the apex (B) The heart is also positioned so that one papillary muscle is visible (top right). The representative M-mode echocardiogram of a WT heart shows a trace is created of dimension (mm) v time (ms) showing boundaries of the heart contracting and relaxing with time. Various parameters are measured including ejection fraction, fractional shortening, systolic and diastolic volume and (a) systolic and (b) diastolic dimension. The program itself calculates an average of three different measurements for systolic and diastolic dimension (red and green lines) and we can calculate the dimensions ourselves by drawing a line on the trace (blue lines on right of trace).

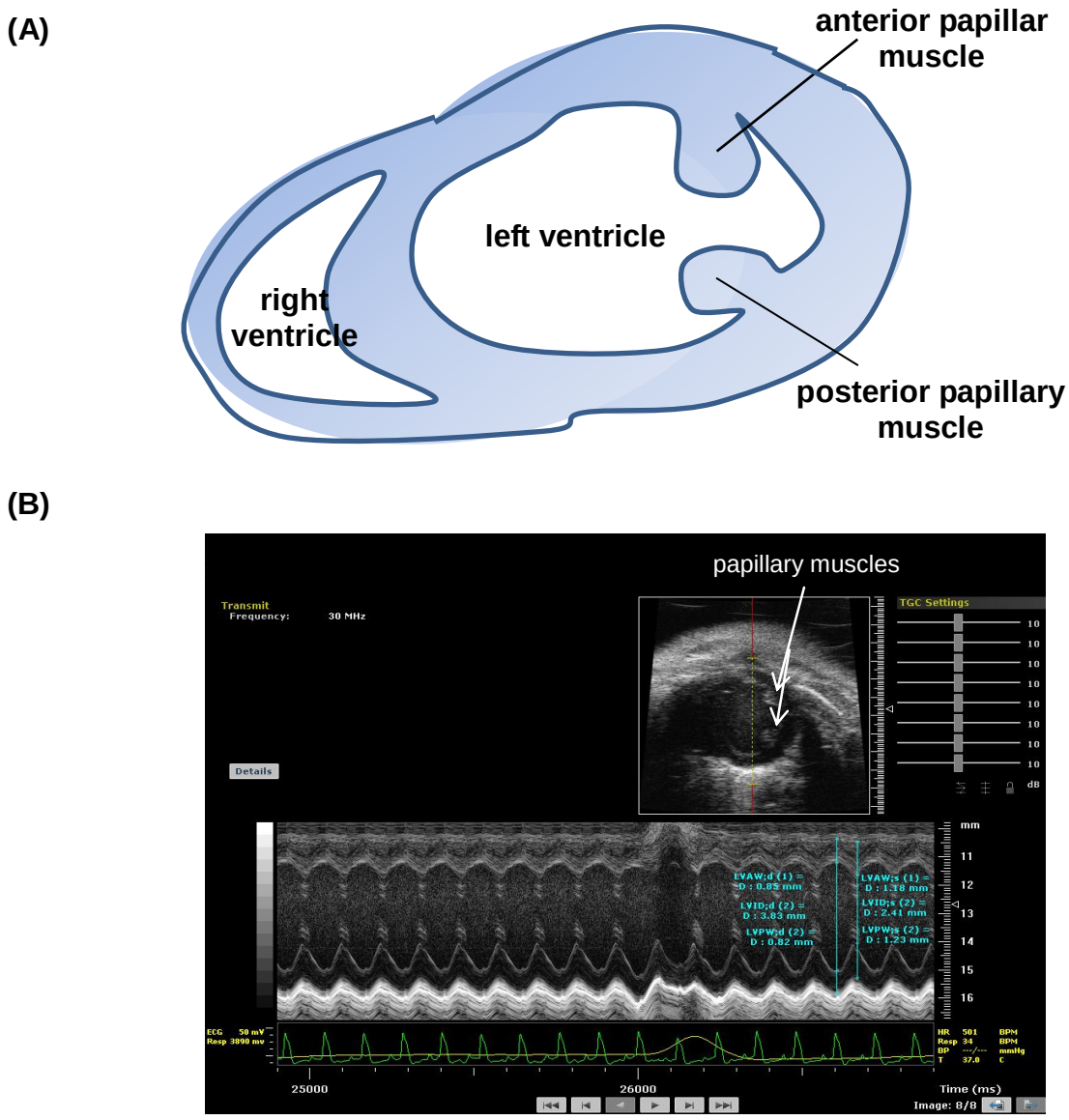

Figure 3.4 Short axis of the heart.

(A) The heart was positioned so that both papillary muscles were visible. (B) The representative M-mode echocardiogram of the short axis of a WT heart shows a trace of dimension (mm) vs time (ms). Parameters measured in this mode include left ventricular anteriolateral and posterior wall thicknesses during diastole and systole as well as left ventricular interior dimension during diastole and systole.

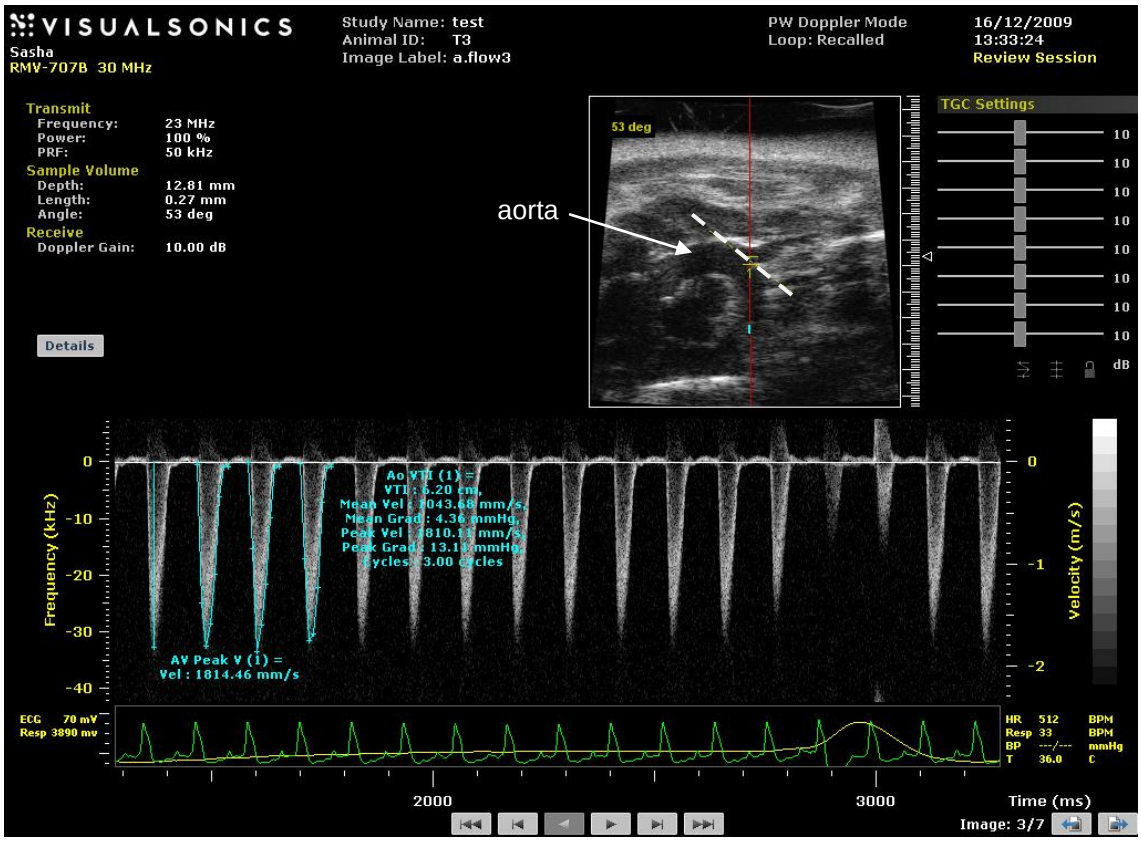

Figure 3.5 Representative Doppler mode echocardiogram of a WT heart.

A trace of velocity (m / s) v time (ms) is created. Parameters measured include aortic root velocity time integral and aortic valve peak velocity.

3.3 Results

3.3.1 Confirmation that KI mouse RIα does not form disulfide *in vitro* or *ex vivo*

The novel Cys17Ser RIα 'redox-dead' KI mouse, in theory, should not form disulfides in response to oxidative stress. Therefore this was assessed *in vitro* and *ex vivo* by comparing the KI RIα response to oxidant to that of RIα in WT littermates.

***In vitro* RIα disulfide formation:** To assess RIα disulfide formation *in vitro*, perfused WT or KI hearts were homogenised and treated with 0.5 mM diamide for 5 min. Figure 3.6A (male hearts) and Figure 3.6B (female hearts) show that in homogenates prepared from WT perfused hearts, both monomer and disulfide dimer were present. In cardiac samples from males the basal disulfide dimer was ~60 % of the total RIα pool, which was similar to females (~65 %). Treatment of WT homogenates with 0.5 mM diamide caused complete loss of monomer and a corresponding increase in RIα disulfide dimer. There was ~40 % increase in disulfide dimer in male which was statistically significant ($p<0.05$) and ~20 % increase in female which was not statistically significant. When reducing agent was added to the preparation (from either sex) in SDS sample buffer, as anticipated the disulfide was fully reduced and so RIα ran at its monomeric weight. In control and diamide-treated male KI heart homogenate there was only reduced monomeric RIα present and no disulfide dimer at all, as anticipated. In females, there were small traces of RIα disulfide in KI hearts but this was most probably an artefact.

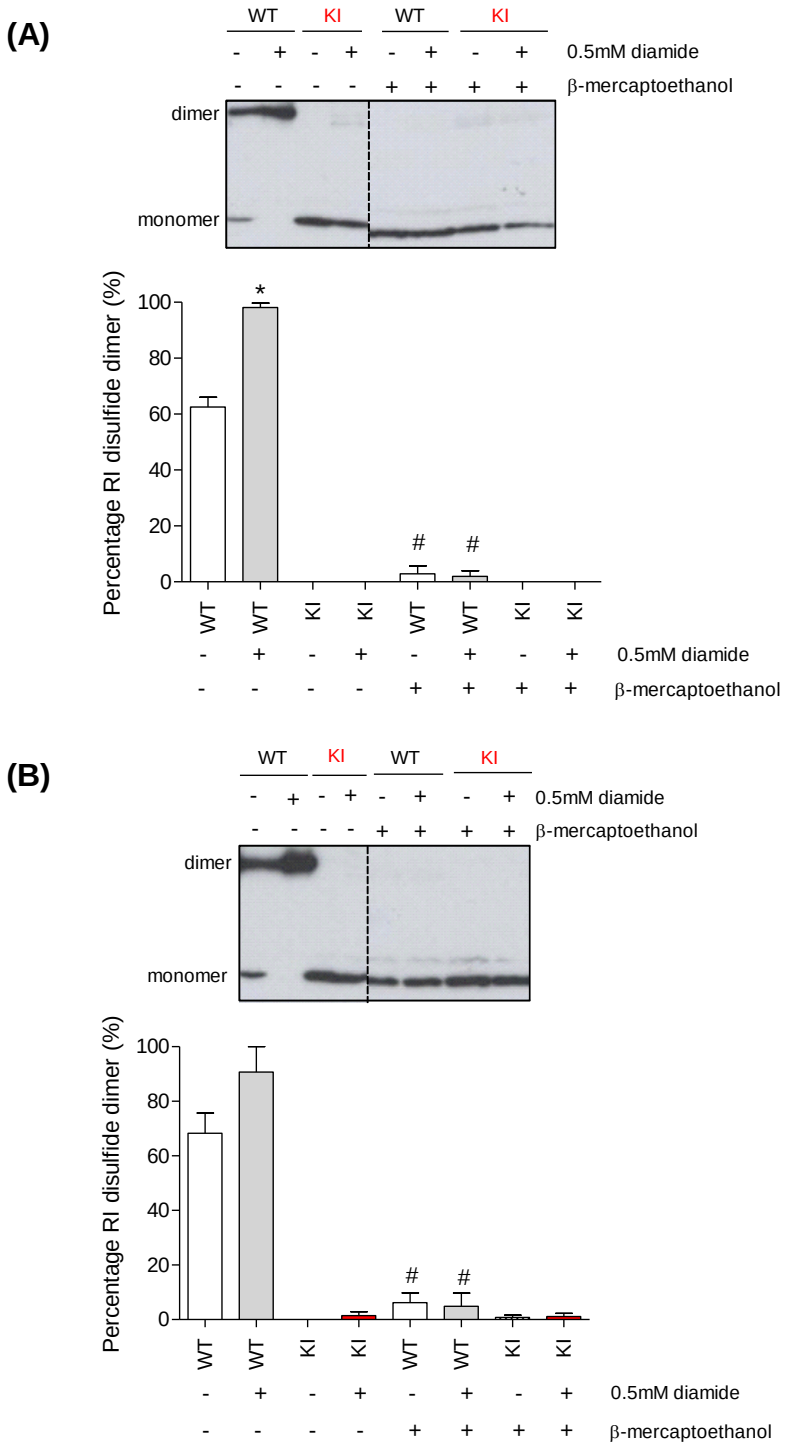

Figure 3.6 Effect of diamide on RIα redox state in WT and KI hearts *in vitro*.

(A) Male hearts were Langendorff-perfused for 45 min, homogenised and treated for 5 min with or without (control) 0.5 mM diamide. Representative blot shows RIα monomer and dimer and graph presents average percentage RIα disulfide dimer for n=4, n=3 ± SEM. * $p<0.05$ compared to untreated WT, # $p<0.05$ with β-mercaptoethanol compared to without. (B) As above but female hearts were studied. Diamide increased disulfide formation in WT hearts but disulfide was completely absent in KI hearts, as anticipated.

***Ex vivo* RIα disulfide formation:** To establish *ex vivo* whether KI mice fail to form RIα disulfide, WT and KI hearts were perfused with K-HB for 40 min followed by 50 μM H_2O_2 for 5 min. Monomer and disulfide dimer were present in perfused WT hearts. There was ~25 % disulfide dimer in female hearts (Figure 3.7A) and ~20 % in male hearts (Figure 3.7B) and perfusion with H_2O_2 increased RIα disulfide in males and females by ~70 %. However, there was no disulfide dimer present at all in female or male control or oxidant-perfused KI hearts, again as expected.

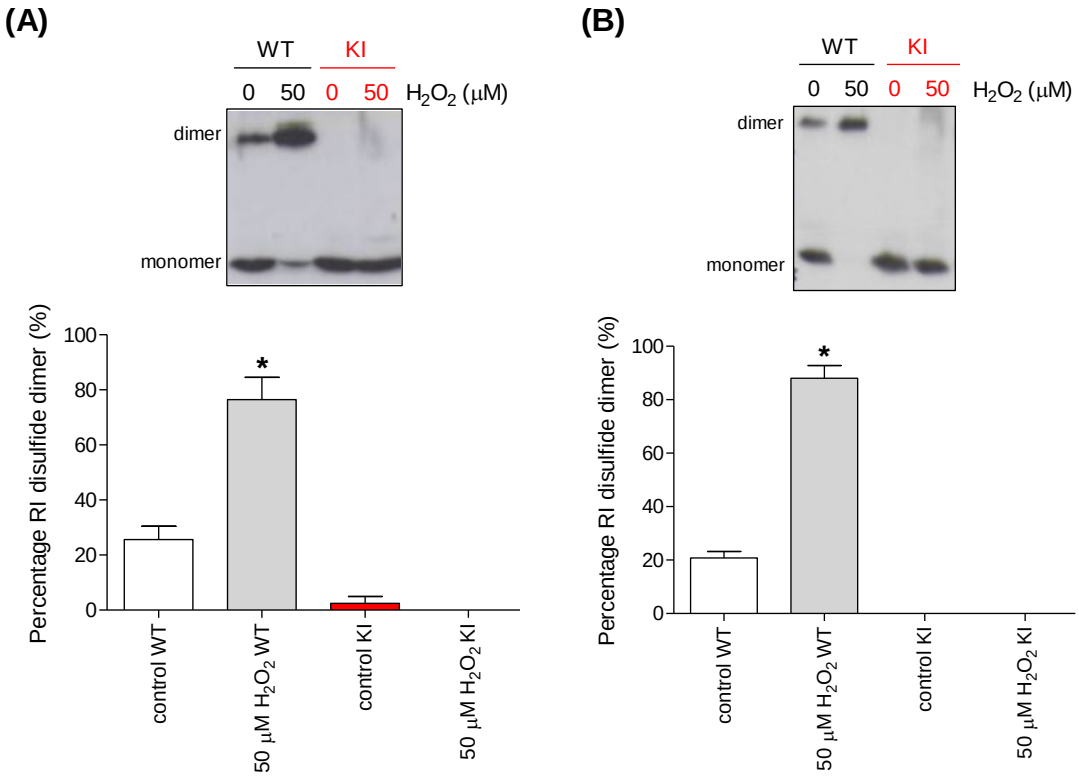

Figure 3.7 PKA RIα redox state in WT and KI hearts Langendorff-perfused with K-HB or H_2O_2.

(A) Female hearts were Langendorff-perfused with K-HB for 45 min or K-HB for 40 min followed by 5 min with or without (control) 50 μM H_2O_2. The representative blot was probed for PKA RIα and graph shows average percentage RIα disulfide for n=6 ± SEM. (B) Same as above but in male hearts. In both male and female, 50 μM H_2O_2 caused a significant increase in RIα disulfide formation in WT which was not seen in the KI where RIα disulfide was completely absent.

3.3.2 RIα abundance in female and male WT and KI organs

To further characterise the novel KI mouse the abundance of PKA RIα in various organs of female (Figure 3.8) and male mice (Figure 3.9) was examined and compared to those in WT of the same sex respectively. KI kidneys had more RIα than WT; with ~3 times more in females and ~4 times more in males. Female KI livers had ~2 times more RIα than WT, and in males there was ~3 times more. However, in lungs, hearts and brains the abundance of RIα was similar between genotypes in both males and females. WT pancreas expressed the same amount of RIα as KI in females; whereas in males the WT tissue expressed twice as much.

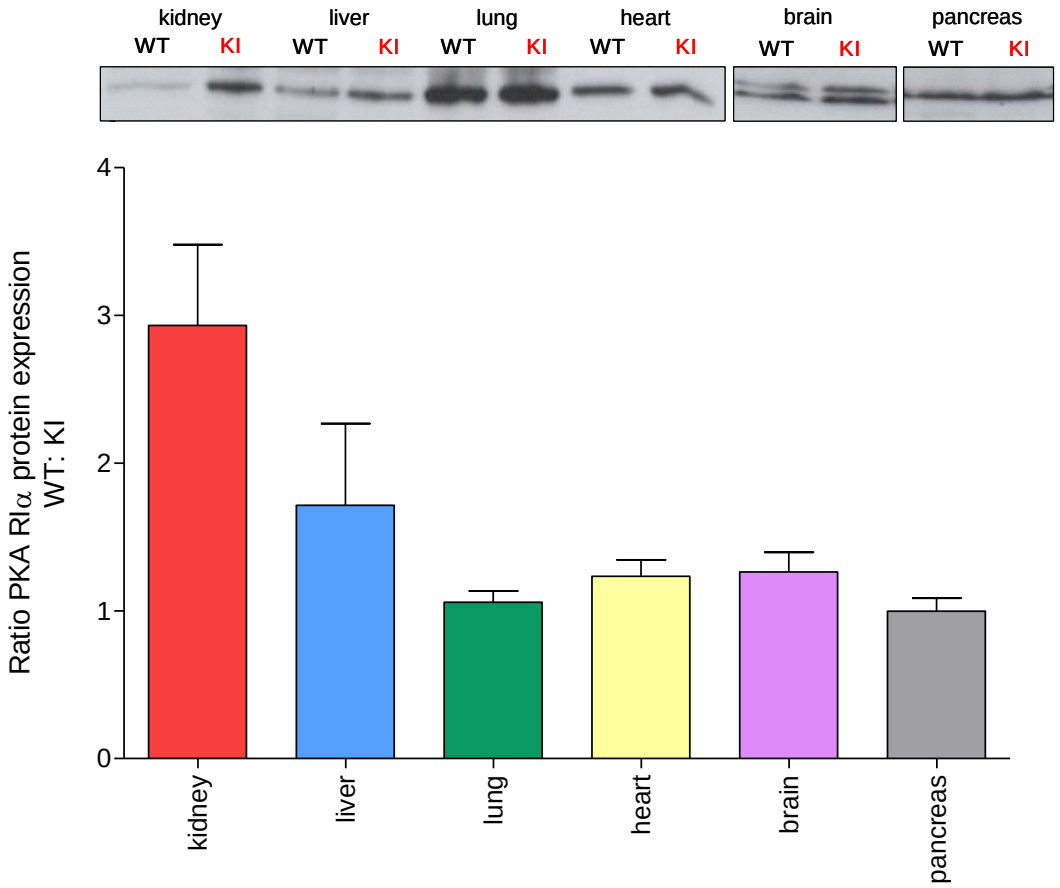

Figure 3.8 RIα abundance in organs from female WT and KI mice.

Organs were homogenised and added to reducing SDS sample buffer. SDS-PAGE and Western blotting were carried out. Top, representative blot showing RIα present in female WT and KI kidney, liver, lung, heart, brain and pancreas. Bottom, graphical representation (kidney n=4 pairs, liver n=5 pairs, lung n=5 pairs, heart n=5 pairs, brain n=3 pairs, pancreas n=4 pairs ± SEM) of the average ratio of RIα present in WT organ compared to KI organ. Lung, heart, brain and pancreas show comparable abundance of RIα in WT and KI but KI kidney and liver has more RIα present than WT.

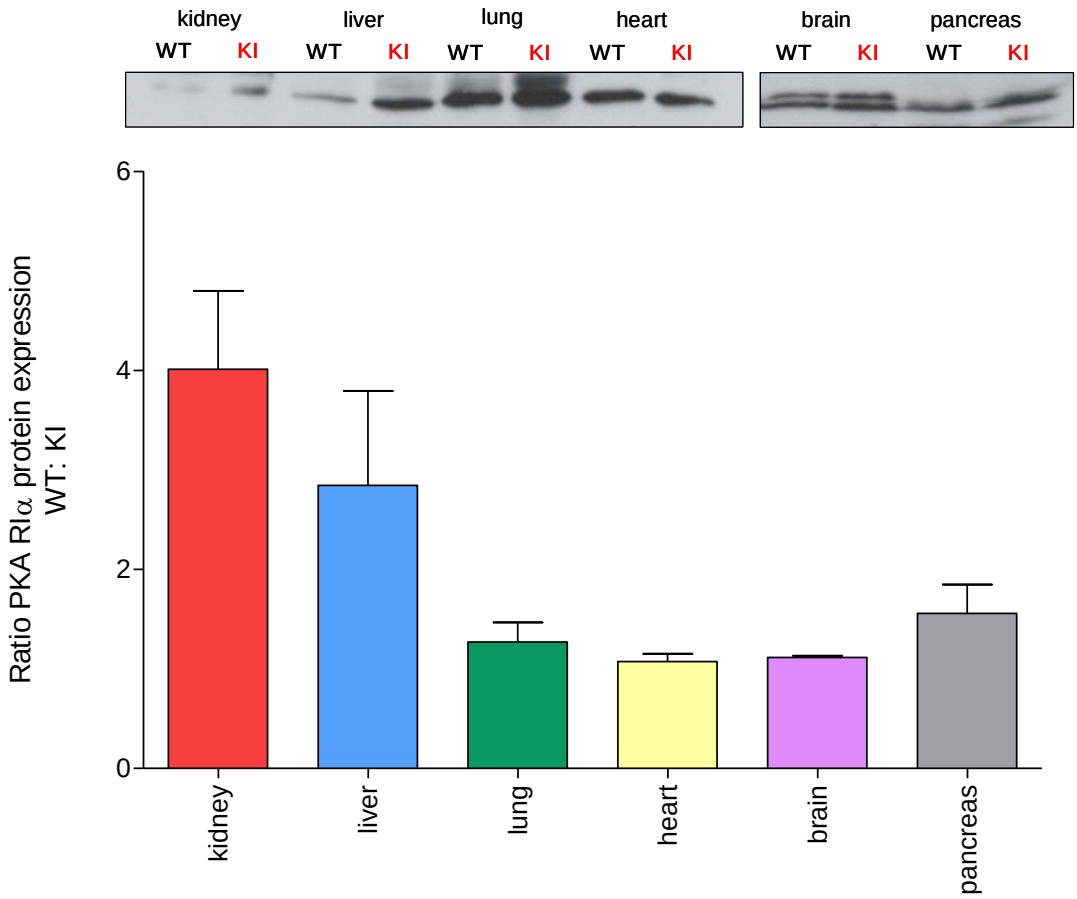

Figure 3.9 Abundance of RIα in organs from male WT and KI mice.

Organs were homogenised and added to reducing SDS sample buffer. SDS-PAGE and Western blotting were carried out. Top, representative blot showing RIα present in WT and KI kidney, liver, lung, heart, brain and pancreas. Bottom, graphical representation of the average ratio of RIα present in WT organ compared to KI organ (kidney n=4 pairs, liver n=6 pairs, lung, brain, pancreas n=4 pairs, heart n=5 pairs ± SEM). Lung, heart, brain showed comparable abundance of RIα in WT to KI but KI kidney, liver and pancreas had more RIα present than WT.

3.3.3 Protein expression in male WT and KI hearts

I am primarily interested in PKA but it was important to determine whether the abundance of other proteins, such as kinases and other PKA subunits are different between WT and KI. Any such compensatory changes could be responsible for any physiological or biochemical difference observed between the genotypes. Figure 3.10 shows the abundance of selected kinases in the hearts of WT and KI mice. It was evident from Western blots and quantitative analysis that there was no statistically significant difference in the abundance of p38 MAPK, PKG Iα, PKCε, PKCα, PKCδ, PKD, ERK, COX-2 or Akt between WT and KI. The abundance of other PKA subunits was also analysed (Figure 3.11); the PKA catalytic subunit and RII were also not different between WT and KI hearts. PKA RIβ could not be detected in WT or KI hearts (results not shown). With a long exposure a band was observed at ~42 kDa perhaps corresponding to PKA RIβ, but there were also a lot of additional non-specific bands near this molecular weight so it is difficult to safely conclude this was RIβ.

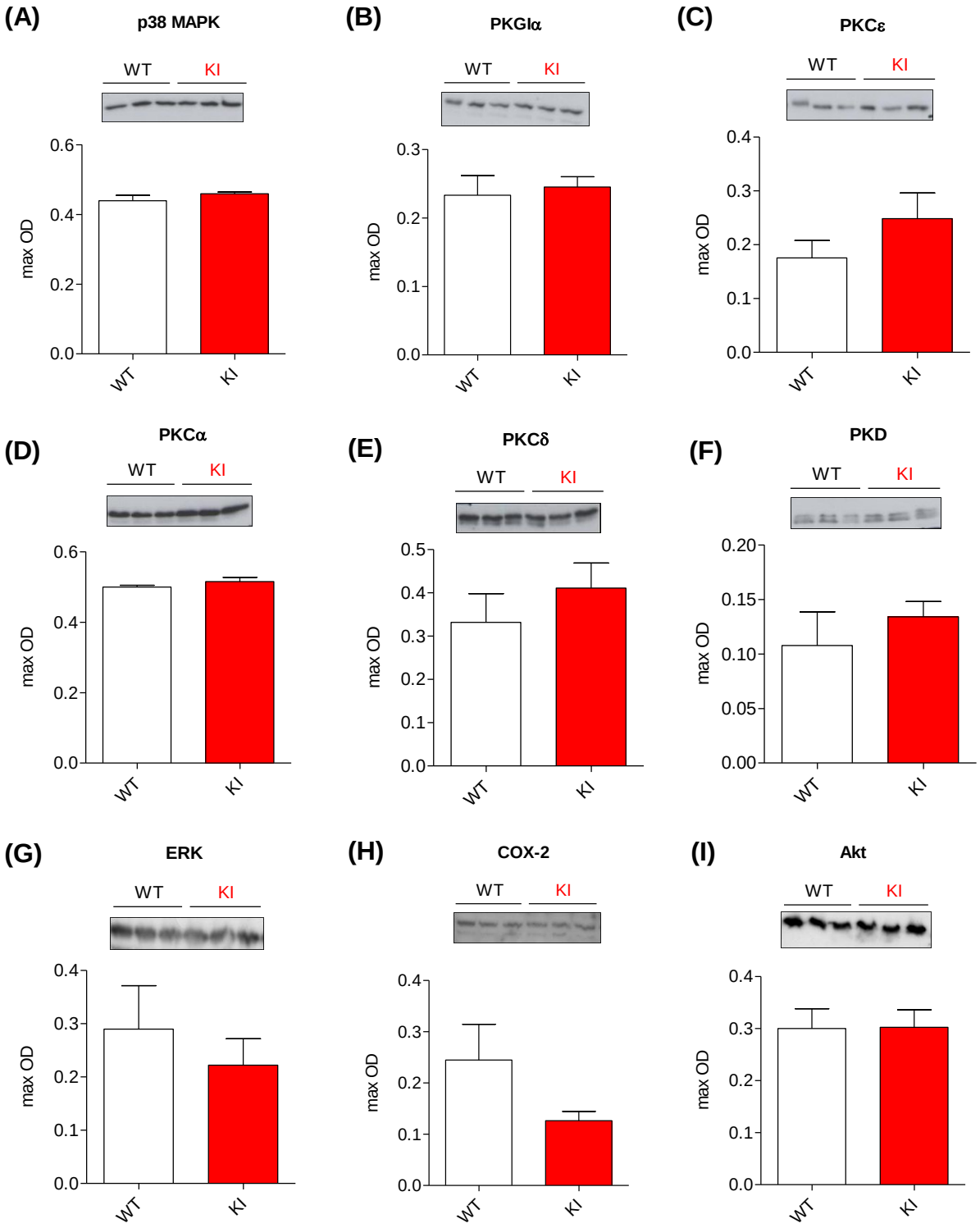

Figure 3.10 Abundance of proteins in WT and KI hearts.

(A) Langendorff-perfused WT and KI hearts were homogenised. SDS-PAGE and Western blotting were performed and blots probed with antibodies to p38 MAPK. Graph shows average max OD for WT and KI hearts (n=3) ± SEM (B) PKG Iα (C) PKCε (D) PKCα(E) PKCδ (F) PKD (G) ERK (H) COX-2 (I) Akt. There were no differences in protein abundance between genotypes.

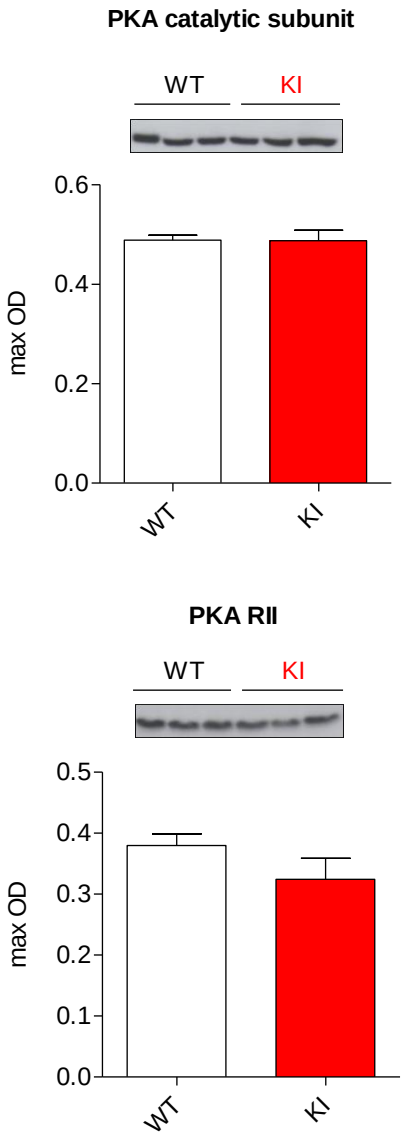

Figure 3.11 Abundance of PKA subunits in WT and KI hearts.

WT and KI hearts were Langendorff-perfused and homogenised. Western blots were probed with antibodies to PKA catalytic subunit and PKA RII. Graphs show average max OD for WT and KI hearts (n=3) ± SEM. There was no difference in abundance of any of the subunits between WT and KI hearts.

3.3.4 Heart weight: body weight ratios for WT and KI mice

To further characterise the KI mouse, the body weights and heart weights of KI mice were compared to WT littermates (Figure 3.12). There was no difference in average body weight between WT and KI mice (28.9 ± 2.4 g and 28.7 ± 2.5 g respectively). In some studies, hearts were weighed after Langendorff perfusion and freezing in liquid nitrogen. Average frozen heart weight to body weight ratio for KI was similar to WT (8.8 ± 0.2 mg / g and 8.6 ± 0.3 mg / g respectively). In other studies hearts were weighed before Langendorff perfusion. Average fresh heart weight to body weight ratios were similar between genotypes (KI, 9.3 ± 0.2 mg / g and WT, 8.9 ± 0.3 mg / g).

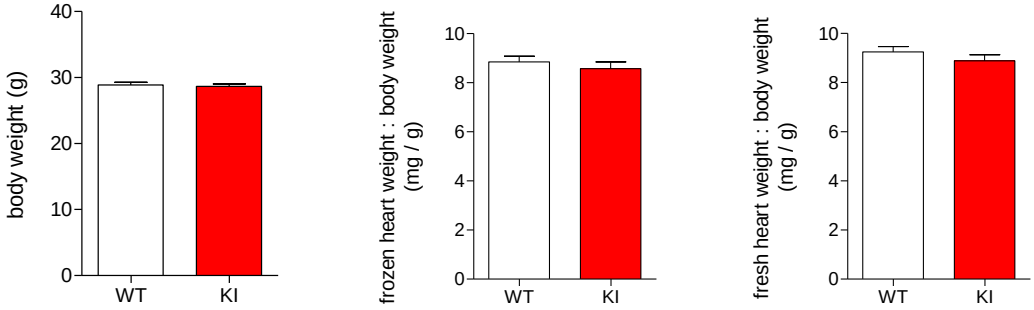

Figure 3.12 Average body weight and heart weight to body weight ratios for WT and KI mice.

Body weights of WT and KI mice (14 - 17 weeks old, WT n=42, KI n=38) were measured as were frozen and fresh heart weights. The ratios of frozen heart weight to body weight (n=33) and fresh heart weight to body weight (WT n=22, KI n=21) were calculated ± SEM. There was no difference in body weight or frozen or fresh heart weight : body weight between WT and KI.

3.3.5 Stability of Langendorff-perfused male WT and KI hearts

The influence of RIα disulfide on cardiac function was analysed in Langendorff-perfused WT and KI hearts. Coronary flow, LVDP and EDP were measured over a 40 min stabilisation period. Figure 3.13 shows these parameters during the last 20 min of this period, during which no adjustments to the preparation were made. Coronary flow (Figure 3.13A) was similar in WT and KI hearts and stayed at ~4 ml / min. The EDP (Figure 3.13B) was different between genotypes for the first 7 min after which it stabilised at ~8 mmHg in both genotypes. Overall, there was not a statistically significant difference in EDP over the 20 min period between WT and KI. There was a trend for average LVDP (Figure 3.13C) in the KI hearts to be ~10 mmHg lower than WT throughout the 20 min period. As the EDP was similar between WT and KI hearts the lower LVDP in KI hearts may be explained by a lower end systolic pressure in KI hearts compared to WT.

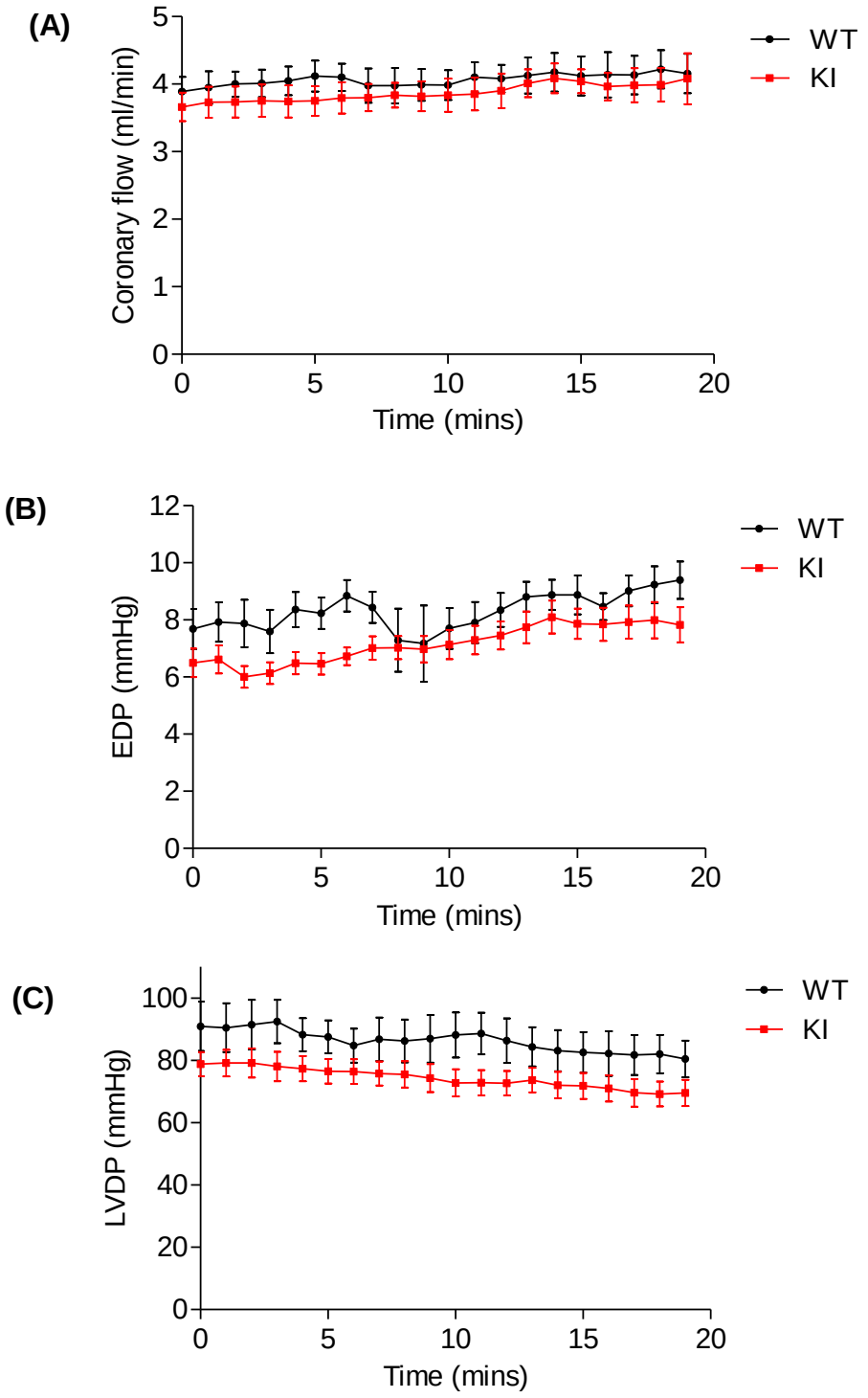

Figure 3.13 Stability of male WT and KI hearts during Langendorff perfusion.

(A) WT and KI hearts were Langendorff-perfused for 40 min. Graph shows average coronary flow during the last 20 min of the stability period (n=6 ± SEM) (B) EDP (C) LVDP. Coronary flow and EDP were similar in WT and KI hearts, but KI hearts showed a trend for a slightly lower LVDP than WT hearts.

3.3.6 Echocardiography in WT and KI mice

Body weights were not different between WT (25.5 ± 0.9 g) and KI (25.1 ± 0.5 g) mice used for echocardiography. The echocardiography software also calculated the left ventricular mass and Figure 3.14 shows that average left ventricular mass: body weight ratios were also not significantly different between genotypes (WT, 3.9 ± 0.1 mg / g and KI, 4.1 ± 0.2 mg / g).

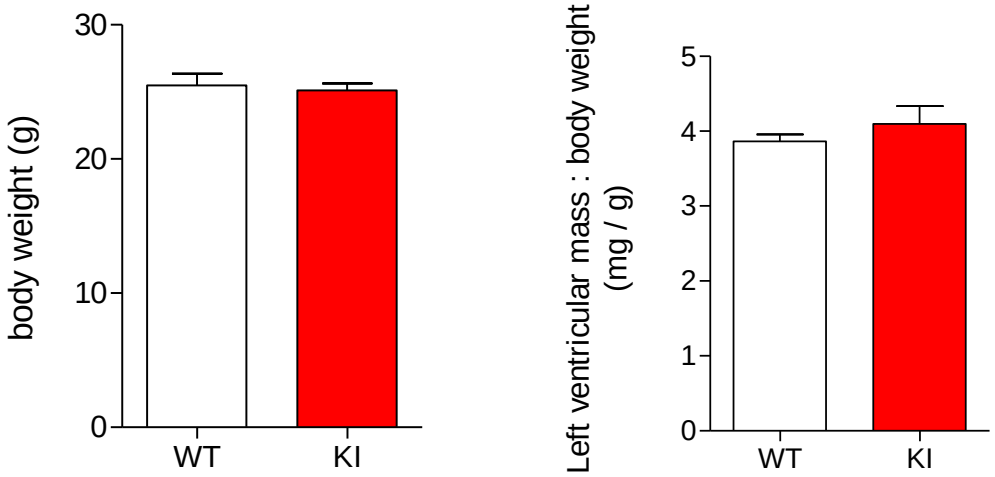

Figure 3.14 Average body weight and left ventricular mass to body weight ratios for WT and KI mice used in echocardiography.

Mice were weighed before they were echocardiographed and the ratio of left ventricular mass to body weight was calculated by the echocardiography software (n=6 ± SEM). There were no statistically significant differences in these measurements between WT and KI.

Echocardiographic analysis of WT and KI mice revealed that KI mice had a larger left ventricular internal dimension during systole (~0.3 mm in M-mode long axis ($p<0.05$, Figure 3.15 and Table 3.2) and ~0.22 mm in M-mode short axis ($p<0.05$, Figure 3.16 and Table 3.3)). Figure 3.15 shows that the left ventricular dimension was ~0.4 mm larger in KI compared to WT during systole and the left ventricular volume was ~9 µl larger in KI compared to WT too, both significant differences ($p<0.05$). KI left ventricles had a ~10 µl larger volume than WT during diastole, and a ~0.2 mm larger dimension, both statistically significant ($p<0.05$). However, the left ventricular internal

dimensions were not different between WT and KI mice during diastole. Intraventricular septal widths and left ventricular posterior wall thicknesses were similar in WT and KI mice during diastole or systole. The cardiac output was similar in WT and KI mice, although ejection fraction and fractional shortening were significantly ($p<0.05$) smaller in KI mice compared to WT mice (~7 % smaller and ~6 % smaller respectively). Doppler mode (Figure 3.17 and Table 3.4) revealed no differences in aortic root velocity time integral or aortic valve peak velocity.

Figure 3.18 presents a schematic which summarises these observations. KI hearts displayed contractile dysfunction as their left ventricular dimensions and volumes were significantly ($p<0.05$) larger in KI than WT during systole. Despite these larger dimensions in the KI, their hearts had the same cardiac output as WT explained by a significantly ($p<0.05$) lower ejection fraction and fractional shortening compared to WT.

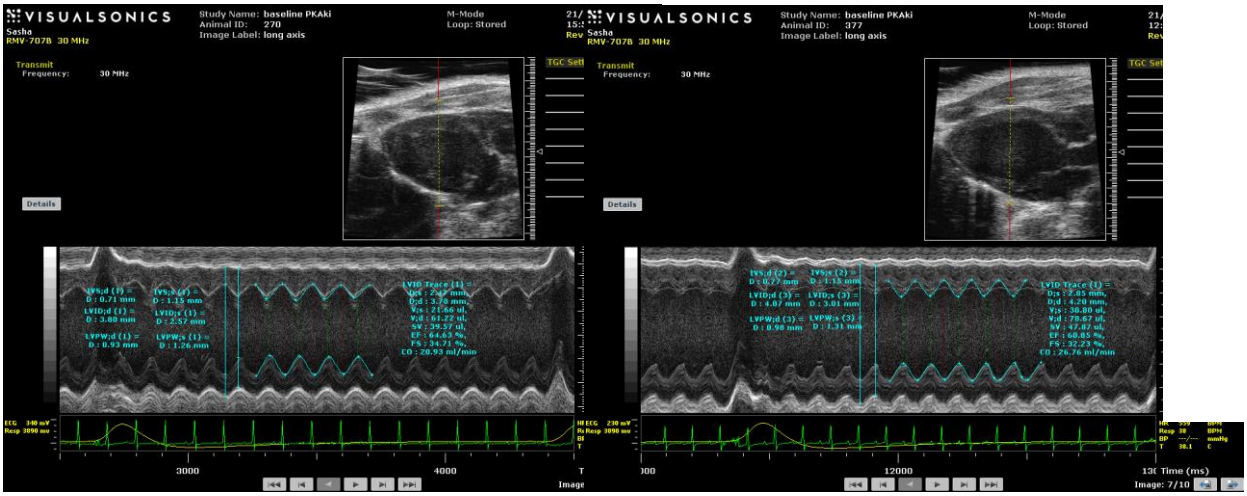

WT **KI**

Figure 3.15 M-mode long axis analysis of WT and KI hearts.

Representative M-mode images of the long axis of WT and KI hearts showing that KI left ventricles were larger than WT during diastole and systole.

Parameter	WT	KI
intraventricular septal width (IVS): diastole (d) (mm)	0.82 ± 0.03	0.93 ± 0.06
left ventricular internal dimension (LVID): d (mm)	3.95 ± 0.09	4.11 ± 0.05
left ventricular posterior wall (LVPW): d (mm)	0.87 ± 0.06	0.85 ± 0.09
IVS: systole (s) (mm)	1.32 ± 0.04	1.28 ± 0.07
LVID: s (mm)	2.57 ± 0.04	2.9 ± 0.09*
LVPW: s (mm)	1.29 ± 0.05	1.21 ± 0.06
dimension; s (mm)	2.38 ± 0.08	2.76 ± 0.08*
dimension; d (mm)	3.88 ± 0.08	4.11 ± 0.07*
volume; s (µl)	20.00 ± 1.53	28.78 ± 1.98*
volume; d (µl)	65.23 ± 3.05	74.94 ± 3.00*
stroke volume (µl)	45.24 ± 1.96	46.16 ± 1.53
ejection fraction (%)	69.49 ± 1.47	61.78 ± 1.49*
fractional shortening (%)	38.60 ± 1.16	32.89 ± 1.03*
cardiac output (ml / min)	23.91 ± 1.07	25.19 ± 0.99
heart rate (bpm)	543.17 ± 7.32	545.3 ± 6.22

Table 3.2. M-mode long axis analysis of WT and KI hearts.

Average values for various echocardiographic parameters in WT and KI mice (n=6 ± SEM *p<0.05 compared to WT) in M-mode long axis. Left ventricular dimension and volume during systole and diastole were significantly larger in KI compared to WT whilst the ejection fraction and fractional shortening were significantly lower in KI than WT.

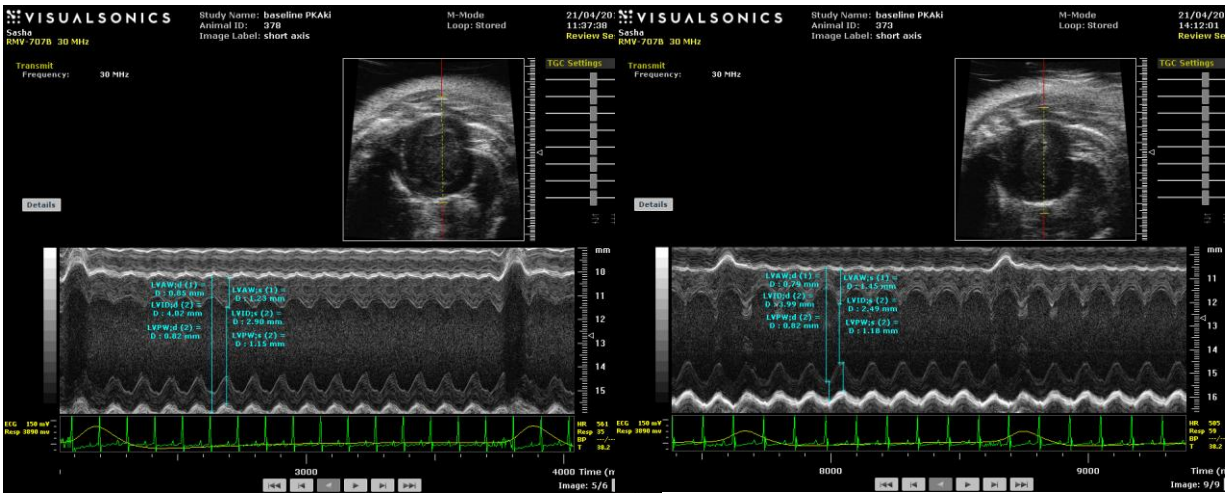

WT **KI**

Figure 3.16 M-mode short axis analysis of WT and KI hearts

Representative M-mode images of the short axis of WT and KI hearts showing that the KI left ventricle was larger than the WT left ventricle during diastole and systole.

Parameter	WT	KI
left ventricular anterolateral wall (LVAW): diastolic (d) (mm)	0.82 ± 0.04	0.9 ± 0.05
left ventricular internal dimension, diastolic (LVID): d (mm)	3.96 ± 0.04	4.03 ± 0.07
left ventricular posterior wall, diastolic (LVPW): d (mm)	0.87 ± 0.05	0.84 ± 0.07
LVAW: systolic (s) (mm)	1.39 ± 0.03	1.31 ± 0.06
LVID: s (mm)	2.55 ± 0.06	2.77 ± 0.06*
LVPW:s (mm)	1.26 ± 0.04	1.18 ± 0.07

Table 3.3. M-mode short axis analysis of WT and KI hearts

Average values for various echocardiographic parameters in WT and KI mice (n=6 ± SEM *p<0.05 compared to WT) in M-mode short axis are shown. Systolic left ventricular internal dimension was significantly larger in KI than WT.

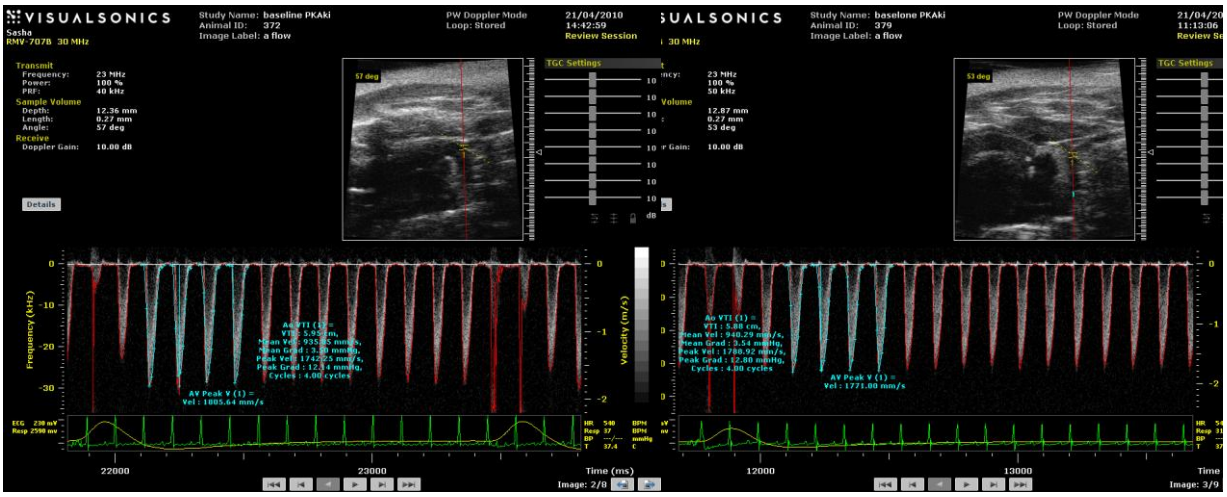

WT **KI**

Figure 3.17 Doppler mode analysis of WT and KI hearts.

Representative images of WT and KI hearts in Doppler mode showing that blood flow velocity in WT and KI hearts was similar.

Parameter	WT	KI
aortic root velocity time integral	1737.31 ± 59.50	1857.27 ± 120.25
aortic valve peak velocity	5.79 ± 0.40	6.11 ± 0.53

Table 3.4. Doppler mode analysis of WT and KI hearts.

Average values for various echocardiographic parameters in WT and KI mice in Doppler mode (n=5, n=6 ± SEM). No differences were observed between WT and KI hearts.

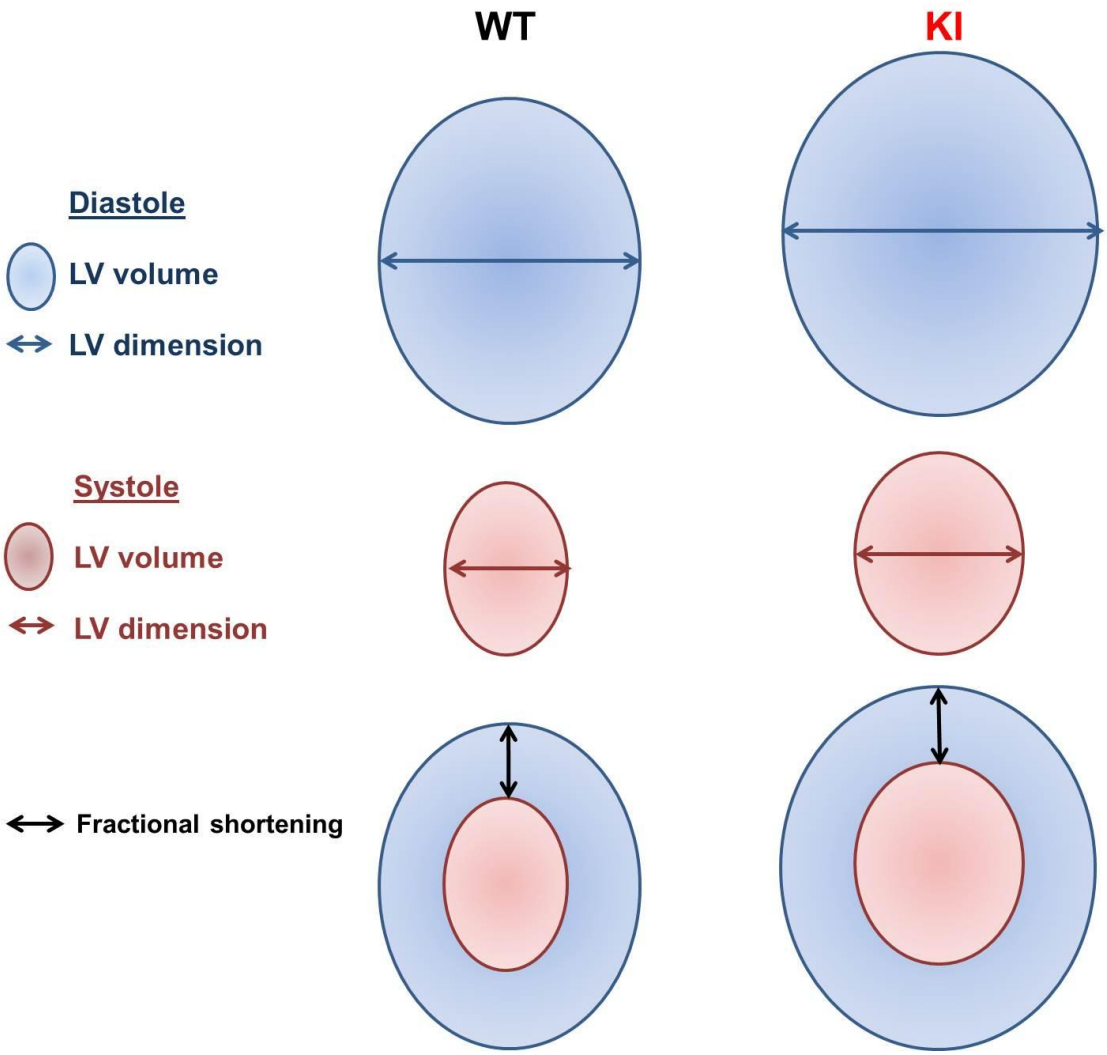

Figure 3.18 Schematic diagram to show the phenotype of WT and KI hearts.

The results of echocardiography suggest that, compared to WT, KI left ventricles were larger in volume and dimension during diastole and systole. However, the cardiac output was the same in both genotypes because KI hearts had a lower ejection fraction and fractional shortening compared to WT.

3.4 Discussion

In this chapter I confirmed that KI RIα does not form disulfide basally or in response to oxidant, unlike in WT, as anticipated. This was observed in *in vitro* and *ex vivo* experimental preparations; although basal WT RIα disulfide was higher *in vitro* than *ex vivo*. This is probably because the *in vitro* heart homogenate was not prepared with maleimide to prevent air oxidation, whereas the *ex vivo* heart homogenate was. Maleimide was absent from the homogenisation buffer used in *in vitro* studies because this alkylates Cys thiols and so would have blocked any disulfide dimerisation induced by the diamide treatment. However, both *in vitro* and *ex vivo* results confirm that the novel Cys17Ser RIα KI mouse is a valid tool for investigating the influence of RIα disulfide on PKA activity and cardiovascular function, as PKA RIα in the tissue of these mice does not form disulfides.

Mutations or KO of PKA regulatory subunits can result in up-regulation of other regulatory subunit isoforms, as well as alter expression of the catalytic subunit. For example, neural specific deletion of the RIβ gene results in a compensatory increase in RIα protein with no change in RII or catalytic subunit protein. When the RIIβ gene is deleted from white adipose and brown adipose tissue of mice, RIα protein increases and catalytic subunit protein reduces slightly. There is no change in RIα mRNA levels however, so the increased protein is likely due to increased stability of RIα by incorporation into Type I PKA holoenzyme.[139] However, the Cys17Ser mutation did not alter the abundance of the PKA RIα, RII or catalytic subunits in the heart. PKA RIβ was not detected in the heart, concurring with others who suggest it is only found in the brain and testes.[100] In addition, the abundance of other selected kinases was similar in WT and KI hearts. Of course, I have not analysed the expression of every kinase known but a number of kinases linked to PKA were assessed and no statistically significant differences were observed between genotypes. I can therefore, be reasonably confident that any physiological differences observed between WT and KI were due to RIα disulfide formation.

Interestingly, RIα abundance was much higher in KI kidney compared to WT kidney in both male and female mice. This was also the case in liver but to a lesser degree. A reason for this may be compensation for the absence of RIα disulfide. RIα disulfide may play a more significant role in the kidney and liver than in the heart, for example so RIα expression was increased in kidney and liver and not in heart. If RIα disulfide is associated with PKA activation, perhaps KI kidney and liver express a higher abundance of RIα (but without disulfide) to achieve the same amount of activity achieved by the WT which basally has a small amount of disulfide present.

The kidney plays a key role in Na^+ balance and regulating blood volume and extracellular fluid volume and so ultimately arterial pressure and hypertension.[140] Hormones such as parathyroid hormone activate PKA which phosphorylates and inhibits Na^+ / H^+ exchanger 3 (NHE-3) in the apical membrane of the proximal tubule of the kidney.[141] Na^+ / H^+ exchanger regulatory co-factor (NHERF, which binds to the A-kinase anchoring protein D-AKAP2,[142] which determines PKA localisation as discussed in Chapter 5) and the anchoring protein ezrin are also required for this inhibition.[143] NHE-3 preferentially exchanges extracellular Na^+ for intracellular H^+ and is important in intravascular volume maintenance and pH homeostasis as demonstrated in NHE-3 null mice which have decreased blood pressure, acidic plasma pH and diarrhoea.[144] In light of this, the higher abundance of RIα in KI mouse kidney could alter blood pressure and this could be investigated *in vivo* by radiotelemetry and with isolated blood vessels using myography. However, the adaptive change in RIα expression in the KI kidney could complicate such studies. Fortunately, no such compensatory expression changes occur in the heart, which is the focus of my studies.

Echocardiography was performed on WT and KI hearts to gain insight into any differences in the structure and function of KI hearts. KI hearts demonstrated some systolic dysfunction, and had a larger left ventricular volume and dimension compared to WT during systole and diastole. The cardiac output was however similar in WT and KI hearts. This was because the KI hearts, despite a larger ventricle, had lower fractional shortening and ejection fraction compared to WT. This could represent an

adaptive response resulting from the chronic inability of RIα in KI to form a disulfide. An alternative is this subtle variation between genotypes could represent a difference in signalling, such that the KI has a deficit in its basal PKA activity, perhaps resulting in the under-phosphorylation of a target protein involved in cardiac contractile function. If the latter explanation was correct, the KI phenotype might be recapitulated in WT if all the basal disulfide could be removed, perhaps pharmacologically with reducing agents. However, such interventions would not be selective for RIα, limiting the information such an approach would provide. The ventricular posterior wall thickness during systole and diastole was not different between WT and KI. Furthermore, the heart weight to body weight ratios were similar between the hearts of either genotype so no hypertrophy was evident in KI hearts.

Langendorff perfusion illustrated that KI hearts had a trend for a lower LVDP than WT hearts. This trend may become statistically significant with a higher *n* number. The EDP was not significantly different between WT and KI hearts but it was slightly lower in KI than WT, despite altering the balloon volume during the first 20 min of the perfusion protocol to repeatedly set the EDP at ~7 mmHg. Frank-Starling's Law states that the greater the preload (pressure in the ventricle at the end of diastole) the greater the contractile force during systole. Therefore a small decrease in EDP can have a marked effect on lowering end systolic pressure and therefore LVDP and this may be what I am observing. I therefore cannot safely say, from these results, that there is a contractile deficit in KI hearts but clearly the LVDP is lower. However, in Chapter 4 I demonstrate that KI LVDP was significantly lower than WT LVDP during the last 5 min of the stabilisation period. Biochemically, a lower LVDP in KI could be due to a basal turnover of RIα disulfide in WT hearts that cannot occur in KI, resulting in higher PKA activity in WT compared to KI. This would occur if thiol oxidants are produced basally in hearts, which is likely as such products are generated in many biochemical processes,[27, 145] and explains the resting disulfide in WT hearts. Whether this small functional change in the KI heart would mean anything in the whole animal is difficult to say and would be something to investigate further. Other methods for assessing contractile function include Frank-Starling curves which demonstrate the relationship between EDP and LVDP in the Langendorff-perfused heart and pressure-volume loops

which, using the Millar ARIA system, measure simultaneous left ventricular pressure and volume.

In conclusion, these results suggest that RIα disulfide may be important in basal heart contractile function, but oxidative stress is likely required for a more pronounced phenotypic difference between WT and KI to be observed. Indeed, a differential response of the two genotypes to oxidative stress is the subject of Chapter 4.

4 RIα DISULFIDE AND cAMP-MEDIATED PKA ACTIVATION

4.1 INTRODUCTION

4.1.1 Adrenergic signalling

Monoamine neurotransmitters are compounds with one amino group connected to an aromatic ring by a two carbon chain (Figure 4.1). Examples include norepinephrine (noradrenaline), epinephrine (adrenaline), phenylephrine and serotonin as well as the drug isoprenaline. Norepinephrine and epinephrine are also classed as catecholamines as they are compounds with a catechol (benzene with two hydroxyl side groups) and a side-chain amine.

Norepinephrine, phenylephrine and epinephrine target the G-protein coupled adrenoceptors, α (α_{1A}, α_{1B}, α_{1D}, α_2) and β (β_1, β_2, β_3), with different affinities and link the sympathetic nervous system to the cardiovascular system. β_1, β_2, β_3 and α_1 adrenoceptors are present in cardiomyocytes. β_1 and β_2 are linked to G_s proteins which activate adenylate cyclase causing the production of 3′,5′-cyclic monophosphate (cAMP). cAMP then binds to the regulatory subunits of cAMP-dependent protein kinase (PKA), enabling catalytic activity and so phosphorylation of PKA substrates (examples described later). The accepted view is that under physiological conditions, catecholamines cause positive inotropy (increased contractility), lusitropy (increased rate of relaxation) and chronotropy (increased heart rate) by β_1 adrenoceptor activation and PKA signalling,[146, 147] but there is also evidence that persistent stimulation of β_1 adrenoceptors activates Ca^{2+} / calmodulin-dependent kinase II independent of PKA activation. This increases intracellular Ca^{2+} and causes myocyte contraction and leads to apoptosis and maladaptive remodelling.[148, 149] β_2 adrenoceptors are linked to both G_s and G_i, which activate and inhibit adenylate cyclase respectively. The switch from G_s to G_i occurs with prolonged stimulation of the β_2 adrenoceptor and this has a cardioprotective effect.[150] β_3 adrenoceptors appear to be responsible for the negative inotropic effects of catecholamines.[151] Isoprenaline is structurally similar to

epinephrine and is a non-selective β adrenoceptor agonist routinely used as a positive control for activation of PKA.

α_1 receptors are associated with G_q proteins and coupled to several signalling pathways such as protein kinase C (PKC), protein kinase D (PKD), mitogen activated protein kinase (MAPK), phospholipase C (PLC), Ca^{2+} channels and phospholipase D.[146, 147] Activation of α_1 receptors is important in smooth muscle contraction,[152] positive inotropy,[153] and negative inotropy.[154, 155] Studies have shown that the outcome of α_1 receptor stimulation depends on extracellular Ca^{2+} concentration which may explain the conflict in the literature over whether α_1 adrenoceptor stimulation increases or reduces myocardial contraction. For example, high extracellular Ca^{2+} can activate PKC which opposes α_1 adrenoceptor-induced positive inotropy.[146, 156]

5-hydroxytryptamine (5-HT, also known as serotonin) is also a monoamine but signals through a different receptor. 5-HT receptors are coupled to various signalling pathways including the PLC pathway. PLC increases inositoltrisphosphate and triggers intracellular Ca^{2+} release and formation of diacylglycerol which activates PKC. This then stimulates the nitric oxide (NO) synthesis pathway generating cGMP which activates cGMP-dependent protein kinase (PKG).[157] In the heart, serotonin causes positive chronotropy and inotropy and mitogenesis (induction of mitosis, the process of cell division) and is a vasoconstrictor or vasodilator depending on the species, blood vessel type or the state of the endothelium cell layer.[158]

4.1.2 Metabolism of monoamines by monoamine oxidases

Monoamine oxidase (MAO) enzymes are located in the outer mitochondrial membrane and catalyse the oxidative deamination (catabolism) of monoamines. There are two types; MAO-A and MAO-B, each having different specificities for substrates and pharmacological inhibitors.[159, 160] Serotonin, norepinephrine and epinephrine are the preferred substrate for MAO-A.[161] The monoamine must first be transported into the cell to be metabolised, as shown in Figure 4.1. An aldehyde intermediate is formed and H_2O_2 is produced as a by-product.[162, 163] The intermediate may then be further

metabolised to an acid by aldehyde dehydrogenase. Metabolism of monoamines is important in regulating neurotransmitter levels and intracellular amine stores.

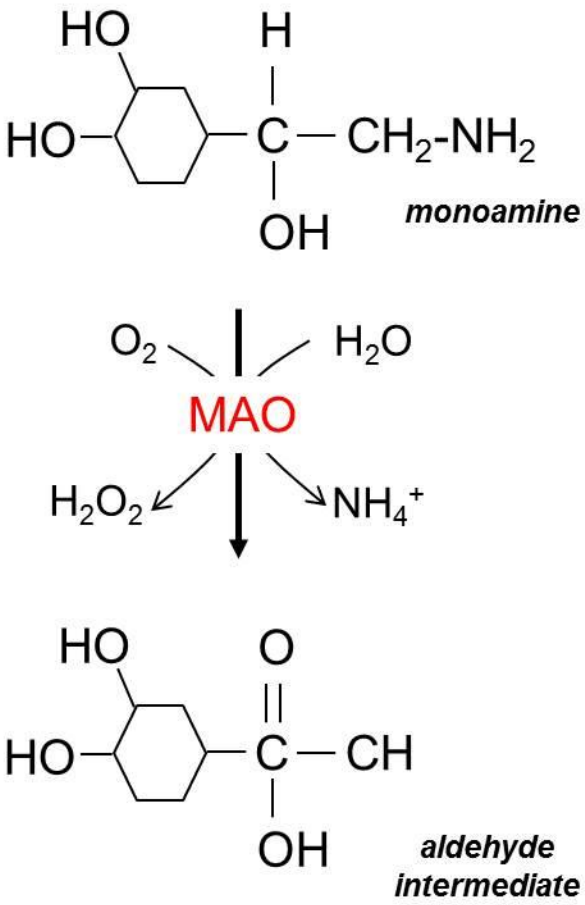

Figure 4.1 Mechanism of MAO-catalysed metabolism of monoamines.

The amine is removed from the monoamine (norepinephrine in this example) and ammonia (NH_4^+) and H_2O_2 are produced as by products as well as the aldehyde intermediate which may then be metabolised by aldehyde dehydrogenase to form the acid.

4.1.3 Mechanism of activation of Type I PKA

As explained in Chapter 1, cAMP binding to the regulatory subunits of PKA causes dissociation of the catalytic subunits which then catalyse the phosphorylation of PKA substrates. Substrate has been shown to sensitise Type I PKA but not Type II PKA to

low concentrations of cAMP. cAMP-induced dissociation of Type I PKA but not Type II was enhanced by substrate and the rate of re-association of the RI subunit with catalytic subunit was inhibited by substrate (which was not the case with RII and catalytic subunit) prolonging PKA activity induced by a given concentration of cAMP.[164-166] The pseudosubstrate inhibitor site and cAMP binding domain A of RI bind to the catalytic subunit,[167] whereas the inhibitor site and both cAMP binding domains (A and B) of RII bind to the catalytic subunit.[168] Vigil *et al.* showed that both substrate and cAMP were required for full activation of Type I PKA. They proposed a mechanism for Type I activation whereby cAMP binds to cAMP binding domain A of RI causing dissociation of some catalytic subunit, then the substrate competes with the pseudosubstrate inhibitor site of the RI subunit for the catalytic subunit causing full dissociation of regulatory subunit-bound catalytic subunits.[165] In comparison, Type II PKA is not sensitised to cAMP by substrate but autophosphorylation of Type II PKA causes RII to have a lower binding affinity for catalytic subunit which increases the dissociation of catalytic subunit caused by cAMP.[166, 169] A role for RIα disulfide in substrate-induced PKA activation is shown in Figure 4.3.

4.1.4 Excitation-contraction coupling

Excitation-contraction (EC) coupling is the series of events that happen from the electrical excitation of the myocyte to contraction of the heart. Ca^{2+} enters the cell during the action potential via depolarization-activated Ca^{2+} channels such as L-type Ca^{2+} channels and the Na^{+} / Ca^{2+} exchanger (NCX, considered to be in reverse mode when pumping Ca^{2+} into cell). This triggers Ca^{2+} release from the sarcoplasmic reticulum (SR) via ryanodine receptors (RyRs). These together raise intracellular concentration of Ca^{2+} which then directly binds to troponin C (TnC) in the myofilament. This causes a conformational change in the troponin complex (TnC together with TnI and cTnT, which anchors the troponin complex to the actin filament). TnI moves away from the myosin binding site of actin so myosin can now bind strongly to actin generating force and causing contraction. To allow relaxation to occur, the intracellular Ca^{2+} concentration must be lowered. This occurs via the NCX (which switches to the

forward mode to extrude Ca^{2+} from the cell), the SR Ca^{2+}-ATPase (SERCA) 2A which pumps Ca^{2+} into the SR, and mitochondrial Ca^{2+} uniport. This lowering of cytosolic Ca^{2+} means less of the ion binds to TnC, allowing the Tn complex to move back to its inactive conformation, blocking the binding of myosin to actin.

Substrates for PKA in EC coupling: Increased circulatory demand leads to β adrenergic stimulation, activation of PKA (considered in more detail in Chapter 1) and enhanced inotropy, lusitropy and chronotropy. PKA achieves this by phosphorylating a number of Ca^{2+}-handling and sarcomeric proteins involved in EC coupling (Figure 4.2). These include the L-type Ca^{2+} channel, the RyR, phospholamban (PLB), phospholemman (PLM), the thin filament protein cardiac TnI (cTnI) and the thick filament protein cardiac myosin binding protein C (cMyBP-C).

PKA phosphorylates and activates L-type Ca^{2+} channels causing Ca^{+} influx.[170] PKA also phosphorylates RyR2, in which two potential PKA phosphorylation sites have been identified; Ser2030 and Ser2808. There is some controversy over the major phosphorylation site upon activation of PKA in response to β adrenergic stimulation. Xiao *et al.*,[171] showed that Ser2030 is the major site and Wehrens *et al.*,[172] used RyR2-Ser2808Ala mice to show that Ser2808 is the major site. Phosphorylation of RyR2 results in activation of the channel,[173] and so Ca^{2+} release from the SR into the cytosol.

PLB inhibits SERCA which prevents SERCA's function of transporting Ca^{2+} into the lumen of the SR from the cytosol, hydrolysing ATP to drive this uptake. Phosphorylation of PLB by PKA at Ser16 reduces its affinity for SERCA, reversing its inhibition on the pump,[174] and so increasing the rate of Ca^{2+} re-uptake into the SR and rate of relaxation.[175]

PLM is an accessory protein that interacts with and inhibits the plasma membrane Na^{+} / K^{+} ATPase (NKA). PKA phosphorylates PLM at Ser68 which activates the NKA reducing intracellular Na^{+}.[176] The NKA transports three Na^{+} ions out in exchange for two K^{+} ions in which is important in generating the resting membrane potential and maintaining the transmembrane Na^{+} gradient which in turn regulates activity of other

ion transporters. These include the NCX which, as already mentioned, is important in regulating the intracellular Ca^{+} concentration and so myocardial contraction. PLM is important in limiting Na^{+} overload at the expense of reduced contraction during β adrenergic stimulation, helping limit arrhythmias and progression to heart failure.[177-179]

As already mentioned, during systole intracellular Ca^{2+} directly binds to TnC in the myofilament. This causes a conformational change in the troponin complex so TnI moves away from the myosin binding site of actin enabling myosin to bind strongly to actin forming cross-bridges and generating force and causing contraction. During diastole, lowering of cytosolic Ca^{2+} means less of the ion binds to TnC, allowing the troponin complex to move back to its inactive conformation, blocking the binding of myosin to actin. PKA phosphorylates cTnI at Ser23 and Ser24. This was shown when cTnI was replaced with slow skeletal (ss) TnI. The ssTnI does not contain the N-terminal region of cTnI that contains the phosphorylatable Ser residues,[180] allowing the role of cTnI phosphorylation to be determined. Phosphorylation of cTnI by PKA results in reduced myofilament Ca^{2+} sensitivity and an increased rate of Ca^{2+} dissociation from TnC contributing to increased rate of relaxation.[181-183] PKA phosphorylation also increases cross-bridge cycling rate,[184] and sarcomere shortening velocity,[185] which is important in increasing rate of relaxation as well as positive inotropy. However, the consequence of cTnI phosphorylation by PKA is controversial as some have failed to show these effects occur.[186, 187] In addition, PKA also phosphorylates cMyBP-C at Ser282, Ser302 and Ser273,[188] which has been shown to play a role in reducing myofilament Ca^{2+} sensitivity,[189] and increasing rate of cross-bridge cycling,[190, 191] although the relative contribution of PKA-mediated cTnI and cMyBP-C phosphorylation to these outcomes is controversial.[192]

PKA also has a role in vascular smooth muscle relaxation and vasodilation, although the mechanism is not fully understood. To achieve this role, PKA phosphorylates and activates the ATP-sensitive K^{+} channels (involved in K^{+} efflux) at multiple sites,[193] and a 20 kDa heat shock-related protein HSP20 at Ser16. HSP20 is an actin binding protein so its phosphorylation may modulate its binding to contractile elements to cause

vasorelaxation.[194-196] PKA also phosphorylates and inhibits RhoA, a protein that indirectly inhibits de-phosphorylation of the myosin light chain by myosin light chain phosphatase, resulting in smooth muscle contraction. Inhibition of RhoA by PKA enables de-phosphorylation of myosin light chain and smooth muscle relaxation.[197]

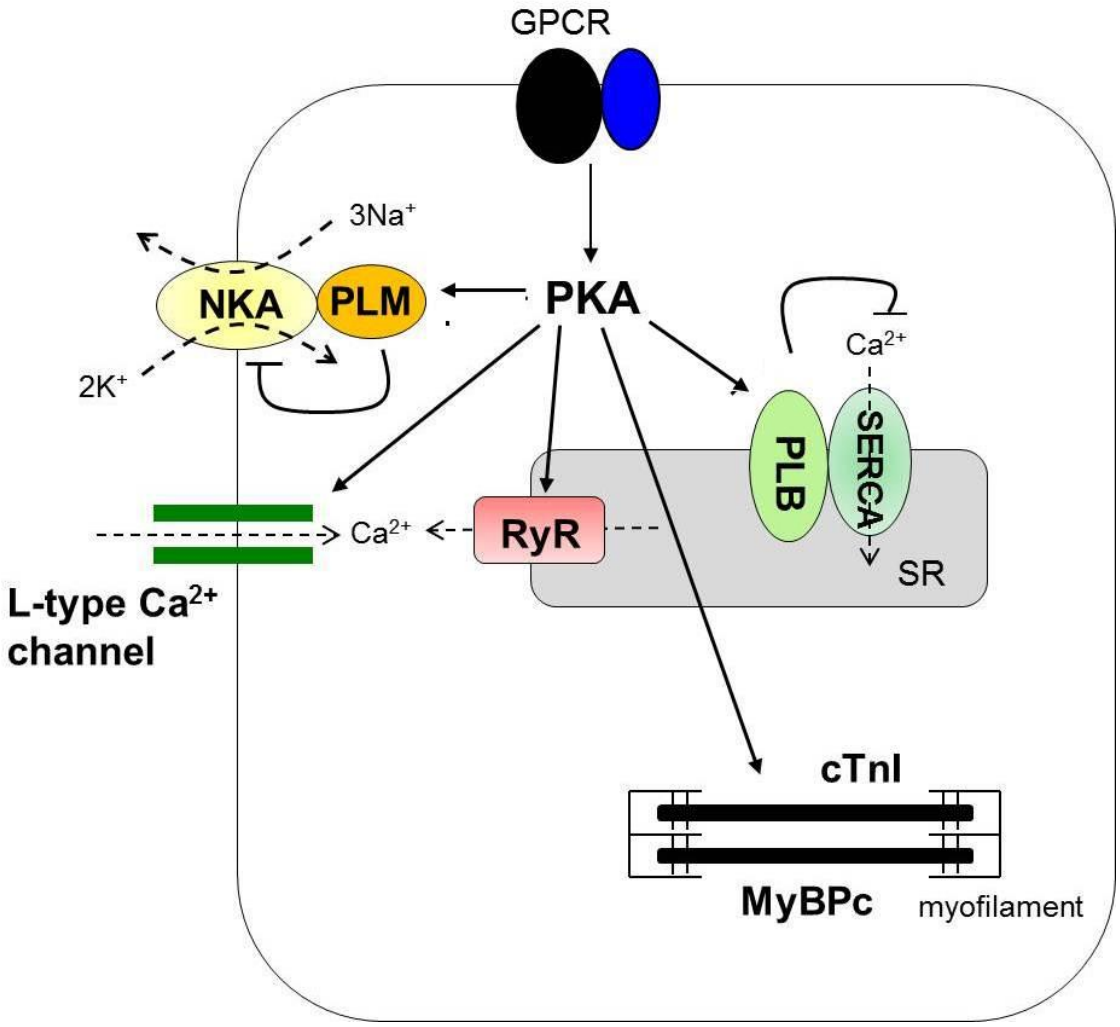

Figure 4.2 Substrates for PKA in cardiomyocytes.

PKA phosphorylates PLM which relieves its inhibition of NKA activity which is important in preventing intracellular Na^+ overload. PKA phosphorylates L-type Ca^{2+} channels and RyRs potentiating Ca^{2+} influx into the cytosol increasing intracellular Ca^{2+} which induces contraction. PKA phosphorylates PLB releasing its inhibitory effect on SERCA, which increases Ca^{2+} uptake into the SR and enhances rate of relaxation. PKA also phosphorylates the myofilament proteins cTnI and cMyBP-C.

4.1.5 Other substrates for PKA

PKA is also able to phosphorylate a number of proteins not directly associated with EC coupling. Glycogen synthase kinase (GSK) 3 is important in cell proliferation, gene expression and cell survival,[198] and has two isoforms, α and β. PKA phosphorylates and inhibits GSK3α at Ser21,[199] and GSK3β at Ser9.[199, 200] PKA also phosphorylates the transcription factor cAMP response element-binding protein (CREB) at Ser133 stimulating transcription of target genes,[201, 202] although one study has demonstrated PKA does not phosphorylate CREB at Ser133 in the mouse heart.[203] Phosphorylation of CREB increases binding of its cofactor, CREB-binding protein which is important for CREB activity.[204]

This chapter focuses on the important issue of the potential inter-relationship of RIα disulfide formation with classical cAMP-dependent PKA activation. For example, they may be mutually-exclusive events or potentially could synergise. The order in which oxidation or cAMP binding occur could also impact on the precise functional consequence of the kinase. The Cys17Ser RIα KI mouse cannot form a disulfide in RIα in response to oxidative stress (discussed in Chapter 3), and so is potentially of immense value in addressing these complexities. The specific aims of this chapter were to address the following:

1. Whether RIα disulfide sensitises PKA to cAMP, which I hypothesise may be the case because others have shown that substrate sensitises Type I but not Type II PKA to cAMP,[164, 165] and Type I can form disulfide but Type II cannot. As considered in detail in Chapter 5, disulfide formation may increase the affinity of RIα for A-kinase anchoring proteins (AKAPs), targeting PKA close to its substrates where the process of substrate-induced activation may then occur (Figure 4.3). Therefore, disulfide may potentiate PKA activity caused by a given concentration of cAMP.

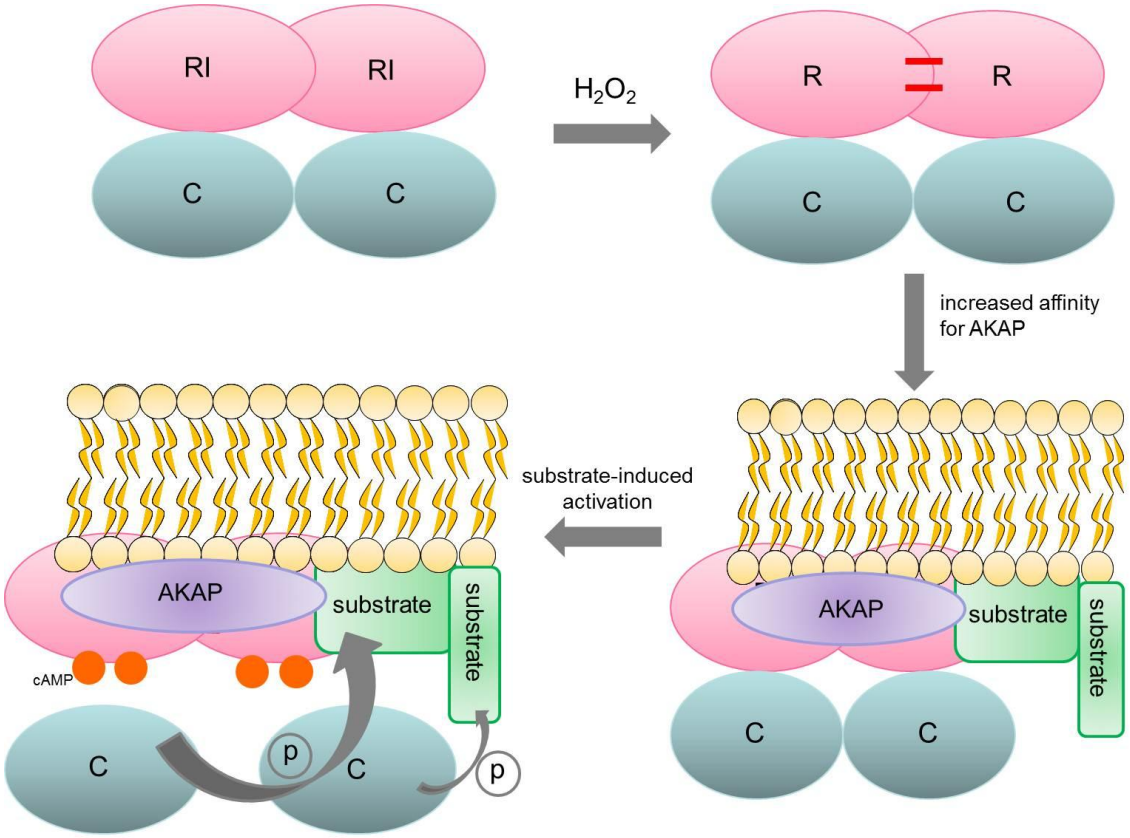

Figure 4.3 Schematic of substrate-induced PKA activation.

RIα disulfide may increase affinity of RIα for AKAPs causing translocation of PKA from the cytosol and targeting of PKA close to its substrates where substrate can sensitise PKA to cAMP. Upon cAMP binding to regulatory subunits, catalytic subunits are released which can phosphorylate target substrates.

2. Whether cAMP modulates RIα disulfide formation which I hypothesise may be the case, as cAMP binding to RIα may cause a conformational change that could alter oxidant-induced disulfide formation. However, whether this is an increase or decrease in disulfide formation is difficult to say.

3. Whether the classical mode of PKA activation by cAMP and potential disulfide-mediated activation of PKA are integrally linked by MAO-mediated breakdown of monoamines. I propose this because catecholamines signal via adrenoceptors to elevate cAMP, but also enter cells to be metabolised by MAO to generate H_2O_2 which may induce RIα oxidation. Thus, monoamines potentially trigger dual events that converge at RIα, as shown in Figure 4.15.

4. Whether RIα disulfide dimerisation modulates cardiac function. I hypothesise this may occur as RIα disulfide is associated with PKA activation,[57] which is associated with positive inotropy, chronotropy and vasorelaxation. Thus cardiac functional responses to oxidants such as H_2O_2 may be different in wild-type (WT) and Cys17Ser RIα KI mice.

5. Whether disulfide-oxidised PKA phosphorylates the same substrates as cAMP-activated PKA, which may occur as RIα disulfide formation has previously been shown to be associated with increased phosphorylation of established cardiac PKA substrates.[57]

4.2 METHODS

4.2.1 Dose-response to isoprenaline in Langendorff-perfused WT mouse hearts

Any differences in sensitivity to cAMP between WT and KI hearts were compared by assessing their respective responses to isoprenaline. One of the classical responses to isoprenaline is an increase in heart rate. Therefore hearts weren't paced at a constant heart rate of 600 bpm which otherwise is my standard procedure when assessing the function of Langendorff-perfused mouse hearts. The rationale was that I could monitor and compare heart rate in WT and KI hearts basally and then after isoprenaline treatment. Another modification to the standard Langendorff procedure in these studies was that K-HB was superfused over the right atrium of the heart, which contains the sinoatrial node (the pacemaker tissue of the heart) that is poorly perfused by normal retrograde perfusion. The standard set-up shown in Chapter 2 was modified so that there were two separate lines emerging from each buffer reservoir rather than one. Each line passed through a peristaltic pump to control coronary flow, with glass heating coils in place to maintain the K-HB at 37 ºC (Figure 4.4A and B). One line from each reservoir supplied K-HB to the heart via a cannula (made from a 20-gauge blunted needle) placed in the aorta (as described in Chapter 2) and the other line from each reservoir superfused the atrium via another cannula placed over the right atrium (Figure 4.4C). Supply to the heart could be switched from one reservoir to another by opening and closing-off lines using clamps.

A pilot study was carried out in WT hearts only to first determine whether a dose-response to isoprenaline could indeed be achieved in un-paced hearts. WT hearts were Langendorff-perfused for 40 min as described in Chapter 2 but were un-paced and the right atrium was superfused, as described above. First, stability of the Langendorff-perfused and atrial-superfused preparation was determined in WT hearts, so that inclusion criteria could be set before subsequent experiments also assessing KI cardiac function.

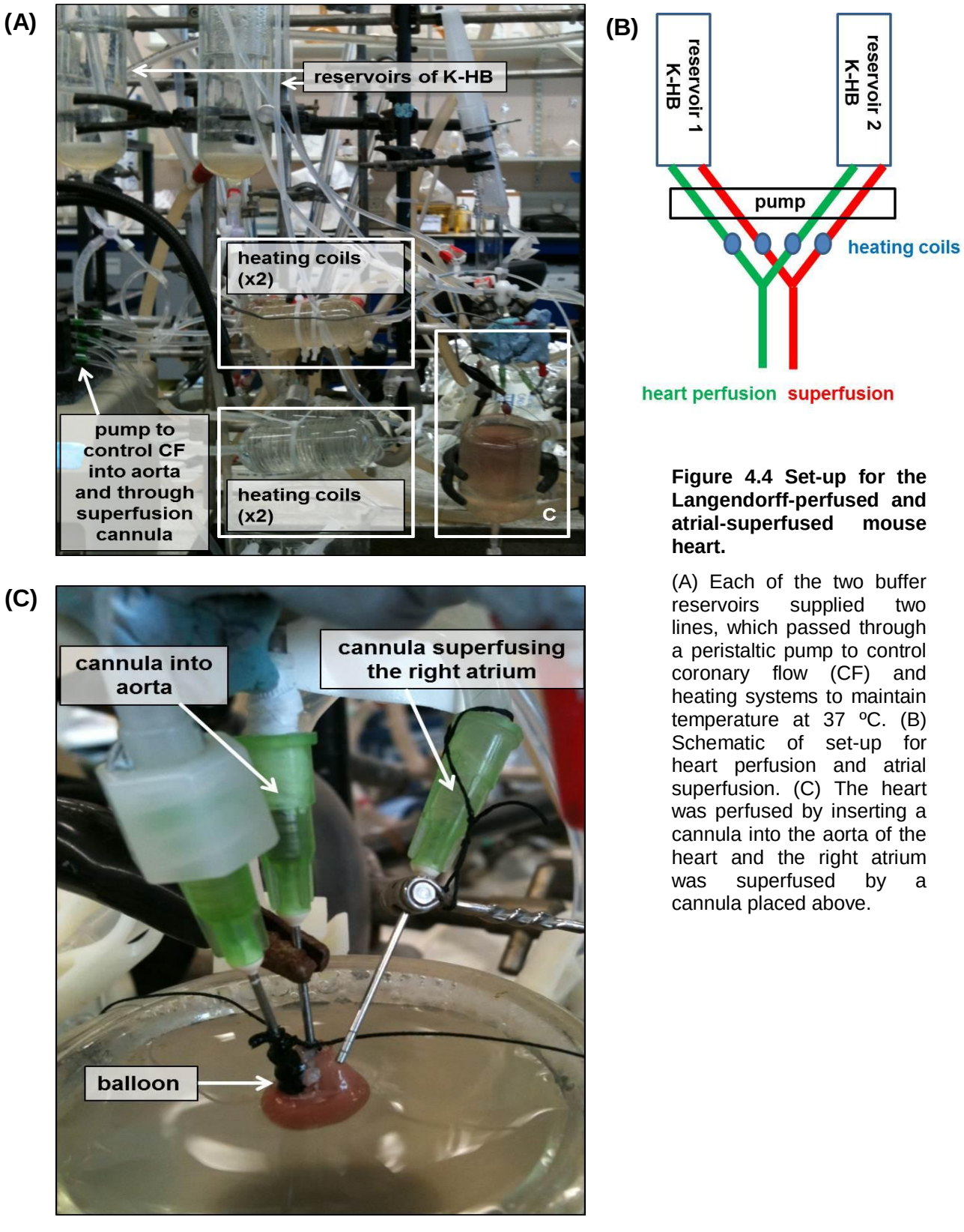

Figure 4.4 Set-up for the Langendorff-perfused and atrial-superfused mouse heart.

(A) Each of the two buffer reservoirs supplied two lines, which passed through a peristaltic pump to control coronary flow (CF) and heating systems to maintain temperature at 37 ºC. (B) Schematic of set-up for heart perfusion and atrial superfusion. (C) The heart was perfused by inserting a cannula into the aorta of the heart and the right atrium was superfused by a cannula placed above.

One buffer reservoir contained K-HB and the other contained isoprenaline in K-HB (prepared immediately before use). Langendorff-perfused and atrial-superfused WT hearts were stabilised for 40 min and if they satisfied the inclusion criteria determined (as described above) they were then simultaneously Langendorff-perfused / atrial-superfused with 0.1 nM isoprenaline for 5 min. The isoprenaline was then washed out of the heart by perfusing with K-HB for 5 min. During this 'wash-out' period, 0.1 nM isoprenaline was drained out of the buffer reservoir and replaced with a higher concentration of 1 nM isoprenaline. The heart was then Langendorff-perfused / atrial-superfused with 1 nM isoprenaline for 5 min followed by another 5 min K-HB 'wash-out'. The heart was then Langendorff-perfused / superfused with 10 nM isoprenaline for 5 min followed by another 5 min wash-out with K-HB and then 100 nM isoprenaline for 5 min.

4.2.2 Assessing the effect of RIα disulfide on activation of PKA by cAMP

The effect of RIα disulfide formation on the cellular response to isoprenaline treatment was investigated in adult rat ventricular myocytes (ARVMs).

Treatment of overnight-cultured ARVMs with diamide then isoprenaline: ARVMs were cultured overnight as described in Chapter 2 and then left untreated or pre-treated with diamide (0.1 or 0.5 mM) for 5 min followed by no further treatment or isoprenaline (10 nM or 1 μM) for 1, 5 or 10 min. The treatment medium was then removed and the cells scraped into SDS sample buffer containing 100 mM maleimide. SDS-PAGE was carried out followed by Western blotting with blots probed for PKA RIα or phospho-PLM (Ser68) as described in Table 4.1.

Treatment of freshly isolated ARVMs with H_2O_2 then isoprenaline: ARVMs were isolated and left to settle as described in Chapter 2. The ARVMs were then left untreated or treated with 10 - 1000 μM H_2O_2 for 10 min and then left without further treatment or treated with 10 nM isoprenaline for a further 5 min. Samples were prepared in SDS sample buffer containing 100 mM maleimide and SDS-PAGE and Western blotting were carried out. Blots were probed for PKA RIα to determine if isoprenaline

altered RIα disulfide formation. They were also probed for phospho-cTnI (Ser23/24), a representative PKA substrate, as described in Table 4.1.

4.2.3 Treatment of ARVMs with 8-Br-cAMP and H_2O_2 to determine whether disulfide formation is effected by cAMP

The classical mode of PKA activation involves cAMP binding to the regulatory subunits of PKA causing dissociation of the catalytic subunits from the PKA tetramer. I wanted to establish whether cAMP-dependent activation of PKA altered oxidant-induced RIα disulfide dimerisation.

ARVMs were isolated and left to settle as described in Chapter 2. They were then left untreated or treated with 100 μM 8-Br-cAMP (a PKA activator which is a cell-permeable cAMP analog with greater resistance to hydrolysis by phosphodiesterases than cAMP itself) for 15 min followed by 0 - 1000 μM H_2O_2 for 15 min. Samples were prepared in SDS sample buffer containing 100 mM maleimide after treatment. SDS-PAGE and Western blotting were carried out and blots were probed for PKA RIα (as described in Chapter 2).

4.2.4 Treatment of ARVMs with monoamines and MAO inhibitor

MAO-catalysed breakdown of monoamines is an endogenous source of H_2O_2,[163] and this may potentially cause RIα disulfide dimerisation. To determine if this is so, ARVMs were isolated and left to settle as described in Chapter 2. The ARVMs were left untreated or treated with 10 μM MAO inhibitor, Clorgyline, for 30 min at 37 ºC followed by monoamine (epinephrine, serotonin, phenylephrine or norepinephrine) at 1, 10, 100 or 500 μM for 30 min. For epinephrine, treatment with a vehicle control (0.5 mM HCl (VWR)) was also carried out. Samples were prepared in SDS sample buffer containing 100 mM maleimide after treatment. SDS-PAGE and Western blotting were carried out and the blots were probed for PKA RIα (as described in Chapter 2) to determine whether treatment with a MAO inhibitor blocked any RIα disulfide dimerisation induced by monoamine treatment.

4.2.5 Measuring phosphorylation of PKA substrates in control and H_2O_2-treated hearts

Brennan *et al.*,[57] showed that oxidation of RIα was associated with increased activity of PKA i.e. increased substrate phosphorylation in freshly isolated and overnight-cultured ARVMs only. Therefore, I determined if this also occurs in isolated WT mouse hearts and whether there was any differential response between WT and KI hearts, so determining whether RIα disulfide formation was associated with or indeed caused PKA activation in this *ex vivo* model system.

WT and KI hearts were Langendorff-perfused with K-HB for 45 min or K-HB for 40 min (stabilisation period) followed by 50 µM H_2O_2 for 5 min (see Chapter 2 for more details). Phosphorylation of PKA substrates in the hearts was analysed by incubating Western blots with specific antibodies; described in Table 4.1. To detect phosphorylation of PLB the sample was boiled at 95 ºC for 6 min to break up the PLB pentamer.

Antibody	Product code	Company	Species	Conc.	Incubation period
phospho-PLM (Ser68)	CP68	gift from M. Shattock (Kings College London)[176]	rabbit	1:10000	1 hour at room temperature
phospho-PLB (Ser16)	A010-12	Badrilla	rabbit	1:5000	3 hours at room temperature
phospho-cTnI (Ser23/24)	#4004	Cell Signalling Technology	rabbit	1:500	overnight at 4 ºC
phospho-MyBP-C (Ser282)	**-**	gift from J. Robbins[205]	rabbit	1:5000	1 hour at room temperature
phospho-MyBP-C (Ser302)	**-**	gift from J. Robbins[205]	rabbit	1:50000	1 hour at room temperature
phospho-CREB (Ser133)	#06-519	Millipore	rabbit	1:1000	overnight at 4 ºC
phospho-GSK-3β (Ser9)	#9336	Cell Signalling Technology	rabbit	1:1000	overnight at 4 ºC

Table 4.1. Phospho-PKA substrate antibodies used in studies.

This table shows the antibodies used to measure phosphorylation of specific PKA substrates in untreated or H_2O_2-treated WT and KI hearts. The table shows the company from which the antibody was purchased and its product code, the species it was raised in and the concentration at which the antibody was used (in 5 % milk in PBS with 0.1 % Tween-20).

4.3 RESULTS

4.3.1 Cardiac function in un-paced and atrial-superfused Langendorff hearts

In order to determine the effects of isoprenaline on heart rate, the preparation was not paced, as mouse hearts are conventionally. During the last 20 min of the 40 min stabilisation period in un-paced hearts, the average EDP remained relatively stable at ~8 mmHg and the LVDP stabilised at ~70 mmHg. However, the heart rate decreased from 380 bpm to 300 bpm and the coronary flow decreased from 2.4 ml / min to 1.8 ml / min (Figure 4.5). Although this lack of stability as a result of not pacing is not ideal, it enables the heart rate response to isoprenaline to be determined. Some hearts were atrial-superfused during the stabilisation period in addition to normal Langendorff coronary perfusion to determine if this attenuated the decline in coronary flow or heart rate observed in un-paced hearts. Indeed atrial superfusion helped maintain heart rate which was ~440 bpm at the end of the 20 min stabilisation period. Heart rate was significantly ($p<0.05$) higher in the Langendorff-perfused and atrial-superfused heart compared to the un-paced Langendorff-perfused preparation. LVDP stabilised at ~80 mmHg in atrial-superfused hearts which was higher than in un-paced hearts (but this was not statistically significant). Atrial superfusion did not affect EDP or coronary flow in un-paced hearts (stabilised at ~6 mmHg and ~3 ml / min respectively) (Figure 4.5). These results suggest that atrial superfusion improved function of un-paced hearts, especially in terms of increasing heart rate. This was important for future studies comparing the effect of different concentrations of isoprenaline on WT and KI heart function.

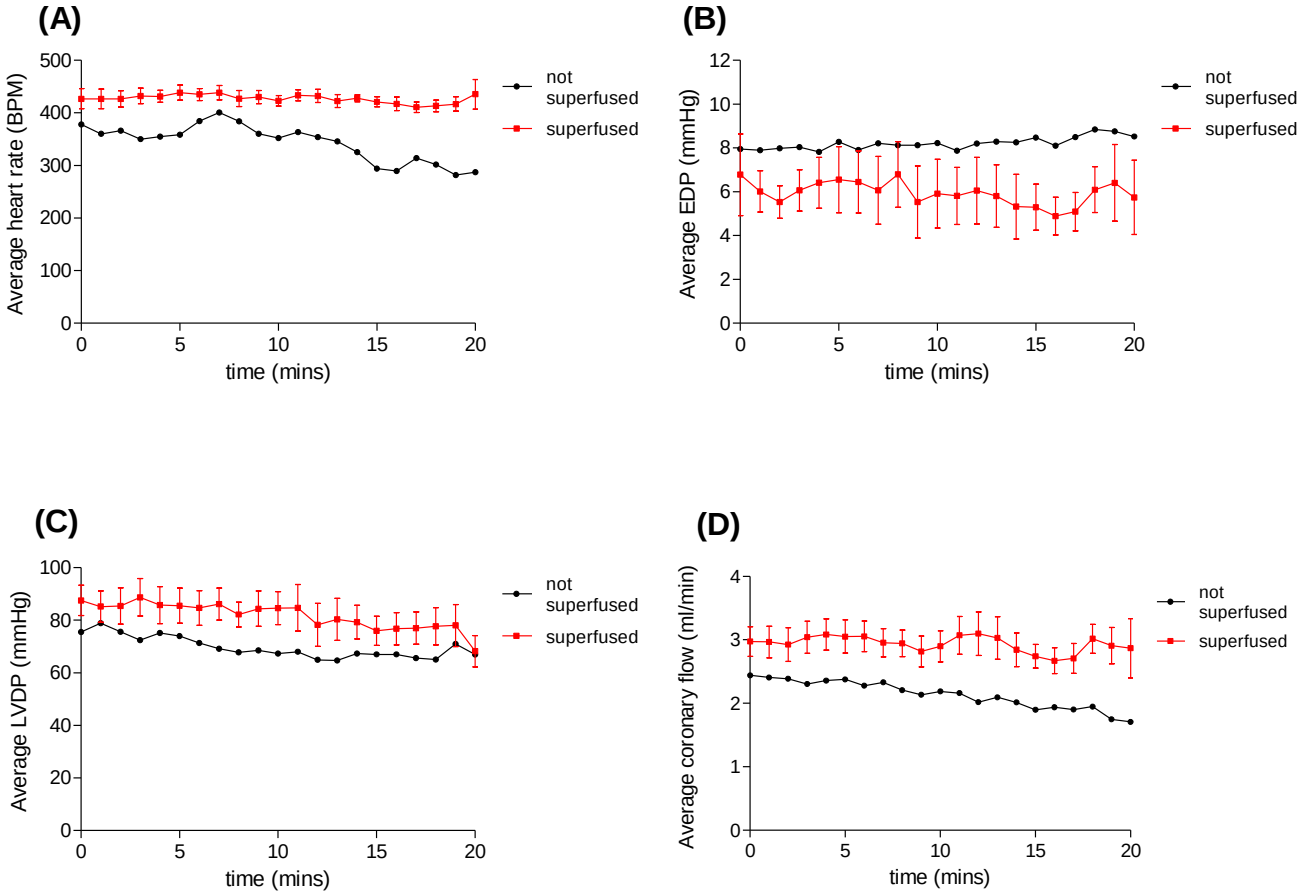

Figure 4.5 Effect of atrial superfusion on function of un-paced Langendorff-perfused WT mouse hearts.

(A) The function of the un-paced WT heart in Langendorff mode with (n=6) or without atrial-superfusion (n=2) was analysed. Graph shows average (± SEM for superfused) heart rate during the last 20 min of the stabilisation period. *p<0.05 AUC not superfused compared to superfused (B) Graph shows average EDP (C) Graph shows average LVDP (D) Graph shows average coronary flow. Atrial superfusion maintained a significantly higher heart rate over the 20 min period compared to when there was no superfusion. It also maintained a higher LVDP and coronary flow.

4.3.2 Dose-response to isoprenaline in Langendorff-perfused WT hearts with or without atrial superfusion

A pilot study was carried out to establish whether a dose-response to isoprenaline could be achieved in the Langendorff-perfused and atrial-superfused WT mouse hearts before experiments were performed using a KI heart preparation.

Figure 4.6 shows a representative trace from LabChart 7 for a WT heart concomitantly Langendorff-perfused and atrial-superfused with K-HB for 40 min followed by successive doses of 0.1, 1, 10 and 100 nM isoprenaline for 5 min with 5 min K-HB 'wash-outs' in between each concentration. Left ventricular pressure (LVP) was relatively stable in the hearts before treatment, although there were a few arrhythmias. However, when 0.1 nM isoprenaline, 1, 10 or 100 nM isoprenaline was administered the heart became highly arrhythmic with a variable heart rate, EDP and LVDP making reliable analysis and therefore quantification of function in these hearts impossible. The periods when isoprenaline was washed out during the protocol reduced the number of arrhythmias but this was accompanied by decreased LVDP which progressively lowered with each successive wash. Indeed, the LVDP was eventually lower than during the stabilisation period making the baseline for LVDP different for each isoprenaline concentration. This lowering of the LVDP together with high incidence of arrhythmias when isoprenaline was present made meaningful analysis essentially impossible.

The Ca^{2+} concentration in the K-HB was reduced from 1.4 mM to 0.7 mM to assess if this reduced the number of arrhythmias during isoprenaline treatment as Ca^{2+} plays a role in arrhythmogenesis.[206] Figure 4.7 shows a representative trace from LabChart 7 for a WT heart Langendorff-perfused and atrial-superfused with K-HB containing 0.7 mM Ca^{2+} for 40 min followed by successive doses of 0.1, 1, 10 and 100 nM isoprenaline for 5 min, with 5 min wash-out periods with K-HB in between each concentration. During the 40 min stabilisation LVDP, EDP, coronary flow and heart rate stabilised with very few arrhythmias. LVDP was lower compared to when 1.4 mM Ca^{2+} was present in the K-HB, which is perhaps expected due to the lower extracellular trigger Ca^{2+}. However, arrhythmias were still induced by isoprenaline, although less so

than with 1.4 mM Ca^{2+}. The wash-outs, again, reduced the number of arrhythmias present compared to during isoprenaline treatment. EDP, coronary flow and heart rate returned to their basal level observed during the stabilisation period, but LVDP again decreased to below baseline. The high incidence of arrhythmias and consequential unstable function, together with the decrease in LVDP with each successive wash-out, again precluded reliable analysis and quantification of these hearts. Ultimately, this meant I could not undertake studies comparing the functional response of the heart in WT and KI mice which had been a primary aim.

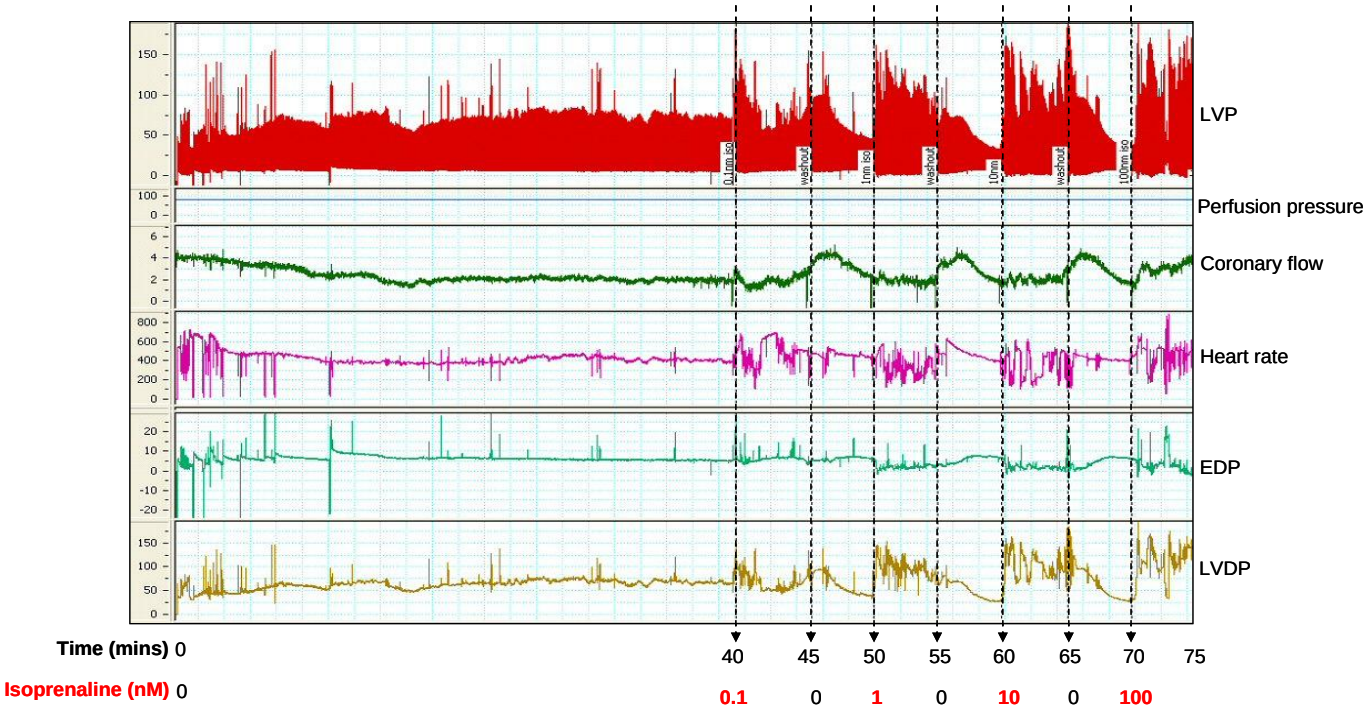

Figure 4.6. Dose-response to isoprenaline in Langendorff-perfused WT mouse heart.

Un-paced hearts were Langendorff-perfused and atrial-superfused for 40 min with K-HB (containing 1.4 mM Ca^{2+}) and then isoprenaline (0.1 - 100 nM) for 5 min with 5 min K-HB wash-outs in between each concentration of isoprenaline. Representative LabChart traces show LVP, perfusion pressure, coronary flow, heart rate, EDP and LVDP during the experiment. LVDP decreased with each successive wash making the baseline different for each isoprenaline concentration. The unstable function and decrease in LVDP meant reliable analysis was impossible.

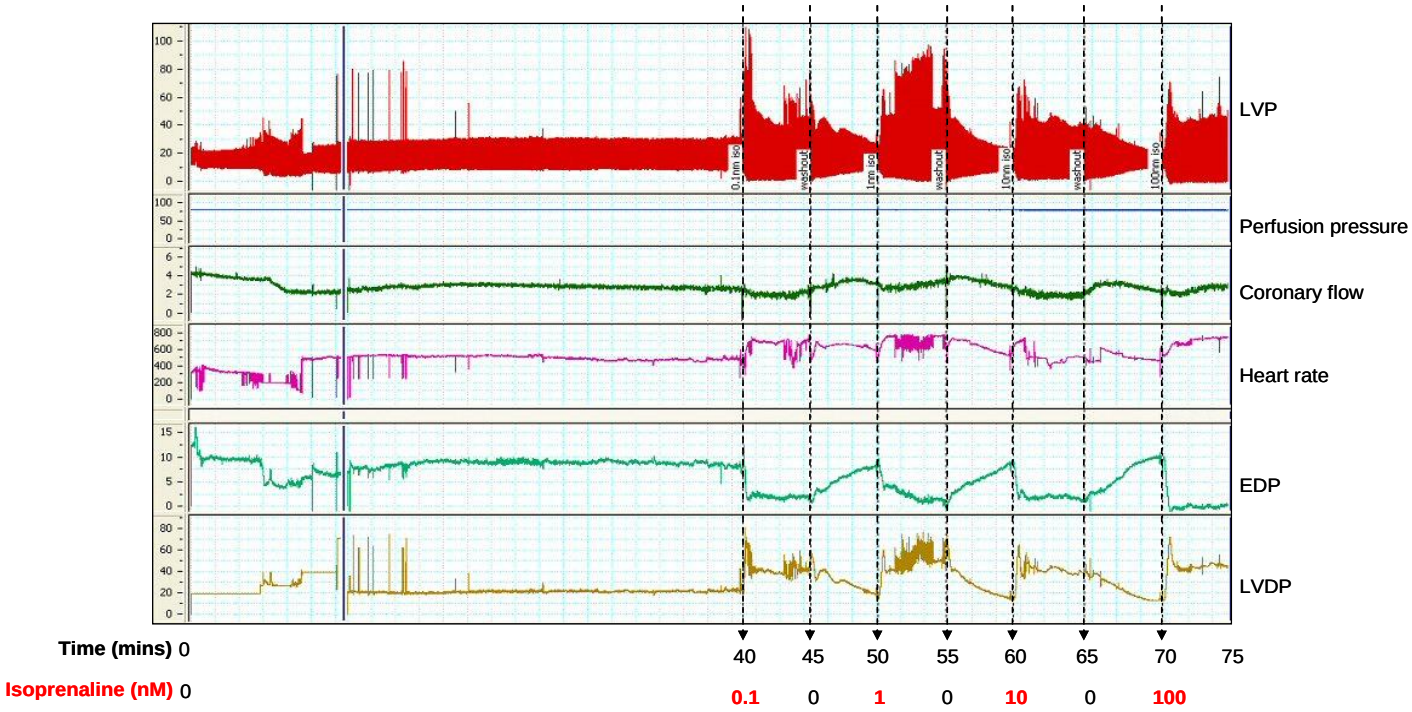

Figure 4.7. Effect of K-HB Ca^{2+} concentration on dose-response to isoprenaline.

Un-paced hearts were Langendorff-perfused and atrial-superfused for 40 min with K-HB (containing 0.7 mM Ca^{2+}) and then isoprenaline (0.1 - 100 nM) for 5 min with 5 min K-HB wash-outs in between each concentration of isoprenaline. Representative LabChart traces show LVP, perfusion pressure, coronary flow, heart rate, EDP and LVDP during the experiment. 0.7 mM Ca^{2+} did not reduce the number of arrhythmias during isoprenaline treatment and LVDP still decreased with each successive wash making the baseline different for each isoprenaline concentration. The unstable function and decrease in LVDP meant reliable analysis was, again, impossible.

4.3.3 Isoprenaline and RIα disulfide formation *ex vivo*

The effect of isoprenaline on RIα disulfide formation when perfused through the Langendorff mouse heart preparation was assessed. 100 nM isoprenaline treatment for 5 min did not significantly alter the percentage RIα disulfide in WT hearts compared to controls, and as expected there was no RIα disulfide present in KI hearts (Figure 4.8).

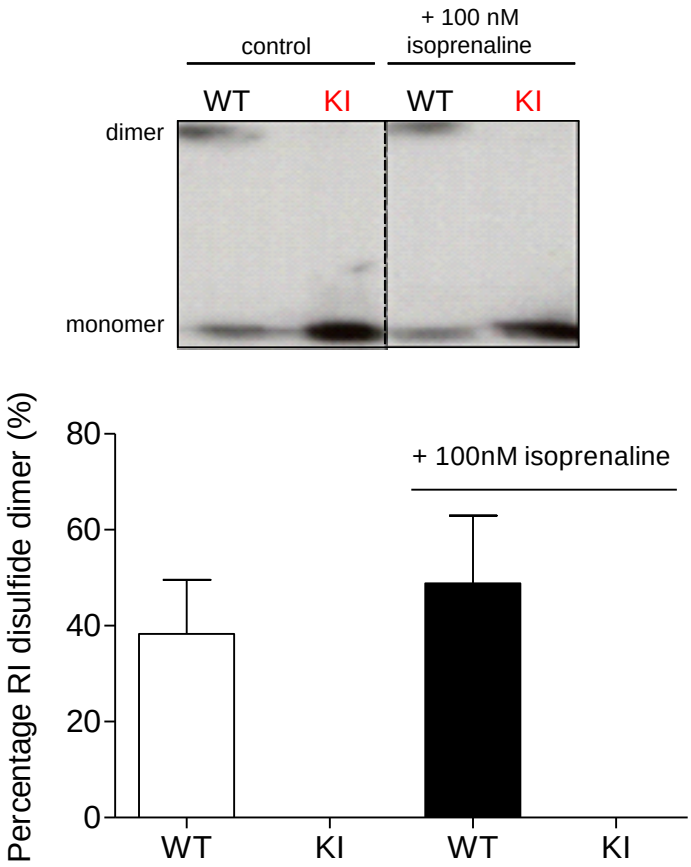

Figure 4.8 Effect of isoprenaline on RIα disulfide in Langendorff-perfused WT and KI hearts.

Hearts were perfused with K-HB for 45 min (control n=3) or K-HB for 40 min followed by 100 nM isoprenaline for 5 min (WT n=4, KI n=2). Western blots were probed for PKA RIα. Top, representative blot (broken line represents a cut in the film) shows RIα monomer and disulfide dimer and bottom, graphical representation of average percentage RIα disulfide ± SEM. These results demonstrate that isoprenaline did not induce RIα disulfide formation.

4.3.4 Effect of diamide on isoprenaline-induced phosphorylation of PLM in overnight-cultured ARVMs

Other research groups,[164, 165] have demonstrated that substrate sensitises Type I, but not Type II, PKA to cAMP. I wanted to determine whether RIα disulfide sensitised PKA to cAMP because the disulfide can form in Type I PKA but not Type II. Disulfide may increase affinity of RIα for AKAPs, which would position it close to substrate and potentially enable substrate-induced sensitisation to cAMP. The RIα protein used in the studies,[164] would have almost certainly been in the disulfide state because of the absence of reducing buffers and the presence of oxygen in the air. The presence of the disulfide may therefore be integral to this sensitisation phenomenon (Figure 4.3). Perhaps if the studies had been carried out with reduced RIα then substrate-induced sensitisation would have been absent, as in the RII preparation. This hypothesis was initially investigated using a cell-based approach. Overnight-cultured ARVMs were treated with diamide (to cause disulfide formation) and then isoprenaline (to produce cAMP and classically activate PKA). PKA RIα disulfide formation was assessed as well as PLM phosphorylation, as a measure of PKA activity. If the disulfide does sensitise PKA to cAMP then I would expect more PLM phosphorylation for a given cAMP concentration when diamide pre-treatment was used compared to control without it. Figure 4.9 shows that the level of basal RIα monomer varies between different cell isolations (A, B or C). The level of disulfide dimer in untreated control cells is higher than expected based on previous work from this lab,[57] and the total signal for RIα does not add up between treatment groups. 0.5 mM diamide induced the anticipated disulfide dimerisation (Figure 4.9A) and caused PLM phosphorylation to a level comparable to isoprenaline (Figure 4.9B), suggesting PKA activation. However, pre-treatment with diamide did not alter the level of isoprenaline-induced PKA activation.

As 0.5 mM diamide caused such a high level of phosphorylation, I assessed the effect of a lower concentration of diamide on isoprenaline-induced PLM phosphorylation. 0.1 mM diamide caused minimal RIα disulfide dimerisation and did not induce PLM phosphorylation whereas 10 nM isoprenaline did induce PLM phosphorylation, as expected (Figure 4.9C). Diamide had a differential effect on isoprenaline-induced PLM

phosphorylation with time where 1 min diamide appeared to reduce phosphorylation induced by isoprenaline, 5 min diamide increased the phosphorylation induced by isoprenaline and 10 min diamide reduced phosphorylation induced by isoprenaline. It should be noted that this experiment was not replicated because of the variable levels of basal RIα monomer between different cell isolations. The variation in RIα redox state and total RIα expression between different isolations (see discussion on this in Chapter 2.2) made it impossible to establish whether disulfide dimerisation effects activation of PKA by cAMP.

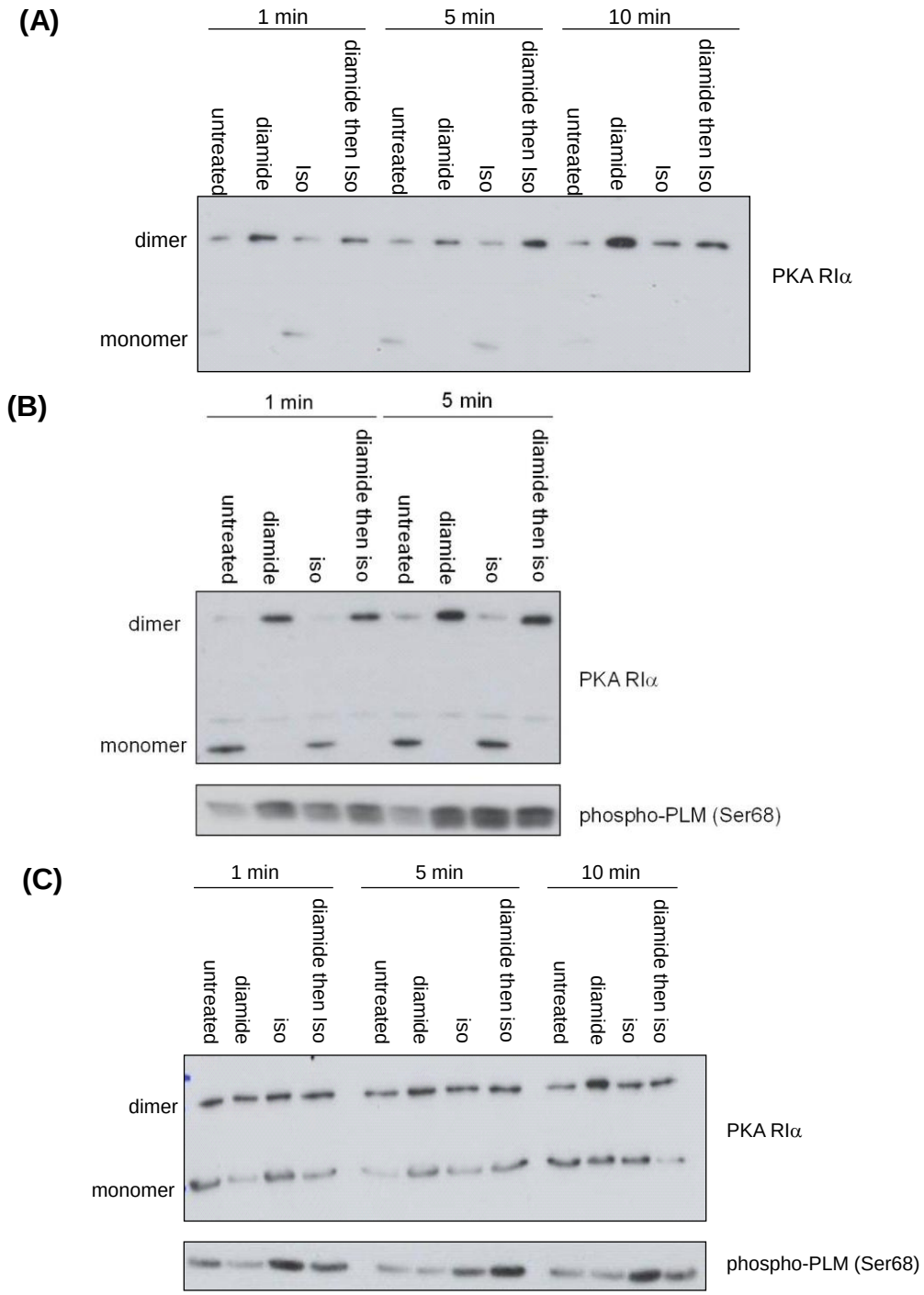

Figure 4.9 Effect of RIα disulfide on isoprenaline-induced PLM phosphorylation.

(A) Overnight-cultured ARVMs were left untreated or pre-treated with 0.5 mM diamide for 5 min. No further treatment or 1 μM isoprenaline was then added (1, 5 or 10 min). Western blots were probed for PKA RIα (B) Same as (A) but in a different ARVM isolation. Western blots were also probed for phospho-PLM (Ser68) (C) Overnight-cultured ARVMs were pre-treated with 0 - 0.1 mM diamide (5 min) and then treated with 10 nM isoprenaline (1, 5 or 10 min). Western blots were probed for PKA RIα or phospho-PLM (Ser68). RIα abundance varied between treatments and presence of RIα monomer varied between isolations making analysis difficult.

4.3.5 Effect of RIα disulfide on isoprenaline-induced phosphorylation of cTnI in freshly isolated ARVMs

As discussed in section 2.2 and section 4.3.4, there are problems with using overnight-cultured ARVMs. To avoid these issues, the effect of RIα disulfide on response to isoprenaline was investigated in freshly isolated ARVMs. Treatment with increasing concentrations of H_2O_2 (10 - 100 µM) caused a trend towards an increase in phosphorylation of cTnI, although 1000 µM caused no increase in phosphorylation compared to isoprenaline alone (Figure 4.10A). Treatment of ARVMs with 10 nM isoprenaline alone caused an increase in cTnI phosphorylation compared to control untreated. This was the positive control to confirm that the ARVMs were responding to this concentration of isoprenaline. Pre-treatment with 10 - 100 µM H_2O_2 potentiated isoprenaline-induced cTnI phosphorylation and caused a trend towards an increase in phosphorylation with increasing concentration of H_2O_2. However, pre-treatment with 1000 µM caused a reduction in isoprenaline-induced phosphorylation of cTnI. Figure 4.10B confirms that treatment of freshly isolated ARVMs with increasing concentrations of H_2O_2 (10 - 1000 µM) caused a trend towards an increase in percentage RIα disulfide dimer, and treatment with isoprenaline after H_2O_2 did not alter this trend. Total RIα protein was similar between treatments unlike in overnight-cultured ARVMs.

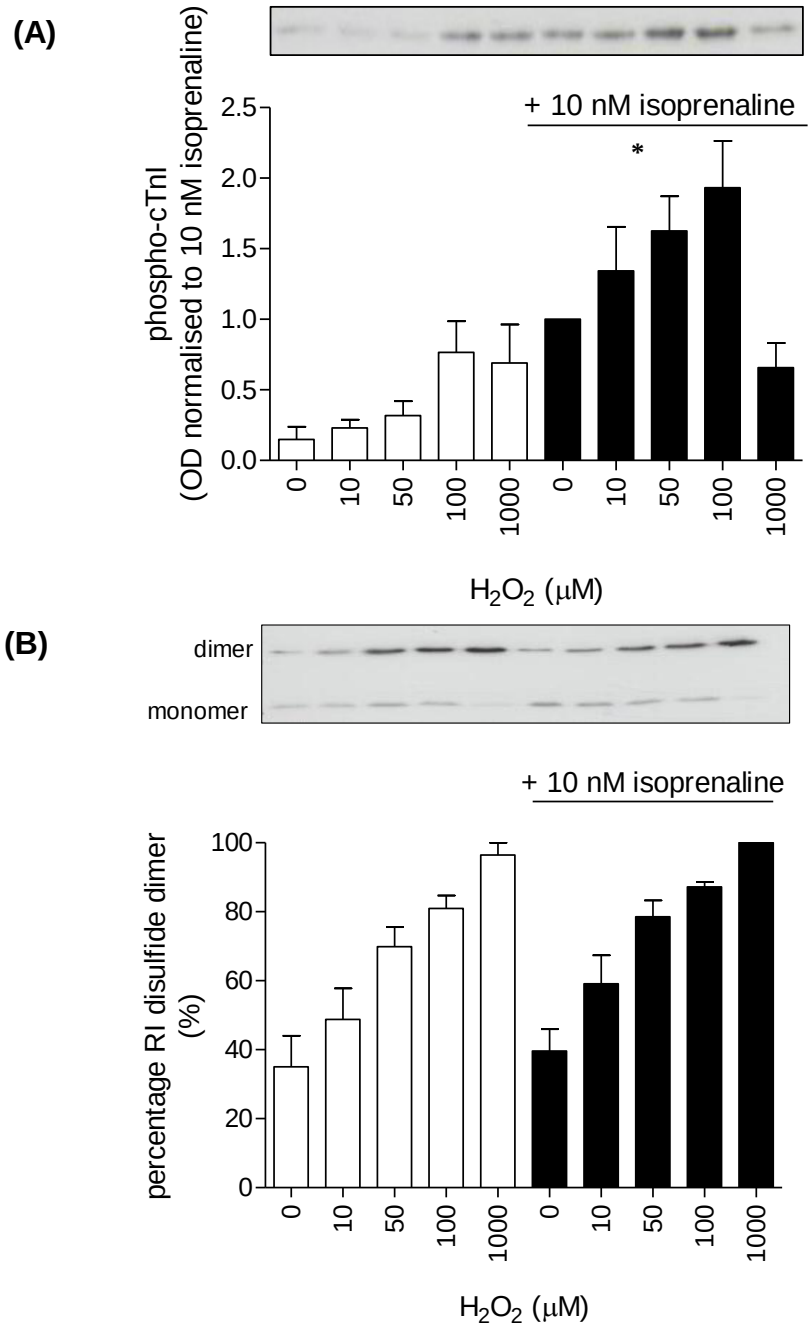

Figure 4.10 Effect of RIα disulfide on response to isoprenaline in freshly isolated ARVMs.

(A) ARVMs were left untreated or treated with 10 - 1000 μM H_2O_2 (10 min) and then left untreated or treated with 10 nM isoprenaline (5 min). Representative Western blot probed for phospho-cTnI (Ser23/24) and quantification of phospho-cTnI normalised to phosphorylation with 10 nM isoprenaline alone (n=4) ± SEM are shown. H_2O_2 caused a trend towards an increase in cTnI phosphorylation and concentrations up to 100 μM potentiated isoprenaline-induced phosphorylation of cTnI. *p<0.05 curve for cTnI phosphorylation with isoprenaline compared to without (2-way ANOVA with repeated measures) (B) Western blots were probed for PKA RIα. Quantification of percentage RIα disulfide for n=4 ± SEM was performed. Isoprenaline did not cause disulfide dimerisation.

4.3.6 Effect of cAMP on RIα disulfide formation

The classical mode of Type I PKA activation involves cAMP binding to the RIα subunits. I wanted to determine whether this event sensitised RIα to disulfide dimerisation. Treatment of freshly isolated ARVMs with increasing concentrations of H_2O_2 up to 1000 µM increased the percentage RIα disulfide dimer, with ~35 % disulfide dimer basally and ~95 % disulfide dimer in 1000 µM H_2O_2-treated ARVMs (Figure 4.11). Pre-treatment of ARVMs with 100 µM Br-cAMP (to activate PKA) caused a trend towards potentiation of the H_2O_2-induced RIα disulfide formation when the vehicle control had no effect. The potentiation was statistically significant ($p<0.05$) at 100 µM H_2O_2 when there was an increase of ~15 %.

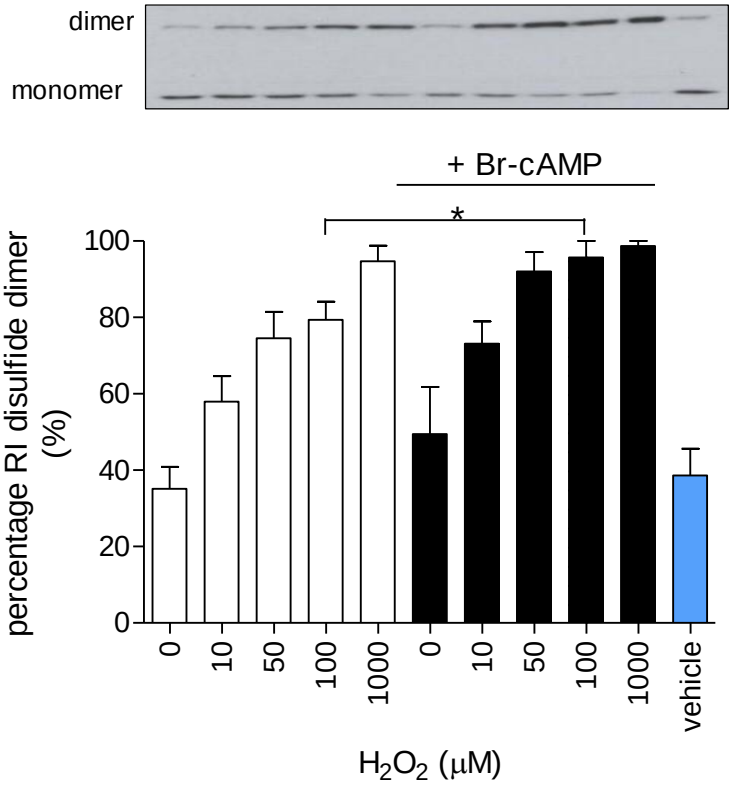

Figure 4.11 Effect of cAMP on RIα disulfide dimerisation.

Freshly isolated ARVMs were left untreated or pre-treated with Br-cAMP (100 µM, 15 min) followed by 0 - 1000 µM H_2O_2 (10 min). Western blots were probed for PKA RIα. Representative blot shows RIα disulfide dimer and reduced monomer. Graph shows quantification (n=6 ± SEM) of percentage RIα disulfide. Increasing concentrations of H_2O_2 caused an increase in RIα disulfide dimerisation and pre-activation of PKA by cAMP potentiated this (significant at 100 µM H_2O_2 (* $p<0.05$)).

4.3.7 MAO as a source of H_2O_2 for RIα disulfide formation

Members of my research laboratory found that monoamines caused PKG Iα disulfide dimerisation and that a MAO inhibitor blocked this effect (*unpublished*). These observations were consistent with breakdown of monoamines by MAO to yield H_2O_2 which then oxidises PKG Iα to disulfide dimer.[60] I therefore hypothesised that monoamines may have the same effect on PKA RIα disulfide dimerisation.

Treatment of freshly isolated ARVMs with increasing concentration of epinephrine up to 10 μM (Figure 4.12A) caused a trend towards a small decrease in the percentage of RIα disulfide (~50 % to ~40 %). However, treatment of ARVMs with epinephrine at higher concentrations (100 μM and 500 μM) increased RIα disulfide over control untreated ARVMs, albeit this was not statistically significant. The vehicle for epinephrine had no effect on basal RIα oxidation. Another monoamine phenylephrine, did not cause RIα disulfide formation in ARVMs at concentrations below 500 μM, with percentage RIα disulfide remaining at ~40 %, although 500 μM phenylephrine caused a small increase (~15 %, not statistically significant) which was inhibited by pre-treatment with the MAO inhibitor Clorgyline (Figure 4.12B). Treatment of ARVMs with increasing concentrations of norepinephrine (1 - 500 μM) caused a clear trend towards an increase in RIα disulfide formation compared to control untreated (~25 % increase at 500 μM), and this increase was blocked by pre-treatment with the MAO inhibitor (Figure 4.12C). This was also observed with serotonin treatment where 100 μM or 500 μM serotonin increased RIα disulfide formation by ~10 % or ~20 % respectively and this was blocked by Clorgyline (Figure 4.12D). There was a significant difference ($P<0.0001$) between the curve for RIα disulfide formation with increasing concentration of serotonin and the curve for disulfide formation with increasing concentration of serotonin and Clorgyline pre-treatment. In all these experiments, treatment with diamide caused ~100 % RIα disulfide dimer formation so ARVMs were responding as expected.

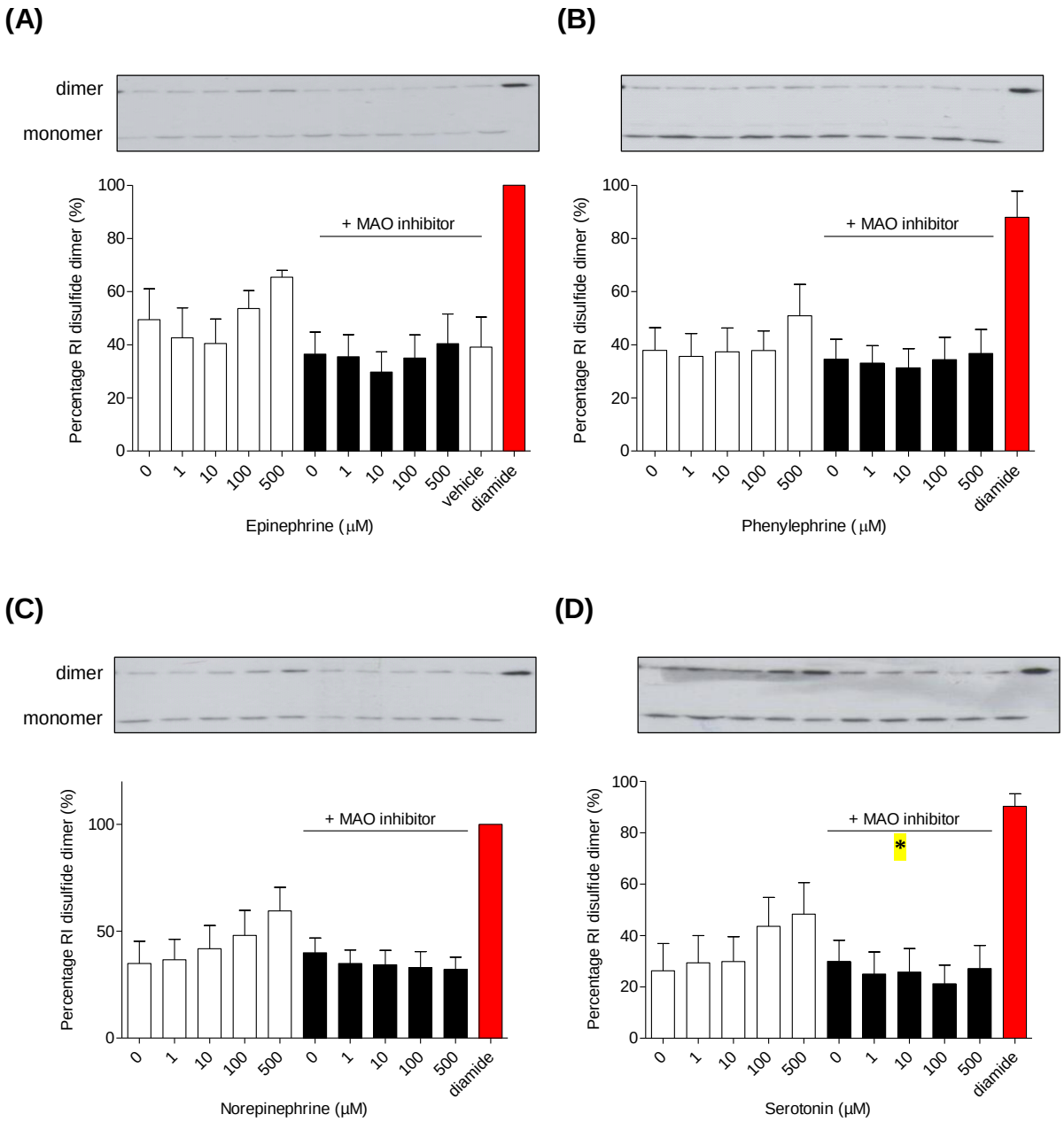

Figure 4.12 Monoamines and PKA RIα disulfide dimer formation.

(A) Freshly isolated ARVMs were left untreated or pre-treated with MAO inhibitor (10 μM, 30 min) followed by 0 - 500 μM epinephrine for 30 min. Western blots were probed for PKA RIα. Representative blot shows RIα monomer and disulfide dimer and graphs present average percentage RIα disulfide dimer for n=5 experiments (± SEM). (B) ARVMs were treated with the monoamine phenylephrine. (C) ARVMs were treated with norepinephrine. (D) ARVMs were treated with serotonin. There was a trend towards an increase in RIα disulfide dimer with increasing concentrations of epinephrine or norepinephrine or serotonin but not phenylephrine and inhibition of MAO blocked the increase in disulfide formation. This effect was statistically significant for serotonin (*P<0.05 curve for RIα disulfide with MAO inhibitor compared to without, 2-way ANOVA with repeated measures).

4.3.8 Effect of RIα disulfide on Langendorff function

Western blotting studies confirmed KI Cys17Ser RIα does not form disulfide basally or in response to oxidative stress (Chapter 4). Therefore, by comparing the responses of WT and KI littermates basally and after oxidative stress (which induces RIα disulfide in WTs), I may be able to determine the role of this single oxidative modification in various cardiovascular 'functional' parameters. Consequently, the isolated heart model was used to assess how H_2O_2 alters coronary flow, LVDP and EDP in WT and KI hearts. A concentration of H_2O_2 was required that had an effect, but was not un-necessarily high. 50 μM H_2O_2 was chosen as the concentration to perfuse WT and KI hearts with to determine the role of RIα disulfide on cardiac function. 50 μM was chosen because results from a pilot study in C57BL/6 mice showed that this concentration altered coronary flow and LVDP similarly to 100 μM H_2O_2 and also increased EDP, albeit to a lesser degree than 100 μM H_2O_2 (data not shown).

Figure 4.13 shows coronary flow, EDP and LVDP in male WT and KI hearts 5 min before and 5 min after 50 μM H_2O_2 Langendorff-perfusion. Basal coronary flow (Figure 4.13A) was similar in WT and KI hearts (~3.9 ml / min). KI hearts showed a statistically significant ($p<0.05$) increase of ~0.4 ml / min in coronary flow with H_2O_2 and in WT hearts, there was an initial trend towards an increase in coronary flow (~0.2 ml / min) when H_2O_2 was perfused, but this decreased again.

Basal EDP (~7 mmHg, Figure 4.13B) was similar in WT and KI hearts, with H_2O_2 causing a statistically significant ($p<0.05$) increase in both genotypes. However, the increase was more pronounced in WT hearts (~8 mmHg) compared to KI (~4 mmHg). H_2O_2 caused a statistically significant ($p<0.05$) decrease in LVDP (Figure 4.13C) in both WT (~77 mmHg to ~56 mmHg) and KI (~64 mmHg to ~59 mmHg) hearts but the effect was less pronounced in the latter. However, this may be because KI hearts also had a significantly ($p<0.05$) lower basal LVDP compared to WT hearts.

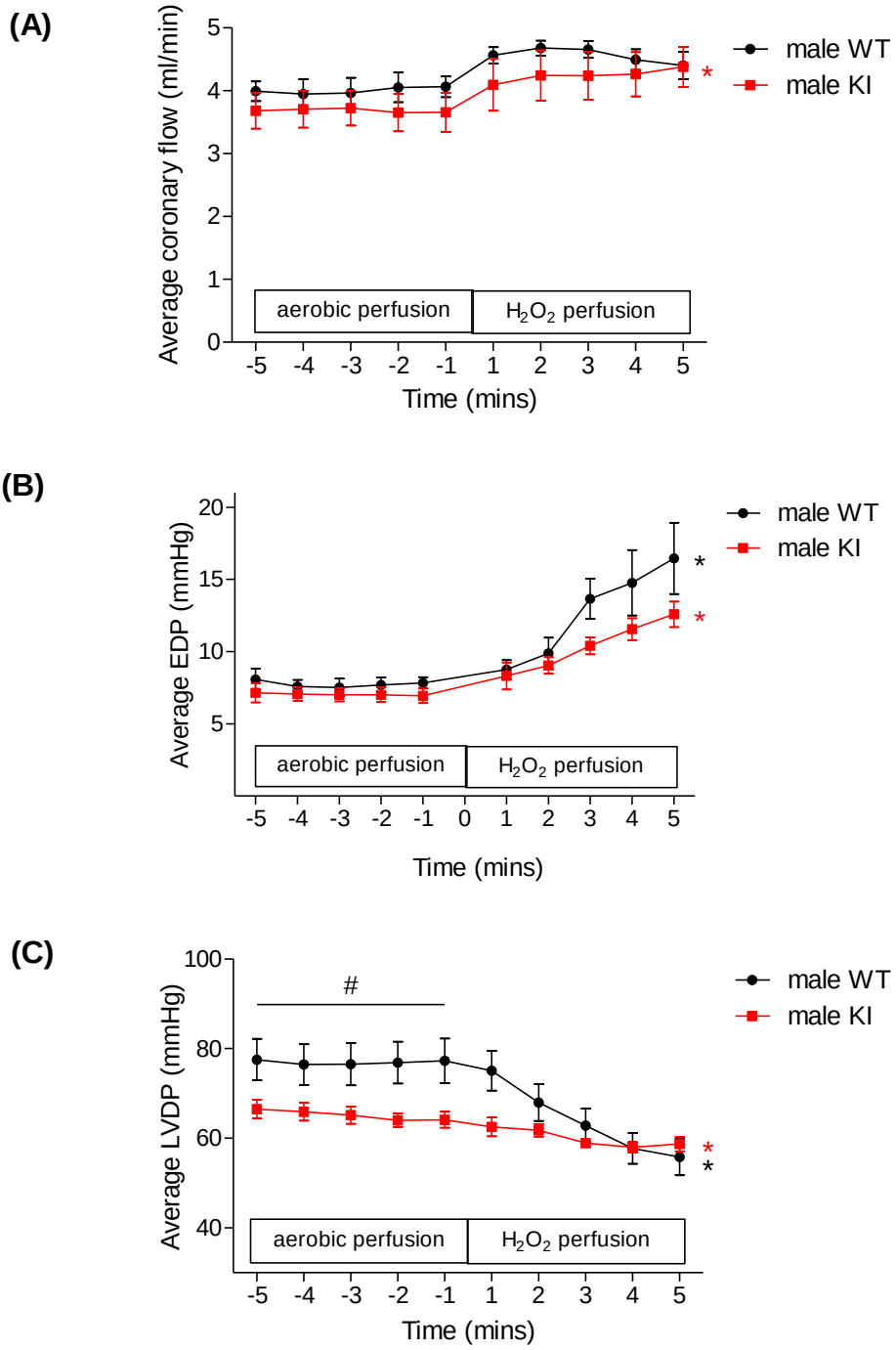

Figure 4.13 Effect of H_2O_2 on function of Langendorff-perfused WT and KI hearts.

(A) WT and KI hearts were Langendorff-perfused with K-HB for 40 min followed by 5 min 50 µM H_2O_2. Graph shows average coronary flow (WT n=6, KI n=7 ± SEM) during the last 5 min of the stabilisation period and then during 5 min perfusion with H_2O_2. * $p<0.05$ area under curve (AUC) for parameter during 5 min H_2O_2 perfusion compared to parameter during 5 min aerobic perfusion. (B) Graph shows average EDP. (C) Graph shows average LVDP. # $p<0.05$ for AUC of LVDP in KI compared to WT. H_2O_2 caused a significant increase in coronary flow and significant decrease in EDP and LVDP in both WT and KI hearts.

4.3.9 RIα disulfide and phosphorylation of PKA substrates in WT and KI hearts

Previous work in our laboratory showed that phosphorylation of PKA substrates increased following H_2O_2 treatment in both freshly isolated ARVMs as well as overnight-cultured ARVMs. The H_2O_2-induced phosphorylation was associated with RIα disulfide formation,[57] but this was not investigated in isolated Langendorff-perfused hearts exposed to H_2O_2.

Phosphorylation of selected PKA substrates (at their established PKA phosphorylation sites) was compared between untreated WT and KI hearts (which cannot form RIα disulfide) to see if RIα disulfide affected basal phosphorylation levels. Some basal differences in PKA activity may have been anticipated as WT hearts contain some basal disulfide dimerised RIα (Figure 4.8). However, Figure 4.14 shows that there were no significant differences in the phosphorylation of any of the PKA substrates (phospho-PLM (Ser68), phospho-PLB (Ser16), phospho-cTnI (Ser23/24), phospho-MyBP-C (Ser302/Ser282), phospho-CREB (Ser133) or phospho-GSK3β (Ser9)) analysed between WT and KI hearts.

In WT hearts phosphorylation of PLB at Ser16 was significantly decreased by 50 μM H_2O_2. There was also a trend for a decreased phosphorylation of cTnI at Ser23/24 and cMyBP-C at Ser282 or Ser302 with H_2O_2 in both WT and KI hearts. No other substrates studied altered their phosphorylation status in WT or KI hearts exposed to H_2O_2.

Both WT and KI hearts responded to 100 nM isoprenaline, as demonstrated by increased phosphorylation of PLM at Ser68, PLB at Ser16, cMyBP-C at Ser282 and Ser302, GSK3β at Ser9 and cTnI at Ser23/24 compared to untreated controls. However unexpectedly, isoprenaline did not cause phosphorylation of CREB at Ser133 in WT or KI hearts.

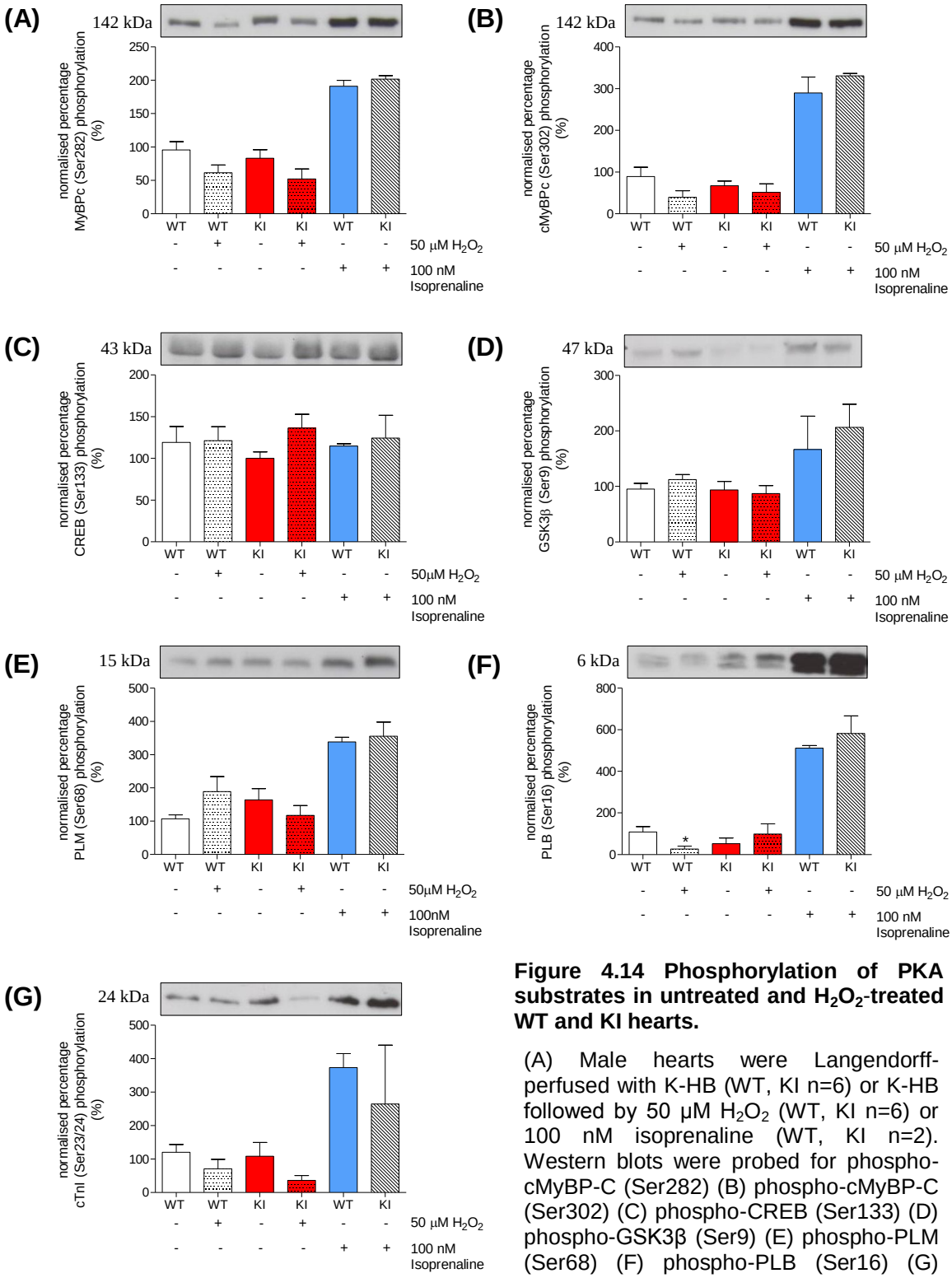

Figure 4.14 Phosphorylation of PKA substrates in untreated and H_2O_2-treated WT and KI hearts.

(A) Male hearts were Langendorff-perfused with K-HB (WT, KI n=6) or K-HB followed by 50 μM H_2O_2 (WT, KI n=6) or 100 nM isoprenaline (WT, KI n=2). Western blots were probed for phospho-cMyBP-C (Ser282) (B) phospho-cMyBP-C (Ser302) (C) phospho-CREB (Ser133) (D) phospho-GSK3β (Ser9) (E) phospho-PLM (Ser68) (F) phospho-PLB (Ser16) (G) phospho-cTnI (Ser23/24). Graphs show average percentage phosphorylation of the substrate normalised to the first control of each set of samples run on the same gel ± SEM. * $p<0.05$ compared to untreated WT. RIα disulfide formation was associated with a significant reduction in PLB phosphorylation at Ser16.

4.4 Discussion

This chapter focused on whether the classical mode of PKA activation by cAMP is effected by, or indeed affects oxidant-induced RIα disulfide formation. The cAMP binding sites and the Cys residues where disulfides form are relatively close to each other in RIα. Certainly cAMP binding causes substantial structural changes (as might a disulfide) and so hypothesising that these events synergise or are mutually exclusive is rational. This is an important issue and trying to better understand the interplay between cAMP binding and RIα disulfide formation may provide insight into the redox regulation of PKA.

Isoprenaline was studied as a positive control for PKA activation as it binds β1 adrenoceptors causing production of cAMP which activates PKA. Isoprenaline did not cause RIα disulfide formation when perfused through WT hearts. It also failed to induce disulfide dimerisation in freshly isolated ARVMs, whereas other monoamines tested did. Epinephrine, serotonin and norepinephrine all induced RIα disulfide formation and this is likely explained by their metabolic decomposition by MAO, during which H_2O_2 is generated.[162, 163] This scenario is supported by the observation that the MAO inhibitor Clorgyline blocked monoamine-induced RIα disulfide formation, consistent with such treatment blocking H_2O_2 production.

Western blotting showed that phenylephrine did not induce RIα disulfide until high concentrations were applied despite being a substrate for MAO.[207] Phenylephrine could be coupling RIα oxidation to disulfide even at low concentrations but not accumulating due to rapid redox recycling by the thioredoxin (Trx) system. Studies in Chapter 6 demonstrate that inhibition of TrxR by auranofin or cisplatin caused accumulation of RIα disulfide showing that even basally that there must be an oxidant stress that couples to RIα oxidation. However, redox cycling prevents us observing this. With higher concentrations of phenylephrine, the disulfide may accumulate because of enhanced H_2O_2 production which overwhelms the cardiac Trx reducing system and so oxidation of RIα is ‘unveiled’.

500 μM was the highest concentration of monoamine that ARVMs were exposed to, which is far beyond the physiological low nanomolar level. It is possible that I would observe RIα disulfide accumulation at lower concentrations of monoamine, if the Trx system was inhibited to prevent reduction of the disulfide (discussed in Chapter 6). Isoprenaline is not a substrate for MAO and is instead metabolised by catechol-O-methyl transferase which involves O-methylation (addition of CH_3 to O) of isoprenaline.[208, 209] Therefore, H_2O_2 is not produced during its metabolism which explains why it did not cause RIα disulfide dimerisation.

I hypothesised that RIα disulfide may sensitise PKA to cAMP as others,[164, 165] showed that Type I, but not Type II, PKA is sensitised to cAMP by substrate. One of the differences between Type I and Type II is that Type II cannot form regulatory subunit disulfides as it does not have the N-terminal Cys residues required for this. As described in Chapter 5 and shown in Figure 4.3, disulfide may increase RIα affinity for AKAPs, which may serve to target PKA close to its substrate which would facilitate the substrate-induced activation mechanism, which does not occur in RII. This may provide a mechanism for sensitisation of PKA to cAMP. It is difficult to replicate such a model in a test tube with just RIα and substrate because the AKAP may not be needed as the RIα and substrate are already together. In contrast, in the cell RIα would have to translocate via AKAP binding due to RIα oxidation. I had anticipated Langendorff-perfused WT and KI mice would differentially respond to given concentrations of isoprenaline (which induces cAMP production) with WT hearts having a larger increase in LVDP and coronary flow and a larger decrease in EDP for a given concentration of isoprenaline compared to KI. This was anticipated as the KI would lack the sensitisation that the disulfide would potentially provide. However, I was unable to construct a dose-response curve to isoprenaline in un-paced Langendorff-perfused WT hearts that could be analysed accurately. This was because the heart became highly arrhythmic during isoprenaline perfusion making analysis inaccurate and unreliable. These arrhythmias were likely caused by Ca^{2+}-overload induced by isoprenaline. A decrease in LDVP was also observed between concentrations of isoprenaline (during the wash-out period) which was not expected and made analysis essentially impossible. This decrease in LVDP has been observed by others in this department and may occur because the heart

is working hard when isoprenaline is administered. Therefore, the heart may become stressed with repeated isoprenaline stimulation and unable to recover during the wash-out period. A dose-response to isoprenaline in un-paced mouse hearts has been achieved by others,[210, 211] but they do not show how stable the un-paced hearts were before isoprenaline treatment. These authors also perfused hearts with isoprenaline in increments rather than having wash-out periods between final isoprenaline concentrations. This may be an alternative protocol for comparing WT and KI heart whereby a dose-response to isoprenaline is given, but due to time constraints I did not attempt such studies.

Another approach to assessing cAMP sensitivity would be to treat vascular aortic rings with different concentrations of isoprenaline. Dose-relaxation response curves (as performed by others,[212]) for WT and KI aortic rings could then be compared to assess any difference in cAMP-sensitivity between genotypes. Also, myocytes could be isolated from WT and KI hearts and treated with different concentrations of isoprenaline, comparing the phosphorylation responses of PKA substrates between genotypes. EC coupling experiments could be performed measuring contractile function and Ca^{2+} transients. These studies are being carried out in the Laboratory of Professor Maier (Goettingham, Germany). In addition, the difference in cAMP-sensitivity with RIα disulfide may be investigated using pure WT and KI Cys17Ser RIα protein in *in vitro* kinase assays.

H_2O_2 has been reported to modulate the response to isoprenaline.[213, 214] Pre-treatment of Langendorff-perfused rat hearts with 200 or 500 μM H_2O_2 for 10 min attenuated their response to 1 μM isoprenaline due to depression of adenylate cyclase activity.[213] A biphasic response to isoprenaline has been shown in rat heart membranes with increasing concentrations of H_2O_2 where low concentrations of H_2O_2 (100 and 200 μM) increased isoprenaline-induced adenylate cyclase activity and high concentrations decreased the enzymes activity.[214]

I assessed the influence of RIα disulfide on response to isoprenaline in ARVMs. This experiment could only be carried out in freshly isolated ARVMs as the total RIα protein abundance varied between treatments in overnight-cultured ARVMs, as discussed in

Chapter 2.2. Increasing the amount of RIα disulfide via treatment with H_2O_2 potentiated isoprenaline-induced phosphorylation of cTnI, with this eventually reaching a peak where-after the phosphorylation level returned to that with isoprenaline alone. There was also a trend towards an increase in cTnI phosphorylation in ARVMs treated with 10 - 100 µM H_2O_2 alone (no isoprenaline present). Although the amount of RIα disulfide increased with 1000 µM H_2O_2 the amount of phosphorylation did not increase above that at 100 µM H_2O_2. This could be due to cell death caused by the higher H_2O_2 concentration and isoprenaline together. However, oxidation of PKA catalytic subunit has been shown by others with 100 µM diamide, inhibiting PKA activity.[58] Consequently, the higher concentrations of H_2O_2 used in my experiments perhaps cause PKA catalytic subunit oxidation, perhaps acting as an off-switch to prevent chronic PKA activation resulting from RIα disulfide formation. As discussed in Chapter 1, the catalytic subunit can also be modified by Cys-targeted oxidation. Humphries *et al.* showed that, during oxidative stress, the catalytic subunit was sensitive to inhibition by intraprotein and interprotein disulfide formation.[58, 113] I have not assessed whether these modifications occur in my samples but my research laboratory has previously screened for proteins susceptible to Cys-targeted oxidation,[120-123] and the PKA catalytic subunit was not identified, although they could have missed it due to low abundance.

Schröder *et al.* suggest that application of 10 µM to 1 mM H_2O_2 is physiological and ARVMs may be treated with these concentrations of H_2O_2 for hours before there is any detrimental effect.[215] Therefore the treatment conditions used in my experiments are potentially physiologically relevant, although the physiological concentration range of H_2O_2 is a matter of debate.

Results in freshly isolated ARVMs showed a trend towards cAMP pre-treatment potentiating H_2O_2-induced RIα disulfide formation suggesting that cAMP sensitises RIα to disulfide formation. This may be because cAMP binding causes a conformational change that alters the Cys thiols such that they are more readily oxidised. RIα disulfide may be redox-cycled to the reduced state by the Trx system at low oxidant concentrations so less of a potentiation by isoprenaline is observed.

One of the aims of this chapter was to establish whether oxidation of RIα to disulfide induces phosphorylation of substrates and alters cardiac function similarly to when PKA is classically activated by cAMP binding to RIα. In terms of contractile function as a comparative read-out of function *ex vivo* this was not readily apparent. For example, I found that H_2O_2 decreases LVDP and increases EDP in WT and KI hearts. If RIα disulfide is directly activating PKA,[57] as occurs via mechanisms that couple to cAMP elevation, I would expect an increase in LVDP and a decrease in EDP in WT hearts. However, one confounding issue is that H_2O_2 will concomitantly activate PKG Iα. Burgoyne *et al*.,[97] showed that isoprenaline-induced activation of PKA increased LVDP in rat hearts and this then slowly decreased with time. This isoprenaline-induced increase in LVDP declined more rapidly, however, when PKG Iα was activated by S-Nitroso-N-Acetyl-D,L-Penicillamine (SNAP)-generated NO. Burgoyne also showed that H_2O_2 did not affect LVDP in rat hearts but when PKG Iα was inhibited a transient increase in LVDP occured. These results suggest that PKG Iα overrides PKA effects and this may also be occurring in my studies. PKG may override PKA by phosphorylating the L-type Ca^{2+} channels to attenuate trigger Ca^{2+} influx and so decrease contractile function.[216] In the future, perfusing hearts with a PKG inhibitor may help confirm this. Another explanation could be H_2O_2-induced inhibition of adenylate cyclase,[213] as already mentioned, and this would mean that cAMP is not generated to activate PKA despite RIα oxidation promoting sensitisation to the second messenger.

The increase in EDP induced by H_2O_2 perfusion was more significant in WT than KI hearts. KI hearts therefore appear to be partially resistant to the diastolic dysfunction induced by H_2O_2. This may, however, be explained by results from echocardiography (see Chapter 3) showing that KI left ventricle volume was larger than WT during diastole, thus at the end of diastole the pressure on a certain sized balloon inserted into the ventricle will be less in KI hearts than WT hearts.

Interestingly, basal LVDP was significantly lower in KI hearts which could be explained by a basal turnover of disulfide in WT hearts that cannot occur in KI, resulting in higher basal PKA activity in WT compared to KI. This would occur if thiol

oxidants are produced basally in control hearts, which is likely as such products are generated in many biochemical processes. As mentioned, I investigated this idea of RIα disulfide turnover by assessing reversal of the RIα disulfide by the Trx system (see Chapter 6).

H_2O_2, like cAMP, induced coronary vasorelaxation but RIα disulfide did not play a role as coronary flow increased to the same extent in both genotypes. Activation of smooth muscle PKG is a principal mechanism of vasorelaxation and blood pressure lowering. As the 1α isoform of PKG is directly activated by H_2O_2,[60] this may explain the increase in coronary flow in both genotypes. In addition, H_2O_2 can activate Ca^{2+} and voltage activated K^+ channels through the phospholipase A2 / arachidonic acid signalling pathway to cause vasorelaxation.[217, 218] The literature on responses to H_2O_2 in the isolated mouse heart is relatively sparse but several studies have been reported in the isolated rat heart with H_2O_2 (180 μM, 10 min) reversibly increasing coronary flow, decreasing LVDP and increasing EDP.[219] The dysfunction with H_2O_2 has been associated with phosphorylation and activation of the Na^+/ H^+ exchanger which increases intracellular Na^+ leading to Ca^{2+} overload.[220, 221]

As discussed above, I found some evidence of increased cTnI phosphorylation with 10-100 μM H_2O_2 in freshly isolated ARVMs after-which there was no further effect on cTnI phosphorylation by H_2O_2. Increased phosphorylation of cTnI in response to 100 μM H_2O_2 was also observed by Brennan *et al.*[57] Others have also shown increased phosphorylation of cTnI in response to H_2O_2, but provided evidence that this was PKC-dependent.[222] I wanted to determine if H_2O_2 increased substrate phosphorylation *ex vivo* in WT and KI hearts and whether there was any difference between genotypes. The only significant difference was in PLB phosphorylation; H_2O_2 decreased Ser16 phosphorylation of PLB in WT but not KI. PLB inhibits sarcoplasmic reticulum (SR) Ca^{2+}-ATPase (SERCA) and phosphorylation of PLB at Ser16 relieves this inhibition. Decreased phosphorylation of PLB after H_2O_2 would attenuate SERCA activity resulting in reduced Ca^{2+} uptake into the SR. This would result in elevated cytosolic Ca^{2+}, causing the heart to relax less during diastole. This may also explain the potential increase in EDP observed in WT compared to KI with H_2O_2 perfusion. Sulakhe *et*

al.,[223] have shown that the hydroxyl radical decreases phosphorylation of PLB in response to β adrenergic stimulation. The mechanism by which H_2O_2 reduces phosphorylation of PLB is unclear but perhaps activation of phosphatases such as protein phosphatase (PP) 2A ,[224] could be responsible. Protein tyrosine phosphatases can be reversibly inhibited by H_2O_2 unlike Ser / threonine phosphatases such as PP2A whose activity was not altered.[225]

Basal substrate phosphorylation was not significantly different between WT and KI hearts which may be expected in the absence of oxidative stress although some basal level of oxidant production is likely. However, yet unpublished studies by Professor Maier's group at the University of Goettingen, Germany found in collaboration studies that SR Ca^{2+} content was lower and diastolic Ca^{2+} concentration was higher in myocytes isolated from the KI mouse compared to WT at baseline. They suggest this may be because oxidant-dependent PKA activation is important for PLB phosphorylation. Although my results suggest there was not a statistically significant difference in PLB phosphorylation between control perfused WT and KI hearts, there was a clear indication of a trend towards lower phosphorylation in KI than WT. These findings conflict with my results in Langendorff-perfused hearts where H_2O_2 significantly decreased PLB phosphorylation at Ser16 in WT but not KI. However, this could be because H_2O_2 may be activating other signalling pathways in the Langendorff heart that over-ride PKA's actions, such as PKG (as discussed above). Brennan *et al.*,[57] showed PLB phosphorylation at Ser16 was increased by H_2O_2 in ARVMs which agrees with the unpublished work from Maier's laboratory. As discussed in Chapter 5, RIα redox state could modulate its interaction with a PLB-associated AKAP, namely AKAP7γ,[226] potentially enabling targeting of PKA to its substrate PLB for phosphorylation.

Although H_2O_2 did not cause any significant differences in phosphorylation of any PKA substrates other than PLB, the large errors in these measurements may mask any disparate responses. The large errors could be due to the Langendorff mouse heart being highly stress-sensitive which could activate kinases to elevate basal phosphorylation of substrates. There was, however, a trend for a decrease in phosphorylation of cMyBP-C and cTnI with H_2O_2 in both genotypes, which may contribute to the decline in

contractile function with H_2O_2 *ex vivo*. Therefore, it seems RIα disulfide did not affect PKA activity in the same way as cAMP in terms of PKA substrate phosphorylation in isolated hearts. KI hearts still responded to cAMP, as shown by similar amounts of substrate phosphorylation in both genotypes in response to isoprenaline. Unexpectedly, CREB was not phosphorylated at Ser133 in response to isoprenaline in either genotype consistent with Li *et al.*,[203] who found that 100 nM isoprenaline did not cause CREB to be phosphorylated at Ser133. They concluded that PKA does not phosphorylate cardiac CREB at Ser133 after isoprenaline treatment, unlike in other tissues, whereas PKCε does after phorbol 12-myristate 13-acetate stimulation.

Experiments using freshly isolated ARVMs generally provide more clear-cut understandable results than the Langendorff mouse heart model in terms of the effect of RIα disulfide on substrate phosphorylation and cAMP sensitisation.

As shown in Figure 4.15, results in ARVMs suggest MAO-catalysed metabolism of monoamines appears to be a source of H_2O_2 for RIα disulfide dimerisation. These monoamines also target β adrenoceptors linked to Gs proteins which activate adenylate cyclase and generate cAMP. Therefore, monoamines have a dual input and may synergise to activate PKA. Disulfide may increase RIα affinity for AKAPs (see Chapter 5) targeting RIα close to its substrate for substrate-induced activation. This potentially increases PKA sensitivity to a given concentration of cAMP and so RIα disulfide is associated with PKA activation. Results suggest cAMP itself sensitises RIα to disulfide dimerisation induced by H_2O_2. The observed increase in substrate phosphorylation to a peak suggests that the above cycle of events lead to increased RIα disulfide formation and PKA activity until a maximum when PKA activity returns to baseline. This suggests there is an off-switch. This off-switch may be catalytic subunit oxidation,[58] or recycling of RIα disulfide by the Trx system (see Chapter 6). It may be interesting to test what happens in cells or a heart exposed to chronic or extreme acute oxidative stress when the system is really pushed as the off-switch could fail. This could be detrimental similarly to when the β adrenergic system is overstimulated in heart failure.[227]

Ex vivo results are more difficult to explain because I expected to observe an increase in contractility and substrate phosphorylation with H_2O_2 in WT hearts associated with increased PKA activity but instead observed decreased contractility and unaltered or decreased substrate phosphorylation. This could be due to activation of other signalling pathways in the Langendorff-perfused heart that are not activated in freshly isolated ARVMs as there are other cell types present but also the heart may just be more sensitive to the effects of H_2O_2 as a whole organ rather than isolated cells.

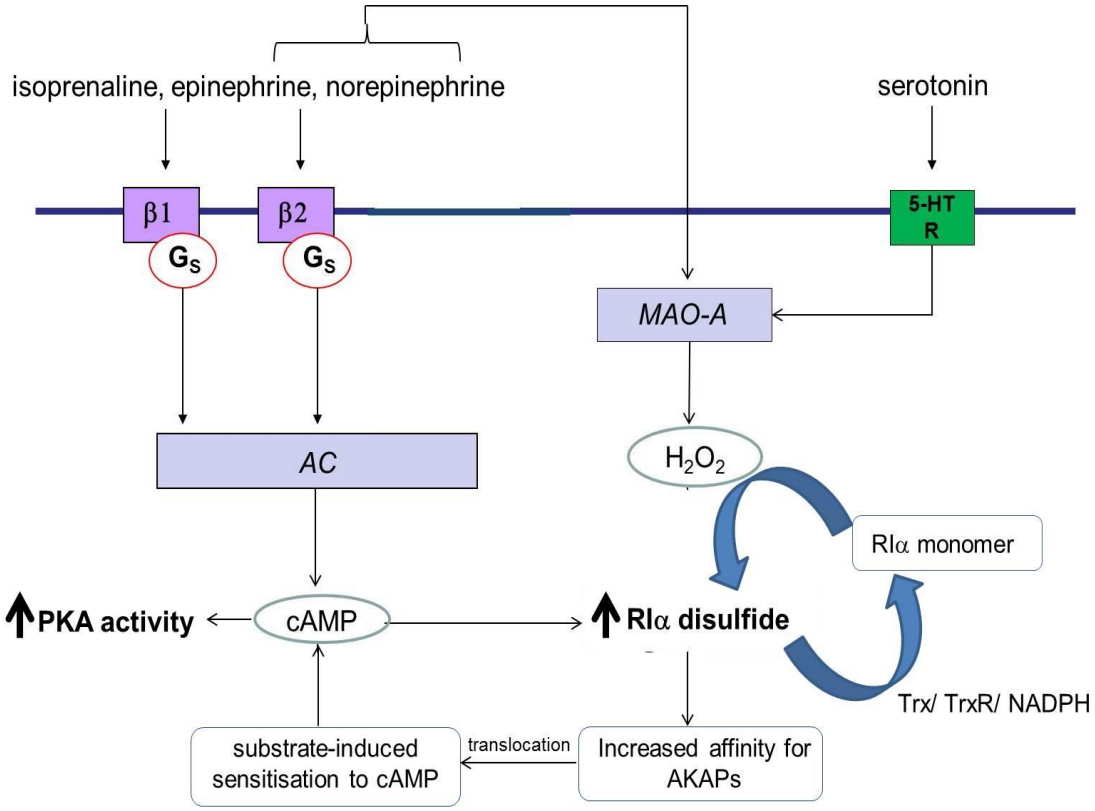

Figure 4.15 Summary of results in freshly isolated ARVMs.

Monoamines target β adrenoceptors which activate adenylate cyclase (AC) generating cAMP which activates PKA. These monoamines are also metabolised by MAO to produce H_2O_2 which oxidises RIα to disulfide, associated with PKA activation. These monoamines therefore have two mechanisms for PKA activation which may synergise. In addition, cAMP sensitises RIα to disulfide formation and RIα disulfide sensitises PKA to cAMP resulting in increased PKA activity. The Trx system may be important in recycling RIα disulfide and preventing chronic PKA activation. Serotonin (which targets the 5-HT receptor) metabolism by MAO is also a source of H_2O_2 for disulfide formation.

5 A ROLE FOR RIα DISULFIDE IN A-KINASE ANCHORING PROTEIN (AKAP) BINDING

5.1 INTRODUCTION

Subcellular localisation of 3′,5′-cyclic monophosphate (cAMP)-dependent protein kinase (PKA) can be determined by its association with scaffolding proteins known as A-kinase anchoring proteins (AKAPs). A 14 - 18 amino acid amphipathic helix in the AKAP interacts with the dimerisation / docking (DD) domain of the PKA regulatory subunit.[228] The AKAP contains a targeting domain (involving protein-protein or protein-lipid interactions) which targets PKA to specific locations.[229, 230] PKA is therefore positioned close to its target substrate and upon cAMP binding to regulatory subunits, catalytic subunits are released and can catalyse phosphorylation of the substrate. AKAPs also form complexes with different cAMP effectors such as phosphodiesterases (PDEs) and phosphatases. PDE's hydrolyse cAMP to terminate activation of PKA and phosphatases dephosphorylate PKA substrates. Therefore, targeting PKA and these cAMP effectors allows specific regulation of cAMP signalling (see reviews [231-233]). AKAPs can also integrate cAMP signalling with other signalling pathways, as shown in the following example.

Muscle-specific AKAP (also known as mAKAP or AKAP6 (Figure 5.1)) forms a complex with Type II PKA and phosphodiesterase 4D3 (PDE4D3).[234] Phosphorylation of serine (Ser) 13 of PDE4D3 by PKA increases its affinity for mAKAP,[235] and phosphorylation of Ser54 of PDE4D3 by PKA leads to its activation.[236] PDE4D3 also recruits extracellular-regulated kinase (ERK) 5 and exchange protein directly activated by cAMP (Epac1) to the mAKAP complex. ERK5 phosphorylates and suppresses PDE4D3 activity and Epac1 is a cAMP acceptor that suppresses ERK5 activity.[237] Ryanodine receptors (RyRs) and protein phosphatase (PP) 2A can also be recruited to the mAKAP-PKA complex. These RyRs may be phosphorylated by mAKAP-targeted PKA and dephosphorylated by mAKAP-targeted

PP2A, providing a mechanism for regulation of RyR activity. mAKAP targets this protein complex to the nuclear envelope.[238]

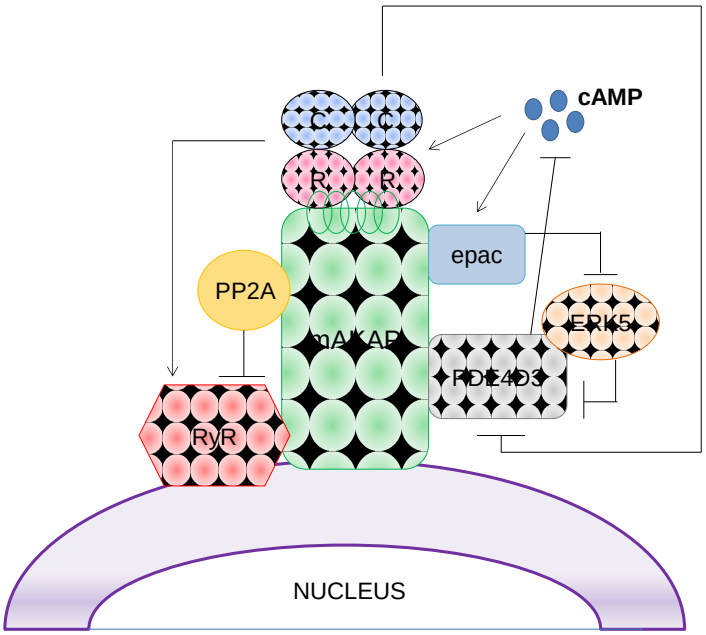

Figure 5.1. mAKAP complex.

mAKAP is tethered to the nucleus. It associates with PKA as well as the RyR and PP2A. When PKA is activated by cAMP it phosphorylates the RyR which is deactivated by PP2A-catalysed dephosphorylation. mAKAP also associates with epac1 and PDE4D3, which recruits ERK5 to the complex. cAMP binds to and activates epac1 which can suppress ERK5 activity which then can inhibit PDE4D3, preventing cAMP hydrolysis. The formation of this complex is important in regulating cAMP signalling as well as ERK signalling.

PKA RII is considered to be non-cytosolic due to binding to AKAPs.[239, 240] RI is generally considered to be soluble and cytosolic but there have been reports of RI in other locations. Upon T-cell activation RIα translocates from the cytoplasm to the T-cell receptor-CD3 complex,[241] and H_2O_2 induces translocation of RIα from cytosol to myofilament in cardiac tissue.[57] RIα has also been identified tightly bound to the membrane of erythrocytes,[242] and bound to the growth factor receptor-bound protein 2.[243] RIα has also been shown to be localised at the neuromuscular junction in skeletal muscle.[244]

This introduction discusses some examples of AKAPs that only bind Type I or Type II PKA, as well as those with dual specificity for the kinase. As mentioned in Chapter 1

and above, the DD domains of RIα and RIIα are each comprised of two helix-turn-helix motifs which dimerise to form a conserved X-type four helix bundle. The amphipathic helix of the AKAP binds across the DD domain. As shown in Figure 5.2, the DD domain of RIα is precisely flanked by the disulfides formed between cysteine (Cys) 16 and Cys37 (Cys17 / Cys38 in mouse) in response to oxidant and so these disulfides may modulate AKAP binding to this region, as discussed later.

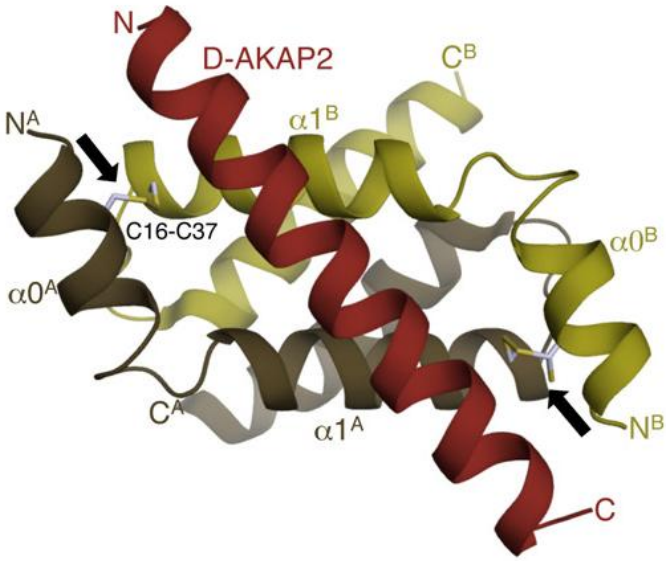

Figure 5.2. Amphipathic helix of D-AKAP 2 binding to DD domain of RIα.[119]

Antiparallel subunits are each made up of two helices (α0 and α1) and form an X-type four helix bundle. The DD domain of each subunit contains two Cys residues (Cys16 and Cys37) which form disulfides during oxidative stress (shown by black arrows). D-AKAPs bind at the region flanked by the two Cys residues and mutating Cys16 or Cys37 has been shown to reduce D-AKAP2 binding.

Despite both RI and RII DD domains being X-type four helix bundles, RIIα provides a shallow hydrophobic surface at its DD domain for the amphipathic helix to bind,[104, 245] whereas RIα provides a compact deep cleft. This is because each RIα subunit has an additional short helix (helix N-1) at its N-terminus shifting the DD domain further from the N-terminus. This helix N-1 folds back on to the X-type four helix bundle altering the protein shape and reducing accessibility to residues for protein interaction and reducing hydrophobicity compared to RIIα.[102] As shown in Figure 5.3, RI and RII therefore provide different surfaces for protein-protein interaction which may

explain differences in AKAP specificity and affinity between the regulatory subunit isoforms. Some dual-specificity AKAPs (D-AKAPs) also have an RI specifier region (RISR) outside the amphipathic helix which acts in synergy with the amphipathic helix to enhance RI binding.[246]

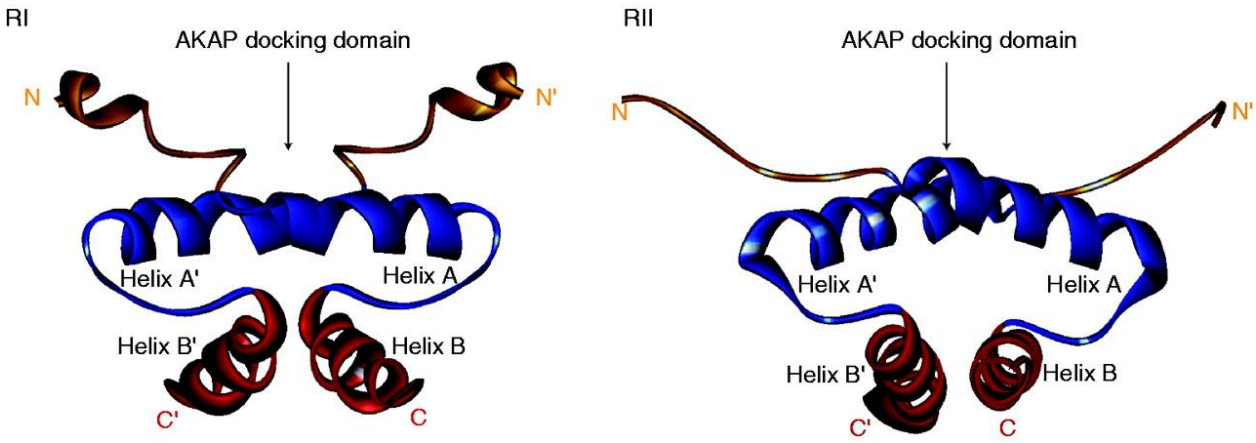

Figure 5.3 Comparison of RIα and RIIα AKAP docking domains.[232]

The DD domain of RIα provides a deep cleft and the DD domain of RIIα provides a shallow hydrophobic groove. Accessibility to the AKAP binding domain is more restricted in RIα due to the helix at the N-terminal which is absent in RIIα. This may explain differences in AKAP specificity and affinity between the regulatory subunit isoforms.

5.1.1 Type II PKA binding AKAPs

An example of an AKAP that binds to RII (Type II PKA) in the heart is AKAP7γ (also known as AKAP18δ) which also co-localises with phospholamban (PLB) and sarcoplasmic reticulum Ca^{2+} ATPase (SERCA) 2. PLB inhibits SERCA2 activity and phosphorylation of PLB at Ser16 by PKA relieves this inhibition.[174] The PKA-mediated phosphorylation of PLB and consequent increased SERCA2 activity is dependent on AKAP18δ function.[226]

Studies with AKAP5 (also known as AKAP79, 150 or 75) knock-out (KO) mice have helped demonstrate that this AKAP targets PKA to the L-type Ca^{2+} channel (LTCC) but protein kinase C (PKC) is also in the complex. The association allows phosphorylation of the α_{1C} subunit of the channel by PKA and therefore channel opening.[247] In ventricular myocytes, AKAP5 associates with adenylate cyclase, PKA RIIα,

calcineurin, β adrenoceptors and caveolin-3-associated LTCCs and is important in enhancing Ca^{2+} transients upon β adrenergic stimulation. During stimulation, only caveolin-3-associated LTCCs are phosphorylated by PKA. However, in AKAP5 KO mice adenylate cyclase fails to associate with AKAP5 with the result that non-caveolin-3-associated LTCCs are also phosphorylated upon β adrenergic stimulation. Phosphorylation of RyR2 and PLB is also reduced as a result of AKAP5 deletion even though these proteins do not directly associate with AKAP5 but this may be due to absence of the microdomain of cAMP created by the AKAP complex.[248]

5.1.2 D-AKAPs

D-AKAPs bind both RI and RII, although in most cases they have a higher affinity for the latter.[228] D-AKAP1 binds PKA RIα, RIIα and RIIβ but not RIβ.[249] For RIIα to bind to D-AKAP1, the DD domain itself is adequate but for RIα to bind to D-AKAP1, the DD domain and residues in regions peripheral to this domain are also required.[116]

S-AKAP84,[250] AKAP121,[251] and D-AKAP1a, b, c and d,[252] are splice variants of the D-AKAP1 gene in mice and AKAP149 is the human homologue.[253] As shown in Figure 5.4, these all have a common 525 amino acid core containing the PKA-binding site but differ at the N-terminus and C-terminus. They also vary in their tissue expression and subcellular localisation. D-AKAP1a, D-AKAP1c, S-AKAP84 and AKAP121 variants have a shorter N-terminus which targets the AKAP to mitochondria whilst D-AKAP1b and D-AKAP1d have a longer N-terminus sequence, containing an additional thirty-three residues, that suppresses mitochondrial targeting and instead targets the AKAP to the endoplasmic reticulum.[254] Asp31 has been identified as essential for this switch from mitochondrial targeting to endoplasmic reticulum targeting.[252] AKAP149 and the longer forms of D-AKAP1 also have a K homology (KH) domain at the C-terminus,[252, 253] which is an ribonucleic acid (RNA) binding motif, discussed in more detail below.

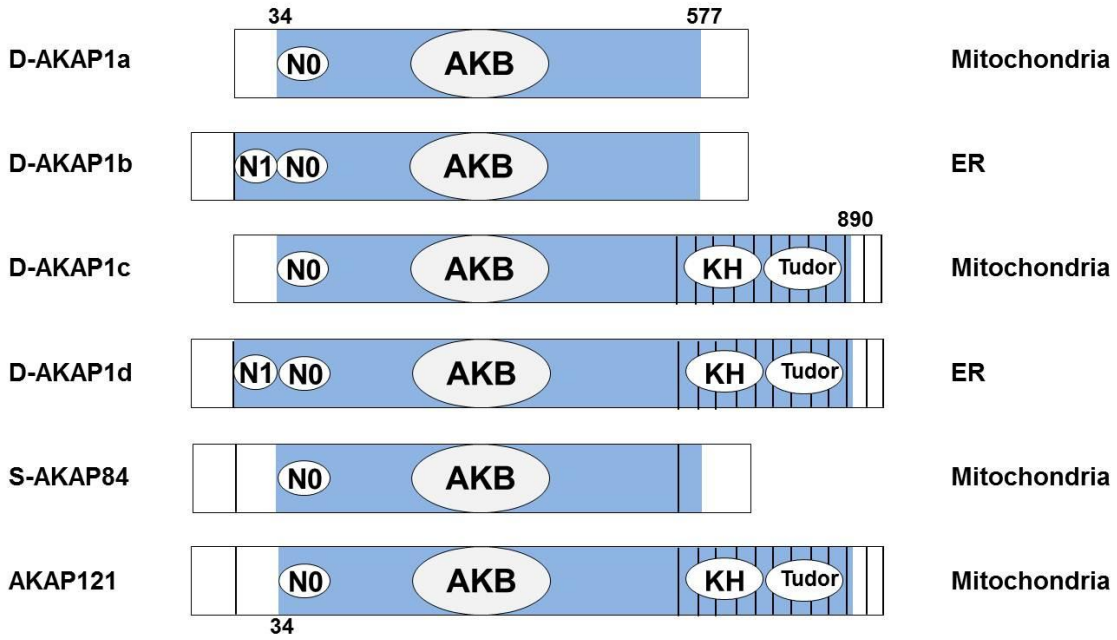

Figure 5.4 Isoforms of D-AKAP1 (modified from Ma *et al.*[252])

The PKA-binding domain (AKB) is common to all isoforms. Isoforms differ at the N-terminus, where some isoforms have the thirty residue mitochondrial (mitochondria) targeting domain (N0) or this region and an additional region of thirty-three residues (N1) that target the AKAP to the ER. The localisation of each AKAP is shown on the right. Isoforms also differ at the C-terminus where they may have KH and Tudor domains, which are RNA binding motifs.

AKAP149 is a trans-membrane protein in the endoplasmic reticulum and nuclear envelope, with most of the protein positioned in the cytosol. At the nuclear envelope, upon nuclear assembly after mitosis, AKAP149 binds PKA by its amphipathic helix and protein phosphatase 1 (PP1) by its arginine-valine-any residue-phenylalanine (RVXF) motif.[255] The AKAP149-PP1 complex dephosphorylates B-type lamins promoting laminin formation and nuclear assembly.[256] In adipocytes, PKA-associated D-AKAP1 binds to the catalytic subunit of PP1 which may regulate PKA's role in lipid metabolism.[257] The RVXF motif in AKAP149 is flanked by Ser residues, which are phosphorylated by PKC to cause dissociation of PP1 and also PKA, although this does not cause dissociation of PP1 and the role of this modification remains unknown.[258]

AKAP121 tethers PKA to the mitochondrial membrane possibly via AKAP121 binding to β tubulin.[259] AKAP121 targeting of PKA (Figure 5.5) enhances PKA signalling in the mitochondria and protects cells from apoptosis through PKA-dependent

phosphorylation of BAD and inhibition of cytochrome c release.[260] AKAP121 is also found in a complex with Src (a tyrosine kinase) and protein-tyrosine phosphatase (PTP) D1. PTPD1 promotes dephosphorylation of Src which increases the kinase's activity. Src phosphorylates the epidermal growth factor (EGF) receptor and leads to increased EGF signalling but binding of AKAP121 to PTPD1 down-regulates this signalling.[261] However, others have shown that AKAP121 increases Src signalling and PKA signalling in the mitochondria, leading to increased phosphorylation of mitochondrial substrates such as cyclooxygenase (COX) and ultimately increased ATP synthesis.[262]

As already mentioned, AKAP149 and the longer forms of D-AKAP1 have a KH domain at their C-terminal,[252, 253] which is an RNA-binding motif that may play a role in localising RNA to a particular cellular compartment. PKA can phosphorylate the KH domain of AKAP121 and increase its binding to the three prime untranslated region (3'-UTR) coding for manganese superoxide dismutase (MnSOD), an antioxidant enzyme, for example. This results in translocation of MnSOD from the cytosol to the mitochondria, which increases its abundance in this cellular compartment.[263] AKAP121 and AKAP149 also bind lipoprotein lipase mRNA which inhibits translation of the enzyme.[264] Lipoprotein lipase plays a role in triglyceride-rich lipoprotein hydrolysis and adipose tissue lipogenesis.

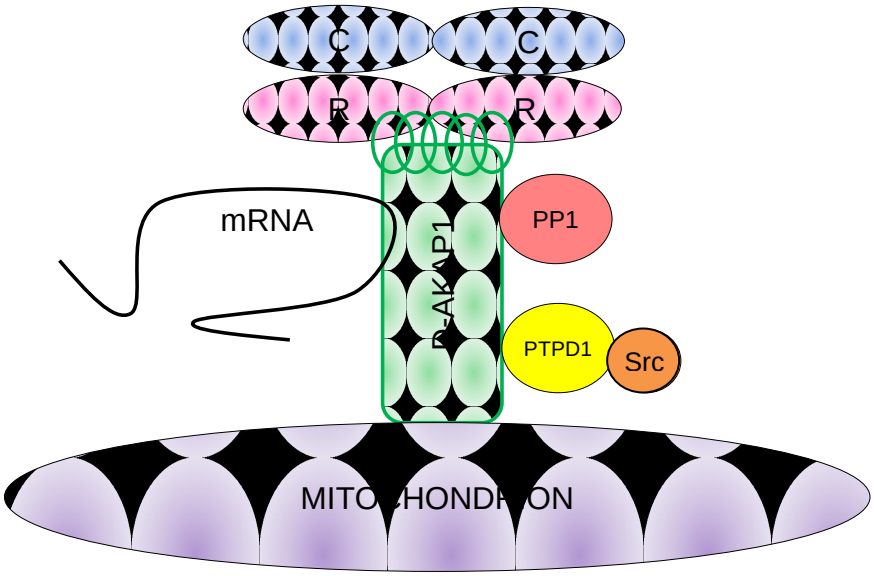

Figure 5.5 D-AKAP1 multi-protein complex.

The amphipathic helix of D-AKAP1 binds to the DD domain of PKA tethering PKA to the mitochondrial membrane. PP1 binds to the RVXF motif in D-AKAP1 and mRNA binds to the KH domain of D-AKAP1. D-AKAP1 also interacts with PTPD1, which recruits Src to the complex.

D-AKAP2 (also known as AKAP10) binds RIα, RIIα and RIIβ but not RIβ.[138] For RIα to bind to D-AKAP2, the DD domain (see Figure 5.2) and regions peripheral to this domain are required.[138] D-AKAP2 has regulator of G-protein-signalling (RGS) domains (RGS-A and RGS-B) which means it can interact with Gα proteins.[138] No D-AKAP2 binding Gα proteins have yet been identified, but the GTPases, Rab11 and GTP-bound Rab4 directly interact with the RGS domains. This causes D-AKAP2 to move from the cytosol to endosomes, regulating recycling of endocytosed proteins back to the membrane.[265]

D-AKAP2 also has a PDZ-binding motif which can bind Na^+ / H^+ exchanger regulator factor 1 (NHERF-1) and 3 (NHERF-3 or PDZK1) in proximal tubular cells of the kidney.[142] Type II Na^+-dependent phosphate co-transporters are important in renal reabsorption of phosphates. NHERF-1 and PDZK1 regulate expression of the co-transporters in the apical membrane of proximal tubules,[266] so D-AKAP2 binding may play a role in this regulation.

AKAP10 also appears to play a role in heart rhythm regulation by altering the sensitivity of cardiac cells to cholinergic stimulation. Cardiac cells of mice with a fifty-one amino acid C-terminal deletion of AKAP10 (removing the PKA-binding site) have increased sensitivity to cholinergic stimulation, leading to a slower heart rate and increased heart rate variability.[267]

AKAP220 (also known as AKAP11) is predominately located in the testes, but it is also found in heart, brain, lung and kidney.[268] The literature mainly focuses on AKAP220 binding to PKA RII, but AKAP220 also binds RI.[269] AKAP220 forms a multi-protein complex with Type II PKA, PP1,[270] and the PKA substrate glycogen synthase kinase (GSK) 3β. PKA in the complex can phosphorylate and inhibit GSK3β, whereas PP1 can dephosphorylate and activate GSK3β.[271] AKAP220 inhibits PP1 activity and this effect is enhanced by PKA RII.[272] AKAP220 can also bind IQ domain GTPase-activating protein 1 (IQGAP1) which is a cytoskeletal scaffolding protein that promotes cell migration by aiding cytoskeleton remodelling. GSK3β inhibits the interaction between IQGAP1 and another protein, CLASP2 by phosphorylating CLASP2. Therefore, PKA in the complex may phosphorylate and inhibit GSK3β thereby allowing IQGAP1 and CLASP2 to interact promoting cell migration. Ca^{2+} also increases binding of IQGAP1 and AKAP220 or IQGAP1 and CLASP2. Ultimately, AKAP220 recruits all these proteins to the leading edge of the cell and promotes cell migration which occurs during tissue development and tumour metastasis.[273] AKAP220 also forms a complex with PKA and aquaporin 2, a water channel in the collecting ducts of the kidney. PKA phosphorylates aquaporin 2 at Ser256 causing its insertion into the apical membrane and water reabsorption.[274]

The splicing factor arginine / Ser-rich 17A **(**SFRS17A**)** is located in splicing factor compartments of the nucleus. It binds RI and RII with a similar affinity, which is atypical for D-AKAPs. SFRS17A binds RI and RII by an amphipathic helix at its N-terminus which is expected, based on how we know AKAPs interact with regulatory subunits (see Figure 5.2 for an example of this). It also binds to RI by the RISR at its C-terminus. The result is targeting of PKA to splicing factor compartments for a potential role in pre-mRNA splicing.[275]

The sarcomeric protein cardiac troponin T (cTnT) is also considered a D-AKAP. It's PKA binding site is an amphipathic helix and displacement of Type II PKA from cTnT leads to reduced PKA activity in the myofilament.[276]

Brefeldin A-inhibited guanine nucleotide-exchange protein 2 **(**BIG2) is a guanine nucleotide-exchange protein (GEP) that is inhibited by brefeldin A, an antibiotic produced by fungi. GEP's accelerate the release of bound GDP from inactive cytosolic adenosine diphosphate (ADP)-ribosylation factor (ARF)-GDP. This promotes binding of guanosine triphosphate (GTP) and formation of active membrane-bound ARF-GTP, and regulates intracellular vesicular trafficking. BIG2 interacts with PKA RIα, PKA RIβ as well as PKA RII and has three different binding sites each with different specificities for the regulatory subunit isoforms. cAMP has been shown to promote translocation of brefeldin A-inhibited guanine nucleotide-exchange protein 1 **(**BIG1) / BIG2 from cytosol to the golgi membrane,[277] where PKA promotes ARF association with the golgi membranes.[278] However others have shown that BIG1, BIG2, RIα and PDE3 form a complex in the cytosol and depletion of PDE3 decreases abundance of BIG1 and BIG2 in membrane and increases their abundance in cytosol.[279] In this situation, cAMP levels increase (due to a decrease in breakdown by PDE3) leading to PKA activation and phosphorylation of BIG1 or BIG2. Phosphorylation decreases GEP activity of BIG1 / 2 and reduces the amount of active ARF-GTP.[279, 280] PP1γ also binds BIG1 or BIG2. After inhibition by PKA-mediated phosphorylation, PP1 dephosphorylates BIG1 or BIG2 which restores GEP activity.[280] Therefore, PDE3, PKA and PP1 all appear to regulate BIG1 or BIG2 activity and therefore ARF function.

5.1.3 Type I PKA binding AKAPs

Most analyses of PKA-AKAP binding have been with Type II PKA. More AKAPs that bind RII have been identified, probably because they can be identified using blot overlay (also known as Far Westerns) in work pioneered by Dr. John Scott.[281, 282] However, this approach is less successful in identifying RI-binding proteins.[283] This is perhaps because during the interaction of AKAPs with RI, the off-rate is faster than the on-rate,[284] making the interaction transient and difficult to catch using solid phase assays.

However, increasingly more AKAPs that only bind RI are being identified. These include α4 integrin, which binds to RI via its cytoplasmic tail and is important in cell motility,[285] and $AKAP_{CE}$, a protein found in *Caenorhabditis elegans.*[286] In neurons, α / β tubulin forms a complex with RI but not with RII. α and β tubulin can form dimers which then form protomers and assemble to form microtubules which are important in cell motility, cell movement and mitosis. The α / β tubulin-RI complex is formed in the cytosol and translocates to the synaptic end. Degradation of this is induced by serotonin allowing long lasting PKA activity in the synapse.[287] As outlined in Chapter 4, I observed monoamine (including serotonin) -induced RIα disulfide formation, which may be a prerequisite to degradation of the α / β tubulin-RI complex. Myosin VIIA is an unconventional myosin located in the outer hair cells of the ear. The DD domain of PKA RIα binds to the C-terminal 4.1, ezrin, radixin, moesin domain of myosin VIIA which may modulate cAMP's regulation of voltage-dependent potassium channels in outer hair cells.[288] Peripheral-type benzodiazepine receptor (PBR) and PKA-associated protein 7 (PAP7) as the name suggests interacts with PBR and PKA RIα. Binding of RIα to PAP7 may target PKA to the mitochondria where, upon cAMP activation, the catalytic subunit is released and can catalyse phosphorylation of steroidogenesis acute regulatory protein (StAR). Phosphorylation causes cholesterol to be transferred from StAR to PBR, a cholesterol binding protein, leading to steroidogenesis.[289]

Sphingosine is a sphingoid base produced by the deacylation of ceramide, an acylated sphingoid base which is a component of the cell membrane. For sphingosine to be catabolised it must be phosphorylated. Sphingosine kinase (SPHK) is an enzyme that catalyses the phosphorylation of sphingosine producing sphingosine 1 phosphate (S1P). S1P is then degraded in the endoplasmic reticulum or can be converted back to ceramide. S1P can also act as a second messenger, activating signalling pathways such as ERK to promote cell survival.[290] Sphingosine kinase interacting protein (SKIP, SPHKAP) interacts with SPHK1 and reduces its activity.[291] SKIP is an RIα–specific AKAP,[292] and has two binding sites with different affinities for RIα dimer so can carry two RIα dimers at one time.[293] The AKAP is cytosolic and highly expressed in

the heart.[292] It is also enriched at the inner mitochondrial membrane where it recruits RIα and associates with coiled-coil-helix-coiled-coil-helix domain-containing protein 3 (ChChd3) for phosphorylation by PKA.[293, 294] ChChd3 is a scaffolding protein that is important in maintaining mitochondria function and mitochondrial cristae structure.[295]

Most recently, a novel RI-specific AKAP termed small membrane (sm) AKAP has been identified in the heart. This AKAP localises at the plasma membrane via potential myristoylation / palmitoylation anchors and the filopodia (cytoplasmic projections on migrating cells), which could be associated with PKA's role in cell migration.[296]

Table 5.1 summarises AKAPs that bind RIα. This chapter focuses on how the interaction between some of these AKAPs and PKA RIα is potentially altered when RIα disulfide formation occurs in the heart. This was primarily determined by comparing cardiac wild-type (WT) and knock-in (KI) Cys17Ser RIα binding to AKAPs. This chapter aims to address the following:

1. Whether disulfide is associated with subcellular translocation of cytosolic RIα to the membrane or myofilament and so determining RIα localisation in mouse hearts. I hypothesise this is so because the disulfide may increase RIα affinity for AKAPs,[119] and so induce cytosolic RIα to move to the AKAPs which may be localised in the membrane or myofilament. In addition, Brennan *et al.* previously showed that 100 μM H_2O_2 caused translocation of PKA RIα from the cytosol to the myofilament in rat hearts,[57] so it is likely that this occurs in mouse hearts too.

2. Whether disulfide modulates RIα interaction with AKAPs. I initially chose to look at RIα binding to D-AKAP1, D-AKAP2, AKAP220 and α / β tubulin as these had been studied extensively. I hypothesise that AKAP interaction will be modulated by RIα redox state because the disulfides precisely flank the AKAP binding site (Figure 5.2) and so they may cause a conformational change that acts as a molecular structural switch to alter AKAP binding to this region. I hypothesise that disulfide will increase binding to AKAPs as Sarma *et al*. demonstrated that RIα disulfide increases its affinity

for D-AKAP2,[119] and so this could be applicable to other AKAPs. However, there is also the idea that disulfide may reduce the association between RIα and some AKAPs.

AKAP	Other proteins in complex	Function of complex	References
D-AKAP1	PP1	nuclear assembly after mitosis Lipid metabolism	[255, 256] [257]
	PTPD1, src	increased EGF signalling ATP synthesis	[261] [262]
	3-UTR of MnSOD	translocation of MnSOD	[263]
	3-UTR of lipoprotein lipase	lipoprotein hydrolysis and adipose tissue lipogenesis	[264]
D-AKAP2	Rab 4, Rab 11	recycling of endocytosed proteins	[265]
	NHERF-1, NHERF-3	renal absorption of phosphates	[142, 266]
AKAP220	PP1		[270, 272]
	GSK3β		[271]
	IQGAP1	cell migration	[273]
SFRS17A		pre-mRNA splicing	[246]
CTnT		regulation of PKA activity in myofilament	[276]
BIG2	BIG1	GEP activity	[279]
	PDE3	regulation of ARF function	[279]
	PP1γ	regulation of ARF function	[280]
α4 integrins		cell motility	[285]
α / β tubulin		regulation of PKA activity in synapse	[287]
Myosin VIIA		regulation of voltage-dependent potassium channels in outer hair cells.	[288]
PAP7	PBR	steroidogenesis	[289]
SKIP	ChChd3	mitochondria structure and function	[293]
smAKAP		cell motility	[296]

Table 5.1. AKAPs that bind PKA RIα.

Proteins shown to interact with the AKAP and the functions that have been associated with the AKAP multi-complexes are also listed.

5.2 METHODS

5.2.1 Fractionation of hearts and analysis of RIα and AKAP abundance

WT and KI hearts were Langendorff-perfused with K-HB for 45 min or K-HB for 40 min followed by 50 μM H_2O_2 for 5 min. Hearts were then homogenised and fractionated into cytosol-enriched, membrane-enriched and myofilament-enriched fractions, as described in Chapter 2. SDS-PAGE and Western blotting were carried out and blots were probed for PKA RIα. Blots were also incubated with antibodies to selected AKAPs that, as described in 5.1.3, have been shown by others to bind RIα. Blots were also incubated with a ChChd3 antibody for reasons discussed later. ChChd3 is a PKA substrate associated with an RIα AKAP.[293] Antibodies and incubation conditions are outlined in Table 5.2 (methods described in more detail in Chapter 2).

Antibody	Product code	Company	Species	Conc.	Incubation period
AKAP220 (L-16)	sc6444	Santa Cruz Biotechnology	Goat	1:1000	3 hours
AKAP10	ab65038	Abcam	Rabbit	1:1000	3 hours
AKAP10 (N-13)	sc-109188	Santa Cruz Biotechnology	Goat	1:1000	3 hours
AKAP149 / 121 (C-20)	sc-6439	Santa Cruz Biotechnology	Goat	1:1000	3 hours
AKAP1	15618-1-AP	Proteintech Group	Rabbit	1:1000	3 hours
α / β tubulin	#2148	Cell Signalling Technology	Rabbit	1:1000	3 hours
SPHKAP	GTX101951	GeneTex	Rabbit	1:500	3 hours
SPHKAP	GTX101952	GeneTex	Rabbit	1:500	3 hours
Myomegalin [N1], N-term	GTX115270	Genetex	Rabbit	1:1000	3 hours
ChChd3	ab99491	Abcam	Goat	1:1000	3 hours

Table 5.2. Details of anti-AKAP antibodies.

This table shows the company each antibody was purchased from and its purchase code, the species it was raised in (and so the secondary antibody to be used), concentration the antibody was used at (in 5 % milk in PBS with 0.1 % Tween-20) and the incubation period at room temperature. D-AKAP1 is also known as AKAP121, AKAP149 and AKAP1. D-AKAP2 is also known as AKAP10.

5.2.2 cAMP affinity capture of cardiac WT and KI RIα

Preparation of heart homogenate: WT and KI hearts were Langendorff-perfused (more detail in Chapter 2) with K-HB for 45 min or K-HB for 40 min followed by 50 µM H_2O_2 for 5 min and homogenised, as described in Chapter 2. 50 µl of 10 % Triton X-100 in homogenisation buffer (100 mM Tris pH 7.4, 1 % Triton X-100, 100 mM maleimide, 1 mM ethylene glycol tetra acetic acid (EGTA), 1 mM ethylenediaminetetraacetic acid (EDTA), 200 µM phenylmethanesulfonylfluoride (PMSF, protease inhibitor) and phosphatase inhibitor cocktail 2 (1:100)) was added to 450 µl of each homogenate, vortexed and left on ice for 5 min. The homogenates were then centrifuged at 25000 rpm for 5 min at 4 ºC. 450 µl of the Triton X-100 soluble fraction from each heart was diluted five-fold by adding 1800 µl of homogenisation buffer. 100 µl of this was added to 100 µl of non-reducing SDS sample buffer containing 100 mM maleimide. This is called the *input.*

Incubation of 8-AEA-cAMP-agarose with heart homogenate: 200 µl of 8-AEA-cAMP-agarose ((2- aminoethylamino) adenosine- 3', 5'- cyclic monophosphate immobilized on agarose, Biolog Life Science Institute) was washed in 500 µl homogenisation buffer. The mixture was vortexed and centrifuged at 1000 rcf for 0.5 min. The supernatant was then removed and discarded and the 8-AEA-cAMP-agarose was washed twice more in homogenisation buffer. After centrifugation, 200 µl of homogenisation buffer was added to the agarose and mixed to give a 50 % slurry. 100 µl of this slurry was added to four 1.5 ml Eppendorf tubes and then centrifuged at 1000 g for 0.5 min. The supernatant was removed and discarded. 2 ml of Triton X-100 soluble fraction from untreated WT, untreated KI, 50 µM H_2O_2-treated WT or 50 µM H_2O_2-treated KI hearts was added to 50 µl 8-AEA-cAMP-agarose (prepared earlier) and incubated overnight (~17 hours) on a rotating wheel at 4 ºC. The next day the samples were centrifuged at 1000 g for 1 min at 4 ºC and 100 µl of each supernatant was added to 100 µl SDS sample buffer containing 100 mM maleimide. This is called the *flow-through*. The remaining supernatant was removed and discarded. 1.5 ml of homogenisation buffer was added to the 8-AEA-cAMP-agarose, gently agitated and then incubated at 4 ºC on a rotating wheel for 15 min. Following this, the supernatant

was removed and discarded and the 8-AEA-cAMP-agarose was washed twice more in the same way. Finally, 100 µl of non-reducing SDS sample buffer containing 100 mM maleimide was added to the 8-AEA-cAMP-agarose and this is called the *capture*.

Optimisation of cAMP affinity capture: The basic method outlined above was systematically modified in an attempt to improve efficiency of RIα capture with AKAP proteins. The first alteration was that 9 ml of diluted Triton X-100 soluble heart fraction was incubated with 200 µl 8-AEA-cAMP-agarose rather than 2 ml Triton X-100 soluble fraction with 50 µl 8-AEA-cAMP-agarose. The second modification was that the Triton X-100 soluble fraction was diluted three-fold rather than five-fold in homogenisation buffer with 8 ml of this added to 250 µl 8-AEA-cAMP-agarose. Experiments in which these alterations were made will be stated.

5.2.3 SDS-PAGE, Western blotting and probing for AKAPs

Input, *flow-through* and *capture* samples were analysed by SDS-PAGE and Western blotting, as described in Chapter 2. Blots were probed with antibodies to D-AKAP1, D-AKAP2, AKAP220 and α / β-tubulin (see Table 5.2). To increase the likelihood of detecting the AKAPs in the cAMP affinity *capture* samples, antibodies were all used at a concentration of 1:500 overnight.

5.2.4 Colloidal Coomassie staining of polyacrylamide gel

Colloidal Coomassie was made up by mixing 784 ml of Solution A (85 % orthophosphoric acid, 0.6 M ammonium sulphate) with 16 ml of Solution B (5 % Coomassie Brilliant Blue G-250). 20 % methanol was then added before use. The polyacrylamide gel was stained in colloidal Coomassie on a shaker overnight. The gels were then de-stained in water until stained bands were clearly observed on the gel against a clear background.

5.2.5 Liquid chromatography-tandem mass spectrometry (LC-MS/MS)

Sections of the colloidal Coomassie stained polyacrylamide gel were excised and analysed by Manuel Mayr and Xiaoke Yin (Kings College, London) who carried out LC-MS/MS to identify the proteins in the gel. This method combines liquid

chromatography, which is the physical separation of chemicals, with mass spectrometry, which involves ionisation of chemicals and determining their mass to charge ratio. In-gel digestion with trypsin was performed following a protocol previously published,[297] with modifications so it could be used with an Investigator ProGest (Genomic Solutions) robotic digestion system. A nanoflow LC system on a reverse-phase column (25 cm C18 PepMap100, Dionex) was used to separate peptides and then these were applied to an LTQ Orbitrap XL mass spectrometer (Thermo Scientific). Full ion scan mode over the mass-to-charge (m / z) range 300-2000 was used to collect spectra. Six independent scans were performed on each ion using dynamic exclusion. Proteins were identified using Mascot 2.3.01 search engine and matching against the mouse UniProt/ Swiss-Prot (version 57.15) database. These results were then validated using Scaffold (version 3.3.1, Proteome software Inc.). Peptide identifications were accepted if they could be established at greater than 95.0 % probability (specified by the Peptide Prophet algorithm).[298, 299] Protein identifications were accepted if they could be established at greater than 99.0 % probability and contained at least two identified peptides with ± 10-ppm mass accuracy. A Fishers Exact test was carried out to compare the number of assigned spectra in WT and KI hearts and differences were considered statistically significant if $p<0.05$. These statistics were carried out by Manuel Mayr and Xiaoke Yin (Kings College, London).

5.3 RESULTS

5.3.1 Localisation of PKA RIα in WT and KI hearts basally and after H_2O_2

Figure 5.6B shows that control WT hearts predominately contain RIα in the reduced monomeric state (~60 %) and this is localised in the cytosol-enriched fraction. There were also small amounts of disulfide dimer in cytosol- (~20 %), membrane- (~13 %) and myofilament- (~7 %) enriched fractions of WT hearts. In comparison, in control KI hearts RIα was all monomer and present in cytosol- and membrane- enriched fractions (~90 % and ~10 % respectively). H_2O_2 increased total disulfide dimer by ~30 % in WT hearts but the increase was not easily observed on Western blots (Figure 5.6A). This was because the film needed to be exposed for long periods to detect RIα in membrane- and myofilament- enriched fractions making the signal for cytosolic RIα monomer or dimer very dense. Figure 5.6 shows that in WT hearts, H_2O_2 increased membrane-associated disulfide by ~10 % and myofilament-associated disulfide by ~5 %. However, H_2O_2 did not affect RIα localisation in KI hearts; RIα monomer was still only present in cytosol- and membrane- enriched fractions These results suggest a role for RIα disulfide in translocation to the membranes and myofilaments.

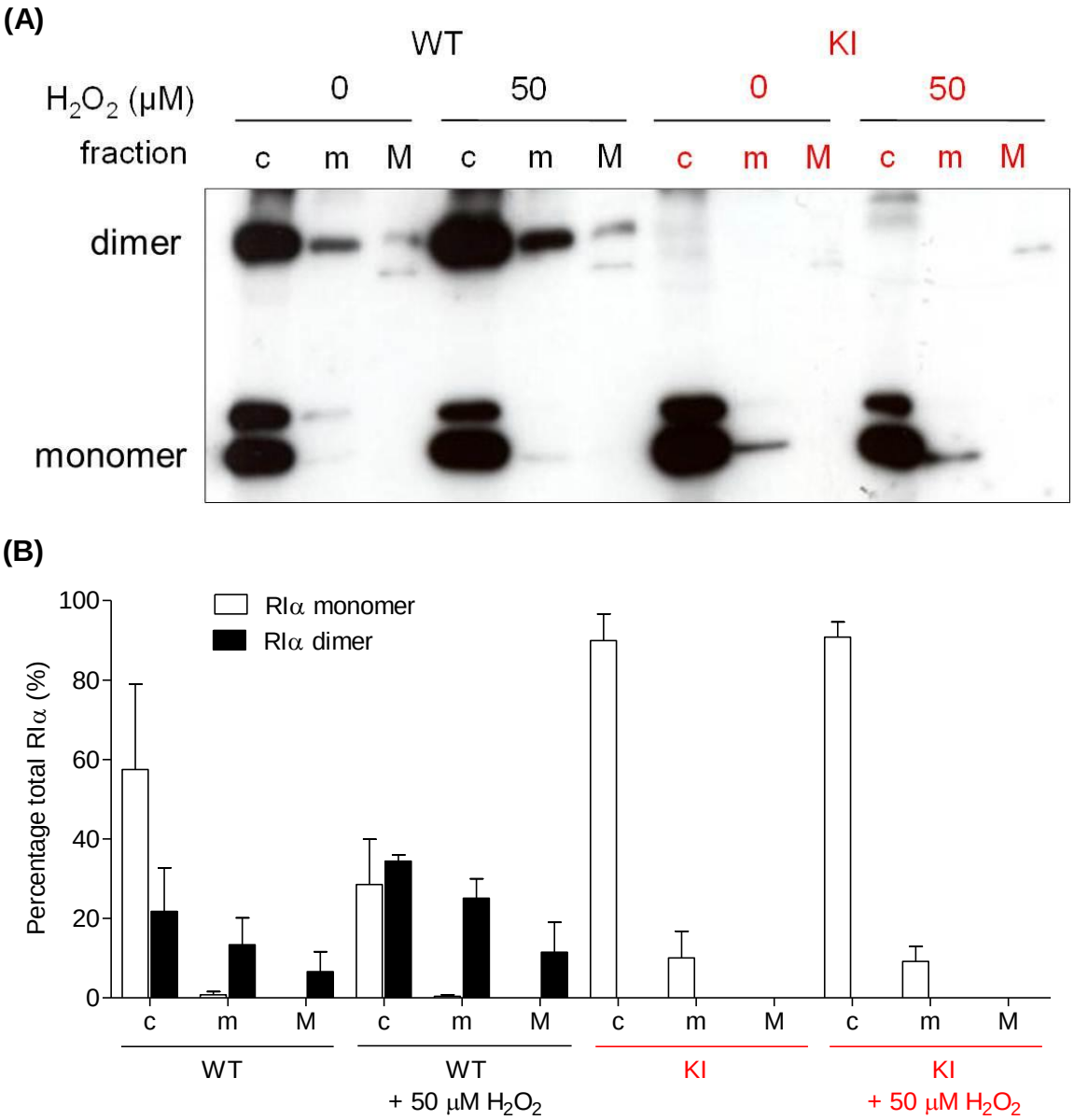

Figure 5.6 Localisation of PKA RIα monomer and dimer in control and H_2O_2 Langendorff-perfused WT and KI hearts.

(A) Male WT / KI hearts were Langendorff-perfused with K-HB or 50 μM H_2O_2 for 5 min and fractionated into cytosol-enriched (c), membrane-enriched (m) and myofilament-enriched (M) fractions. Redox state of PKA RIα was determined by immunoblotting as shown in the representative blot (B) Quantification (n=3 ± SEM) of percentage of total RIα abundance in each fraction. RIα disulfide translocated to membrane- and myofilament- enriched fractions.

5.3.2 Localisation of PKA catalytic subunit in WT and KI hearts basally and after H_2O_2

Figure 5.7 shows that, as expected, most PKA catalytic subunit was in the cytosol-enriched fraction of WT hearts (~50 % of total catalytic subunit in the heart) with smaller amounts of catalytic subunit in the membrane- (~40 %) and myofilament-enriched (~10 %) fractions. However, in KI hearts, ~25 % more catalytic subunit was localised in the cytosol-enriched fraction compared to WT. Consequently, there was ~10 % less catalytic subunit in the membrane and myofilament fractions of KI hearts compared to WT. When RIα disulfide was increased by oxidant treatment in WT hearts, abundance of catalytic subunit in the cytosol-enriched fraction was not altered. However, catalytic subunit localisation in the membrane increased with a corresponding decrease in the myofilament such that the difference in catalytic subunit abundance between membrane and myofilament fractions now became statistically significant ($p<0.05$, ~40 % compared to ~15 % in control WT hearts). In contrast, oxidant treatment of KI hearts did not alter localisation of PKA catalytic subunit.

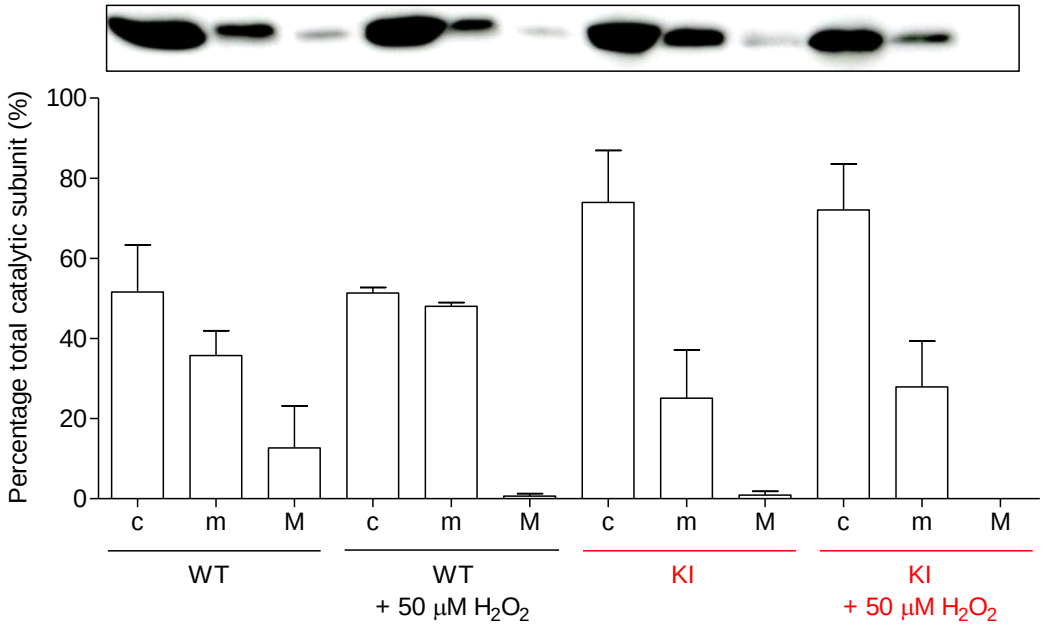

Figure 5.7 Localisation of PKA catalytic subunit in control and H_2O_2-perfused WT and KI hearts.

Hearts were Langendorff-perfused with K-HB or 50 μM H_2O_2 for 5 min and fractionated into cytosol-enriched (c), membrane-enriched (m) and myofilament-enriched (M) fractions. Western blots were probed for PKA catalytic subunit as shown in the representative blot. Average percentage of total catalytic subunit in each fraction was calculated for n=3 hearts ± SEM * $p<0.05$ compared to membrane-enriched fraction of WT + 50 μM H_2O_2. The catalytic subunit was mostly localised in the cytosol-enriched fraction in all hearts with some catalytic subunit in the membrane-enriched fraction. H_2O_2 caused an increase in catalytic subunit abundance in WT membrane but not KI membrane.

5.3.3 Screening for antibodies that detect selected AKAPs

Screening for an antibody to D-AKAP1: Figure 5.8A shows that antibody sc-6439 detected a protein at ~149 kDa in control or H_2O_2-treated WT or KI hearts, as well as in liver which was used as a positive control known to abundantly express this AKAP. This was the correct molecular weight for D-AKAP1 but non-specific bands were also seen at ~135 kDa and ~175 kDa. In WT or KI hearts (control or H_2O_2-treated) and in liver, antibody 15618-1-AP (Figure 5.8B) detected proteins at ~180 kDa, ~90 kDa and ~149 kDa, the latter corresponding to D-AKAP1. Antibody 15618-1-AP was the chosen antibody to probe blots for D-AKAP1 because it generated fewer interfering non-specific bands near to 149 kDa that might otherwise complicate the detection of D-AKAP1 at 149 kDa.

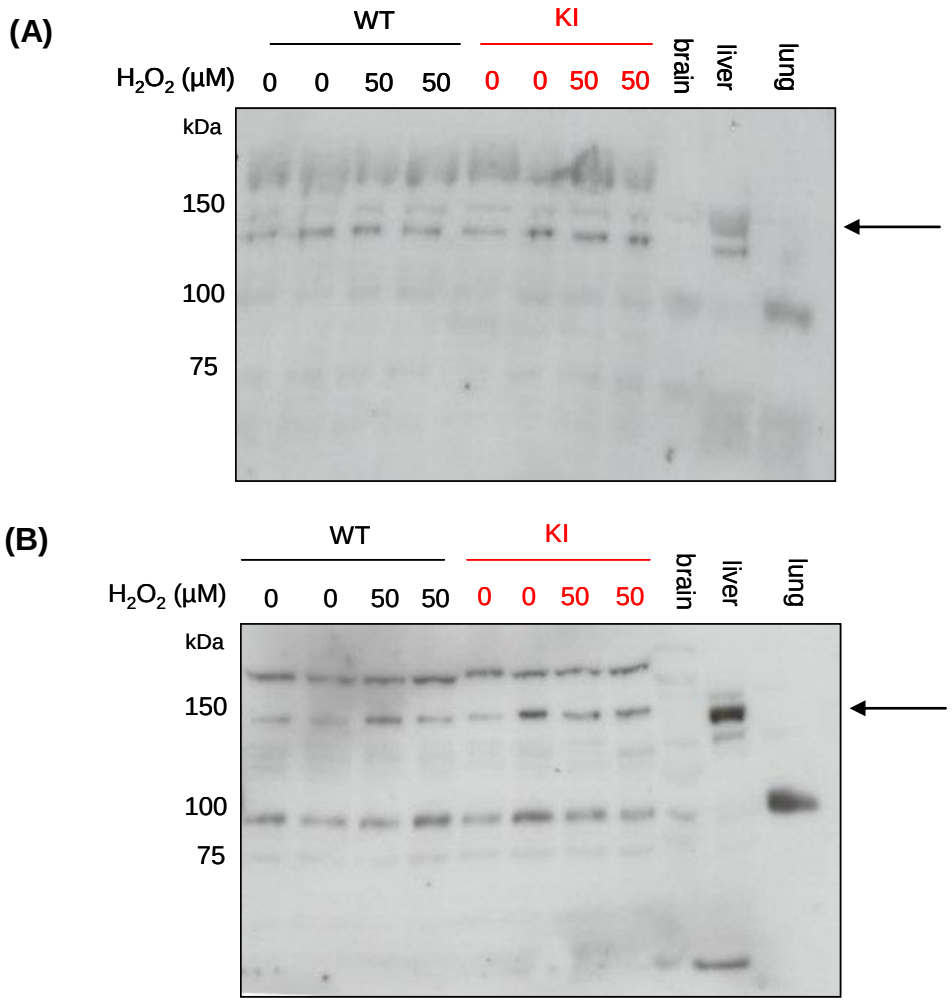

Figure 5.8 Immunoblot detection of D-AKAP1 in male WT and KI hearts.

(A) WT and KI hearts were Langendorff-perfused with K-HB or H_2O_2. Western blot was probed for D-AKAP1 using antibody sc-6439 which detected a protein at the correct molecular weight (149 kDa) for D-AKAP1, as indicated by the arrow. (B) Western blots were also incubated with the D-AKAP1 antibody 15618-1-AP which detected a band at the correct molecular weight for D-AKAP1 (as indicated by the arrow) and fewer non-specific interfering bands near to 149 kDa. Antibody 15618-1-AP was therefore chosen when probing for D-AKAP1 in future studies.

Screening for an antibody to D-AKAP2: Figure 5.9A shows that the first antibody purchased from Abcam (ab65038) detected proteins at ~50 kDa, ~100 kDa and ~250 kDa but did not detect a protein at the correct molecular weight for D-AKAP2 (74 kDa) in hearts. D-AKAP2 was not detected in lung, kidney, liver or brain either so this was not because it is not present in heart but because the antibody did not detect D-AKAP2. Antibody sc-109188 (Figure 5.9B) detected the AKAP at 74 kDa in WT or KI hearts (control or H_2O_2-perfused) as well as in lung, kidney and liver. Sc-109188 was therefore the antibody chosen to probe blots for D-AKAP2 in future studies.

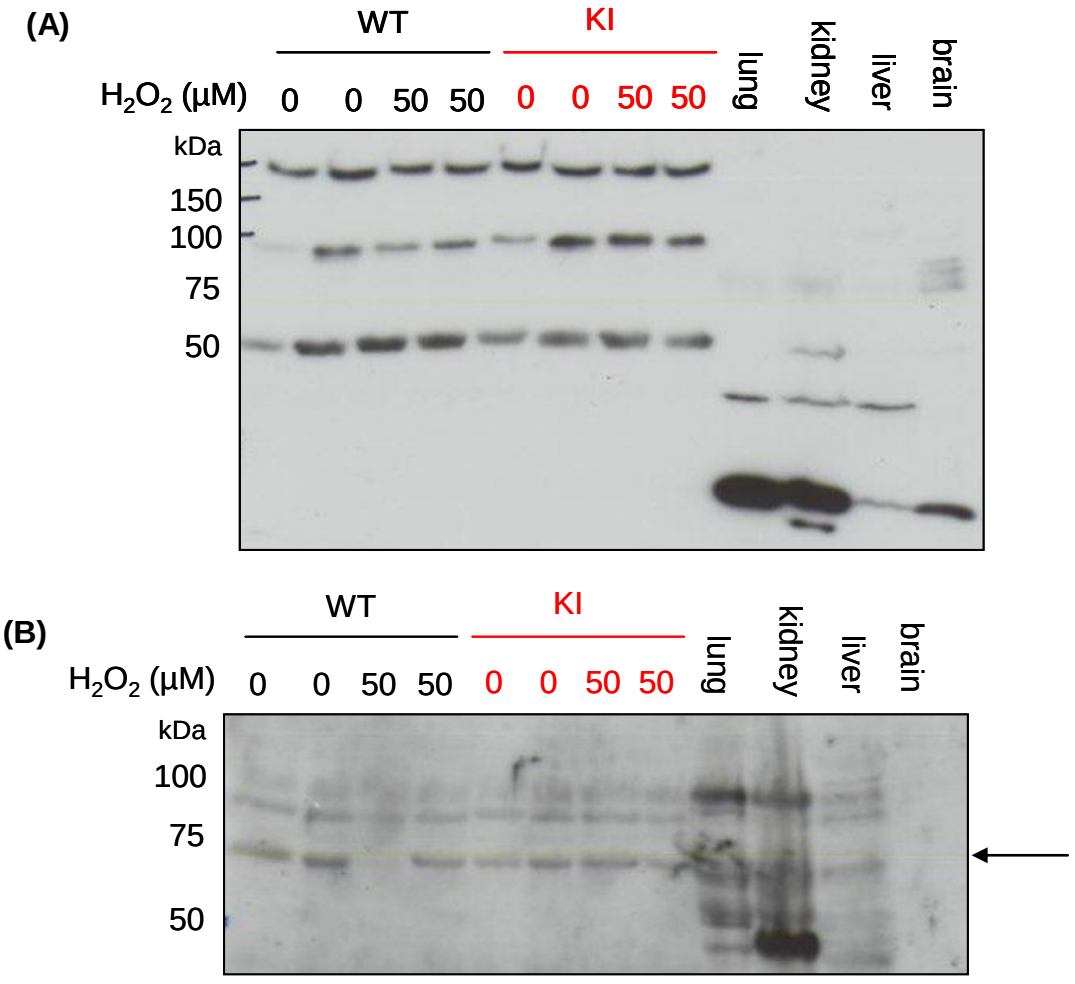

Figure 5.9 Immunoblot detection of D-AKAP2 in male WT and KI hearts.

(A) WT and KI hearts were Langendorff-perfused with K-HB or 50 μM H_2O_2 for 5 min. Western blots were probed for D-AKAP2 with antibody ab65038 which failed to detect a protein at the correct molecular weight (74 kDa) (B) Western blots were incubated with antibody sc-109188 which showed the presence of a band at ~74 kDa (indicated by the arrow) corresponding to D-AKAP2.

Screening for an antibody to AKAP220: Figure 5.10 shows that antibody sc6444 to AKAP220 detected a band at ~220 kDa in control as well as H_2O_2-perfused WT or KI hearts. This band was also observed in lung, kidney and liver, but not brain and corresponded to AKAP220. Therefore, this antibody was to be used in subsequent studies assessing the subcellular localisation of AKAP220 in WT and KI hearts.

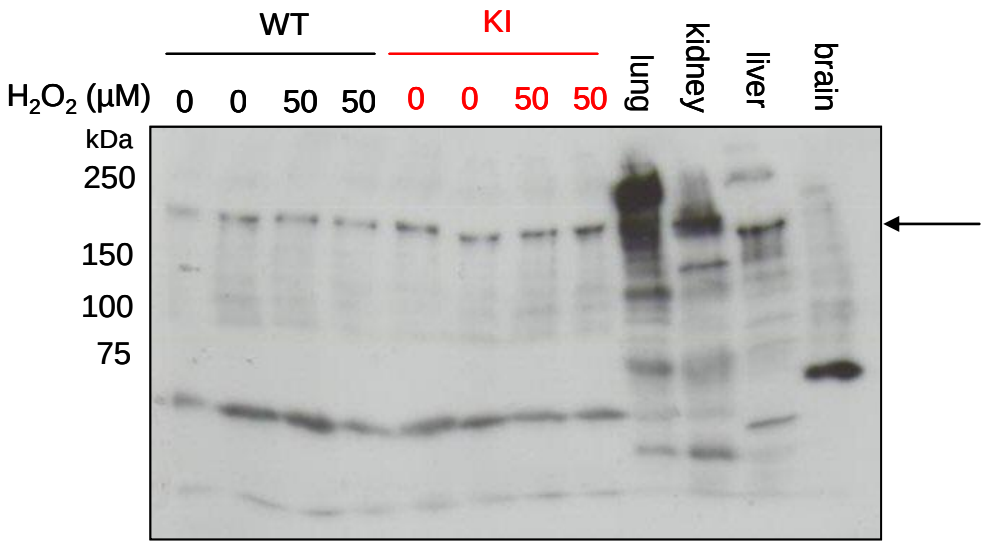

Figure 5.10 Immunoblot detection of AKAP220 in WT and KI hearts.

WT and KI hearts were Langendorff-perfused for 45 min with K-HB or 40 min with K-HB followed by 50 μM H_2O_2. After SDS-PAGE, the Western blot was probed for AKAP220 (L-16, sc6444). AKAP220 was detected in all hearts and lung, kidney and liver but not brain, as indicated by the arrow.

Screening for an antibody to α / β tubulin: Figure 5.11 shows that antibody #2148 detected a doublet at ~55 kDa corresponding to α (lower band) and β (upper band) tubulin in all organs. This antibody was used when probing blots for α / β tubulin.

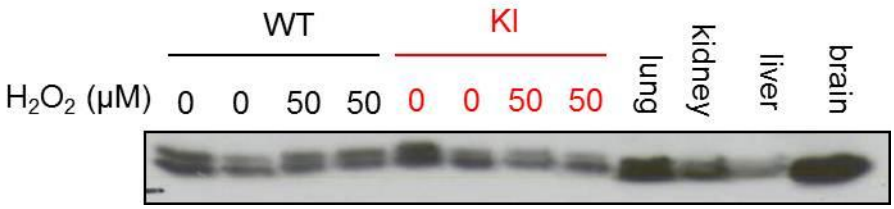

Figure 5.11 Immunoblot detection of α / β tubulin in male WT and KI hearts.

WT and KI hearts were Langendorff-perfused with K-HB or K-HB followed by 5 min H_2O_2. The Western blot was probed for α / β tubulin (antibody #2148). α (lower band) and β (upper band) tubulin were present in WT and KI hearts and lung, kidney, liver and brain.

5.3.4 Localisation of AKAPs in WT and KI hearts

Only binding of WT and KI RIα to AKAPs localised in the Triton X-100 soluble fraction of WT and KI hearts could be assessed using the cAMP affinity capture method. Figure 5.12A shows that D-AKAP1 was most abundant in the membrane-enriched fractions of WT and KI hearts with only small amounts in the cytosol- and myofilament- enriched fractions of hearts. In contrast, D-AKAP2 was most abundant in the cytosol-enriched fractions of untreated control or H_2O_2-perfused WT and KI hearts. A small amount of the D-AKAP2 localised to myofilament-enriched fractions with even less in membrane-enriched fractions (Figure 5.12B). AKAP220 was clearly most abundant in cytosol-enriched fractions of control WT and KI hearts and H_2O_2-perfused WT and KI hearts with small variable amounts in membrane- or myofilament-enriched fractions (Figure 5.12C). α / β tubulin was predominately in the cytosol- and myofilament- enriched fractions of control and H_2O_2-treated WT and KI hearts (Figure 5.12D). In summary, there were no differences in the localisation of any of these AKAPs between genotypes or between oxidant-treated and control untreated hearts.

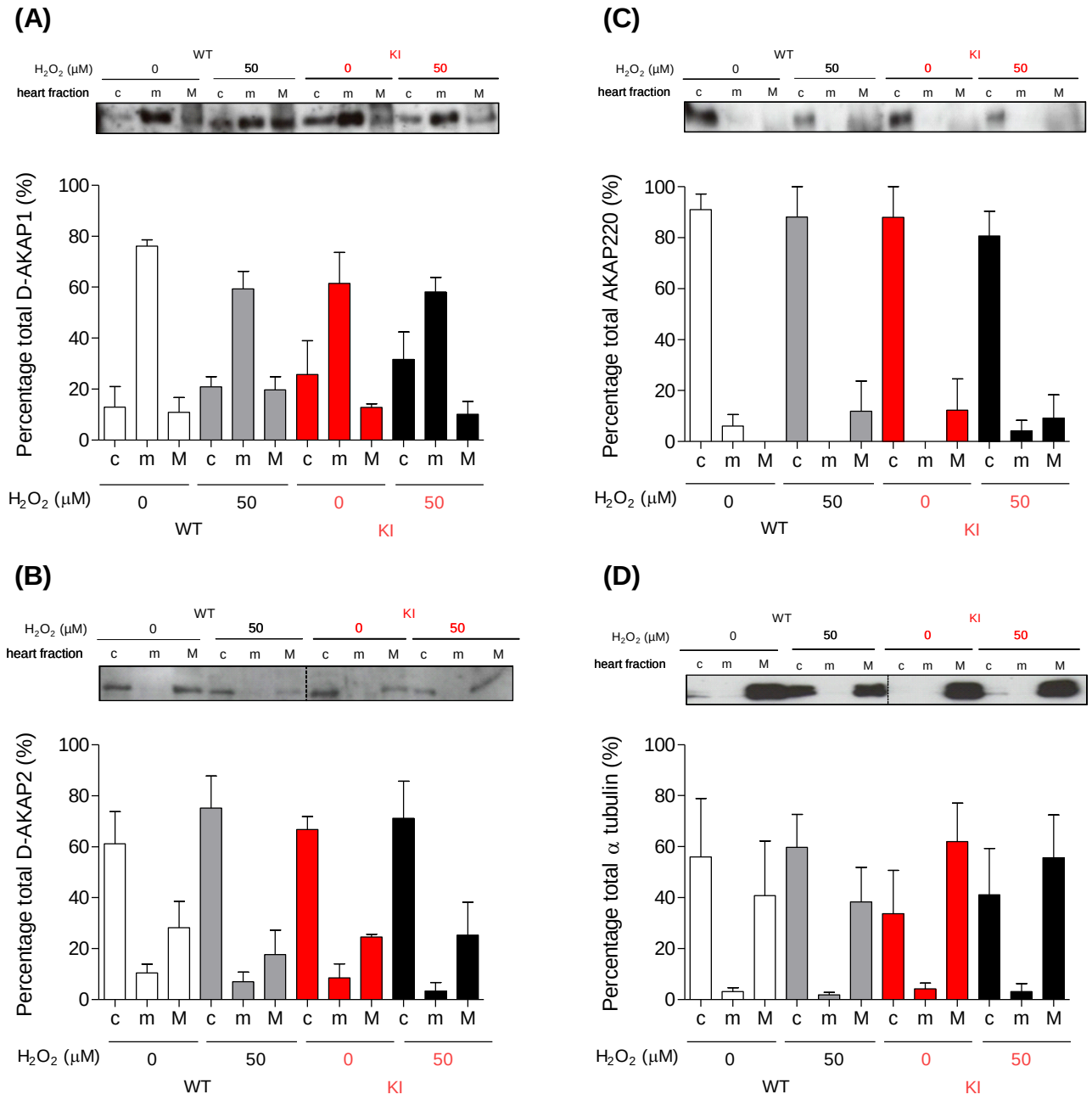

Figure 5.12 Subcellular localisation of selected AKAPs in WT and KI hearts.

(A) Hearts were Langendorff-perfused for 45 min with K-HB or 40 min with K-HB followed by 5 min with H_2O_2. They were fractionated into cytosol- (c), membrane- (m) and myofilament- (M) enriched fractions. After SDS-PAGE, Western blots were probed for D-AKAP1 as shown in the representative blot. Percentage of total AKAP in each fraction (n=3) ± SEM was calculated (B) Western blots were probed for D-AKAP2 (C) Western blots were probed for AKAP220 (D) Western blots were probed for α / β tubulin. All of these AKAPs were present in the cytosol- or membrane-enriched fractions of WT and KI hearts so their binding to RIα could be assessed using the cAMP affinity capture method.

5.3.5 Role for disulfide in modulation of AKAP binding to RIα

Pilot study to determine whether RIα and R-bound AKAPs were 'captured': The cAMP affinity capture was considered successful if RIα abundance was higher in *capture* samples than *input* samples, with *flow-through* being depleted of RIα. RIα in the *input* sample (Figure 5.13A) was monomeric (reduced) in untreated WT heart and shifted almost completely to disulfide dimer with H_2O_2 treatment. In untreated control and H_2O_2-treated KI hearts RIα was only present in its reduced monomeric form, as expected. No RIα was present in *flow-through* samples and RIα signal intensity for all *capture* samples was higher than for their corresponding *input* sample, demonstrating the cAMP affinity capture had worked efficiently. The redox state of control *capture* RIα was the same as the *input* sample so overnight incubation of heart homogenate with cAMP-agarose in air did not oxidise WT RIα. However, an increase in monomeric RIα was observed in the oxidant-treated WT *capture* sample compared to *input* which lowered percentage disulfide dimer to ~50 % which was unexpected. In addition, more RIα was observed in the H_2O_2-treated KI heart compared to the other hearts, which would make any differences in AKAP binding between this sample and others difficult to analyse. However, this was not a reproducible result. A colloidal Coomassie stained polyacrylamide gel containing these *capture* samples revealed only a couple of faint bands in KI *capture* samples at ~50 kDa (Figure 5.13B, indicated by arrows). Therefore, the protocol needed to be optimised so that more proteins bound to RI / RII might be detected by colloidal Coomassie staining.

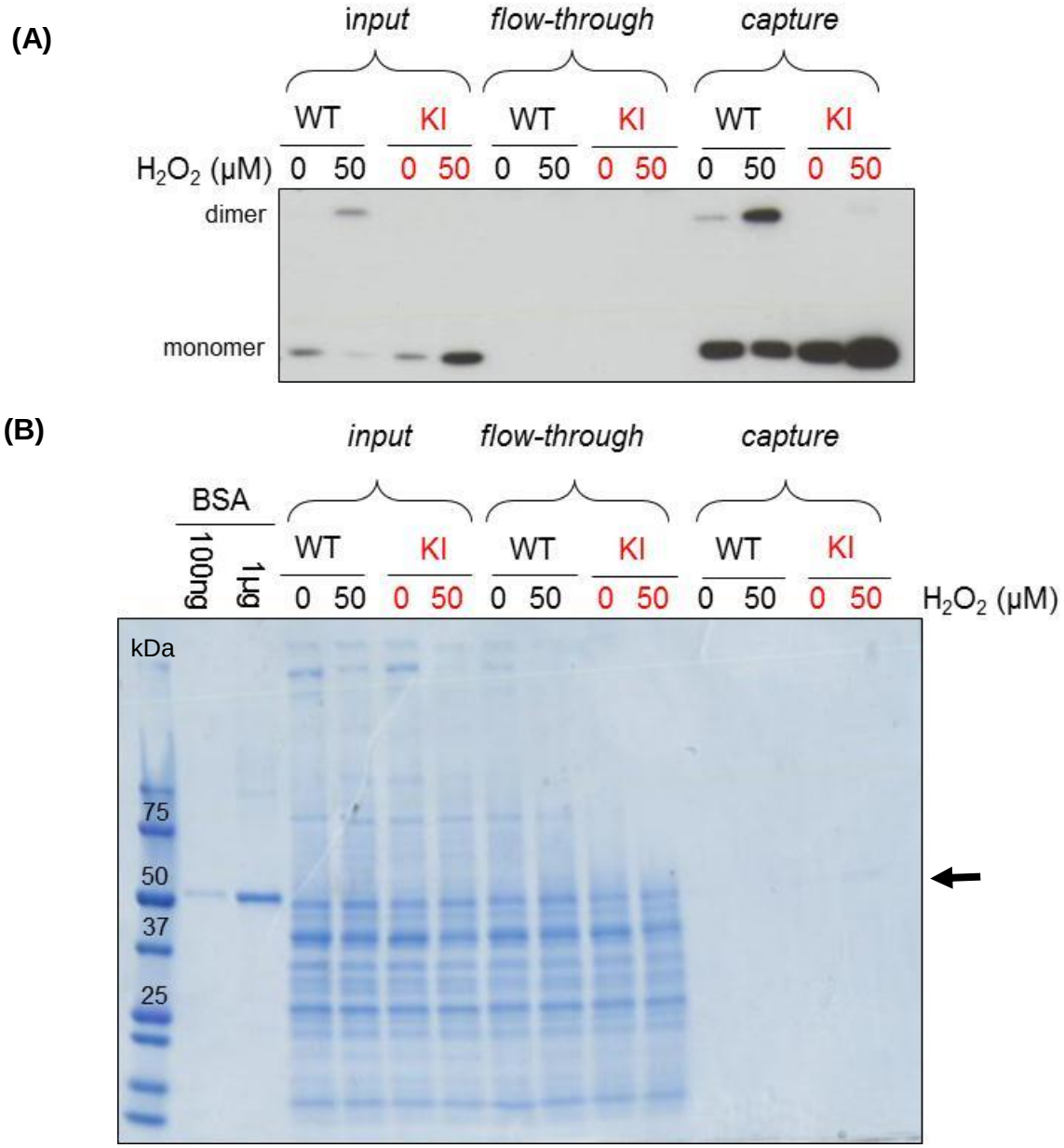

Figure 5.13 cAMP affinity capture of PKA RIα.

(A) The Triton X-100 soluble fraction of WT and KI hearts (Langendorff-perfused with K-HB or 50 μM H_2O_2) was incubated with 8-AEA-cAMP-agarose. Western blotting and probing for PKA RIα demonstrated that RIα was captured. (B) *Capture* samples were run on a gradient gel and the gel was stained with colloidal Coomassie to show proteins that were bound to RI / RII. However, only two bands were identified (indicated by arrow) and were not very abundant, generating less signal than the staining achieved by the 100 ng bovine serum albumin (BSA) standard.

'Capture' of RIα and R-bound proteins after optimisation of the method: The total volume of Triton X-100 soluble heart fraction and the volume of 8-AEA-cAMP-agarose were increased with the aim of enhancing capture and detection of candidate proteins by colloidal Coomassie staining and specific antibodies. In control WT *input*, RIα was ~46 % dimer and with H_2O_2 treatment this percentage increased to ~59 % (Figure 5.14A). This change was not as large as expected based on previous experiments (for example in Figure 5.13). In KI *input* samples no disulfide dimer at all was present, which was expected. The modified capture method was still efficient as there was no RIα present in *flow-through* samples. After a 15 min film exposure time, it was evident that there was no disulfide dimer present at all in 50 μM H_2O_2-perfused KI *capture* but, unexpectedly, there was a small amount in control KI *capture*. It was difficult to see any difference in RIα disulfide dimerisation with H_2O_2 in WT hearts but after a shorter film exposure time (10 secs), control WT *capture* had ~13 % disulfide dimer and with H_2O_2 treatment this increased to ~41 %, which was a bigger difference than seen in *input* samples. Abundance of RIα monomer appeared to stay the same with H_2O_2 treatment in *capture* WT samples as observed in the previous experiment. The redox state of RIα was as expected in all *capture* samples so a comparison of AKAP binding could be performed between samples. Another important aspect of the solid-phase cAMP studies was the possibility that AKAPs might be captured as determined by immunoblotting. This would also allow me to assess whether there were differences in AKAP binding to WT or KI RIα and whether oxidation to the disulfide modulated this. Figure 5.14B shows that D-AKAP1 was only just detectable in *input, flow-through* and *capture* samples so any differences between genotypes could not be observed. D-AKAP2 and AKAP220 were not detected in any of the samples. The Triton X-100 soluble fraction was diluted 5-fold before incubation with the 8-AEA-cAMP-agarose overnight so this dilution would explain why the AKAPs were not detected in these samples, but were in Figure 5.12. α / β tubulin was present in the *input* samples and *flow-through* samples, but were absent from *capture* samples suggesting that RI / RII did not bind to α / β tubulin. *Capture* samples were also run on a polyacrylamide gel which was then colloidal Coomassie-stained to reveal proteins bound to RI / RII. Figure 5.14C shows that some proteins were detected in the *capture* samples at amounts of ~100 ng or less.

The most prominent band was at ~50 kDa, which was probably RIα and some bands were seen below 50 kDa but were very faint so the changes to the protocol did not significantly improve detection of regulatory subunit-bound proteins by Coomassie staining.

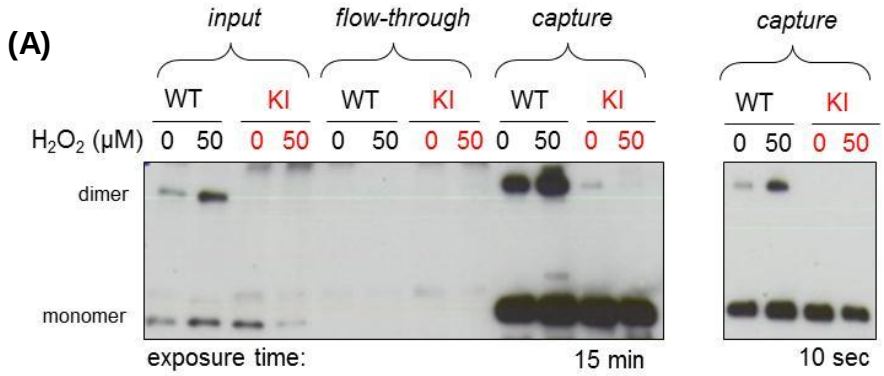

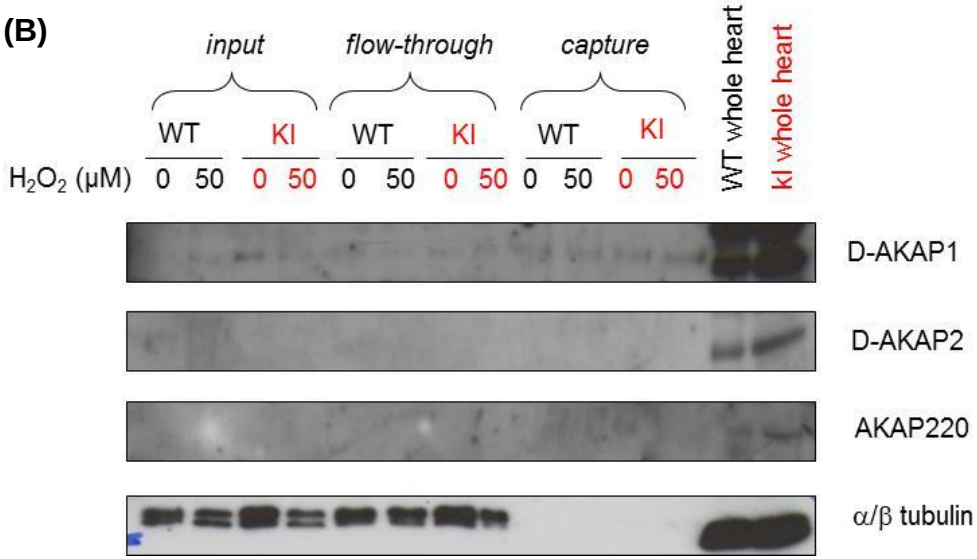

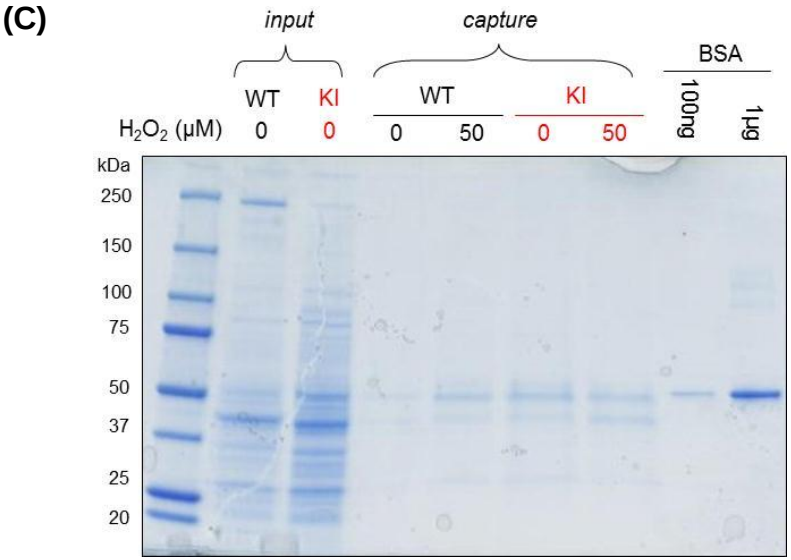

Figure 5.14 cAMP affinity capture of PKA RIα.

(A) The Triton X-100 soluble fraction of WT and KI hearts Langendorff-perfused for 45 min with K-HB or 40 min with K-HB followed by 5 min with 50 μM H_2O_2 were incubated with 8-AEA-cAMP-agarose. The success of the capture was shown by SDS-PAGE followed by Western blotting and probing for PKA RIα. (B) Samples were also probed for D-AKAP1, D-AKAP2, AKAP220 and α / β tubulin. α / β tubulin and D-AKAP1 were detected in the *input*, *flow-through* and *capture* samples. (C) The *capture* samples were also concentrated down and run on a gradient gel which was then stained with colloidal Coomassie. Faint bands were observed in all samples.

'Capture' of RIα and R-bound proteins after further optimisation of the method: The total volume of Triton X-100 soluble heart fraction and the volume of 8-AEA-cAMP-agarose were increased with the aim of enhancing the capture (and therefore detection of candidate proteins as assessed by immunoblotting) that leads into proteomic studies.

In Triton X-100 soluble *input* samples (Figure 5.16A) RIα was present as ~35 % disulfide dimer in control WT and ~40 % disulfide dimer in H_2O_2-treated WT. As expected, KI RIα was 100 % monomer in control and H_2O_2-treated *input* samples. RIα was absent from the *flow-through* samples. RIα redox state in *capture* samples was similar to that for *input* samples, but a faint band was detected at ~100 kDa in KI hearts. To determine if this was a PKA catalytic subunit (42 kDa) bound to a PKA RIα subunit (50 kDa) the blot was probed with an antibody specific for PKA catalytic subunit (Figure 5.16B). The antibody indeed detected a band at ~100 kDa in the *capture* samples, which may provide some evidence for this complex forming between the RIα subunit and a catalytic subunit. Blots were also probed for specific candidate AKAPs (Figure 5.16A). D-AKAP1 was present in all *input* samples but abundance was lower in control WT compared to other samples. There was no D-AKAP1 in the *flow-through* suggesting this protein bound to RI / RII and *capture* samples suggest that D-AKAP1 bound to the regulatory subunit in H_2O_2-treated WT, control KI and H_2O_2-treated KI hearts. However, there was no evidence for D-AKAP1 binding to the regulatory subunit in control WT heart but this was probably because of the lower abundance of D-AKAP1 in the control WT *input* sample. Despite this, these results suggest that RIα disulfide is not involved in D-AKAP1 binding as the amount of D-AKAP1 pulled out was similar in H_2O_2-treated WT and H_2O_2-treated KI *capture* samples. D-AKAP2 and AKAP220 were present in *flow-through* samples but not *capture* samples suggesting that these AKAPs did not bind RI / RII. However, the band intensities for potential D-AKAP2 and AKAP220 were weak and limit confidence in them being RI / RII AKAPs, although of course we know from the literature that they are indeed RI / RII binding proteins. α / β tubulin was detected well in *input* samples and was present in *flow-through* samples suggesting α / β tubulin is not an RI / RII AKAP, consistent with results in Figure

5.14B. Colloidal Coomassie staining revealed a number of proteins bound to RIα (Figure 5.16B); more than identified in Figure 5.14C. Again, a prominent band was seen at ~50 kDa, which was probably PKA RIα and other prominent bands (more than 100 ng) were seen at ~25 kDa, ~37 kDa and ~150 kDa.

Overall increasing the volume of Triton X-100 soluble fraction and 8-AEA-cAMP-agarose did increase detection of some selected AKAPs by antibodies and proteins bound to RI / RII by colloidal Coomassie staining but the results were still inconsistent so a more sensitive method was required.

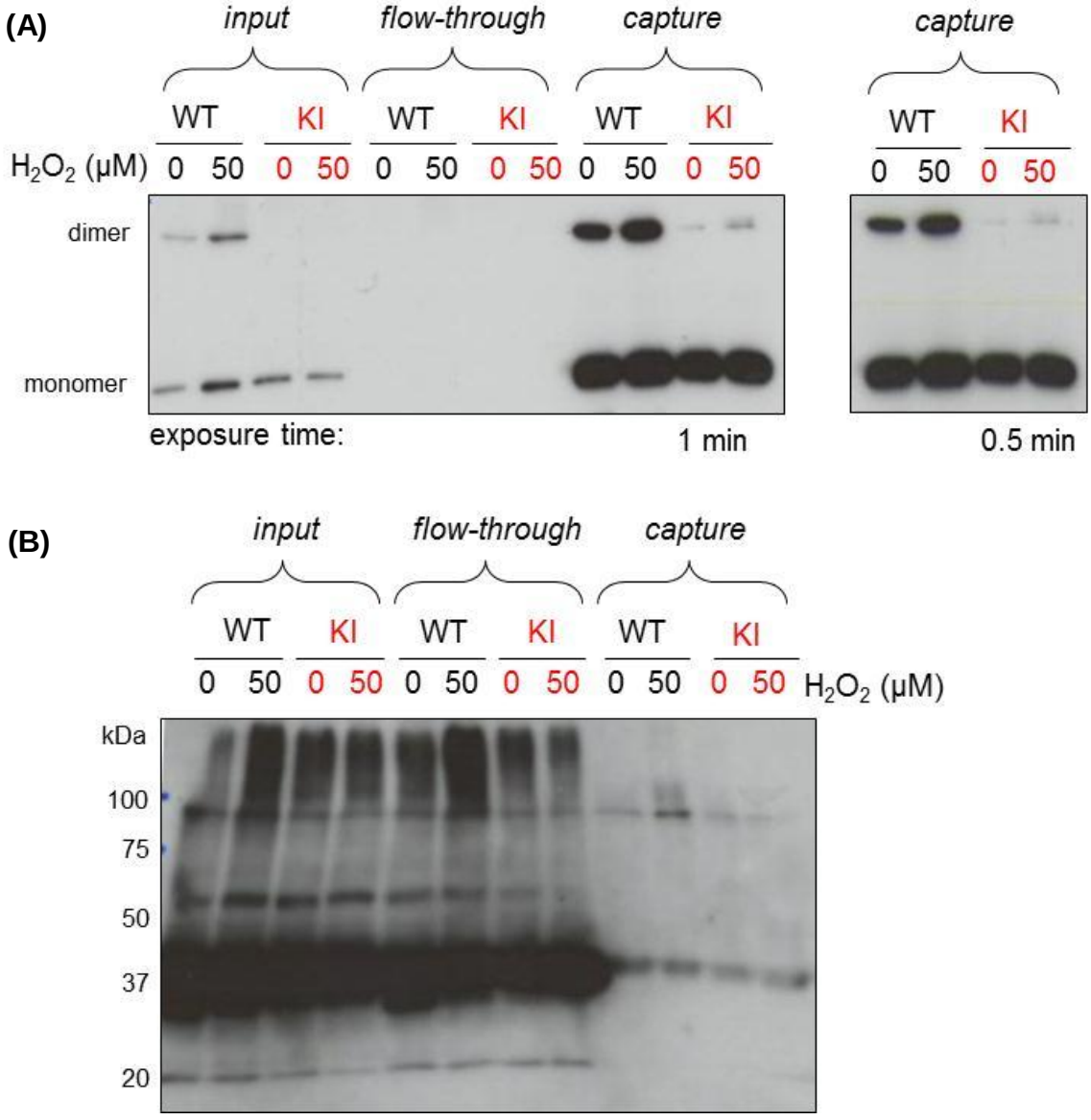

Figure 5.15 cAMP affinity capture of PKA RIα.

(A) 8-AEA-cAMP-agarose was incubated with the Triton X-100 soluble fraction of WT and KI hearts Langendorff-perfused with K-HB or 50 μM H_2O_2. Western blotting and probing for PKA RIα showed that RIα was captured. (B) Western blots were incubated with a PKA catalytic subunit antibody to show a band at 100 kDa which could be an RIα-catalytic subunit complex.

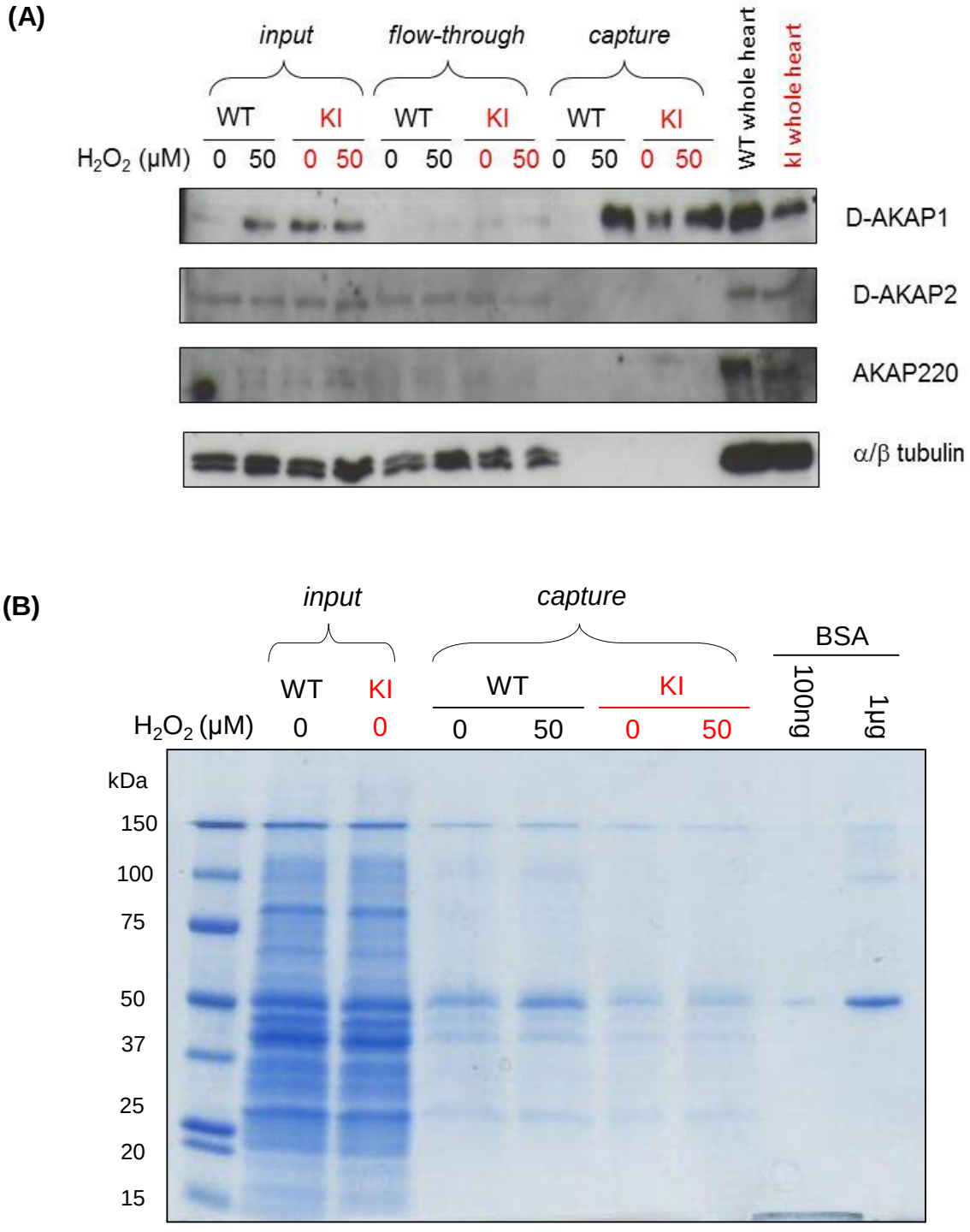

Figure 5.16 cAMP affinity capture of PKA RIα.

(A) Western blots were probed for D-AKAP1, D-AKAP2, AKAP220 and α / β tubulin to see if these were captured. Only D-AKAP1 was identified in *capture* samples (B) *Capture* samples were also run on a gradient gel which was then stained with colloidal Coomassie but only faint bands were identified in all *capture* samples.

5.3.6 Proteomics analysis by LC-MS/MS

Preparation of colloidal Coomassie stained gel bands for analysis by LC-MS/MS: Figure 5.16B shows only a few weakly-stained bands and certainly the pattern is virtually identical between groups and so staining provides no evidence that RIα redox state modulates the presence of RIα binding proteins such as AKAPs. Proteomic methods are hampered by the high abundance proteins, that are often non-specific proteins or proteins that bind but are not modulated by RIα oxidation state. However, it is possible that there is a sub-proteome 'below' these dominant bands that cannot be detected by Coomassie. As LC-MS/MS is more sensitive, it may be used to detect and identify these proteins. If this could be achieved the samples could be re-analysed using immunoblotting to examine the relative abundance of these proteins. Indeed the MS provides some information about the abundance of these proteins, as measured by spectral counting. Figure 5.17 shows the bands cut out of the colloidal Coomassie stained gel (previously shown in Figure 5.16B) for analysis by LC-MS/MS. As already stated, there were only a few prominent bands stained on the gel and due to restrictions on the length of time the mass spectrometer could be used for, areas of the gel where these stained bands could be observed were prioritised for analysis.

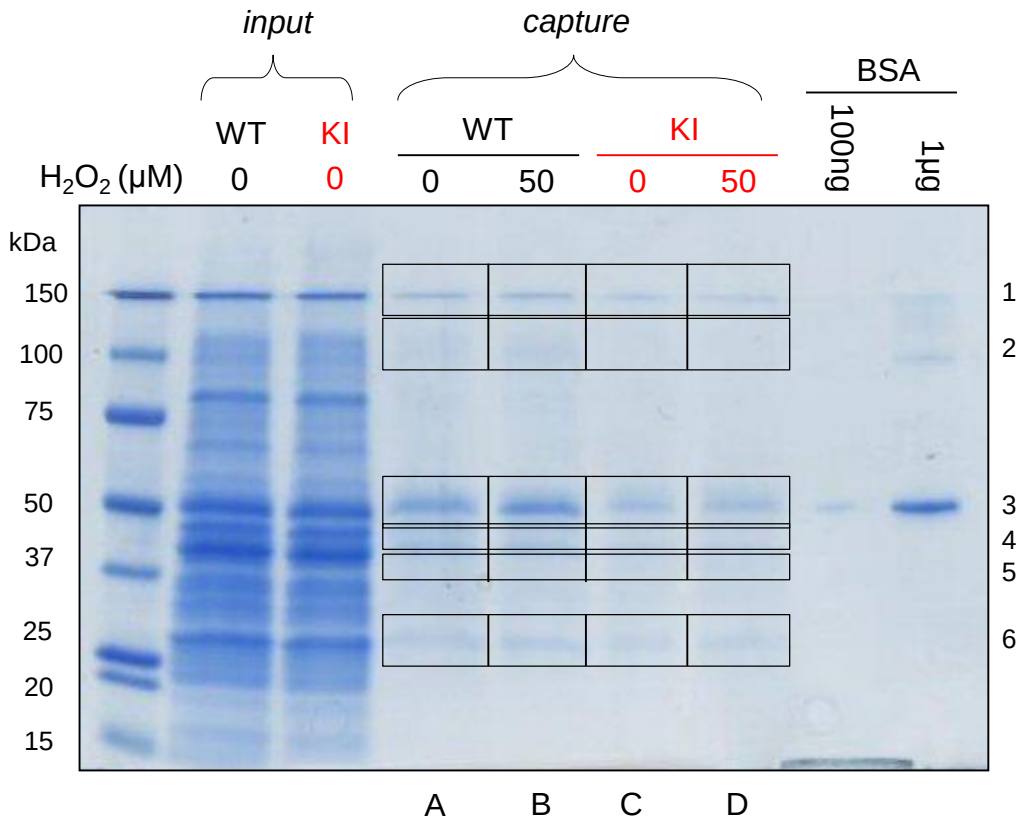

Figure 5.17 Bands cut out of a colloidal Coomassie stained gel to be analysed by LC-MS/MS.

Capture samples were run on a SDS polyacrylamide gradient gel which was stained with colloidal Coomassie. The bands cut out are outlined and were labelled according to which lane (A, B, C or D) and molecular weight level (1, 2, 3, 4, 5 or 6) they were cut from. A total of twenty-four bands were cut out and proteins in these bands were identified by LC-MS/MS.

RI / RII-binding proteins identified by LC-MS/MS: LC-MS/MS identified 158 RI / RII binding proteins (see Appendix A). The data was also analysed for any proteins in which there was a trend for the spectral count to increase or decrease with H_2O_2 in WT but not KI, as shown in Appendix B. A Fishers Exact test was performed to identify statistically significant differences ($p<0.05$) in the abundance of the identified proteins between WT and KI *captures*. Appendix C summarises the proteins of which abundance was significantly different between WT and KI *captures*. Finally, Table 5.3 below summarises some of these proteins that are of particular interest due to their potential association with PKA or an AKAP as described in the literature. Very long chain specific acyl-CoA dehydrogenase, SERCA2, ChChd3, alpha-enolase, D-AKAP1 and D-AKAP2 were proteins of particular interest.

Genotype/ treatment	WT vs KI	WT	WT H_2O_2	KI	KI H_2O_2			
Identified protein	**Fishers Exact Test (p value)**	**A**	**B**	**C**	**D**	**Function**	**Substrate for PKA?**	**AKAP association?**
Alpha-enolase	0.013	12	12	9	3	glycolysis enzyme	no but it is phosphorylated by Src,[300] which is a PKA substrate (Ser17).[301]	in a complex with myomegalin isoform 4 (an AKAP) and PKA RI.[302] Src signalling is linked to D-AKAP1.[262]
ChChd3	0.024	13	13	5	8	forms protein complexes important in maintaining crista architecture and protein import.[295]	yes (Thr10).[294]	interacts with SKIP which is an RI AKAP.[293]
D-AKAP2	0.27	0	13	6	8	anchoring protein for PKA	No	yes (see 5.1.2)
D-AKAP1	0.25	12	23	18	18	anchoring protein for PKA	No	yes (see 5.1.2)
SERCA2	3.7E-06	81	74	97	122	Ca^{2+}-ATPase, regulates Ca^{2+} entry into the sarcoplasmic reticulum.	no but it is inhibited by PLB which is a PKA substrate (Ser16).[174]	in a complex with PKA RIIα, AKAP18 and PLB.[226]
Very long-chain specific acyl-CoA dehydrogenase, mitochondria	0.00039	8	4	17	16	fatty acid β oxidation and lipid metabolism	yes (Ser586).[303]	No

Table 5.3. Proteins of particular interest identified by LC-MS/MS.

The table shows the number of assigned spectra for each protein in *capture* samples from control or 50 µM H_2O_2-perfused (5 min) WT or KI hearts. p values are given for a Fishers Exact test comparing WT and KI hearts (statistically significant if $p<0.05$). The function of each protein, whether it is a PKA substrate or associated with a PKA substrate and whether it is an AKAP or associated with an AKAP are also described.

5.3.7 Determining whether disulfide modulates RIα binding to candidate proteins identified from LC-MS/MS

SKIP, ChChd3 and RIα complex: ChdChd3, a protein identified in LC-MS/MS, is a novel substrate for PKA,[294] that has been identified in a complex with SKIP and RI.[293] SKIP is an AKAP for Type I PKA and present in the heart.[292, 293] The spectral count for ChChd3 in WT *capture* samples was significantly higher than for KI *capture* samples suggesting more ChChd3 was captured in the WT than KI samples. Therefore, RIα disulfide could be important in binding of RIα to SKIP, potentially serving to position PKA close to ChdChd3 to enable targeted phosphorylation.

An antibody to SKIP was required in order to determine its subcellular localisation in the heart and to determine a potential association with RIα and ChChd3. Antibody GTX101952 detected a protein at ~183 kDa consistent with the predicted molecular weight of SKIP, but there were several additional non-specific bands present (Figure 5.18A). Antibody GTX101951 detected proteins at ~80 kDa and ~183 kDa in cardiac samples, the latter being consistent with the detection of SKIP (Figure 5.18B). Therefore, GTX101951 was the chosen antibody when probing blots for SKIP as there were less non-specific bands that could complicate detection of SKIP at 183 kDa.

SKIP was present in the Triton X-100 insoluble fraction and ChChd3 was present in the Triton X-100 soluble fraction of WT and KI hearts (Figure 5.19). This is consistent with the LC-MS/MS identification of ChChd3 in Triton X-100 soluble *capture* samples. There was also a hint of more ChChd3 in the Triton X-100 insoluble fraction of WT hearts exposed to H_2O_2 but fractionation of WT and KI hearts revealed that SKIP was only present in the myofilament-enriched fraction of H_2O_2-treated WT hearts even after long film exposures times. ChChd3 was predominately localised in membrane-enriched fractions and only after long film exposures times were small amounts observed in cytosol- and myofilament-enriched fractions (Figure 5.20). Therefore, SKIP and ChChd3 may potentially interact with disulfide RIα in the myofilament (but not reduced monomeric RIα as this is not present in the myofilament (Figure 5.6)).

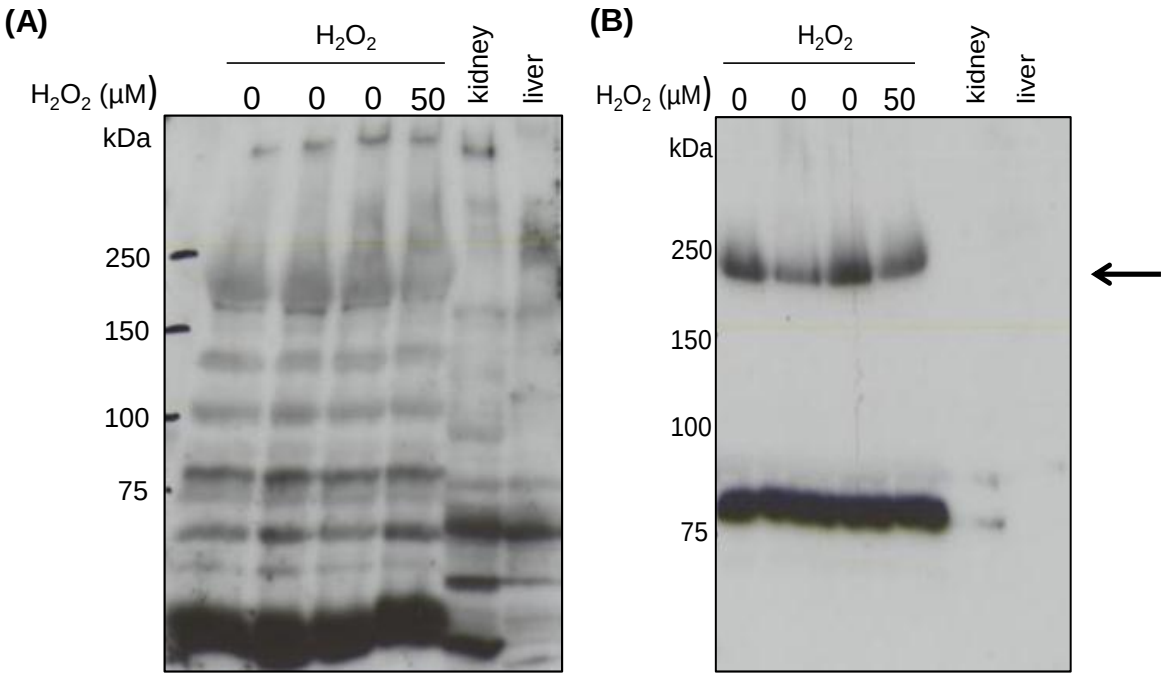

Figure 5.18 Screening for an antibody to SKIP.

(A) WT hearts were Langendorff-perfused for 45 min with K-HB or 40 min with K-HB followed by 5 min with 50 μM H_2O_2. A Western blot was probed for SKIP with antibody GTX101952. This detected a protein at ~183 kDa corresponding to SKIP but also a lot of non-specific bands (B) A Western blot was incubated with SKIP antibody GTX101951 which detected a significant band at ~183 kDa (indicated by the arrow) corresponding to SKIP and was the antibody of choice when now probing for SKIP.

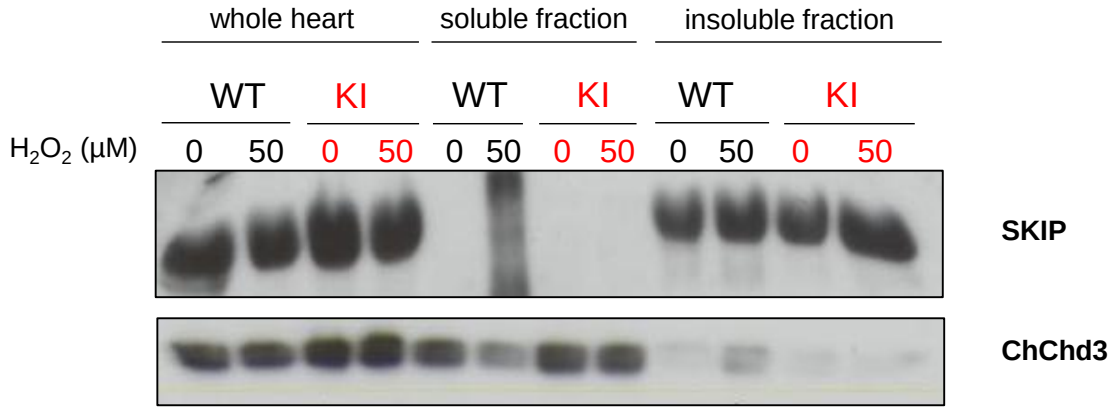

Figure 5.19 Localisation of SKIP and ChChd3 in WT and KI hearts.

Langendorff-perfused (K-HB for 45 min or K-HB for 40 min followed by 50 μM H_2O_2 for 5 min) WT and KI hearts were homogenised, separated into Triton X-100 soluble and Triton X-100 insoluble fractions and added to SDS sample buffer. SDS-PAGE and Western blotting were performed and blots were probed for SKIP or ChChd3. SKIP was only present in the insoluble fraction and ChChd3 was predominately in the soluble fraction.

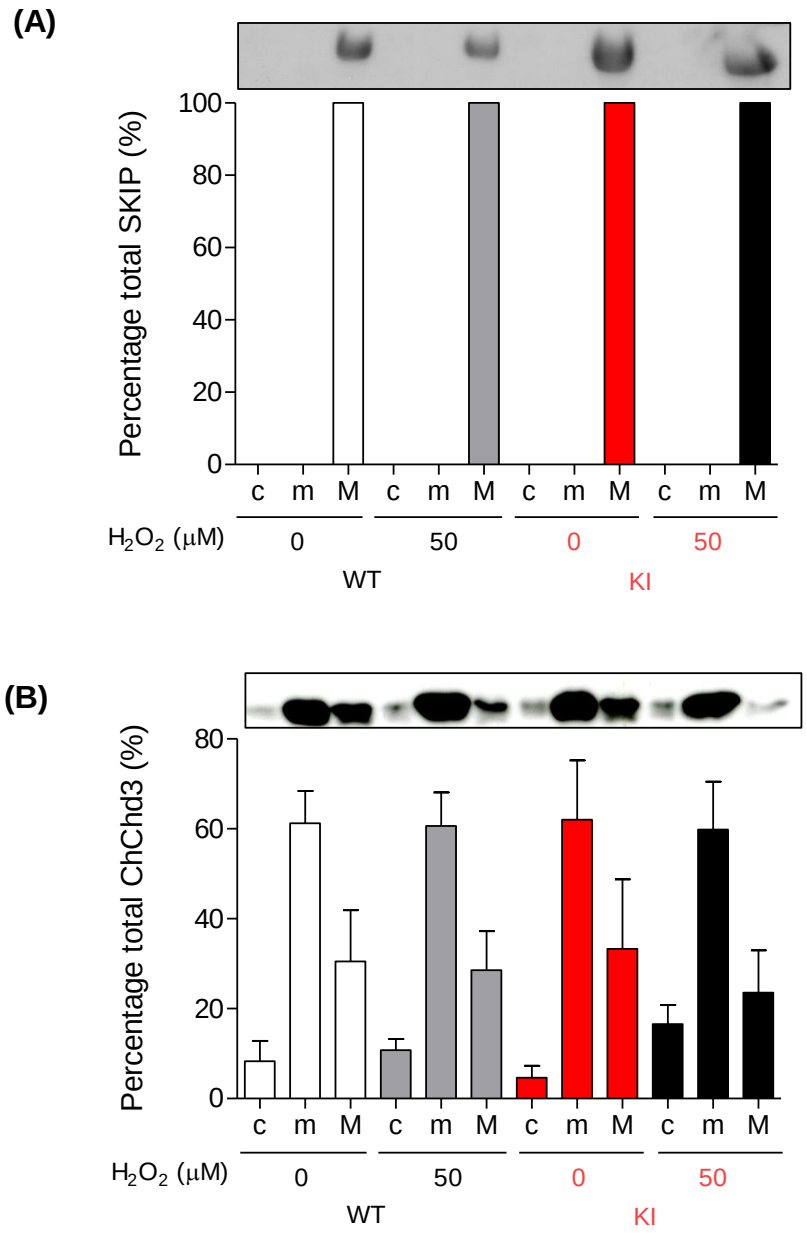

Figure 5.20 Localisation of SKIP and ChChd3 in WT and KI hearts.

(A) Langendorff-perfused WT and KI hearts were fractionated into cytosol-, membrane- and myofilament- enriched fractions. Western blots were probed for SKIP as shown in the representative blot. Average percentage of total SKIP in each fraction was calculated for n=3 hearts ± SEM. (B) Western blots were probed for ChChd3, as shown in the representative blot. Average percentage of total ChChd3 in each fraction was calculated for n=3 hearts ± SEM. SKIP was only present in the myofilament-enriched fraction and ChChd3 was mainly in the membrane.

Alpha-enolase, myomegalin and RIα complex: Human isoform 4 of myomegalin is an AKAP that associates with PKA RIα and RIIα as well as cardiac troponin I (cTnI), alpha-enolase (enolase 1) and enolase 2.[302] LC-MS/MS (by spectral counting) revealed alpha-enolase was significantly more abundant in WT than KI *capture* samples. Therefore myomegalin (isoform 4) could serve to localise PKA RIα with alpha-enolase, a process that could be regulated by RIα disulfide status altering its interaction with myomegalin. LC-MS/MS did not identify myomegalin but I found myomegalin (isoform 4, molecular weight of 267 kDa) was predominately localised in the myofilament-enriched fraction (Triton X-100 insoluble fraction) of hearts (Figure 5.21) which may explain this. There is potential for oxidation status of RIα to modulate its binding to myomegalin, as RIα is only present in the myofilament in WT hearts and not KI hearts (Figure 5.6). However, results suggest myomegalin, RIα and alpha-enolase cannot associate as LC-MS/MS revealed alpha-enolase was in the Triton X-100 soluble fraction when myomegalin is in the Triton X-100 insoluble fraction.

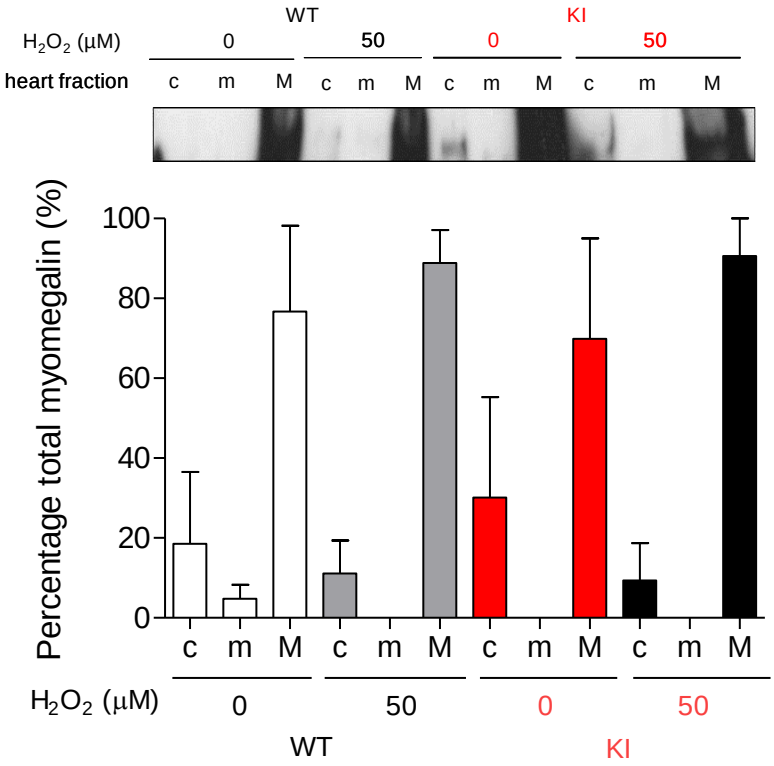

Figure 5.21 Myomegalin localisation in WT and KI hearts.

WT and KI hearts were Langendorff-perfused with K-HB or 50 μM H_2O_2. Western blots were incubated with myomegalin antibody (GeneTex) as shown in the representative blot. Average percentage of total myomegalin in each fraction was calculated for n=3 hearts ± SEM. Myomegalin was predominately localised in myofilament-enriched fraction of all hearts.

5.4 DISCUSSION

This chapter focused on the role of RIα disulfide in modulating binding to AKAPs and determining RIα localisation. As the disulfides that can form in RIα precisely flank the AKAP-binding domain of the kinase, I thought it is highly likely that the interaction between RIα and the AKAP will be modulated by disulfide formation. Heart fractionation and immunoblotting studies demonstrated that RIα was mostly cytosolic and this was regardless of its redox state. This is consistent with the historical view that RIα is soluble and cytosolic,[304] with the RII isoforms being in the particulate fraction due to association with AKAPs.[239, 240] The percentage RIα disulfide in WT hearts basally was higher than expected based on previous work,[57] and Western blots in Chapter 4 illustrating basal disulfide abundance in WT hearts but this may be a partial over-estimation due to the long film exposure times required to detect RIα in other fractions of the heart.

Others have also observed RI in the membrane fraction of cardiac ventricular tissue,[305] and associated with the cardiac myocyte sarcolemma.[306] A small amount of RIα was present in the membrane-enriched fraction of WT and KI hearts basally. Boeshans *et al.*,[307] used MS to determine whether RIα is membrane-associated because of a post-translational modification such as palmitoylation, which is the covalent attachment of fatty acids to Cys, Ser or threonine residues.[308] They concluded that there were no structural differences between cytosolic and membrane associated RIα that could explain the membrane localisation rather than cytosolic localisation of RIα. They did discover that membrane-associated RIα had a higher abundance of disulfide than cytosolic RIα. This is consistent with more RIα monomer than disulfide dimer in the cytosol and mostly disulfide dimer in the membrane of WT hearts. However, I found that KI heart tissue also had monomeric RIα in the membrane but this could be non-specific as the membrane-enriched fraction was not washed after separation from the cytosol-enriched fraction so there could be a small amount of RIα remaining from the cytosol fraction.

Increased localisation of PKA RIα at membrane and myofilament was associated with increased PKA RIα disulfide in response to oxidant and suggested translocation. It appears that only disulfide dimeric RIα can translocate to the membrane (consistent with Boeshans *et al.*,[307]) or myofilament. Translocation of RIα to the membrane- and myofilament-enriched fractions in response to H_2O_2 has been observed by others in rat hearts.[57] Peroxiredoxins (Prxs), which like PKA RIα form double disulfides during oxidative stress, also translocate from cytosol to membrane in response to H_2O_2, with Prx peroxidative thiol hyperoxidation to the sulfinate state causing translocation to the myofilament.[309]

The PKA catalytic subunit has been shown to translocate to the nucleus.[310, 311] I did not observe catalytic subunit translocation concomitant with RIα disulfide dimer to the myofilament. However, I have evidence to suggest that catalytic subunit translocated to the membrane in response to oxidant. Western blotting analysis suggested that the catalytic subunit translocated from the myofilament to the membrane, however. This is inconsistent with RIα translocation, which was from cytosol to membrane. When RIα and the catalytic subunit are both localised in the membrane they may first associate to form the inactive PKA tetramer. Following disulfide dimer formation there may be an increase in RIα affinity for membrane-associated AKAPs which may serve to position the PKA tetramer close to its substrates for substrate-induced sensitisation of PKA to cAMP, of which I have provided some evidence in Chapter 4 (Figure 5.22). This would increase release of catalytic subunits from the PKA tetramer leaving AKAP bound RIα. Others have shown that membrane-associated RI is unbound to catalytic subunit,[305, 306] which would support this hypothesis. I would therefore expect increased phosphorylation of membrane-associated PKA substrates with H_2O_2. However, as discussed in Chapter 4, increased phosphorylation of membrane-associated PKA substrates such as phospholemman (PLM) and PLB was not observed in oxidant-perfused WT hearts. Disulfide may also *reduce* RIα affinity for some AKAPs, which may explain the significant reduction in PLB phosphorylation observed in oxidant-treated WT hearts, as discussed further below. In addition, binding of RIα to some

AKAPs may not be altered by disulfide as may be the case for the membrane-associated substrate, PLM, the phosphorylation state of which was not altered by H_2O_2.

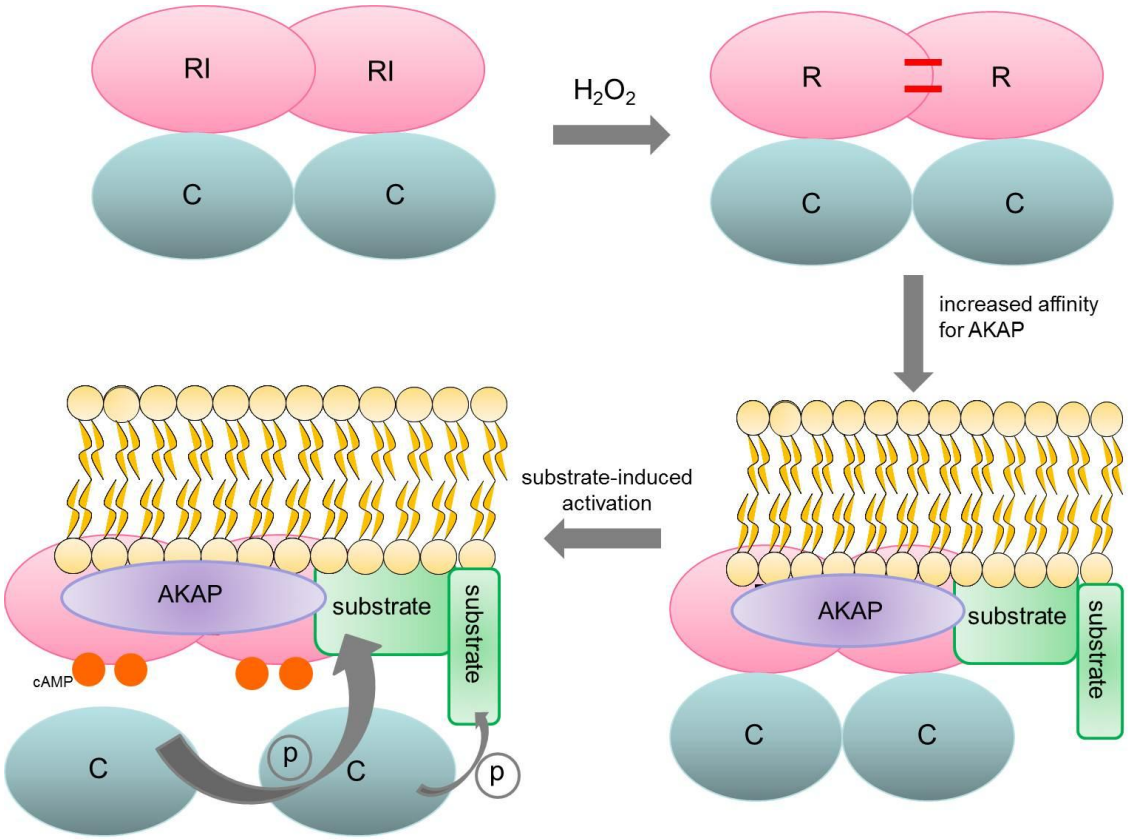

Figure 5.22 Schematic of substrate-induced PKA activation.

RIα disulfide may increase affinity of RIα for AKAPs causing translocation of PKA from the cytosol and targeting of PKA close to its substrates where substrate can sensitise PKA to cAMP. Upon cAMP binding to regulatory subunits, catalytic subunits are released and can phosphorylate target substrate.

I found that AKAP220 was predominately a cytosol-associated AKAP which agrees with another study,[274] but another study shows that it is membrane-associated.[273] I also demonstrated that D-AKAP2 was predominately cytosolic with a small amount in the membrane and others have also shown that D-AKAP2 is primarily cytosolic but can associate with membranes of endosomes,[265] and is also mitochondrial.[312] I observed a high abundance of α / β tubulin in the cytosol which is consistent with another study illustrating that α / β tubulin is cytosolic.[313] I demonstrated that D-

AKAP1 was predominately membrane-associated with small amounts in the cytosol in WT or KI hearts which agrees with a study showing D-AKAP1 is on the cytosolic surface of the mitochondrial membrane.[252] It is likely that RIα predominately binds to cytosol-associated AKAPs such as AKAP220, D-AKAP2, α / β tubulin or D-AKAP1 under control conditions as it is predominately localised in the cytosol. A smaller amount of RIα may also bind to membrane-associated AKAPs such as D-AKAP1 and D-AKAP2 as a small amount of RIα is also localised here. However, when RIα is oxidised to the disulfide form its affinity for membrane- and myofilament-associated AKAPs may increase inducing the observed translocation to the membrane and myofilament. As already mentioned, D-AKAP1 and D-AKAP2 were found in the membrane so are candidate AKAPs responsible for translocation of RIα to membrane from cytosol. Small amounts of D-AKAP1, D-AKAP2 and α / β tubulin were found in the myofilament-enriched fraction so these are candidate AKAPs responsible for the observed translocation of RIα to myofilament.

A solid-phase cAMP affinity capture method was implemented to assess whether disulfide increases RIα affinity for membrane-associated AKAPs, which could underlie the translocation of RIα from the cytosol. A similar approach has been used successfully by others,[275, 312] for analysis of AKAP binding. A variety of cAMP analogues with different affinities for RI and RII AKAPs have been used to identify RI / RII-specific AKAPs and D-AKAPs.[314] This method relies on the premise that WT or KI PKA RI / RII (with bound AKAPs) will bind to cAMP so that captured AKAPs can be identified using antibodies to specific AKAPs. This method could only be used to analyse AKAPs in the Triton X-100 soluble fraction (cytosol-enriched and membrane-enriched fractions) of the heart. If AKAPs are not Triton X-100 soluble (i.e. in the myofilament-enriched fraction) this precludes their detection using this approach. In the pioneering work of Dr. Scott,[281, 282] AKAPs were identified using radiolabelled RII in blot overlays and of course the entire cell / tissue fraction is present, including the Triton X-100 insoluble fraction. Unfortunately, as discussed elsewhere, capturing RIα AKAPs in this way is more difficult. This cAMP affinity capture method, therefore,

excludes AKAPs responsible for oxidant-induced translocation of WT PKA RIα to myofilament.

The cAMP affinity captures generated variable results which may be explained by a number of issues encountered. Firstly, not all the antibodies purchased to assess the presence of AKAPs were specific; antibodies to D-AKAP1, D-AKAP2 and AKAP220 detected other proteins of variable molecular weights which were most likely to be splice variants, which are highly prevalent in AKAPs,[232, 252] but regardless complicated interpretation of results. Some of the antibodies, namely the AKAP220 and D-AKAP2 antibodies, were not sensitive enough either. Even when the antibody concentration was increased and longer incubation periods were used, D-AKAP2 and AKAP220 were not easily detected in many *input* samples. Often the film had to be exposed for long periods, leading to high background signal; this particularly made the detection of D-AKAP1 unreliable. This AKAP detection issue may be because the affinity capture studies used diluted heart homogenates; although the idea was that if they were indeed captured by the cAMP-agarose the AKAPs would be enriched and so easily detected by immunoblotting.

Another issue was that the cAMP affinity capture process appeared to chemically reduce RIα disulfide. Hearts where RIα was mostly disulfide dimer in *input* samples then had similar amounts of disulfide dimer and monomer in *capture* samples consistent with reduction of RIα. This decrease in percentage disulfide in H_2O_2-treated hearts may result in less of a difference in AKAP binding between control and H_2O_2-treated hearts as the difference in percentage disulfide is smaller. In some examples, there also appeared to be an increase in total RIα protein because of this reduction to monomer which is difficult to explain as there is no sensible basis for *de novo* protein synthesis.

Another issue was that a band at ~100 kDa (the same mass as RIα disulfide dimer) was observed in some KI *capture* samples. KI RIα cannot form RIα disulfide so this was not expected and was not observed previously. I have provided some evidence that this could be the PKA catalytic subunit bound to RIα subunit (shown to occur with RII and

catalytic subunit,[59]) but as this was only explored in one experiment it is possible that the 100 kDa band in the KI hearts is an artefact from over-exposure of the film as it is not observed on a shorter exposure that is adequate to generate a strong RIα signal.

I expected to see a number of significantly stained bands on colloidal Coomassie-stained gels of *capture* samples. It is unclear why only a few faint bands were observed as the affinity capture appeared to work well in terms of capturing RIα. Although optimisation of the protocol was attempted, perhaps further optimising is required to increase the amount of RIα captured and so RIα-bound proteins. Although it is possible that AKAPs are in insufficient abundance to generate Coomassie stained bands even if captures are highly efficient. For this reason and because of lack of success with specific AKAP antibodies, LC-MS/MS was used to identify AKAPs in the cAMP-agarose *capture* samples. This was considered a more sensitive technique.

LC-MS/MS identified a number of cAMP-binding proteins captured in similar abundance between genotypes and with oxidant treatment. These could be RII-specific binding proteins or targets simply not effected by RIα disulfide formation. Western blotting demonstrated that AKAP220 and α / β tubulin were both in the Triton X-100 soluble fraction of WT and KI hearts but they were not identified by LC-MS/MS. However, they may not have been detected by LC-MS/MS because they were present in the part of the colloidal Coomassie stained gel that was not analysed or the LC-MS/MS was not sensitive enough to detect them. AKAP220 was difficult to detect in *input* samples using antibodies but where visible was not detected in *capture* samples, which agrees with LC-MS/MS results that AKAP220 does not bind RI / RII. However, this conflicts with a study showing it binds RI and RII.[269] α / β tubulin was easily detected in *input* samples but was generally not detected in *capture* samples. This further conflicts with literature showing RI binds tubulin specifically.[287] Possible explanations for this are considered below.

ChChd3 is a substrate for PKA,[294] and forms a complex with SKIP, an AKAP that binds Type I PKA.[293] LC-MS/MS identified significantly more ChChd3 was

captured for WT compared to KI. I hypothesised that there was more ChChd3 in WT because WT RIα can form disulfide that may increase binding to SKIP. ChChd3 was localised in the membrane-enriched fraction of WT and KI hearts which agrees with others who found ChChd3 is located in the inner mitochondrial membrane.[295] They show it may be synthesised in the cytosol and associated with HSP70 to keep it in its reduced form before being transported to the mitochondria. Therefore, ChChd3 can potentially be phosphorylated by membrane-localised PKA. Perhaps ChChd3 phosphorylation is increased in oxidant-treated WT hearts as a result of translocation of RIα disulfide and so catalytic subunit to the membrane. However, there is no antibody to phospho-ChChd3 (Thr10) available commercially and the one generated by Taylor's lab (San Diego, USA) is no longer available. Future studies could implement the Phos-tag method,[315] to assess phosphorylation status or immunoprecipitation of ChChd3 with subsequent probing with a pan-specific PKA phospho-substrate antibody may be valuable.

SKIP was not identified by LC-MS/MS but this could be for reasons already mentioned; because it was present in the part of the colloidal Coomassie stained gel that was not analysed or the LC-MS/MS was not sensitive enough to detect it. Fractionation revealed SKIP was located in the myofilament-enriched fraction of WT and KI hearts whereas others have reported SKIP localisation to the cytosol.[292] This conflict in results may be due to differences in sample preparation although I am confident with my fractionation protocol as I showed presence of respective marker proteins that are indicative of each fraction (shown in Chapter 2). If SKIP is localised in the myofilament, it would not have been detected by LC-MS/MS because the *capture* sample analysed was only the Triton X-100 soluble fraction of the heart.

Overall, the reason for increased ChChd3 binding to WT RIα does not appear to be due to increased RIα binding to SKIP. I reason this is because SKIP is only in the Triton X-100 insoluble fraction of the heart whereas ChChd3 is predominately present in the Triton X-100 soluble fraction. ChChd3 is a scaffolding protein that forms complexes with proteins other than PKA including the inner mitochondrial membrane proteins,

mitofilin and optic atrophy 1 (OPA1) and the outer mitochondrial membrane protein Sam50. These are GTPases involved in mitochondrial fusion (merging of mitochondria before division).[295] Interestingly, OPA1 has been identified as a D-AKAP that has a slightly higher specificity for RI than RII. It has been shown to localise with PKA (Type I or Type II) and perilipin in lipid droplets. Perilipin is a PKA substrate and its phosphorylation regulates access of lipases and so formation of this complex is important in control of lipolysis.[316] Therefore OPA1 may also function as a D-AKAP in mitochondria and form a complex with ChChd3 and RIα and disulfide may alter the interaction of RIα with OPA1.

AKAP7γ (also known as AKAP18δ) binds PKA RI and RII and is located in the cytoplasm and nucleus.[317] It forms a multi-protein complex with PLB, SERCA2 and PKA RII. However, the presence of PKA RI in this complex was not analysed despite AKAP7γ being a D-AKAP. Lygren *et al.* demonstrated that the interaction between AKAP7γ and PLB was inhibited by phosphorylation of PLB at Ser16, a known PKA phosphorylation site. AKAP7γ interaction with PLB was necessary to recruit PKA for phosphorylation of PLB and Ca^{2+} re-uptake into the SR.[226] LC-MS/MS identified SERCA2 as a protein that bound KI RIα more than WT RIα. This may suggest that RIα disulfide reduces binding of PKA RIα to an AKAP (e.g. AKAP7γ) and so reduces complex formation with SERCA2 and PLB too. I found (see Chapter 4) that phosphorylation of PLB, the inhibitory protein for SERCA2, was significantly decreased by oxidant treatment in WT but not KI. This is consistent with the hypothesis; if AKAP binding is reduced in response to oxidant, less PKA is anticipated to associate with its substrate PLB, so phosphorylation of PLB would be less. This highlights the possibility that disulfide may reduce RIα-AKAP binding as well as increase it. Reduced AKAP binding may be a mechanism to increase the amount of free RIα in the cytosol- / membrane- enriched fractions of the heart so it can then translocate to myofilament.

Alpha-enolase is a glycolysis enzyme present in the cytosol as well as on the cell membrane where it can function as a plasminogen receptor.[318] LC-MS/MS revealed this bound more to WT RIα than KI RIα. Although it is not a substrate for PKA there is

evidence it may be a substrate for Src,[300] which as mentioned in 5.1.2, is associated with D-AKAP1. Work by Banky *et al.*,[116] showed that mutating Cys16 did not affect D-AKAP1 binding to RI. LC-MS/MS demonstrated an increase in D-AKAP1 abundance in the WT *capture* sample with H_2O_2 but not in the KI. D-AKAP1 was detected in *capture* samples using a D-AKAP1 antibody and its binding appeared to increase with oxidant treatment in both genotypes. This is interesting but the *n* number for both these analyses needs to be increased to form a confident conclusion on whether disulfide alters RIα binding to D-AKAP1.

Isoform 4 of myomegalin interacts with PKA RI and RII and also alpha-enolase.[302] Perhaps RIα disulfide increases binding to myomegalin which recruits alpha-enolase. However, the function of this complex formation is unclear as alpha-enolase is not an established PKA substrate. Absence of myomegalin in *capture* samples could indicate it was present in the Triton X-100 soluble fraction of the heart but doesn't bind RI / RII, it was present in the section of the colloidal Coomassie stained gel that was not analysed or the LC-MS/MS was not sensitive enough to detect the protein. However, Western blotting showed it to be abundant in the myofilament-enriched fraction of WT and KI hearts which is consistent with studies showing its presence in the sarcomere,[302] so its detection by LC-MS/MS would not be expected. Overall, I am unable to suggest a specific AKAP linking PKA RIα and alpha-enolase in the cytosol and membrane as this is not an area well studied.

Very long-chain specific acyl-CoA dehydrogenase (VLCD) is an enzyme involved in fatty acid β oxidation and lipid metabolism. Ser586 of VLCD is phosphorylated by PKA. A VLCD Ser586 mutant has increased apoptosis, increased reactive oxygen species production and decreased enzyme activity.[303] VLCD preferentially bound to redox-dead RIα suggesting that disulfide may reduce binding of RIα to this AKAP. It may be interesting in further work to determine whether VLCD phosphorylation is increased in KI hearts to further test the idea that RIα redox status regulates its interaction with this dehydrogenase. There are, however, no commercially available antibodies to monitor phosphorylation status of this site. Kabuyama *et al.*,[303]

produced their own antibody, which could be sought in future studies. The literature does not describe any specific AKAPs associated with VLCD but there may be a novel AKAP associated with this protein that recruits PKA to VLCD to coordinate its phosphorylation.

The effect of mutating the Cys residues flanking the DD domain in RIα on binding to D-AKAP2 has been studied by others. Huang *et al*.,[138] showed that mutating Cys17 in RI did not affect D-AKAP2 binding, whereas mutating Cys38 abolished D-AKAP2 binding. Sarma *et al*. found that mutating Cys17 reduced RIα-D-AKAP2 binding 3-fold compared to WT protein, and mutating Cys38 reduced binding 16-fold. They suggest D-AKAP2 binding may be reduced because disulfide bond formation decreases flexibility of the N-terminal helix N-1 of RIα so the structure is more ordered and so residues critical for D-AKAP2 binding are positioned in close proximity to the AKAP for improved binding.[119] D-AKAP2 was identified in cAMP affinity *capture* samples by LC-MS/MS and there was a trend for an increase in spectral count with H_2O_2 in WT *capture* but not KI. Unfortunately, D-AKAP2 was not detected or only weakly detected in *input* samples or *flow-through* samples using a D-AKAP2 specific antibody. The work of others showed mutating Cys17 did not have as big an effect on D-AKAP2 binding as mutating Cys38.[119] This may be why I am unable to detect any difference between WT and KI, as Cys17 was mutated in the KI mouse rather than Cys38. In addition, the apparent chemical reduction of the RIα disulfide to reduced monomer by the cAMP affinity capture process (described earlier) may compromise the ability to assay the effect of H_2O_2 on RIα redox state in WT hearts. This may also prevent a difference being observed between WT and KI in terms of AKAP binding and may apply to the other AKAPs assessed too. Perhaps when this chemical RIα reduction by the cAMP affinity capture method happens, AKAP binding that occurred previous is lost so I am unable to observe it.

LC-MS/MS was only carried out on one sample of each band from each genotype and each treatment so the *n* number should be increased in the future to gain more information on RIα disulfide and AKAP binding. Inconsistencies in results could also

be due to some of the complexities of the cAMP affinity capture method, some of which have already been discussed above. The method is artificial as the concentration of cAMP is very high and so not physiological. This may affect binding of AKAPs to RIα but even if it was low and physiological the same issues could be present. The effect of cAMP and H_2O_2 together on RIα binding to AKAPs is not known and which order these events happen in physiologically is not known. In addition, PKG can bind cAMP,[319] so may bind directly to the cAMP agarose. This kinase has its own binding proteins that may then be identified in *capture* samples, complicating results. LC-MS/MS showed that PKG I was significantly more abundant in KI than WT *capture* samples and there was a trend for an increase with oxidant treatment in both genotypes. The difference between genotypes is difficult to explain as the PKA RIα mutation should not alter PKG I interaction with cAMP. However, PKG Iα forms disulfide in response to H_2O_2,[60] so this may increase its affinity for cAMP and explain the increase in its abundance in H_2O_2-treated *capture* samples for both genotypes.

There are alternative methods that may be used to demonstrate the influence of disulfide on AKAP binding which avoid the use of AKAP specific antibodies and the numerous complexities of cAMP affinity capture. One example is adding a FLAG tag to the specific AKAP in WT and KI heart homogenate, isolating the immune complexes by FLAG agarose and then carrying out SDS-PAGE and Western blotting and probing for PKA RIα. The cAMP affinity capture method is a solid-phase binding assay similar to Far Westerns which do not identify RI AKAPs as easily as RII AKAPs; one reason being that the RI-AKAP binding off-rate is faster than the on-rate,[284] making the interaction transient and difficult to catch using solid phase assays. Susan Taylor's group showed that WT disulfide RIα has increased D-AKAP2 affinity by surface plasma resonance.[119] This most probably worked because it involves real time monitoring of AKAP binding and release. Therefore, this is a method that could be used in my studies. Another method that could be used is confocal microscopy, to show co-localisation of RIα and specific AKAPs.

Although I was unable to determine any association between RIα disulfide and AKAP binding I did identify a number of proteins that potentially interact with RIα. I have attempted to provide links between some of these proteins and AKAPs described in the literature but there may be novel AKAPs that we do not know about yet that may explain some of the results. In conclusion, disulfide causes translocation of RIα to the myofilament but whether this is as a result of increased AKAP binding is yet to be confirmed.

6 DOES THE THIOREDOXIN SYSTEM REDUCE RIα DISULFIDE?

6.1 INTRODUCTION

6.1.1 Thioredoxin

The thioredoxin (Trx) system is important in maintaining a reduced intracellular state. In this chapter I assessed whether Trx has a role in reduction of PKA RIα disulfide. Trx was originally identified in *Escherichia coli (E. coli),* as a hydrogen donor for ribonucleotide reductase.[320] It is also known as adult T-cell leukaemia-derived factor because a Trx-homologue was identified in the supernatant of human T-lymphotropic virus-I-infected T cells.[321] Trx is a 12 kDa protein that catalyses the reduction of protein disulfides and S-nitrosothiols,[322] as discussed below.

Forms of Trx and their structure: Mammalian cells contain Trx1 and Trx2 which are encoded by different genes.[323] Trxs from archaea to humans show 27 - 69 % sequence identity to Trx from *E.coli*. All Trxs have the same overall 3D structure,[324] and have the same structural motif called the 'Trx fold'. This consists of a four stranded β-sheet and three flanking α-helices or more specifically, an N-terminal βαβ motif and a C-terminal ββα motif connected by a loop of residues making up another α helix. The active site motif is Cysteine (Cys) - Glycine (Gly) - Proline (Pro) - Cys and this redox active dithiol, which interacts with the disulfide of the target protein, is located at the N-terminus of the α1 helix.[325] Human Trx1 has the two Cys residues (Cys32 and Cys35) located in the active site, and an additional three Cys residues located outside of the active site; Cys62, Cys69 and Cys73.

There is less information on Trx2 than Trx1. Trx2 contains the Trx fold and the conserved active site Cys residues but not the structural Cys residues that Trx1 has in its C-terminus.[326] This makes it resistant to oxidation (which occurs in Trx1 as discussed below). It also has a sixty amino acid extension at the N-terminal that is

involved in mitochondrial translocation and contains a protease cleavage site where cleavage produces the mature protein.[327]

Localisation and expression of Trx: Trx1 is mostly cytosolic but can also be found in the nucleus.[321] Phorbol 12-myristate 13-acetate (PMA), ultra-violet radiation and tumour necrosis factor (TNF) α are examples of stimuli that cause Trx1 translocation from the cytoplasm to the nucleus.[328] In contrast, Trx2 is mitochondrial.[327, 329]

Trx is ubiquitous in all living cells but a comparison of expression of Trx1 and Trx2 reveals differences in their abundances in various organs.[327]. Expression of Trx can be altered by a variety of stresses. Taniguchi *et al.*,[330] showed that oxidant stresses such as diamide (5 µM for 6 hours), or H_2O_2 (1 - 100 µM for 6 hours) increased Trx gene expression in Jurkat cells. Trx1 expression was also increased in endothelial cells by low doses of H_2O_2 (10 or 50 µM) and short term shear stress.[331] Expression of Trx1 was reduced after ischaemia and reperfusion and adaption to the ischaemic stress (by short preconditioning episodes of ischaemia and reperfusion) followed by ischaemia and reperfusion resulted in an increase in Trx1 expression.[332] In contrast, it has also been shown in human umbilical vein endothelial cells that H_2O_2 (100 µM or 200 µM for 6 hours) can induce degradation of Trx1 and apoptosis.[333]

How Trx reduces its substrate and is regenerated by Trx reductase: Trx does not target and reduce all disulfide proteins. It has selective substrates due to specific protein-protein interactions. The crystal structures of human Trx1 and human Trx2, both reduced and oxidised states have been described.[326, 334, 335] Trx is generally thought to interact with its substrates in its reduced monomeric form, but there is also evidence for a reduced dimeric Trx1 species where the two monomers of the dimer are linked by a hydrogen bond and the linkage stabilised by a disulfide between Cys73 residues of each monomer. The reduced dimer may be Trx's inactive state as it is not a substrate for Trx reductase (TrxR), perhaps acting as a regulatory mechanism.[335] As mentioned, Trx2 does not contain Cys73, but has Ala73 in its place which precludes

disulfide formation. There is evidence, however, that Trx2 can still form a dimer due to hydrophobic interactions and hydrogen bonds.[326]

As mentioned, Trx has a consensus redox-active dithiol (Cys32-Gly-Pro-Cys35) in its active site. The Cys thiol at the N-terminal (Cys32 in human Trx) has a reduced pKa (~6.3 compared to ~8.7 in a 'typical' Cys thiol).[335] This thiol therefore exists in the deprotonated thiolate state at physiological pH and reacts with the target protein disulfide, becoming disulfide-linked to the target. This interprotein disulfide is short-lived because it is rapidly reduced by the C-terminal thiol (Cys35 in human) of Trx. Overall this results in formation of a reduced target protein, and intraprotein disulfide in the active site of Trx between Cys32 and Cys35. This Trx intraprotein disulfide is reduced by TrxR using NADPH, as explained in more detail below.[336] The mechanism of Trx-catalysed reduction is shown in Figure 6.1.

The crystal structure of human Trx complexed with TrxR1 has been solved and shows that TrxR1 has a flexible C-terminal arm, which enables the transfer of electrons to Trx.[337] Trx can only be reduced by TrxR, no other enzyme has been identified that can replace TrxR in this role.[338]

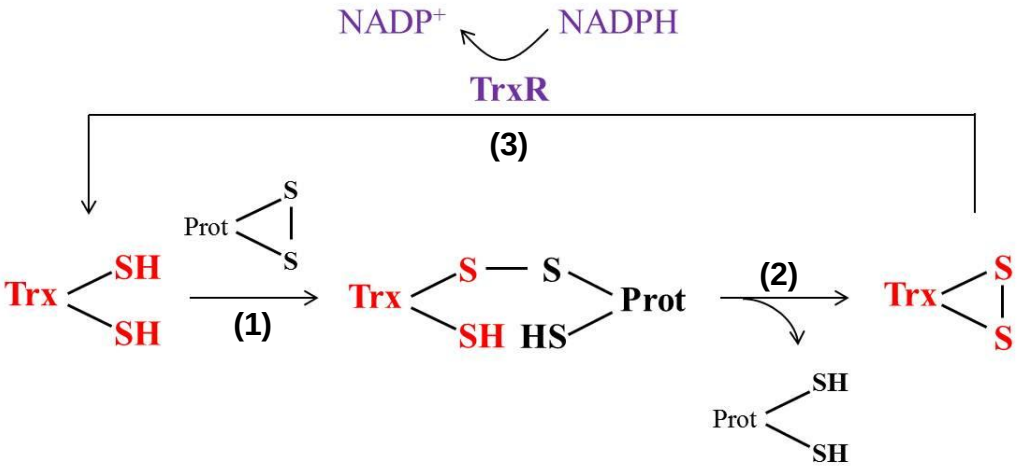

Figure 6.1 Mechanism of reduction of a target protein disulfide by Trx and regeneration of Trx by TrxR.

(1) Reduced Trx interacts with the target protein disulfide. An interprotein disulfide forms between one of the active site Cys residues of Trx and a Cys in the target protein. (2) The other Cys residue in the active site of Trx then reduces this disulfide. The target protein disulfide is fully reduced and an intraprotein disulfide forms in Trx. (3) The disulfide is then reduced by TrxR using NADPH.

Functions of Trx and its substrates: Enzymes that form a disulfide during their catalytic cycle were the first substrates described for Trx1. These include peroxiredoxin (Prx, described in Chapter 1),[339] ribonucleotide reductase,[340] and methionine sulfoxide reductase.[341]

The function of Trx1 has been well-studied, but less is known about the functions of Trx2, so unless stated otherwise I am specifically referring to Trx1 from here on. Trx is not only important for its reducing activity and protecting cells from oxidative stress, but also has an important role in redox signalling, as considered below. Trx interacts with and reduces proteins important in cell growth and proliferation, apoptosis and gene expression. In addition to these well studied functions, Trx has more recently been shown to be important in cardiac muscle contraction and cardiac energy dynamics by targeting substrates such as components of the mitochondrial permeability transition

pore, important in supplying ATP to the heart.[342] Further examples of the substrates and functions of Trx are provided below.

Trx in cell growth and survival: Knockout Trx mice die early in embryogenesis suggesting an essential role for Trx in morphogenesis and differentiation of the embryo and highlighting a crucial role in cell growth.[343] Trx has been shown to be excreted by normal and transformed cells such as monocytes, fibroblasts and airway epithelial cells,[344] and exhibit chemo-attractant properties.[345] It has also been described as a growth factor stimulating growth of lymphocytes, fibroblasts and some tumour cell lines, and it is overexpressed in a number of tumours.[346] Trx inhibits apoptosis by targeting a number of proteins such as p53 and apoptosis signal-relating kinase (ASK-1).

ASK1 is a mitogen activated protein kinase (MAPK) kinase kinase (MAPKKK) activated by reactive oxygen species (ROS), Fas and TNF. Its downstream targets include p38 MAPK and c-Jun N-terminal kinase (JNK) which induce apoptosis.[347] Under normal conditions, ASK1 is found in the cytoplasm and forms a complex with Trx1.[348] Reduced Trx1 inhibits ASK1 activity by binding to ASK1 at its N-terminus,[349] with amino acids 46 - 277 of ASK1 being necessary and sufficient for this interaction.[350] Cys250 in ASK1 has been shown to be particularly important for binding to Trx1,[50] as has another single Cys (Cys35 or Cys32) in Trx.[351] Binding of Trx to ASK1 prevents the TNF receptor associated factor 2 (TRAF2) binding to ASK1 which is important in TNF-induced activation of ASK1.[352] Trx also inhibits the homophilic interaction (ASK1 binding to ASK1) of ASK1 at its N-terminal which was shown to be necessary for H_2O_2-induced ASK1 activation,[350] and induces ASK1 ubiquitination / degradation.[351] When Trx is oxidised by H_2O_2, it dissociates from ASK1, leading to ASK1 activation and apoptosis.[349, 351, 352] ASK1 may also be oxidised directly by H_2O_2 to form a disulfide linked multimer (up to tetramer), which is then reduced by Trx. Oxidation of ASK1 to the multimer was required after dissociation of Trx from ASK1 (ASK1 activation) for full activation of ASK1's downstream target JNK and ultimately H_2O_2-induced apoptosis.[353] ASK1 is not only located in the

cytoplasm but is also located in the mitochondria. Under resting conditions, reduced Trx1 is bound to ASK1 in the cytoplasm (as already stated) and reduced Trx2 is bound to ASK1 in the mitochondria. Cys30 in ASK1 is important for binding to Trx2. Stimuli such as ROS and TNF cause dissociation of Trx1 and Trx2 leading to mitochondrial-dependent apoptosis.[348] Trx1 and Trx2 can work cooperatively to inhibit ASK1-induced apoptosis. This is because when Trx1 dissociates from cytoplasmic ASK1, activation of a JNK-dependent apoptotic pathway occurs, involving activation of JNK, BID cleavage and Bax translocation. When Trx2 dissociates from mitochondrial ASK1 at the same time as dissociation of Trx1 from cytoplasmic ASK1, activation of a JNK-independent apoptotic pathway occurs. Both apoptotic pathways merge at cytochrome c release (Trx2 interacts with cytochrome c),[323] and result in caspase 3 activation and apoptosis.[348]

Trx in gene expression: Trx enhances the deoxyribonucleic acid (DNA) binding of transcription factors important in the response to apoptosis, oxidative stress and tumorigenesis.[354] Activator protein 1 (AP-1), nuclear factor kappa-light-chain-enhancer of activated B cells (NFκB) and p53 are examples of substrates involved in this function of Trx.

AP-1 is a dimeric transcription factor composed of members of the Fos, Jun, activating transcription factors and Jun dimerisation partners families. AP-1 has important roles in cell proliferation, apoptosis and neoplastic transformation.[355] The binding of Fos and Jun to the AP-1 DNA sequence motif is regulated by oxidation and reduction. The reduction of a conserved Cys residue in the DNA binding domains of Fos and Jun increases DNA binding activity.[356] Certain stimuli cause Trx translocation from the cytoplasm to the nucleus where it directly associates (through Cys residues in the active site of Trx) with a protein called redox factor 1 (Ref-1).[357] Ref-1 then stimulates DNA binding activity of AP-1 by reduction, although the mechanism is poorly understood.[358, 359] There is evidence for and against Cys65 / Cys64 (human / mouse) being the redox catalytic site in Ref-1.[360, 361] More recently, Ref-1 has been described as a ‘redox chaperone’ that, independently of its Cys residues, facilitates the

chemical reduction of various transcription factors by GSH and Trx. AP-1 is suggested to be one of these transcription factors.[362]

NFκB is a dimeric transcription factor composed of members of the Rel family including p50, p65 and p52. Inactive NFκB is present in the cytoplasm bound to an I kappa B (IκB) inhibitory protein. Stimuli such as TNFα trigger an intracellular kinase cascade resulting in phosphorylation and proteosomal degradation of IκB. This means the p50 - p65 heterodimer can translocate to the nucleus, bind to DNA and activate transcription of target genes involved in functions such as inflammation, nitric oxide (NO) production, apoptosis and proliferation.[363] NFκB DNA binding is regulated by reduction and oxidation of the p50 subunit. p50 subunits form disulfide dimers and formation is dependent on Cys62. Oxidation abolishes DNA binding whereas reduction by Trx stimulates DNA binding.[364, 365] Direct physical interaction between an oligopeptide from the p50 DNA-binding loop and Trx has been shown.[366] Ref-1 can act as a 'redox chaperone' to facilitate the reduction of NFκB by Trx,[362] as well as act alone to reduce Cys62 of the p50 subunit.[367] As mentioned earlier, Trx can translocate from the cytoplasm to the nucleus under certain conditions. Cys62 of the p50 subunit is strongly reduced in the nucleus and highly oxidised in the cytoplasm.[367] Hirota *et al.* suggest that Trx in the cytoplasm and nucleus have opposing effects on NFκB activity. Trx in the cytoplasm blocks the degradation of IκB and Trx in the nucleus increases NFκB's DNA binding activity by direct association.[328]

Functions of Trx2: The mitochondrial respiratory chain is a major source of ROS, so mitochondrial antioxidant systems (including the Trx2 system, manganese superoxide dismutase (MnSOD) and Trx peroxidase) are important in preventing irreversible oxidative damage.[348] Trx2 is essential for embryonic development and cellular respiration,[368] and plays a role in protection against oxidant-induced apoptosis, as already discussed.[369, 370]

The role of Trx in de-nitrosylation and S-nitrosylation: In addition to reducing protein disulfides, Trx promotes S-nitrosylation and de-nitrosylation of target proteins depending on the redox state of the cell. The mechanism of de-nitrosylation of a protein involves trans-S-nitrosylation of Cys32 of Trx, intraprotein disulfide formation between Cys32 and Cys35 in Trx and release of nitroxyl (HNO). Reduction of disulfide Trx by TrxR and NADPH follows. In addition, the intraprotein disulfide form of Trx may be S-nitrosylated at Cys62, 69 or 73 (in human) and under certain conditions, S-nitrosylated Trx may trans-S-nitrosylate other proteins.[322, 371-373] This mechanism is presented in Figure 6.2.

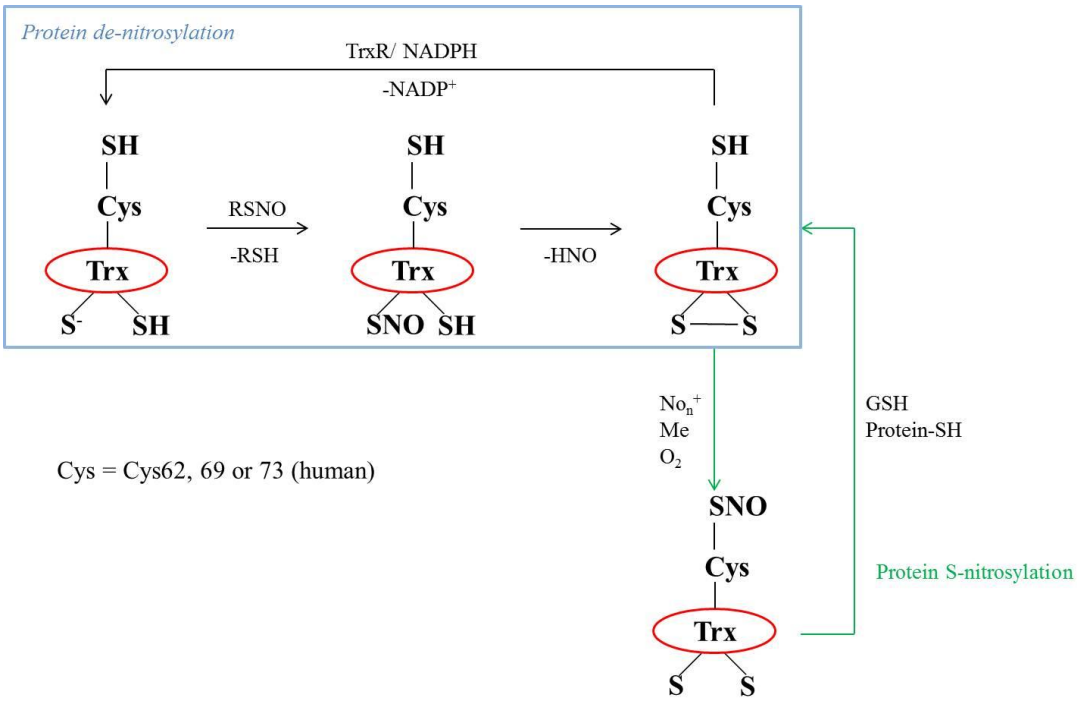

Figure 6.2 Mechanism of protein de-nitrosylation and S-nitrosylation by Trx1.

Trx1 de-nitrosylates its target protein (RSNO to RSH) by being S-nitrosylated itself at Cys32. Cys35 then forms an intraprotein disulfide with Cys32 releasing nitroxyl (HNO). Under certain conditions i.e. when the intraprotein disulfide in Trx1 cannot be reduced, Cys62, 69 or 73 of Trx1 (not in active site) is S-nitrosylated. Trx1 can then S-nitrosylate other protein thiols (protein-SH) such as GSH.

Substrates for Trx1-mediated denitrosylation and S-nitrosylation have been identified. Prx-1 was a substrate for trans-S-nitrosylation but not denitrosylation. Glyceraldehyde 3-phosphate dehydrogenase (GAPDH) and α-tubulin were substrates for both S-nitrosylation and denitrosylation.[374] Cys163 of caspase 3, a mitochondrial enzyme, is a target for S-nitrosylation by Trx-Cys73 and this leads to inactivation of caspase 3 and inhibition of apoptosis.[375, 376] Denitrosylation of S-nitrosylated caspase 3 is induced by stimulation of the Fas receptor (death receptor) and this is mediated by Trx2 / TrxR2. Denitrosylation is required for full activation of caspase 3 and apoptosis.[377]

Trx interacting protein: Trx interacting protein (TXNIP) is also known as vitamin D3-upregulated protein and Trx binding protein 2. It's only known function is to bind and inhibit Trx. When TXNIP is oxidised it forms an intraprotein disulfide between Cys63 and Cys247. TXNIP then interacts with reduced Trx, with Cys247 of TXNIP forming an interprotein disulfide with Cys32 of Trx.[378] Overexpression of TXNIP has been shown to reduce Trx activity and its nuclear translocation, inhibit proliferation,[379] enhance ROS production and attenuate cardiac hypertrophy.[380] Knockdown of TXNIP also abolishes high glucose-induced apoptosis and ASK1 activation.[381]

6.1.2 Thioredoxin reductase

Members of the TrxR family: TrxR was first cloned and sequenced from *E.coli* in the late 1980s.[382, 383] In the late 1990s a human TrxR (named TrxR1) was cloned and sequenced from placenta. Human TrxR1 has a molecular mass of 54 kDa and only has 31 % sequence identity with prokaryotic TrxRs. It is bigger than prokaryotic TrxRs and lower eukaryotic TrxR enzymes due to the dimer interface domain (explained later).[384] Bovine TrxR1 and rat liver TrxR1 have also been purified,[385, 386] and sequenced.[387] TrxR1 is cytosolic.[388]

The identification of a mitochondrial Trx2 (as described in earlier) prompted work investigating the existence of a mitochondrial TrxR. Cloning and expression of complementary deoxyribonucleic acid (cDNA) for a mitochondrial human TrxR, TrxR2, with a molecular weight of 56 kDa have been described. TrxR2 cDNA had 56 %

identity to TrxR1 and there was 84 % similarity at the amino acid level.[389] Cloning and expression of cDNA for mouse and rat TrxR2 have also been described.[390, 391]

Another member of the TrxR family is Trx - oxidised glutathione (GSSG) reductase (TR2 or Txnrd3). This demonstrates specificity for both the Trx system and GSSG system as it can reduce Trx, GSSG and a GSH-linked disulfide.[392] A partial sequence for Txnrd3 cDNA has been identified in humans,[393] and the full sequence for mouse Txnrd3 cDNA has been identified. This showed 88 % identity to the partial human sequence, 73 % identity to human TrxR1 and 56 % identity to human TrxR2. This form of TrxR is found mainly in the testis.[392]

Structure of members of the TrxR family: TrxR1, TrxR2 and Txnrd3 are members of the pyridine nucleotide-disulfide oxidoreductase family. Other members of this group include lipoamide dehydrogenase, mercuric ion reductase, glutathione reductase and NADH peroxidase. Members of this group are homodimeric (except NADH peroxidase which is a homotetramer) and each monomer has a redox-active disulfide and FAD protein bound.[394] TrxR also contains an NADPH-binding domain.[338] *E.coli* TrxR does not contain the dimer interface domain i.e. the site of interaction between subunits found in mammalian TrxR. This explains why mammalian TrxR is larger than *E.coli* TrxR.[384] The structure of mammalian TrxR can be seen in Figure 6.3.

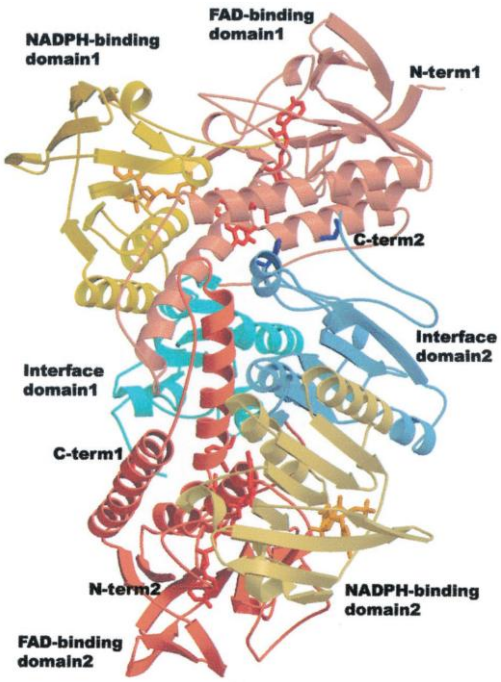

Figure 6.3 Ribbon representation of rat TrxR.

The two subunits are shown in light or dark colours, respectively. (Red = FAD binding domain; yellow = NADP binding domain; blue = interface domain. NADP = orange ball-and-stick model and bound FAD = red ball and stick model.[394]

Mammalian TrxR contains an active site with the sequence; Cys-Val-Asn-Val-Gly-Cys, which is located in the FAD binding domain.[394] In *E.coli* this sequence is located in the NADPH-binding domain and has a two amino acid bridge between the Cys residues rather than the four amino acid bridge seen in mammalian TrxR1.[384] Mammalian TrxR also contains a C-terminal extension with the unique sequence Gly-Cys-SeCys-Gly,[395] where SeCys is selenocysteine. This is where the S has been replaced with Se which lowers the pKa, which is essential for the enzymes catalytic mechanism.[338, 396]

TrxR2 has a similar structure to TrxR1 with a conserved active site, FAD-binding and NADPH-binding domains but also has a thirty-three amino acid extension at the N-terminus which when removed abolishes mitochondrial translocation.[389] Txnrd3 contains the TrxR1 domains and an N-terminal glutaredoxin (Grx) domain.[392]

Mechanism of TrxR-catalysed reduction of its substrates: The NADPH and FAD domains of *E.coli* TrxR are positioned so that when NADPH binds it is not in close contact with FAD, preventing electrons being transferred from NADPH to FAD. This is not the case in other members of the pyridine nucleotide-disulfide oxidoreductase family. To overcome this issue of the NADPH and FAD domains not being close together, a conformational change occurs where the NADPH domain is rotated 66 º with respect to the FAD domain. Now when NADPH binds to the NADPH domain it is in close contact with FAD so electrons can be transferred from NADPH to FAD. Following this, reduction of the active site disulfide of TrxR can occur. The conformational change also exposes the reduced active site dithiol of TrxR so it can reduce Trx. During reduction of Trx, an active site disulfide is formed in TrxR, allowing TrxR to move back into its original conformation and the catalytic cycle can start again.[338, 397-399]

The mechanism for mammalian TrxR catalysis relies on a head-to-tail orientation of the homodimer so that the C-terminal Cys497-SeCys498 (in rat, absent in *E.coli* TrxR) residues of each subunit are opposite the N-terminal active site dithiol (Cys59 and Cys64 in rat) of the other subunit of the dimer.[400] In oxidised TrxR, Cys497 and SeCys498 form a selenenylsulfide and the active site Cys59 and Cys64 residues form an intraprotein disulfide. The active site disulfide is reduced by NADPH via FAD. Electrons from NADPH are then transferred to the selenenylsulfide to form a selenolthiol.[394, 400-402] Tyrosine (Tyr)116 (its side chain is located above SeCys) is also important in the reduction of selenenylsulfide.[403] The resulting selenolthiol then acts as the active site for reduction of substrates such as Trx.[394, 400-402] Electrons may be offered to the final substrate by movement of the reduced C-terminal arm away from the catalytic site to the surface.[394, 404] SeCys498 forms a mixed selenenylsulfide with Trx which is then reduced by Cys497 in the C-terminal active site to form a selenenylsulfide between Cys497 and SeCys498. The cycle then starts again,[394] as shown schematically in Figure 6.4.

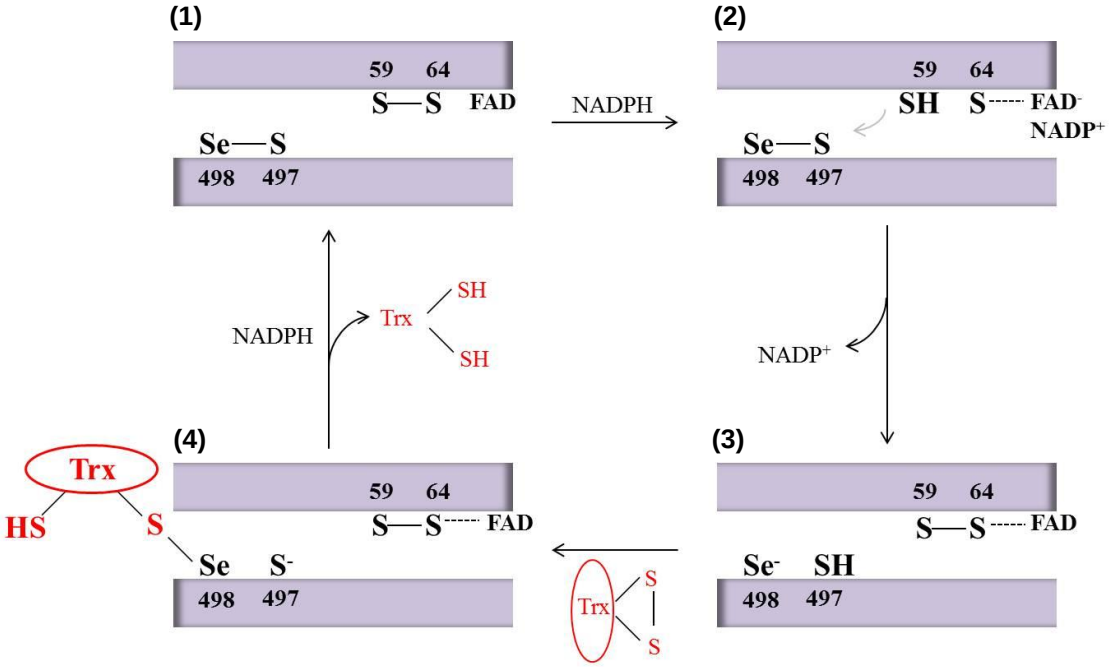

Figure 6.4 Postulated mechanism of reduction of Trx by mammalian (example is rat) TrxR.

(1) The mammalian TrxR homodimer is in a head-to-tail orientation so the active site Cys59 and Cys64 and the C-terminal Cys497-SeCys498 are close to each other. The active site Cys residues are oxidised to a disulfide and the C-terminal Cys residues are oxidised to a selenenylsulfide. (2) NADPH transfers its electrons to the active site disulfide via FAD reducing this disulfide. (3) The C-terminal selenenylsulfide is then reduced and the active site Cys residues form a disulfide. (4) Oxidised Trx forms an interprotein disulfide with SeCys498 of TrxR which is then reduced by Cys497 to form the oxidised TrxR homodimer again (1) and reduced Trx.

Substrates for TrxR: Although knock-out (KO) TrxR1 mice die during embryogenesis, interestingly mice with a heart-specific KO of TrxR1 develop normally.[405] Mice lacking functional TrxR2 also die during embryogenesis with mice with a heart-specific inactivation of TrxR2 dying soon after birth from dilated cardiomyopathy and congestive heart failure. This shows the importance of TrxR2 in heart development and function. Overall TrxR1 and TrxR2 appear to have non-redundant functions.[406]

In addition to being bigger than *E. coli* TrxR, mammalian TrxRs have a different and wider substrate specificity; reducing proteins other than just Trx.[385] The endoplasmic reticulum proteins protein disulfide isomerase, Ca^{2+} binding protein 1 (CaBP1) and Ca^{2+} binding protein 2 (CaBP2) are also substrates and these have Trx-like activity.[407, 408] TrxR can also reduce non-disulfide substrates such as lipid hydroperoxides and H_2O_2.[409]

If RIα disulfide formation is a form of redox regulation of PKA then I would anticipate that it can be reversed, and most probably this would be enzymatically. This chapter investigates whether the Trx system is indeed capable of reducing RIα disulfide. I hypothesise that the Trx system does reduce oxidised RIα because bands at ~62 kDa and ~75 kDa have been observed on some non-reducing Western blots,[57] consistent with RIα monomer and one Trx or RIα monomer and two Trx's, respectively (Figure 6.5). Consequently, this chapter aims to address the following:

1. Whether the Trx-TrxR-NADPH system reduces PKA RIα disulfide. This will be assessed by monitoring NADPH consumption indexed by measuring a decrease in NADPH fluorescence. I hypothesise that PKA RIα disulfide is a substrate for the Trx system and so I anticipate an increase in Trx-TrxR activity and consequent increase in NADPH consumption.

2. Whether 3′,5′-cyclic monophosphate (cAMP) modulates Trx-TrxR dependent reduction of RIα disulfide. cAMP binding to RIα may cause a conformational change in RIα that may reduce or increase Trx's access to RIα disulfide and so Trx-mediated reduction of disulfide. The altered activity of Trx in turn alters the amount of oxidised Trx present and therefore amount of substrate for TrxR thereby altering TrxR activity.

3. If pharmacological inhibition of TrxR alters basal RIα redox state or RIα disulfide formation in response to a low concentration of oxidant. Inhibition of TrxR will cause an accumulation of oxidised Trx, which then can't reduce its substrates. I hypothesise

that PKA RIα disulfide is a substrate for Trx and so I expect to observe an accumulation of RIα disulfide when TrxR is pharmacologically inhibited.

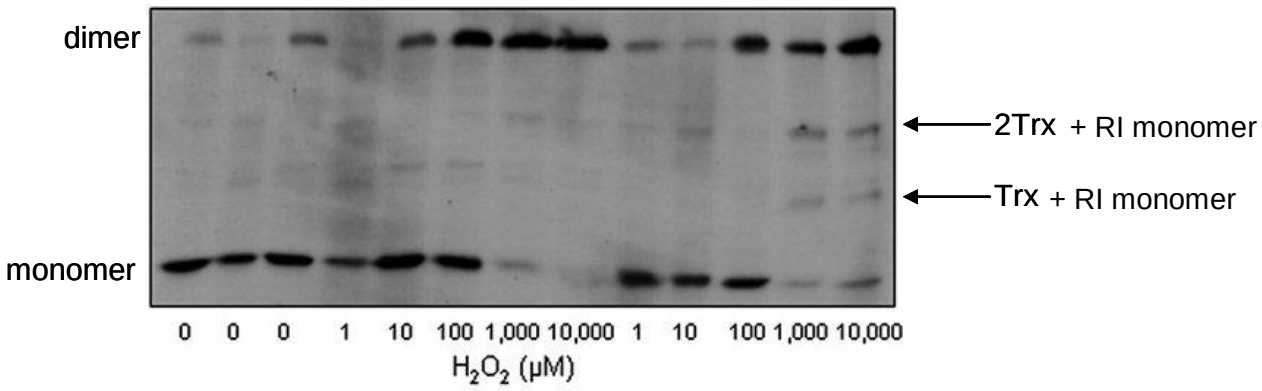

Figure 6.5 Brennans,[57] Western blot probed with anti - PKA RI.

Isolated perfused rat hearts were perfused with 0 - 10000 μM H_2O_2 (5 min). I hypothesise that the two bands indicated by arrows for hearts perfused with 1000 and 10000 μM H_2O_2 are the RIα subunit conjugated to one Trx or two Trx units.

6.2 METHODS

6.2.1 NADPH fluorescence

RIα protein is expensive to purchase, so to determine if the Trx system (TrxR, Trx, NADPH) reduced RIα disulfide a method was used that was sensitive enough such that only a small amount of RIα was required. This approach also keeps the concentration of proteins and reducing molecules at concentrations similar to what they are in the cell. As fluorescence spectroscopy is suitably sensitive, a method based on NADPH which is intrinsically fluorescent was chosen. The reduced form of NADPH is fluorescent but the non-reduced form is not. Therefore if RIα disulfide is reduced by Trx-TrxR, NADPH would be consumed as a substrate and therefore oxidised and so I would expect to observe a decrease in NADPH fluorescence (Figure 6.6).

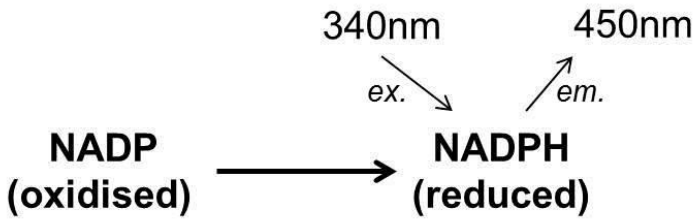

Figure 6.6 NADPH fluorescence.

Schematic showing that reduced NADPH, but not oxidised $NADP^+$, fluoresces at a 340 nm excitation (ex.) wavelength and a 450 nm emission (em.) wavelength.

Construction of a NADPH standard curve and determining assay sensitivity: First, a standard curve was constructed. 20 µl of each NADPH standard concentration (0.05, 0.1, 0.5, 1, 2.5, 5, 7.5, 10, 12.5, 25 and 50 µM in 100 µM diethylene triamine pentaacetic acid (DTPA) in 100 mM Tris pH 7.4) was added in duplicate to wells of a black 384-well optical bottom plate. The plate was placed in a fluorescence reader (FLUOstar Omega (BMG Labtech)) set at 37 ºC and a 340 nm excitation wavelength and a 450 nm emission wavelength. Fluorescence readings were recorded every minute for 5 min. An NADPH standard curve was then constructed using average values at 5

min. A low concentration of NADPH that was detected by the reader but with little error was then selected for studies assessing RIα disulfide reduction. A low concentration of NADPH was chosen to sensitise the fluorescence experiment assessing Trx-dependent RIα reduction, as a limited amount of recombinant RIα was available.

RIα or Prx-1 modulated NADPH consumption by Trx-TrxR: To determine if the Trx system was involved in RIα disulfide reduction, NADPH fluorescence was measured as above. The assay mixture in a final volume of 20 µl comprised of 5 µM NADPH, 635 nM TrxR (purified from rat liver), 150 nM recombinant human Trx1 (R&D Systems) and 1.4 µM PKA RIα (human recombinant, Biaffin GmbH & Co KG) or 1.5 µM recombinant human Prx-1 (Sigma Aldrich) in 100 µM DTPA in 100 mM Tris pH 7.4. A 5 min stability period with just Trx, TrxR and NADPH was carried out first before RIα or Prx-1 was added. Fluorescence of a blank (100 µM DTPA in 100 mM Tris pH 7.4) was also measured throughout so that this value could be subtracted from the values for the other reaction mixtures to give normalised values. The intrinsic fluorescence of each component (Trx, TrxR, RIα or Prx-1) was measured to check whether these interfere with NADPH fluorescence measurements.

Effect of cAMP on RIα-modulated NADPH fluorescence: I assessed whether cAMP altered Trx-dependent RIα reduction. cAMP binding to RIα may cause a conformational change which may enhance or inhibit Trx1 binding to RIα and therefore alter RIα disulfide reduction. NADPH fluorescence was measured as above. In addition, NADPH fluorescence in the presence of cAMP-saturated RIα was measured. RIα was incubated with 150 µM cAMP before both being added to the reaction mixture.

6.2.2 Monitoring disulfide RIα or disulfide Prx-1 reduction by Western immunoblotting

The redox status of RIα or Prx-1 in the samples from the fluorescence assays (described above) was analysed by immunoblotting. 20 µl SDS sample buffer (with 100 mM maleimide) was immediately added to the samples at the end of the fluorescence assay

and SDS-PAGE and Western blotting were carried out as described in Chapter 2. Blots were probed for RIα or Prx-1. The Prx-1 antibody (ab41906, Abcam) was incubated with the blots for 1 hour at 1:1000 in 5 % milk in PBS with 0.1 % Tween-20 (PBS-T) at room temperature then washed for an hour and incubated with anti-rabbit secondary antibody for 1 hour at room temperature.

6.2.3 Adult rat ventricular myocyte treatment with TrxR inhibitors: auranofin and cisplatin

Another method for determining whether Trx1 reduced RIα disulfide involved treating adult rat ventricular myocytes (ARVMs) with the TrxR inhibitors, cisplatin or auranofin. As described in Chapter 2, ARVMs were isolated from male Wistar rats and either cultured overnight and treated or left to settle at room temperature for two hours (freshly isolated) then treated.

Treatment of overnight-cultured ARVMs: Pilot experiments were carried out in overnight-cultured ARVMs. ARVMs were left untreated or pre-treated with a TrxR inhibitor (20 nM auranofin or 100 μM cisplatin) or vehicle (ethanol for auranofin and dimethyl sulfoxide (DMSO) for cisplatin) for 5 min. ARVMs were then left untreated or treated with 0.5 mM diamide for a further 1, 5 or 10 min. The culture medium was then removed and 300 μl SDS sample buffer with 100 mM maleimide was added to the wells and the cells were scraped off the plate using a cell scraper. The mixture was then pipetted into an Eppendorf tube.

Treatment of freshly isolated ARVMs: Myocytes were aliquoted into Eppendorf tubes and left untreated or treated with auranofin (50, 250 or 500 nM) or its vehicle (500 nM ethanol) or cisplatin (20, 50 or 75 μM) or its vehicle (75 μM DMSO) for 30 min at 37 ºC. Treatment with diamide (1, 5, 10 or 50 μM) for 5 min then followed. Samples were centrifuged at 1000 g for 0.5 min, the supernatant was removed and then the pellet was re-suspended in 250 μl SDS sample buffer containing 100 mM maleimide. In additional experiments, ARVMs were treated with 150, 300, 500 or 750 μM cisplatin or

750 nM, 1, 2 or 3 μM auranofin or the vehicles for 30 min using the same protocol described.

6.2.4 Monitoring redox status of PKA RIα, cGMP-dependent protein kinase Iα and Prx-1 in freshly isolated ARVMs treated with TrxR inhibitors

The redox state of PKA RIα in auranofin / cisplatin treated ARVMs was determined by SDS-PAGE and Western blotting and probing the blots for PKA RIα, as described in Chapter 2. cGMP-dependent protein kinase (PKG) Iα redox state was also determined by incubating the blots with cGKIα (E-17) (sc-10338, Santa Cruz) for 1 hour (1:1000) followed by a one hour wash and incubation with anti-goat secondary (1:1000 in 5% milk in PBS-T) for 1 hour at room temperature. The redox state of Prx-1 was also determined by probing the blot for Prx-1 (as described in 6.2.2).

6.2.5 Determining redox state of Prx-1 in Langendorff-perfused wild-type mouse hearts by Western immunoblotting

Wild-type (WT) hearts were Langendorff-perfused for 40 min with K-HB and then homogenised. SDS-PAGE and Western blotting were carried out (as described in Chapter 2). Blots were probed for Prx-1 (ab41905, Abcam) as described in 6.2.2.

6.3 RESULTS

6.3.1 NADPH fluorescence as a measure of RIα disulfide reduction by the Trx system

NADPH fluorescence standard curve and stability of NADPH fluorescence over time: A standard curve was constructed for NADPH fluorescence at 5 min (Figure 6.7A). From the standard curve, a low concentration of NADPH was chosen that gave a relatively small error but a relatively high relative fluorescence units (RFU) value as this allows the RIα reduction assay to be sensitive. After magnification of the standard curve between 0 and 10 μM NADPH (Figure 6.7B), 5 μM NADPH was chosen which fluoresced at ~27000 relative fluorescence units (RFU). Figure 6.8 shows that fluorescence for all concentrations of NADPH stayed quite stable over the 5 min period which was important when assessing how other proteins affect NADPH fluorescence over time. Fluorescence for 5 μM NADPH only changed from 49000 ± 8200 RFU at 0 min to 48000 ± 8400 RFU at 5 min.

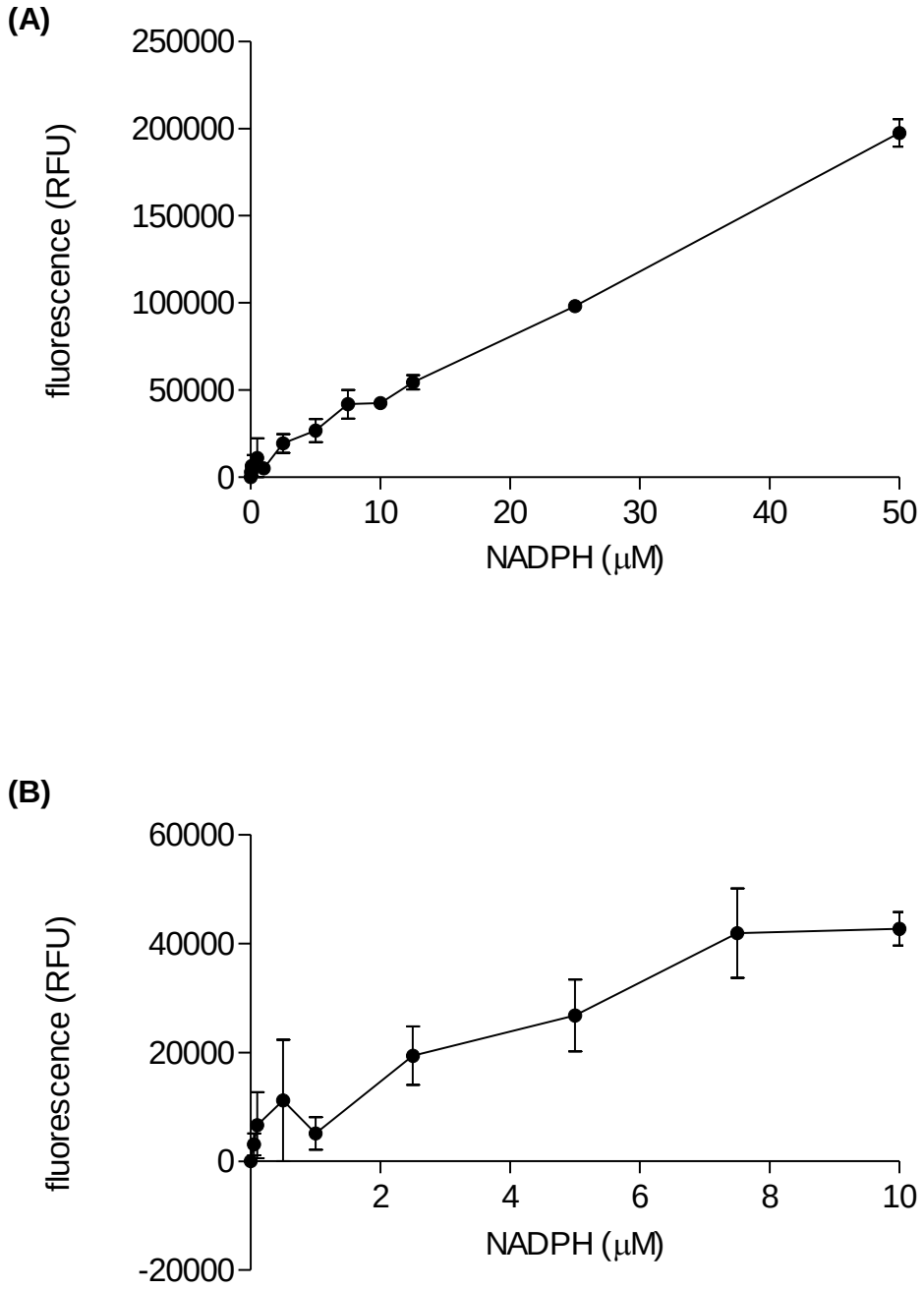

Figure 6.7 Standard curve for NADPH fluorescence.

(A) 0 - 50 μM NADPH standards were prepared and fluorescence (RFU) was read after 5 min. Values are normalised where the RFU value for the blank (0 μM) was subtracted from each value. Graph shows average fluorescence values ± SEM where n=9/10 (B) The graph was magnified between 0 – 10 μM NADPH.

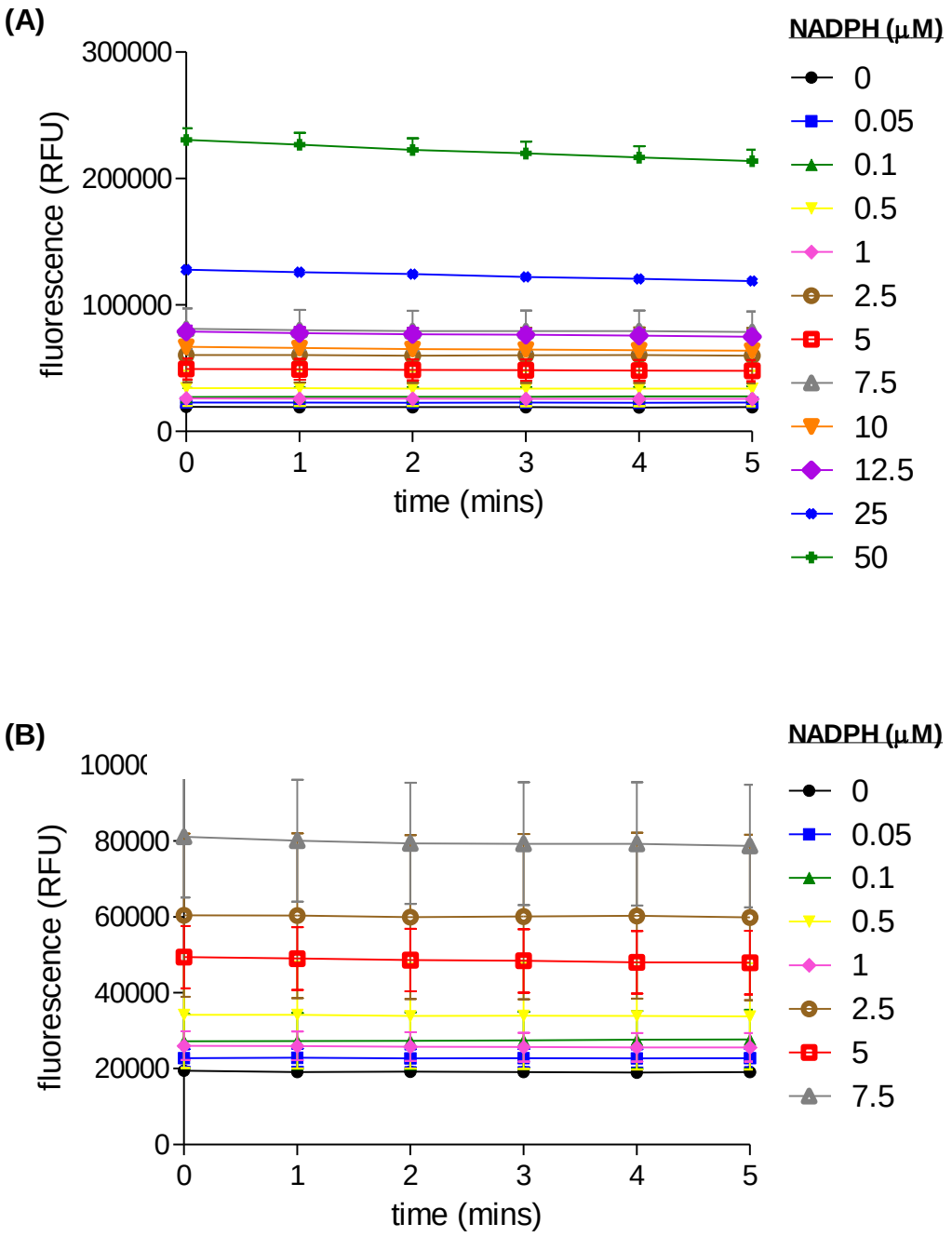

Figure 6.8 Stability of NADPH fluorescence over time.

(A) 0 - 50 µM NADPH standards were prepared and fluorescence (RFU) was measured over 5 min. Graphs show average fluorescence (raw values) ± SEM where n=9/10 (B) Magnification of average fluorescence over 5 min for 0 - 7.5 µM NADPH. Fluorescence was stable over 5 min.

Effect of assay components on NADPH consumption: It was important to check that the individual components of the Trx system (Trx alone, TrxR alone) and RIα itself did not affect NADPH fluorescence over time. This allows me to be sure that any effect seen when all the components were incubated together was definitely due to the presence of substrate. Prx-1 was used as a positive control to verify the assay was working, being selected as it is a known substrate for Trx.[410] Therefore, the effect of Prx-1 alone on NADPH fluorescence was also analysed.

Trx caused a trend for an increase in NADPH fluorescence over time, but this was not significantly different from fluorescence for NADPH alone at any time point (Figure 6.9A). This increase was not expected. It is difficult to explain NADPH production but perhaps Trx auto-fluoresces under these conditions. TrxR caused NADPH to be consumed and this was significantly different ($p<0.05$) from NADPH consumption for NADPH alone at each time point (Figure 6.9B). This may be due to auto-oxidation of TrxR in air requiring reduction by NADPH and so NADPH to be consumed. Prx-1 did not affect NADPH fluorescence (Figure 6.10A) and neither did RIα (Figure 6.10B).

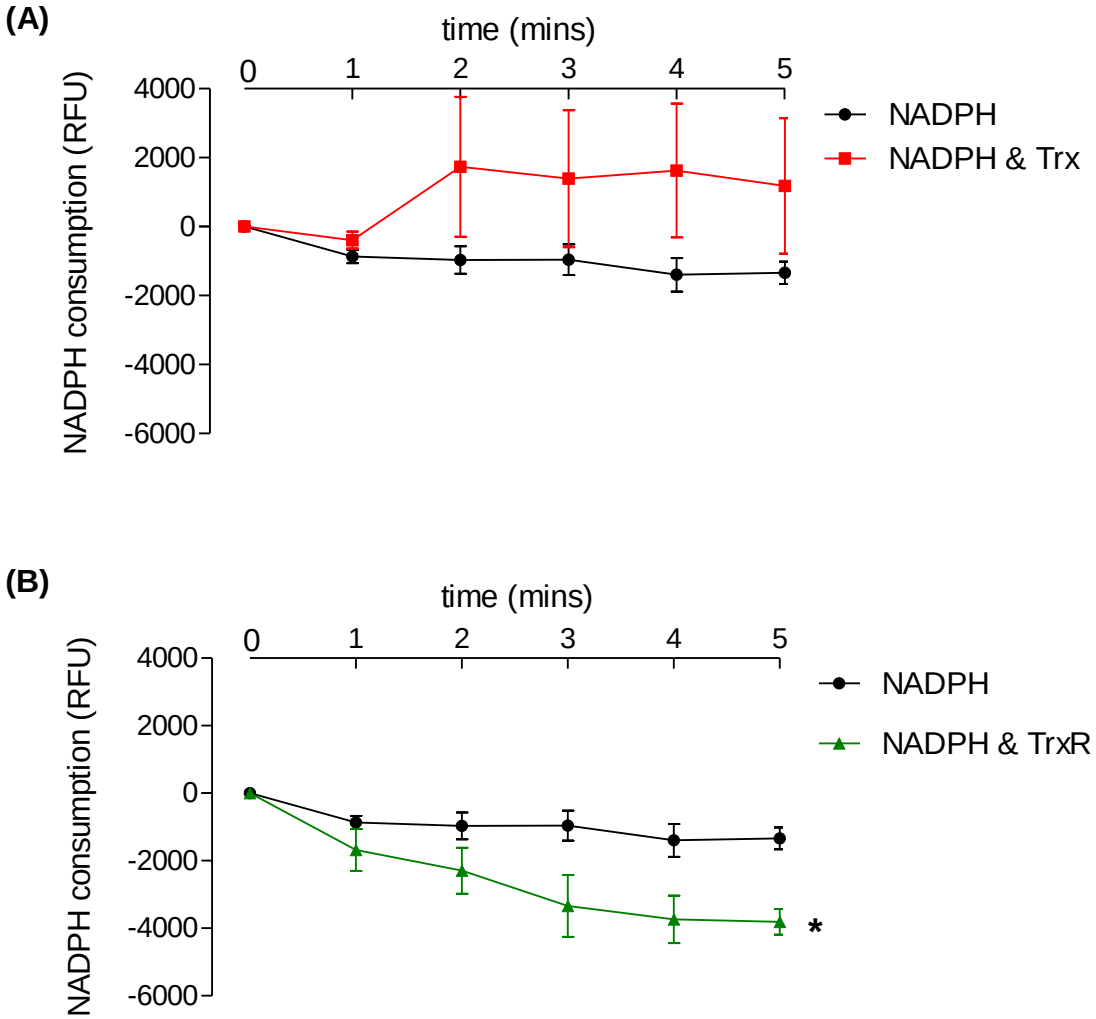

Figure 6.9 Effect of Trx or TrxR on NADPH consumption.

(A) Fluorescence of 5 µM NADPH alone (n=7) or with 150 nM Trx (n=6) was measured over 5 min. Graph shows the change in fluorescence (NADPH consumption) from time = 0 min (minus blank) ± SEM. (B) Fluorescence of 5 µM NADPH alone (n=7) or with 635 nM TrxR (n=5) was measured over 5 min. $^{*}p<0.05$ compared to NADPH alone. Trx caused a trend for an increase in NADPH fluorescence and TrxR caused a significant decrease.

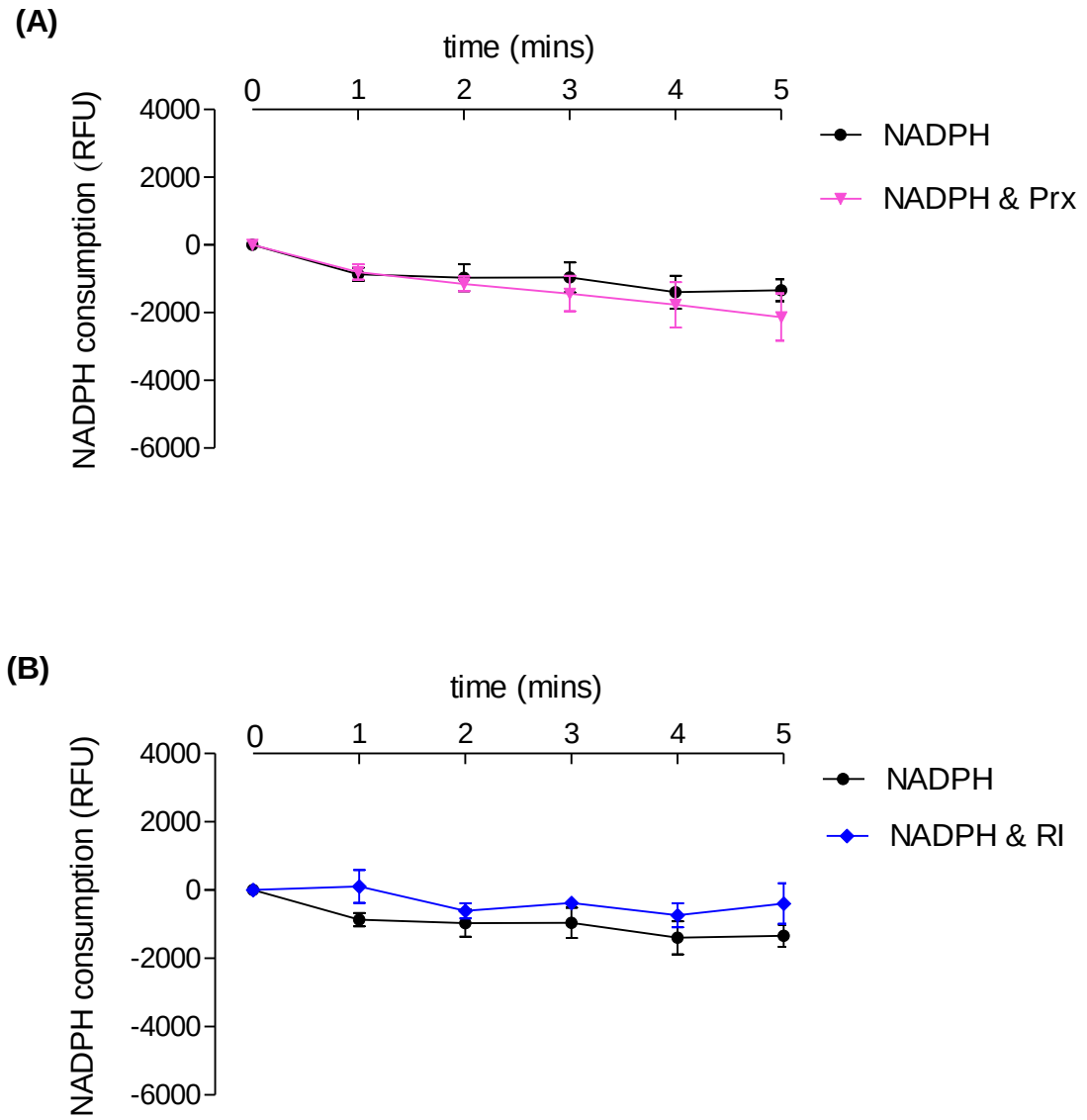

Figure 6.10 The effect of oxidised Prx-1 or oxidised RIα on NADPH consumption.

(A) Fluorescence of 5 µM NADPH alone (n=6) and with 1.5 µM Prx-1 (n=7) was read over 5 min. Graph shows change in fluorescence (NADPH consumption) from time = 0 min (minus blank) ± SEM (B) Fluorescence of 5 µM NADPH alone (n=6) and with 1.4 µM RIα (n=5). NADPH fluorescence was not altered by RIα or Prx-1.

Effect of RIα and Prx-1 on NADPH consumption by Trx-TrxR: In order to determine whether the Trx system reduces RIα disulfide, the effect of oxidised RIα on NADPH consumption by Trx-TrxR was analysed over 5 min. NADPH fluorescence only decreased by 2700 ± 430 RFU when NADPH was mixed with Trx and TrxR for 5 min (Figure 6.11). This minor time-dependent consumption of NADPH is likely to be because Trx and TrxR are auto-oxidised in air to provide a basal activity of TrxR (consuming NADPH). Prx-1, a recognised substrate of the Trx system, served as a positive control and confirmed that the assay was working. Oxidised Prx-1 caused 3-fold more NADPH to be consumed compared to the control (significant, $p<0.05$). Oxidised RIα similarly caused 3-fold more NADPH to be consumed compared to control (significant, $p<0.05$) consistent with RIα being a substrate for the Trx system.

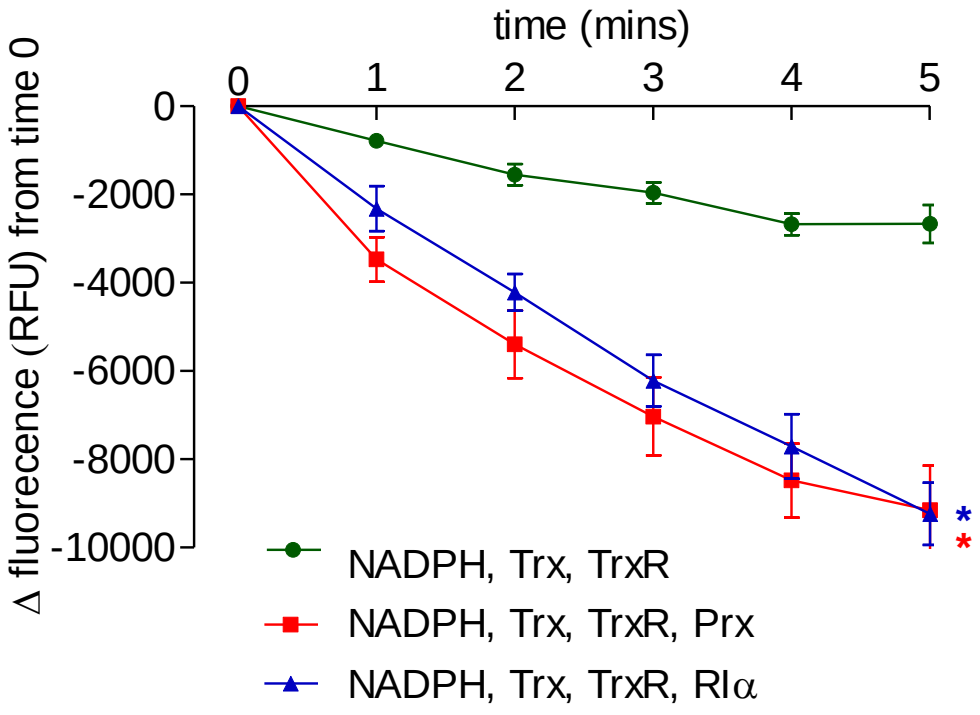

Figure 6.11 Effect of oxidised Prx-1 or oxidised RIα on NADPH consumption by Trx-TrxR.

The fluorescence of 5 µM NADPH, 150 nM Trx and 635 nM TrxR alone or together with 1.5 µM Prx-1 (oxidised) or 1.4 µM RIα (oxidised) was read over 5 min. This graph shows the change in NADPH fluorescence (NADPH consumption, minus blank) from time 0 min ± SEM. Prx-1 (n=8) and RIα (n=6) caused a significant (*$p<0.05$) reduction in NADPH fluorescence over 5 min compared to when no substrate was present (n=7).

Confirmation that Prx-1 and RIα were indeed reduced by Trx-TrxR: Although the consumption of NADPH in the assay containing disulfide RIα or Prx-1 together with Trx and TrxR was consistent with reduction of the substrate, further confirmation of this was sought. Consequently, the oxidation state of RIα before and after incubation with NADPH alone or NADPH, Trx and TrxR was determined by Western immunoblotting. Figure 6.12 confirms that Prx-1 was oxidised at the start of the assay. When Prx-1 was mixed with NADPH alone for 10 min, it remained in its oxidised form (no monomer). However, when mixed with NADPH / Trx / TrxR, more Prx-1 was present in its reduced monomeric state, confirming that the Trx system did reduce Prx-1. Figure 6.13 confirms that RIα was also oxidised at the start of the experiments. When RIα was mixed with NADPH alone, there was a relatively small amount of reduced monomeric RIα present in comparison to oxidised dimeric RIα. When Trx and TrxR were also in the reaction mixture, the abundance of reduced monomeric RIα did not change, which is inconsistent with the fluorescence results suggesting RIα disulfide is reduced by the Trx system.

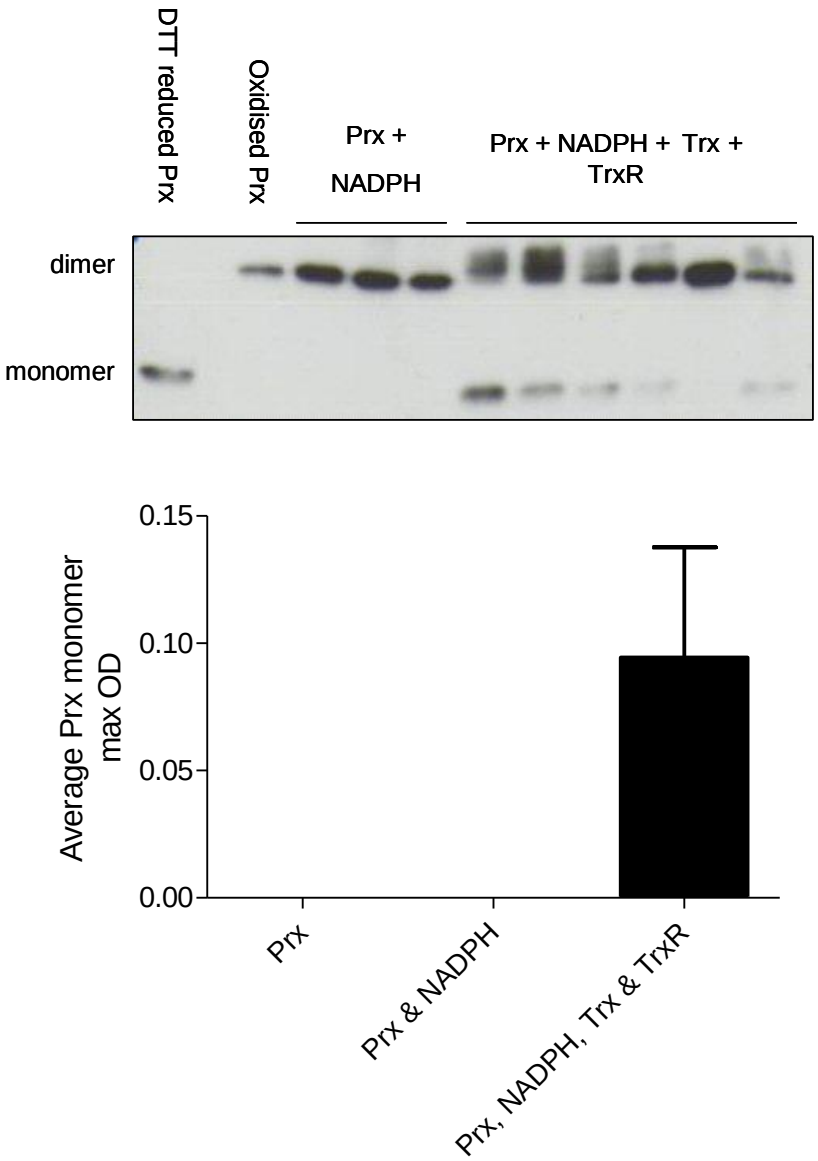

Figure 6.12 Reduction of Prx-1 by the Trx system.

5 μM NADPH, 150 nM Trx, 635 nM TrxR and 1.5 μM Prx-1 (non-reduced / oxidised form) were incubated together for 5 min. Western blotting was carried out to show Prx-1 redox state and average reduced Prx-1 max OD was presented graphically (n=1, 3, 6 ± SEM). Prx-1 was reduced by the Trx system.

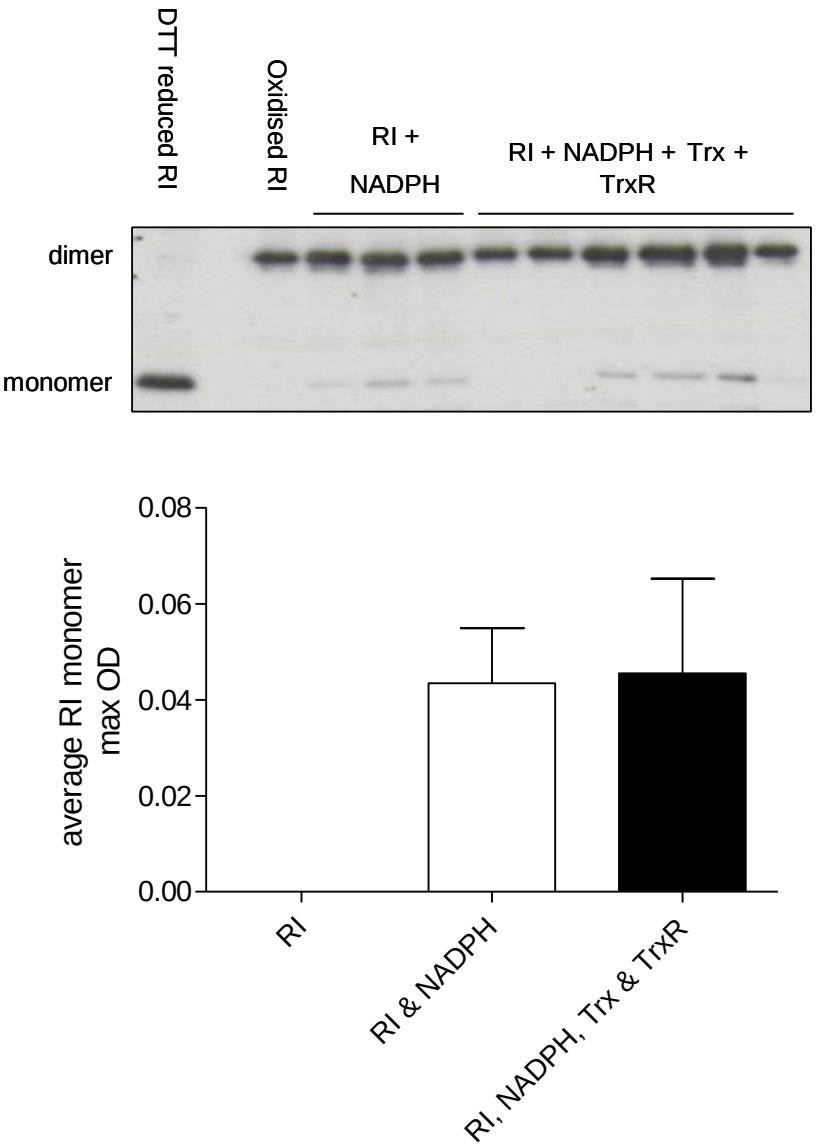

Figure 6.13 Reduction of PKA RIα by the Trx system.

5 μM NADPH, 150 nM Trx, 635 nM TrxR and 1.4 μM RIα (non-reduced form) were incubated together for 5 min. Western blot was probed for PKA RIα and average max OD of reduced RIα was calculated (n=1, 3, 6 ± SEM). Reduced RIα formed when oxidised RIα was incubated with NADPH, Trx and TrxR but RIα was also unexpectedly reduced when incubated with NADPH alone.

6.3.2 Effect of cAMP on RIα reduction by the Trx system

cAMP was added to the fluorescence assay to establish whether this altered Trx-TrxR activity induced by oxidised RIα.

Effect of cAMP on disulfide RIα-mediated NADPH consumption: cAMP was now an additional component in the assay, and so I needed to determine whether cAMP auto-fluorescence interfered with the assay. cAMP alone did not significantly alter NADPH fluorescence over 5 min (Figure 6.14A). RIα caused a decrease (5500 ± 1300 RFU) in NADPH fluorescence over the 5 min period which was significantly different ($p<0.05$) from when substrate was absent (1500 ± 1100 RFU) (Figure 6.14B). When cAMP-bound RIα was added to the Trx / TrxR / NADPH mixture a decrease in NADPH fluorescence (6300 ± 1100 RFU) occurred which was significantly ($p<0.05$) different from when substrate was absent. This decrease was similar to the decrease in NADPH consumption for RIα with no cAMP (consistent with results in Figure 6.11). Therefore, cAMP did not alter NADPH consumption in an assay assessing RIα reduction by the Trx system.

Effect of cAMP on redox state of RIα: Although reduction of RIα by the Trx system was not detected by immunoblotting studies (Figure 6.13), I wanted to check this was also the case for RIα with cAMP. Figure 6.14C demonstrates, again, that RIα with NADPH alone is present mainly in its oxidised disulfide dimeric form and the addition of Trx / TrxR with or without cAMP did not change RIα redox state. Only at a long exposure of the immunoblot was any reduced monomeric RIα observed, and this was minimal compared to RIα disulfide dimer. Therefore, again this method could not detect RIα disulfide reduction by the Trx system.

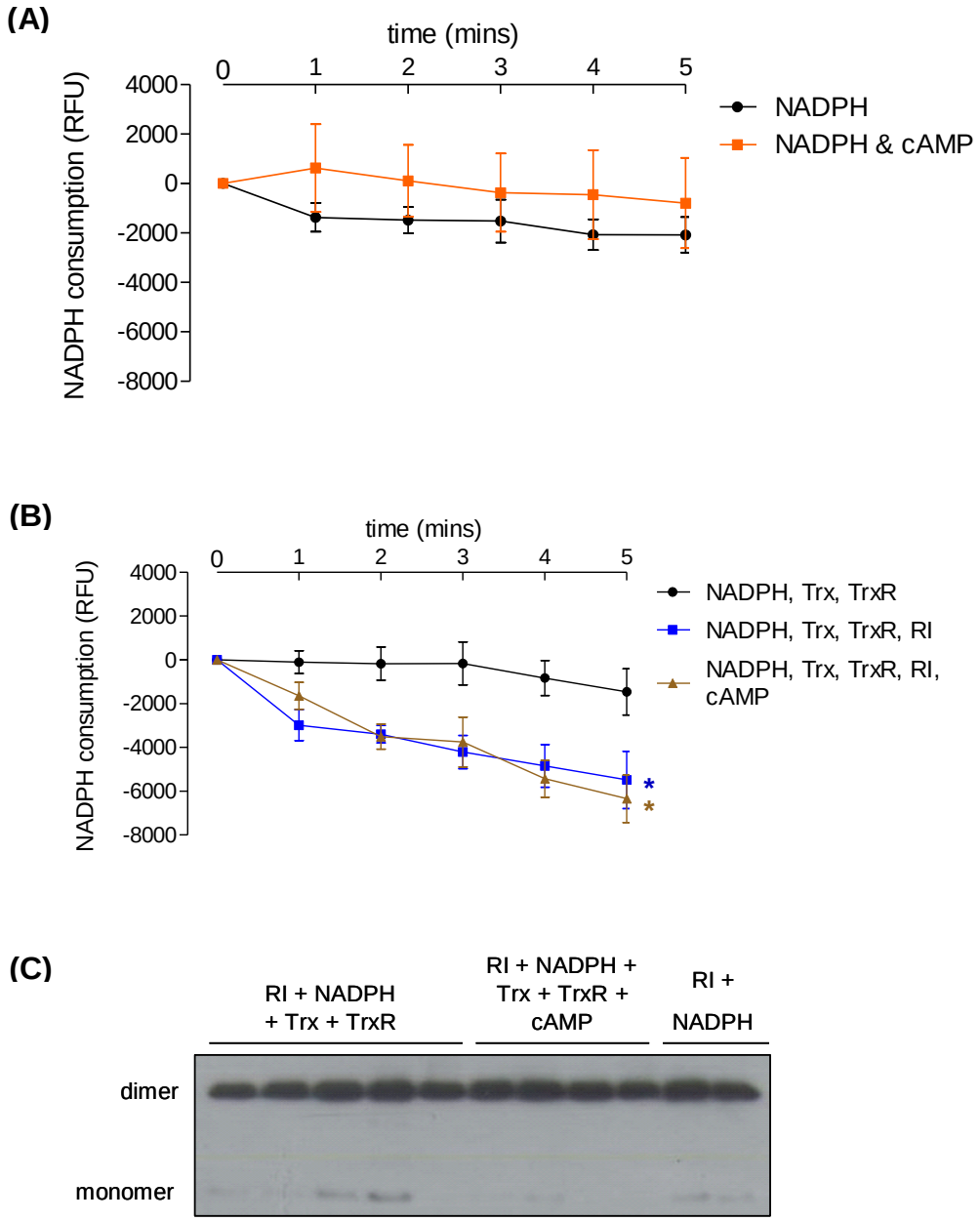

Figure 6.14 Effect of cAMP on NADPH consumption by RIα and the Trx system.

(A) Fluorescence was measured for 5 µM NADPH alone or with 150 µM cAMP for 5 min and average change in fluorescence (NADPH consumption) from time = 0 (n=4 ± SEM) was calculated. (B) Fluorescence was measured over 5 min for NADPH, TrxR and Trx alone or these components with RIα or RIα and cAMP and average NADPH consumption quantified (n=5 ± SEM, * $p<0.05$ AUC compared to AUC for no substrate). cAMP did not affect the significant NADPH consumption caused by oxidised RIα. (C) Redox state of PKA RIα in fluorescence samples was identified by Western blotting but no reduction of RIα by the Trx system was observed.

6.3.3 Using TrxR inhibitors to assess reduction of RIα disulfide by the Trx system in ARVMs

Effect of TrxR inhibition on RIα redox state in overnight-cultured ARVMs: Experiments were initially carried out in ARVMs cultured overnight for reasons discussed in Chapter 2.2.

Figure 6.15 shows representative blots for overnight-cultured ARVMs treated with diamide or the TrxR inhibitors, auranofin (A) or cisplatin (B) for 1 or 5 min. The blots illustrate the general finding that the reduced RIα monomer was fully absent even in control untreated cells. The abundance of RIα seemingly varied between treatments despite confirmation of equal total protein loading by Coomassie blue staining (not shown). This observation of a low abundance of reduced monomeric RIα was unexpected and complicated studies I had anticipated undertaking. Diamide increased RIα disulfide compared to control which is consistent with RIα monomer being oxidised. However, overnight culture caused the 'disappearance' of the reduced kinase. Possible explanations for this are discussed in Chapter 2.2. Consequently, these findings hindered my ability to establish whether the Trx system reverses RIα disulfide.

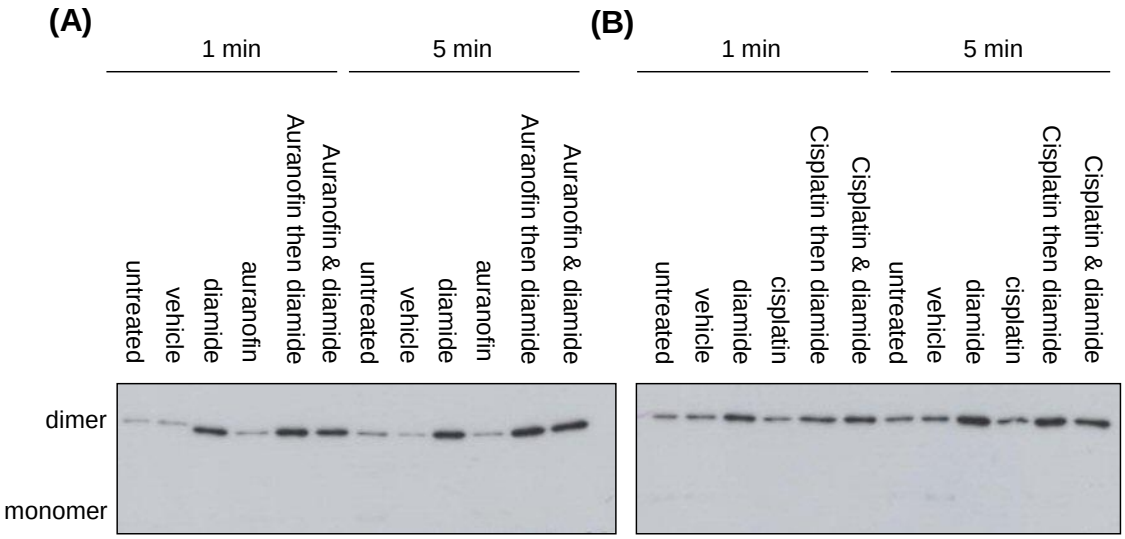

Figure 6.15 Effect of TrxR inhibitors (auranofin and cisplatin) on PKA RIα redox state in overnight-cultured ARVMs.

(A) Overnight-cultured ARVMs were left untreated or pre-treated with vehicle (ethanol) or TrxR inhibitor (auranofin) for 5 min. ARVMs were then left untreated or treated with diamide (1 or 5 min). Western blots were probed for PKA RI□. (B) As above but vehicle was DMSO and TrxR inhibitor was cisplatin. Unexpectedly there was no reduced monomeric RI□ present in overnight-cultured ARVMs.

Effect of TrxR inhibition on RIα redox state in freshly isolated ARVMs: As discussed in Chapter 2.2, loss of monomeric reduced RIα and variable RIα protein abundance between samples in overnight-cultured ARVMs appeared to be associated with changing the cell culture medium, which is a step routinely carried out when culturing ARVMs overnight. In contrast, in freshly isolated ARVMs reduced monomeric RIα was present and the total RIα protein abundance was similar between control and treated cells. Therefore, the effect of TrxR inhibition on RIα redox state could be investigated in freshly isolated ARVMs.

Figure 6.16 shows representative immunoblots probed for RIα with corresponding graphs showing the percentage RIα disulfide in freshly isolated ARVMs before and after treatment with cisplatin. Treatment with concentrations of cisplatin up to 75 μM

(Figure 6.16A) did not alter the percentage RIα disulfide, which stayed at ~35 %. When this was repeated with diamide pre-treatment, an increase in disulfide RIα above basal was again not observed. Treatment of freshly isolated ARVMs with higher concentrations of cisplatin (150, 300, 500 or 750 µM, Figure 6.16B) caused a trend towards an increase in percentage RIα disulfide, from 33 ± 6 % to 59 ± 10 %. An increase was also seen when these cisplatin-treated ARVMs were pre-treated with 5 µM diamide (36 ± 12 % to 75 ± 6 %). This suggests that inhibiting TrxR caused an accumulation of RIα disulfide.

Treatment of freshly isolated ARVMs with concentrations of another TrxR inhibitor, auranofin (50 - 500 nM) did not alter RIα disulfide levels, which was basally ~25 % (Figure 6.17A). 50 nM auranofin did not alter RIα disulfide in ARVMs pre-treated with 5 µM diamide (~25 %) but 250 nM and 500 nM caused a small increase to ~40 % and ~35 % respectively. In comparison, treatment of ARVMs with 750 nM up to 3 µM auranofin alone (Figure 6.17B) caused a trend towards an increase in RIα disulfide formation (29 ± 6 % to 61 ± 7 %). This trend was also observed when ARVMs were pre-treated with 5 µM diamide then treated with 750 nM up to 3 µM auranofin (40 ± 10 % to 68 ± 7 %). When ARVMs were pre-treated with diamide then 1 or 2 µM auranofin there appeared to be a synergistic effect on increasing RIα disulfide formation.

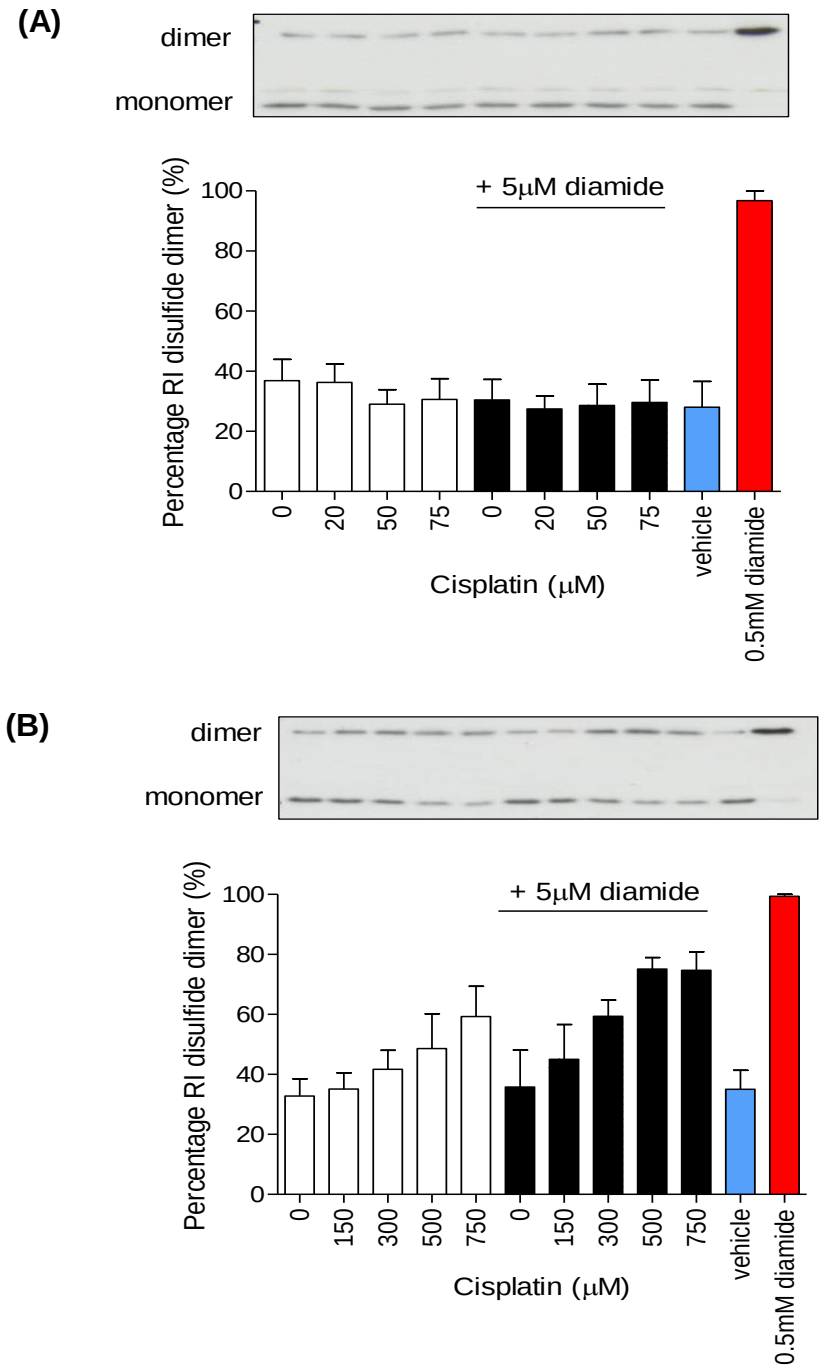

Figure 6.16 Effect of cisplatin on PKA RIα redox state in freshly isolated ARVMs.

(A) ARVMs were left untreated or treated with cisplatin (0 - 75 μM), vehicle or 0.5 mM diamide for 30 min -/+ post-treatment with 5 μM diamide. Blots were probed for PKA RIα and percentage PKA RIα disulfide dimer was calculated (n=5 ± SEM). (B) ARVMs were treated with cisplatin (150 – 750 μM), vehicle or diamide -/+ post-treatment with diamide. There was a trend towards an increase in RIα disulfide with 150 - 750 μM cisplatin with and without diamide treatment.

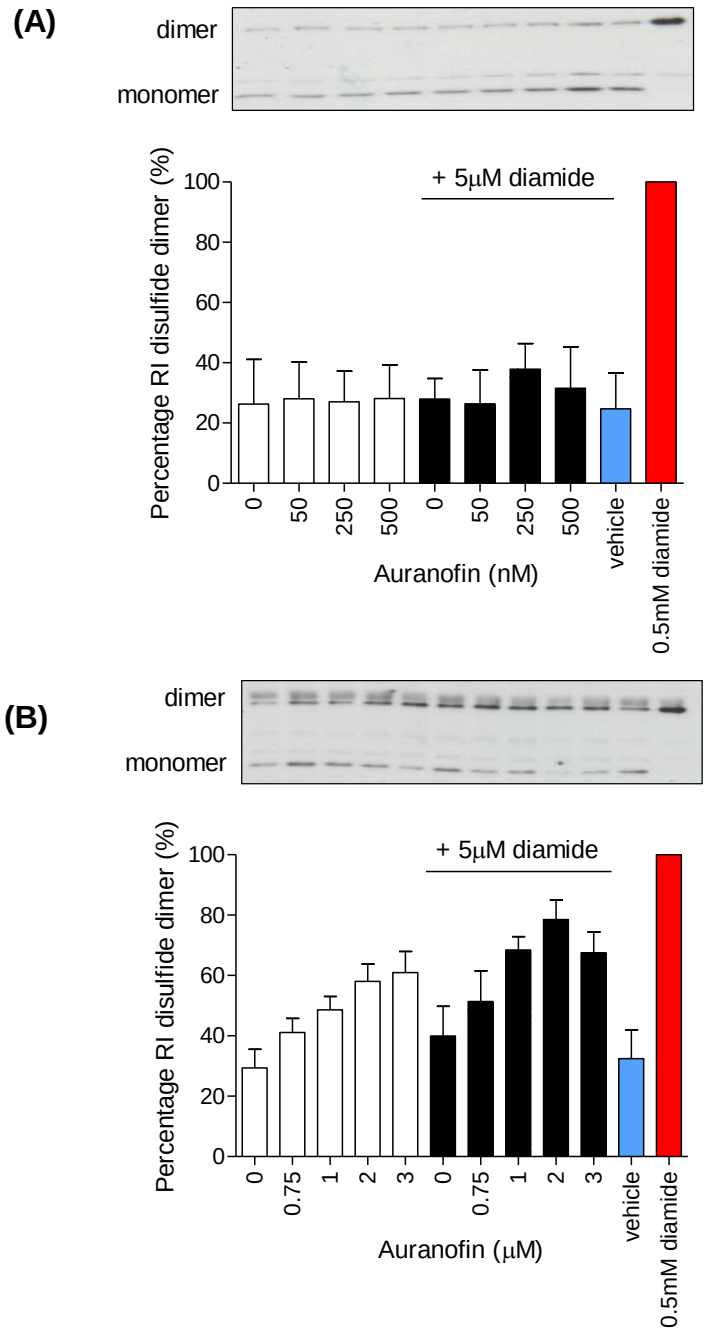

Figure 6.17. Effect of auranofin on PKA RIα redox state in freshly isolated ARVMs.

(A) ARVMs were treated with auranofin (0 - 500 nM), vehicle or 0.5 mM diamide for 30 min -/+ post-treatment with 5 μM diamide (5 min). Blots were probed for PKA RIα as shown in representative blot. Percentage PKA RIα disulfide dimer is shown graphically (n=5 ± SEM). (B) ARVMs were treated with 0 - 3 μM auranofin, vehicle or 0.5 mM diamide (30 min) -/+ post-treatment with 5 μM diamide (5 min). There was a trend towards an increase in RIα disulfide with 0.75 - 3 μM auranofin with and without diamide.

PKG Iα redox state in freshly isolated ARVMs treated with TrxR inhibitors: PKG Iα can also be oxidised to a disulfide,[60] (as outlined in Chapter 1). The redox state of PKG Iα was determined in the samples previously probed for PKA RIα to determine whether PKG Iα disulfide was also reduced by the Trx system. There was a trend towards an increase PKG Iα disulfide in ARVMs treated with 0 – 750 μM cisplatin (as observed with PKA RIα) but it was not statistically significant. The percentage PKG Iα disulfide increased by ~20 % with 750 μM cisplatin treatment (Figure 6.18A). This trend also occurred in cisplatin-treated ARVMs then treated with 5 μM diamide. There was also a trend towards an increase in percentage PKG Iα disulfide in ARVMs treated with 0 – 3 μM auranofin albeit statistically insignificant (Figure 6.18B), mirroring what was observed with PKA RIα. Treatment with the maximum auranofin concentration (3 μM) increased PKG Iα disulfide by ~13 %. Again, this trend was also observed in auranofin-treated ARVMs then treated with 5 μM diamide. 5 μM diamide alone increased percentage PKG Iα disulfide by ~10 % in both data sets.

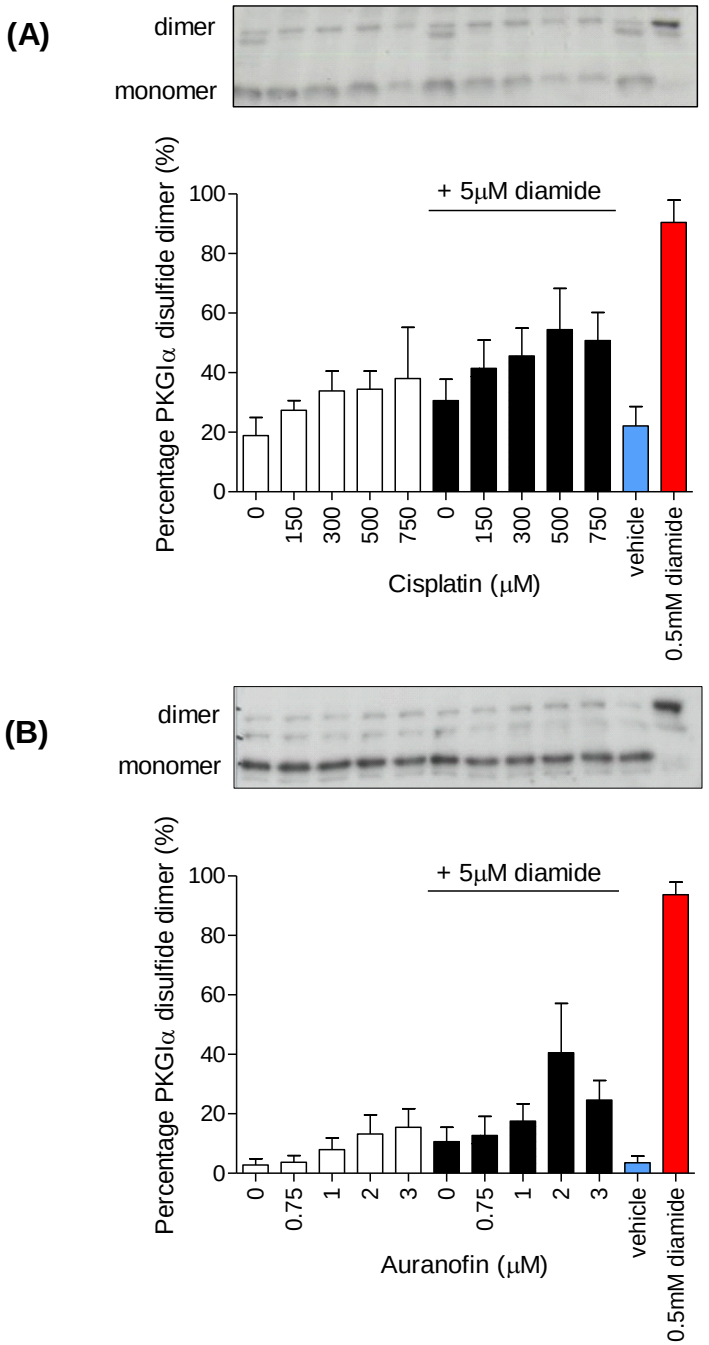

Figure 6.18 Effect of cisplatin or auranofin on PKG Iα redox state in freshly isolated ARVMs.

(A) ARVMs were treated with 0 - 750 μM cisplatin, DMSO vehicle or 0.5 mM diamide (30 min) -/+ post-treatment with 5 μM diamide (5 min). Western blots were probed for PKG Iα and percentage PKG Iα disulfide dimer was presented graphically (n=5 ± SEM). (B) ARVMs were treated with 0 – 3 μM auranofin, ethanol vehicle or 0.5 mM diamide (30 min) -/+ post-treatment with diamide (5 μM, 5 min). There was a trend towards an increase in PKG Iα disulfide with increasing concentration of auranofin or cisplatin.

Effect of TrxR inhibition on Prx-1 redox state: Prx-1 is a known substrate for Trx-catalysed reduction. I wanted to confirm that cisplatin and auranofin were indeed efficiently inhibiting TrxR under the treatment conditions used. Consequently, Prx-1 oxidation to the disulfide dimer was monitored, serving as a positive control.

Prx-1 was present basally as a disulfide dimer (50 kDa) in untreated ARVMs, as well as after 150 - 750 µM cisplatin treatment (Figure 6.19). No reduced monomeric Prx-1 (25 kDa) was observed in untreated ARVMs, even after long film exposure times. This suggests that ARVMs were under substantive oxidative stress under basal conditions. However, there was also a band at ~150 kDa after 50 µM or 75 µM cisplatin treatment (Figure 6.19A) and this band increased in intensity as the concentration of cisplatin increased from 150 µM to 750 µM (Figure 6.19B). This band was present in the positive control (0.5 mM diamide, Figure 6.19A), and absent in the vehicle-only sample (Figure 6.19B). It may therefore indicate an oxidative modification of Prx-1 which is reduced by Trx, such that this oxidised form of Prx-1 accumulated when TrxR was inhibited.

The redox state of Prx-1 was also analysed in freshly isolated ARVMs treated with auranofin (Figure 6.20). Again, in untreated and auranofin-treated ARVMs, Prx-1 was present only as dimer at 50 kDa suggesting that the ARVMs were already under significant oxidative stress. There was a faint band at ~150 kDa in 0.5 mM diamide-treated ARVMs, but this was not seen in any other treatments. As shown in Figure 6.20C, Prx-1 was not present as disulfide dimer under control conditions in other model systems such as Langendorff-perfused hearts. In these samples Prx-1 was predominately a reduced monomer at 25 kDa under basal conditions.

Overall I was unable to determine whether cisplatin or auranofin inhibited TrxR, because Prx-1 was found to be basally oxidised (present as a disulfide dimer) in control ARVMs. However, a Prx-1 complex of ~150 kDa may be evidence for inhibition of TrxR in cisplatin-treated ARVMs.

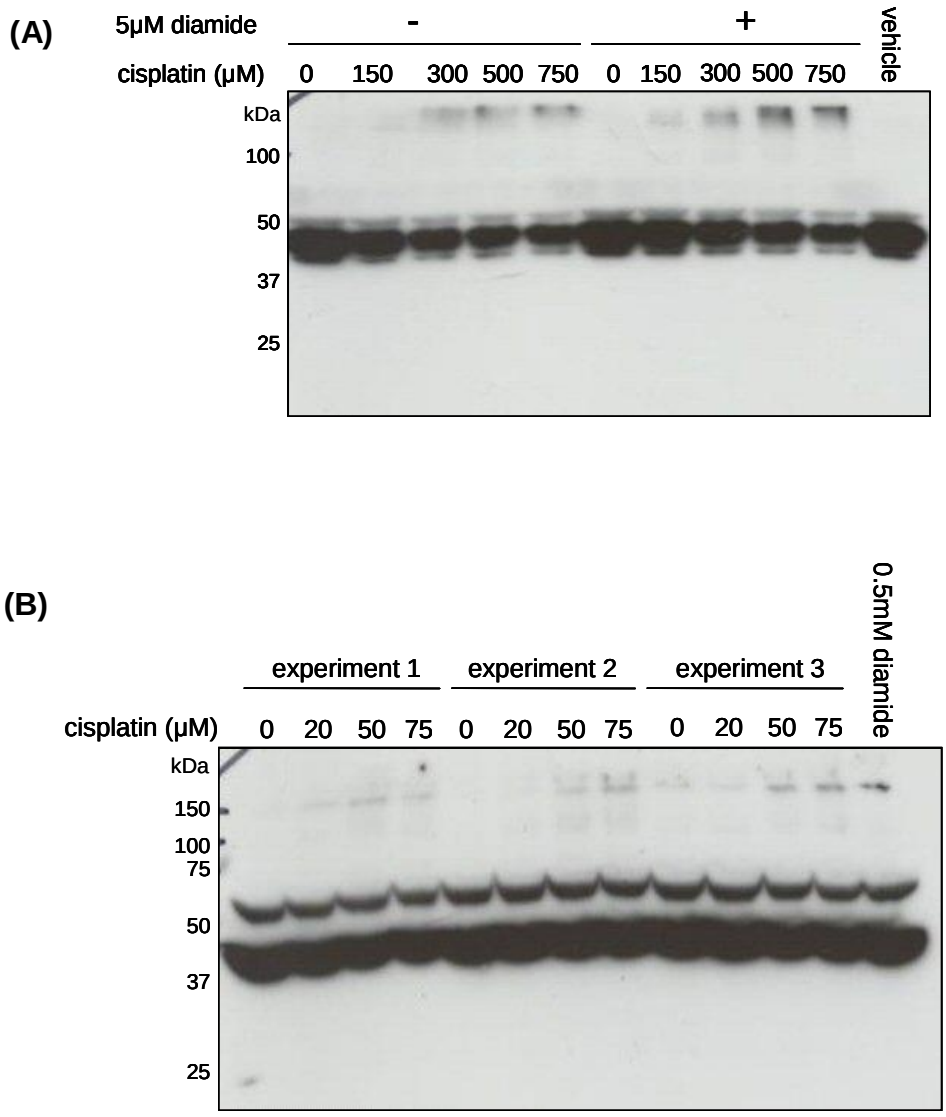

Figure 6.19 Effect of cisplatin on redox state of Prx-1.

(A) ARVMs were left untreated or treated with 150 - 750 μM cisplatin or DMSO vehicle for 30 min -/+ post-treatment with diamide (5 μM, 5 min). Western blot was probed for Prx-1. (B) ARVMs from three different cell isolations (experiments 1 - 3) were treated with 20 - 75 μM cisplatin or 0.5 mM diamide for 30 min. Western blot was probed for Prx-1. Unexpectedly, Prx-1 was present as disulfide dimer in control conditions as well as treated cells.

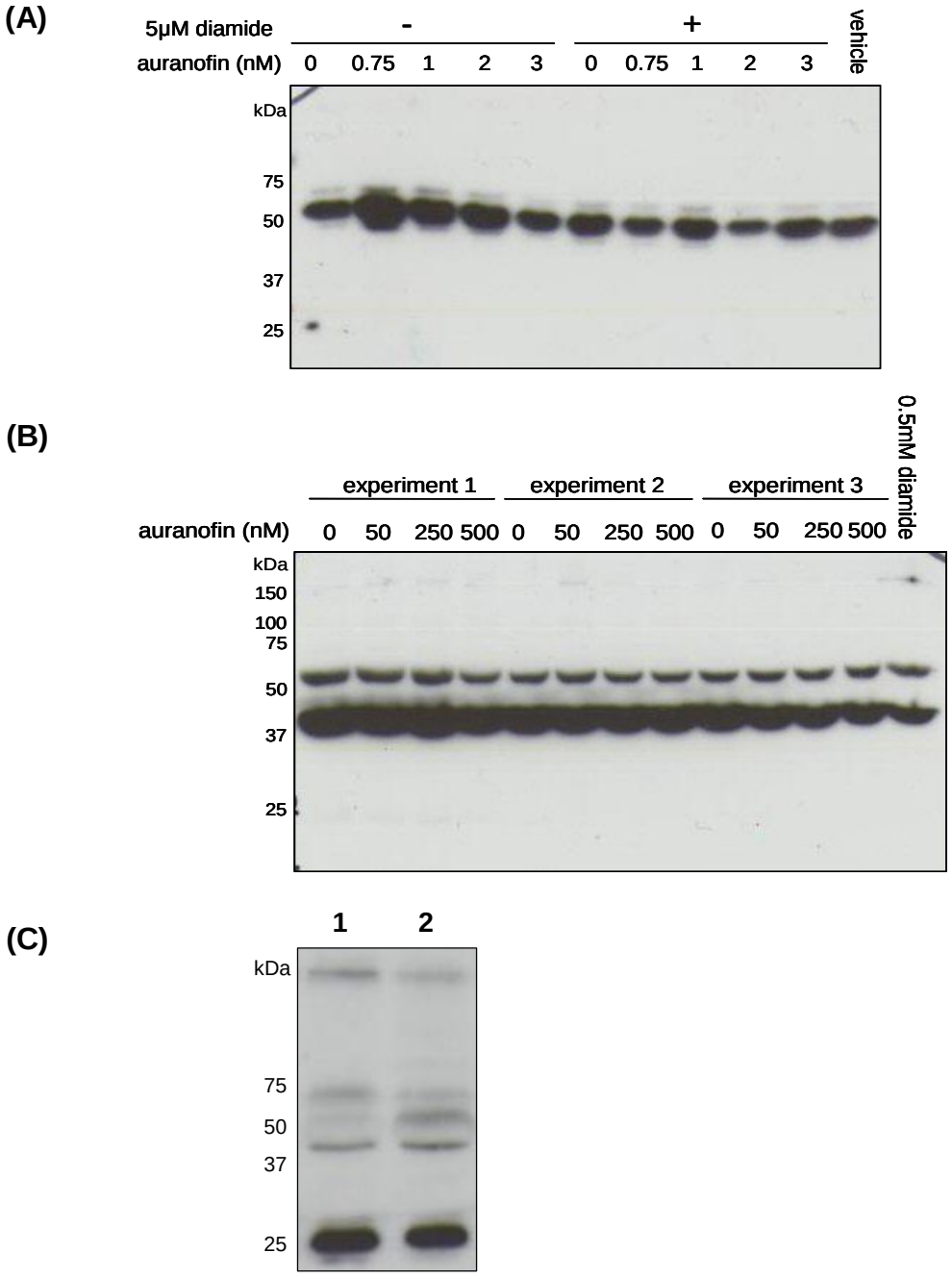

Figure 6.20 Effect of auranofin on redox state of Prx-1.

(A) Freshly isolated ARVMs were left untreated or treated with 0.75 - 3 μM auranofin or ethanol vehicle (30 min) -/+ post-treatment with diamide (5 μM, 5 min) (B) ARVMs were treated with 0 - 500 nM auranofin or 0.5 mM diamide for 30 min. Redox state of Prx-1 in three different experiments was observed by Western blotting. Prx-1 was unexpectedly diimeric in untreated ARVMs as well as treated (C) Mouse hearts (heart 1 and 2) were Langendorff-perfused with K-HB for 40 min. Western blots were probed for Prx-1, which was present as monomer in both hearts.

6.4 DISCUSSION

The aim of this chapter was to determine whether the Trx system reduces RIα disulfide. If it does, it suggests that the RIα disulfide is a reversible regulatory modification that potentially occurs physiologically. One approach was to determine if the Trx system reduces RIα disulfide *in vitro* by measuring TrxR activity. This was indexed by measuring a decrease in NADPH absorbance, a common approach used by others.[411] When Trx reduces its substrate and becomes oxidised itself, it is then reduced by TrxR which in doing so becomes oxidised. Oxidised TrxR is then reduced by NADPH, causing NADPH to be oxidised to $NADP^+$. NADPH absorbs light at 340 nm but $NADP^+$ does not. Pilot studies (results not shown) were carried out which measured NADPH absorbance when NADPH, Trx and TrxR were incubated with oxidised RIα. However, by using GSSG and Prx-1 as positive controls, it was calculated that large amounts of RIα would be required to drive the reaction and see a change in absorbance. RIα is expensive to buy and the kinase concentration would not be physiologically relevant, so an alternative method was required.

Instead, NADPH fluorescence was measured as fluorescence is more sensitive and so allows a smaller amount of RIα to be used in the reaction assay. Fluorescence-monitoring was carried out with the idea that TrxR activity would increase if the Trx system reduces RIα disulfide. This would be demonstrated by a decrease in NADPH fluorescence, as NADPH is oxidised to the $NADP^+$ form (during TrxR activity), which does not fluoresce. This method has been used by others to monitor TrxR activity.[412]

Trx or TrxR alone altered NADPH fluorescence. The increased fluorescence with Trx was potentially due to Trx auto-fluorescence, and the decrease with TrxR addition may have been due to auto-oxidation of TrxR in air causing NADPH consumption. However, these possibilities were excluded as control assays without RIα or Prx-1 were measured alongside the RIα or Prx-1 assays for comparison, so RIα or Prx-1-dependent changes could be identified.

Oxidised Prx-1 and RIα were used at a similar concentration in the fluorescence assays. Prx-1 is a well-known substrate for Trx,[410] and so the similarity in rate of NADPH consumption between Prx-1 and RIα suggests the Trx system is involved in RIα disulfide reduction.

TrxR can alone reduce some low molecular weight proteins, as described in section 6.1.2, but Trx1 has a wider range of substrates than TrxR (see section 6.1.1) and TrxR has not been shown to reduce any kinases directly. Consequently, it is unlikely that TrxR directly reduces RIα disulfide but instead it's more likely to reduce oxidised Trx. However, I cannot be certain about this in these experiments. A control should have been carried out in which oxidised RIα and NADPH and TrxR were incubated together and NADPH consumption monitored.

Although the NADPH consumption assay suggests RIα disulfide is reduced by the Trx system, this could not be corroborated by biochemical experiments in which RIα redox state was measured by Western immunoblotting. RIα was still disulfide dimer after incubation with components of the Trx system, and this may be because the interaction between Trx and its substrate (in this case RIα) is only a transient one. This has been suggested by Hirota *et al.* when demonstrating the direct interaction between Trx and redox factor 1 (Ref-1) by immunoprecipitation.[357] So once RIα is reduced and Trx released, RIα may then be quickly re-oxidised by oxygen in air back to the disulfide, making it difficult to 'catch' RIα in its reduced form. However, it could be argued that if this is happening then the same would be expected for Prx-1. Clearly it does not, leaving this issue unresolved.

Surprisingly, there was reduced monomeric RIα present in some samples where only NADPH was also present. This is difficult to explain as NADPH is generally described as a reducing equivalent for reduction-catalysing enzymes such as TrxR (see 6.1.2), glutathione reductase,[45] and the enzyme NADPH-cytochrome P450 reductase, which accepts electrons from NADPH and transfers them to microsomal cytochrome P450s.[413] RIα does not have any NADPH binding sites, the amount of reduced

monomeric RIα detected in these samples was relatively insignificant and the immunoblots had to be exposed for a long time for the monomer to be observed, so the observed reduced monomer is unlikely to be indicative of RIα reduction by NADPH directly.

cAMP binds to RIα causing release of catalytic subunits and therefore PKA activation. Substrate can affect the sensitivity of PKA RIα to cAMP (see Chapter 4). Viste *et al.*,[164] showed that for full activation of PKA ~1 μM cAMP was required which was approximately 200-fold excess cAMP compared to RIα. I incubated RIα with 100-fold excess cAMP, so consider this to be pertinent to physiology. I hypothesised that cAMP may modulate the ability of the Trx system to reduce oxidised RIα because it causes a substantial conformational change in RIα, and this may affect access of Trx to the RIα disulfide. In Chapter 4, Western immunoblotting revealed that cAMP increased H_2O_2-induced RIα disulfide. In this chapter, I found cAMP did not alter RIα-modulated NADPH consumption, suggesting that the mechanism by which cAMP induces the increased disulfide formation does not involve inhibiting the regulatory reduction of RIα disulfide by the Trx system.

Another approach to assess whether RIα disulfide is reduced by the Trx system involved treating ARVMs with the TrxR inhibitors auranofin or cisplatin and looking for an accumulation of RIα disulfide. However, there are issues to consider when inhibiting TrxR. TrxR has other substrates apart from Trx (described in section 6.1.2) such as protein disulfide isomerase,[407] CaBP1 or CaBP2,[408] so when TrxR is inhibited these proteins may no longer be reduced and so their activity affected. In addition, because Trx is reduced by TrxR, inhibition of TrxR means that Trx may no longer be reduced and unable to reduce its downstream substrates, and so their activity may be altered. For example, ASK1 may not be activated and NF-κ B may not be inhibited (as described in section 6.1.1).

Cisplatin is a Pt-containing compound (Figure 6.21A) that irreversibly inhibits TrxR.[414] Cisplatin is thought to target the SeCys in TrxR because cisplatin cannot

inhibit glutathione reductase, a structurally related non-selenoprotein.[415] About 1 % of intracellular cisplatin reacts with DNA but cisplatin can also react with and form an adduct with GSH. The cell exports this adduct but when in the cell it can inhibit both the Trx system and the Grx system.[416] Cisplatin forms complexes with DNA resulting in DNA damage and cell death, and is therefore, used to treat a wide range of cancers.[415] Cisplatin has been shown to cause apoptosis at the concentrations used in my experiments, but the treatment time was a lot longer (48 hours) than the 30 min treatment used here and so perhaps apoptosis is not expected.[414]

Auranofin is a compound used for the treatment of rheumatoid arthritis, inhibiting the reduced form of TrxR. Auranofin is also used in anti-cancer therapy where it inhibits DNA synthesis.[417] Auranofin contains gold (Figure 6.21B), which itself has a high affinity for thiols. Auranofin's mechanism of TrxR inhibition involves targeting the SeCys in TrxR, as demonstrated by its inability to inhibit glutathione reductase, a structurally related non-selenoprotein.[418] Auranofin also causes apoptosis, a LD_{50} of 1.4 μM during 24 hours treatment,[419] which is at the top of the concentration range I treated ARVMs with, although this was only for 30 min. Thus it is unlikely that apoptosis occurred in my experiments.

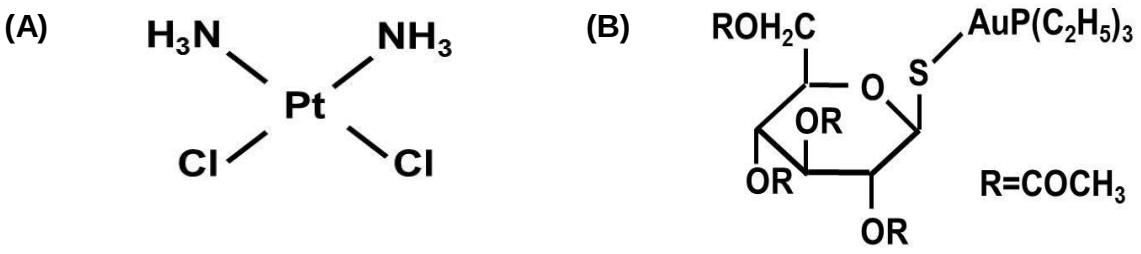

Figure 6.21 Structure of cisplatin and auranofin.

(A) Cisplatin is a Pt containing compound. (B) auranofin is an Au containing compound.

My experiments with TrxR inhibitors were initially carried out using overnight-cultured ARVMs; however the reduced monomeric RIα was absent in control untreated ARVMs

and RIα protein abundance varied between treatments. These issues were considered in detail in Chapter 2.2. Fortunately, these problems did not occur in freshly isolated ARVMs. However, untreated cells still had the issue that RIα disulfide dimer level was high basally. This high basal dimer is likely due to the stress of cell isolation because RIα disulfide is low basally in control isolated hearts.

I hypothesised that in some circumstances such as treatment with low concentrations of oxidant (e.g. 5 μM H_2O_2), RIα disulfide formation is occurring but it's not detected by Western immunoblotting because the RIα disulfide is rapidly reduced by the Trx system. There was evidence of this as auranofin and cisplatin both caused RIα disulfide accumulation. At some concentrations of auranofin (1 μM and 2 μM) there also appeared to be a synergistic effect with diamide, i.e. RIα disulfide formation was larger with diamide and auranofin treatment together than the sum of the amounts of disulfide formation for auranofin treatment alone and diamide treatment alone. This was not observed with cisplatin treatment however. It is difficult to compare effects of cisplatin with effects of auranofin because the concentrations of inhibitors I used were different. The concentrations of cisplatin were 250-fold higher than auranofin, yet auranofin synergised with diamide and cisplatin did not. However, others have compared cisplatin and auranofin and observed that auranofin is a more effective inhibitor than cisplatin.[420] This means that in my experiments, auranofin may be more effective at inhibiting TrxR than cisplatin, and so the effect of a low concentration of oxidant on RIα disulfide would be greater in auranofin-treated cells than cisplatin-treated cells. This synergy may further support the hypothesis that RIα is being recycled by the Trx system, such that RIα disulfide fails to accumulate at low concentrations of oxidant. Synergy was only observed at the highest concentrations of auranofin suggesting that it was necessary for TrxR activity to be inhibited to a large degree in order for the 'real' percentage RIα disulfide formation induced by 5 μM diamide to be observed i.e. to stop the Trx system recycling RIα disulfide formed in response to 5 μM diamide back to the reduced state.

PKG Iα oxidation was also assessed in ARVMs treated with TrxR inhibitors as this kinase can also be oxidised to a disulfide dimer.[60] There was a trend towards an increase in PKG Iα disulfide accumulation in control and diamide pre-treated ARVMs with increasing concentrations of auranofin or cisplatin. However, as observed for PKA RIα, the increases in PKG Iα oxidation were relatively minor and non-significant. Again, a reason for this could be the significant background oxidant stress the ARVMs appear to be under.

Unfortunately, I could not 'prove' that the TrxR inhibitors were inhibiting TrxR activity at the concentrations used in my experiments, as assessed by monitoring Prx-1 oxidation to the disulfide dimer. The ARVMs were already under oxidative stress under resting conditions as shown by presence of Prx-1 disulfide dimer only. No reduced monomer was present at all in control untreated ARVMs. In other systems such as the Langendorff-perfused rat heart, under resting conditions, Prx-1 is mainly present as reduced monomer although Prx-2 is 50:50 monomer:dimer,[309] and others have shown Prx-1 to be mostly present as a reduced monomer in untreated fresh ARVMs.[421] Again, the high basal Prx-1 dimer could be due to the stress of ARVM isolation. Another reason may be that the ARVM population used in the experiments does contain some dead and dying ARVMs (depending on the success of the ARVM isolation) which may release ROS, to elevate basal oxidative stress. Accumulation of a possible Prx-1 complex at ~150 kDa was observed in cisplatin-treated ARVMs which may be indicative of TrxR inhibition. Typical 2-Cys Prxs such as Prx-1 have only been suggested to form decamers, and atypical 2-Cys Prxs have been suggested to form hexamers and a lower degree of polymerization compared to typical 2-Cys Prxs.[422] Therefore, formation of a Prx-1 complex at ~150 kDa (suggesting a hexamer) may not be possible. It may therefore, be interesting to look at the oxidation state of other Prx types such as the atypical 2-Cys Prxs in these ARVMs.

Although I could not confirm that the inhibitors were inhibiting TrxR activity at the concentrations used, others have. Cox *et al*.,[419] showed that TrxR activity decreased to ~60 % of the control after 30 min of ~150 nM auranofin treatment. I observed an

increase in RIα disulfide in diamide-treated ARVMs at 250 nM auranofin, but this effect was not sustained when auranofin was increased to 500 nM in the first set of experiments. Cox *et al.* also showed that TrxR activity was reduced to ~15 % of the control with 750 nM auranofin treatment. I observed an increase in RIα disulfide in ARVMs treated with 750 nM auranofin alone and treated with both 750 nM auranofin and diamide. Arnér *et al.* showed that 25 μM cisplatin for 30 min reduced TrxR activity to ~40 %, 50 μM cisplatin reduced TrxR activity to ~30 % and 100 μM cisplatin reduced activity to ~5 % of basal.[401] I failed to observe any effect on RIα disulfide until 150 μM cisplatin was used, although in my experiments there was a jump from 75 μM to 150 μM cisplatin treatments so the increase might have been observed at lower untested concentrations. It appears that TrxR activity needs to be inhibited to a high degree if RIα disulfide accumulation is to be observed. Auranofin and cisplatin did not only increase RIα disulfide in diamide-treated ARVMs, but also control ARVMs which supports the conclusion from the Prx-1 data that the ARVMs were under oxidative stress basally.

Overall, the TrxR inhibitor results show a trend towards an increase in RIα disulfide formation with increasing concentration of TrxR inhibitor. With more replicates, significant differences could potentially be unveiled and whether the Trx system is involved in RIα disulfide reduction could be determined. Only small amounts of disulfide accumulation were caused by the TrxR inhibitors but the fact that the cells were under significant oxidative stress already means that there was less reduced RIα available to form a disulfide dimer during oxidant treatment. Thus only small changes with the inhibitors may be anticipated.

The methods used to determine if the Trx system reduces RIα disulfide were ‘indirect’. It would be useful to mutate the individual catalytic Cys residues in Trx1 and assess if accumulation of RIα disulfide occurs in the presence of the mutants and oxidant. This would not only potentially help determine whether Trx1 specifically interacts with RIα, but would also confirm which Cys residues are involved.

In conclusion, a significant decrease in NADPH fluorescence, i.e. increased NADPH consumption by the Trx system, occurred in the presence of oxidised RIα suggesting that it is indeed reduced by the Trx system. Furthermore, a trend for an increase in RIα disulfide formation in ARVMs after treatment with TrxR inhibitors also suggests that the Trx system is involved in RIα reduction. The proposed mechanism for RIα reduction by the Trx system is presented in Figure 6.22. If RIα disulfide formation is a regulatory mechanism involved in redox signalling it is likely to be a reversible process to enable the signalling to be switched off. As far as I know, no other work has been carried out assessing the relationship between Trx and RIα. H_2O_2 treatment has been reported to inhibit PKA, a process in which Trx-TrxR re-activated the kinase.[59] However, this occurred in Type II PKA which cannot form the disulfide that forms in RIα as it does not contain the necessary N-terminal Cys residues. Further experiments investigating the direct interaction between Trx and RIα would be a valuable supplement to the findings of this chapter.

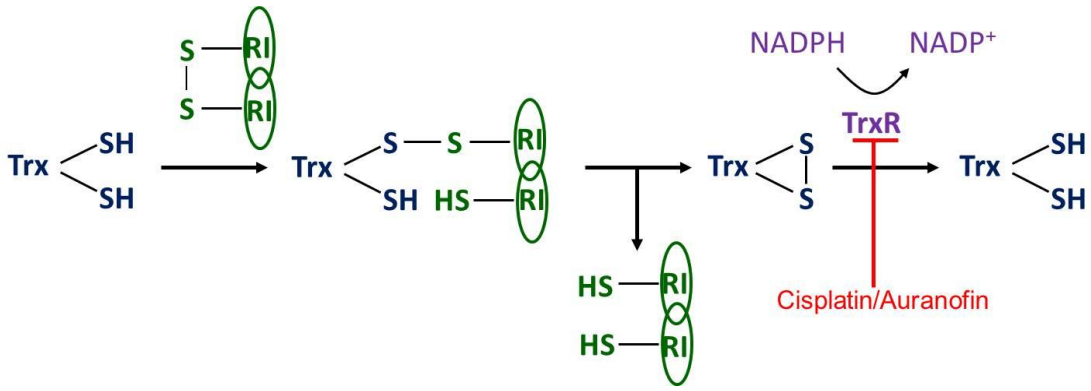

Figure 6.22 Proposed mechanism of RIα reduction by the Trx system.

Trx first forms an interprotein disulfide with RIα which is then resolved by the other catalytic Cys in Trx, releasing reduced RIα and forming an intraprotein disulfide in Trx. This is then reduced by TrxR using NADPH. Cisplatin and auranofin inhibit TrxR causing an accumulation of RIα disulfide.

7 GENERAL DISCUSSION

Although a number of oxidative modifications of PKA have been reported,[58, 59] my research laboratory has only observed one such alteration, namely disulfide formation between the two RIα subunits which was associated with kinase activation.[57] The main objective of my studies was to discover more about the regulation of PKA by RIα disulfide formation and the functional consequences of this event in the heart. A novel RIα Cys17Ser knock-in (KI) mouse which cannot form disulfides in RIα was generated on the basis that it would be a useful tool for discovering more about the role of RIα disulfide formation in the heart.

As outlined in Chapters 3-6, a series of hypotheses were postulated regarding the role of RIα disulfide in PKA activation. Previous work showed that treatment of isolated rat hearts with H_2O_2 caused translocation of RIα disulfide from cytosol to myofilament.[57] I also found that cytosolic disulfide RIα translocated to the membrane and myofilament in response to H_2O_2 in isolated mouse hearts. RIα translocation was most pronounced in the myofilament fraction, where after oxidant treatment RIα was present in wild-type (WT) myofilament but completely absent in KI myofilament. In addition, it was only disulfide RIα that was present in the WT myofilament after oxidant treatment; there was no reduced monomeric RIα. These observations indicate that disulfide formation is a key event in RIα translocation to myofilament. A-kinase anchoring proteins (AKAPs) target PKA to distinct subcellular locations in the cell. For example, Muscle-specific AKAP (mAKAP) can target PKA to the nuclear envelope,[238] and dual-specificity AKAP (D-AKAP) 1 can target PKA to the mitochondrial membrane.[259] Sarma *et al.* showed that disulfide increased RIα affinity for D-AKAP2,[119] which I hypothesised could also be applicable to other AKAPs because the disulfides that form in the dimerisation / docking (DD) domain of RIα precisely flank the AKAP binding site. Thus RIα disulfide formation may cause a conformational change that acts as a molecular structural switch to modulate AKAP binding to this region. I hypothesised that RIα disulfide formation enhances the affinity

of cytosolic RIα for AKAPs in the membrane or myofilament inducing its translocation to these fractions of the heart (Figure 7.1). However, I failed to determine whether disulfide alters RIα affinity for AKAPs using a 3′,5′-cyclic monophosphate (cAMP) affinity capture method, probing for the presence of AKAPs using specific antibodies or binding proteins generally using liquid chromatography-tandem mass spectrometry (LC-MS/MS). Consequently, I was unable to confirm an increase in affinity with AKAP(s) underlies RIα translocation upon oxidation. This was disappointing but inconsistent results, most probably because of complexities with the cAMP affinity capture method, were a significant issue. These complexities include the non-physiologically high concentration of cAMP on the affinity beads and capture of proteins other than PKA regulatory subunits. The antibodies used to identify captured AKAPs were unreliable also detecting non-specific proteins and in some cases not detecting the AKAP at all. Another confounding complexity was that incubation of RIα with the cAMP agarose appeared to cause chemical reduction of RIα disulfide to reduced monomer i.e. increased RIα monomer abundance and total RIα protein. This was highly unexpected as oxidising conditions prevail during the capture procedure (due to being carried out in air), so it was anticipated that RIα disulfide would increase rather than decrease. The consequence of this chemical RIα disulfide reduction may be that AKAP binding that occurred previous to the cAMP affinity capture protocol (i.e. because of oxidation) may be lost. This may be the major reason why this approach to investigating the role of disulfide in RIα-AKAP interaction failed. At the outset of these studies, this could not have been foreseen. However, that cAMP can lead to reduction of RIα disulfide is an intriguing observation worthy of future study. Nonetheless, LC-MS/MS analysis did identify a number of candidate RIα-binding proteins which warrant further investigation. These candidates include coiled-coil-helix-coiled-coil-helix domain-containing protein 3 (ChChd3) which is a PKA substrate important in maintaining mitochondria function and mitochondrial cristae structure.[295] LC-MS/MS showed more ChChd3 bound to WT RIα than KI RIα. ChChd3 has been shown to be associated with sphingosine kinase interacting protein (SKIP),[293] which

interestingly is an RIα-specific AKAP.[292] Similarly, the glycolytic enzyme, alpha-enolase was identified by LC-MS/MS as a protein that bound more WT RIα than KI RIα. Isoform 4 of myomegalin interacts with PKA RI and RII and also alpha-enolase,[302] so there is potential for disulfide to alter the affinity of RIα for myomegalin, which may recruit PKA to alpha-enolase. However, the function of this complex formation is unclear and alpha-enolase is not an established PKA substrate. I was unable to further investigate the interaction of RIα with SKIP or myomegalin (and whether this may be redox regulated) due to the lack of solubility of SKIP and myomegalin (both are in the Triton X-100 insoluble fraction), precluding cAMP affinity capture or immunoprecipitation methods.

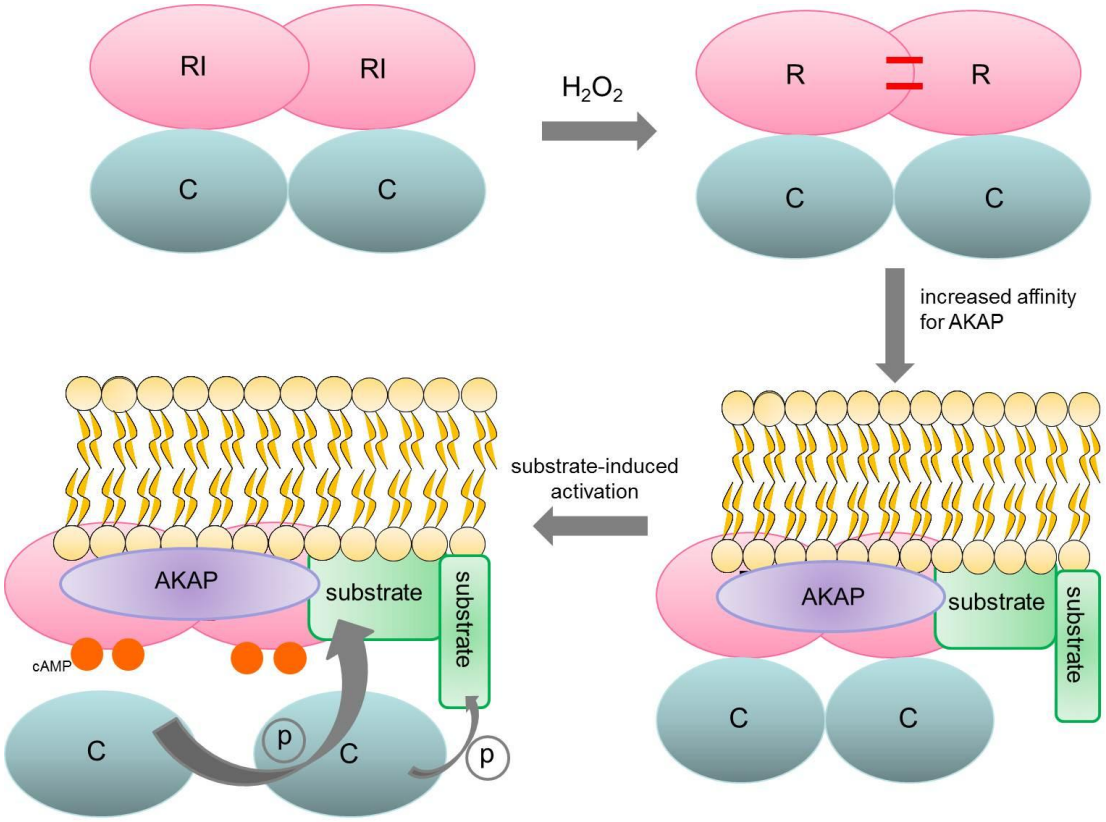

Figure 7.1 Schematic of substrate-induced PKA activation.

RIα disulfide may increase affinity of RIα for AKAPs causing PKA translocation from the cytosol and targeting of PKA close to its substrates where substrate can sensitise PKA to cAMP. Upon cAMP binding to regulatory (R) subunits, catalytic (C) subunits are released and phosphorylate target substrates.

Type I PKA is sensitised to cAMP by presence of substrate, whereas Type II is not.[164, 165] This is of particular note, given Type I can form disulfides but Type II cannot as it does not have the necessary Cys residues. Therefore, I hypothesised that the disulfide-induced increase in affinity of RIα for AKAPs, as reported by Sarma *et al.*,[119] serves to position PKA close to its substrates to facilitate substrate-induced sensitisation of PKA to cAMP, resulting in kinase activation. Therefore, in adult rat ventricular myocytes (ARVMs) I expected to observe an increase in PKA activity (i.e. increased phosphorylation of PKA substrates) after oxidant treatment or increased

sensitivity to a β-adrenoceptor agonist (i.e. isoprenaline, generating cAMP) after treatment with an oxidant (Figure 7.1). I demonstrated that disulfide potentiated isoprenaline-induced cardiac troponin I (cTnI) phosphorylation in freshly isolated ARVMs, consistent with sensitisation of PKA to cAMP by disulfide. In addition, cAMP potentiated oxidant-induced disulfide formation suggesting a positive feedback system in which cAMP increases RIα disulfide formation which then increases PKA sensitivity to cAMP. Treatment of ARVMs with H_2O_2 increased RIα disulfide formation and this disulfide formation was associated with increased phosphorylation of cTnI, which is consistent with Brennan *et al.* showing that RIα disulfide was associated with PKA activation.[57] These results suggest that RIα disulfide causes PKA to be sensitised to basal levels of cAMP, such that PKA is activated in the absence of increased β-adrenoceptor stimulation. However, I was unable to demonstrate a similar oxidant-induced activation of PKA in isolated mouse hearts. In fact, oxidant-induced disulfide formation wasn't associated with altered phosphorylation of any substrate tested apart from the membrane-associated target phospholamban (PLB). However, PLB's phosphorylation was unexpectedly significantly *reduced* by H_2O_2 which I speculate could be because disulfide may in some cases decrease RIα affinity for an AKAP such as that associated with PLB. In addition, LC-MS/MS analysis of cAMP affinity captures demonstrated significantly less binding of sarcoplasmic reticulum (SR) Ca^{2+} ATPase (SERCA) 2 to WT RIα than KI RIα. PLB basally inhibits SERCA2, but when PLB is phosphorylated at Ser16 by PKA this relieves the inhibition to enhance Ca^{2+} uptake into the SR.[174, 175] The reduced SERCA2 binding to WT RIα could be indicative of oxidant-induced RIα disulfide translocation away from the membrane to the myofilaments. This translocation may result in decreased interaction of RIα with a membrane-localised AKAP associated with PLB and SERCA2, AKAP7γ being a possible candidate.[226] This decreased AKAP interaction would reduce targeting of PKA close to PLB, so attenuating substrate-induced PKA activation and phosphorylation of PLB. Therefore I would expect RIα disulfide formation to be associated with reduced phosphorylation of PLB which, as already stated, was found to

occur in WT hearts after oxidant treatment. Again these observations highlight the possibility that disulfide may lower the affinity of RIα for some AKAPs rather than enhance affinity, as occurs for D-AKAP2.[119] Whether oxidation increases RIα binding to AKAP and targets PKA close to substrate for substrate-induced cAMP sensitisation and substrate phosphorylation cannot readily be investigated *in vitro* with purified proteins, as the substrate and kinase will already be co-localised, lacking the compartmentalisation found in cells. However whether RIα disulfide activates PKA could be determined in the future using *in vitro* kinase assays. For example, phosphorylation of the PKA substrate kemptide by gamma-^{32}P-ATP (ATP in which radioactive phosphorus-32 has been incorporated into the triphosphate) can be used to assay activity of PKA with disulfide or dithiothreitol-reduced recombinant RIα protein.

A previous unpublished observation in my research laboratory found that monoamine oxidase (MAO)-catalysed metabolism of catecholamines induced PKG Iα disulfide formation as a result of generation of H_2O_2. It is known that the metabolic decomposition pathway of monoamines yields H_2O_2,[162, 163] and so it was logical that the oxidant generated may also target PKA RIα to induce disulfide formation. This was indeed the case, RIα was oxidised via this pathway. Treatment of freshly isolated ARVMs with the MAO inhibitor Clorgyline blocked monoamine-induced RIα disulfide formation. This observation therefore provides a link between β adrenergic signalling (the classical mode of PKA activation) and potential oxidant-induced PKA activation (Figure 7.2). Monoamines may serve as dual inputs and may synergise to activate PKA, as considered further below.

I also hypothesised that RIα disulfide may be recycled back to the reduced state by the thioredoxin (Trx) system as outlined in Figure 7.2. Indeed evidence for redox cycling of RIα was identified, supporting the idea that PKA RIα oxidation to disulfide and any associated alteration in kinase activity is reversible. NADPH fluorescence assays and experiments in which freshly isolated ARVMs were treated with TrxR inhibitors both provided strong evidence for recycling of RIα disulfide by the Trx system. This is

important as such reversal is an anticipated feature of a regulatory system. It has been reported that H_2O_2 treatment inhibits PKA, and the Trx-TrxR system re-activated the kinase.[59] However, this was for Type II PKA which does not contain the N-terminal Cys residues that enable the disulfides to form in RIα.

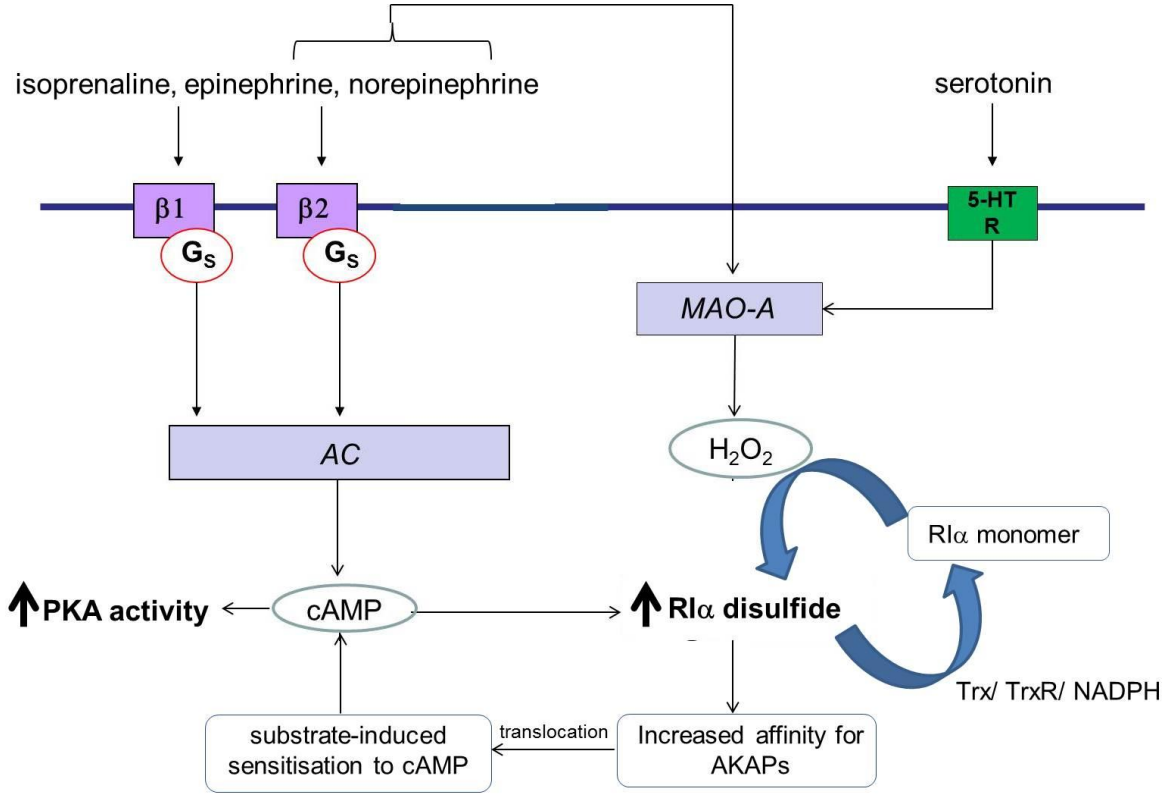

Figure 7.2 Redox regulation of PKA.

Catecholamines classically activate β adrenergic signalling in which adenylate cyclase is activated, generating cAMP which activates PKA. However, these catecholamines and other monoamines are also transported into the cell and metabolised by MAO generating H_2O_2. This oxidises RIα to the disulfide form, which may increase affinity of RIα for AKAPs causing its translocation and positioning of PKA closer to substrates. This may facilitate substrate-induced sensitisation of PKA to cAMP and PKA activation. RIα disulfide formation is also potentiated by cAMP and RIα disulfide can be recycled back to the monomeric form by the Trx system.

The studies reported in this thesis highlight inconsistencies between freshly isolated ARVMs and Langendorff perfused WT isolated hearts. For example H_2O_2 treatment

increased phosphorylation of PKA substrates in freshly isolated ARVMs, but not in isolated mouse hearts. It may be that Langendorff perfusion is not an optimal model for studying the role of RIα disulfide in regulating PKA activity because of presence of cell types other than ventricular myocytes. Perhaps myocytes isolated from WT and KI mouse hearts would be a good complementary model for future studies. In addition, perhaps *in vivo* studies would be a valuable next step for studying the RIα Cys17Ser KI mouse in the context of furthering understanding of the oxidation of this kinase. Interestingly, the KI kidney expressed substantially more PKA RIα than WT, which may be a compensatory mechanism for absence of RIα disulfide. In the kidney, PKA phosphorylates proteins important in blood pressure regulation such as Na^+ / H^+ exchanger 3,[141] which in turn effects cardiac function, and so this must be taken into consideration with future *in vivo* studies. It also has to be carefully considered whether the RIα Cys17Ser KI mouse was the optimal mutation to use in generating a 'redox-dead' PKA mouse. One key consideration regarding the RIα Cys17Ser KI mouse is that it is not known for certain whether Cys17 or Cys38 is the sensing thiol i.e. the thiol that is oxidised first. If Cys17 is the oxidant sensing thiol (which we think is the case, as discussed in Chapter 1) it is anticipated to be initially oxidised to a sulfenic acid before being resolved by Cys38 of the adjacent monomer to generate an interprotein disulfide. This potentially happens on Cys17 of both RIα subunits, so a double disulfide is anticipated to form (Figure 7.3A). Therefore, if Cys17 is mutated to become a Ser17, neither disulfide can form, as shown in Figure 7.3B. If Cys38 is the sensing thiol, the outcome will be the same, namely no RIα disulfides can form. However, if Cys38 reacts with the oxidant to form a sulfenic acid, as this cannot then be resolved by Ser17, there would be the potential for further stepwise oxidation to the sulfinic acid and then the sulfonic acid (Figure 7.3C) which are irreversible modifications and may themselves alter the activity of PKA. Future studies could determine whether Cys38 is indeed the sensing thiol by labelling sulfenic groups with dimedone,[423] a method established in our research laboratory. I would expect more dimedone labelling in the oxidatively stressed KI heart compared to the WT heart if Cys38 is the sensing thiol, as sulfenates in the WT would rapidly form disulfides. Perhaps, the double Cys mutant would have

been the optimal mutant mouse to generate, as this would overcome the issues relating to thiol hyperoxidation discussed. However, the double mutation (albeit to Ala instead of Ser) abolished D-AKAP1 binding to RIα,[116] and D-AKAP2 binding to RIα,[138] suggesting that the dual amino acid change caused a conformational change that itself altered normal PKA function. Perhaps, ideally but unlikely due to the high expense of generating and maintaining the mouse colonies, it would be best if the Cys17Ser, Cys38Ser and double Cys mutant mice were generated and comparisons made between all of these.

(A) WT RIα

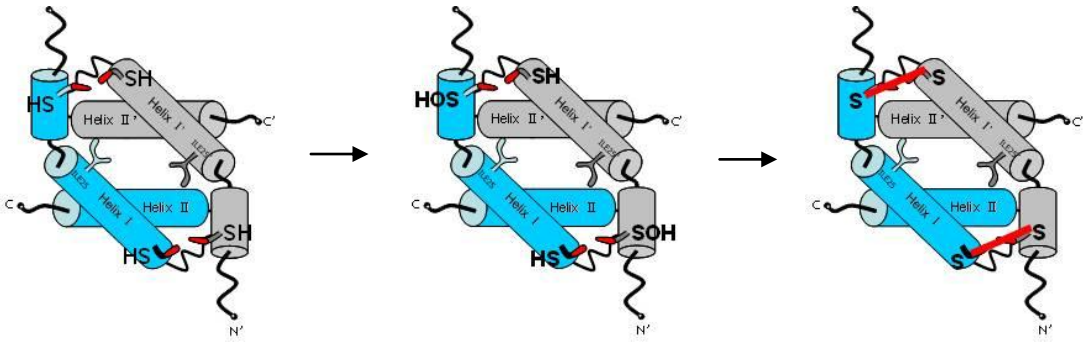

reduced monomer | sulfenic acid | disulfide

(B) KI RIα if Cys17 is sensing thiol

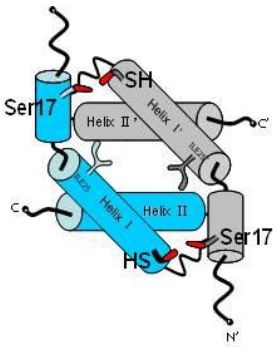

reduced monomer

(C) KI RIα if Cys38 is sensing thiol

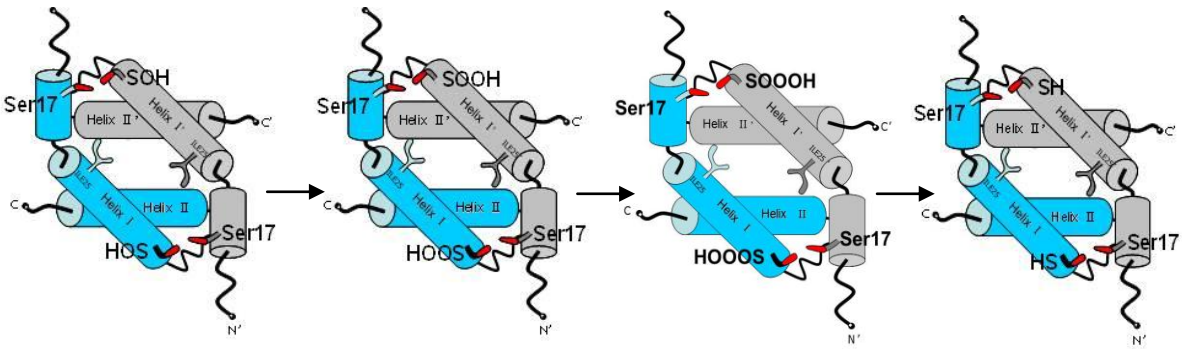

reduced monomeric | sulfenic acid | sulfinic acid | sulfonic acid

Figure 7.3 Oxidation of WT and KI RIα.

(A) If Cys17 is the sensing thiol WT RIα is oxidised to a sulfenic acid which is then resolved by Cys38 to form a disulfide. This also occurs in WT if Cys38 is the sensing thiol. (B) If Cys17 is the sensing thiol KI RIα cannot be oxidised as it is mutated to a Ser17 and Cys38 will not be reactive. Therefore, this KI RIα is termed 'redox dead'. (C) If Cys38 is the sensing thiol KI RIα may be oxidised to a sulfenic which can't be resolved by Cys17 as it is mutated to Ser17. The sulfenic acid may be further oxidised to a sulfinic or sulfonic acid which may alter PKA function.

One of the obvious questions to consider is whether RIα disulfide actually occurs in the 'real world'. The concentrations of oxidant required to observe RIα disulfide in ARVMs are possibly higher than those that occur physiologically. However, if as my results suggest, the Trx system is recycling RIα disulfide, it is likely that RIα disulfide forms continuously at low levels of oxidant, but I just don't observe it as it is quickly reduced back to monomeric RIα. Low levels of oxidants causing disulfide formation may be important in basal, regulatory redox signalling, important for homeostatic maintenance. Such a regulatory role would be different than in oxidant-response pathways, such as that involving nuclear factor erythroid-derived 2 (Nrf2),[424] which predominately serves to combat oxidative stress by up-regulating antioxidant gene expression. I consider such adaptive signalling is a counter measure to injurious levels of oxidative stress, and that this is different to the oxidation of PKA which the evidence suggests occurs basally in healthy tissue. I am primarily interested in PKA oxidation in the heart as PKA plays a key role in the positive inotropic, lusitropic and chronotropic response to β adrenergic signalling,[146, 147] and is important in protein transcription.[425, 426] The cardiac phenotype of the Cys17Ser KI mouse perhaps provides the most insight into the role of RIα disulfide under basal conditions. Echocardiography revealed that the KI heart had a slightly larger left ventricular volume than WT during diastole and systole. However, as the KI also had a reduced fractional shortening and ejection fraction than WT, this resulted in an essentially identical cardiac output as WT. As discussed in Chapter 3, this could be a chronic adaptive response to an inability to form RIα disulfide or may represent a PKA-signalling difference that could potentially be reproduced in WT by removing all basal disulfide. These results suggest a subtle role for RIα disulfide in basal heart contractility. In addition, I observed a reduced LVDP in the Langendorff perfused KI heart compared to WT. However, whether this reduction is significant enough to impact on cardiac function is arguable. The Langendorff heart is very sensitive to changes in EDP (which is determined by the volume in the balloon inserted into the left ventricle) according to the Frank-Starling mechanism. An increased volume in the balloon stretches the ventricular wall, causing cardiac muscle to contract more forcefully and so increase systolic and developed pressure. Therefore, a small difference in EDP between WT and KI hearts could result

in a potentiated difference in LVDP between genotypes so the difference in LVDP between WT and KI hearts may not be as a result of RIα disulfide formation.

The concentrations of monoamines that induced RIα disulfide were well above the low nanomolar range occurring physiologically. However, RIα disulfide may have been evident at lower physiological concentrations of monoamine if the Trx system wasn't recycling the disulfide. The prospect that monoamines (epinephrine and norepinephrine being catecholamines) not only classically activate PKA via β adrenergic signalling but also activate PKA via RIα disulfide formation due to H_2O_2 production during their metabolism by MAO is interesting, but requires further study. At low concentrations of monoamine it is therefore possible that the PKA-mediated response to catecholamines is not just due to activation of β adrenoceptors and cAMP signalling but also due to H_2O_2-induced RIα disulfide formation.

If oxidative stress occurs due to increased production of reactive oxygen species (ROS) or decreased antioxidant levels then RIα disulfide formation will most likely accumulate when a threshold oxidative stress level is exceeded, perhaps when the Trx system can't recycle the disulfide back to monomeric RIα fast enough. The accumulation of RIα disulfide may occur at the membranes and myofilaments of the heart, which my studies in ARVMs suggest may result in enhanced phosphorylation of PKA substrates. The mechanism for this potentiated phosphorylation likely being increased RIα affinity for AKAPs after RIα oxidation, leading to substrate-induced PKA activation. When flux through this pathway is persistently high, this may lead to disease such as heart failure. This condition is associated with abnormalities in Ca^{2+}-handling,[427] altered β adrenoceptor signalling,[428] and depressed cardiac contractility. For example, phosphorylation of ryanodine receptor (RyR) 2 by PKA is increased in the human failing heart,[429] and more specifically dilated cardiomyopathy.[430, 431] Although my findings with ARVMs suggest increased phosphorylation of PKA substrates with oxidant treatment, my observations with isolated hearts do not support this, although the phosphorylation status of RyR2 was not analysed.

In terms of PKA regulatory subunit-binding AKAPs, the literature is primarily focused on the RII isoform. Although, as considered throughout this thesis, RIα-interacting AKAPs are being increasingly appreciated, the wealth of studies on RII is largely because early studies predominately identified AKAPs that only bound this isoform. Solid phase assays (such as blot overlay) generally failed to identify RIα binding targets. In addition, a peptide known as Ht31 (derived from a human thyroid AKAP) that binds to the RII subunit with high affinity to compete with AKAPs for RII has been a powerful tool in these studies. An equivalent selective peptide for studying RIα–AKAP binding has not been generated. In ARVMs expressing Ht31, reduced phosphorylation of PKA substrates and increased rate of amplitude of cell shortening and relaxation in response to isoprenaline were observed, with concomitant loss of RII compartmentalisation.[432] RII-AKAP interactions are also altered in the failing heart.[433] As already mentioned, sphingosine kinase interacting protein (SKIP) is an RIα-specific AKAP,[292] associated with the PKA substrate ChChd3,[293] which I found bound more to WT RIα than KI RIα suggesting disulfide may increase RIα interaction with SKIP and so ChChd3. Interestingly, binding of PKA regulatory subunits (isoform not specified) to SKIP was increased in human failing hearts.[434] It would be therefore be fascinating to determine whether RIα disulfide formation is increased in human failing hearts and then if so to assess whether more RIα interacted with SKIP in these hearts to supplement the findings by Aye e*t al*.[434]

The potential for MAO-catalysed metabolism of monoamines to be a source of H_2O_2 for RIα disulfide formation suggests that the associated enhanced PKA activity could be involved in conditions where MAO activity or levels of monoamines are increased. Kaludercic *et al.*,[435] showed that in pressure overloaded hearts, norepinephrine metabolism by MAO-A was increased as was ROS production and the hearts showed adverse remodelling and dysfunction. I hypothesise that RIα disulfide may be highly abundant in these hearts. Mice expressing a dominant negative MAO-A were protected against pressure overload,[435] and I hypothesise that RIα disulfide abundance may be lower in these hearts. Therefore, it may be interesting to assess whether Cys17Ser RIα KI mice are protected against pressure overload-induced hypertrophy too. In contrast,

removal of MAO-A has been shown to increase serotonin-dependent ventricular hypertrophy in pressure overloaded hearts.[436] However, as discussed by Kaludercic *et al.*,[435, 437] the discrepancy between these two studies could be due to differences in the severity of the pressure overload or adaptive changes in the mice. Either way, the importance of RIα disulfide in this model would be interesting to study.

The transcription factor cAMP response element-binding protein (CREB) is an established substrate for PKA,[201, 202] and the monoamine phenylephrine has been shown to activate CREB in ARVMs via a number of signalling pathways involving PKA, extracellular signal-regulated kinase (ERK) 1/2, p38 mitogen activated protein kinase and mitogen- and stress-activated protein kinase 1 (MSK1). MSK1 was important in regulating expression of atrial natriuretic peptide messenger RNA (mRNA), which is a marker gene of cardiac hypertrophy.[438] Therefore, my results suggest that phenylephrine may also activate CREB via the following proposed mechanism. Phenylephrine is transported into the cell and metabolised by MAO generating H_2O_2 which induces RIα disulfide formation. This increases RIα affinity for AKAPs which target PKA close to CREB for substrate-induced sensitisation to cAMP and therefore, upon cAMP binding to RIα, catalytic subunits are released to phosphorylate and activate CREB. This mechanism may therefore contribute to hypertrophic growth. MAOs are also a source of H_2O_2 in ischaemia-reperfusion,[163] so RIα disulfide abundance may also be interesting to analyse in this model, potentially contributing to the pathogenesis of ischaemia-reperfusion injury.

Excessive amounts of catecholamines (e.g. norepinephrine or epinephrine) are secreted by tumours such as pheochromocytomas, which are most frequently formed from chromaffin cells in the adrenal glands, although they can also occur outside of these glands. Chromaffin cells can also be found along the aorta, blood vessel walls and in the heart, but primary pheochromocytomas of the heart are extremely rare.[439, 440] Patients with a pheochromocytoma can have a number of life-threatening cardiovascular complications and these can depend on which catecholamine the tumour is secreting. Epinephrine-secreting tumours are associated with episodic symptoms such as headaches, palpatations and hyperglycaemia whereas norepinephrine-secreting tumours

are associated with sustained hypertension. Other cardiovascular manifestations of pheochromocytomas are tachycardia, intermittent hypertension, orthostatic hypotension (occurs when standing up) and arrhythmias.[441] These symptoms are due to the excessive circulating concentrations of catecholamines which are well known to activate adrenoceptors but, as shown in my thesis, these catecholamines are also metabolised by MAOs generating H_2O_2 which then induces RIα disulfide formation. Disulfide formation is associated with PKA activation and so increased PKA activity by this mechanism together with β adrenoceptor stimulation may play a role in the symptoms of pheochromocytomas.

As already discussed in Chapter 3, Carney Complex is a multiple endocrine neoplasia characterised by spotty skin pigmentation typically on the face, schwannomas and myxomas, which occur anywhere in the body but those on the heart are the major cause of mortality. Most of the mutations identified in these patients are in the dimerisation / docking (DD) domain of PKA RIα and result in inactivation of the regulatory subunit.[131] The effects of this mutation are due to excess PKA activity due to de-regulation of the Cα subunit.[442] Therefore, the increased PKA activity associated with RIα disulfide may also contribute to signalling leading to the myxomas in the heart. One study showed that, in tumours with these inactivating RIα mutations, basal PKA activity was not altered but activity induced by cAMP was enhanced i.e. the tumours were more sensitive to cAMP.[135] Therefore, it could be that in Carney Complex, mutations cause PKA RIα to have a heightened sensitivity to oxidation to disulfide making PKA more sensitive to cAMP via substrate-induced sensitisation.

In summary, cardiac RIα disulfide formation is an important post-translational modification that inter-relates with the classical mode of PKA activation by cAMP. Catecholamines which activate β adrenergic signalling to elevate cAMP and stimulate PKA are also transported into the cell and metabolised by MAO generating H_2O_2 which can then oxidise RIα to disulfide. Disulfide formation causes translocation of RIα to the membrane and myofilament. Whether this is as a result of increased affinity of RIα for AKAPs is yet to be fully elucidated, but this event may serve to position PKA close to substrates to enable substrate-induced sensitisation of PKA to cAMP and PKA

activation. Therefore, catecholamines activate PKA by two pathways which potentially synergise. In addition, cAMP sensitises RIα to disulfide formation which together with disulfide / substrate-induced sensitisation to cAMP forms a positive feedback loop. Importantly the oxidation of RIα to disulfide may be reversed by the Trx sytem suggesting that RIα disulfide formation is a regulatory mechanism. This mechanism is particularly important in the heart where PKA plays a prominent role in the positive inotropic, lusitropic and chronotropic response to β adrenergic signalling. Future work might assess whether disulfide directly activates PKA by *in vitro* kinase assays and whether RIα-AKAP binding is modulated by disulfide. Ultimately, because of the major roles of PKA in the heart, experiments investigating the role of RIα disulfide in diseases such as heart failure, hypertrophy and ischaemia-reperfusion would be warranted.

REFERENCES

1. Geiszt, M. and T.L. Leto, *The Nox Family of NAD(P)H Oxidases: Host Defense and Beyond.* Journal of Biological Chemistry, 2004. **279**(50): p. 51715-51718.

2. Rotrosen, D. and T.L. Leto, *Phosphorylation of neutrophil 47-kDa cytosolic oxidase factor. Translocation to membrane is associated with distinct phosphorylation events.* Journal of Biological Chemistry, 1990. **265**(32): p. 19910-5.

3. Bae, Y.S., et al., *Platelet-derived Growth Factor-induced H_2O_2 Production Requires the Activation of Phosphatidylinositol 3-Kinase.* Journal of Biological Chemistry, 2000. **275**(14): p. 10527-10531.

4. Park, H.S., et al., *Sequential Activation of Phosphatidylinositol 3-Kinase, βPix, Rac1, and Nox1 in Growth Factor-Induced Production of H2O2.* Molecular and Cellular Biology, 2004. **24**(10): p. 4384-4394.

5. Bae, Y.S., et al., *Epidermal Growth Factor (EGF)-induced Generation of Hydrogen Peroxide.* Journal of Biological Chemistry, 1997. **272**(1): p. 217-221.

6. Yang, D., et al., *Pro-inflammatory cytokines increase reactive oxygen species through mitochondria and NADPH oxidase in cultured RPE cells.* Experimental Eye Research, 2007. **85**(4): p. 462-472.

7. Rajagopalan, S., Kurz, S., Münzel, T., Tarpey, M., Freeman, B.A., Griendling, K.K., Harrison, D.G., *Angiotensin II-mediated hypertension in the rat increases vascular superoxide production via membrane NADH/NADPH oxidase activation. Contribution to alterations of vasomotor tone.* The Journal of Clinical Investigation 1996. **97**(8): p. 1916-1923.

8. Faraci, F.M. and S.P. Didion, *Vascular Protection.* Arteriosclerosis, Thrombosis, and Vascular Biology, 2004. **24**(8): p. 1367-1373.

9. Guzik, T.J., et al., *Vascular Superoxide Production by NAD(P)H Oxidase.* Circulation Research, 2000. **86**(9): p. e85-e90.

10. Davignon, J. and P. Ganz, *Role of Endothelial Dysfunction in Atherosclerosis.* Circulation, 2004. **109**(23 suppl 1): p. III-27-III-32.

11. Thomas, C., et al., *Hydroxyl radical is produced via the Fenton reaction in submitochondrial particles under oxidative stress: implications for diseases associated with iron accumulation.* Redox Report, 2009. **14**(3): p. 102-108.

12. Berry, C.E. and J.M. Hare, *Xanthine oxidoreductase and cardiovascular disease: molecular mechanisms and pathophysiological implications.* The Journal of Physiology, 2004. **555**(3): p. 589-606.

13. Landmesser, U., et al., *Vascular Oxidative Stress and Endothelial Dysfunction in Patients With Chronic Heart Failure.* Circulation, 2002. **106**(24): p. 3073-3078.

14. Raha, S. and B.H. Robinson, *Mitochondria, oxygen free radicals, disease and ageing.* Trends in Biochemical Sciences, 2000. **25**(10): p. 502-508.

15. Muller, F.L., Y. Liu, and H. Van Remmen, *Complex III Releases Superoxide to Both Sides of the Inner Mitochondrial Membrane.* Journal of Biological Chemistry, 2004. **279**(47): p. 49064-49073.

16. Kussmaul, L. and J. Hirst, *The mechanism of superoxide production by NADH:ubiquinone oxidoreductase (complex I) from bovine heart mitochondria.* Proceedings of the National Academy of Sciences, 2006. **103**(20): p. 7607-7612.

17. Liu, Y., G. Fiskum, and D. Schubert, *Generation of reactive oxygen species by the mitochondrial electron transport chain.* Journal of Neurochemistry, 2002. **80**(5): p. 780-787.

18. Kushnareva, Y., Murphy, A.N., Andreyev, A., *Complex I-mediated reactive oxygen species generation: modulation by cytochrome c and NAD(P)+ oxidation-reduction state.* Biochemical Journal. , 2002. **368 (Pt 2)**(2): p. 545-553.

19. Genova, M.L., et al., *The site of production of superoxide radical in mitochondrial Complex I is not a bound ubisemiquinone but presumably iron–sulfur cluster N2.* FEBS Letters, 2001. **505**(3): p. 364-368.

20. Ohnishi, S.T., et al., *A Possible Site of Superoxide Generation in the Complex I Segment of Rat Heart Mitochondria.* Journal of Bioenergetics and Biomembranes, 2005. **37**(1): p. 1-15.

21. Treberg, J.R., C.L. Quinlan, and M.D. Brand, *Evidence for Two Sites of Superoxide Production by Mitochondrial NADH-Ubiquinone Oxidoreductase (Complex I).* Journal of Biological Chemistry, 2011. **286**(31): p. 27103-27110.

22. Turrens, J.F., A. Alexandre, and A.L. Lehninger, *Ubisemiquinone is the electron donor for superoxide formation by complex III of heart mitochondria.* Archives of Biochemistry and Biophysics, 1985. **237**(2): p. 408-414.

23. Muller, F., A.R. Crofts, and D.M. Kramer, *Multiple Q-Cycle Bypass Reactions at the Qo Site of the Cytochrome bc1 Complex†.* Biochemistry, 2002. **41**(25): p. 7866-7874.

24. Schaffer, S.W., C.J. Jong, and M. Mozaffari, *Role of oxidative stress in diabetes-mediated vascular dysfunction: Unifying hypothesis of diabetes revisited.* Vascular Pharmacology, 2012. **57**(5–6): p. 139-149.

25. Salvi, M., et al., *Catalase Takes Part in Rat Liver Mitochondria Oxidative Stress Defense.* Journal of Biological Chemistry, 2007. **282**(33): p. 24407-24415.

26. Esworthy, R.S., Y.-S. Ho, and F.-F. Chu, *The Gpx1 Gene Encodes Mitochondrial Glutathione Peroxidase in the Mouse Liver.* Archives of Biochemistry and Biophysics, 1997. **340**(1): p. 59-63.

27. Dröge, W., *Free Radicals in the Physiological Control of Cell Function.* Physiological Reviews, 2002. **82**(1): p. 47-95.

28. Förstermann, U., *Endothelial NO synthase as a source of NO and superoxide.* European Journal of Clinical Pharmacology, 2006. **62**(0): p. 5-12.

29. Ziolo, M.T., *The fork in the nitric oxide road: Cyclic GMP or nitrosylation?* Nitric Oxide, 2008. **18**(3): p. 153-156.

30. Behrendt, D. and P. Ganz, *Endothelial function: From vascular biology to clinical applications.* The American Journal of Cardiology, 2002. **90**(10, Supplement 3): p. L40-L48.

31. Milstien, S. and Z. Katusic, *Oxidation of Tetrahydrobiopterin by Peroxynitrite: Implications for Vascular Endothelial Function.* Biochemical and Biophysical Research Communications, 1999. **263**(3): p. 681-684.

32. Raman, C.S., et al., *Crystal Structure of Constitutive Endothelial Nitric Oxide Synthase: A Paradigm for Pterin Function Involving a Novel Metal Center.* Cell, 1998. **95**(7): p. 939-950.

33. Ming-Hui Zou, C.S., Richard A. Cohen, *Oxidation of the zinc-thiolate complex and uncoupling of endothelial nitric oxide synthase by peroxynitrite.* The Journal of Clinical Investigation, 2002. **109**(6): p. 817-826.

34. Antoniades, C., et al., *Association of plasma asymmetrical dimethylarginine (ADMA) with elevated vascular superoxide production and endothelial nitric oxide synthase uncoupling: implications for endothelial function in human atherosclerosis.* European Heart Journal, 2009. **30**(9): p. 1142-1150.

35. Chen, C.-A., et al., *S-glutathionylation uncouples eNOS and regulates its cellular and vascular function.* Nature, 2010. **468**(7327): p. 1115-1118.

36. Landmesser, U., Dikalov, S., Price, S.R., McCann, L., Fukai, T., Holland, S.M., Mitch, W.E., Harrison, D.G., *Oxidation of tetrahydrobiopterin leads to uncoupling of endothelial cell nitric oxide synthase in hypertension.* The Journal of Clinical Investigation 2003. **111**(8): p. 1201-1209.

37. Törnwall, M.E., et al., *Effect of α-tocopherol and β-carotene supplementation on coronary heart disease during the 6-year post-trial follow-up in the ATBC study.* European Heart Journal, 2004. **25**(13): p. 1171-1178.

38. Leppälä, J.m., Virtamo, J., Fogelholm, R., Albanes, D., Taylor, P. R., Heinonen, O. P., *Vitamin e and beta carotene supplementation in high risk for stroke: A*

subgroup analysis of the alpha-tocopherol, beta-carotene cancer prevention study. Archives of Neurology, 2000. **57**(10): p. 1503-1509.

39. Hoshi, T. and S.H. Heinemann, *Regulation of cell function by methionine oxidation and reduction.* The Journal of Physiology, 2001. **531**(1): p. 1-11.

40. Kamisaki, Y., et al., *An activity in rat tissues that modifies nitrotyrosine-containing proteins.* Proceedings of the National Academy of Sciences, 1998. **95**(20): p. 11584-11589.

41. Reth, M., *Hydrogen peroxide as second messenger in lymphocyte activation.* Nat Immunol, 2002. **3**(12): p. 1129-1134.

42. Hess, D.T., et al., *Protein S-nitrosylation: purview and parameters.* Nat Rev Mol Cell Biol, 2005. **6**(2): p. 150-166.

43. Bindoli, A., Fukuto, J.M., Forman, H.J., *Thiol Chemistry in Peroxidase Catalysis and Redox Signaling.* Antioxidants & Redox Signaling, 2008. **10**(9): p. 1549-1564.

44. Poole, L.B. and K.J. Nelson, *Discovering mechanisms of signaling-mediated cysteine oxidation.* Current Opinion in Chemical Biology, 2008. **12**(1): p. 18-24.

45. Lillig, C.H., C. Berndt, and A. Holmgren, *Glutaredoxin systems.* Biochimica et Biophysica Acta (BBA) - General Subjects, 2008. **1780**(11): p. 1304-1317.

46. Jönsson, T.J., et al., *Reduction of Cysteine Sulfinic Acid in Peroxiredoxin by Sulfiredoxin Proceeds Directly through a Sulfinic Phosphoryl Ester Intermediate.* Journal of Biological Chemistry, 2008. **283**(35): p. 23846-23851.

47. Cross, J.V. and D.J. Templeton, *Oxidative stress inhibits MEKK1 by site-specific glutathionylation in the ATP-binding domain.* Biochem. J., 2004. **381**(3): p. 675-683.

48. Kang, Y.J., et al., *Multiple Activation Mechanisms of p38α Mitogen-activated Protein Kinase.* Journal of Biological Chemistry, 2006. **281**(36): p. 26225-26234.

49. Park, H.-S., et al., *Nitric oxide negatively regulates c-Jun N-terminal kinase/stress-activated protein kinase by means of S-nitrosylation.* Proceedings of the National Academy of Sciences, 2000. **97**(26): p. 14382-14387.

50. Nadeau, P.J., S.J. Charette, and J. Landry, *REDOX Reaction at ASK1-Cys250 Is Essential for Activation of JNK and Induction of Apoptosis.* Molecular Biology of the Cell, 2009. **20**(16): p. 3628-3637.

51. Park, H.-S., et al., *Inhibition of Apoptosis Signal-regulating Kinase 1 by Nitric Oxide through a Thiol Redox Mechanism.* Journal of Biological Chemistry, 2004. **279**(9): p. 7584-7590.

52. Lin, D. and D.J. Takemoto, *Oxidative Activation of Protein Kinase Cγ through the C1 Domain.* Journal of Biological Chemistry, 2005. **280**(14): p. 13682-13693.

53. Knapp, L.T. and E. Klann, *Superoxide-induced Stimulation of Protein Kinase C via Thiol Modification and Modulation of Zinc Content.* Journal of Biological Chemistry, 2000. **275**(31): p. 24136-24145.

54. Chu, F., N.E. Ward, and C.A. O'Brian, *Potent inactivation of representative members of each PKC isozyme subfamily and PKD via S-thiolation by the tumor-promotion/progression antagonist glutathione but not by its precursor cysteine.* Carcinogenesis, 2001. **22**(8): p. 1221-1229.

55. Ward, N.E., et al., *Oxidant-Induced S-Glutathiolation Inactivates Protein Kinase C-α (PKC-α): A Potential Mechanism of PKC Isozyme Regulation†.* Biochemistry, 2000. **39**(33): p. 10319-10329.

56. Gopalakrishna, R., Z.H. Chen, and U. Gundimeda, *Nitric oxide and nitric oxide-generating agents induce a reversible inactivation of protein kinase C activity and phorbol ester binding.* Journal of Biological Chemistry, 1993. **268**(36): p. 27180-27185.

57. Brennan, J.P., et al., *Oxidant-induced Activation of Type I Protein Kinase A Is Mediated by RI Subunit Interprotein Disulfide Bond Formation.* Journal of Biological Chemistry, 2006. **281**(31): p. 21827-21836.

58. Humphries, K.M., C. Juliano, and S.S. Taylor, *Regulation of cAMP-dependent Protein Kinase Activity by Glutathionylation.* Journal of Biological Chemistry, 2002. **277**(45): p. 43505-43511.

59. de Piña, M.Z., et al., *Signaling the Signal, Cyclic AMP-dependent Protein Kinase Inhibition by Insulin-formed H_2O_2 and Reactivation by Thioredoxin.* Journal of Biological Chemistry, 2008. **283**(18): p. 12373-12386.

60. Burgoyne, J.R., et al., *Cysteine Redox Sensor in PKGIa Enables Oxidant-Induced Activation.* Science, 2007. **317**(5843): p. 1393-1397.

61. Salmeen, A., et al., *Redox regulation of protein tyrosine phosphatase 1B involves a sulphenyl-amide intermediate.* Nature, 2003. **423**(6941): p. 769-773.

62. van Montfort, R.L.M., et al., *Oxidation state of the active-site cysteine in protein tyrosine phosphatase 1B.* Nature, 2003. **423**(6941): p. 773-777.

63. Barrett, W.C., et al., *Regulation of PTP1B via Glutathionylation of the Active Site Cysteine 215.* Biochemistry, 1999. **38**(20): p. 6699-6705.

64. Seth, D. and J. Rudolph, *Redox Regulation of MAP Kinase Phosphatase 3†.* Biochemistry, 2006. **45**(28): p. 8476-8487.

65. van der Wijk, T., J. Overvoorde, and J. den Hertog, *H_2O_2-induced Intermolecular Disulfide Bond Formation between Receptor Protein-tyrosine Phosphatases.* Journal of Biological Chemistry, 2004. **279**(43): p. 44355-44361.

66. van der Wijk, T., C. Blanchetot, and J. den Hertog, *Regulation of receptor protein-tyrosine phosphatase dimerization.* Methods, 2005. **35**(1): p. 73-79.

67. Yang, J., et al., *Reversible Oxidation of the Membrane Distal Domain of Receptor PTPα Is Mediated by a Cyclic Sulfenamide†.* Biochemistry, 2007. **46**(3): p. 709-719.

68. Lee, S.-R., et al., *Reversible Inactivation of the Tumor Suppressor PTEN by H_2O_2.* Journal of Biological Chemistry, 2002. **277**(23): p. 20336-20342.

69. Yu, C.-X., S. Li, and A.R. Whorton, *Redox Regulation of PTEN by S-Nitrosothiols.* Molecular Pharmacology, 2005. **68**(3): p. 847-854.

70. Okazaki, S., et al., *Multistep Disulfide Bond Formation in Yap1 Is Required for Sensing and Transduction of H_2O_2 Stress Signal.* Molecular Cell, 2007. **27**(4): p. 675-688.

71. Tachibana, T., et al., *A Major Peroxiredoxin-induced Activation of Yap1 Transcription Factor Is Mediated by Reduction-sensitive Disulfide Bonds and Reveals a Low Level of Transcriptional Activation.* Journal of Biological Chemistry, 2009. **284**(7): p. 4464-4472.

72. Lee, C., et al., *Redox regulation of OxyR requires specific disulfide bond formation involving a rapid kinetic reaction path.* Nat Struct Mol Biol, 2004. **11**(12): p. 1179-1185.

73. Zheng, M., F. Åslund, and G. Storz, *Activation of the OxyR Transcription Factor by Reversible Disulfide Bond Formation.* Science, 1998. **279**(5357): p. 1718-1722.

74. Tao, K., *In vivo oxidation-reduction kinetics of OxyR, the transcriptional activator for an oxidative stress-inducible regulon in Escherichia coli.* FEBS Letters, 1999. **457**(1): p. 90-92.

75. KLATT, P., et al., *Redox regulation of c-Jun DNA binding by reversible S-glutathiolation.* The FASEB Journal, 1999. **13**(12): p. 1481-1490.

76. Klatt, P., E.P. Molina, and S. Lamas, *Nitric Oxide Inhibits c-Jun DNA Binding by Specifically TargetedS-Glutathionylation.* Journal of Biological Chemistry, 1999. **274**(22): p. 15857-15864.

77. Manalo, D.J., Z. Lin, and A.Y.C. Liu, *Redox-Dependent Regulation of the Conformation and Function of Human Heat Shock Factor 1†.* Biochemistry, 2002. **41**(8): p. 2580-2588.

78. Lu, M., et al., *Two Distinct Disulfide Bonds Formed in Human Heat Shock Transcription Factor 1 Act in Opposition To Regulate Its DNA Binding Activity†.* Biochemistry, 2008. **47**(22): p. 6007-6015.

79. Herscovitch, M., et al., *Intermolecular disulfide bond formation in the NEMO dimer requires Cys54 and Cys347.* Biochemical and Biophysical Research Communications, 2008. **367**(1): p. 103-108.

80. Reynaert, N.L., et al., *Nitric oxide represses inhibitory κB kinase through S-nitrosylation.* Proceedings of the National Academy of Sciences of the United States of America, 2004. **101**(24): p. 8945-8950.

81. Kelleher, Z.T., et al., *NOS2 Regulation of NF-κB by S-Nitrosylation of p65.* Journal of Biological Chemistry, 2007. **282**(42): p. 30667-30672.

82. Kelleher, Z.T., et al., *NOS2 regulation of LPS-induced airway inflammation via S-nitrosylation of NF-κB p65.* American Journal of Physiology - Lung Cellular and Molecular Physiology, 2011. **301**(3): p. L327-L333.

83. Marshall, H.E. and J.S. Stamler, *Inhibition of NF-κB by S-Nitrosylation.* Biochemistry, 2001. **40**(6): p. 1688-1693.

84. Yang, P., et al., *Oxidant-mediated Akt Activation in Human RPE Cells.* Investigative Ophthalmology & Visual Science, 2006. **47**(10): p. 4598-4606.

85. Wood, Z.A., et al., *Structure, mechanism and regulation of peroxiredoxins.* Trends in Biochemical Sciences, 2003. **28**(1): p. 32-40.

86. Woo, H.A., et al., *Reduction of Cysteine Sulfinic Acid by Sulfiredoxin Is Specific to 2-Cys Peroxiredoxins.* Journal of Biological Chemistry, 2005. **280**(5): p. 3125-3128.

87. Yang, K.-S., et al., *Inactivation of Human Peroxiredoxin I during Catalysis as the Result of the Oxidation of the Catalytic Site Cysteine to Cysteine-sulfinic Acid.* Journal of Biological Chemistry, 2002. **277**(41): p. 38029-38036.

88. Jeong, W., et al., *Molecular Mechanism of the Reduction of Cysteine Sulfinic Acid of Peroxiredoxin to Cysteine by Mammalian Sulfiredoxin.* Journal of Biological Chemistry, 2006. **281**(20): p. 14400-14407.

89. Jonsson, T.J., L.C. Johnson, and W.T. Lowther, *Structure of the sulphiredoxin-peroxiredoxin complex reveals an essential repair embrace.* Nature, 2008. **451**(7174): p. 98-101.

90. Biteau, B., J. Labarre, and M.B. Toledano, *ATP-dependent reduction of cysteine-sulphinic acid by S. cerevisiae sulphiredoxin.* Nature, 2003. **425**(6961): p. 980-984.

91. Jönsson, T.J., et al., *Identification of Intact Protein Thiosulfinate Intermediate in the Reduction of Cysteine Sulfinic Acid in Peroxiredoxin by Human Sulfiredoxin.* Journal of Biological Chemistry, 2008. **283**(34): p. 22890-22894.

92. Budanov, A.V., et al., *Regeneration of Peroxiredoxins by p53-Regulated Sestrins, Homologs of Bacterial AhpD.* Science, 2004. **304**(5670): p. 596-600.

93. González, D.R., et al., *Differential role of S-nitrosylation and the NO–cGMP–PKG pathway in cardiac contractility.* Nitric Oxide, 2008. **18**(3): p. 157-167.

94. Hartzell, H.C., *The Stress of Relaxation.* Science, 2007. **317**(5843): p. 1331-1332.

95. Hofmann, F., et al., *cGMP Regulated Protein Kinases (cGK) cGMP: Generators, Effectors and Therapeutic Implications*, H.H.H.W. Schmidt, F. Hofmann, and J.-P. Stasch, Editors. 2009, Springer Berlin Heidelberg. p. 137-162.

96. Schnell, J.R., et al., *Rapid and accurate structure determination of coiled-coil domains using NMR dipolar couplings: Application to cGMP-dependent protein kinase Iα.* Protein Science, 2005. **14**(9): p. 2421-2428.

97. Burgoyne, J.R. and P. Eaton, *Transnitrosylating Nitric Oxide Species Directly Activate Type I Protein Kinase A, Providing a Novel Adenylate Cyclase-independent Cross-talk to β-Adrenergic-like Signaling.* Journal of Biological Chemistry, 2009. **284**(43): p. 29260-29268.

98. Prysyazhna, O., O. Rudyk, and P. Eaton, *Single atom substitution in mouse protein kinase G eliminates oxidant sensing to cause hypertension.* Nat Med, 2012. **18**(2): p. 286-290.

99. Rudyk, O., et al., *Nitroglycerin Fails to Lower Blood Pressure in Redox-Dead Cys42Ser PKG1α Knock-In Mouse / Clinical Perspective.* Circulation, 2012. **126**(3): p. 287-295.

100. Clegg, C.H., G.G. Cadd, and G.S. McKnight, *Genetic characterization of a brain-specific form of the type I regulatory subunit of cAMP-dependent protein kinase.* Proceedings of the National Academy of Sciences, 1988. **85**(11): p. 3703-3707.

101. Taylor, S.S., et al., *Dynamics of signaling by PKA.* Biochimica et Biophysica Acta (BBA) - Proteins & Proteomics, 2005. **1754**(1–2): p. 25-37.

102. Banky, P., et al., *Related Protein–Protein Interaction Modules Present Drastically Different Surface Topographies Despite A Conserved Helical Platform.* Journal of Molecular Biology, 2003. **330**(5): p. 1117-1129.

103. Newlon, M.G., et al., *The A-kinase Anchoring Domain of Type IIα cAMP-dependent Protein Kinase Is Highly Helical.* Journal of Biological Chemistry, 1997. **272**(38): p. 23637-23644.

104. Kinderman, F.S., et al., *A Dynamic Mechanism for AKAP Binding to RII Isoforms of cAMP-Dependent Protein Kinase.* Molecular Cell, 2006. **24**(3): p. 397-408.

105. Herberg, F.W., S.S. Taylor, and W.R.G. Dostmann, *Active Site Mutations Define the Pathway for the Cooperative Activation of cAMP-Dependent Protein Kinase†.* Biochemistry, 1996. **35**(9): p. 2934-2942.

106. Humphries, K.M., J.K. Pennypacker, and S.S. Taylor, *Redox Regulation of cAMP-dependent Protein Kinase Signaling.* Journal of Biological Chemistry, 2007. **282**(30): p. 22072-22079.

107. Jiang, G. and B.B. Zhang, *Glucagon and regulation of glucose metabolism.* American Journal of Physiology - Endocrinology And Metabolism, 2003. **284**(4): p. E671-E678.

108. Wang, X., et al., *Regulation of Neuroprotective Activity of Myocyte-enhancer Factor 2 by cAMP-Protein Kinase A Signaling Pathway in Neuronal Survival.* Journal of Biological Chemistry, 2005. **280**(17): p. 16705-16713.

109. Zhang, L. and P.A. Insel, *The Pro-apoptotic Protein Bim Is a Convergence Point for cAMP/Protein Kinase A- and Glucocorticoid-promoted Apoptosis of Lymphoid Cells.* Journal of Biological Chemistry, 2004. **279**(20): p. 20858-20865.

110. Moujalled, D., et al., *Cyclic-AMP-dependent protein kinase A regulates apoptosis by stabilizing the BH3-only protein Bim.* EMBO Rep, 2011. **12**(1): p. 77-83.

111. Bellis, A., et al., *Cross-Talk Between PKA and Akt Protects Endothelial Cells From Apoptosis in the Late Ischemic Preconditioning.* Arteriosclerosis, Thrombosis, and Vascular Biology, 2009. **29**(8): p. 1207-1212.

112. Bolli, R., *The Late Phase of Preconditioning.* Circulation Research, 2000. **87**(11): p. 972-983.

113. Humphries, K.M., M.S. Deal, and S.S. Taylor, *Enhanced Dephosphorylation of cAMP-dependent Protein Kinase by Oxidation and Thiol Modification.* Journal of Biological Chemistry, 2005. **280**(4): p. 2750-2758.

114. Cheng, X., et al., *Phosphorylation and activation of cAMP-dependent protein kinase by phosphoinositide-dependent protein kinase.* Proceedings of the National Academy of Sciences, 1998. **95**(17): p. 9849-9854.

115. Moore, M.J., et al., *Phosphorylation of the Catalytic Subunit of Protein Kinase A.* Journal of Biological Chemistry, 2002. **277**(49): p. 47878-47884.

116. Banky, P., Huang, L.J-S., Taylor, S.S., *Dimerization/Docking Domain of the Type Iα Regulatory Subunit of cAMP-dependent Protein Kinase.* Journal of Biological Chemistry, 1998. **273**(52): p. 35048-35055.

117. León, D.A., et al., *A Stable α-Helical Domain at the N Terminus of the RIα Subunits of cAMP-dependent Protein Kinase Is a Novel Dimerization/Docking Motif.* Journal of Biological Chemistry, 1997. **272**(45): p. 28431-28437.

118. Bubis, J., T.S. Vedvick, and S.S. Taylor, *Antiparallel alignment of the two protomers of the regulatory subunit dimer of cAMP-dependent protein kinase I.* Journal of Biological Chemistry, 1987. **262**(31): p. 14961-6.

119. Sarma, G.N., et al., *Structure of D-AKAP2:PKA RI Complex: Insights into AKAP Specificity and Selectivity.* Structure, 2010. **18**(2): p. 155-166.

120. Eaton, P. and M.J. Shattock, *Purification of Proteins Susceptible to Oxidation at Cysteine Residues: Identification of Malate Dehydrogenase as a Target for S-Glutathiolation.* Annals of the New York Academy of Sciences, 2002. **973**(1): p. 529-532.

121. Eaton, P., et al., *Reversible Cysteine-Targeted Oxidation of Proteins during Renal Oxidative Stress.* Journal of the American Society of Nephrology, 2003. **14**(suppl 3): p. S290-S296.

122. Brennan, J.P., et al., *Detection and Mapping of Widespread Intermolecular Protein Disulfide Formation during Cardiac Oxidative Stress Using Proteomics with Diagonal Electrophoresis.* Journal of Biological Chemistry, 2004. **279**(40): p. 41352-41360.

123. Saurin, A.T., Neubert, H., Brennan, J.P., Eaton, P, *Widespread sulfenic acid formation in tissues in response to hydrogen peroxide.* Proceedings of the National Academy of Sciences 2004 **101**(52): p. 17982-17987.

124. Sutherland, F.J., et al., *Mouse isolated perfused heart: Characteristics and cautions.* Clinical and Experimental Pharmacology and Physiology, 2003. **30**(11): p. 867-878.

125. Wang, Q.D., et al., *Cyclic fluctuations in the cardiac performance of the isolated Langendorff-perfused mouse heart: pyruvate abolishes the fluctuations and has an anti-ischaemic effect.* Acta Physiologica Scandinavica, 2002. **175**(4): p. 279-287.

126. Burgoyne, J.R., *Thiol-dependent redox regulation in the cardiovascular system: An investigation of protein S-nitrosylation and a novel oxidant-induced activation of protein kinase G.* . Thesis, 2008.

127. Boerth, N.J., et al., *Cyclic GMP-Dependent Protein Kinase Regulates Vascular Smooth Muscle Cell Phenotype.* Journal of Vascular Research, 1997. **34**(4): p. 245-259.

128. Amieux, P.S., et al., *Increased Basal cAMP-dependent Protein Kinase Activity Inhibits the Formation of Mesoderm-derived Structures in the Developing Mouse Embryo.* Journal of Biological Chemistry, 2002. **277**(30): p. 27294-27304.

129. Amieux, P.S. and G.S. McKnight, *The Essential Role of RIα in the Maintenance of Regulated PKA Activity.* Annals of the New York Academy of Sciences, 2002. **968**(1): p. 75-95.

130. Skålhegg, B.S., et al., *Mutation of the Cα Subunit of PKA Leads to Growth Retardation and Sperm Dysfunction.* Molecular Endocrinology, 2002. **16**(3): p. 630-639.

131. Kirschner, L.S., *Use of mouse models to understand the molecular basis of tissue-specific tumorigenesis in the Carney complex.* Journal of Internal Medicine, 2009. **266**(1): p. 60-68.

132. Boikos, S.A. and C.A. Stratakis, *Carney Complex: Pathology and Molecular Genetics.* Neuroendocrinology, 2006. **83**(3-4): p. 189-199.

133. Bertherat, J., et al., *Mutations in Regulatory Subunit Type 1A of Cyclic Adenosine 5′-Monophosphate-Dependent Protein Kinase (PRKAR1A): Phenotype Analysis in 353 Patients and 80 Different Genotypes.* Journal of Clinical Endocrinology & Metabolism, 2009. **94**(6): p. 2085-2091.

134. Kirschner, L.S., et al., *Genetic heterogeneity and spectrum of mutations of the PRKAR1A gene in patients with the Carney complex.* Human Molecular Genetics, 2000. **9**(20): p. 3037-3046.

135. Kirschner, L.S., et al., *Mutations of the gene encoding the protein kinase A type I-[alpha] regulatory subunit in patients with the Carney complex.* Nat Genet, 2000. **26**(1): p. 89-92.

136. Kirschner, L.S., et al., *A Mouse Model for the Carney Complex Tumor Syndrome Develops Neoplasia in Cyclic AMP–Responsive Tissues.* Cancer Research, 2005. **65**(11): p. 4506-4514.

137. Yin, Z., et al., *Heart-Specific Ablation of Prkar1a Causes Failure of Heart Development and Myxomagenesis.* Circulation, 2008. **117**(11): p. 1414-1422.

138. Huang, L.J.-s., et al., *D-AKAP2, a novel protein kinase A anchoring protein with a putative RGS domain.* Proceedings of the National Academy of Sciences, 1997. **94**(21): p. 11184-11189.

139. Amieux, P.S., et al., *Compensatory Regulation of RIα Protein Levels in Protein Kinase A Mutant Mice.* Journal of Biological Chemistry, 1997. **272**(7): p. 3993-3998.

140. Adamczak, M., et al., *Kidney and hypertension.* Kidney Int, 2002. **61**(S80): p. S62-S67.

141. Moe, O.W., M. Amemiya, and Y. Yamaji, *Activation of protein kinase A acutely inhibits and phosphorylates Na/H exchanger NHE-3.* The Journal of Clinical Investigation, 1995. **96**(5): p. 2187-2194.

142. Gisler, S.M., et al., *PDZK1: II. An anchoring site for the PKA-binding protein D-AKAP2 in renal proximal tubular cells.* Kidney Int, 2003. **64**(5): p. 1746-1754.

143. Weinman, E.J., D. Steplock, and S. Shenolikar, *Acute regulation of NHE3 by protein kinase A requires a multiprotein signal complex.* Kidney International, 2001. **60**(2): p. 450-454.

144. Alexander, R.T. and S. Grinstein, *Tethering, recycling and activation of the epithelial sodium–proton exchanger, NHE3.* Journal of Experimental Biology, 2009. **212**(11): p. 1630-1637.

145. Valko, M., et al., *Free radicals and antioxidants in normal physiological functions and human disease.* The International Journal of Biochemistry & Cell Biology, 2007. **39**(1): p. 44-84.

146. Xiao, R.-P., et al., *Subtype-specific α1- and β-adrenoceptor signaling in the heart.* Trends in Pharmacological Sciences, 2006. **27**(6): p. 330-337.

147. Xiang, Y. and B.K. Kobilka, *Myocyte Adrenoceptor Signaling Pathways.* Science, 2003. **300**(5625): p. 1530-1532.

148. Wang, W., et al., *Sustained β1-Adrenergic Stimulation Modulates Cardiac Contractility by Ca^{2+}/Calmodulin Kinase Signaling Pathway.* Circulation Research, 2004. **95**(8): p. 798-806.

149. Zhu, W.-Z., et al., *Linkage of β1-adrenergic stimulation to apoptotic heart cell death through protein kinase A–independent activation of Ca^{2+}/calmodulin kinase II.* The Journal of Clinical Investigation, 2003. **111**(5): p. 617-625.

150. Zhu, W.-Z., et al., *Dual modulation of cell survival and cell death by β2-adrenergic signaling in adult mouse cardiac myocytes.* Proceedings of the National Academy of Sciences, 2001. **98**(4): p. 1607-1612.

151. Gauthier, C., et al., *Functional beta3-adrenoceptor in the human heart.* The Journal of Clinical Investigation, 1996. **98**(2): p. 556-562.

152. Han, C., P.W. Abel, and K.P. Minneman, *[alpha]1Adrenoceptor subtypes linked to different mechanisms for increasing intracellular Ca^{2+} in smooth muscle.* Nature, 1987. **329**(6137): p. 333-335.

153. Fedida, D. and R.A. Bouchard, *Mechanisms for the positive inotropic effect of alpha 1-adrenoceptor stimulation in rat cardiac myocytes.* Circulation Research, 1992. **71**(3): p. 673-88.

154. Heubach, J.F., et al., *Physiological antagonism between ventricular β1-adrenoceptors and α1-adrenoceptors but no evidence for β2- and β3-adrenoceptor function in murine heart.* British Journal of Pharmacology, 2002. **136**(2): p. 217-229.

155. Kissling, G., et al., *alpha 1-adrenoceptor-mediated negative inotropy of adrenaline in rat myocardium.* The Journal of Physiology, 1997. **499**(Pt 1): p. 195-205.

156. Capogrossi, M.C., et al., *Ca^{2+} dependence of alpha-adrenergic effects on the contractile properties and Ca^{2+} homeostasis of cardiac myocytes.* Circulation Research, 1991. **69**(2): p. 540-50.

157. Nebigil, C.G. and L. Maroteaux, *A Novel Role for Serotonin in Heart.* Trends in Cardiovascular Medicine, 2001. **11**(8): p. 329-335.

158. Ni, W. and S.W. Watts, *5-hydroxytryptamine in the cardiovascular system: focus on the serotonin transporter (SERT).* Clinical and Experimental Pharmacology and Physiology, 2006. **33**(7): p. 575-583.

159. Geha, R.M., et al., *Substrate and Inhibitor Specificities for Human Monoamine Oxidase A and B Are Influenced by a Single Amino Acid.* Journal of Biological Chemistry, 2001. **276**(13): p. 9877-9882.

160. Shih, J.C., Chen, K., Ridd, M.J., *MONOAMINE OXIDASE: From Genes to Behavior.* Annual Review of Neuroscience 1999 **22**: p. 197-217.

161. Fowler, C.J., T.J. Mantle, and K.F. Tipton, *The nature of the inhibition of rat liver monoamine oxidase types A and B by the acetylenic inhibitors clorgyline, l-deprenyl and pargyline.* Biochemical Pharmacology, 1982. **31**(22): p. 3555-3561.

162. Pizzinat, N., et al., *Reactive oxygen species production by monoamine oxidases in intact cells.* Naunyn-Schmiedeberg's Archives of Pharmacology, 1999. **359**(5): p. 428-431.

163. Kunduzova, O.R., et al., *Hydrogen peroxide production by monoamine oxidase during ischemia/reperfusion.* European Journal of Pharmacology, 2002. **448**(2–3): p. 225-230.

164. Viste, K., et al., *Substrate Enhances the Sensitivity of Type I Protein Kinase A to cAMP*. Journal of Biological Chemistry, 2005. **280**(14): p. 13279-13284.

165. Vigil, D., et al., *Differential Effects of Substrate on Type I and Type II PKA Holoenzyme Dissociation†.* Biochemistry, 2004. **43**(19): p. 5629-5636.

166. Anand, G., S.S. Taylor, and D.A. Johnson, *Cyclic-AMP and Pseudosubstrate Effects on Type-I A-Kinase Regulatory and Catalytic Subunit Binding Kinetics†.* Biochemistry, 2007. **46**(32): p. 9283-9291.

167. Huang, L.J.-s. and S.S. Taylor, *Dissecting cAMP Binding Domain A in the RIα Subunit of cAMP-dependent Protein Kinase.* Journal of Biological Chemistry, 1998. **273**(41): p. 26739-26746.

168. Anand, G.S., et al., *R-subunit Isoform Specificity in Protein Kinase A: Distinct Features of Protein Interfaces in PKA Types I and II by Amide H/2H Exchange Mass Spectrometry.* Journal of Molecular Biology, 2007. **374**(2): p. 487-499.

169. Martin, B.R., et al., *Isoform-Specific PKA Dynamics Revealed by Dye-Triggered Aggregation and DAKAP1α-Mediated Localization in Living Cells.* Chemistry and Biology, 2007. **14**(9): p. 1031-1042.

170. Kamp, T.J. and J.W. Hell, *Regulation of Cardiac L-Type Calcium Channels by Protein Kinase A and Protein Kinase C.* Circulation Research, 2000. **87**(12): p. 1095-1102.

171. Xiao, B., et al., *Ser-2030, but not Ser-2808, is the major phosphorylation site in cardiac ryanodine receptors responding to protein kinase A activation upon β-adrenergic stimulation in normal and failing hearts.* Biochemical Journal, 2006. **396**(1): p. 7-16.

172. Wehrens, X.H.T., et al., *Ryanodine receptor/calcium release channel PKA phosphorylation: A critical mediator of heart failure progression.* Proceedings of the National Academy of Sciences of the United States of America, 2006. **103**(3): p. 511-518.

173. Xiao, B., et al., *Functional Consequence of Protein Kinase A-dependent Phosphorylation of the Cardiac Ryanodine Receptor.* Journal of Biological Chemistry, 2007. **282**(41): p. 30256-30264.

174. Chen, Z., B.L. Akin, and L.R. Jones, *Mechanism of Reversal of Phospholamban Inhibition of the Cardiac Ca^{2+}-ATPase by Protein Kinase A and by Anti-phospholamban Monoclonal Antibody 2D12.* Journal of Biological Chemistry, 2007. **282**(29): p. 20968-20976.

175. Frank, K.F., et al., *Sarcoplasmic reticulum Ca^{2+}-ATPase modulates cardiac contraction and relaxation.* Cardiovascular Research, 2003. **57**(1): p. 20-27.

176. Silverman, B.d.Z., et al., *Serine 68 phosphorylation of phospholemman: acute isoform-specific activation of cardiac Na/K ATPase.* Cardiovascular Research, 2005. **65**(1): p. 93-103.

177. Shattock, M.J., *Phospholemman: its role in normal cardiac physiology and potential as a drugable target in disease.* Current Opinion in Pharmacology, 2009. **9**(2): p. 160-166.

178. Bell, J.R., et al., *Characterization of the phospholemman knockout mouse heart: depressed left ventricular function with increased Na-K-ATPase activity.* American Journal of Physiology - Heart and Circulatory Physiology, 2008. **294**(2): p. H613-H621.

179. Cheung, J.Y., et al., *Review Article: Phospholemman: A Novel Cardiac Stress Protein.* Clinical and Translational Science, 2010. **3**(4): p. 189-196.

180. Fentzke, R.C., et al., *Impaired cardiomyocyte relaxation and diastolic function in transgenic mice expressing slow skeletal troponin I in the heart.* The Journal of Physiology, 1999. **517**(1): p. 143-157.

181. Pi, Y., et al., *Protein kinase C and A sites on troponin I regulate myofilament Ca^{2+} sensitivity and ATPase activity in the mouse myocardium.* The Journal of Physiology, 2003. **552**(3): p. 845-857.

182. Kooij, V., et al., *Effect of troponin I Ser23/24 phosphorylation on Ca^{2+}-sensitivity in human myocardium depends on the phosphorylation background.* Journal of Molecular and Cellular Cardiology, 2010. **48**(5): p. 954-963.

183. Zhang, R., J. Zhao, and J.D. Potter, *Phosphorylation of Both Serine Residues in Cardiac Troponin I Is Required to Decrease the Ca Affinity of Cardiac Troponin C.* Journal of Biological Chemistry, 1995. **270**(51): p. 30773-30780.

184. Herron, T.J., F.S. Korte, and K.S. McDonald, *Power Output Is Increased After Phosphorylation of Myofibrillar Proteins in Rat Skinned Cardiac Myocytes.* Circulation Research, 2001. **89**(12): p. 1184-1190.

185. Strang, K.T., et al., *Beta-adrenergic receptor stimulation increases unloaded shortening velocity of skinned single ventricular myocytes from rats.* Circulation Research, 1994. **74**(3): p. 542-9.

186. Janssen, P.M.L. and P.P. De Tombe, *Protein kinase A does not alter unloaded velocity of sarcomere shortening in skinned rat cardiac trabeculae.* American Journal of Physiology - Heart and Circulatory Physiology, 1997. **273**(5): p. H2415-H2422.

187. Johns, E.C., et al., *Troponin I phosphorylation does not increase the rate of relaxation following laser flash photolysis of diazo-2 in guinea-pig skinned trabeculae.* Pflügers Archiv European Journal of Physiology, 1997. **433**(6): p. 842-844.

188. Sadayappan, S., et al., *A Critical Function for Ser-282 in Cardiac Myosin Binding Protein-C Phosphorylation and Cardiac Function / Novelty and Significance.* Circulation Research, 2011. **109**(2): p. 141-150.

189. Chen, P.P., et al., *Protein kinase A–induced myofilament desensitization to Ca2+ as a result of phosphorylation of cardiac myosin–binding protein C.* The Journal of General Physiology, 2010. **136**(6): p. 615-627.

190. Tong, C.W., et al., *Acceleration of Crossbridge Kinetics by Protein Kinase A Phosphorylation of Cardiac Myosin Binding Protein C Modulates Cardiac Function.* Circulation Research, 2008. **103**(9): p. 974-982.

191. Colson, B.A., et al., *Protein Kinase A–Mediated Phosphorylation of cMyBP-C Increases Proximity of Myosin Heads to Actin in Resting Myocardium.* Circulation Research, 2008. **103**(3): p. 244-251.

192. Stelzer, J.E., et al., *Differential Roles of Cardiac Myosin-Binding Protein C and Cardiac Troponin I in the Myofibrillar Force Responses to Protein Kinase A Phosphorylation.* Circulation Research, 2007. **101**(5): p. 503-511.

193. Quinn, K.V., J.P. Giblin, and A. Tinker, *Multisite Phosphorylation Mechanism for Protein Kinase A Activation of the Smooth Muscle ATP-Sensitive K+ Channel*. Circulation Research, 2004. **94**(10): p. 1359-1366.

194. Beall, A., et al., *The Small Heat Shock-related Protein, HSP20, Is Phosphorylated on Serine 16 during Cyclic Nucleotide-dependent Relaxation.* Journal of Biological Chemistry, 1999. **274**(16): p. 11344-11351.

195. Beall, A.C., et al., *Cyclic Nucleotide-dependent Vasorelaxation Is Associated with the Phosphorylation of a Small Heat Shock-related Protein.* Journal of Biological Chemistry, 1997. **272**(17): p. 11283-11287.

196. Komalavilas, P., Penn, R.B., Flynn, C.R., Thresher, Lopes, J.B., Furnish, E.J., Guo, M', Pallero, M.A., Murphy-Ullrich, J.E., Brophy, C.M., *The small heat shock-related protein, HSP20, is a cAMP-dependent protein kinase substrate that is involved in airway smooth muscle relaxation.* American Journal of Physiology. Lung Cellular and Molecular Physiology 2008. **294**(1): p. L69–L78.

197. Murthy, K.S., et al., *Inhibition of sustained smooth muscle contraction by PKA and PKG preferentially mediated by phosphorylation of RhoA.* American Journal of Physiology - Gastrointestinal and Liver Physiology, 2003. **284**(6): p. G1006-G1016.

198. Doble, B.W. and J.R. Woodgett, *GSK-3: tricks of the trade for a multi-tasking kinase.* Journal of Cell Science, 2003. **116**(7): p. 1175-1186.

199. Fang, X., et al., *Phosphorylation and inactivation of glycogen synthase kinase 3 by protein kinase A.* Proceedings of the National Academy of Sciences, 2000. **97**(22): p. 11960-11965.

200. Li, M., et al., *Cyclic AMP Promotes Neuronal Survival by Phosphorylation of Glycogen Synthase Kinase 3β.* Molecular and Cellular Biology, 2000. **20**(24): p. 9356-9363.

201. Gonzalez, G.A. and M.R. Montminy, *Cyclic AMP stimulates somatostatin gene transcription by phosphorylation of CREB at serine 133.* Cell, 1989. **59**(4): p. 675-680.

202. Johannessen, M., M.P. Delghandi, and U. Moens, *What turns CREB on?* Cellular Signalling, 2004. **16**(11): p. 1211-1227.

203. Li, B., M.A. Kaetzel, and J.R. Dedman, *Signaling pathways regulating murine cardiac CREB phosphorylation.* Biochemical and Biophysical Research Communications, 2006. **350**(1): p. 179-184.

204. Parker, D., et al., *Phosphorylation of CREB at Ser-133 induces complex formation with CREB-binding protein via a direct mechanism.* Molecular and Cellular Biology, 1996. **16**(2): p. 694-703.

205. Sadayappan, S., et al., *Cardiac Myosin Binding Protein-C Phosphorylation in a β-Myosin Heavy Chain Background.* Circulation, 2009. **119**(9): p. 1253-1262.

206. Clusin, W.T., *Calcium and Cardiac Arrhythmias: DADs, EADs, and Alternans.* Critical Reviews in Clinical Laboratory Sciences, 2003. **40**(3): p. 337-375.

207. Raffel, D.M., et al., *Clinical Evaluation of Carbon-11-Phenylephrine: MAO-Sensitive Marker of Cardiac Sympathetic Neurons.* Journal of Nuclear Medicine, 1996. **37**(12): p. 1923-1931.

208. Conolly, M.E., Davies, D. S., Dollery, C. T., Morgan, C. D., Paterson, J. W., Sandler, M., *Metabolism of isoprenaline in dog and man.* British Journal of Pharmacology, 1972. **46**(3): p. 458-472.

209. Raxworthy, M.J., I.R. Youde, and P.A. Gulliver, *Catechol-O-methyltransferase: substrate-specificity and stereoselectivity for β-adrenoceptor agents.* Xenobiotica, 1986. **16**(1): p. 47-52.

210. Zhai, J., et al., *Cardiac-specific Overexpression of a Superinhibitory Pentameric Phospholamban Mutant Enhances Inhibition of Cardiac Function in Vivo.* Journal of Biological Chemistry, 2000. **275**(14): p. 10538-10544.

211. Gyurko, R., et al., *Modulation of mouse cardiac function in vivo by eNOS and ANP*. American Journal of Physiology - Heart and Circulatory Physiology, 2000. **278**(3): p. H971-H981.

212. Chan, S.L. and R.R. Fiscus, *Vasorelaxant response to isoprenaline, nitric oxide donor, calcitonin gene-related peptide and vasoactive intestinal peptide in aortic rings of adult C57BL/6J mice.* European Journal of Pharmacology, 2001. **431**(2): p. 229-236.

213. Persad, S., V. Panagia, and N.S. Dhalla, *Role of H_2O_2 in changing β-adrenoceptor and adenylyl cyclase in ischemia-reperfused hearts.* Molecular and Cellular Biochemistry, 1998. **186**(1): p. 99-106.

214. Persad, S., et al., *Modification of cardiac β-adrenoceptor mechanisms by H_2O_2.* American Journal of Physiology - Heart and Circulatory Physiology, 1998. **274**(2): p. H416-H423.

215. Schröder, E. and P. Eaton, *Hydrogen peroxide as an endogenous mediator and exogenous tool in cardiovascular research: issues and considerations.* Current Opinion in Pharmacology, 2008. **8**(2): p. 153-159.

216. Yang, L., et al., *Protein Kinase G Phosphorylates Cav1.2 α1c and β2 Subunits.* Circulation Research, 2007. **101**(5): p. 465-474.

217. Barlow, R.S. and R.E. White, *Hydrogen peroxide relaxes porcine coronary arteries by stimulating BKCa channel activity.* American Journal of Physiology - Heart and Circulatory Physiology, 1998. **275**(4): p. H1283-H1289.

218. Barlow, R.S., A.M. El-Mowafy, and R.E. White, *H_2O_2 opens BKCa channels via the PLA2-arachidonic acid signaling cascade in coronary artery smooth muscle.* American Journal of Physiology - Heart and Circulatory Physiology, 2000. **279**(2): p. H475-H483.

219. Skjelbakken, T., Valen, G., Vaage, J., *Perfusing isolated rat hearts with hydrogen peroxide: an experimental model of cardiac dysfunction caused by reactive oxygen species.* Scandinavian Journal of Clinical and Laboratory Investigation 1996. **56**(5): p. 431-9.

220. Snabaitis, A.K., D.J. Hearse, and M. Avkiran, *Regulation of sarcolemmal Na^+/H^+ exchange by hydrogen peroxide in adult rat ventricular myocytes.* Cardiovascular Research, 2002. **53**(2): p. 470-480.

221. Hoque, A.N., Karmazyn, M., *Effect of sodium-hydrogen exchange inhibition on functional and metabolic impairment produced by oxidative stress in the isolated rat heart.* Canadian Journal of Physiology and Pharmacology 1997. **75**(4): p. 326-34.

222. Avner, B.S., et al., *H_2O_2 alters rat cardiac sarcomere function and protein phosphorylation through redox signaling.* American Journal of Physiology - Heart and Circulatory Physiology, 2010. **299**(3): p. H723-H730.

223. Sulakhe, P.V., X.T. Vo, and T.E. Morris, *Phosphorylation of inhibitory subunit of troponin and phospholamban in rat cardiomyocytes: Modulation by exposure of cardiomyocytes to hydroxyl radicals and sulfhydryl group reagents.* Molecular and Cellular Biochemistry, 1997. **175**(1): p. 99-107.

224. Deshmukh, P.A., B.C. Blunt, and P.A. Hofmann, *Acute modulation of PP2a and troponin I phosphorylation in ventricular myocytes: studies with a novel PP2a*

peptide inhibitor. American Journal of Physiology - Heart and Circulatory Physiology, 2007. **292**(2): p. H792-H799.

225. Denu, J.M. and K.G. Tanner, *Specific and Reversible Inactivation of Protein Tyrosine Phosphatases by Hydrogen Peroxide: Evidence for a Sulfenic Acid Intermediate and Implications for Redox Regulation†.* Biochemistry, 1998. **37**(16): p. 5633-5642.

226. Lygren, B., et al., *AKAP complex regulates Ca^{2+} re-uptake into heart sarcoplasmic reticulum.* EMBO Rep, 2007. **8**(11): p. 1061-1067.

227. Feldman, D.S., Elton, T.S., Sun, B., Martin, M.M., Ziolo, M.T., *Mechanisms of Disease: detrimental adrenergic signaling in acute decompensated heart failure.* Nature Clinical Practice Cardiovascular Medicine 2008. **5**(4): p. 208-218.

228. Carr, D.W., et al., *Interaction of the regulatory subunit (RII) of cAMP-dependent protein kinase with RII-anchoring proteins occurs through an amphipathic helix binding motif.* Journal of Biological Chemistry, 1991. **266**(22): p. 14188-14192.

229. Dell'Acqua, M.L., et al., *Membrane-targeting sequences on AKAP79 bind phosphatidylinositol-4,5-bisphosphate.* EMBO J, 1998. **17**(8): p. 2246-2260.

230. Trotter, K.W., et al., *Alternative Splicing Regulates the Subcellular Localization of a-Kinase Anchoring Protein 18 Isoforms.* The Journal of Cell Biology, 1999. **147**(7): p. 1481-1492.

231. Kritzer, M.D., et al., *AKAPs: The architectural underpinnings of local cAMP signaling.* Journal of Molecular and Cellular Cardiology, 2012. **52**(2): p. 351-358.

232. Pidoux, G. and K. Taskén, *Specificity and spatial dynamics of protein kinase A signaling organized by A-kinase-anchoring proteins.* Journal of Molecular Endocrinology, 2010. **44**(5): p. 271-284.

233. McConnachie, G., L.K. Langeberg, and J.D. Scott, *AKAP signaling complexes: getting to the heart of the matter.* Trends in Molecular Medicine, 2006. **12**(7): p. 317-323.

234. Dodge, K.L., et al., *mAKAP assembles a protein kinase A/PDE4 phosphodiesterase cAMP signaling module.* EMBO J, 2001. **20**(8): p. 1921-1930.

235. Carlisle Michel, J.J., et al., *PKA-phosphorylation of PDE4D3 facilitates recruitment of the mAKAP signalling complex.* Biochem. J., 2004. **381**(3): p. 587-592.

236. Sette, C. and M. Conti, *Phosphorylation and Activation of a cAMP-specific Phosphodiesterase by the cAMP-dependent Protein Kinase.* Journal of Biological Chemistry, 1996. **271**(28): p. 16526-16534.

237. Dodge-Kafka, K.L., et al., *The protein kinase A anchoring protein mAKAP coordinates two integrated cAMP effector pathways.* Nature, 2005. **437**(7058): p. 574-578.

238. Kapiloff, M.S., Jackson, N., Airhart, N., *mAKAP and the ryanodine receptor are part of a multi-component signaling complex on the cardiomyocyte nuclear envelope.* Journal of Cell Science, 2001. **114**(17): p. 3167-3176.

239. Yang, J., et al., *A-kinase Anchoring Protein 100 (AKAP100) is Localized in Multiple Subcellular Compartments in the Adult Rat Heart.* The Journal of Cell Biology, 1998. **142**(2): p. 511-522.

240. Colledge, M. and J.D. Scott, *AKAPs: from structure to function.* Trends in Cell Biology, 1999. **9**(6): p. 216-221.

241. Zhou, W., L. Vergara, and R. König, *T cell receptor induced intracellular redistribution of type I protein kinase A.* Immunology, 2004. **113**(4): p. 453-459.

242. Rubin, C.S., Erlichman, J., Rosen, O.M., *Cyclic Adenosine 3',5'-Monophosphate-dependent Protein Kinase of Human Erythrocyte Membranes.* Journal of Biological Chemistry, 1972. **247**(19): p. 6135-6139.

243. Ciardiello, F., Tortora, G., *Interactions between the epidermal growth factor receptor and type I protein kinase A: biological significance and therapeutic implications.* Clinical Cancer Research, 1998. **4**(4): p. 821-828.

244. Imaizumi-Scherrer, T., Faust, D.M., Bénichou, J.C., Hellio, R., Weiss, M.C., *Accumulation in fetal muscle and localization to the neuromuscular junction of cAMP-dependent protein kinase A regulatory and catalytic subunits RI alpha and C alpha.* The Journal of Cell Biology, 1996. **134**(5): p. 1241-1254.

245. Gold, M.G., et al., *Molecular Basis of AKAP Specificity for PKA Regulatory Subunits.* Molecular Cell, 2006. **24**(3): p. 383-395.

246. Jarnaess, E., et al., *Dual specificity A-kinase anchoring proteins (AKAPs) contain an additional binding region that enhances targeting of protein kinase A type I.* The Journal of biological chemistry, 2008. **283**(48): p. 33708-33718.

247. Gao, T., et al., *cAMP-Dependent Regulation of Cardiac L-Type Ca2+ Channels Requires Membrane Targeting of PKA and Phosphorylation of Channel Subunits.* Neuron, 1997. **19**(1): p. 185-196.

248. Nichols, C.B., et al., *Sympathetic Stimulation of Adult Cardiomyocytes Requires Association of AKAP5 With a Subpopulation of L-Type Calcium Channels / Novelty and Significance.* Circulation Research, 2010. **107**(6): p. 747-756.

249. Huang, L.J.-s., et al., *Identification of a Novel Protein Kinase A Anchoring Protein That Binds Both Type I and Type II Regulatory Subunits.* Journal of Biological Chemistry, 1997. **272**(12): p. 8057-8064.

250. Lin, R.-Y., S.B. Moss, and C.S. Rubin, *Characterization of S-AKAP84, a Novel Developmentally Regulated A Kinase Anchor Protein of Male Germ Cells.* Journal of Biological Chemistry, 1995. **270**(46): p. 27804-27811.

251. Chen, Q., Lin, R-Y., Rubin, C.S., *Organelle-specific Targeting of Protein Kinase AII (PKAII).* Journal of Biological Chemistry, 1997. **272**(24): p. 15247-15257.

252. Ma, Y., Taylor, S.S., *A Molecular Switch for Targeting between Endoplasmic Reticulum (ER) and Mitochondria.* Journal of Biological Chemistry, 2008. **283**(17): p. 11743-11751.

253. Trendelenburg, G., et al., *Molecular Characterization of AKAP149, a Novel A Kinase Anchor Protein with a KH Domain.* Biochemical and Biophysical Research Communications, 1996. **225**(1): p. 313-319.

254. Huang, L.J.-s., et al., *NH2-Terminal Targeting Motifs Direct Dual Specificity A-Kinase–anchoring Protein 1 (D-AKAP1) to Either Mitochondria or Endoplasmic Reticulum.* The Journal of Cell Biology, 1999. **145**(5): p. 951-959.

255. Steen, R.L., et al., *Recruitment of Protein Phosphatase 1 to the Nuclear Envelope by a-Kinase Anchoring Protein Akap149 Is a Prerequisite for Nuclear Lamina Assembly.* The Journal of Cell Biology, 2000. **150**(6): p. 1251-1262.

256. Steen, R.L., et al., *AKAP149 is a novel PP1 specifier required to maintain nuclear envelope integrity in G1 phase.* Journal of Cell Science, 2003. **116**(11): p. 2237-2246.

257. Bridges, D., et al., *Identification and characterization of D-AKAP1 as a major adipocyte PKA and PP1 binding protein.* Biochemical and Biophysical Research Communications, 2006. **346**(1): p. 351-357.

258. Küntziger, T., et al., *Association of PP1 with Its Regulatory Subunit AKAP149 Is Regulated by Serine Phosphorylation Flanking the RVXF Motif of AKAP149†.* Biochemistry, 2006. **45**(18): p. 5868-5877.

259. Cardone, L., et al., *A-Kinase Anchor Protein 84/121 are Targeted to Mitochondria and Mitotic Spindles by Overlapping Amino-terminal Motifs.* Journal of Molecular Biology, 2002. **320**(3): p. 663-675.

260. Affaitati, A., et al., *Essential Role of A-kinase Anchor Protein 121 for cAMP Signaling to Mitochondria.* Journal of Biological Chemistry, 2003. **278**(6): p. 4286-4294.

261. Cardone, L., et al., *Mitochondrial AKAP121 Binds and Targets Protein Tyrosine Phosphatase D1, a Novel Positive Regulator of src Signaling.* Molecular and Cellular Biology, 2004. **24**(11): p. 4613-4626.

262. Livigni, A., et al., *Mitochondrial AKAP121 Links cAMP and src Signaling to Oxidative Metabolism.* Molecular Biology of the Cell, 2006. **17**(1): p. 263-271.

263. Ginsberg, M.D., et al., *PKA-dependent Binding of mRNA to the Mitochondrial AKAP121 Protein.* Journal of Molecular Biology, 2003. **327**(4): p. 885-897.

264. Ranganathan, G., et al., *Role of A Kinase Anchor Proteins in the Tissue-Specific Regulation of Lipoprotein Lipase.* Molecular Endocrinology, 2005. **19**(10): p. 2527-2534.

265. Eggers, C.T., et al., *D-AKAP2 Interacts with Rab4 and Rab11 through Its RGS Domains and Regulates Transferrin Receptor Recycling.* Journal of Biological Chemistry, 2009. **284**(47): p. 32869-32880.

266. Giral, H., et al., *Role of PDZK1 Protein in Apical Membrane Expression of Renal Sodium-coupled Phosphate Transporters.* Journal of Biological Chemistry, 2011. **286**(17): p. 15032-15042.

267. Tingley, W.G., et al., *Gene-trapped mouse embryonic stem cell-derived cardiac myocytes and human genetics implicate AKAP10 in heart rhythm regulation.* Proceedings of the National Academy of Sciences, 2007. **104**(20): p. 8461-8466.

268. Lester, L.B., et al., *Cloning and Characterization of a Novel A-kinase Anchoring Protein.* Journal of Biological Chemistry, 1996. **271**(16): p. 9460-9465.

269. Reinton, N., et al., *Localization of a Novel Human A-Kinase-Anchoring Protein, hAKAP220, during Spermatogenesis.* Developmental Biology, 2000. **223**(1): p. 194-204.

270. Schillace, R.V. and J.D. Scott, *Association of the type 1 protein phosphatase PP1 with the A-kinase anchoring protein AKAP220.* Current biology : CB, 1999. **9**(6): p. 321-324.

271. Tanji, C., et al., *A-Kinase Anchoring Protein AKAP220 Binds to Glycogen Synthase Kinase-3β (GSK-3β) and Mediates Protein Kinase A-dependent Inhibition of GSK-3β.* Journal of Biological Chemistry, 2002. **277**(40): p. 36955-36961.

272. Schillace, R.V., et al., *Multiple Interactions within the AKAP220 Signaling Complex Contribute to Protein Phosphatase 1 Regulation.* Journal of Biological Chemistry, 2001. **276**(15): p. 12128-12134.

273. Logue, J.S., et al., *AKAP220 Protein Organizes Signaling Elements That Impact Cell Migration.* Journal of Biological Chemistry, 2011. **286**(45): p. 39269-39281.

274. Okutsu, R., et al., *AKAP220 colocalizes with AQP2 in the inner medullary collecting ducts.* Kidney Int, 2008. **74**(11): p. 1429-1433.

275. Jarnæss, E., et al., *Splicing Factor Arginine/Serine-rich 17A (SFRS17A) Is an A-kinase Anchoring Protein That Targets Protein Kinase A to Splicing Factor Compartments.* Journal of Biological Chemistry, 2009. **284**(50): p. 35154-35164.

276. Sumandea, C.A., et al., *Cardiac Troponin T, a Sarcomeric AKAP, Tethers Protein Kinase A at the Myofilaments.* Journal of Biological Chemistry, 2011. **286**(1): p. 530-541.

277. Li, H., et al., *Protein kinase A-anchoring (AKAP) domains in brefeldin A-inhibited guanine nucleotide-exchange protein 2 (BIG2).* Proceedings of the National Academy of Sciences, 2003. **100**(4): p. 1627-1632.

278. , M.E., et al., *Effect of Protein Kinase A Activity on the Association of ADP-ribosylation Factor 1 to Golgi Membranes.* Journal of Biological Chemistry, 2000. **275**(25): p. 19050-19059.

279. Puxeddu, E., et al., *Interaction of phosphodiesterase 3A with brefeldin A-inhibited guanine nucleotide-exchange proteins BIG1 and BIG2 and effect on ARF1 activity.* Proceedings of the National Academy of Sciences, 2009. **106**(15): p. 6158-6163.

280. Kuroda, F., J. Moss, and M. Vaughan, *Regulation of brefeldin A-inhibited guanine nucleotide-exchange protein 1 (BIG1) and BIG2 activity via PKA and protein phosphatase 1γ.* Proceedings of the National Academy of Sciences, 2007. **104**(9): p. 3201-3206.

281. Logue, J.S., et al., *Anchored Protein Kinase A Recruitment of Active Rac GTPase.* Journal of Biological Chemistry, 2011. **286**(25): p. 22113-22121.

282. Scott, J.D., et al., *Type II regulatory subunit dimerization determines the subcellular localization of the cAMP-dependent protein kinase.* Journal of Biological Chemistry, 1990. **265**(35): p. 21561-6.

283. Miki, K. and E.M. Eddy, *Single Amino Acids Determine Specificity of Binding of Protein Kinase A Regulatory Subunits by Protein Kinase A Anchoring Proteins.* Journal of Biological Chemistry, 1999. **274**(41): p. 29057-29062.

284. Herberg, F.W., et al., *Analysis of A-kinase anchoring protein (AKAP) interaction with protein kinase A (PKA) regulatory subunits: PKA isoform specificity in AKAP binding.* Journal of Molecular Biology, 2000. **298**(2): p. 329-339.

285. Lim, C.J., et al., *[alpha]4 Integrins are Type I cAMP-dependent protein kinase-anchoring proteins.* Nat Cell Biol, 2007. **9**(4): p. 415-421.

286. Angelo, R. and C.S. Rubin, *Molecular Characterization of an Anchor Protein (AKAPCE) That Binds the RI Subunit (RCE) of Type I Protein Kinase A from Caenorhabditis elegans.* Journal of Biological Chemistry, 1998. **273**(23): p. 14633-14643.

287. Kurosu, T., et al., *α/β-tubulin are A kinase anchor proteins for type I PKA in neurons.* Brain Research, 2009. **1251**(0): p. 53-64.

288. Küssel-Andermann, P., et al., *Unconventional Myosin VIIA Is a Novel A-kinase-anchoring Protein.* Journal of Biological Chemistry, 2000. **275**(38): p. 29654-29659.

289. Liu, J., H. Li, and V. Papadopoulos, *PAP7, a PBR/PKA-RIα-associated protein: a new element in the relay of the hormonal induction of steroidogenesis.* The Journal of Steroid Biochemistry and Molecular Biology, 2003. **85**(2–5): p. 275-283.

290. Maceyka, M., et al., *Sphingosine kinase, sphingosine-1-phosphate, and apoptosis.* Biochimica et Biophysica Acta (BBA) - Molecular and Cell Biology of Lipids, 2002. **1585**(2–3): p. 193-201.

291. Lacaná, E., et al., *Cloning and Characterization of a Protein Kinase A Anchoring Protein (AKAP)-related Protein That Interacts with and Regulates Sphingosine Kinase 1 Activity.* Journal of Biological Chemistry, 2002. **277**(36): p. 32947-32953.

292. Kovanich, D., et al., *Sphingosine Kinase Interacting Protein is an A-Kinase Anchoring Protein Specific for Type I cAMP-Dependent Protein Kinase.* ChemBioChem, 2010. **11**(7): p. 963-971.

293. Means, C.K., et al., *An entirely specific type I A-kinase anchoring protein that can sequester two molecules of protein kinase A at mitochondria.* Proceedings of the National Academy of Sciences, 2011. **108**(48): p. E1227-E1235.

294. Schauble, S., et al., *Identification of ChChd3 as a Novel Substrate of the cAMP-dependent Protein Kinase (PKA) Using an Analog-sensitive Catalytic Subunit.* Journal of Biological Chemistry, 2007. **282**(20): p. 14952-14959.

295. Darshi, M., et al., *ChChd3, an Inner Mitochondrial Membrane Protein, Is Essential for Maintaining Crista Integrity and Mitochondrial Function.* Journal of Biological Chemistry, 2011. **286**(4): p. 2918-2932.

296. Burgers, P.P., Ma, Y., Margarucci, L., Mackey, M., van der Heyden, M.A., Ellisman, M., Scholten, A., Taylor, S.S., Heck, A.J., *A Small Novel A-Kinase Anchoring Protein (AKAP) That Localizes Specifically Protein Kinase A-Regulatory Subunit I (PKA-RI) to the Plasma Membrane.* The Journal of Biological Chemistry, 2012. **epub ahead of print**.

297. Shevchenko, A., Wilm, M., Vorm, O., Mann, M., *Mass spectrometric sequencing of proteins silver-stained polyacrylamide gels.* Analytical Chemistry, 1996. **68**(5): p. 850-8.

298. Nesvizhskii, A., Keller, A., Kolker, E., Aebersold, R., *A statistical model for identifying proteins by tandem mass spectrometry.* Analytical Chemistry, 2003. **75**(17): p. 4646-4658.

299. Keller, A., Nesvizhskii, AI., Kolker E., Aebersold, R., *Empirical statistical model to estimate the accuracy of peptide identifications made by MS/MS and database search.* Analytical Chemistry, 2002. **74**(20): p. 5383-92.

300. Tanaka, M., K. Maeda, and K. Nakashima, *Chicken α-Enolase but Not β-Enolase Has a Src-Dependent Tyrosine-Phosphorylation Site: cDNA Cloning and Nucleotide Sequence Analysis.* Journal of Biochemistry, 1995. **117**(3): p. 554-559.

301. Schmitt, J.M. and P.J.S. Stork, *PKA Phosphorylation of Src Mediates cAMP's Inhibition of Cell Growth via Rap1.* Molecular Cell, 2002. **9**(1): p. 85-94.

302. Uys, G.M., et al., *Myomegalin is a novel A-kinase anchoring protein involved in the phosphorylation of cardiac myosin binding protein C.* BMC cell biology, 2011. **12**: p. 18.

303. Kabuyama, Y., et al., *Dysregulation of very long chain acyl-CoA dehydrogenase coupled with lipid peroxidation.* American Journal of Physiology - Cell Physiology, 2010. **298**(1): p. C107-C113.

304. Corbin, J.D., et al., *Compartmentalization of adenosine 3':5'-monophosphate and adenosine 3':5'-monophosphate-dependent protein kinase in heart tissue.* Journal of Biological Chemistry, 1977. **252**(11): p. 3854-61.

305. Reinitz, C.A., R.A. Bianco, and J.B. Shabb, *Compartmentation of the Type I Regulatory Subunit of cAMP-Dependent Protein Kinase in Cardiac Ventricular Muscle.* Archives of Biochemistry and Biophysics, 1997. **348**(2): p. 391-402.

306. Robinson, M.L., et al., *Association of the Type I Regulatory Subunit of cAMP-Dependent Protein Kinase with Cardiac Myocyte Sarcolemma.* Archives of Biochemistry and Biophysics, 1996. **330**(1): p. 181-187.

307. Boeshans, K.M., Resing, K.A., Hunt, J.B., Ahn, N.G., Shabb, J.B., *Structural characterization of the membrane-associated regulatory subunit of type I cAMP-dependent protein kinase by mass spectrometry: identification of Ser81 as the in vivo phosphorylation site of RIalpha.* Protein Science, 1999 **8**(7): p. 1515-1522.

308. Resh, M.D., *Palmitoylation of Ligands, Receptors, and Intracellular Signaling Molecules.* Sci. STKE, 2006. **2006**(359): p. re14-.

309. Schröder, E., J.P. Brennan, and P. Eaton, *Cardiac peroxiredoxins undergo complex modifications during cardiac oxidant stress.* American Journal of Physiology - Heart and Circulatory Physiology, 2008. **295**(1): p. H425-H433.

310. Dohrman, D.P., I. Diamond, and A.S. Gordon, *Ethanol causes translocation of cAMP-dependent protein kinase catalytic subunit to the nucleus.* Proceedings of the National Academy of Sciences, 1996. **93**(19): p. 10217-10221.

311. Gao, Z., et al., *Protein kinase A translocation and insulin secretion in pancreatic beta-cells: studies with adenylate cyclase toxin from Bordetella pertussis.* Biochem. J., 2002. **368**(2): p. 397-404.

312. Wang, L., et al., *Cloning and mitochondrial localization of full-length D-AKAP2, a protein kinase A anchoring protein.* Proceedings of the National Academy of Sciences, 2001. **98**(6): p. 3220-3225.

313. Akoumianaki, T., et al., *Nucleocytoplasmic shuttling of soluble tubulin in mammalian cells.* Journal of Cell Science, 2009. **122**(8): p. 1111-1118.

314. Aye, T.T., et al., *Selectivity in Enrichment of cAMP-dependent Protein Kinase Regulatory Subunits Type I and Type II and Their Interactors Using Modified cAMP Affinity Resins.* Molecular & Cellular Proteomics, 2009. **8**(5): p. 1016-1028.

315. Kinoshita, E., et al., *Phosphate-binding Tag, a New Tool to Visualize Phosphorylated Proteins.* Molecular & Cellular Proteomics, 2006. **5**(4): p. 749-757.

316. Pidoux, G., et al., *Optic atrophy 1 is an A-kinase anchoring protein on lipid droplets that mediates adrenergic control of lipolysis.* EMBO J, 2011. **30**(21): p. 4371-4386.

317. Brown, R.L., et al., *AKAP7γ is a nuclear RI-binding AKAP*. Biochemical and Biophysical Research Communications, 2003. **306**(2): p. 394-401.

318. Moscato, S., et al., *Surface expression of a glycolytic enzyme, α-enolase, recognized by autoantibodies in connective tissue disorders.* European Journal of Immunology, 2000. **30**(12): p. 3575-3584.

319. Osborne, B.W., et al., *Crystal Structure of cGMP-Dependent Protein Kinase Reveals Novel Site of Interchain Communication.* Structure, 2011. **19**(9): p. 1317-1327.

320. Laurent, T.C., E.C. Moore, and P. Reichard, *Enzymatic Synthesis of Deoxyribonucleotides.* Journal of Biological Chemistry, 1964. **239**(10): p. 3436-3444.

321. Tagaya Y, M.Y., Mitsui A, Kondo N, Matsui H, Hamuro J, Brown N, Arai K, Yokota T, Wakasugi H, *ATL-derived factor (ADF), an IL-2 receptor/Tac inducer homologous to thioredoxin; possible involvement of dithiol-reduction in the IL-2 receptor induction.* EMBO J., 1989. **8**(3): p. 757-64.

322. Sengupta, R. and A. Holmgren, *The role of thioredoxin in the regulation of cellular processes by S-nitrosylation.* Biochimica et Biophysica Acta (BBA) - General Subjects, 2011. **1820**(6): p. 689-700.

323. Tanaka, T., et al., *Thioredoxin-2 (TRX-2) is an essential gene regulating mitochondria-dependent apoptosis.* EMBO J, 2002. **21**(7): p. 1695-1703.

324. Eklund, H., F.K. Gleason, and A. Holmgren, *Structural and functional relations among thioredoxins of different species.* Proteins: Structure, Function, and Bioinformatics, 1991. **11**(1): p. 13-28.

325. Jennifer L, M., *Thioredoxin —a fold for all reasons.* Structure, 1995. **3**(3): p. 245-250.

326. Smeets, A., et al., *Crystal structures of oxidized and reduced forms of human mitochondrial thioredoxin 2.* Protein Science, 2005. **14**(10): p. 2610-2621.

327. Spyrou, G., et al., *Cloning and Expression of a Novel Mammalian Thioredoxin.* Journal of Biological Chemistry, 1997. **272**(5): p. 2936-2941.

328. Hirota, K., et al., *Distinct Roles of Thioredoxin in the Cytoplasm and in the Nucleus.* Journal of Biological Chemistry, 1999. **274**(39): p. 27891-27897.

329. Bodenstein J, F.H., *Characterization of two thioredoxins in pig heart including a new mitochondrial protein.* Z Naturforsch C. , 1991. **46**(3-4): p. 270-9.

330. Taniguchi, Y., et al., *A Novel Promoter Sequence Is Involved in the Oxidative Stress-Induced Expression of the Adult T-Cell Leukemia-Derived Factor (ADF)/Human Thioredoxin (Trx) Gene.* Nucleic Acids Research, 1996. **24**(14): p. 2746-2752.

331. Haendeler, J., et al., *Low doses of reactive oxygen species protect endothelial cells from apoptosis by increasing thioredoxin-1 expression.* FEBS Letters, 2004. **577**(3): p. 427-433.

332. Turoczi, T., et al., *Thioredoxin redox signaling in the ischemic heart: an insight with transgenic mice overexpressing Trx1.* Journal of Molecular and Cellular Cardiology, 2003. **35**(6): p. 695-704.

333. Haendeler, J., et al., *Cathepsin D and H_2O_2 Stimulate Degradation of Thioredoxin-1.* Journal of Biological Chemistry, 2005. **280**(52): p. 42945-42951.

334. Hall, G. and J. Emsley, *Structure of human thioredoxin exhibits a large conformational change.* Protein Science, 2010. **19**(9): p. 1807-1811.

335. Weichsel, A., et al., *Crystal structures of reduced, oxidized, and mutated human thioredoxins: evidence for a regulatory homodimer.* Structure, 1996. **4**(6): p. 735-751.

336. Berndt, C., C.H. Lillig, and A. Holmgren, *Thiol-based mechanisms of the thioredoxin and glutaredoxin systems: implications for diseases in the cardiovascular system.* American Journal of Physiology - Heart and Circulatory Physiology, 2007. **292**(3): p. H1227-H1236.

337. Fritz-Wolf, K., et al., *Crystal structure of the human thioredoxin reductase-thioredoxin complex.* Nat Commun, 2011. **2**: p. 383.

338. Mustacich, D. and G. Powis, *Thioredoxin reductase.* Biochem. J., 2000. **346**(1): p. 1-8.

339. Rhee, S.G., H.Z. Chae, and K. Kim, *Peroxiredoxins: A historical overview and speculative preview of novel mechanisms and emerging concepts in cell signaling.* Free Radical Biology and Medicine, 2005. **38**(12): p. 1543-1552.

340. Holmgren, A. and R. Sengupta, *The use of thiols by ribonucleotide reductase.* Free Radical Biology and Medicine, 2010. **49**(11): p. 1617-1628.

341. Boschi-Muller, S., et al., *The enzymology and biochemistry of methionine sulfoxide reductases.* Biochimica et Biophysica Acta (BBA) - Proteins & Proteomics, 2005. **1703**(2): p. 231-238.

342. Fu, C., et al., *Elucidation of Thioredoxin Target Protein Networks in Mouse.* Molecular & Cellular Proteomics, 2009. **8**(7): p. 1674-1687.

343. Matsui, M., et al., *Early Embryonic Lethality Caused by Targeted Disruption of the Mouse Thioredoxin Gene.* Developmental Biology, 1996. **178**(1): p. 179-185.

344. Rubartelli, A., et al., *Secretion of thioredoxin by normal and neoplastic cells through a leaderless secretory pathway.* Journal of Biological Chemistry, 1992. **267**(34): p. 24161-24164.

345. Bertini, R., et al., *Thioredoxin, a Redox Enzyme Released in Infection and Inflammation, Is a Unique Chemoattractant for Neutrophils, Monocytes, and T Cells.* The Journal of Experimental Medicine, 1999. **189**(11): p. 1783-1789.

346. Powis, G., D. Mustacich, and A. Coon, *The role of the redox protein thioredoxin in cell growth and cancer.* Free Radical Biology and Medicine, 2000. **29**(3–4): p. 312-322.

347. Tobiume, K., et al., *ASK1 is required for sustained activations of JNK/p38 MAP kinases and apoptosis* EMBO reports 2001. **2**(3): p. 222-228.

348. Zhang, R., et al., *Thioredoxin-2 Inhibits Mitochondria-Located ASK1-Mediated Apoptosis in a JNK-Independent Manner.* Circulation Research, 2004. **94**(11): p. 1483-1491.

349. Saitoh, M., et al., *Mammalian thioredoxin is a direct inhibitor of apoptosis signal-regulating kinase (ASK) 1.* EMBO J, 1998. **17**(9): p. 2596-2606.

350. Fujino, G., et al., *Thioredoxin and TRAF Family Proteins Regulate Reactive Oxygen Species-Dependent Activation of ASK1 through Reciprocal Modulation of the N-Terminal Homophilic Interaction of ASK1.* Mol. Cell. Biol., 2007. **27**(23): p. 8152-8163.

351. Liu, Y. and W. Min, *Thioredoxin Promotes ASK1 Ubiquitination and Degradation to Inhibit ASK1-Mediated Apoptosis in a Redox Activity-Independent Manner.* Circulation Research, 2002. **90**(12): p. 1259-1266.

352. Liu, H., et al., *Activation of Apoptosis Signal-Regulating Kinase 1 (ASK1) by Tumor Necrosis Factor Receptor-Associated Factor 2 Requires Prior Dissociation of the ASK1 Inhibitor Thioredoxin.* Molecular and Cellular Biology, 2000. **20**(6): p. 2198-2208.

353. Nadeau, P.J., et al., *Disulfide Bond-mediated Multimerization of Ask1 and Its Reduction by Thioredoxin-1 Regulate H2O2-induced c-Jun NH2-terminal Kinase Activation and Apoptosis.* Molecular Biology of the Cell, 2007. **18**(10): p. 3903-3913.

354. Yamawaki, H., J. Haendeler, and B.C. Berk, *Thioredoxin.* Circulation Research, 2003. **93**(11): p. 1029-1033.

355. Shaulian, E.K., Michael, *AP-1 in cell proliferation and survival.* Oncogene, 2001. **20**(19): p. 2390-2400.

356. Abate, C.P., L; Rauscher, FJ 3rd; Curran, T., *Redox regulation of fos and jun DNA-binding activity in vitro.* Science, 1990. **249**(4973): p. 1157-61.

357. Hirota, K., et al., *AP-1 transcriptional activity is regulated by a direct association between thioredoxin and Ref-1.* Proceedings of the National Academy of Sciences, 1997. **94**(8): p. 3633-3638.

358. Xanthoudakis, S.M., G; Wang, F; Pan, Y C; Curran, T, *Redox activation of Fos-Jun DNA binding activity is mediated by a DNA repair enzyme.* The EMBO Journal, 1992. **11**(9): p. 3323-3335.

359. Xanthoudakis, S.C., T, *Identification and characterization of Ref-1, a nuclear protein that facilitates AP-1 DNA-binding activity.* The EMBO Journal, 1992. **11**(2): p. 653-665.

360. Walker, L.J., et al., *Identification of residues in the human DNA repair enzyme HAP1 (Ref-1) that are essential for redox regulation of Jun DNA binding.* Molecular and Cellular Biology, 1993. **13**(9): p. 5370-5376.

361. Ordway, J.M., D. Eberhart, and T. Curran, *Cysteine 64 of Ref-1 Is Not Essential for Redox Regulation of AP-1 DNA Binding.* Molecular and Cellular Biology, 2003. **23**(12): p. 4257-4266.

362. Ando, K., et al., *A new APE1/Ref-1-dependent pathway leading to reduction of NF-κB and AP-1, and activation of their DNA-binding activity.* Nucleic Acids Research, 2008. **36**(13): p. 4327-4336.

363. Janssen-Heininger, Y.M.W., M.E. Poynter, and P.A. Baeuerle, *Recent advances torwards understanding redox mechanisms in the activation of nuclear factor κb.* Free Radical Biology and Medicine, 2000. **28**(9): p. 1317-1327.

364. Matthews, J.R., et al., *Thiordoxin regulates the DNA binding activity of NF-χB by reduction of a disulphid bond involving cysteine 62.* Nucleic Acids Research, 1992. **20**(15): p. 3821-3830.

365. Hayashi, T., Y. Ueno, and T. Okamoto, *Oxidoreductive regulation of nuclear factor kappa B. Involvement of a cellular reducing catalyst thioredoxin.* Journal of Biological Chemistry, 1993. **268**(15): p. 11380-8.

366. Qin, J., et al., *Solution structure of human thioredoxin in a mixed disulfide intermediate complex with its target peptide from the transcription factor NFκB.* Structure, 1995. **3**(3): p. 289-297.

367. Nishi, T., et al., *Spatial Redox Regulation of a Critical Cysteine Residue of NF-κB in Vivo.* Journal of Biological Chemistry, 2002. **277**(46): p. 44548-44556.

368. Nonn, L., et al., *The Absence of Mitochondrial Thioredoxin 2 Causes Massive Apoptosis, Exencephaly, and Early Embryonic Lethality in Homozygous Mice.* Molecular and Cellular Biology, 2003. **23**(3): p. 916-922.

369. Chen, Y., et al., *Overexpressed Human Mitochondrial Thioredoxin Confers Resistance to Oxidant-induced Apoptosis in Human Osteosarcoma Cells.* Journal of Biological Chemistry, 2002. **277**(36): p. 33242-33248.

370. Chen, Y., et al., *Protection against oxidant-induced apoptosis by mitochondrial thioredoxin in SH-SY5Y neuroblastoma cells.* Toxicology and Applied Pharmacology, 2006. **216**(2): p. 256-262.

371. Sengupta, R., et al., *Thioredoxin Catalyzes the Denitrosation of Low-Molecular Mass and Protein S-Nitrosothiols†.* Biochemistry, 2007. **46**(28): p. 8472-8483.

372. Weichsel, A., M. Kem, and W.R. Montfort, *Crystal structure of human thioredoxin revealing an unraveled helix and exposed S-nitrosation site.* Protein Science, 2010. **19**(9): p. 1801-1806.

373. Wu, C., et al., *Redox Regulatory Mechanism of Transnitrosylation by Thioredoxin.* Molecular & Cellular Proteomics, 2010. **9**(10): p. 2262-2275.

374. Wu, C., et al., *Distinction of thioredoxin transnitrosylation and denitrosylation target proteins by the ICAT quantitative approach.* Journal of Proteomics, 2011. **74**(11): p. 2498-2509.

375. Mitchell, D.A. and M.A. Marletta, *Thioredoxin catalyzes the S-nitrosation of the caspase-3 active site cysteine.* Nat Chem Biol, 2005. **1**(3): p. 154-158.

376. Mitchell, D.A., et al., *Thioredoxin is required for S-nitrosation of procaspase-3 and the inhibition of apoptosis in Jurkat cells.* Proceedings of the National Academy of Sciences, 2007. **104**(28): p. 11609-11614.

377. Benhar, M., et al., *Regulated Protein Denitrosylation by Cytosolic and Mitochondrial Thioredoxins.* Science, 2008. **320**(5879): p. 1050-1054.

378. Patwari, P., et al., *The Interaction of Thioredoxin with Txnip.* Journal of Biological Chemistry, 2006. **281**(31): p. 21884-21891.

379. Schulze, P.C., et al., *Vitamin D3–Upregulated Protein-1 (VDUP-1) Regulates Redox-Dependent Vascular Smooth Muscle Cell Proliferation Through Interaction With Thioredoxin.* Circulation Research, 2002. **91**(8): p. 689-695.

380. Yoshioka, J., et al., *Thioredoxin-Interacting Protein Controls Cardiac Hypertrophy Through Regulation of Thioredoxin Activity.* Circulation, 2004. **109**(21): p. 2581-2586.

381. Shi, Y., et al., *Knockdown of thioredoxin interacting protein attenuates high glucose-induced apoptosis and activation of ASK1 in mouse mesangial cells.* FEBS Letters, 2011. **585**(12): p. 1789-1795.

382. Russel, M. and P. Model, *Direct cloning of the trxB gene that encodes thioredoxin reductase.* Journal of Bacteriology, 1985. **163**(1): p. 238-242.

383. Russel, M. and P. Model, *Sequence of thioredoxin reductase from Escherichia coli. Relationship to other flavoprotein disulfide oxidoreductases.* Journal of Biological Chemistry, 1988. **263**(18): p. 9015-9019.

384. Gasdaska, P.Y., et al., *Cloning and sequencing of a human thioredoxin reductase.* FEBS Letters, 1995. **373**(1): p. 5-9.

385. Holmgren, A., *Bovine thioredoxin system. Purification of thioredoxin reductase from calf liver and thymus and studies of its function in disulfide reduction.* Journal of Biological Chemistry, 1977. **252**(13): p. 4600-4606.

386. Luthman, M.H., A., *Rat liver thioredoxin and thioredoxin reductase: purification and characterization.* Biochemistry, 1982. **21**(26): p. 6628-6633.

387. Zhong, L., et al., *Rat and Calf Thioredoxin Reductase Are Homologous to Glutathione Reductase with a Carboxyl-terminal Elongation Containing a*

Conserved Catalytically Active Penultimate Selenocysteine Residue. Journal of Biological Chemistry, 1998. **273**(15): p. 8581-8591.

388. Rozell, B., et al., *Immunohistochemical localization of thioredoxin and thioredoxin reductase in adult rats.* Eur J Cell Biol, 1985. **38**(1): p. 79-86.

389. Miranda-Vizuete, A., et al., *Human mitochondrial thioredoxin reductase.* European Journal of Biochemistry, 1999. **261**(2): p. 405-412.

390. Miranda-Vizuete, A., A.E. Damdimopoulos, and G. Spyrou, *cDNA cloning, expression and chromosomal localization of the mouse mitochondrial thioredoxin reductase gene.* Biochimica et Biophysica Acta (BBA) - Gene Structure and Expression, 1999. **1447**(1): p. 113-118.

391. Lee, S.-R., et al., *Molecular Cloning and Characterization of a Mitochondrial Selenocysteine-containing Thioredoxin Reductase from Rat Liver.* Journal of Biological Chemistry, 1999. **274**(8): p. 4722-4734.

392. Sun, Q.-A., et al., *Selenoprotein oxidoreductase with specificity for thioredoxin and glutathione systems.* Proceedings of the National Academy of Sciences, 2001. **98**(7): p. 3673-3678.

393. Sun, Q.-A., et al., *Redox Regulation of Cell Signaling by Selenocysteine in Mammalian Thioredoxin Reductases.* Journal of Biological Chemistry, 1999. **274**(35): p. 24522-24530.

394. Sandalova, T., et al., *Three-dimensional structure of a mammalian thioredoxin reductase: Implications for mechanism and evolution of a selenocysteine-dependent enzyme.* Proceedings of the National Academy of Sciences, 2001. **98**(17): p. 9533-9538.

395. Gladyshev, V.N., K.T. Jeang, and T.C. Stadtman, *Selenocysteine, identified as the penultimate C-terminal residue in human T-cell thioredoxin reductase, corresponds to TGA in the human placental gene.* Proceedings of the National Academy of Sciences, 1996. **93**(12): p. 6146-6151.

396. Zhong, L. and A. Holmgren, *Essential Role of Selenium in the Catalytic Activities of Mammalian Thioredoxin Reductase Revealed by Characterization of Recombinant Enzymes with Selenocysteine Mutations.* Journal of Biological Chemistry, 2000. **275**(24): p. 18121-18128.

397. Waksman, G., et al., *Crystal Structure of Escherichia coli Thioredoxin Reductase Refined at 2 Å Resolution: Implication for a Large Conformational Change during Catalysis.* Journal of Molecular Biology, 1994. **236**(3): p. 800-816.

398. Williams, C., *Mechanism and structure of thioredoxin reductase from Escherichia coli.* The FASEB Journal, 1995. **9**(13): p. 1267-1276.

399. Mulrooney, S.B. and C.H. Williams, *Evidence for two conformational states of thioredoxin reductase from Escherichia coli: Use of intrinsic and extrinsic quenchers of flavin fluorescence as probes to observe domain rotation.* Protein Science, 1997. **6**(10): p. 2188-2195.

400. Zhong, L., E.S.J. Arnér, and A. Holmgren, *Structure and mechanism of mammalian thioredoxin reductase: The active site is a redox-active selenolthiol/selenenylsulfide formed from the conserved cysteine-selenocysteine sequence.* Proceedings of the National Academy of Sciences, 2000. **97**(11): p. 5854-5859.

401. Arnér, E.S.J. and A. Holmgren, *Physiological functions of thioredoxin and thioredoxin reductase.* European Journal of Biochemistry, 2000. **267**(20): p. 6102-6109.

402. Fujiwara, N., et al., *Roles of N-Terminal Active Cysteines and C-Terminal Cysteine-Selenocysteine in the Catalytic Mechanism of Mammalian Thioredoxin Reductase.* Journal of Biochemistry, 2001. **129**(5): p. 803-812.

403. Cheng, Q., et al., *Crystal Structure and Catalysis of the Selenoprotein Thioredoxin Reductase 1.* Journal of Biological Chemistry, 2009. **284**(6): p. 3998-4008.

404. Gromer, S., et al., *A hypothesis on the catalytic mechanism of the selenoenzyme thioredoxin reductase.* Biochem J., 1998. **332 (pt 2)**: p. 591-592.

405. Jakupoglu, C., et al., *Cytoplasmic Thioredoxin Reductase Is Essential for Embryogenesis but Dispensable for Cardiac Development.* Molecular and Cellular Biology, 2005. **25**(5): p. 1980-1988.

406. Conrad, M., et al., *Essential Role for Mitochondrial Thioredoxin Reductase in Hematopoiesis, Heart Development, and Heart Function.* Molecular and Cellular Biology, 2004. **24**(21): p. 9414-9423.

407. Lundström, J. and A. Holmgren, *Protein disulfide-isomerase is a substrate for thioredoxin reductase and has thioredoxin-like activity.* Journal of Biological Chemistry, 1990. **265**(16): p. 9114-9120.

408. Lundström-Ljung, J., et al., *Two resident ER-proteins, CaBP1 and CaBP2, with thioredoxin domains, are substrates for thioredoxin reductase: comparison with protein disulfide isomerase.* FEBS Letters, 1995. **357**(3): p. 305-308.

409. Björnstedt, M., et al., *Human Thioredoxin Reductase Directly Reduces Lipid Hydroperoxides by NADPH and Selenocystine Strongly Stimulates the Reaction via Catalytically Generated Selenols.* Journal of Biological Chemistry, 1995. **270**(20): p. 11761-11764.

410. Chae, H.Z., Kim, H.J., Kang, S.W., Rhee, S.G., *Characterization of three isoforms of mammalian peroxiredoxin that reduce peroxides in the presence of thioredoxin.* Diabetes Research and Clinical Practice, 1999. **45**(2-3): p. 101-112.

411. Chew, E.-H., et al., *Thioredoxin reductase inhibition by antitumor quinols: a quinol pharmacophore effect correlating to antiproliferative activity.* The FASEB Journal, 2008. **22**(6): p. 2072-2083.

412. Prast-Nielsen, S., et al., *Inhibition of thioredoxin reductase 1 by porphyrins and other small molecules identified by a high-throughput screening assay.* Free Radical Biology and Medicine, 2011. **50**(9): p. 1114-1123.

413. Wang, M., et al., *Three-dimensional structure of NADPH–cytochrome P450 reductase: Prototype for FMN- and FAD-containing enzymes.* Proceedings of the National Academy of Sciences, 1997. **94**(16): p. 8411-8416.

414. Sasada, T., et al., *Possible involvement of thioredoxin reductase as well as thioredoxin in cellular sensitivity to cis-diamminedichloroplatinum (II).* Free Radical Biology and Medicine, 1999. **27**(5–6): p. 504-514.

415. Tonissen, K.F. and G. Di Trapani, *Thioredoxin system inhibitors as mediators of apoptosis for cancer therapy.* Molecular Nutrition & Food Research, 2009. **53**(1): p. 87-103.

416. Arnér, E.S.J., et al., *Analysis of the inhibition of mammalian thioredoxin, thioredoxin reductase, and glutaredoxin by cis-diamminedichloroplatinum (II) and its major metabolite, the glutathione-platinum complex.* Free Radical Biology and Medicine, 2001. **31**(10): p. 1170-1178.

417. McKeage, M.J., L. Maharaj, and S.J. Berners-Price, *Mechanisms of cytotoxicity and antitumor activity of gold(I) phosphine complexes: the possible role of mitochondria.* Coordination Chemistry Reviews, 2002. **232**(1–2): p. 127-135.

418. Gromer, S., et al., *Human Placenta Thioredoxin Reductase.* Journal of Biological Chemistry, 1998. **273**(32): p. 20096-20101.

419. Cox, A.G., et al., *The thioredoxin reductase inhibitor auranofin triggers apoptosis through a Bax/Bak-dependent process that involves peroxiredoxin 3 oxidation.* Biochemical Pharmacology, 2008. **76**(9): p. 1097-1109.

420. Rackham, O., et al., *Substrate and inhibitor specificities differ between human cytosolic and mitochondrial thioredoxin reductases: Implications for development of specific inhibitors.* Free Radical Biology and Medicine, 2011. **50**(6): p. 689-699.

421. Maller, C., Schröder, E., Eaton, P., *Glyceraldehyde 3-phosphate dehydrogenase is unlikely to mediate hydrogen peroxide signaling: studies with a novel anti-dimedone sulfenic acid antibody.* Antioxidant Redox Signal. , 2011. **14**(1): p. 49-60.

422. Barranco-Medina, S., J.-J. Lázaro, and K.-J. Dietz, *The oligomeric conformation of peroxiredoxins links redox state to function.* FEBS Letters, 2009. **583**(12): p. 1809-1816.

423. Charles, R.L., et al., *Protein Sulfenation as a Redox Sensor.* Molecular & Cellular Proteomics, 2007. **6**(9): p. 1473-1484.

424. Nguyen, T., P. Nioi, and C.B. Pickett, *The Nrf2-Antioxidant Response Element Signaling Pathway and Its Activation by Oxidative Stress.* Journal of Biological Chemistry, 2009. **284**(20): p. 13291-13295.

425. Zolk, O., et al., *β-Adrenergic stimulation induces cardiac ankyrin repeat protein expression: involvement of protein kinase A and calmodulin-dependent kinase.* Cardiovascular Research, 2003. **59**(3): p. 563-572.

426. Gupta, M.P., P. Kogut, and M. Gupta, *Protein kinase-A dependent phosphorylation of transcription enhancer factor-1 represses its DNA-binding activity but enhances its gene activation ability.* Nucleic Acids Research, 2000. **28**(16): p. 3168-3177.

427. Houser, S.R., V. Piacentino Iii, and J. Weisser, *Abnormalities of Calcium Cycling in the Hypertrophied and Failing Heart.* Journal of Molecular and Cellular Cardiology, 2000. **32**(9): p. 1595-1607.

428. Port, J.D. and M.R. Bristow, *Altered Beta-adrenergic Receptor Gene Regulation and Signaling in Chronic Heart Failure.* Journal of Molecular and Cellular Cardiology, 2001. **33**(5): p. 887-905.

429. Marx, S.O., et al., *PKA Phosphorylation Dissociates FKBP12.6 from the Calcium Release Channel (Ryanodine Receptor): Defective Regulation in Failing Hearts.* Cell, 2000. **101**(4): p. 365-376.

430. Antos, C.L., et al., *Dilated Cardiomyopathy and Sudden Death Resulting From Constitutive Activation of Protein Kinase A.* Circulation Research, 2001. **89**(11): p. 997-1004.

431. Movsesian, M.A., *Altered cAMP-mediated signalling and its role in the pathogenesis of dilated cardiomyopathy.* Cardiovascular Research, 2004. **62**(3): p. 450-459.

432. Fink, M.A., et al., *AKAP-Mediated Targeting of Protein Kinase A Regulates Contractility in Cardiac Myocytes.* Circulation Research, 2001. **88**(3): p. 291-297.

433. Zakhary, D.R., C.S. Moravec, and M. Bond, *Regulation of PKA Binding to AKAPs in the Heart.* Circulation, 2000. **101**(12): p. 1459-1464.

434. Aye, T.-T., et al., *Reorganized PKA-AKAP associations in the failing human heart.* Journal of Molecular and Cellular Cardiology, 2012. **52**(2): p. 511-518.

435. Kaludercic, N., et al., *Monoamine Oxidase A–Mediated Enhanced Catabolism of Norepinephrine Contributes to Adverse Remodeling and Pump Failure in Hearts With Pressure Overload.* Circulation Research, 2010. **106**(1): p. 193-202.

436. Lairez, O., et al., *Genetic deletion of MAO-A promotes serotonin-dependent ventricular hypertrophy by pressure overload.* Journal of Molecular and Cellular Cardiology, 2009. **46**(4): p. 587-595.

437. Kaludercic, N., et al., *Monoamine oxidases (MAO) in the pathogenesis of heart failure and ischemia/reperfusion injury.* Biochimica et Biophysica Acta (BBA) - Molecular Cell Research, 2011. **1813**(7): p. 1323-1332.

438. Markou, T., M. Hadzopoulou-Cladaras, and A. Lazou, *Phenylephrine induces activation of CREB in adult rat cardiac myocytes through MSK1 and PKA signaling pathways.* Journal of Molecular and Cellular Cardiology, 2004. **37**(5): p. 1001-1011.

439. Meunier, J.-P., et al., *Cardiac pheochromocytoma.* Ann Thorac Surg, 2001. **71**(2): p. 712-713.

440. Jebara, V.A., et al., *Cardiac pheochromocytomas.* Ann Thorac Surg, 1992. **53**(2): p. 356-361.

441. Prejbisz, A., Lenders, J.W.M., Eisenhofer, G., Januszewicz, A., *Cardiovascular manifestations of phaeochromocytoma.* Journal of Hypertension, 2011. **29**(11): p. 2049-2060.

442. Yin, Z., et al., *Differential Role of PKA Catalytic Subunits in Mediating Phenotypes Caused by Knockout of the Carney Complex Gene Prkar1a.* Molecular Endocrinology, 2011. **25**(10): p. 1786-1793.

APPENDICES

Appendix A. Proteins identified in cAMP affinity capture *capture* samples by LC-MS/MS. *Capture* samples were run on a gradient gel and the gel was stained with colloidal Coomassie. Selected stained bands were cut out of the gel and analysed by LC-MS/MS. The table shows the band ID in which the named protein was identified where A is control WT heart, B is 50 µM H_2O_2-perfused WT heart, C is control KI heart and D is 50 µM H_2O_2-perfused KI heart and 1 – 6 is the different molecular weight levels on the gel.

Band ID	Protein name	Protein accession no.	Mw (Da)	Protein ID probability (%)	No. of unique peptides	No. of unique spectra	No. of total spectra	Percentage sequence coverage (%)
A1	Keratin, type II cytoskeletal 5	K2C5_MOUSE	61,768.0	100.0	3	3	5	7.76
	Protein KIAA0664	K0664_MOUSE	148,071.4	100.0	5	5	9	4.11
	Clathrin heavy chain 1	CLH_MOUSE	191,560.9	100.0	4	5	8	3.46
	Long-chain specific acyl-CoA dehydrogenase, mitochondrial	ACADL_MOUSE	47,908.7	100.0	3	3	4	8.37
	Sodium/potassium-transporting ATPase subunit alpha-1	AT1A1_MOUSE	112,985.3	100.0	3	3	6	3.91
	cAMP-dependent protein kinase type II-alpha regulatory subunit	KAP2_MOUSE	45,389.4	100.0	3	3	5	8.23
	ATP synthase subunit alpha, mitochondrial	ATPA_MOUSE	59,754.1	100.0	7	8	14	15.90
	Keratin, type II cytoskeletal 6A	K2C6A_MOUSE	59,336.7	100.0	5	5	8	10.50
	Cytoplasmic dynein 1 heavy chain 1	DYHC1_MOUSE	532,023.0	100.0	6	6	7	1.87
	Isocitrate dehydrogenase [NADP], mitochondrial	IDHP_MOUSE	50,907.2	100.0	5	5	9	13.10
	Superoxide dismutase [Cu-Zn]	SODC_MOUSE	15,941.9	99.9	2	2	4	15.60
	Filamin-C	FLNC_MOUSE	291,111.8	100.0	8	8	10	4.29

	Leucine-rich PPR motif-containing protein, mitochondrial	LPPRC_MOUSE	156,622.2	100.0	18	19	34	13.90
	A kinase anchor protein 1, mitochondrial	AKAP1_MOUSE	92,164.5	100.0	6	6	8	13.10
	Actin, alpha cardiac muscle 1	ACTC_MOUSE	42,020.1	100.0	3	3	5	10.30
	Trifunctional enzyme subunit alpha, mitochondrial	ECHA_MOUSE	82,671.5	100.0	5	5	7	8.78
	Keratin, type I cytoskeletal 10	K1C10_MOUSE	57,771.3	100.0	3	3	6	5.96
	Pyruvate carboxylase, mitochondrial	PYC_MOUSE	129,685.9	100.0	5	5	9	5.77
	Aconitate hydratase, mitochondrial	ACON_MOUSE	85,465.9	100.0	12	12	21	18.50
	Vinculin	VINC_MOUSE	116,719.4	100.0	5	5	7	5.72
	Sarcoplasmic/endoplasmic reticulum calcium ATPase 2	AT2A2_MOUSE	114,860.0	100.0	13	15	26	14.10
	ATP synthase subunit beta, mitochondrial	ATPB_MOUSE	56,301.2	100.0	9	10	18	26.30
	Bifunctional aminoacyl-tRNA synthetase	SYEP_MOUSE	170,054.3	100.0	3	3	3	2.84
	Glycogen phosphorylase, muscle form	PYGM_MOUSE	97,289.4	100.0	2	2	3	3.44
	Collagen alpha-2(VI) chain	CO6A2_MOUSE	110,335.2	99.9	2	2	3	2.90
	Sarcalumenin	SRCA_MOUSE	99,186.0	100.0	3	3	5	4.07
	Carnitine O-palmitoyltransferase 1, muscle isoform	CPT1B_MOUSE	88,220.0	100.0	4	4	6	5.31
	cAMP-dependent protein kinase type I-alpha regulatory subunit	KAP0_MOUSE	43,185.8	100.0	5	6	11	15.70
	Valyl-tRNA synthetase	SYVC_MOUSE	140,217.1	100.0	2	2	4	2.22

	Myosin-binding protein C, cardiac-type	MYPC3_MOUSE	140,631.8	100.0	17	18	30	17.90
	Dystrophin	DMD_MOUSE	425,816.3	100.0	5	5	6	1.71
	3-ketoacyl-CoA thiolase, mitochondrial	THIM_MOUSE	41,858.2	100.0	2	2	3	8.06
	Keratin, type I cytoskeletal 42	K1C42_MOUSE	50,133.6	100.0	3	3	4	9.51
	Keratin, type I cytoskeletal 16	K1C16_MOUSE	51,607.7	99.9	2	2	3	6.82
	NAD(P) transhydrogenase, mitochondrial	NNTM_MOUSE	113,841.3	100.0	4	4	6	4.42
	Myomesin-1	MYOM1_MOUSE	185,464.6	100.0	35	41	65	26.50
	Uncharacterized protein KIAA0564 homolog	K0564_MOUSE	213,424.4	100.0	17	17	29	10.30
	ADP/ATP translocase 1	ADT1_MOUSE	32,905.4	100.0	4	4	8	11.70
	Myosin-6	MYH6_MOUSE	223,571.2	100.0	33	37	61	20.70
A2	Lon protease homolog, mitochondrial	LONM_MOUSE	105,843.9	100.0	8	8	11	11.50
	Sodium/potassium-transporting ATPase subunit alpha-1	AT1A1_MOUSE	112,985.3	100.0	19	19	34	23.40
	cAMP-dependent protein kinase type II-alpha regulatory subunit	KAP2_MOUSE	45,389.4	100.0	10	10	16	34.70
	ATP synthase subunit alpha, mitochondrial	ATPA_MOUSE	59,754.1	100.0	7	8	12	17.50
	Keratin, type II cytoskeletal 6A	K2C6A_MOUSE	59,336.7	100.0	8	9	17	14.50
	2-oxoglutarate dehydrogenase E1 component, mitochondrial	ODO1_MOUSE	116,450.6	100.0	18	22	39	23.10
	Medium-chain specific acyl-CoA dehydrogenase, mitochondrial	ACADM_MOUSE	46,482.4	100.0	4	4	5	11.90

	Sodium/potassium-transporting ATPase subunit alpha-2	AT1A2_MOUSE	112,220.7	99.9	2	2	3	12.60
	Isocitrate dehydrogenase [NADP], mitochondrial	IDHP_MOUSE	50,907.2	100.0	6	6	11	17.70
	Superoxide dismutase [Cu-Zn]	SODC_MOUSE	15,941.9	99.9	2	2	3	15.60
	LIM domain-binding protein 3	LDB3_MOUSE	76,432.1	100.0	5	5	7	9.13
	A kinase anchor protein 1, mitochondrial	AKAP1_MOUSE	92,164.5	100.0	2	2	4	2.57
	Actin, alpha cardiac muscle 1	ACTC_MOUSE	42,020.1	100.0	5	6	12	15.90
	Keratin, type I cytoskeletal 10	K1C10_MOUSE	57,771.3	100.0	3	3	6	6.49
	Aconitate hydratase, mitochondrial	ACON_MOUSE	85,465.9	100.0	15	17	31	23.10
	Trifunctional enzyme subunit beta, mitochondrial	ECHB_MOUSE	51,388.0	100.0	3	3	6	6.95
	Sarcoplasmic/endoplasmic reticulum calcium ATPase 2	AT2A2_MOUSE	114,860.0	100.0	23	27	49	24.40
	ATP synthase subunit beta, mitochondrial	ATPB_MOUSE	56,301.2	100.0	8	9	17	22.50
	Very long-chain specific acyl-CoA dehydrogenase, mitochondrial	ACADV_MOUSE	70,877.0	100.0	4	4	6	7.62
	Fumarate hydratase, mitochondrial	FUMH_MOUSE	54,371.1	100.0	3	3	5	8.68
	Trifunctional enzyme subunit alpha, mitochondrial	ECHA_MOUSE	82,671.5	100.0	5	5	10	9.17
	3-ketoacyl-CoA thiolase, mitochondrial	THIM_MOUSE	41,858.2	100.0	3	3	5	11.30
	Glycogen phosphorylase, muscle form	PYGM_MOUSE	97,289.4	100.0	2	2	4	2.38
	Sarcalumenin	SRCA_MOUSE	99,186.0	100.0	2	2	3	2.86
	Creatine kinase M-type	KCRM_MOUSE	43,045.6	100.0	3	3	4	9.45

	Presequence protease, mitochondrial	PREP_MOUSE	117,374.4	100.0	2	2	2	2.41
	Pyruvate dehydrogenase E1 component subunit beta, mitochondrial	ODPB_MOUSE	38,937.0	99.9	2	2	4	6.41
	cAMP-dependent protein kinase type I-alpha regulatory subunit	KAP0_MOUSE	43,185.8	100.0	14	16	31	35.40
	Myosin-binding protein C, cardiac-type	MYPC3_MOUSE	140,631.8	100.0	6	6	10	5.51
	Glyceraldehyde-3-phosphate dehydrogenase	G3P_MOUSE	35,810.1	100.0	3	3	4	15.00
	Kinesin-1 heavy chain	KINH_MOUSE	109,550.6	100.0	9	9	14	9.97
	Myosin-Ic	MYO1C_MOUSE	121,947.9	100.0	3	3	3	3.10
	Keratin, type I cytoskeletal 42	K1C42_MOUSE	50,133.6	100.0	7	7	11	19.00
	Alpha-actinin-2	ACTN2_MOUSE	103,657.2	100.0	7	7	9	9.96
	NAD(P) transhydrogenase, mitochondrial	NNTM_MOUSE	113,841.3	100.0	12	16	28	13.50
	NADH-ubiquinone oxidoreductase 75 kDa subunit, mitochondrial	NDUS1_MOUSE	79,749.6	100.0	2	2	3	3.99
	Myomesin-1	MYOM1_MOUSE	185,464.6	100.0	11	11	16	7.92
	Uncharacterized protein KIAA0564 homolog	K0564_MOUSE	213,424.4	100.0	3	3	4	2.41
	Isoleucyl-tRNA synthetase, mitochondrial	SYIM_MOUSE	112,805.9	100.0	4	4	6	5.73
	Hexokinase-2	HXK2_MOUSE	102,536.6	100.0	12	13	24	16.70
	ADP/ATP translocase 1	ADT1_MOUSE	32,905.4	100.0	3	3	5	10.10
	Hexokinase-1	HXK1_MOUSE	108,304.7	100.0	4	4	8	6.06

A3	Keratin, type II cytoskeletal 5	K2C5_MOUSE	61,768.0	100.0	3	3	5	7.93
	Pyruvate kinase isozymes M1/M2	KPYM_MOUSE	57,845.6	100.0	6	7	11	16.90
	cAMP-dependent protein kinase type II-alpha regulatory subunit	KAP2_MOUSE	45,389.4	100.0	18	27	58	48.10
	ATP synthase subunit alpha, mitochondrial	ATPA_MOUSE	59,754.1	100.0	14	17	33	32.20
	Keratin, type II cytoskeletal 6A	K2C6A_MOUSE	59,336.7	100.0	8	9	18	17.20
	2-oxoglutarate dehydrogenase E1 component, mitochondrial	ODO1_MOUSE	116,450.6	100.0	3	3	4	3.62
	Tubulin beta-2C chain	TBB2C_MOUSE	49,830.7	100.0	7	7	12	18.40
	Isocitrate dehydrogenase [NADP], mitochondrial	IDHP_MOUSE	50,907.2	100.0	13	15	30	32.70
	Alpha-enolase	ENOA_MOUSE	47,141.7	100.0	3	3	5	18.90
	Methylmalonate-semialdehyde dehydrogenase [acylating], mitochondrial	MMSA_MOUSE	57,916.3	100.0	8	9	16	23.60
	Aldehyde dehydrogenase, mitochondrial	ALDH2_MOUSE	56,537.6	100.0	8	9	12	16.80
	Actin, alpha cardiac muscle 1	ACTC_MOUSE	42,020.1	100.0	3	4	6	13.30
	Aconitate hydratase, mitochondrial	ACON_MOUSE	85,465.9	100.0	3	3	5	4.10
	Trifunctional enzyme subunit beta, mitochondrial	ECHB_MOUSE	51,388.0	100.0	9	9	18	21.10
	ATP synthase subunit beta, mitochondrial	ATPB_MOUSE	56,301.2	100.0	15	20	35	43.30
	Fumarate hydratase, mitochondrial	FUMH_MOUSE	54,371.1	100.0	5	6	11	11.60
	Trifunctional enzyme subunit alpha, mitochondrial	ECHA_MOUSE	82,671.5	100.0	4	4	6	7.08

	Sarcalumenin	SRCA_MOUSE	99,186.0	100.0	7	7	12	10.40
	Cytochrome b-c1 complex subunit 1, mitochondrial	QCR1_MOUSE	52,768.8	100.0	5	5	9	11.50
	Pyruvate dehydrogenase E1 component subunit alpha, somatic form, mitochondrial	ODPA_MOUSE	43,232.5	100.0	2	2	8	5.13
	Beta-enolase	ENOB_MOUSE	47,025.9	100.0	4	4	9	14.70
	Dihydrolipoyl dehydrogenase, mitochondrial	DLDH_MOUSE	54,272.4	100.0	6	7	10	16.10
	Succinyl-CoA:3-ketoacid-coenzyme A transferase 1, mitochondrial	SCOT1_MOUSE	55,990.2	100.0	5	6	10	15.00
	cAMP-dependent protein kinase type I-alpha regulatory subunit	KAP0_MOUSE	43,185.8	100.0	14	20	62	38.80
	Propionyl-CoA carboxylase beta chain, mitochondrial	PCCB_MOUSE	58,394.5	100.0	3	3	5	8.13
	Keratin, type I cytoskeletal 42	K1C42_MOUSE	50,133.6	100.0	5	5	9	13.90
	Keratin, type I cytoskeletal 16	K1C16_MOUSE	51,607.7	100.0	2	3	5	9.59
	Tubulin alpha-4A chain	TBA4A_MOUSE	49,924.6	100.0	5	6	11	15.20
	ADP/ATP translocase 1	ADT1_MOUSE	32,905.4	100.0	4	4	6	12.80
A4	NADH dehydrogenase [ubiquinone] iron-sulfur protein 2, mitochondrial	NDUS2_MOUSE	52,626.8	100.0	6	6	12	18.10
	Cysteine desulfurase, mitochondrial	NFS1_MOUSE	50,001.8	100.0	3	3	5	8.65
	Long-chain specific acyl-CoA dehydrogenase, mitochondrial	ACADL_MOUSE	47,908.7	100.0	6	6	9	17.70
	cAMP-dependent protein kinase type II-alpha regulatory subunit	KAP2_MOUSE	45,389.4	100.0	10	12	19	36.70

	ATP synthase subunit alpha, mitochondrial	ATPA_MOUSE	59,754.1	100.0	5	6	11	11.20
	Keratin, type II cytoskeletal 6A	K2C6A_MOUSE	59,336.7	100.0	5	5	8	7.96
	Medium-chain specific acyl-CoA dehydrogenase, mitochondrial	ACADM_MOUSE	46,482.4	100.0	4	5	9	11.60
	Isocitrate dehydrogenase [NADP], mitochondrial	IDHP_MOUSE	50,907.2	100.0	17	22	50	39.80
	Alpha-enolase	ENOA_MOUSE	47,141.7	100.0	5	5	7	23.00
	Mannose-6-phosphate isomerase	MPI_MOUSE	46,575.9	100.0	3	3	5	10.20
	2-oxoisovalerate dehydrogenase subunit alpha, mitochondrial	ODBA_MOUSE	50,371.5	100.0	3	4	7	11.10
	Phosphoglycerate kinase 1	PGK1_MOUSE	44,551.1	100.0	4	4	8	13.40
	Elongation factor Tu, mitochondrial	EFTU_MOUSE	49,508.9	100.0	6	7	11	15.00
	Sodium/potassium-transporting ATPase subunit beta-1	AT1B1_MOUSE	35,196.4	100.0	3	4	6	12.50
	Citrate synthase, mitochondrial	CISY_MOUSE	51,738.1	100.0	3	3	4	6.47
	Aconitate hydratase, mitochondrial	ACON_MOUSE	85,465.9	100.0	4	4	5	6.79
	Trifunctional enzyme subunit beta, mitochondrial	ECHB_MOUSE	51,388.0	100.0	7	8	14	16.20
	ATP synthase subunit beta, mitochondrial	ATPB_MOUSE	56,301.2	100.0	5	5	8	11.20
	Fumarate hydratase, mitochondrial	FUMH_MOUSE	54,371.1	100.0	6	7	12	17.80
	Cytochrome b-c1 complex subunit 1, mitochondrial	QCR1_MOUSE	52,768.8	100.0	8	9	18	22.50
	Pyruvate dehydrogenase E1 component subunit alpha, somatic form, mitochondrial	ODPA_MOUSE	43,232.5	100.0	7	7	13	18.70

	Beta-enolase	ENOB_MOUSE	47,025.9	100.0	9	13	27	29.70
	Creatine kinase M-type	KCRM_MOUSE	43,045.6	100.0	3	3	5	9.97
	Trifunctional enzyme subunit alpha, mitochondrial	ECHA_MOUSE	82,671.5	100.0	3	3	5	5.90
	[Pyruvate dehydrogenase [lipoamide]] kinase isozyme 1, mitochondrial	PDK1_MOUSE	48,926.8	100.0	2	2	3	8.06
	Eukaryotic initiation factor 4A-I	IF4A1_MOUSE	46,155.3	100.0	5	5	8	14.00
	Kynurenine--oxoglutarate transaminase 3	KAT3_MOUSE	51,127.9	99.9	2	2	3	5.27
	cAMP-dependent protein kinase type I-alpha regulatory subunit	KAP0_MOUSE	43,185.8	100.0	8	9	14	23.10
	Succinyl-CoA ligase [ADP-forming] subunit beta, mitochondrial	SUCB1_MOUSE	50,114.7	100.0	4	4	7	11.20
	Keratin, type I cytoskeletal 42	K1C42_MOUSE	50,133.6	100.0	5	5	9	13.50
	[Pyruvate dehydrogenase [lipoamide]] kinase isozyme 2, mitochondrial	PDK2_MOUSE	46,070.1	100.0	5	5	5	15.20
	Actin, alpha cardiac muscle 1	ACTC_MOUSE	42,020.1	100.0	6	6	12	20.40
	Cytochrome b-c1 complex subunit 2, mitochondrial	QCR2_MOUSE	48,236.0	100.0	9	9	14	25.60
	ADP/ATP translocase 1	ADT1_MOUSE	32,905.4	100.0	4	4	7	12.80
	Creatine kinase S-type, mitochondrial	KCRS_MOUSE	47,474.7	100.0	7	7	10	17.90
A5	NADH dehydrogenase [ubiquinone] iron-sulfur protein 2, mitochondrial	NDUS2_MOUSE	52,626.8	100.0	3	3	4	6.26
	Long-chain specific acyl-CoA dehydrogenase, mitochondrial	ACADL_MOUSE	47,908.7	100.0	11	13	23	35.30

	cAMP-dependent protein kinase type II-alpha regulatory subunit	KAP2_MOUSE	45,389.4	100.0	7	7	13	22.90
	Dihydrolipoyllysine-residue acetyltransferase component of pyruvate dehydrogenase complex, mitochondrial	ODP2_MOUSE	67,942.6	100.0	3	3	5	7.32
	ATP synthase subunit alpha, mitochondrial	ATPA_MOUSE	59,754.1	100.0	4	4	7	9.40
	Keratin, type II cytoskeletal 6A	K2C6A_MOUSE	59,336.7	100.0	3	3	5	4.34
	Aspartate aminotransferase, mitochondrial	AATM_MOUSE	47,412.3	100.0	4	4	6	10.00
	Medium-chain specific acyl-CoA dehydrogenase, mitochondrial	ACADM_MOUSE	46,482.4	100.0	4	6	12	12.40
	Keratin, type II cytoskeletal 1	K2C1_MOUSE	65,607.1	100.0	3	4	8	3.77
	Succinyl-CoA ligase [GDP-forming] subunit beta, mitochondrial	SUCB2_MOUSE	46,841.0	100.0	3	3	4	9.01
	Actin, cytoplasmic 1	ACTB_MOUSE, ACTG_MOUSE	41,737.8	100.0	4	6	12	41.10
	Isocitrate dehydrogenase [NADP], mitochondrial	IDHP_MOUSE	50,907.2	100.0	9	11	20	23.90
	Mannose-6-phosphate isomerase	MPI_MOUSE	46,575.9	100.0	3	3	5	10.20
	Phosphoglycerate kinase 1	PGK1_MOUSE	44,551.1	100.0	8	8	13	21.30
	Aconitate hydratase, mitochondrial	ACON_MOUSE	85,465.9	100.0	3	3	5	4.10
	Elongation factor Tu, mitochondrial	EFTU_MOUSE	49,508.9	100.0	4	5	9	10.40
	NADH dehydrogenase [ubiquinone] 1 alpha subcomplex subunit 10, mitochondrial	NDUAA_MOUSE	40,604.7	100.0	6	6	8	15.50

	Actin, alpha cardiac muscle 1	ACTC_MOUSE	42,020.1	100.0	16	20	40	54.10
	Beta-enolase	ENOB_MOUSE	47,025.9	100.0	3	4	5	10.10
	Citrate synthase, mitochondrial	CISY_MOUSE	51,738.1	100.0	4	4	8	11.40
	Trifunctional enzyme subunit beta, mitochondrial	ECHB_MOUSE	51,388.0	100.0	3	3	4	5.47
	Acetyl-CoA acetyltransferase, mitochondrial	THIL_MOUSE	44,816.4	100.0	8	13	22	26.40
	ATP synthase subunit beta, mitochondrial	ATPB_MOUSE	56,301.2	100.0	6	6	11	15.70
	Trifunctional enzyme subunit alpha, mitochondrial	ECHA_MOUSE	82,671.5	100.0	4	4	6	6.16
	3-ketoacyl-CoA thiolase, mitochondrial	THIM_MOUSE	41,858.2	100.0	7	8	15	30.20
	Pyruvate dehydrogenase E1 component subunit alpha, somatic form, mitochondrial	ODPA_MOUSE	43,232.5	100.0	3	3	6	8.97
	Creatine kinase M-type	KCRM_MOUSE	43,045.6	100.0	4	4	8	13.10
	Eukaryotic initiation factor 4A-I	IF4A1_MOUSE	46,155.3	100.0	2	2	3	5.67
	cAMP-dependent protein kinase type I-alpha regulatory subunit	KAP0_MOUSE	43,185.8	100.0	9	12	20	26.20
	Succinyl-CoA ligase [ADP-forming] subunit beta, mitochondrial	SUCB1_MOUSE	50,114.7	100.0	11	13	23	24.00
	Keratin, type I cytoskeletal 42	K1C42_MOUSE	50,133.6	100.0	6	7	11	11.30
	Isovaleryl-CoA dehydrogenase, mitochondrial	IVD_MOUSE	46,326.5	100.0	5	6	11	13.70
	Cytochrome b-c1 complex subunit 2, mitochondrial	QCR2_MOUSE	48,236.0	100.0	9	14	25	25.60
	Fructose-bisphosphate aldolase A	ALDOA_MOUSE	39,356.5	100.0	5	5	8	20.30

	ADP/ATP translocase 1	ADT1_MOUSE	32,905.4	100.0	4	4	8	12.80
	Creatine kinase S-type, mitochondrial	KCRS_MOUSE	47,474.7	100.0	7	7	9	20.00
A6	Prohibitin	PHB_MOUSE	29,820.6	100.0	4	4	7	15.80
	ATP synthase subunit alpha, mitochondrial	ATPA_MOUSE	59,754.1	100.0	7	7	13	17.70
	Enoyl-CoA hydratase, mitochondrial	ECHM_MOUSE	31,475.3	100.0	6	8	16	23.80
	Medium-chain specific acyl-CoA dehydrogenase, mitochondrial	ACADM_MOUSE	46,482.4	100.0	6	6	11	15.90
	Keratin, type II cytoskeletal 1	K2C1_MOUSE	65,607.1	100.0	3	4	7	3.77
	Isocitrate dehydrogenase [NADP], mitochondrial	IDHP_MOUSE	50,907.2	100.0	4	4	7	11.10
	Phosphoglycerate kinase 1	PGK1_MOUSE	44,551.1	100.0	2	2	4	7.91
	Sepiapterin reductase	SPRE_MOUSE	27,883.8	100.0	4	4	6	23.80
	Citrate lyase subunit beta-like protein, mitochondrial	CLYBL_MOUSE	37,549.1	100.0	3	3	5	9.76
	Electron transfer flavoprotein subunit alpha, mitochondrial	ETFA_MOUSE	35,009.8	100.0	6	7	12	28.50
	L-lactate dehydrogenase A chain	LDHA_MOUSE	36,498.9	100.0	6	6	8	19.00
	Malate dehydrogenase, mitochondrial	MDHM_MOUSE	35,611.9	100.0	6	6	11	21.90
	Actin, alpha cardiac muscle 1	ACTC_MOUSE	42,020.1	100.0	6	6	10	19.60
	Trifunctional enzyme subunit alpha, mitochondrial	ECHA_MOUSE	82,671.5	100.0	3	3	4	4.72
	Pyruvate kinase isozymes M1/M2	KPYM_MOUSE	57,845.6	100.0	3	3	6	5.84

	NADH dehydrogenase [ubiquinone] iron-sulfur protein 3, mitochondrial	NDUS3_MOUSE	30,149.4	100.0	4	6	10	15.20
	Electron transfer flavoprotein subunit beta	ETFB_MOUSE	27,623.2	100.0	3	3	3	14.10
	Cytochrome b-c1 complex subunit Rieske, mitochondrial	UCRI_MOUSE	29,367.2	100.0	3	3	5	8.39
	3-hydroxyisobutyrate dehydrogenase, mitochondrial	3HIDH_MOUSE	35,440.6	100.0	4	4	7	20.00
	Coiled-coil-helix-coiled-coil-helix domain-containing protein 3, mitochondrial	CHCH3_MOUSE	26,334.4	100.0	7	8	13	18.90
	Trifunctional enzyme subunit beta, mitochondrial	ECHB_MOUSE	51,388.0	100.0	6	6	10	14.30
	Acetyl-CoA acetyltransferase, mitochondrial	THIL_MOUSE	44,816.4	100.0	4	4	8	13.20
	ATP synthase subunit beta, mitochondrial	ATPB_MOUSE	56,301.2	100.0	3	3	5	8.32
	Prohibitin-2	PHB2_MOUSE	33,297.6	100.0	3	3	5	9.70
	Aconitate hydratase, mitochondrial	ACON_MOUSE	85,465.9	100.0	4	4	7	7.44
	3-ketoacyl-CoA thiolase, mitochondrial	THIM_MOUSE	41,858.2	100.0	4	4	6	12.60
	Cytochrome c1, heme protein, mitochondrial	CY1_MOUSE	35,328.4	100.0	4	5	8	20.90
	Mitochondrial carnitine/acylcarnitine carrier protein	MCAT_MOUSE	33,028.2	100.0	4	4	7	11.00
	Pyruvate dehydrogenase E1 component subunit alpha, somatic form, mitochondrial	ODPA_MOUSE	43,232.5	100.0	3	3	4	4.87
	Cytochrome b-c1 complex subunit 2, mitochondrial	QCR2_MOUSE	48,236.0	100.0	5	5	9	13.50

	Mitochondrial 2-oxoglutarate/malate carrier protein	M2OM_MOUSE	34,156.3	100.0	4	4	8	14.00
	Pyruvate dehydrogenase E1 component subunit beta, mitochondrial	ODPB_MOUSE	38,937.0	100.0	5	5	9	17.50
	Dihydropteridine reductase	DHPR_MOUSE	25,570.2	100.0	3	3	5	17.80
	ATP synthase subunit gamma, mitochondrial	ATPG_MOUSE	32,887.4	100.0	4	4	11	15.80
	cAMP-dependent protein kinase type I-alpha regulatory subunit	KAP0_MOUSE	43,185.8	100.0	4	4	6	14.40
	Methylglutaconyl-CoA hydratase, mitochondrial	AUHM_MOUSE	33,396.2	100.0	3	3	5	11.10
	Glyceraldehyde-3-phosphate dehydrogenase	G3P_MOUSE	35,810.1	100.0	4	4	6	19.20
	Succinate dehydrogenase [ubiquinone] iron-sulfur subunit, mitochondrial	DHSB_MOUSE	31,815.0	100.0	5	6	11	19.50
	Triosephosphate isomerase	TPIS_MOUSE	26,712.2	100.0	7	8	16	36.10
	Phosphate carrier protein, mitochondrial	MPCP_MOUSE	39,633.1	100.0	10	12	21	27.70
	3,2-trans-enoyl-CoA isomerase, mitochondrial	D3D2_MOUSE	32,079.2	100.0	5	5	10	21.50
	NAD-dependent deacetylase sirtuin-5	SIRT5_MOUSE	34,134.1	99.9	2	2	2	5.81
	Voltage-dependent anion-selective channel protein 3	VDAC3_MOUSE	30,754.0	100.0	3	3	3	12.00
	Malate dehydrogenase, cytoplasmic	MDHC_MOUSE	36,512.1	100.0	4	4	8	16.50
	Myosin light chain 3	MYL3_MOUSE	22,422.2	100.0	5	6	10	38.20
	Dehydrogenase/reductase SDR family member 4	DHRS4_MOUSE	27,754.0	100.0	3	3	4	11.50

	ADP/ATP translocase 2	ADT2_MOUSE	32,932.6	100.0	4	4	7	20.80
	14-3-3 protein zeta/delta	1433Z_MOUSE	27,771.9	100.0	3	3	5	14.70
	ADP/ATP translocase 1	ADT1_MOUSE	32,905.4	100.0	14	15	28	39.30
B1	Protein KIAA0664	K0664_MOUSE	148,071.4	100.0	4	4	7	3.73
	Cullin-associated NEDD8-dissociated protein 2	CAND2_MOUSE	135,636.3	100.0	3	3	5	3.32
	Clathrin heavy chain 1	CLH_MOUSE	191,560.9	100.0	5	6	9	4.00
	cAMP-dependent protein kinase type II-alpha regulatory subunit	KAP2_MOUSE	45,389.4	100.0	4	4	6	13.50
	ATP synthase subunit alpha, mitochondrial	ATPA_MOUSE	59,754.1	100.0	7	7	11	15.90
	2-oxoglutarate dehydrogenase E1 component, mitochondrial	ODO1_MOUSE	116,450.6	99.9	2	2	3	3.23
	Fatty acid synthase	FAS_MOUSE	272,429.3	100.0	8	8	15	4.27
	Isocitrate dehydrogenase [NADP], mitochondrial	IDHP_MOUSE	50,907.2	100.0	5	5	9	14.80
	Dihydrolipoyllysine-residue acetyltransferase component of pyruvate dehydrogenase complex, mitochondrial	ODP2_MOUSE	67,942.6	99.9	2	2	3	5.45
	Superoxide dismutase [Cu-Zn]	SODC_MOUSE	15,941.9	100.0	3	3	5	22.10
	Filamin-C	FLNC_MOUSE	291,111.8	99.9	2	2	2	0.95
	Leucine-rich PPR motif-containing protein, mitochondrial	LPPRC_MOUSE	156,622.2	100.0	19	20	35	14.60
	A kinase anchor protein 1, mitochondrial	AKAP1_MOUSE	92,164.5	100.0	9	9	15	16.90

	Valyl-tRNA synthetase	SYVC_MOUSE	140,217.1	100.0	6	6	9	6.25
	Actin, alpha cardiac muscle 1	ACTC_MOUSE	42,020.1	100.0	3	3	6	10.30
	Keratin, type I cytoskeletal 10	K1C10_MOUSE	57,771.3	100.0	3	3	6	5.96
	Pyruvate carboxylase, mitochondrial	PYC_MOUSE	129,685.9	100.0	8	9	15	9.08
	Aconitate hydratase, mitochondrial	ACON_MOUSE	85,465.9	100.0	12	13	24	18.50
	Trifunctional enzyme subunit beta, mitochondrial	ECHB_MOUSE	51,388.0	100.0	2	2	4	4.00
	Sarcoplasmic/endoplasmic reticulum calcium ATPase 2	AT2A2_MOUSE	114,860.0	100.0	9	10	19	11.30
	ATP synthase subunit beta, mitochondrial	ATPB_MOUSE	56,301.2	100.0	8	9	16	23.60
	Trifunctional enzyme subunit alpha, mitochondrial	ECHA_MOUSE	82,671.5	100.0	6	6	10	9.96
	Sarcalumenin	SRCA_MOUSE	99,186.0	100.0	4	4	7	4.95
	Cytochrome c1, heme protein, mitochondrial	CY1_MOUSE	35,328.4	100.0%	3	3	5	17.20
	Carnitine O-palmitoyltransferase 1, muscle isoform	CPT1B_MOUSE	88,220.0	100.0%	3	3	6	4.27
	cAMP-dependent protein kinase type I-alpha regulatory subunit	KAP0_MOUSE	43,185.8	100.0%	4	6	10	9.45
	Myosin-binding protein C, cardiac-type	MYPC3_MOUSE	140,631.8	100.0	20	23	43	20.40
	Vinculin	VINC_MOUSE	116,719.4	100.0	2	2	3	2.25
	A-kinase anchor protein 2	AKAP2_MOUSE	98,578.4	100.0	5	7	11	9.41
	Sodium/potassium-transporting ATPase subunit alpha-1	AT1A1_MOUSE	112,985.3	100.0	5	5	6	5.96
	NAD(P) transhydrogenase, mitochondrial	NNTM_MOUSE	113,841.3	100.0	8	8	14	8.84

	Myomesin-1	MYOM1_MOUSE	185,464.6	100.0	38	46	75	30.20
	Uncharacterized protein KIAA0564 homolog	K0564_MOUSE	213,424.4	100.0	15	15	27	9.45
	Myosin-6	MYH6_MOUSE	223,571.2	100.0	30	35	57	19.50
	ADP/ATP translocase 1	ADT1_MOUSE	32,905.4	100.0	4	4	8	11.70
B2	cAMP-dependent protein kinase type II-alpha regulatory subunit	KAP2_MOUSE	45,389.4	100.0	7	7	9	25.20
	ATP-citrate synthase	ACLY_MOUSE	119,731.4	100.0	3	3	4	3.76
	ATP synthase subunit alpha, mitochondrial	ATPA_MOUSE	59,754.1	100.0	6	7	13	13.60
	2-oxoglutarate dehydrogenase E1 component, mitochondrial	ODO1_MOUSE	116,450.6	100.0	20	22	37	27.40
	Medium-chain specific acyl-CoA dehydrogenase, mitochondrial	ACADM_MOUSE	46,482.4	100.0	4	4	5	11.90
	Heat shock 70 kDa protein 4	HSP74_MOUSE	94,133.4	100.0	3	3	5	4.04
	Isocitrate dehydrogenase [NADP], mitochondrial	IDHP_MOUSE	50,907.2	100.0	8	9	17	19.20
	Long-chain-fatty-acid--CoA ligase 1	ACSL1_MOUSE	77,926.2	100.0	3	3	5	5.15
	LIM domain-binding protein 3	LDB3_MOUSE	76,432.1	100.0	4	4	6	6.92
	Lon protease homolog, mitochondrial	LONM_MOUSE	105,843.9	100.0	7	7	13	8.75
	A kinase anchor protein 1, mitochondrial	AKAP1_MOUSE	92,164.5	100.0	5	5	8	7.82
	Actin, alpha cardiac muscle 1	ACTC_MOUSE	42,020.1	100.0	3	4	7	9.81
	Keratin, type I cytoskeletal 10	K1C10_MOUSE	57,771.3	100.0	5	5	9	8.07

	Myosin-binding protein C, cardiac-type	MYPC3_MOUSE	140,631.8	100.0	3	3	4	3.07
	Aconitate hydratase, mitochondrial	ACON_MOUSE	85,465.9	100.0	14	17	30	21.20
	Trifunctional enzyme subunit beta, mitochondrial	ECHB_MOUSE	51,388.0	100.0	4	4	5	8.21
	Sarcoplasmic/endoplasmic reticulum calcium ATPase 2	AT2A2_MOUSE	114,860.0	100.0	23	28	55	22.50
	ATP synthase subunit beta, mitochondrial	ATPB_MOUSE	56,301.2	100.0	9	10	18	26.10
	Very long-chain specific acyl-CoA dehydrogenase, mitochondrial	ACADV_MOUSE	70,877.0	100.0	3	3	4	5.79
	Trifunctional enzyme subunit alpha, mitochondrial	ECHA_MOUSE	82,671.5	100.0	6	6	11	10.70
	3-ketoacyl-CoA thiolase, mitochondrial	THIM_MOUSE	41,858.2	100.0	5	5	7	19.10
	Glycogen phosphorylase, muscle form	PYGM_MOUSE	97,289.4	100.0	3	3	6	3.68
	Carnitine O-palmitoyltransferase 1, muscle isoform	CPT1B_MOUSE	88,220.0	100.0	2	2	4	3.24
	Presequence protease, mitochondrial	PREP_MOUSE	117,374.4	100.0	4	4	8	4.73
	cAMP-dependent protein kinase type I-alpha regulatory subunit	KAP0_MOUSE	43,185.8	100.0	16	18	43	41.70
	Kinesin-1 heavy chain	KINH_MOUSE	109,550.6	100.0	9	9	16	10.80
	Myosin-Ic	MYO1C_MOUSE	121,947.9	100.0	2	2	3	2.63
	Alpha-actinin-2	ACTN2_MOUSE	103,657.2	100.0	4	4	7	5.37
	NADH-ubiquinone oxidoreductase 75 kDa subunit, mitochondrial	NDUS1_MOUSE	79,749.6	100.0	3	3	4	4.81

	Keratin, type II cytoskeletal 1	K2C1_MOUSE	65,607.1	100.0	3	4	8	3.77
	Sodium/potassium-transporting ATPase subunit alpha-1	AT1A1_MOUSE	112,985.3	100.0	16	16	31	19.60
	NAD(P) transhydrogenase, mitochondrial	NNTM_MOUSE	113,841.3	100.0	12	15	26	12.70
	Dihydrolipoyllysine-residue acetyltransferase component of pyruvate dehydrogenase complex, mitochondrial	ODP2_MOUSE	67,942.6	100.0	3	3	4	7.79
	Uncharacterized protein KIAA0564 homolog	K0564_MOUSE	213,424.4	100.0	6	6	11	4.04
	Isoleucyl-tRNA synthetase, mitochondrial	SYIM_MOUSE	112,805.9	100.0	4	4	7	5.24
	Hexokinase-2	HXK2_MOUSE	102,536.6	100.0	14	16	25	19.00
	Hexokinase-1	HXK1_MOUSE	108,304.7	100.0	3	3	6	5.13
	ADP/ATP translocase 1	ADT1_MOUSE	32,905.4	100.0	6	6	11	20.10
B3	Succinyl-CoA:3-ketoacid-coenzyme A transferase 1, mitochondrial	SCOT1_MOUSE	55,990.2	100.0	3	3	5	10.20
	cAMP-dependent protein kinase type II-alpha regulatory subunit	KAP2_MOUSE	45,389.4	100.0	19	27	46	50.60
	ATP synthase subunit alpha, mitochondrial	ATPA_MOUSE	59,754.1	100.0	15	18	33	34.20
	Cytochrome b-c1 complex subunit 1, mitochondrial	QCR1_MOUSE	52,768.8	99.9	2	2	3	6.25
	Fumarate hydratase, mitochondrial	FUMH_MOUSE	54,371.1	100.0	4	5	9	11.20
	cAMP-dependent protein kinase type II-beta regulatory subunit	KAP3_MOUSE	46,167.7	100.0	3	3	5	22.60

	ATP synthase subunit beta, mitochondrial	ATPB_MOUSE	56,301.2	100.0	17	23	41	43.30
	Methylmalonate-semialdehyde dehydrogenase [acylating], mitochondrial	MMSA_MOUSE	57,916.3	100.0	11	12	22	28.40
	cAMP-dependent protein kinase type I-beta regulatory subunit	KAP1_MOUSE	43,224.4	100.0	3	3	5	16.50
	Dihydrolipoyl dehydrogenase, mitochondrial	DLDH_MOUSE	54,272.4	100.0	4	4	5	9.82
	Sarcalumenin	SRCA_MOUSE	99,186.0	100.0	8	8	13	12.90
	Tubulin beta-2C chain	TBB2C_MOUSE	49,830.7	100.0	7	7	12	18.90
	cAMP-dependent protein kinase type I-alpha regulatory subunit	KAP0_MOUSE	43,185.8	100.0	18	25	79	42.50
	Pyruvate dehydrogenase E1 component subunit alpha, somatic form, mitochondrial	ODPA_MOUSE	43,232.5	100.0	5	5	8	13.10
	Pyruvate kinase isozymes M1/M2	KPYM_MOUSE	57,845.6	100.0	7	8	15	20.50
	Epoxide hydrolase 2	HYES_MOUSE	62,516.8	100.0	3	3	5	6.50
	Tubulin alpha-4A chain	TBA4A_MOUSE	49,924.6	100.0	5	6	9	16.70
	Aconitate hydratase, mitochondrial	ACON_MOUSE	85,465.9	100.0	3	3	3	5.13
	Actin, alpha cardiac muscle 1	ACTC_MOUSE	42,020.1	100.0	4	4	8	13.30
	Propionyl-CoA carboxylase beta chain, mitochondrial	PCCB_MOUSE	58,394.5	100.0	4	4	8	9.98
	Aldehyde dehydrogenase, mitochondrial	ALDH2_MOUSE	56,537.6	100.0	6	6	9	11.40
	Isocitrate dehydrogenase [NADP], mitochondrial	IDHP_MOUSE	50,907.2	100.0	7	9	18	19.20

	Trifunctional enzyme subunit beta, mitochondrial	ECHB_MOUSE	51,388.0	100.0	10	10	18	22.90
B4	NADH dehydrogenase [ubiquinone] iron-sulfur protein 2, mitochondrial	NDUS2_MOUSE	52,626.8	100.0	6	7	12	14.90
	Long-chain specific acyl-CoA dehydrogenase, mitochondrial	ACADL_MOUSE	47,908.7	100.0	3	3	5	7.67
	cAMP-dependent protein kinase type II-alpha regulatory subunit	KAP2_MOUSE	45,389.4	100.0	4	4	8	12.20
	ATP synthase subunit alpha, mitochondrial	ATPA_MOUSE	59,754.1	100.0	5	6	9	11.60
	Isocitrate dehydrogenase [NADP], mitochondrial	IDHP_MOUSE	50,907.2	100.0	18	22	43	37.80
	Alpha-enolase	ENOA_MOUSE	47,141.7	100.0	5	6	11	27.60
	Elongation factor Tu, mitochondrial	EFTU_MOUSE	49,508.9	100.0	4	4	7	10.20
	Sodium/potassium-transporting ATPase subunit beta-1	AT1B1_MOUSE	35,196.4	100.0	3	4	7	12.50
	Actin, alpha cardiac muscle 1	ACTC_MOUSE	42,020.1	100.0	3	3	5	9.81
	Keratin, type I cytoskeletal 10	K1C10_MOUSE	57,771.3	100.0	3	3	5	5.96
	Trifunctional enzyme subunit beta, mitochondrial	ECHB_MOUSE	51,388.0	100.0	11	13	19	25.90
	ATP synthase subunit beta, mitochondrial	ATPB_MOUSE	56,301.2	100.0	5	5	8	15.10
	Fumarate hydratase, mitochondrial	FUMH_MOUSE	54,371.1	100.0	8	10	16	27.20
	Elongation factor 1-gamma	EF1G_MOUSE	50,061.3	100.0	5	6	10	10.80
	Cytochrome b-c1 complex subunit 1, mitochondrial	QCR1_MOUSE	52,768.8	100.0	9	10	20	22.70

	Pyruvate dehydrogenase E1 component subunit alpha, somatic form, mitochondrial	ODPA_MOUSE	43,232.5	100.0	7	8	15	16.90
	Beta-enolase	ENOB_MOUSE	47,025.9	100.0	10	14	24	33.20
	Kynurenine--oxoglutarate transaminase 3	KAT3_MOUSE	51,127.9	100.0	5	5	8	13.00
	Elongation factor 1-alpha 1	EF1A1_MOUSE	50,114.2	100.0	3	3	4	7.58
	cAMP-dependent protein kinase type I-alpha regulatory subunit	KAP0_MOUSE	43,185.8	100.0	12	15	26	28.30
	Tetratricopeptide repeat protein 38	TTC38_MOUSE	52,224.8	100.0	3	3	3	7.31
	26S protease regulatory subunit 7	PRS7_MOUSE	48,649.6	100.0	2	2	3	4.62
	Lactation elevated protein 1	LACE1_MOUSE	54,314.8	100.0	3	3	3	5.83
	Creatine kinase S-type, mitochondrial	KCRS_MOUSE	47,474.7	100.0	2	2	4	5.49
	ADP/ATP translocase 1	ADT1_MOUSE	32,905.4	100.0	5	5	8	15.80
B5	NADH dehydrogenase [ubiquinone] iron-sulfur protein 2, mitochondrial	NDUS2_MOUSE	52,626.8	100.0	3	3	4	6.48
	Cysteine desulfurase, mitochondrial	NFS1_MOUSE	50,001.8	100.0	5	6	9	14.40
	Long-chain specific acyl-CoA dehydrogenase, mitochondrial	ACADL_MOUSE	47,908.7	100.0	8	9	15	24.70
	cAMP-dependent protein kinase type II-alpha regulatory subunit	KAP2_MOUSE	45,389.4	100.0	6	6	10	18.00
	Medium-chain specific acyl-CoA dehydrogenase, mitochondrial	ACADM_MOUSE	46,482.4	100.0	6	8	13	17.10
	Keratin, type II cytoskeletal 1	K2C1_MOUSE	65,607.1	100.0	3	4	8	3.77

	Succinyl-CoA ligase [GDP-forming] subunit beta, mitochondrial	SUCB2_MOUSE	46,841.0	100.0	5	5	8	14.10
	Actin, cytoplasmic 1	ACTB_MOUSE, ACTG_MOUSE	41,737.8	100.0	3	4	7	32.80
	Isocitrate dehydrogenase [NADP], mitochondrial	IDHP_MOUSE	50,907.2	100.0	18	22	43	42.00
	Phosphoglycerate kinase 1	PGK1_MOUSE	44,551.1	100.0	11	12	18	31.40
	Elongation factor Tu, mitochondrial	EFTU_MOUSE	49,508.9	100.0	8	9	16	23.00
	Sodium/potassium-transporting ATPase subunit beta-1	AT1B1_MOUSE	35,196.4	100.0	3	4	6	12.50
	NADH dehydrogenase [ubiquinone] 1 alpha subcomplex subunit 10, mitochondrial	NDUAA_MOUSE	40,604.7	100.0	3	3	5	8.73
	Actin, alpha cardiac muscle 1	ACTC_MOUSE	42,020.1	100.0	16	21	44	51.70
	Beta-enolase	ENOB_MOUSE	47,025.9	100.0	6	6	11	16.40
	Citrate synthase, mitochondrial	CISY_MOUSE	51,738.1	100.0	3	3	5	7.97
	Trifunctional enzyme subunit beta, mitochondrial	ECHB_MOUSE	51,388.0	100.0	7	7	14	15.80
	Acetyl-CoA acetyltransferase, mitochondrial	THIL_MOUSE	44,816.4	100.0	8	11	20	27.40
	[Pyruvate dehydrogenase [lipoamide]] kinase isozyme 1, mitochondrial	PDK1_MOUSE	48,926.8	100.0	2	2	4	5.99
	3-ketoacyl-CoA thiolase, mitochondrial	THIM_MOUSE	41,858.2	100.0	7	8	12	32.00
	Cytochrome b-c1 complex subunit 1, mitochondrial	QCR1_MOUSE	52,768.8	100.0	5	5	7	14.00
	Pyruvate dehydrogenase E1 component subunit alpha, somatic form, mitochondrial	ODPA_MOUSE	43,232.5	100.0	7	7	14	17.40

	Creatine kinase M-type	KCRM_MOUSE	43,045.6	100.0	4	4	7	13.10
	Eukaryotic initiation factor 4A-I	IF4A1_MOUSE	46,155.3	100.0	5	5	9	14.30
	cAMP-dependent protein kinase type I-alpha regulatory subunit	KAP0_MOUSE	43,185.8	100.0	8	11	18	23.40
	Glyceraldehyde-3-phosphate dehydrogenase	G3P_MOUSE	35,810.1	100.0	3	3	5	12.90
	Phosphate carrier protein, mitochondrial	MPCP_MOUSE	39,633.1	100.0	3	3	5	9.52
	Succinyl-CoA ligase [ADP-forming] subunit beta, mitochondrial	SUCB1_MOUSE	50,114.7	100.0	12	13	23	26.30
	[Pyruvate dehydrogenase [lipoamide]] kinase isozyme 2, mitochondrial	PDK2_MOUSE	46,070.1	100.0	3	3	4	9.09
	Isovaleryl-CoA dehydrogenase, mitochondrial	IVD_MOUSE	46,326.5	100.0	5	6	10	13.40
	Cytochrome b-c1 complex subunit 2, mitochondrial	QCR2_MOUSE	48,236.0	100.0	9	13	25	29.60
	ADP/ATP translocase 1	ADT1_MOUSE	32,905.4	100.0	3	3	5	10.10
	Creatine kinase S-type, mitochondrial	KCRS_MOUSE	47,474.7	100.0	9	10	18	23.90
B6	Prohibitin	PHB_MOUSE	29,820.6	100.0	4	4	8	15.80
	Enoyl-CoA hydratase, mitochondrial	ECHM_MOUSE	31,475.3	100.0	9	12	20	37.20
	ATP synthase subunit alpha, mitochondrial	ATPA_MOUSE	59,754.1	100.0	3	3	4	7.41
	Medium-chain specific acyl-CoA dehydrogenase, mitochondrial	ACADM_MOUSE	46,482.4	100.0	3	3	5	7.60
	Prohibitin-2	PHB2_MOUSE	33,297.6	100.0	5	6	9	17.70

	Succinyl-CoA ligase [GDP-forming] subunit alpha, mitochondrial	SUCA_MOUSE	36,155.2	100.0	2	2	4	8.38
	Isocitrate dehydrogenase [NADP], mitochondrial	IDHP_MOUSE	50,907.2	100.0	3	3	3	6.42
	Sepiapterin reductase	SPRE_MOUSE	27,883.8	100.0	3	3	4	18.80
	Citrate lyase subunit beta-like protein, mitochondrial	CLYBL_MOUSE	37,549.1	100.0	6	6	11	23.10
	Electron transfer flavoprotein subunit alpha, mitochondrial	ETFA_MOUSE	35,009.8	100.0	5	7	12	24.90
	L-lactate dehydrogenase A chain	LDHA_MOUSE	36,498.9	100.0	6	6	10	21.10
	Actin, alpha cardiac muscle 1	ACTC_MOUSE	42,020.1	100.0	6	7	13	20.20
	NADH dehydrogenase [ubiquinone] 1 alpha subcomplex subunit 9, mitochondrial	NDUA9_MOUSE	42,509.5	100.0	5	6	10	15.10
	Malate dehydrogenase, mitochondrial	MDHM_MOUSE	35,611.9	100.0	8	8	14	28.40
	NADH dehydrogenase [ubiquinone] iron-sulfur protein 3, mitochondrial	NDUS3_MOUSE	30,149.4	100.0	4	6	11	15.20
	Electron transfer flavoprotein subunit beta	ETFB_MOUSE	27,623.2	100.0	5	6	10	23.90
	3-hydroxyisobutyrate dehydrogenase, mitochondrial	3HIDH_MOUSE	35,440.6	100.0	5	5	9	24.20
	Coiled-coil-helix-coiled-coil-helix domain-containing protein 3, mitochondrial	CHCH3_MOUSE	26,334.4	100.0	6	7	13	18.50
	Trifunctional enzyme subunit beta, mitochondrial	ECHB_MOUSE	51,388.0	100.0	4	4	5	9.05
	3-ketoacyl-CoA thiolase, mitochondrial	THIM_MOUSE	41,858.2	100.0	3	3	5	11.30

	D-beta-hydroxybutyrate dehydrogenase, mitochondrial	BDH_MOUSE	38,286.0	99.9	2	2	3	6.12
	Cytochrome c1, heme protein, mitochondrial	CY1_MOUSE	35,328.4	100.0	4	5	8	20.90
	Mitochondrial carnitine/acylcarnitine carrier protein	MCAT_MOUSE	33,028.2	100.0	4	4	6	11.30
	Mitochondrial 2-oxoglutarate/malate carrier protein	M2OM_MOUSE	34,156.3	100.0	3	4	7	8.92
	Pyruvate dehydrogenase E1 component subunit beta, mitochondrial	ODPB_MOUSE	38,937.0	100.0	5	5	8	19.80
	Dihydropteridine reductase	DHPR_MOUSE	25,570.2	100.0	3	3	5	17.80
	ATP synthase subunit gamma, mitochondrial	ATPG_MOUSE	32,887.4	100.0	5	6	14	19.50
	L-lactate dehydrogenase B chain	LDHB_MOUSE	36,572.4	99.9	2	2	4	7.78
	Methylglutaconyl-CoA hydratase, mitochondrial	AUHM_MOUSE	33,396.2	100.0	3	3	4	14.00
	Succinate dehydrogenase [ubiquinone] iron-sulfur subunit, mitochondrial	DHSB_MOUSE	31,815.0	100.0	4	5	10	15.20
	Ubiquinone biosynthesis methyltransferase COQ5, mitochondrial	COQ5_MOUSE	37,336.0	100.0	4	4	7	13.10
	Triosephosphate isomerase	TPIS_MOUSE	26,712.2	100.0	4	5	9	21.30
	Phosphate carrier protein, mitochondrial	MPCP_MOUSE	39,633.1	100.0	12	14	25	32.20
	3,2-trans-enoyl-CoA isomerase, mitochondrial	D3D2_MOUSE	32,079.2	100.0	5	5	9	21.50
	Regulator of microtubule dynamics protein 1	RMD1_MOUSE	35,001.6	99.9	2	2	2	7.21

	6-phosphogluconolactonase	6PGL_MOUSE	27,255.3	100.0	3	4	5	18.70
	Voltage-dependent anion-selective channel protein 3	VDAC3_MOUSE	30,754.0	100.0	3	3	5	15.20
	Malate dehydrogenase, cytoplasmic	MDHC_MOUSE	36,512.1	100.0	4	4	8	16.50
	Myosin light chain 3	MYL3_MOUSE	22,422.2	100.0	3	3	6	19.10
	ADP/ATP translocase 1	ADT1_MOUSE	32,905.4	100.0	14	15	28	35.90
	ADP/ATP translocase 2	ADT2_MOUSE	32,932.6	100.0	3	3	6	17.80
C1	Long-chain specific acyl-CoA dehydrogenase, mitochondrial	ACADL_MOUSE	47,908.7	100.0	4	4	6	11.40
	cAMP-dependent protein kinase type II-alpha regulatory subunit	KAP2_MOUSE	45,389.4	100.0	5	5	8	16.70
	ATP synthase subunit alpha, mitochondrial	ATPA_MOUSE	59,754.1	100.0	9	9	17	19.20
	Medium-chain specific acyl-CoA dehydrogenase, mitochondrial	ACADM_MOUSE	46,482.4	100.0	4	5	6	10.90
	Keratin, type II cytoskeletal 1	K2C1_MOUSE	65,607.1	100.0	3	4	8	3.77
	Isocitrate dehydrogenase [NADP], mitochondrial	IDHP_MOUSE	50,907.2	100.0	5	5	7	12.60
	Filamin-C	FLNC_MOUSE	291,111.8	100.0	3	3	6	1.47
	LIM domain-binding protein 3	LDB3_MOUSE	76,432.1	100.0	3	3	4	4.98
	Malate dehydrogenase, mitochondrial	MDHM_MOUSE	35,611.9	100.0	3	3	5	12.10
	Leucine-rich PPR motif-containing protein, mitochondrial	LPPRC_MOUSE	156,622.2	100.0	10	10	17	7.97

	A kinase anchor protein 1, mitochondrial	AKAP1_MOUSE	92,164.5	100.0	7	7	10	12.40
	Actin, alpha cardiac muscle 1	ACTC_MOUSE	42,020.1	100.0	6	6	10	18.80
	2-oxoglutarate dehydrogenase E1 component, mitochondrial	ODO1_MOUSE	116,450.6	100.0	3	3	5	3.91
	Keratin, type I cytoskeletal 10	K1C10_MOUSE	57,771.3	100.0	3	3	6	5.96
	Aconitate hydratase, mitochondrial	ACON_MOUSE	85,465.9	100.0	13	15	26	19.90
	ATP synthase subunit beta, mitochondrial	ATPB_MOUSE	56,301.2	100.0	9	10	18	26.30
	Trifunctional enzyme subunit alpha, mitochondrial	ECHA_MOUSE	82,671.5	100.0	5	5	8	7.86
	Sarcalumenin	SRCA_MOUSE	99,186.0	100.0	3	3	5	3.74
	Creatine kinase M-type	KCRM_MOUSE	43,045.6	100.0	3	3	6	9.45
	cAMP-dependent protein kinase type I-alpha regulatory subunit	KAP0_MOUSE	43,185.8	100.0	6	7	11	19.20
	Myosin-binding protein C, cardiac-type	MYPC3_MOUSE	140,631.8	100.0%	13	14	23	13.90
	Vinculin	VINC_MOUSE	116,719.4	100.0	2	2	2	2.25
	A-kinase anchor protein 2	AKAP2_MOUSE	98,578.4	100.0	4	4	6	6.27
	Sodium/potassium-transporting ATPase subunit alpha-1	AT1A1_MOUSE	112,985.3	100.0	5	5	8	6.84
	Fatty acid synthase	FAS_MOUSE	272,429.3	100.0	2	2	2	0.88
	NAD(P) transhydrogenase, mitochondrial	NNTM_MOUSE	113,841.3	100.0	4	4	6	5.34
	Myomesin-1	MYOM1_MOUSE	185,464.6	100.0	15	16	26	12.70
	Sarcoplasmic/endoplasmic reticulum calcium ATPase 2	AT2A2_MOUSE	114,860.0	100.0	14	15	29	14.90

	Uncharacterized protein KIAA0564 homolog	K0564_MOUSE	213,424.4	100.0	4	4	5	2.94
	Myosin-6	MYH6_MOUSE	223,571.2	100.0	33	40	71	19.00
	ADP/ATP translocase 1	ADT1_MOUSE	32,905.4	100.0	6	6	11	19.80
C2	Long-chain specific acyl-CoA dehydrogenase, mitochondrial	ACADL_MOUSE	47,908.7	100.0	3	3	6	8.14
	cAMP-dependent protein kinase type II-alpha regulatory subunit	KAP2_MOUSE	45,389.4	100.0	6	6	10	19.70
	ATP synthase subunit alpha, mitochondrial	ATPA_MOUSE	59,754.1	100.0	9	10	19	19.20
	Aspartate aminotransferase, mitochondrial	AATM_MOUSE	47,412.3	99.9	2	2	3	6.74
	Medium-chain specific acyl-CoA dehydrogenase, mitochondrial	ACADM_MOUSE	46,482.4	100.0	3	3	3	9.03
	Keratin, type II cytoskeletal 1	K2C1_MOUSE	65,607.1	100.0	3	4	8	3.77
	Heat shock 70 kDa protein 4	HSP74_MOUSE	94,133.4	100.0	4	4	7	5.71
	Isocitrate dehydrogenase [NADP], mitochondrial	IDHP_MOUSE	50,907.2	100.0	6	6	10	15.50
	LIM domain-binding protein 3	LDB3_MOUSE	76,432.1	100.0	5	5	8	7.75
	Lon protease homolog, mitochondrial	LONM_MOUSE	105,843.9	100.0	4	4	6	5.16
	Malate dehydrogenase, mitochondrial	MDHM_MOUSE	35,611.9	100.0	3	3	5	12.10
	ATP synthase subunit O, mitochondrial	ATPO_MOUSE	23,364.4	100.0	2	2	2	11.70
	A kinase anchor protein 1, mitochondrial	AKAP1_MOUSE	92,164.5	100.0	5	5	7	7.35

	Actin, alpha cardiac muscle 1	ACTC_MOUSE	42,020.1	100.0	8	9	14	28.90
	2-oxoglutarate dehydrogenase E1 component, mitochondrial	ODO1_MOUSE	116,450.6	100.0	17	21	33	23.00
	Keratin, type I cytoskeletal 10	K1C10_MOUSE	57,771.3	100.0	4	4	6	5.79
	Pyruvate kinase isozymes M1/M2	KPYM_MOUSE	57,845.6	100.0	3	3	5	5.65
	Heat shock protein HSP 90-beta	HS90B_MOUSE	83,328.4	100.0	3	3	5	5.25
	Aconitate hydratase, mitochondrial	ACON_MOUSE	85,465.9	100.0	16	18	32	24.60
	Trifunctional enzyme subunit beta, mitochondrial	ECHB_MOUSE	51,388.0	100.0	4	4	7	8.00
	Sarcoplasmic/endoplasmic reticulum calcium ATPase 2	AT2A2_MOUSE	114,860.0	100.0	20	22	37	21.20
	ATP synthase subunit beta, mitochondrial	ATPB_MOUSE	56,301.2	100.0	10	12	21	27.60
	Very long-chain specific acyl-CoA dehydrogenase, mitochondrial	ACADV_MOUSE	70,877.0	100.0	7	7	11	13.00
	Fumarate hydratase, mitochondrial	FUMH_MOUSE	54,371.1	100.0	3	3	6	8.68
	3-ketoacyl-CoA thiolase, mitochondrial	THIM_MOUSE	41,858.2	100.0	4	4	7	14.10
	Glycogen phosphorylase, muscle form	PYGM_MOUSE	97,289.4	100.0	2	2	2	2.02
	Sarcalumenin	SRCA_MOUSE	99,186.0	100.0	2	2	4	2.31
	Long-chain-fatty-acid--CoA ligase 1	ACSL1_MOUSE	77,926.2	99.9	2	2	2	3.15
	Creatine kinase M-type	KCRM_MOUSE	43,045.6	100.0	3	3	6	9.45
	Trifunctional enzyme subunit alpha, mitochondrial	ECHA_MOUSE	82,671.5	100.0	8	8	12	13.60
	Pyruvate dehydrogenase E1 component subunit beta, mitochondrial	ODPB_MOUSE	38,937.0	100.0	3	3	4	10.90

	Succinate dehydrogenase [ubiquinone] flavoprotein subunit, mitochondrial	DHSA_MOUSE	72,585.6	100.0	3	3	4	5.57
	L-lactate dehydrogenase B chain	LDHB_MOUSE	36,572.4	100.0	3	3	4	10.50
	Myosin-binding protein C, cardiac-type	MYPC3_MOUSE	140,631.8	100.0	3	3	5	2.99
	Kinesin-1 heavy chain	KINH_MOUSE	109,550.6	100.0	6	6	9	7.27
	Heat shock cognate 71 kDa protein	HSP7C_MOUSE	70,872.8	100.0	3	3	3	6.19
	cAMP-dependent protein kinase type I-alpha regulatory subunit	KAP0_MOUSE	43,185.8	100.0	12	13	22	36.50
	Alpha-actinin-2	ACTN2_MOUSE	103,657.2	100.0	4	4	7	5.70
	Glyceraldehyde-3-phosphate dehydrogenase	G3P_MOUSE	35,810.1	100.0	4	4	7	12.30
	Cytochrome b-c1 complex subunit 2, mitochondrial	QCR2_MOUSE	48,236.0	100.0	3	3	4	8.83
	Sodium/potassium-transporting ATPase subunit alpha-1	AT1A1_MOUSE	112,985.3	100.0	12	12	20	14.20
	NAD(P) transhydrogenase, mitochondrial	NNTM_MOUSE	113,841.3	100.0	11	13	20	11.50
	NADH-ubiquinone oxidoreductase 75 kDa subunit, mitochondrial	NDUS1_MOUSE	79,749.6	100.0	5	5	7	7.43
	Dihydrolipoyllysine-residue acetyltransferase component of pyruvate dehydrogenase complex, mitochondrial	ODP2_MOUSE	67,942.6	100.0	2	2	4	5.45
	Myomesin-1	MYOM1_MOUSE	185,464.6	100.0	12	12	20	9.24
	Uncharacterized protein KIAA0564 homolog	K0564_MOUSE	213,424.4	100.0	4	4	4	2.78

	Myosin-6	MYH6_MOUSE	223,571.2	100.0	14	15	23	9.60
	Hexokinase-1	HXK1_MOUSE	108,304.7	100.0	3	3	5	4.31
	Hexokinase-2	HXK2_MOUSE	102,536.6	100.0	5	5	7	6.98
	ADP/ATP translocase 1	ADT1_MOUSE	32,905.4	100.0	6	6	12	19.50
C3	3-ketoacyl-CoA thiolase, mitochondrial	THIM_MOUSE	41,858.2	100.0	4	4	6	16.40
	Pyruvate kinase isozymes M1/M2	KPYM_MOUSE	57,845.6	100.0	8	8	13	20.50
	cAMP-dependent protein kinase type II-alpha regulatory subunit	KAP2_MOUSE	45,389.4	100.0	15	21	40	43.90
	ATP synthase subunit alpha, mitochondrial	ATPA_MOUSE	59,754.1	100.0	12	14	25	25.30
	Epoxide hydrolase 2	HYES_MOUSE	62,516.8	100.0	5	5	9	13.00
	Aspartate aminotransferase, mitochondrial	AATM_MOUSE	47,412.3	99.9	2	2	3	6.05
	Medium-chain specific acyl-CoA dehydrogenase, mitochondrial	ACADM_MOUSE	46,482.4	100.0	4	5	7	11.90
	Aldehyde dehydrogenase X, mitochondrial	AL1B1_MOUSE	57,553.5	100.0	2	2	3	4.62
	Tubulin beta-2C chain	TBB2C_MOUSE	49,830.7	100.0	5	5	7	13.00
	Isocitrate dehydrogenase [NADP], mitochondrial	IDHP_MOUSE	50,907.2	100.0	9	11	19	21.20
	Long-chain-fatty-acid--CoA ligase 1	ACSL1_MOUSE	77,926.2	100.0	5	5	8	7.87
	Calsequestrin-2	CASQ2_MOUSE	48,199.1	100.0	3	4	6	7.71
	Methylmalonate-semialdehyde dehydrogenase [acylating], mitochondrial	MMSA_MOUSE	57,916.3	100.0	5	6	9	14.20

	Aldehyde dehydrogenase, mitochondrial	ALDH2_MOUSE	56,537.6	100.0	6	6	10	13.90
	Actin, alpha cardiac muscle 1	ACTC_MOUSE	42,020.1	100.0	8	9	16	26.80
	Malate dehydrogenase, mitochondrial	MDHM_MOUSE	35,611.9	100.0	3	3	3	9.47
	Aconitate hydratase, mitochondrial	ACON_MOUSE	85,465.9	100.0	10	12	22	14.10
	Trifunctional enzyme subunit beta, mitochondrial	ECHB_MOUSE	51,388.0	100.0	6	7	12	14.50
	cAMP-dependent protein kinase type II-beta regulatory subunit	KAP3_MOUSE	46,167.7	100.0	3	3	6	22.60
	Sarcoplasmic/endoplasmic reticulum calcium ATPase 2	AT2A2_MOUSE	114,860.0	100.0	7	8	14	8.05
	ATP synthase subunit beta, mitochondrial	ATPB_MOUSE	56,301.2	100.0	13	17	29	38.80
	Fumarate hydratase, mitochondrial	FUMH_MOUSE	54,371.1	99.9	2	2	4	6.31
	Trifunctional enzyme subunit alpha, mitochondrial	ECHA_MOUSE	82,671.5	100.0	6	6	11	10.60
	Sarcalumenin	SRCA_MOUSE	99,186.0	100.0	6	6	10	8.90
	Carnitine O-palmitoyltransferase 1, muscle isoform	CPT1B_MOUSE	88,220.0	100.0	4	4	7	5.57
	Pyruvate dehydrogenase E1 component subunit alpha, somatic form, mitochondrial	ODPA_MOUSE	43,232.5	100.0	3	3	4	7.44
	Succinate dehydrogenase [ubiquinone] flavoprotein subunit, mitochondrial	DHSA_MOUSE	72,585.6	100.0	2	2	3	4.22
	L-lactate dehydrogenase B chain	LDHB_MOUSE	36,572.4	99.9	2	2	4	5.69
	Dihydrolipoyl dehydrogenase, mitochondrial	DLDH_MOUSE	54,272.4	100.0	5	6	8	12.40

	Glyceraldehyde-3-phosphate dehydrogenase	G3P_MOUSE	35,810.1	100.0	3	3	4	12.90
	Succinyl-CoA:3-ketoacid-coenzyme A transferase 1, mitochondrial	SCOT1_MOUSE	55,990.2	100.0	6	6	11	17.70
	Sodium/potassium-transporting ATPase subunit beta-1	AT1B1_MOUSE	35,196.4	100.0	3	3	4	12.50
	cAMP-dependent protein kinase type I-alpha regulatory subunit	KAP0_MOUSE	43,185.8	100.0	13	17	47	36.00
	Phosphate carrier protein, mitochondrial	MPCP_MOUSE	39,633.1	100.0	2	2	4	7.28
	Electron transfer flavoprotein-ubiquinone oxidoreductase, mitochondrial	ETFD_MOUSE	68,091.8	100.0	4	4	6	6.82
	Vimentin	VIME_MOUSE	53,688.8	100.0	2	2	3	4.94
	Cytochrome b-c1 complex subunit 2, mitochondrial	QCR2_MOUSE	48,236.0	100.0	3	3	5	9.05
	Tubulin alpha-4A chain	TBA4A_MOUSE	49,924.6	100.0	4	5	9	11.80
	Dihydrolipoyllysine-residue acetyltransferase component of pyruvate dehydrogenase complex, mitochondrial	ODP2_MOUSE	67,942.6	100.0	4	4	7	9.19
	Myomesin-1	MYOM1_MOUSE	185,464.6	100.0	4	4	6	2.70
	ADP/ATP translocase 1	ADT1_MOUSE	32,905.4	100.0	3	3	6	8.72
C4	NADH dehydrogenase [ubiquinone] iron-sulfur protein 2, mitochondrial	NDUS2_MOUSE	52,626.8	100.0	3	4	7	6.05
	Long-chain specific acyl-CoA dehydrogenase, mitochondrial	ACADL_MOUSE	47,908.7	100.0	3	3	5	7.91

	cAMP-dependent protein kinase type II-alpha regulatory subunit	KAP2_MOUSE	45,389.4	100.0	4	4	6	12.20
	ATP synthase subunit alpha, mitochondrial	ATPA_MOUSE	59,754.1	100.0	6	6	11	12.80
	Medium-chain specific acyl-CoA dehydrogenase, mitochondrial	ACADM_MOUSE	46,482.4	100.0	5	5	7	14.00
	Keratin, type II cytoskeletal 1	K2C1_MOUSE	65,607.1	100.0	3	4	8	3.77
	Isocitrate dehydrogenase [NADP], mitochondrial	IDHP_MOUSE	50,907.2	100.0	16	20	43	36.90
	Alpha-enolase	ENOA_MOUSE	47,141.7	100.0	4	4	7	23.30
	Phosphoglycerate kinase 1	PGK1_MOUSE	44,551.1	100.0	3	3	4	10.60
	Elongation factor Tu, mitochondrial	EFTU_MOUSE	49,508.9	99.9	2	2	4	4.20
	Mitochondrial-processing peptidase subunit beta	MPPB_MOUSE	54,615.4	100.0	2	2	3	4.50
	Sodium/potassium-transporting ATPase subunit beta-1	AT1B1_MOUSE	35,196.4	100.0	2	3	4	9.87
	Trifunctional enzyme subunit alpha, mitochondrial	ECHA_MOUSE	82,671.5	100.0	5	5	9	9.04
	Keratin, type I cytoskeletal 10	K1C10_MOUSE	57,771.3	100.0	3	3	6	5.96
	Aconitate hydratase, mitochondrial	ACON_MOUSE	85,465.9	100.0	7	7	11	11.40
	Trifunctional enzyme subunit beta, mitochondrial	ECHB_MOUSE	51,388.0	100.0	7	8	15	16.40
	Sarcoplasmic/endoplasmic reticulum calcium ATPase 2	AT2A2_MOUSE	114,860.0	100.0	2	2	3	2.20
	Fumarate hydratase, mitochondrial	FUMH_MOUSE	54,371.1	100.0	4	5	10	12.40
	Elongation factor 1-gamma	EF1G_MOUSE	50,061.3	100.0	4	4	6	10.80

	Cytochrome b-c1 complex subunit 1, mitochondrial	QCR1_MOUSE	52,768.8	100.0	8	8	15	20.40
	Pyruvate dehydrogenase E1 component subunit alpha, somatic form, mitochondrial	ODPA_MOUSE	43,232.5	100.0	4	5	9	8.72
	Beta-enolase	ENOB_MOUSE	47,025.9	100.0	9	14	26	26.30
	Creatine kinase M-type	KCRM_MOUSE	43,045.6	100.0	2	2	4	6.30
	cAMP-dependent protein kinase type I-alpha regulatory subunit	KAP0_MOUSE	43,185.8	100.0	10	12	17	31.20
	Kynurenine--oxoglutarate transaminase 3	KAT3_MOUSE	51,127.9	100.0	5	5	8	13.00
	Keratin, type I cytoskeletal 42	K1C42_MOUSE	50,133.6	100.0	3	3	6	6.64
	Actin, alpha cardiac muscle 1	ACTC_MOUSE	42,020.1	100.0	6	7	12	20.20
	Cytochrome b-c1 complex subunit 2, mitochondrial	QCR2_MOUSE	48,236.0	100.0	3	3	5	9.05
	Creatine kinase S-type, mitochondrial	KCRS_MOUSE	47,474.7	100.0	3	3	4	11.20
	ADP/ATP translocase 1	ADT1_MOUSE	32,905.4	100.0	5	5	7	15.80
C5	NADH dehydrogenase [ubiquinone] iron-sulfur protein 2, mitochondrial	NDUS2_MOUSE	52,626.8	100.0	3	3	6	6.26
	Cysteine desulfurase, mitochondrial	NFS1_MOUSE	50,001.8	100.0	3	3	5	8.65
	Succinyl-CoA ligase [ADP-forming] subunit beta, mitochondrial	SUCB1_MOUSE	50,114.7	100.0	10	10	18	23.30
	Long-chain specific acyl-CoA dehydrogenase, mitochondrial	ACADL_MOUSE	47,908.7	100.0	7	7	11	22.10
	cAMP-dependent protein kinase type II-alpha regulatory subunit	KAP2_MOUSE	45,389.4	100.0	10	10	17	35.20

	ATP synthase subunit alpha, mitochondrial	ATPA_MOUSE	59,754.1	100.0	6	6	12	13.60
	Aspartate aminotransferase, mitochondrial	AATM_MOUSE	47,412.3	100.0	3	3	5	9.77
	Medium-chain specific acyl-CoA dehydrogenase, mitochondrial	ACADM_MOUSE	46,482.4	100.0	5	6	11	14.00
	Actin, cytoplasmic 1	ACTB_MOUSE, ACTG_MOUSE	41,737.8	100.0	3	5	7	28.50
	Isocitrate dehydrogenase [NADP], mitochondrial	IDHP_MOUSE	50,907.2	100.0	15	18	32	37.80
	2-oxoisovalerate dehydrogenase subunit alpha, mitochondrial	ODBA_MOUSE	50,371.5	99.9	2	3	5	6.56
	Phosphoglycerate kinase 1	PGK1_MOUSE	44,551.1	100.0	9	10	19	27.80
	Calcium-binding mitochondrial carrier protein Aralar1	CMC1_MOUSE	74,571.8	100.0	3	3	4	4.87
	Elongation factor Tu, mitochondrial	EFTU_MOUSE	49,508.9	100.0	5	6	11	14.20
	Sodium/potassium-transporting ATPase subunit beta-1	AT1B1_MOUSE	35,196.4	100.0	3	4	6	12.50
	Trifunctional enzyme subunit beta, mitochondrial	ECHB_MOUSE	51,388.0	100.0	7	7	13	15.80
	Acetyl-CoA acetyltransferase, mitochondrial	THIL_MOUSE	44,816.4	100.0	6	7	12	23.30
	Sarcoplasmic/endoplasmic reticulum calcium ATPase 2	AT2A2_MOUSE	114,860.0	100.0	5	5	9	6.51
	ATP synthase subunit beta, mitochondrial	ATPB_MOUSE	56,301.2	100.0	3	3	6	7.37
	3-ketoacyl-CoA thiolase, mitochondrial	THIM_MOUSE	41,858.2	100.0	6	7	13	23.40
	Cytochrome b-c1 complex subunit 1, mitochondrial	QCR1_MOUSE	52,768.8	100.0	3	3	5	5.42

	Pyruvate dehydrogenase E1 component subunit alpha, somatic form, mitochondrial	ODPA_MOUSE	43,232.5	100.0	7	7	16	19.00
	Beta-enolase	ENOB_MOUSE	47,025.9	100.0	5	5	8	15.70
	Aconitate hydratase, mitochondrial	ACON_MOUSE	85,465.9	100.0	10	10	19	17.60
	Creatine kinase M-type	KCRM_MOUSE	43,045.6	100.0	4	4	8	13.10
	Trifunctional enzyme subunit alpha, mitochondrial	ECHA_MOUSE	82,671.5	100.0	3	4	7	4.59
	Eukaryotic initiation factor 4A-I	IF4A1_MOUSE	46,155.3	100.0	4	4	6	10.60
	Glyceraldehyde-3-phosphate dehydrogenase	G3P_MOUSE	35,810.1	100.0	3	3	5	12.90
	cAMP-dependent protein kinase type I-alpha regulatory subunit	KAP0_MOUSE	43,185.8	100.0	7	9	16	19.70
	Keratin, type I cytoskeletal 42	K1C42_MOUSE	50,133.6	100.0	2	2	4	4.65
	Isovaleryl-CoA dehydrogenase, mitochondrial	IVD_MOUSE	46,326.5	100.0	5	5	8	13.70
	Actin, alpha cardiac muscle 1	ACTC_MOUSE	42,020.1	100.0	10	15	32	30.80
	Cytochrome b-c1 complex subunit 2, mitochondrial	QCR2_MOUSE	48,236.0	100.0	10	12	16	28.00
	ADP/ATP translocase 1	ADT1_MOUSE	32,905.4	100.0	4	4	7	12.80
	Creatine kinase S-type, mitochondrial	KCRS_MOUSE	47,474.7	100.0	8	8	12	20.50
C6	Prohibitin	PHB_MOUSE	29,820.6	100.0	4	4	7	15.80
	Long-chain specific acyl-CoA dehydrogenase, mitochondrial	ACADL_MOUSE	47,908.7	100.0	3	3	5	8.37
	cAMP-dependent protein kinase type II-alpha regulatory subunit	KAP2_MOUSE	45,389.4	100.0	3	3	5	10.70

	ATP synthase subunit alpha, mitochondrial	ATPA_MOUSE	59,754.1	100.0	7	9	15	17.20
	Enoyl-CoA hydratase, mitochondrial	ECHM_MOUSE	31,475.3	100.0	6	10	18	30.30
	Medium-chain specific acyl-CoA dehydrogenase, mitochondrial	ACADM_MOUSE	46,482.4	100.0	4	4	7	11.40
	Prohibitin-2	PHB2_MOUSE	33,297.6	100.0	5	5	9	17.70
	Isocitrate dehydrogenase [NADP], mitochondrial	IDHP_MOUSE	50,907.2	100.0	8	8	10	20.80
	Mitochondrial carnitine/acylcarnitine carrier protein	MCAT_MOUSE	33,028.2	100.0	4	4	5	13.30
	Citrate lyase subunit beta-like protein, mitochondrial	CLYBL_MOUSE	37,549.1	100.0	5	5	8	16.90
	Electron transfer flavoprotein subunit alpha, mitochondrial	ETFA_MOUSE	35,009.8	100.0	6	7	13	28.50
	L-lactate dehydrogenase A chain	LDHA_MOUSE	36,498.9	100.0	5	5	9	16.60
	Estradiol 17-beta-dehydrogenase 8	DHB8_MOUSE	26,645.3	100.0	3	4	6	15.40
	Actin, alpha cardiac muscle 1	ACTC_MOUSE	42,020.1	100.0	7	8	14	21.80
	NADH dehydrogenase [ubiquinone] 1 alpha subcomplex subunit 9, mitochondrial	NDUA9_MOUSE	42,509.5	100.0	2	2	4	6.10
	Malate dehydrogenase, mitochondrial	MDHM_MOUSE	35,611.9	100.0	9	10	17	31.40
	NADH dehydrogenase [ubiquinone] iron-sulfur protein 3, mitochondrial	NDUS3_MOUSE	30,149.4	100.0	3	4	8	14.80
	Electron transfer flavoprotein subunit beta	ETFB_MOUSE	27,623.2	100.0	3	3	5	12.20

	3-hydroxyisobutyrate dehydrogenase, mitochondrial	3HIDH_MOUSE	35,440.6	100.0	4	4	8	20.00
	Cytochrome b-c1 complex subunit Rieske, mitochondrial	UCRI_MOUSE	29,367.2	100.0	2	2	3	8.03
	Coiled-coil-helix-coiled-coil-helix domain-containing protein 3, mitochondrial	CHCH3_MOUSE	26,334.4	100.0	3	3	5	12.80
	Trifunctional enzyme subunit beta, mitochondrial	ECHB_MOUSE	51,388.0	100.0	6	6	9	13.90
	Acetyl-CoA acetyltransferase, mitochondrial	THIL_MOUSE	44,816.4	100.0	5	5	8	17.70
	Sarcoplasmic/endoplasmic reticulum calcium ATPase 2	AT2A2_MOUSE	114,860.0	100.0	3	3	5	4.02
	Apolipoprotein O-like	APOOL_MOUSE	29,262.0	100.0	3	3	5	14.70
	3-ketoacyl-CoA thiolase, mitochondrial	THIM_MOUSE	41,858.2	100.0	5	6	9	19.60
	D-beta-hydroxybutyrate dehydrogenase, mitochondrial	BDH_MOUSE	38,286.0	99.9	2	2	3	6.12
	Pyruvate dehydrogenase E1 component subunit alpha, somatic form, mitochondrial	ODPA_MOUSE	43,232.5	100.0	3	3	4	7.44
	Mitochondrial 2-oxoglutarate/malate carrier protein	M2OM_MOUSE	34,156.3	100.0	5	5	9	21.70
	Pyruvate dehydrogenase E1 component subunit beta, mitochondrial	ODPB_MOUSE	38,937.0	100.0	5	5	10	16.20
	Dihydropteridine reductase	DHPR_MOUSE	25,570.2	100.0	3	3	5	17.80
	ATP synthase subunit gamma, mitochondrial	ATPG_MOUSE	32,887.4	100.0	6	7	14	20.50
	cAMP-dependent protein kinase type I-alpha regulatory subunit	KAP0_MOUSE	43,185.8	100.%	9	9	18	28.30

	L-lactate dehydrogenase B chain	LDHB_MOUSE	36,572.4	99.9	2	2	4	7.78
	Glyceraldehyde-3-phosphate dehydrogenase	G3P_MOUSE	35,810.1	100.0	3	3	6	12.30
	Succinate dehydrogenase [ubiquinone] iron-sulfur subunit, mitochondrial	DHSB_MOUSE	31,815.0	100.0	5	6	11	18.40
	Triosephosphate isomerase	TPIS_MOUSE	26,712.2	100.0	3	3	3	15.70
	Phosphate carrier protein, mitochondrial	MPCP_MOUSE	39,633.1	100.0	8	10	19	20.70
	3,2-trans-enoyl-CoA isomerase, mitochondrial	D3D2_MOUSE	32,079.2	100.0	4	5	10	18.70
	Cytochrome b-c1 complex subunit 2, mitochondrial	QCR2_MOUSE	48,236.0	100.0	7	7	13	16.30
	Succinate dehydrogenase [ubiquinone] flavoprotein subunit, mitochondrial	DHSA_MOUSE	72,585.6	99.9	2	3	6	3.92
	2,4-dienoyl-CoA reductase, mitochondrial	DECR_MOUSE	36,215.2	100.0	3	3	6	13.40
	Malate dehydrogenase, cytoplasmic	MDHC_MOUSE	36,512.1	100.0	4	4	7	16.50
	Myosin light chain 3	MYL3_MOUSE	22,422.2	100.0	4	5	9	27.00
	ADP/ATP translocase 2	ADT2_MOUSE	32,932.6	100.0	2	2	4	17.80
	ADP/ATP translocase 1	ADT1_MOUSE	32,905.4	100.0	12	13	24	34.90
D1	ADP/ATP translocase 1	ADT1_MOUSE	32,905.4	100.0	5	5	9	15.80
	Actin, alpha cardiac muscle 1	ACTC_MOUSE	42,020.1	100.0	5	5	10	15.40
	Aconitate hydratase, mitochondrial	ACON_MOUSE	85,465.9	100.0	14	15	24	21.90
	NADH-ubiquinone oxidoreductase 75 kDa subunit, mitochondrial	NDUS1_MOUSE	79,749.6	99.9	2	2	4	3.58

	A-kinase anchor protein 2	AKAP2_MOUSE	98,578.4	100.0	4	4	6	6.16
	Isocitrate dehydrogenase [NADP], mitochondrial	IDHP_MOUSE	50,907.2	100.0	2	2	3	3.98
	Sarcoplasmic/endoplasmic reticulum calcium ATPase 2	AT2A2_MOUSE	114,860.0	100.0	11	12	23	12.30
	A kinase anchor protein 1, mitochondrial	AKAP1_MOUSE	92,164.5	100.0	6	6	10	12.80
	Creatine kinase M-type	KCRM_MOUSE	43,045.6	100.0	3	3	5	9.45
	Myosin-binding protein C, cardiac-type	MYPC3_MOUSE	140,631.8	100.0	15	16	28	15.50
	Medium-chain specific acyl-CoA dehydrogenase, mitochondrial	ACADM_MOUSE	46,482.4	100.0	3	4	6	9.50
	Long-chain specific acyl-CoA dehydrogenase, mitochondrial	ACADL_MOUSE	47,908.7	100.0	3	3	5	8.37
	ATP synthase subunit beta, mitochondrial	ATPB_MOUSE	56,301.2	100.0	10	11	17	28.20
	Trifunctional enzyme subunit alpha, mitochondrial	ECHA_MOUSE	82,671.5	100.0	7	7	10	12.30
	Leucine-rich PPR motif-containing protein, mitochondrial	LPPRC_MOUSE	156,622.2	100.0	11	11	20	8.98
	Kinesin-1 heavy chain	KINH_MOUSE	109,550.6	100.0	5	5	8	6.54
	Keratin, type II cytoskeletal 1	K2C1_MOUSE	65,607.1	100.0	3	3	6	3.77
	cAMP-dependent protein kinase type I-alpha regulatory subunit	KAP0_MOUSE	43,185.8	100.0	6	6	8	20.20
	2-oxoglutarate dehydrogenase E1 component, mitochondrial	ODO1_MOUSE	116,450.6	100.0	3	4	7	3.32

	NAD(P) transhydrogenase, mitochondrial	NNTM_MOUSE	113,841.3	100.0	4	4	7	4.79
	Malate dehydrogenase, mitochondrial	MDHM_MOUSE	35,611.9	100.0	2	2	2	6.21
	Sodium/potassium-transporting ATPase subunit alpha-1	AT1A1_MOUSE	112,985.3	100.0	8	8	12	10.90
	Vinculin	VINC_MOUSE	116,719.4	100.0	3	3	3	3.10
	Uncharacterized protein KIAA0564 homolog	K0564_MOUSE	213,424.4	100.0	5	5	6	3.52
	Myomesin-1	MYOM1_MOUSE	185,464.6	100.0	13	14	23	8.88
	Keratin, type I cytoskeletal 10	K1C10_MOUSE	57,771.3	100.0	4	4	7	6.49
	Superoxide dismutase [Cu-Zn]	SODC_MOUSE	15,941.9	100.0	2	2	4	15.60
	cAMP-dependent protein kinase type II-alpha regulatory subunit	KAP2_MOUSE	45,389.4	100.0	4	4	7	11.70
	ATP synthase subunit alpha, mitochondrial	ATPA_MOUSE	59,754.1	100.0	8	9	15	19.20
	Myosin-6	MYH6_MOUSE	223,571.2	100.0	32	39	63	18.40
	Sarcalumenin	SRCA_MOUSE	99,186.0	100.0	3	3	5	3.74
D2	Calcium-binding mitochondrial carrier protein Aralar1	CMC1_MOUSE	74,571.8	100.0	3	3	5	4.87
	Sarcoplasmic/endoplasmic reticulum calcium ATPase 2	AT2A2_MOUSE	114,860.0	100.0	21	25	45	22.10
	Kinesin-1 heavy chain	KINH_MOUSE	109,550.6	100.0	4	4	7	4.67
	ADP/ATP translocase 1	ADT1_MOUSE	32,905.4	100.0	6	6	12	20.10
	L-lactate dehydrogenase B chain	LDHB_MOUSE	36,572.4	100.0	3	3	4	10.50
	Heat shock cognate 71 kDa protein	HSP7C_MOUSE	70,872.8	100.0	5	5	7	10.40

	Superoxide dismutase [Cu-Zn]	SODC_MOUSE	15,941.9	100.0	3	3	4	22.10
	Trifunctional enzyme subunit beta, mitochondrial	ECHB_MOUSE	51,388.0	100.0	5	5	8	10.10
	Carnitine O-palmitoyltransferase 1, muscle isoform	CPT1B_MOUSE	88,220.0	100.0	3	3	6	4.27
	Aspartate aminotransferase, mitochondrial	AATM_MOUSE	47,412.3	100.0	2	2	3	6.28
	Succinate dehydrogenase [ubiquinone] flavoprotein subunit, mitochondrial	DHSA_MOUSE	72,585.6	100.0	3	3	5	5.57
	NADH-ubiquinone oxidoreductase 75 kDa subunit, mitochondrial	NDUS1_MOUSE	79,749.6	100.0	4	4	6	6.60
	A kinase anchor protein 1, mitochondrial	AKAP1_MOUSE	92,164.5	100.0	4	4	8	5.95
	Pyruvate dehydrogenase E1 component subunit beta, mitochondrial	ODPB_MOUSE	38,937.0	100.0	3	3	4	10.90
	Malate dehydrogenase, mitochondrial	MDHM_MOUSE	35,611.9	100.0	4	4	6	18.00
	Myomesin-1	MYOM1_MOUSE	185,464.6	100.0	7	7	13	4.74
	2-oxoglutarate dehydrogenase E1 component, mitochondrial	ODO1_MOUSE	116,450.6	100.0	14	18	28	18.60
	Long-chain-fatty-acid--CoA ligase 1	ACSL1_MOUSE	77,926.2	100.0	4	4	6	6.44
	ATP synthase subunit beta, mitochondrial	ATPB_MOUSE	56,301.2	100.0	11	12	22	31.20
	Fumarate hydratase, mitochondrial	FUMH_MOUSE	54,371.1	100.0	3	3	5	8.68
	Dihydrolipoyllysine-residue acetyltransferase component of pyruvate dehydrogenase complex, mitochondrial	ODP2_MOUSE	67,942.6	100.0	2	2	3	4.83

	ATP synthase subunit alpha, mitochondrial	ATPA_MOUSE	59,754.1	100.0	8	9	18	19.20
	Uncharacterized protein KIAA0564 homolog	K0564_MOUSE	213,424.4	100.0	3	3	3	2.05
	Actin, alpha cardiac muscle 1	ACTC_MOUSE	42,020.1	100.0	7	9	17	23.10
	ATP synthase subunit gamma, mitochondrial	ATPG_MOUSE	32,887.4	99.9	2	2	3	7.38
	Keratin, type I cytoskeletal 10	K1C10_MOUSE	57,771.3	100.0	3	3	6	5.61
	Stress-70 protein, mitochondrial	GRP75_MOUSE	73,529.1	100.0	3	3	5	5.89
	Hexokinase-2	HXK2_MOUSE	102,536.6	100.0	6	6	8	8.51
	Creatine kinase M-type	KCRM_MOUSE	43,045.6	100.0	3	3	5	9.45
	Heat shock protein HSP 90-beta	HS90B_MOUSE	83,328.4	100.0	5	5	7	8.56
	Lon protease homolog, mitochondrial	LONM_MOUSE	105,843.9	100.0	4	4	5	5.16
	LIM domain-binding protein 3	LDB3_MOUSE	76,432.1	100.0	3	3	5	4.84
	Hexokinase-1	HXK1_MOUSE	108,304.7	100.0	3	3	4	4.31
	cAMP-dependent protein kinase type I-alpha regulatory subunit	KAP0_MOUSE	43,185.8	100.0	10	11	21	32.00
	Endoplasmin	ENPL_MOUSE	92,478.6	100.0	3	3	5	5.74
	NAD(P) transhydrogenase, mitochondrial	NNTM_MOUSE	113,841.3	100.0	9	10	14	10.00
	Myosin-binding protein C, cardiac-type	MYPC3_MOUSE	140,631.8	100.0	5	5	7	5.91
	3-ketoacyl-CoA thiolase, mitochondrial	THIM_MOUSE	41,858.2	100.0	4	4	8	16.40
	Alpha-actinin-2	ACTN2_MOUSE	103,657.2	100.0	5	5	6	7.49

	Sodium/potassium-transporting ATPase subunit alpha-1	AT1A1_MOUSE	112,985.3	100.0	12	12	19	15.60
	Very long-chain specific acyl-CoA dehydrogenase, mitochondrial	ACADV_MOUSE	70,877.0	100.0	4	4	6	7.62
	Myosin-6	MYH6_MOUSE	223,571.2	100.0	14	15	21	8.82
	Aconitate hydratase, mitochondrial	ACON_MOUSE	85,465.9	100.0	15	19	36	23.60
	Sarcalumenin	SRCA_MOUSE	99,186.0	100.0	4	4	6	4.95
	Citrate synthase, mitochondrial	CISY_MOUSE	51,738.1	100.0	3	3	5	6.47
	cGMP-dependent protein kinase 1	KGP1_MOUSE	76,353.9	100.0	2	2	2	3.28
	Medium-chain specific acyl-CoA dehydrogenase, mitochondrial	ACADM_MOUSE	46,482.4	100.0	3	3	6	9.03
	Glyceraldehyde-3-phosphate dehydrogenase	G3P_MOUSE	35,810.1	100.0	4	4	7	12.30
	Isocitrate dehydrogenase [NADP], mitochondrial	IDHP_MOUSE	50,907.2	100.0%	6	6	11	15.50
	Trifunctional enzyme subunit alpha, mitochondrial	ECHA_MOUSE	82,671.5	100.0	9	9	16	15.20
	cAMP-dependent protein kinase type II-alpha regulatory subunit	KAP2_MOUSE	45,389.4	100.0	7	7	11	24.40
D3	ADP/ATP translocase 1	ADT1_MOUSE	32,905.4	100.0	3	3	6	8.72
	cAMP-dependent protein kinase type II-alpha regulatory subunit	KAP2_MOUSE	45,389.4	100.0	15	22	41	43.90
	Pyruvate kinase isozymes M1/M2	KPYM_MOUSE	57,845.6	100.0	6	6	9	15.40
	Isocitrate dehydrogenase [NADP], mitochondrial	IDHP_MOUSE	50,907.2	100.0	9	11	19	21.20

	Malate dehydrogenase, mitochondrial	MDHM_MOUSE	35,611.9	100.0	3	3	4	9.47
	Actin, alpha cardiac muscle 1	ACTC_MOUSE	42,020.1	100.0	6	7	12	19.10
	Glycogen phosphorylase, muscle form	PYGM_MOUSE	97,289.4	100.0	2	2	3	2.49
	L-lactate dehydrogenase B chain	LDHB_MOUSE	36,572.4	99.9	2	2	3	5.69
	Medium-chain specific acyl-CoA dehydrogenase, mitochondrial	ACADM_MOUSE	46,482.4	100.0	3	4	6	9.03
	Succinyl-CoA:3-ketoacid-coenzyme A transferase 1, mitochondrial	SCOT1_MOUSE	55,990.2	100.0	3	3	5	7.69
	3-ketoacyl-CoA thiolase, mitochondrial	THIM_MOUSE	41,858.2	100.0	3	3	5	13.10
	Dihydrolipoyllysine-residue acetyltransferase component of pyruvate dehydrogenase complex, mitochondrial	ODP2_MOUSE	67,942.6	100.0	3	4	7	7.79
	Long-chain-fatty-acid--CoA ligase 1	ACSL1_MOUSE	77,926.2	100.0	9	9	15	13.60
	Sarcoplasmic/endoplasmic reticulum calcium ATPase 2	AT2A2_MOUSE	114,860.0	100.0	9	10	18	10.50
	Sarcalumenin	SRCA_MOUSE	99,186.0	100.0	6	6	11	8.90
	ATP synthase subunit beta, mitochondrial	ATPB_MOUSE	56,301.2	100.0	12	14	25	33.50
	Aldehyde dehydrogenase, mitochondrial	ALDH2_MOUSE	56,537.6	100.0	4	4	6	8.67
	cGMP-dependent protein kinase 1	KGP1_MOUSE	76,353.9	100.0	3	3	4	5.51
	Epoxide hydrolase 2	HYES_MOUSE	62,516.8	100.0	3	3	6	5.96
	Phosphate carrier protein, mitochondrial	MPCP_MOUSE	39,633.1	100.0	3	3	5	9.52

	Long-chain specific acyl-CoA dehydrogenase, mitochondrial	ACADL_MOUSE	47,908.7	100.0	3	3	4	7.91
	Electron transfer flavoprotein-ubiquinone oxidoreductase, mitochondrial	ETFD_MOUSE	68,091.8	100.0	3	3	3	4.87
	Dihydrolipoyl dehydrogenase, mitochondrial	DLDH_MOUSE	54,272.4	100.0	5	6	9	11.40
	Tubulin beta-2C chain	TBB2C_MOUSE	49,830.7	100.0	6	6	10	14.40
	Vimentin	VIME_MOUSE	53,688.8	100.0	4	4	5	9.01
	Trifunctional enzyme subunit alpha, mitochondrial	ECHA_MOUSE	82,671.5	100.0	8	10	17	14.80
	Fumarate hydratase, mitochondrial	FUMH_MOUSE	54,371.1	100.0	5	6	9	16.00
	Succinate dehydrogenase [ubiquinone] flavoprotein subunit, mitochondrial	DHSA_MOUSE	72,585.6	100.0	5	5	8	9.34
	cAMP-dependent protein kinase type II-beta regulatory subunit	KAP3_MOUSE	46,167.7	100.0	3	3	6	22.60
	cAMP-dependent protein kinase type I-alpha regulatory subunit	KAP0_MOUSE	43,185.8	100.0	14	18	40	34.10
	Heat shock cognate 71 kDa protein	HSP7C_MOUSE	70,872.8	100.0	6	6	8	12.70
	Aspartate aminotransferase, mitochondrial	AATM_MOUSE	47,412.3	100.0	3	3	6	9.77
	Propionyl-CoA carboxylase beta chain, mitochondrial	PCCB_MOUSE	58,394.5	100.0	6	6	11	14.40
	Cytochrome b-c1 complex subunit 1, mitochondrial	QCR1_MOUSE	52,768.8	100.0	3	3	6	8.12
	Methylmalonate-semialdehyde dehydrogenase [acylating], mitochondrial	MMSA_MOUSE	57,916.3	100.0	6	8	14	16.80

	ATP synthase subunit alpha, mitochondrial	ATPA_MOUSE	59,754.1	100.0	11	13	22	23.10
	Aconitate hydratase, mitochondrial	ACON_MOUSE	85,465.9	100.0	12	13	24	16.70
	Tubulin alpha-4A chain	TBA4A_MOUSE	49,924.6	100.0	5	6	11	15.20
	NADH-ubiquinone oxidoreductase 75 kDa subunit, mitochondrial	NDUS1_MOUSE	79,749.6	100.0	2	2	2	3.58
	Trifunctional enzyme subunit beta, mitochondrial	ECHB_MOUSE	51,388.0	100.0	8	9	15	18.30
	Acetyl-coenzyme A synthetase 2-like, mitochondrial	ACS2L_MOUSE	74,623.5	100.0	3	3	5	4.40
	Calcium-binding mitochondrial carrier protein Aralar1	CMC1_MOUSE	74,571.8	100.0	3	3	6	4.73
	Carnitine O-palmitoyltransferase 1, muscle isoform	CPT1B_MOUSE	88,220.0	100.0	3	3	6	4.15
	Pyruvate dehydrogenase E1 component subunit alpha, somatic form, mitochondrial	ODPA_MOUSE	43,232.5	100.0	3	3	6	7.18
	Beta-enolase	ENOB_MOUSE	47,025.9	100.0	2	3	5	7.14
	Myomesin-1	MYOM1_MOUSE	185,464.6	100.0	3	3	6	1.74
	Adenylosuccinate lyase	PUR8_MOUSE	54,809.3	100.0	2	2	2	4.13
D4	ATP synthase subunit beta, mitochondrial	ATPB_MOUSE	56,301.2	100.0	3	3	5	7.37
	26S protease regulatory subunit 8	PRS8_MOUSE	45,627.2	100.0	3	3	3	9.61
	Creatine kinase S-type, mitochondrial	KCRS_MOUSE	47,474.7	100.0	7	8	11	17.40
	Beta-enolase	ENOB_MOUSE	47,025.9	100.0	8	10	17	23.00
	Phosphoglycerate kinase 1	PGK1_MOUSE	44,551.1	100.0	9	9	15	26.60

	Succinate dehydrogenase [ubiquinone] flavoprotein subunit, mitochondrial	DHSA_MOUSE	72,585.6	100.0	3	3	6	5.87
	3-ketoacyl-CoA thiolase, mitochondrial	THIM_MOUSE	41,858.2	100.0	2	3	5	8.31
	Carnitine O-palmitoyltransferase 1, muscle isoform	CPT1B_MOUSE	88,220.0	100.0	2	2	4	2.85
	Sarcoplasmic/endoplasmic reticulum calcium ATPase 2	AT2A2_MOUSE	114,860.0	100.0	10	11	18	11.80
	Cytochrome b-c1 complex subunit 1, mitochondrial	QCR1_MOUSE	52,768.8	100.0	6	6	11	15.40
	Elongation factor Tu, mitochondrial	EFTU_MOUSE	49,508.9	100.0	6	7	12	17.90
	[Pyruvate dehydrogenase [lipoamide]] kinase isozyme 1, mitochondrial	PDK1_MOUSE	48,926.8	100.0	5	5	6	15.90
	NADH dehydrogenase [ubiquinone] iron-sulfur protein 2, mitochondrial	NDUS2_MOUSE	52,626.8	100.0	3	3	6	6.05
	Long-chain-fatty-acid--CoA ligase 1	ACSL1_MOUSE	77,926.2	100.0	5	5	8	7.01
	Keratin, type I cytoskeletal 10	K1C10_MOUSE	57,771.3	99.9	2	2	4	3.86
	Medium-chain specific acyl-CoA dehydrogenase, mitochondrial	ACADM_MOUSE	46,482.4	100.0	4	5	9	11.60
	Very long-chain specific acyl-CoA dehydrogenase, mitochondrial	ACADV_MOUSE	70,877.0	100.0	2	2	4	3.20
	Fumarate hydratase, mitochondrial	FUMH_MOUSE	54,371.1	100.0	3	3	5	10.50
	Creatine kinase M-type	KCRM_MOUSE	43,045.6	100.0	3	3	6	9.45
	Succinyl-CoA ligase [ADP-forming] subunit beta, mitochondrial	SUCB1_MOUSE	50,114.7	100.0	8	8	14	20.70

	Cysteine desulfurase, mitochondrial	NFS1_MOUSE	50,001.8	100.0	3	3	6	8.65
	L-lactate dehydrogenase B chain	LDHB_MOUSE	36,572.4	100.0	3	3	6	10.50
	Citrate synthase, mitochondrial	CISY_MOUSE	51,738.1	100.0	4	4	5	9.91
	Electron transfer flavoprotein-ubiquinone oxidoreductase, mitochondrial	ETFD_MOUSE	68,091.8	100.0	4	4	7	7.31
	cAMP-dependent protein kinase type II-alpha regulatory subunit	KAP2_MOUSE	45,389.4	100.0	11	11	21	37.20
	Isocitrate dehydrogenase [NADP], mitochondrial	IDHP_MOUSE	50,907.2	100.0	15	20	41	36.10
	[Pyruvate dehydrogenase [lipoamide]] kinase isozyme 2, mitochondrial	PDK2_MOUSE	46,070.1	100.0	5	5	5	16.50
	Actin, alpha cardiac muscle 1	ACTC_MOUSE	42,020.1	100.0	9	9	17	28.40
	ADP/ATP translocase 1	ADT1_MOUSE	32,905.4	100.0	6	6	10	20.10
	Long-chain specific acyl-CoA dehydrogenase, mitochondrial	ACADL_MOUSE	47,908.7	100.0	7	7	12	20.00
	Aconitate hydratase, mitochondrial	ACON_MOUSE	85,465.9	100.0	12	12	22	20.10
	2-oxoisovalerate dehydrogenase subunit alpha, mitochondrial	ODBA_MOUSE	50,371.5	99.9	2	2	4	6.56
	Eukaryotic initiation factor 4A-I	IF4A1_MOUSE	46,155.3	100.0	7	7	10	19.70
	Cytochrome b-c1 complex subunit 2, mitochondrial	QCR2_MOUSE	48,236.0	100.0	8	8	15	22.30
	Trifunctional enzyme subunit alpha, mitochondrial	ECHA_MOUSE	82,671.5	100.0	9	10	19	15.20

	Adenosylhomocysteinase	SAHH_MOUSE	47,689.1	99.9	2	2	3	5.56
	ATP synthase subunit alpha, mitochondrial	ATPA_MOUSE	59,754.1	100.0	8	8	13	18.40
	cAMP-dependent protein kinase type I-alpha regulatory subunit	KAP0_MOUSE	43,185.8	100.0	6	6	12	16.50
	Pyruvate dehydrogenase E1 component subunit alpha, somatic form, mitochondrial	ODPA_MOUSE	43,232.5	100.0	5	5	8	13.80
	Trifunctional enzyme subunit beta, mitochondrial	ECHB_MOUSE	51,388.0	100.0	7	7	11	16.20
	Succinyl-CoA ligase [GDP-forming] subunit beta, mitochondrial	SUCB2_MOUSE	46,841.0	100.0	3	3	5	8.31
	Calcium-binding mitochondrial carrier protein Aralar1	CMC1_MOUSE	74,571.8	100.0	6	6	10	10.90
D5	cAMP-dependent protein kinase type II-alpha regulatory subunit	KAP2_MOUSE	45,389.4	100.0	7	8	15	22.90
	Pyruvate dehydrogenase E1 component subunit beta, mitochondrial	ODPB_MOUSE	38,937.0	100.0	3	3	4	10.90
	Aspartate aminotransferase, mitochondrial	AATM_MOUSE	47,412.3	100.0	3	3	5	6.28
	Aconitate hydratase, mitochondrial	ACON_MOUSE	85,465.9	100.0	8	8	15	11.80
	Acetyl-CoA acetyltransferase, mitochondrial	THIL_MOUSE	44,816.4	100.0	9	12	19	29.50
	Electron transfer flavoprotein-ubiquinone oxidoreductase, mitochondrial	ETFD_MOUSE	68,091.8	100.0	3	3	6	5.52
	Actin, alpha cardiac muscle 1	ACTC_MOUSE	42,020.1	100.0	16	21	46	55.70
	Long-chain specific acyl-CoA dehydrogenase, mitochondrial	ACADL_MOUSE	47,908.7	100.0	12	13	22	31.90

	ADP/ATP translocase 1	ADT1_MOUSE	32,905.4	100.0	5	5	8	15.80
	Trifunctional enzyme subunit alpha, mitochondrial	ECHA_MOUSE	82,671.5	100.0	3	3	6	5.37
	ATP synthase subunit beta, mitochondrial	ATPB_MOUSE	56,301.2	100.0	5	5	7	13.60
	Glyceraldehyde-3-phosphate dehydrogenase	G3P_MOUSE	35,810.1	100.0	3	3	6	12.90
	Creatine kinase M-type	KCRM_MOUSE	43,045.6	100.0	4	4	7	13.10
	Sarcoplasmic/endoplasmic reticulum calcium ATPase 2	AT2A2_MOUSE	114,860.0	100.0	5	6	9	6.32
	Citrate synthase, mitochondrial	CISY_MOUSE	51,738.1	100.0	4	4	6	11.40
	3-ketoacyl-CoA thiolase, mitochondrial	THIM_MOUSE	41,858.2	100.0	10	12	20	42.60
	Mannose-6-phosphate isomerase	MPI_MOUSE	46,575.9	100.0	3	3	5	10.20
	Elongation factor Tu, mitochondrial	EFTU_MOUSE	49,508.9	100.0	3	3	3	8.41
	NADH dehydrogenase [ubiquinone] 1 alpha subcomplex subunit 10, mitochondrial	NDUAA_MOUSE	40,604.7	100.0	5	5	7	20.00
	Actin, cytoplasmic 1	ACTB_MOUSE, ACTG_MOUSE	41,737.8	100.0	3	4	7	37.90
	Succinyl-CoA ligase [ADP-forming] subunit beta, mitochondrial	SUCB1_MOUSE	50,114.7	100.0	8	10	15	22.00
	Cysteine desulfurase, mitochondrial	NFS1_MOUSE	50,001.8	100.0	2	2	3	4.66
	Phosphate carrier protein, mitochondrial	MPCP_MOUSE	39,633.1	100.0	2	2	4	7.28
	Creatine kinase S-type, mitochondrial	KCRS_MOUSE	47,474.7	100.0	5	5	5	14.80
	Long-chain-fatty-acid--CoA ligase 1	ACSL1_MOUSE	77,926.2	100.0	4	4	6	5.87

	ATP synthase subunit alpha, mitochondrial	ATPA_MOUSE	59,754.1	100.0	8	8	14	19.30
	Medium-chain specific acyl-CoA dehydrogenase, mitochondrial	ACADM_MOUSE	46,482.4	100.0	3	5	10	9.50
	Myomesin-1	MYOM1_MOUSE	185,464.6	100.0	3	3	5	1.98
	Succinate dehydrogenase [ubiquinone] flavoprotein subunit, mitochondrial	DHSA_MOUSE	72,585.6	100.0	4	4	8	7.23
	cAMP-dependent protein kinase type I-alpha regulatory subunit	KAP0_MOUSE	43,185.8	100.0	7	9	16	20.70
	Isovaleryl-CoA dehydrogenase, mitochondrial	IVD_MOUSE	46,326.5	100.0	5	6	11	13.70
	Fructose-bisphosphate aldolase A	ALDOA_MOUSE	39,356.5	100.0	3	3	5	9.62
	Isocitrate dehydrogenase [NADP], mitochondrial	IDHP_MOUSE	50,907.2	100.0	7	8	12	19.20
	Cytochrome b-c1 complex subunit 2, mitochondrial	QCR2_MOUSE	48,236.0	100.0	11	16	27	30.50
	Phosphoglycerate kinase 1	PGK1_MOUSE	44,551.1	100.0	11	12	18	29.00
D6	Pyruvate dehydrogenase E1 component subunit beta, mitochondrial	ODPB_MOUSE	38,937.0	100.0	3	3	4	10.00
	cAMP-dependent protein kinase type I-alpha regulatory subunit	KAP0_MOUSE	43,185.8	100.0	8	9	15	27.60
	Medium-chain specific acyl-CoA dehydrogenase, mitochondrial	ACADM_MOUSE	46,482.4	100.0	5	5	8	14.50
	Pyruvate dehydrogenase E1 component subunit alpha, somatic form, mitochondrial	ODPA_MOUSE	43,232.5	100.0	5	5	6	10.00

	NADH dehydrogenase [ubiquinone] iron-sulfur protein 3, mitochondrial	NDUS3_MOUSE	30,149.4	100.0	3	4	8	14.80
	Isocitrate dehydrogenase [NADP], mitochondrial	IDHP_MOUSE	50,907.2	100.0	6	6	9	15.50
	Succinate dehydrogenase [ubiquinone] iron-sulfur subunit, mitochondrial	DHSB_MOUSE	31,815.0	100.0	3	4	7	11.00
	D-beta-hydroxybutyrate dehydrogenase, mitochondrial	BDH_MOUSE	38,286.0	100.0	3	3	4	11.40
	ADP/ATP translocase 2	ADT2_MOUSE	32,932.6	100.0	3	3	4	22.50
	Electron transfer flavoprotein subunit alpha, mitochondrial	ETFA_MOUSE	35,009.8	100.0	6	8	14	27.30
	Actin, alpha cardiac muscle 1	ACTC_MOUSE	42,020.1	100.0	8	10	16	24.70
	2,4-dienoyl-CoA reductase, mitochondrial	DECR_MOUSE	36,215.2	100.0	3	3	6	13.40
	Malate dehydrogenase, cytoplasmic	MDHC_MOUSE	36,512.1	100.0	4	4	7	16.50
	Mitochondrial 2-oxoglutarate/malate carrier protein	M2OM_MOUSE	34,156.3	100.0	6	6	10	22.30
	Triosephosphate isomerase	TPIS_MOUSE	26,712.2	100.0	3	4	7	17.70
	Malate dehydrogenase, mitochondrial	MDHM_MOUSE	35,611.9	100.0	4	4	7	13.30
	ATP synthase subunit alpha, mitochondrial	ATPA_MOUSE	59,754.1	100.0	7	8	16	17.40
	ADP/ATP translocase 1	ADT1_MOUSE	32,905.4	100.0	14	15	26	40.30
	Sepiapterin reductase	SPRE_MOUSE	27,883.8	100.0	3	4	6	18.00
	Sarcoplasmic/endoplasmic reticulum calcium ATPase 2	AT2A2_MOUSE	114,860.0	100.0	5	5	9	5.94

	Citrate lyase subunit beta-like protein, mitochondrial	CLYBL_MOUSE	37,549.1	100.0	3	3	5	9.76
	Myosin light chain 3	MYL3_MOUSE	22,422.2	100.0	3	3	6	19.60
	Myomesin-1	MYOM1_MOUSE	185,464.6	100.0	3	3	4	2.28
	ATP synthase subunit gamma, mitochondrial	ATPG_MOUSE	32,887.4	100.0	4	5	12	15.80
	Aconitate hydratase, mitochondrial	ACON_MOUSE	85,465.9	100.0	3	4	6	5.26
	Cytochrome b-c1 complex subunit 2, mitochondrial	QCR2_MOUSE	48,236.0	100.0	7	7	13	18.30
	3-hydroxyisobutyrate dehydrogenase, mitochondrial	3HIDH_MOUSE	35,440.6	100.0	3	3	6	15.20
	Glyceraldehyde-3-phosphate dehydrogenase	G3P_MOUSE	35,810.1	100.0	3	3	5	12.90
	3,2-trans-enoyl-CoA isomerase, mitochondrial	D3D2_MOUSE	32,079.2	100.0	3	4	7	13.50
	cAMP-dependent protein kinase type II-alpha regulatory subunit	KAP2_MOUSE	45,389.4	100.0	5	5	8	16.20
	Coiled-coil-helix-coiled-coil-helix domain-containing protein 3, mitochondrial	CHCH3_MOUSE	26,334.4	100.0	4	5	8	12.80
	Succinate dehydrogenase [ubiquinone] flavoprotein subunit, mitochondrial	DHSA_MOUSE	72,585.6	100.0	3	4	7	5.27
	Trifunctional enzyme subunit alpha, mitochondrial	ECHA_MOUSE	82,671.5	100.0	4	5	7	7.08
	Trifunctional enzyme subunit beta, mitochondrial	ECHB_MOUSE	51,388.0	100.0	6	6	10	14.30
	Long-chain specific acyl-CoA dehydrogenase, mitochondrial	ACADL_MOUSE	47,908.7	100.0	3	3	5	8.37

	Electron transfer flavoprotein subunit beta	ETFB_MOUSE	27,623.2	100.0	6	6	11	24.30
	Acetyl-CoA acetyltransferase, mitochondrial	THIL_MOUSE	44,816.4	100.0	5	5	7	17.20
	L-lactate dehydrogenase A chain	LDHA_MOUSE	36,498.9	100.0	3	3	5	8.73
	ATP synthase subunit beta, mitochondrial	ATPB_MOUSE	56,301.2	100.0	4	4	7	11.30
	Enoyl-CoA hydratase, mitochondrial	ECHM_MOUSE	31,475.3	100.0	6	8	14	28.60
	3-ketoacyl-CoA thiolase, mitochondrial	THIM_MOUSE	41,858.2	100.0	7	9	14	25.70
	Estradiol 17-beta-dehydrogenase 8	DHB8_MOUSE	26,645.3	100.0	3	4	6	15.40
	Phosphate carrier protein, mitochondrial	MPCP_MOUSE	39,633.1	100.0	10	13	19	23.80
	Cytochrome b-c1 complex subunit Rieske, mitochondrial	UCRI_MOUSE	29,367.2	100.0	3	4	6	8.39

Appendix B. Proteins of which abundance increased or decreased with H_2O_2 in WT *capture* but not KI *capture*. cAMP affinity capture samples were run on a gradient gel and the gel was stained with colloidal Coomassie. Selected stained bands were cut out of the gel and analysed by LC-MS/MS. The table lists identified proteins in which abundance increased or decreased between control and H_2O_2-treated WT hearts but not between KI control and H_2O_2-treated hearts. The accession no., molecular weight (Mw) and no. of assigned spectra for each *capture* sample are also shown.

Displaying: no. of assigned spectra			WT	WT	KI	KI
Identified proteins	**Accession no.**	**Mw (kDa)**	**control**	**H_2O_2**	**control**	**H_2O_2**
Aspartate aminotransferase, mitochondrial	AATM_MOUSE	47	11	8	17	17
Medium-chain specific acyl-CoA dehydrogenase, mitochondrial	ACADM_MOUSE	46	44	28	41	45
Very long-chain specific acyl-CoA dehydrogenase, mitochondrial	ACADV_MOUSE	71	8	4	17	16
ATP-citrate synthase	ACLY_MOUSE	120	0	4	0	0
A kinase anchor protein 1, mitochondrial	AKAP1_MOUSE	92	12	23	18	18
A-kinase anchor protein 2	AKAP2_MOUSE	99	0	13	6	8
ATP synthase subunit alpha, mitochondrial	ATPA_MOUSE	60	90	74	99	98
Citrate lyase subunit beta-like protein, mitochondrial	CLYBL_MOUSE	38	5	11	8	5
Ubiquinone biosynthesis methyltransferase COQ5, mitochondrial	COQ5_MOUSE	37	3	7	1	3
Estradiol 17-beta-dehydrogenase 8	DHB8_MOUSE	27	6	3	6	6
Dihydrolipoyl dehydrogenase, mitochondrial	DLDH_MOUSE	54	10	5	10	13
Fatty acid synthase	FAS_MOUSE	272	1	15	2	4
Lactation elevated protein 1	LACE1_MOUSE	54	0	3	0	0
NADH dehydrogenase [ubiquinone] 1 alpha subcomplex subunit 9, mitochondrial	NDUA9_MOUSE	43	0	10	4	0
Dihydrolipoyllysine-residue acetyltransferase component of pyruvate dehydrogenase complex, mitochondrial	ODP2_MOUSE	68	14	7	15	14
Pyruvate dehydrogenase E1 component subunit beta, mitochondrial	ODPB_MOUSE	39	16	12	20	19
Phosphoglycerate kinase 1	PGK1_MOUSE	45	25	19	26	36
26S protease regulatory subunit 7	PRS7_MOUSE	49	0	3	0	0
Pyruvate carboxylase, mitochondrial	PYC_MOUSE	130	9	15	0	1

Valyl-tRNA synthetase	SYVC_MOUSE	140	4	9	1	0
Tetratricopeptide repeat protein 38	TTC38_MOUSE	52	0	3	0	0
Voltage-dependent anion-selective channel protein 3	VDAC3_MOUSE	31	3	5	2	2

Appendix C. Proteins of which abundance was significantly (p<0.05) different between WT and KI *capture* samples. cAMP affinity capture samples were run on a gradient gel and the gel was stained with colloidal Coomassie. Selected stained bands were cut out of the gel and analysed by LC-MS/MS. The table lists identified proteins in which abundance was significantly (p<0.05) different between WT (control and H_2O_2-treated) and KI (control and H_2O_2-treated) hearts. The accession no., molecular weight (Mw) and no. of assigned spectra for each *capture* sample are shown as well as the p-value from a Fishers Exact Test.

Displaying: no. of assigned spectra			**WT vs KI**	**WT**	**WT**	**KI**	**KI**
Identified proteins	**Accession no.**	**Mw (kDa)**	**Fisher's Exact Test (p-value)**	**control**	**H_2O_2**	**control**	**H_2O_2**
Aspartate aminotransferase, mitochondrial	AATM_MOUSE	47	0.033	11	8	17	17
Long-chain specific acyl-CoA dehydrogenase, mitochondrial	ACADL_MOUSE	48	0.038	40	25	35	51
Very long-chain specific acyl-CoA dehydrogenase, mitochondrial	ACADV_MOUSE	71	0.00039	8	4	17	16
Aconitate hydratase, mitochondrial	ACON_MOUSE	85	2.5E-11	74	61	116	127
Acetyl-coenzyme A synthetase 2-like, mitochondrial	ACS2L_MOUSE	75	0.018	0	2	2	9
Long-chain-fatty-acid--CoA ligase 1	ACSL1_MOUSE	78	0.000000033	4	8	15	38
Actin, alpha cardiac muscle 1	ACTC_MOUSE	42	0.0044	85	83	98	118
Aldehyde dehydrogenase X, mitochondrial	AL1B1_MOUSE	58	0.03	0	0	3	3
Sarcoplasmic/endoplasmic reticulum calcium ATPase 2	AT2A2_MOUSE	115	0.0000037	81	74	97	122
ATP synthase subunit alpha, mitochondrial	ATPA_MOUSE	60	0.028	90	74	99	98
Coiled-coil-helix-coiled-coil-helix domain-containing protein 3, mitochondrial	CHCH3_MOUSE	26	0.024	13	13	5	8
Clathrin heavy chain 1	CLH_MOUSE	192	0.042	8	9	2	4
Calcium-binding mitochondrial carrier protein Aralar1	CMC1_MOUSE	75	0.0000059	3	6	13	25
Ubiquinone biosynthesis methyltransferase COQ5, mitochondrial	COQ5_MOUSE	37	0.041	3	7	1	3
Carnitine O-palmitoyltransferase 1, muscle isoform	CPT1B_MOUSE	88	0.032	9	10	12	19

Cytochrome c1, heme protein, mitochondrial	CY1_MOUSE	35	0.00031	11	14	4	2
Dehydrogenase/reductase SDR family member 4	DHRS4_MOUSE	28	0.02	4	5	0	2
Succinate dehydrogenase [ubiquinone] flavoprotein subunit, mitochondrial	DHSA_MOUSE	73	0.0000068	11	9	23	35
Cytoplasmic dynein 1 heavy chain 1	DYHC1_MOUSE	532	0.011	7	3	0	1
Trifunctional enzyme subunit alpha, mitochondrial	ECHA_MOUSE	83	0.00000069	38	26	50	75
Elongation factor Tu, mitochondrial	EFTU_MOUSE	50	0.049	22	25	16	18
Alpha-enolase	ENOA_MOUSE	47	0.013	12	12	9	3
Beta-enolase	ENOB_MOUSE	47	0.034	41	37	36	22
Electron transfer flavoprotein subunit alpha, mitochondrial	ETFA_MOUSE	35	0.043	13	14	21	22
Electron transfer flavoprotein-ubiquinone oxidoreductase, mitochondrial	ETFD_MOUSE	68	0.0000032	5	7	20	24
Stress-70 protein, mitochondrial	GRP75_MOUSE	74	0.0029	0	1	5	7
Heat shock protein HSP 90-beta	HS90B_MOUSE	83	0.036	4	3	7	9
Heat shock cognate 71 kDa protein	HSP7C_MOUSE	71	3.5E-10	0	0	11	21
Hexokinase-2	HXK2_MOUSE	103	0.00011	24	25	7	8
Isocitrate dehydrogenase [NADP], mitochondrial	IDHP_MOUSE	51	0.022	127	133	121	95
Uncharacterized protein KIAA0564 homolog	K0564_MOUSE	213	0.00000053	33	38	9	9
Protein KIAA0664	K0664_MOUSE	148	0.022	9	7	3	2
cAMP-dependent protein kinase type I-alpha regulatory subunit	KAP0_MOUSE	43	0.00045	144	179	131	112
cAMP-dependent protein kinase type I-beta regulatory subunit	KAP1_MOUSE	43	0.0000017	3	10	6	2
cGMP-dependent protein kinase 1	KGP1_MOUSE	76	0.00066	0	4	6	12
L-lactate dehydrogenase B chain	LDHB_MOUSE	37	0.0033	6	8	15	19
Methylmalonate-semialdehyde dehydrogenase [acylating], mitochondrial	MMSA_MOUSE	58	0.029	16	22	10	15
Myosin-6	MYH6_MOUSE	224	0.00000042	61	57	94	84
Myomesin-1	MYOM1_MOUSE	185	0.041	83	75	58	51

NADH dehydrogenase [ubiquinone] 1 alpha subcomplex subunit 9, mitochondrial	NDUA9_MOUSE	43	0.041	0	10	4	0
NADH-ubiquinone oxidoreductase 75 kDa subunit, mitochondrial	NDUS1_MOUSE	80	0.0065	3	4	9	12
NADH dehydrogenase [ubiquinone] iron-sulfur protein 2, mitochondrial	NDUS2_MOUSE	53	0.032	17	16	13	7
Phosphoglycerate kinase 1	PGK1_MOUSE	45	0.036	25	19	26	36
Presequence protease, mitochondrial	PREP_MOUSE	117	0.021	2	8	1	0
Pyruvate carboxylase, mitochondrial	PYC_MOUSE	130	0.0000063	9	15	0	1
Cytochrome b-c1 complex subunit 1, mitochondrial	QCR1_MOUSE	53	0.0033	30	34	21	17
Valyl-tRNA synthetase	SYVC_MOUSE	140	0.0034	4	9	1	0
3-ketoacyl-CoA thiolase, mitochondrial	THIM_MOUSE	42	0.012	33	31	39	53
Triosephosphate isomerase	TPIS_MOUSE	27	0.011	16	9	3	7